Technical Report Documentation Page

1. Report No.	2. Government Accession No.	3. Recipient's Catalog No.
FHWA-SC-14-02		

4. Title and Subtitle	5. Report Date
Seismic Site Coefficients and Acceleration Design Response Spectra Based on Conditions in South Carolina	November 15, 2014
	6. Performing Organization Code
7. Author(s)	8. Performing Organization Report No.
Ronald D. Andrus, Nadarajah Ravichandran, Shimelies A. Aboye, Ariful H. Bhuiyan, and James R. Martin II	
9. Performing Organization Name and Address	10. Work Unit No. (TRAIS)
Clemson University Glenn Department of Civil Engineering Clemson, SC 29634-0911	
	11. Contract or Grant No.
	SC-DOT Research Project No. 686
12. Sponsoring Agency Name and Address	13. Type of Report and Period Covered
South Carolina Department of Transportation P. O. Box 191 Columbia, SC 29202-0191	Final Report December 01, 2009 to November 30, 2014
	14. Sponsoring Agency Code

15. Supplementary Notes

16. Abstract

The simplified procedure in design codes for determining earthquake response spectra involves estimating site coefficients to adjust available rock accelerations to site accelerations. Several investigators have noted concerns with the site coefficients recommended in current codes, herein called the 1994 National Earthquake Hazard Reduction Program (NEHRP) site coefficients, including (1) the suitability of the 1994 NEHRP coefficients for conditions different from Western United States geology; (2) the appropriateness of using a single coefficient for a wide range of soil stiffnesses; and (3) the suitability of using coefficients that are independent of depth to top of rock.

This report describes a systematic ground response study to determined site coefficients (F) appropriate for South Carolina's geologic and seismic conditions. The study involves assuming conditions at seven locations in the Atlantic Coastal Plain and four locations in the South Carolina Piedmont. Over 60,000 total stress, one-dimensional equivalent linear (SHAKE2000) and nonlinear (DMOD2000) ground response simulations are conducted using numerous representative shear wave velocity profiles and a suite of over 130 synthetic rock outcrop motions generated with the computer program Scenario_PC assuming return periods of 475 and 2,475 years.

Results of the ground response analyses are compiled into over 400 plots of computed values of F versus average shear wave velocity in the top 100 ft (V_{S100ft}) grouped by site location, depth to top of soft rock ($H_{B\text{-}C}$) or hard rock (H_{HR}), spectral period (T), and spectral acceleration of the rock input motion ($S_{outcrop}$). In nearly all the plots, the following three distinct features can be seen—(1) an increasing trend in F as V_{S100ft} increases from zero; (2) a zone of peak values of F; and (3) a decreasing trend in F as V_{S100ft} increases to the velocity of the reference rock.

17. Key Words	18. Distribution Statement
Earthquakes; ground motion; ground response analysis; material damping; seismic site coefficients; shear wave velocity; site effects; shear modulus; South Carolina	No restrictions.

19. Security Classif. (of this report)	20. Security Classif. (of this page)	21. No. Of Pages	22. Price
Unclassified	Unclassified	367	$45

16. Abstract (continued)

A new mathematical model for F is developed from the results to capture these three distinct features. Development of the model begins by estimating the peak site coefficient (F_P) and the corresponding average shear wave velocity ($V_{S100ftP}$) for each plot. Next, the values of F_P and $V_{S100ftP}$ are studied to determine the most significant influencing variables. In addition to V_{S100ft}, variables found to be most influential are: $H_{B\text{-}C}$, H_{HR}, $S_{outcrop}$, mean predominant period of the rock input motion (T_m), and average shear wave velocity in the top 330 ft (V_{S330ft}). Finally, overall median relationships for F that are functions of F_P, $V_{S100ftP}$, and the most influential variables are derived from regression analysis.

The amount of variability within the plotted values of F is characterized by 95% upper bound and 5% lower bound relationships. The 95% upper bounds are, on average, 42% higher than the median relationships; and the 5% low bounds are, on average, 36% lower than the median relationships.

Computed values of F are generally higher for the Piedmont than for the Coastal Plain. This difference can be explained by the fact that the Piedmont site coefficients are referenced to hard rock, instead of soft rock, and because of the higher impedance contrasts between soil and hard rock in the Piedmont.

The median F relationships for spectral periods of 0.0, 0.2 and 1.0 s are compared with the 1994 NEHRP site coefficients. The 1994 NEHRP coefficients are found to be often over conservative for NEHRP Site Class E sites; and sometimes unconservative for NEHRP Site Class C and D sites, particularly where the top of rock lies at shallow depths. Based on this comparison, the model of F developed in this study is recommended for seismic design in South Carolina.

Because the recommended model of F is based on a very broad range of soil/rock conditions and general rock motion properties, it can be directly applied to other areas with similar geologic and seismic conditions. In areas outside of South Carolina, calibration or modification of model variables may be required.

The simplified procedure for determining acceleration design response spectrum (ADRS), sometimes called the 3-point ADRS method, is found to be generally valid when $V_{S100ft} > 650$ ft/s. However, when $V_{S100ft} \leq 650$ ft/s, the results of this and other studies indicate that significant spectral peaks may occur at periods greater than 1.0 s. For this reason, it is recommended that a multi-point ADRS be plotted with the 3-point ADRS to check if long-period accelerations are under predicted. The objective of the multi-point ADRS is not to replace the design code philosophy, but to present an option for the designer to check that longer period accelerations are not under-predicted by the 3-point ADRS.

It is also found that 3-point ADRS curves predicted by the site coefficients for the Coastal Plain and the Piedmont exhibit some differences when applied to sites near the boundary of these two physiographic areas, called the Fall Line. It is recommended that ADRS curves based on the Piedmont site coefficients be used at sites near the Fall Line where $H_{HR} < 330$ ft; and the Coastal Plain site coefficients be used at sites in the Coastal Plain where $H_{HR} \geq 330$ ft.

Finally, a discussion of the repercussions of the new seismic site coefficients on structural analysis of highway bridges in South Carolina is presented. The discussion is based on the analysis results of two sample bridges using the 1994 NEHRP site coefficients, the site coefficients of this study, and the computer program SAP2000 or CSiBridge.

ACKNOWLEDGMENTS

The South Carolina Department of Transportation (SCDOT) and the Federal Highway Administration (FHWA) funded this work under SCDOT Research Project No. 686. The Steering and Implementation Committee for this project consisted of: Nicholas Harman, chair, Lucero E. Mesa and Chris Gaskins of SCDOT; and Kenneth Johnson of FHWA. The support of the SCDOT/FHWA and the guidance of the Steering and Implementation Committee are sincerely appreciated.

We thank WeiChiang Pang of Clemson University for his assistance with some of the statistical interpretations. We also thank James Kaklamanos of Merrimack College and anonymous reviewers of the *Earthquake Spectra* and the *Bulletin of the Seismological Society of America* manuscripts prepared from this work for their many constructive and insightful comments. Finally, we thank Michael Esposito of Clemson University for his editorial review of the report, and the staff at Clemson University for their administrative support.

TABLE OF CONTENTS

LIST OF TABLES

LIST OF FIGURES

CHAPTER ONE

INTRODUCTION

1.1 Background

Local site conditions can greatly influence ground surface motions and structural damage caused by earthquakes (Kramer 1996). Two earthquakes that emphasized the influence of local site conditions on ground response and had a major impact on seismic building codes were the 1985 Michoacán, Mexico, and the 1989 Loma Prieta, California, earthquakes (Idriss 1990; Borcherdt 1994). Local site conditions of importance include the travel path geology, the underlying basin structure, the thicknesses of soil layers, the small-strain stiffness and material damping of each layer, the variation of stiffness and material damping with shearing strain amplitude of each layer, and the site topography.

Presented in Figure 1.1 is a schematic of earthquake motion propagation from source to site. The rupture at the fault initiates stress waves that propagate through the bedrock to the soil layers beneath the project site, and finally through the soil layers to reach the ground surface. The rupture mechanism and wave passage effects through the bedrock are often modeled in a seismic hazard analysis study (e.g., U.S. Geological Survey hazard maps, S.C. Department of Transportation hazard maps), which provides ground motion parameters at the top of the bedrock. Site response analysis mainly deals with the ground motion propagation through the soil layers.

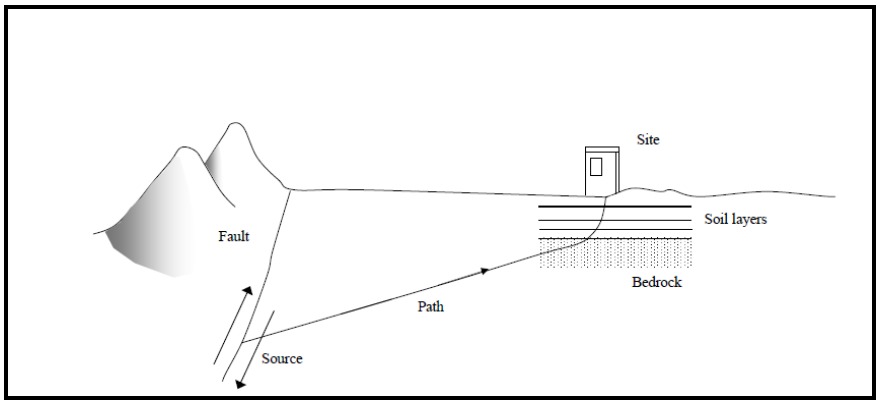

Figure 1.1 Schematic ground motion propagation from source to site (after Kramer 1996).

Several investigators have noted the particular significance of small-strain stiffness represented by shear modulus or shear wave velocity on dynamic behavior (Idriss 1990; Borcherdt 1994; Boore et al. 1994; Joyner et al. 1994). Because a complete characterization of small-strain shear wave velocity (V_S) to bedrock and a site-specific ground response analysis are often not economically feasible for routine projects, the average V_S in the top 100 ft (V_{S100ft}) has been adopted for determining seismic site classification (Borcherdt 1994; Seed et al. 1994; Dobry et al. 2000). The value of V_{S100ft} is computed by:

$$V_{S100ft} = \frac{100}{\sum_{i=1}^{m} H_i / V_{si}} \tag{1.1}$$

where H_i is the thickness in feet of layer i; V_{Si} is the shear wave velocity in ft/s of layer i; and m is the number of layers in the top 100 ft.

Profiles with $V_{S100ft} > 5{,}000$ ft/s, $2{,}500 < V_{S100ft} \leq 5{,}000$ ft/s, $1200 < V_{S100ft} \leq 2{,}500$ ft/s, $600 < V_{S100ft} \leq 1{,}200$ ft/s and $V_{S100ft} \leq 600$ ft/s correspond to seismic site classes designated as A, B, C, D and E, respectively, assuming no special condition (e.g., peats, highly organic clays, very high plasticity clays, very thick soft/medium stiff clay) that are designated as Site Class F. These site classes are often referred to as the National Earthquake Hazard Reduction Program (NEHRP) seismic site classes after the study where they were first introduced (BSSC 1995).

One of the outputs of ground response analysis is the site acceleration response spectrum, which is a plot of the maximum spectral acceleration responses of a series of single degree-of-freedom systems, typically with 5% damping, for a given base motion. From the site response spectrum and the input rock outcrop response spectrum, the site coefficient (F) is computed by:

$$F = \frac{S_{site}}{S_{outcrop}} \tag{1.2}$$

where S_{site} is the site spectral acceleration at a selected period; and $S_{outcrop}$ is the soft rock outcrop spectral acceleration at the same period.

The site coefficients for short-period or 0.2 s (F_a) and long-period or 1.0 s (F_v) adopted in the American Society of Civil Engineers Standard ASCE 7-10 (ASCE 2010), the International Building Code (ICC 2012), and the AASHTO guide (AASHTO 2011a) first appeared in the 1994 NEHRP provisions (BSSC 1995). Original values of F_a and F_v at small levels of shaking (peak ground accelerations ≈ 0.1 g) were derived from empirical investigations using strong motion data recorded in the San Francisco Bay area during the 1989 Loma Prieta earthquake (Borcherdt 1994; Joyner et al. 1994). At stronger levels of shaking, original values of F_a and F_v were derived from the results of one-dimensional equivalent linear and nonlinear site response analyses assuming Western United States geologic and seismic conditions (Seed et al. 1994; Dobry et al. 2000). These site coefficients are herein referred to as the 1994 NEHRP F_a and F_v values. The 1994 NEHRP F_a values are also often assumed for the site coefficients for the free-field or 0.0 s (F_{PGA}) condition.

1.2 Problem Statement

The problem statement of this study is conceived from concerns highlighted by a number of investigators regarding the 1994 NEHRP F_a and F_v values as well as the recommended site-class based procedure. Some of these concerns include: (1) significant differences between the 1994 NEHRP values and computed mean values from site-specific response analysis; (2) the appropriateness of using the 1994 NEHRP site coefficients for soil conditions different from Western United States; (3) the appropriateness of using a single value for a site class with a wide range of V_{S100ft}; (4) the appropriateness of using a single value that is independent of the depth to top of rock; and (5) the appropriateness of assuming $F_{PGA} = F_a$.

Several studies using non-Loma Prieta strong motion data sets have provided F_a and F_v values that are somewhat different from the 1994 NEHRP. Borcherdt (2002) obtained F_a and F_v that are slightly greater based on amplifications observed during the 1994 Northridge, California earthquake. Stewart et al. (2003) obtained slightly higher F_a and F_v values using various California earthquakes. Park and Hashash (2005) showed that the 1994 NEHRP F_a and F_v values may be over conservative at short periods and unconservative at long periods for thick soil deposits. Silva et al. (2000) obtained higher F_a and F_v for C and D site classes, and significantly lower F_a and F_v for E site class using point-source model stochastic ground motions. Crouse (2011) indicated that the commonly used procedure for constructing design

response spectra based just on the F_a and F_v values may not always capture acceleration response at periods > 2.0 s. Matasovic and Hashash (2012) indicated concerns about using the 1994 NEHRP values in evaluating response of both short-period (T < 0.5 s) and long-period (T > 1.0 s) structures.

In South Carolina, studies also have shown that the 1994 NEHRP F_a and F_v may not be applicable to conditions in the state (Power et al. 1998; Lester and Chapman 2005; Chapman et al. 2006). Lester and Chapman (2005) obtained peak spectral accelerations around Columbia that significantly exceed values predicted by the 1994 NEHRP coefficients, especially at periods around 1.0 s. Chapman et al. (2006) presented results of a ground response study for conditions in Charleston where F_a and F_v exceeded the 1994 NEHRP coefficients.

Recognizing the limitations of the 1994 NEHRP site coefficients, the authors of AASHTO (2011b) wrote: "Site response analyses have also shown that response of deep soil basins (i.e., basins with over 500 ft of sediments) and soil sites with a bedrock interface or other layer interface across which there is a significant contrast in soil stiffness and density within 150 to 200 ft of the ground surface is not properly described by the NEHRP soil site coefficients. These deep soil basin and shallow bedrock conditions can be accounted for using appropriate one-dimensional site response analysis." The deep soil basin condition is typical of the South Carolina Coastal Plain. The significant contrast in soil stiffness and density condition is typical of the South Carolina Piedmont. Thus, new site coefficients based on conditions in South Carolina are needed.

1.3 Objectives

The objectives of this report are:

1. To derive a new generalized mathematical model of $F_{PGA,}$ F_a and F_v, as well as site coefficients at other periods based on conditions typical of South Carolina. Conditions typical of Aiken, Charleston, Columbia, Florence, Lake Marion, Myrtle Beach, and the South Carolina side of Savannah (Georgia) will be considered for the Coastal Plain. For the Piedmont, conditions typical of Columbia, Greenville, Greenwood and Rock Hill areas will be considered. The site coefficients will be derived as a function of amplitude, V_{S100ft} (or stiffness of the soil in top 100 ft), mean-predominant period of the base motion (T_m), and

fundamental period of the soil in the top 330 ft (T_{330ft}). Computed mean values of F will be plotted versus V_{S100ft} and grouped by amplitude and period. The derived site coefficients will be compared with the 1994 NEHRP F_a and F_v values and previous studies.

2. To identify conditions where the commonly used (and sometimes called 3-point) simplified procedure for constructing acceleration design response spectra may not be appropriate, and to recommend modifications to the procedure where needed.
3. To investigate and quantify the effect of depth to soft rock ($H_{B\text{-}C}$) and depth to hard rock (H_{HR}) on the derived site coefficients. The effect of $H_{B\text{-}C}$ will be investigated by assuming hypothetical $H_{B\text{-}C}$ values of 5, 16, 33, 66, 100, 165, and 330 ft.
4. To investigate and quantify the effect of duration of earthquake motion on the derived site coefficients by using synthetic motions generated assuming earthquake moment magnitude (M_w) of 5, 6, 7, and 8.

1.4 Report Overview

Discussed in Chapter 2 is a ground response study performed based on conditions in the Charleston area. From the results, a continuous V_{S100ft}- and amplitude-dependent seismic site coefficient model is developed. The site coefficient model for Charleston developed in Chapter 2 is extended to the South Carolina Coastal Plain in Chapter 3 and the South Carolina Piedmont in Chapter 4. Presented in Chapter 5 are tabulated maximum median site coefficients within a seismic site class computed from the generalized models developed in Chapters 3 and 4. Also presented in Chapter 5 is a discussion on the site coefficients and the acceleration design response spectra (ADRS) procedure recommended in the South Carolina Department of Transportation Geotechnical Design Manual (SCDOT 2010). Presented in Chapter 6 is a discussion on the repercussion of the new seismic site coefficients on structural analysis. Finally, a summary of this study and recommendations for future study are given in Chapter 7.

CHAPTER TWO

SEISMIC SITE COEFFICIENTS AND DESIGN RESPONSE SPECTRA BASED ON CONDITIONS IN CHARLESTON[1]

2.1 Geology and Seismology

The Charleston area, as displayed in Figure 2.1, is located within the lower part of the Atlantic Coastal Plain. Gridlines in Figure 2.1 represent 7.5-minute quadrangle boundaries. Major rivers flowing through the area into the Atlantic Ocean include the Ashley, the Cooper, the Stono and the Wando. Ground surface elevations range from sea level along the coast to about 105 ft above sea level in the northwestern most quadrangle shown in Figure 2.1.

The subsurface geology consists of ocean-ward thickening Cretaceous and younger sediments down to depths of 2,300-3,300 ft (Chapman and Talwani 2002). Near-surface sediments are typically unconsolidated Quaternary deposits ranging from beach/barrier island sand to estuarine sand and clay to fluvial sand and silt (McCartan et al. 1984). Exposures of Tertiary sediments exist in limited areas along the stream banks in the northwestern half of Figure 2.1. Tertiary and Cretaceous sediments are compacted, but weakly lithified. Beneath the Tertiary and Cretaceous sediments are hard Mesozoic/Paleozoic basement rock.

The Charleston earthquake of August 31, 1886 with moment magnitude of ~7.0 is the largest historic earthquake to have occurred in the southeastern U.S. (Bollinger 1977). The epicentral area was located near Summerville, Ladson and Middleton Place. The source was likely the Woodstock fault zone shown in Figure 2.1, as delineated by Durá-Gómez and Talwani (2009). Shaking was felt as far as Boston, Massachusetts; Havana, Cuba; Bermuda; and Iowa City, Iowa (Dutton, 1889). Côté (2006) estimated 124 deaths were caused by the earthquake. Talwani and Schaeffer (2001) estimated from paleoliquefaction investigations the recurrence rate for 1886-like earthquakes to be about 500 years.

[1] A similar version of this chapter is published in EERI's *Earthquake Spectra*; Aboye, S.A., Andrus, R.D., Ravichandran, N., Bhuiyan, A.H., and Harman, N., "Seismic Site Factors for Constructing Response Spectra Based on Conditions in Charleston, South Carolina", 2015, Vol. 31, doi: 10.1193/041912eqs163m, in press. (Published online ahead of print 25 November 2013.)

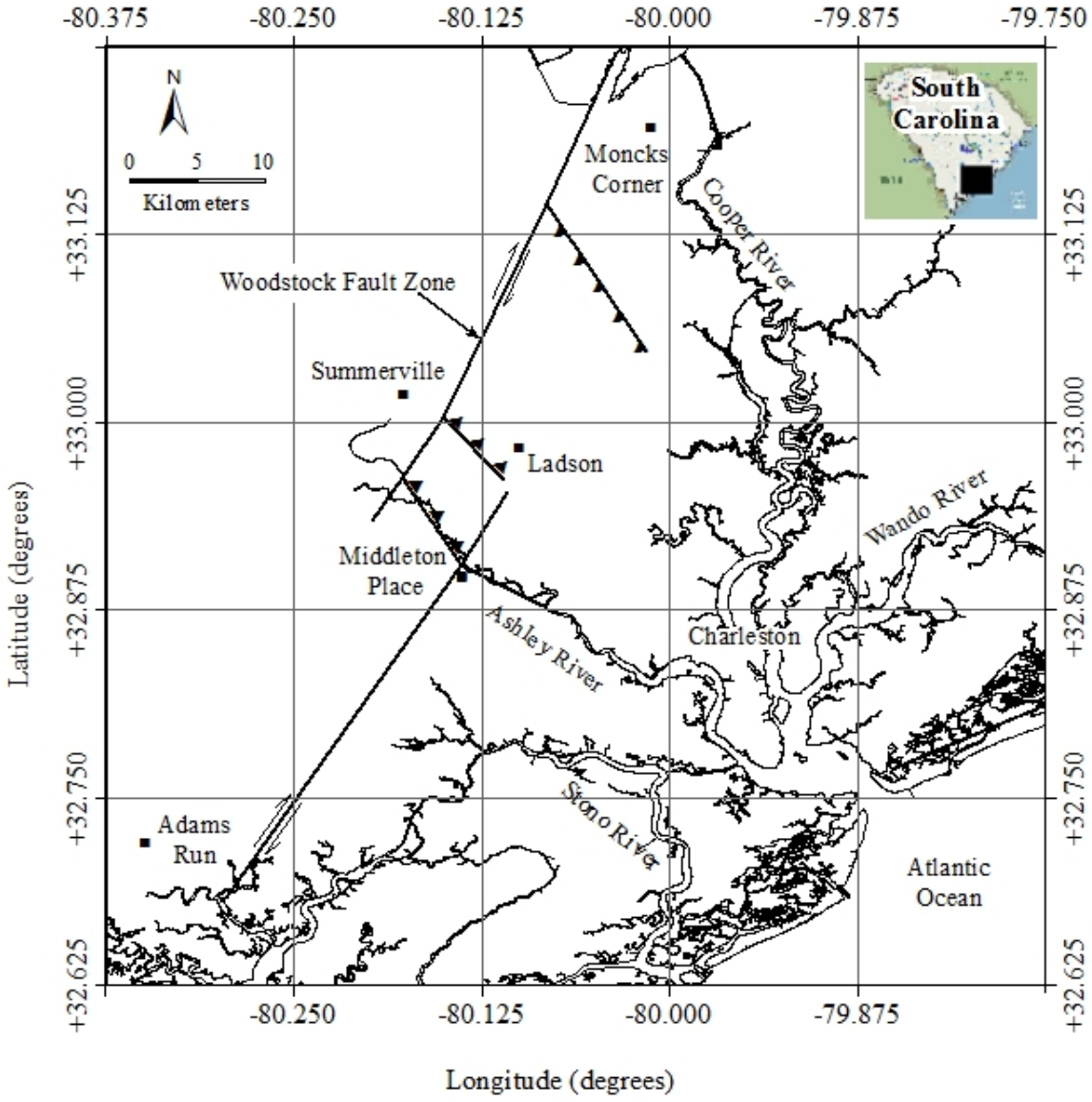

Figure 2.1 Map of the Charleston area showing the Woodstock fault zone as delineated in Durá-Gómez and Talwani (2009).

2.2 Dynamic Soil/Rock Model

Fifty-six V_S profiles are used to represent the variations of small-strain soil/rock stiffnesses in the Charleston area. Presented in Figure 2.2a are twenty-eight V_S profiles that extend to a soft rock (V_S = 2,300 ft/s) half space at a depth of 450 ft. These twenty-eight V_S profiles consist of a reference profile, established by averaging in situ measurements, and twenty-seven variations of the reference profiles.

Tabulated V_S values for the reference profile shown in Figure 2.2a are given in Table 2.1. Above the depth of 260 ft, values of V_S are taken from the statistical study by Andrus et al. (2006) based on compiled in situ measurements conducted by different investigators during the years of 1998-2004. Most of the V_S measurements were made by the seismic cone penetration test method. Some were conducted by the seismic downhole, spectral-analysis-of-surface-waves, suspension logger and seismic refraction methods. Above the depth of 33 ft, the V_S value of 620 ft/s is the average for the 100,000-year-old Wando Formation. Between the depths of 33 ft and 260 ft, the values of V_S ranging from 1,300 to 1,700 ft/s are averages of measurements from the Tertiary-age sediments. Between the depths of 260 and 450 ft, the values of V_S are averages of measurements made by the suspension logger method for the South Carolina Department of Transportation (SCDOT) in 2006.

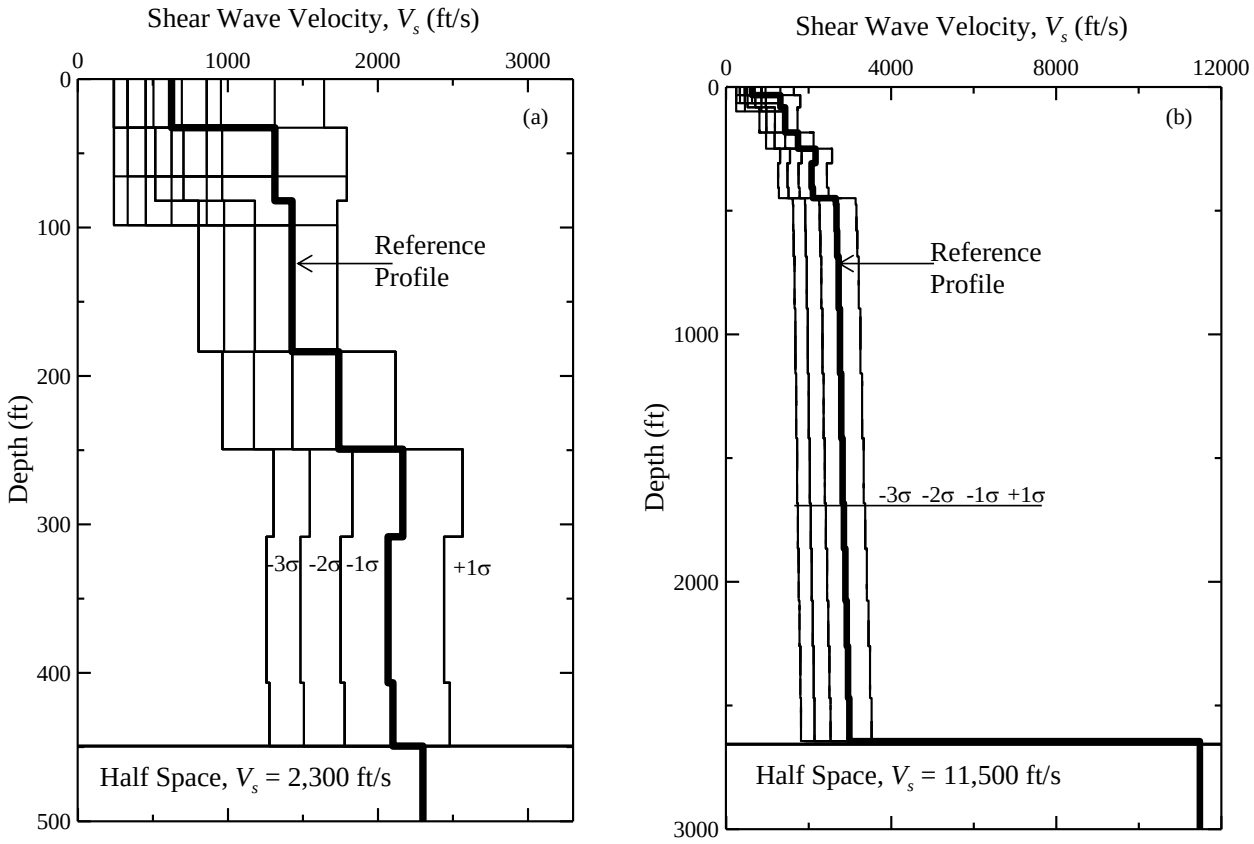

Figure 2.2 Shear wave velocity profiles considered for (a) the soft rock outcropping condition, and (b) the hard rock outcropping condition.

Table 2.1 Reference soil/soft rock profile with top of half space at a depth of 450 ft (modified from Andrus et al. 2006).

Layer number(s)	Layer thickness (ft)	Total unit weight (lb/ft^3)	Shear wave velocity, V_S (ft/s)	Standard deviation of ln(V_S)	Plasticity index, *PI* (%)	Mean effective stress, σ_m' (lb/in^2)	Geologic age
1-3	3.3	116	623	0.32	15	2.2	Quaternary (Wando Formation)
4-10	3.3	116	623	0.32	15	7.2	
11-25	3.3	118	1312	0.31	50	32	Tertiary
26-37	3.3	118	1427	0.19			
38-41	16.4	120	1738	0.20	15	87	Tertiary
42-44	19.7	120	2165	0.17			
45-49	19.7	120	2066	0.26			
50-52	11.5	125	2099	0.26	15	203	Tertiary
53	8.2	125	2099	0.14			
54	Half space	143	2300				Tertiary and older

The V_S profiles plotted in Figure 2.2a are created to represent the range of likely variations in thickness of the Quaternary deposits and V_S of the Quaternary and Tertiary deposits within the Charleston area. Quaternary thicknesses are assumed to be 0, 33, 66 and 100 ft. Variations in V_S are included by applying ±1, -2 and -3 standard deviations of ln(V_S) to the reference profile above the half space. Profiles based on +2 and +3 standard deviations of ln(V_S) are not considered to avoid unrealistic conditions. The standard deviation (σ) of ln(V_S) is used because V_S data typically follow lognormal distributions. As given in Table 2.1, the average values of σ of ln(V_S) are 0.32 for the Wando, and 0.14 to 0.31 for the Tertiary-age sediments.

The twenty-eight V_S profiles plotted in Figure 2.2b are considered to investigate spectral response differences that result from propagating hard rock outcrop motions from a depth of 2,644 ft, versus propagating soft rock outcrop motions from a depth of 450 ft. The V_S profiles presented in Figures 2.2a and 2.2b are identical in the top 450 ft. Below 450 ft in Figure 2.2b, commonly assumed values of V_S in soft rock for Charleston are used (Andrus et al. 2006).

Displayed in Figure 2.3 are the V_S profiles shown in Figure 2.2a grouped by NEHRP site classes. Also plotted is the reference V_S profile which has a V_{S100ft} of 968 ft/s. The number of V_S profiles corresponding to the NEHRP Site Class E, D and C are 12, 13 and 3, respectively. It can be seen in the V_{S100ft} histogram plot presented in Figure 2.4 that the systematically-generated V_S profiles have adequate representation of the NEHRP E and D site classes, which is important for the development of the site coefficient model. The lognormal mean V_{S100ft} value of the generated V_S profiles is 682 ft/s.

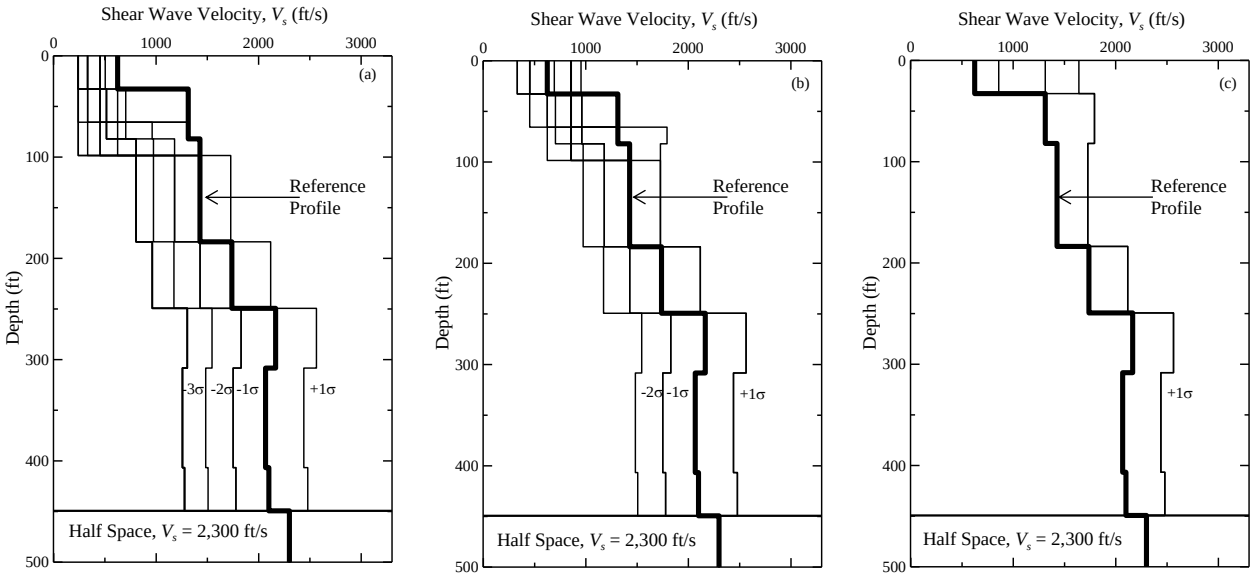

Figure 2.3 V_S profiles grouped by NEHRP Site Class (a) E, (b) D, and (c) C.

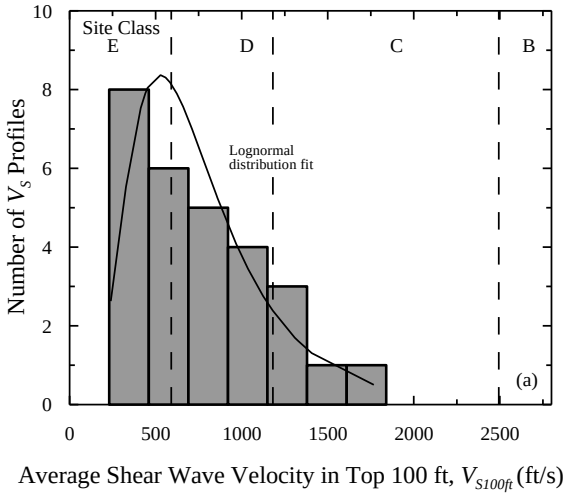

Figure 2.4 Histogram of V_{S100ft} for the twenty-eight V_S profiles.

The Zhang et al. (2005, 2008) relationships that expressed variations of G/G_{max} and D with shearing strain amplitude (γ) in terms of geologic age, mean effective confining pressure, and soil plasticity index are used to account for stiffness degradation during cyclic loading. Sample G/G_{max}-γ and D-γ relationships for Tertiary deposits with mean effective confining stresses of 32 psi (depth ≈ 79 ft) and 102 psi (depth ≈ 427 ft) are displayed in Figure 2.5. Also displayed in Figure 2.5 are the ±1σ G/G_{max}-γ and D-γ relationships. For the half space with V_{S100ft} = 2,300 ft/s, linear or constant relationships of G/G_{max}-γ and D-γ are assumed. This is done by entering G/G_{max} = 1 and D = 0.5% for all γ values. A value of D = 0.5% is taken to be representative for soft rock in the South Carolina Coastal Plain (SCDOT 2008a).

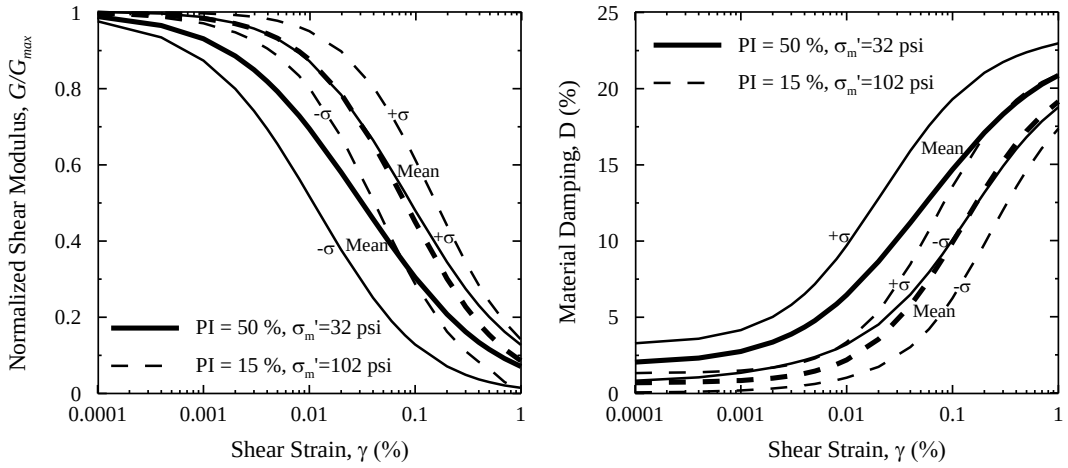

Figure 2.5 Sample G/G_{max}-γ and D-γ relationships (Zhang et al. 2005, 2008).

2.3 Input Ground Motions

A computer program called Scenario_PC was used to simulate outcrop motions, because actual strong motion records are not available for the Charleston area. Scenario_PC was developed by Chapman (2006) for seismic hazard analysis in South Carolina. The program generates acceleration time histories based on a point-source stochastic model (Atkinson and Boore 1995). Necessary inputs for Scenario_PC include: (1) rock model; (2) earthquake moment magnitude; (3) site-to-source distance; and (4) return period.

Chapman and Talwani (2002) defined two rock models for South Carolina in the program Scenario_PC. The first model is referred to as the geologic realistic condition and consists of a very thick, outcropping soft rock (V_S = 2,300 ft/s) layer over hard rock. The thickness of the soft rock layer is equal to the thickness of Tertiary and Cretaceous sediments (e.g., 2,300-3,200 ft in the Charleston area). The second model is referred to as the hard rock outcropping condition, which consists of 820 ft of weathered hard rock (V_S = 8,200 ft/s) underlain by a half space of unweathered hard rock (V_S = 11,500 ft/s). Scenario_PC uses a B-C boundary amplification function to transfer the hard rock motions to geologic realistic soft rock motions (Chapman 2006). The two main advantages of performing ground response analysis based on the geologic realistic condition are: (1) the input V_S profiles need only to extend to about 450 ft in Charleston, and (2) the computed site coefficients can be applied to the USGS B-C boundary rock accelerations to construct the design response spectra.

Deaggregation analyses of the seismic hazard at six oscillator frequencies (0, 0.5, 1, 2, 3.33, 5 Hz) are performed for the centers of the twenty-four 7.5-minute quadrangles shown in Figure 2.1 using the 2002 USGS interactive seismic hazard analysis online tools (https://geohazards.usgs.gov/deaggint/2002/index.php; accessed March 26, 2010). The return periods considered are 10% and 2% probabilities of exceedance in 50 years (or return periods of 475 and 2475 years, respectively). These return periods are referred to in SCDOT (2008a) as the Functional Evaluation Earthquake (FEE) and the Safety Evaluation Earthquake (SEE), respectively. For a given quadrangle and return period, the predominant moment magnitude (M_w) and modal site-to-source distance (R) are found to be practically the same for all of the six spectral periods. This observation agrees with Chapman (2006) and SCDOT (2008a). Sample deaggregated M_w and R values for the Charleston quadrangle at the six spectral periods are

presented in Table 2.2. For the Charleston area and both return periods, the deaggregated data suggest that the hazard at all spectral periods is dominated by events with M_w between 7.2 and 7.4, and R between 3.8 and 22.4 miles.

Table 2.2 Sample predominant moment magnitude and site-to-source distance pairs for six spectral periods for the Charleston quadrangle.

Period of interest	Modal Moment Magnitude, M_w	Source to site distance, R (miles)
PGA	7.37	15.6
0.1 sec	7.37	15.7
0.2 sec	7.37	15.7
0.3 sec	7.37	15.7
1.0 sec	7.38	15.7
2.0 sec	7.38	15.6

Presented in Figure 2.6 are sample synthetic input motions generated for the center of the Charleston quadrangle and three other neighboring quadrangles (i.e., Johns Island, North Charleston and Fort Moultrie) for the FEE and SEE conditions. The synthetic motions are generated to match with the uniform hazard spectra points. Displayed in Figure 2.7 are the respective response spectra plots for the motion shown in Figure 2.6. It can be seen that the relative differences in period contents between the SEE and FEE motions are small, and periods at which peak accelerations occur are about 0.15 s.

Because one of the objectives of this study is to provide site coefficients that are comparable with the 1994 NEHRP coefficients, the peak ground acceleration at the soft rock outcrop surface ($PGA_{B\text{-}C}$) of the motions need to match the range provided in the NEHRP. This is achieved by scaling the $PGA_{B\text{-}C}$ of the motions to match with the NEHRP $PGA_{B\text{-}C}$. Even though this step removes the association between the scaled motion and the stated probability of exceedance (P_E) value, it is acceptable because it does not bring an additional bias to the response predicted. This is confirmed by a sensitivity analysis performed using the FEE motion and a scaled SEE motion, as presented in Figure 2.8. The scaled SEE motion predicts the same surface spectral accelerations as the FEE motion. This is an expected observation, because the seismic hazard is dominated by a single earthquake source. Park et al. (2012) suggested that such arbitrary scaling may be used when the seismic hazard is dominated by a single earthquake source zone.

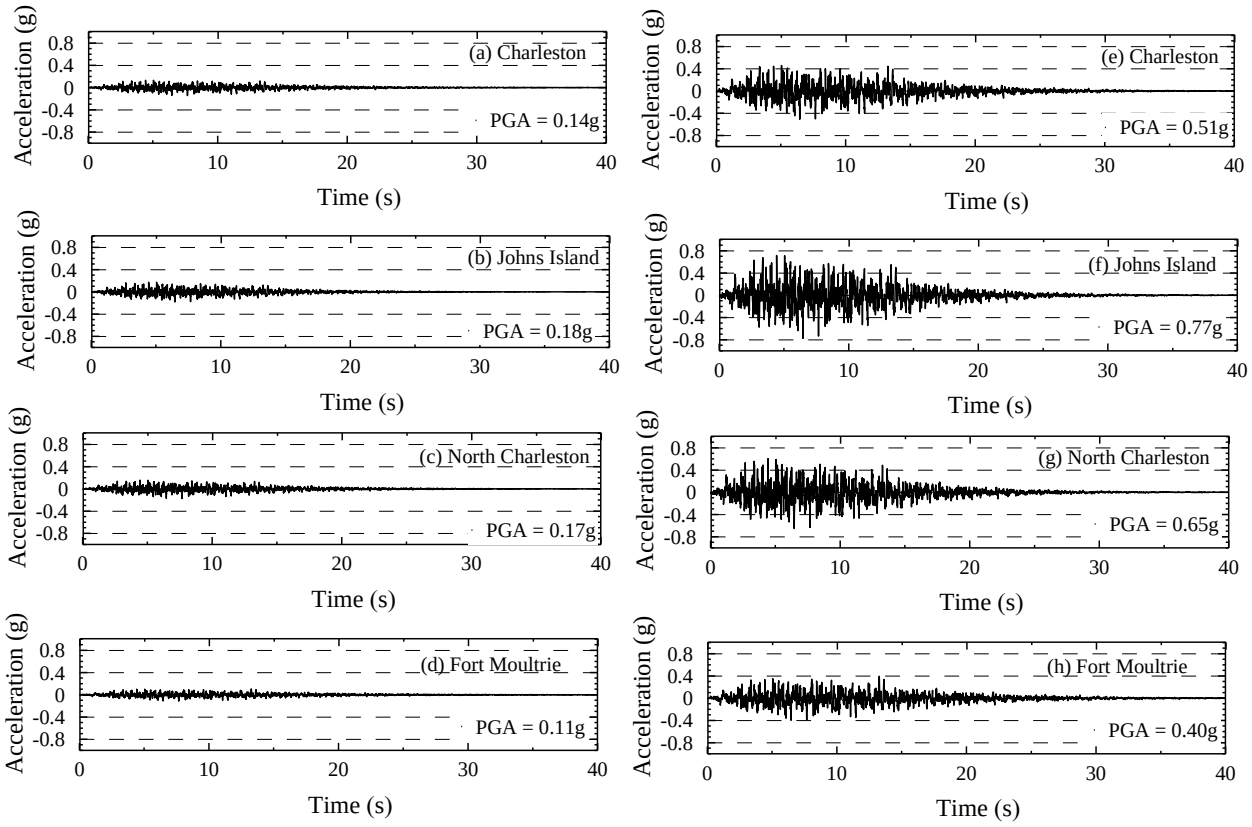

Figure 2.6 Sample synthetic soft rock outcrop motions generated by Scenario_PC for (a-d) 10% and (e-h) 2% probability of exceedance in 50 years.

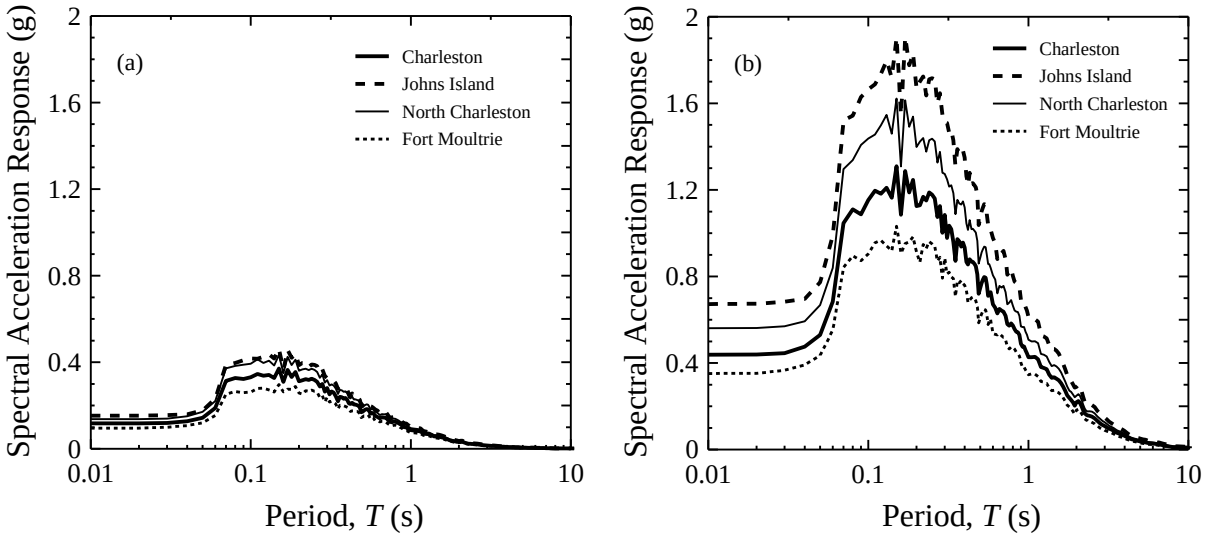

Figure 2.7 Response spectra of soft rock outcrop ground motions for (a) 10% and (b) 2% probability of exceedance in 50 years for the time histories shown in Figure 2.6.

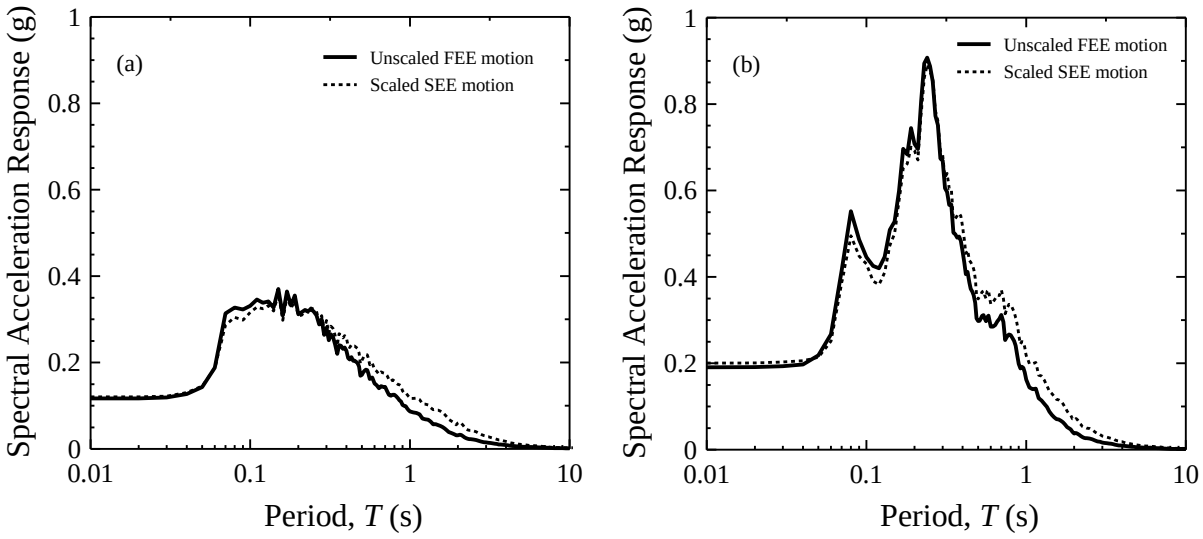

Figure 2.8 Sensitivity of the response acceleration to arbitrary scaling at (a) soft rock, and (b) ground surface.

Input soft rock outcrop motions for twelve quadrangles, two return periods, and six $PGA_{B\text{-}C}$ scaling values are used with the V_S profiles presented in Figure 2.2a. This is a total of 144 acceleration time histories. After a depth transformation, the soft rock motions are applied at the half space located at a depth of 450 ft in Figure 2.2a.

For the analyses involving the deeper V_S profiles presented in Figure 2.2b, twenty-four acceleration time histories representing the hard rock outcropping condition are generated by Scenario_PC and applied at the hard rock half space located at a depth of 2,644 ft. Sample hard rock acceleration time histories are presented in Figure 2.9.

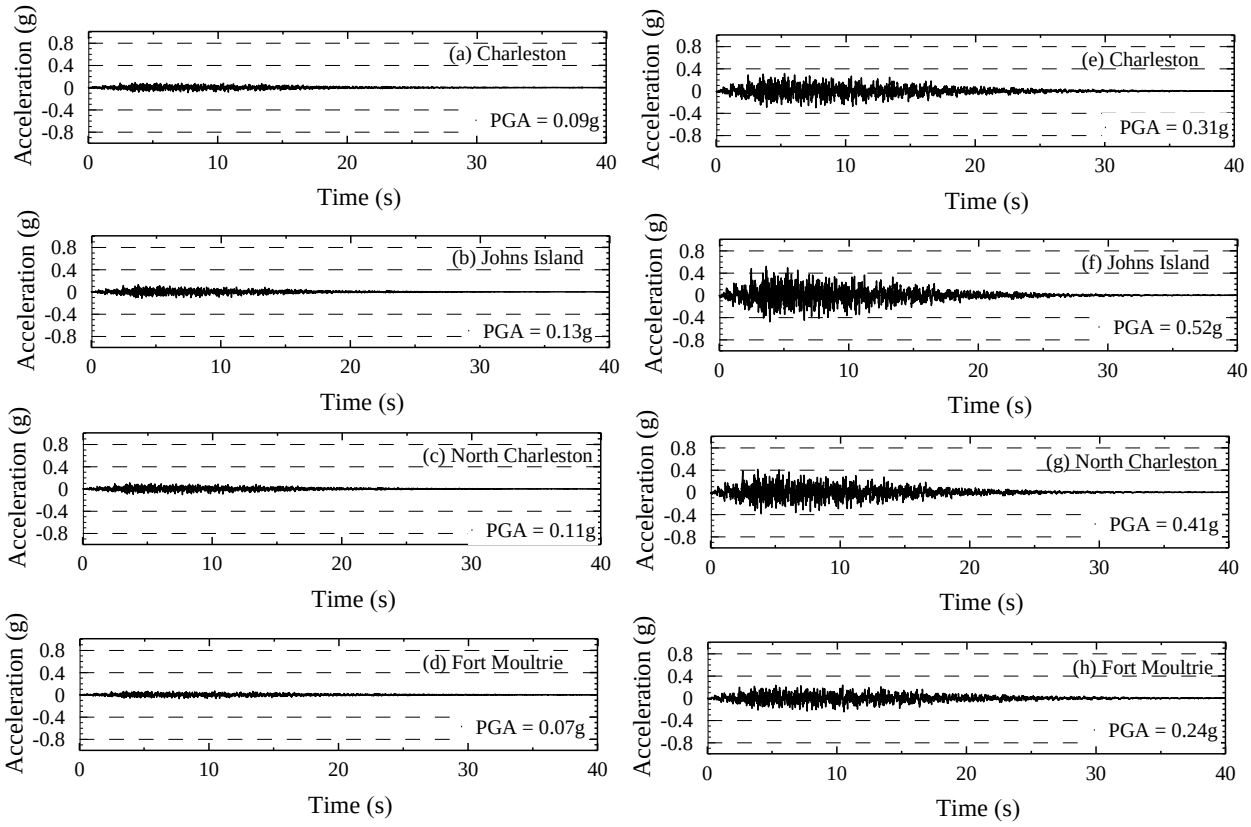

Figure 2.9 Sample synthetic hard rock outcrop motions generated by Scenario_PC for (a-d) 10% and (e-h) 2% probability of exceedance in 50 years.

2.4 Ground Response Analysis

The computer programs SHAKE2000 (Ordóñez 2011) and DMOD2000 (Matasović and Ordóñez 2011) are used to perform one-dimensional, total stress ground response analysis. The one-dimensionality assumption is taken to be appropriate for three reasons. First, due to subsequent refractions by the soil layers, stress waves propagate from the earthquake focus to the earth's surface in a nearly vertical path, especially close to the surface. Second, much of the Charleston area is flat within the source-to-site distance range. Third, soil properties generally vary more rapidly in the vertical direction than in the horizontal direction making the vertical soil/rock column more important. The stated justifications for one-dimensional analysis do not take into account topography of the bedrock or earthquake directivity effects, which are not well established for the Charleston area. Thus, one-dimensional analysis is considered valid.

SHAKE2000 is based on the original SHAKE program by Schnabel et al. (1972) and uses the equivalent linear method of modeling the nonlinear response of a one dimensional horizontally layered soil profile to vertically propagating shear waves. Although a nonlinear formulation is preferred for modeling nonlinear systems, SHAKE2000 is considered valid when computed peak ground acceleration is less than 0.4 g and computed values of γ are less than 2% (Kramer and Paulsen 2004). The major advantage of SHAKE2000 is that it takes much less computation time and has less input needs than computer programs based on a nonlinear formulation.

DMOD2000 is an enhanced version of D-MOD (Matasović 1993) and uses a nonlinear formulation where the stress-strain hysteretic response of soil is modeled by a degraded backbone curve generated by unloading-reloading rules developed by Masing (1926) and extended by Pyke (1979). Because this type of formulation considers only hysteretic damping, an external viscous damping formulation is incorporated in the form of Rayleigh damping. This requires an initial calibration step for DMOD2000 to obtain suitable values of the viscous damping (ξ) and an odd integer (n) related to the modes at which target damping is matched. The calibration involves running DMOD2000 at a low input value of $PGA_{B\text{-}C}$ and adjusting ξ and n until the response spectrum from DMOD2000 matches the response spectrum from SHAKE2000. At low loading, the hysteretic damping is insignificant because the material behaves linearly even with non-linear material model. The ξ and n that produces the best match between spectra are then used in running DMOD2000 at the desired high $PGA_{B\text{-}C}$ level.

Non-linear time domain analysis also requires special attention to layer thicknesses. Subdividing of major layers is often done by requiring a minimum fundamental frequency of 15-25 Hz for sublayers, because higher frequencies contain a relatively small amount of energy in an earthquake loading (Schnabel et al. 1972). The fundamental frequency of a layer is computed by $V_S/4h$, where h is the thickness of the sublayer.

For this study, SHAKE2000 is used when $PGA_{B\text{-}C} \leq 0.3$ g; and DMOD2000 is mainly used when $PGA_{B\text{-}C} > 0.3$ g. Values of ξ and n for use in DMOD2000 are determined by running both programs mostly with $PGA_{B\text{-}C} = 0.1$ g. The best frequency calibration pairs are found to be either ($\xi = 0.75$, $n = 7$); ($\xi = 0.5$, $n = 7$); or ($\xi = 0.5$, $n = 5$). The criterion of layer frequency ≥ 25 Hz is shown to be sufficient to ensure ‘‘layer-independent’’ results, based on analyses performed

with assumed cutoff frequencies of 15, 20 and 25 Hz. Thus, sublayer thicknesses could not exceed $V_S/100$.

2.5 Results

Average values of F are computed for six spectral period ranges (T): ≤ 0.01, 0.01-0.4, 0.41-0.8, 0.81-1.2, 1.21-2.0 and 2.01-4.0 s, respectively based on the geologic realistic, soft rock condition. These ranges are referred to by their middle range periods. The respective site coefficients are denoted as $F_{PGA,}$ $F_{0.2}$ (or F_a), $F_{0.6}$, F_1 (or F_v), $F_{1.6}$ and F_3. Presented in Figures 2.10-2.12 are computed $F_{PGA,}$ F_a and F_v values, respectively, plotted versus V_{S100ft}. Each data point is determined by calculating the arithmetic mean from twelve simulations involving twelve different time histories. The data plotted in Figures 2.10-2.12 are results of over 9,000 SHAKE and 4,500 DMOD simulations.

Averaging values of F over a spectral period range is consistent with the development of the NEHRP F_a and F_v recommended values. It should be noted, however, that the NEHRP F_a and F_v were determined assuming the spectral period ranges of 0.1-0.5 s and 0.4-2.0 s, respectively (Borcherdt 1994). Narrower period ranges allow for better predictions of spectral accelerations, because the periods at which spectral peaks occur can vary greatly from site to site and can exceed 1.0 s.

The plotted V_{S100ft} -F data pairs exhibit three general features--(1) an increasing trend in F as V_{S100ft} increases from zero; (2) a zone of peak F values, depending on $S_{outcrop}$; and (3) a decreasing trend in F as V_{S100ft} increases beyond the zone of peak F values. Similar general features can be observed in data reported by other investigators (Silva et al. 2000; Chapman et al. 2006; Fairbanks et al. 2008) and are supported by vibration theory, where V_{S100ft} is an index for site period. These three general features are assumed in developing the mathematical model of F.

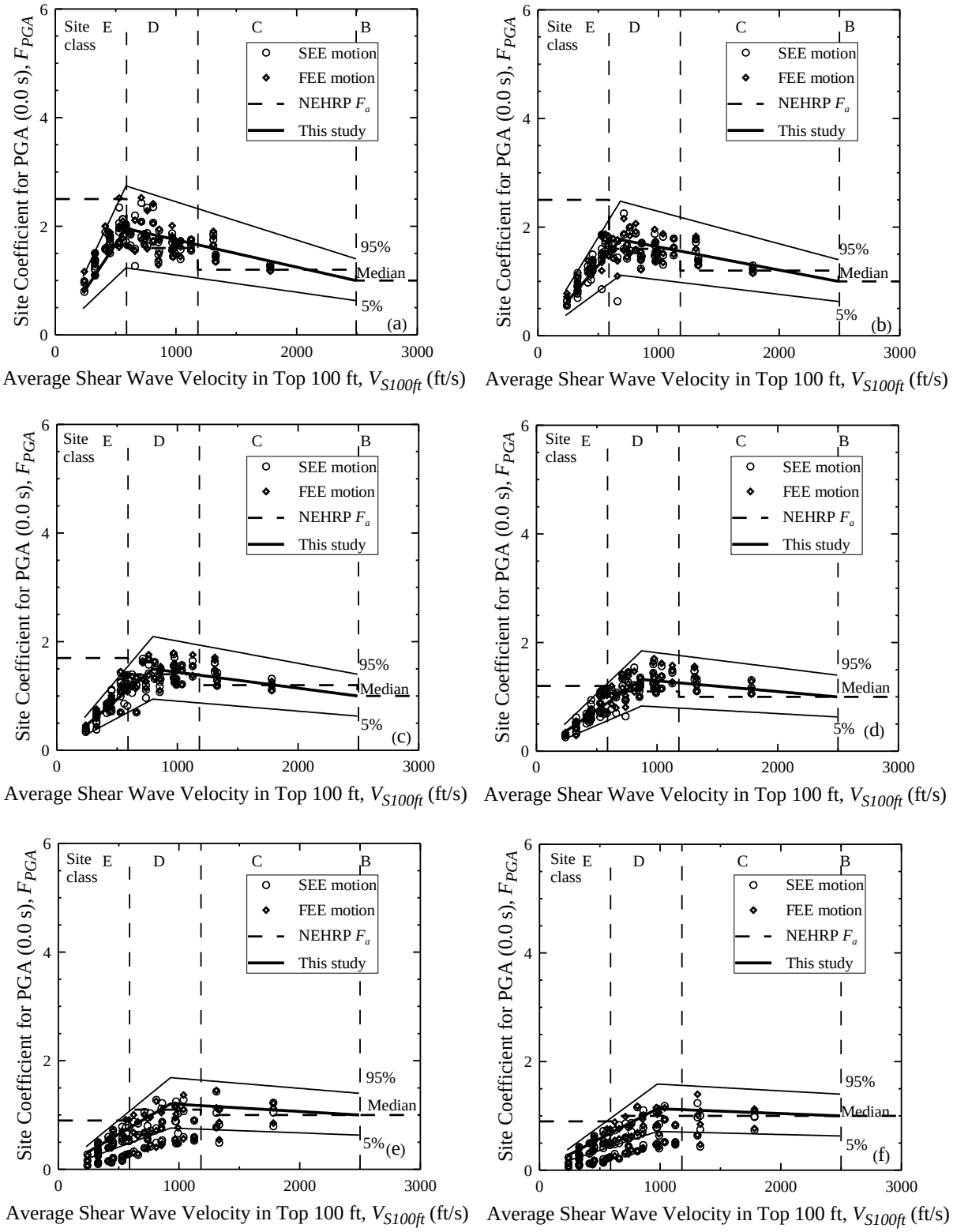

Figure 2.10 Site coefficients for 0.0 s spectral period (free-field) with $PGA_{outcrop}$ equal to (a) 0.05 g, (b) 0.1 g, (c) 0.2 g, (d) 0.3 g, (e) 0.4 g, and (f) 0.5 g.

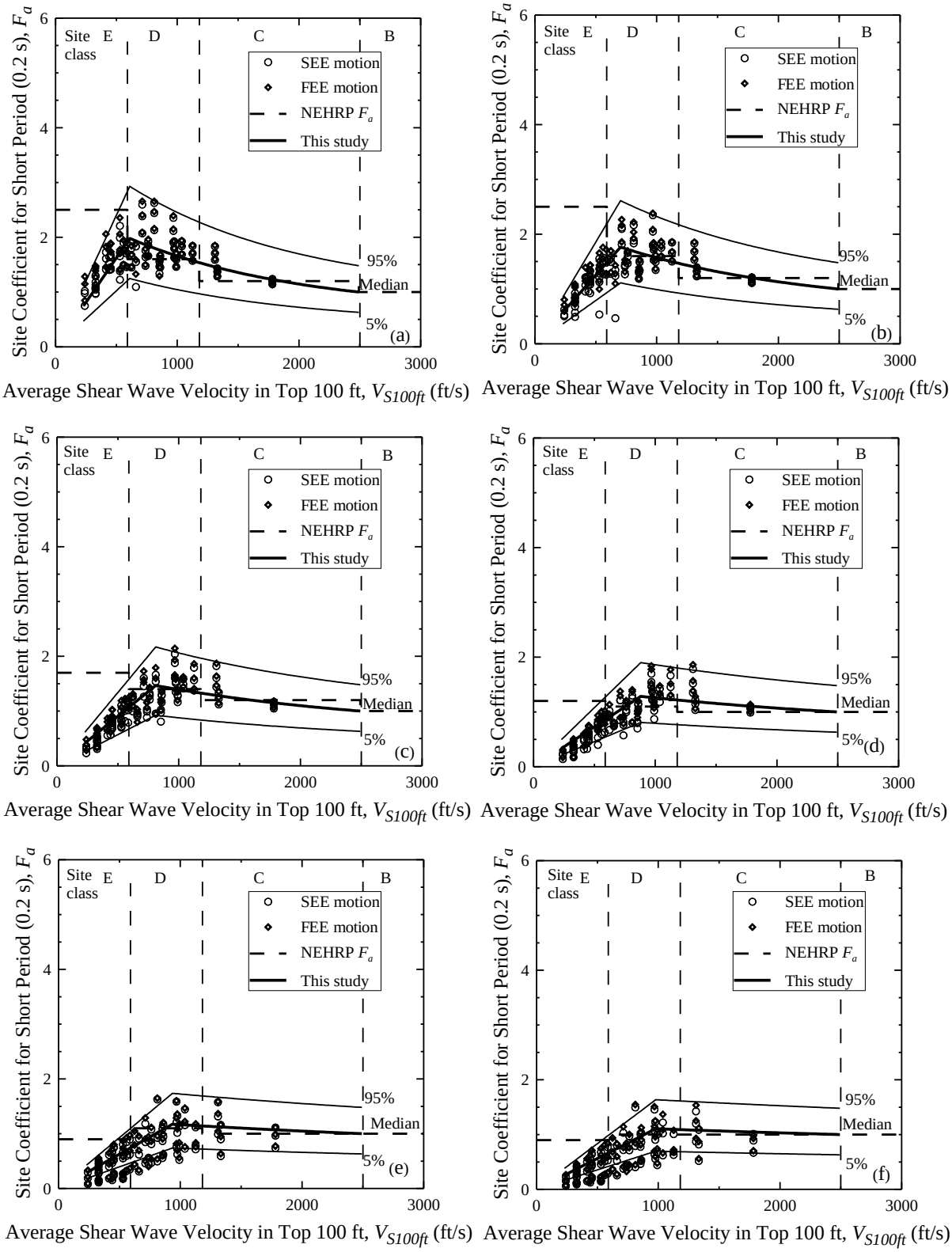

Figure 2.11 Site coefficients for 0.2 s (short) spectral period with S_S equal to (a) 0.125 g, (b) 0.25 g, (c) 0.50 g, (d) 0.75 g, (e) 1.0 g, and (f) 1.25 g.

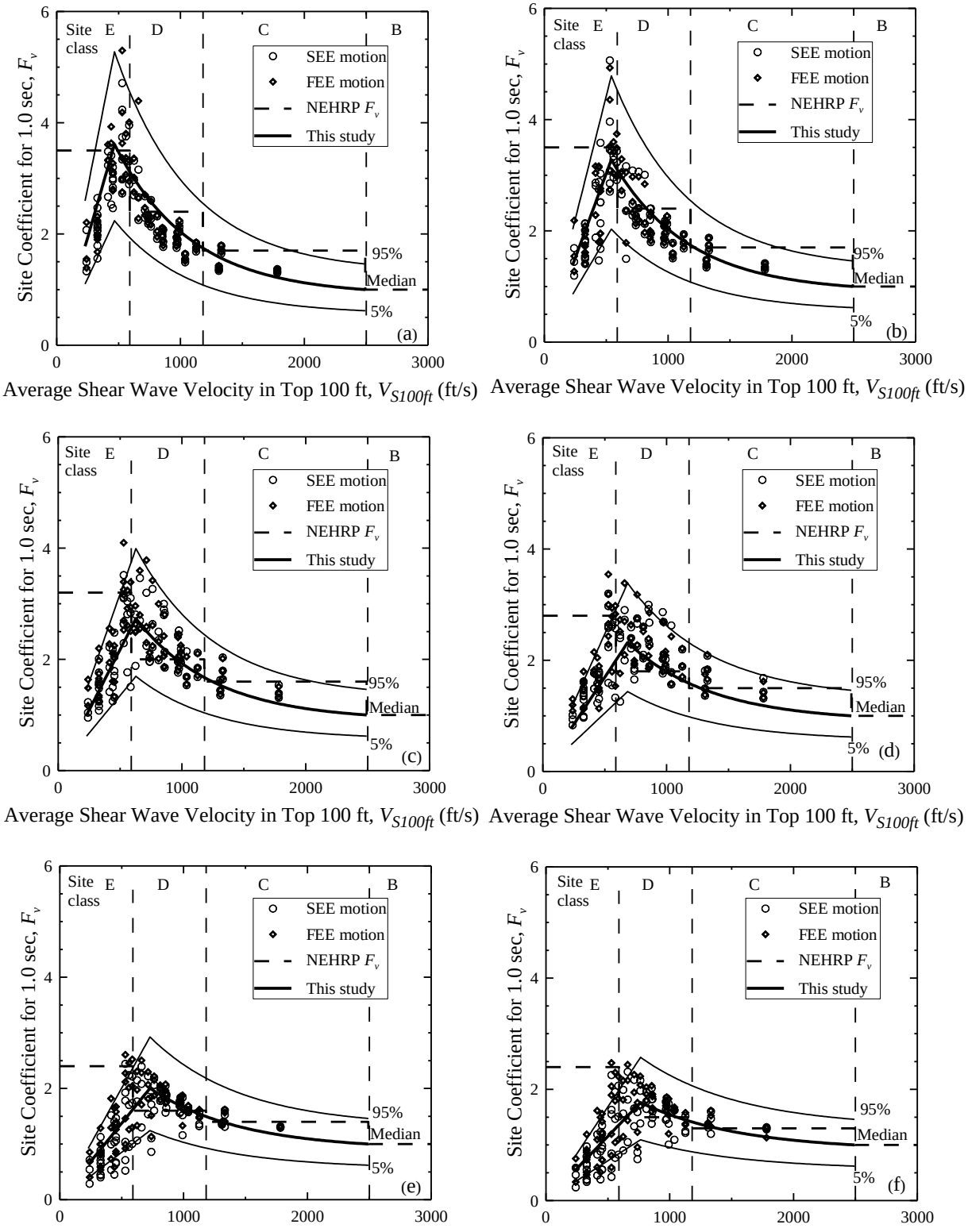

Figure 2.12 Site coefficients for 1.0 s (long) spectral period with S_1 equal to (a) 0.05 g, (b) 0.1 g, (c) 0.2 g, (d) 0.3 g, (e) 0.4 g, and (f) 0.5 g.

When V_{S100ft} is less than the estimated V_{S100ft} corresponding to the peak F value ($V_{S100ftP}$), the median F curves plotted in Figures 2.10-2.12 can be expressed by the following linear relationship:

$$F = \left(\frac{F_P}{V_{S100ftP}} \right) V_{S100ft} \qquad \text{for all values } T \text{ and } V_{S100ft} < V_{S100ftP} \tag{2.1}$$

where F_P is the estimated peak F value. F_P and $V_{S100ftP}$ are calculated by:

$$F_P = x_1 S_{outcrop} + x_2 \tag{2.2a}$$

$$V_{S100ftP} = x_3 S_{outcrop} + x_4 \tag{2.2b}$$

where x_1, x_2, x_3 *and* x_4 are regression coefficients given in Table 2.3.

When $V_{S100ft} \geq V_{S100ftP}$, the median F curves plotted in Figures 2.10-2.12 can be expressed by the following linear or exponential relationships:

$$F = \frac{(F_P - 1)(2500 - V_{S100ft})}{2500 - V_{S100ftP}} + 1 \qquad \text{for } T < 0.2 \text{ s and } V_{S100ft} \geq V_{S100ftP} \tag{2.3a}$$

$$F = a + b\, e^{cV_{S100ft}} \qquad \text{for } T \geq 0.2 \text{ s and } V_{S100ft} \geq V_{S100ftP} \tag{2.3b}$$

where a is a regression coefficient given in Table 2.3; and b and c are regression coefficients calculated from:

$$b = \frac{1 - a}{e^{2500c}} \tag{2.4a}$$

$$c = \left(\frac{1}{2500 - V_{S100ftP}} \right) \ln \left(\frac{1 - a}{F_P - a} \right) \tag{2.4b}$$

Equations 2.1 and 2.3 are formulated to satisfy three conditions. First, Equations 2.1 and 2.3 provide the same F values at $V_{S100ftP}$. Second, Equation 2.1 assumes F = 0 when V_{S100ft} = 0 ft/s. This assumption agrees with the fact that material with zero stiffness cannot support shear waves and, for this reason, F should be zero regardless of $S_{outcrop}$. Third, Equation 2.3 satisfies the condition that F = 1.0 when V_{S100ft} = 2,500 ft/s, which is the assumed reference soft rock outcrop site used in the design codes and 1994 NEHRP provisions.

Table 2.3 Regression coefficients for estimating seismic site coefficients.

Spectral period, T (s)	$S_{outcrop}$	x_1 (g^{-1})	x_2	x_3 (g^{-1}. ft/s)	x_4 (ft/s)	a	$Z_{0.95}$	$Z_{0.05}$
0.0	$PGA_{outcrop}$	-1.88	1.99	1178	466	--*	1.38	0.64
0.2	S_S	-0.83	2.05	344	577	0.65	1.48	0.63
0.6	$S_{0.6}$	-3.53	3.09	679	512	0.85	1.40	0.70
1.0	S_1	-4.16	3.76	417	505	0.90	1.40	0.68
1.6	$S_{1.6}$	-5.36	3.86	649	397	0.97	1.40	0.68
3.0	$S_{3.0}$	-8.20	2.80	1292	262	0.99	1.30	0.65

*T < 0.2 s, calculate F using Equation 2.3a.

The development of Equations 2.1 and 2.3 involved a two-step procedure. First, median curves are derived based on residual analysis of the individual subset of data in Figures 2.10-2.12. The appropriateness of the median curves is checked by studying residuals. The residual, ε, is defined here as F of the plotted data divided by F of the median curve. Probability plots shown in Figure 2.13 and 2.14 indicate that ε better follows a lognormal distribution than a normal distribution. As displayed in Figure 2.15, the computed median values of ε are approximately equal to 1.0, which indicates that the median relationships are unbiased in predicting F and the models have central tendencies. In other words, the predictions underestimate the response just as often as they overestimate. The second step involves obtaining linear regression approximations of F_p and $V_{S100ftP}$ as a function of $S_{outcrop}$ (Equation 2.2). Based on F_p and $V_{S100ftP}$, Equations 2.1 and 2.3 are established using the entire data set for a given F. The predictor variable V_{S100ft} is shown to have little or no overall bias in the median relationships expressed by Equations 2.1 and 2.3, because plots of V_{S100ft} -ε do not show any systematic structure.

The upper and lower bound curves shown in Figures 2.10-2.12 are drawn to bound 95% and 5%, respectively, of all the data points for a given F. They are drawn by multiplying Equations 2.1 and 2.3 by the average standard Z-scores (i.e., $Z_{0.95}$ or $Z_{0.05}$) listed in Table 2.3. The Z-scores are obtained from lognormal cumulative distribution of F-residuals for each set of data.

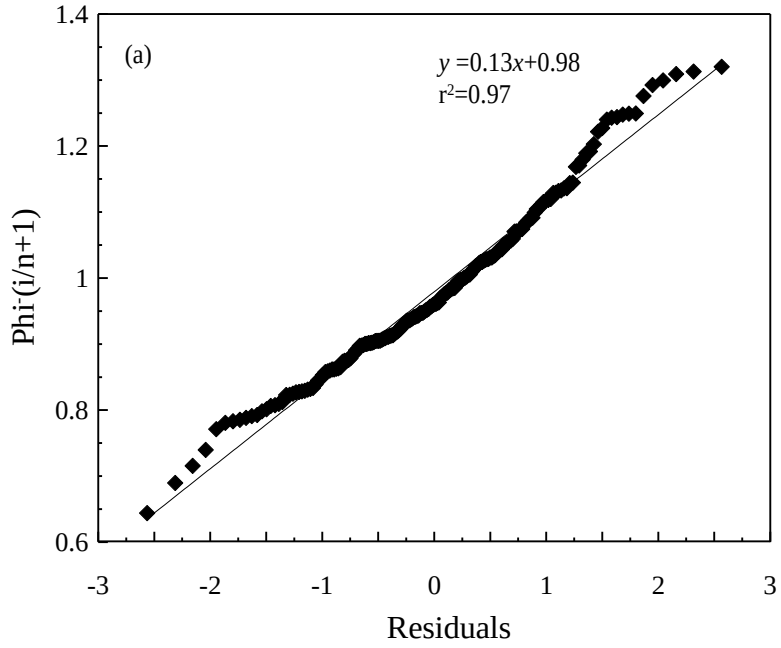

Figure 2.13 Probability plot assuming normal distribution of the residuals.

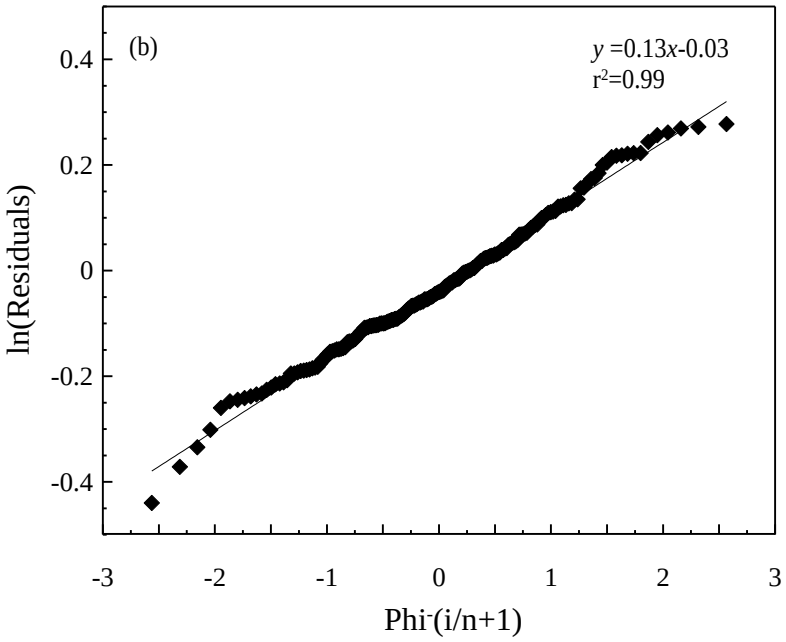

Figure 2.14 Probability plot assuming lognormal distribution of the residuals.

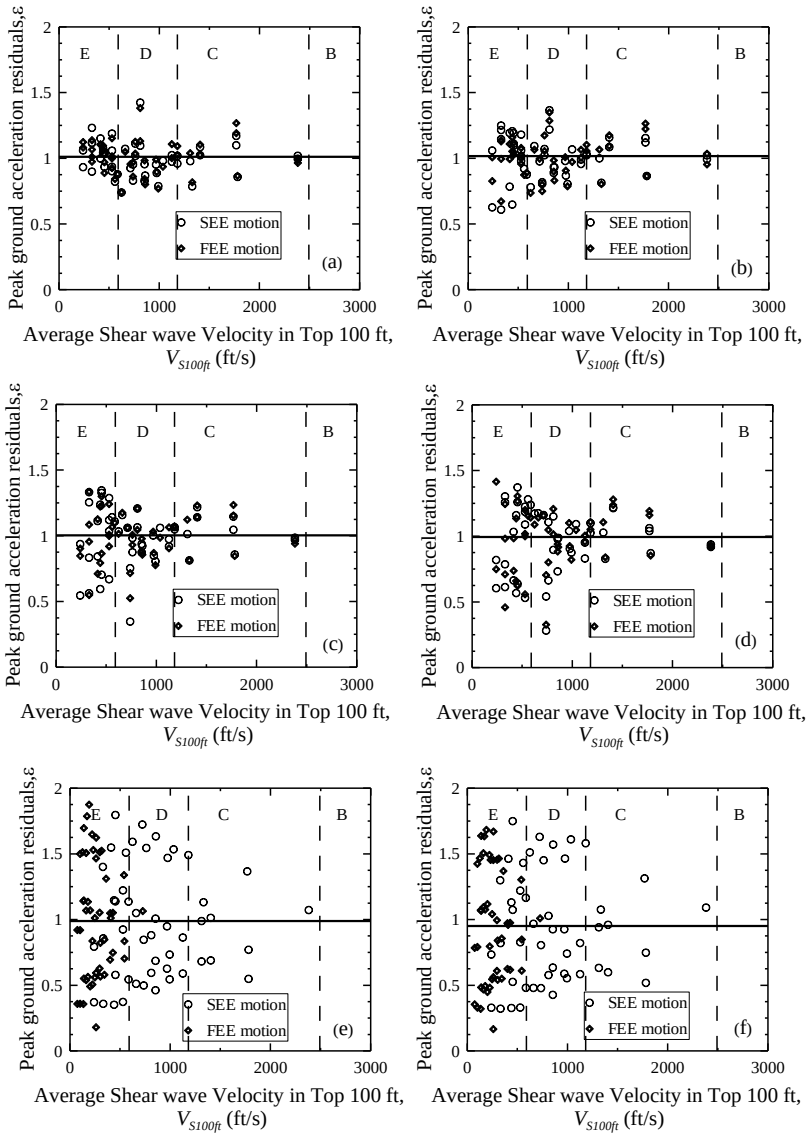

Figure 2.15 Sample residual-V_{S100ft} plots for F_{PGA} equal to (a) 0.05 g, (b) 0.1 g, (c) 0.2 g, (d) 0.3 g, (e) 0.4 g, and (f) 0.5 g.

Additional analyses using DMOD2000 with $PGA_{B\text{-}C}$ = 0.3 g provide results that are similar to the results obtained from SHAKE2000 with $PGA_{B\text{-}C}$ = 0.3 g. Values of F_{PGA} and F_a based on SHAKE2000 are, on average, 10% lower than values based on DMOD2000. On the other hand, F_v values based on SHAKE2000 are 10% higher than F_v values based on DMOD2000. At $PGA_{B\text{-}C}$ = 0.2 g, the difference is expected to be less, because the values of ξ and n use in DMOD2000 are determined by running both programs mostly with $PGA_{B\text{-}C}$ = 0.1 g.

2.6 Discussion

2.6.1 Recommended Site Coefficients

The 1994 NEHRP F_a and F_v values are also plotted in Figures 2.10, 2.11, and 2.12 for comparison with the computed coefficients. AASHTO (2011a), ICC (2012) and SCDOT (2008a) adopted the 1994 NEHRP F_a values for the peak horizontal ground acceleration site coefficient F_{PGA}. It can be seen in Figures 2.10-2.11 that there is good general agreement between the NEHRP F_a values and the computed F_{PGA} and F_a median values. Computed F_{PGA} and F_a median values are, however, slightly higher than the NEHRP F_a for Site Class D, when the spectral accelerations at the soft rock outcrop for 0.2 s (S_S) are less than 1.25 g (Figures 2.10a-2.10d and 2.10a-2.10d). This finding generally agrees with Silva et al. (2000) and Borcherdt (2002), who also obtained F_a values slightly greater than the NEHRP values for Site Class D. For Site Class E, the computed F_{PGA} and F_a median values are, on average, significantly lower than the NEHRP value.

Concerning F_v, it can be seen in Figure 2.12 that there is good general agreement between the computed median F_v values and the NEHRP value. For Site Class C, computed median F_v values are higher than the NEHRP value in 3 out of 6 of the plots. For Site Class D, computed median F_v values are more often higher than the NEHRP value. This observation generally agrees with Silva et al. (2000), Borcherdt (2002), Stewart et al. (2003) and Choi and Stewart (2005) who also obtained F_v values greater than the NEHRP for Site class D. For Site Class E, the computed median F_v values are often significantly lower than the NEHRP value.

Based on the findings discussed above and because conditions typical of Charleston are used, the relationships defined by Equations 2.1 and 2.3 are recommended for constructing design response spectra curves, in the Charleston area. Differences in F_a and F_v values obtained in this study and the 1994 NEHRP may be explained by (1) differences in assumed soil/rock conditions; (2) differences in applied ground motions; and (3) the fact that the NEHRP uses a single site coefficient value for a given site class. The 95% upper bound and 5% lower bound curves shown in Figures 2.10-2.12 represent the variations that are likely for a given value of V_{S100ft}. The variables affecting F (in order of decreasing relative contribution) are V_{S100ft}, G/G_{max}-γ and D-γ, earthquake time history (return periods of 475 or 2,475 years), and V_S below 100 ft.

While the functional forms proposed for the site coefficient model (Equations 2.1 and 2.3) may not lend themselves well to code applications, they do provide a more accurate representation of the computed coefficients than do the NEHRP coefficients for given values of V_{S100ft}. The use of Equation 2.1 at very low values of V_S profiles is supported by the results plotted in Figures 2.10-2.12, extending to V_{S100ft} as low as 240 ft/s, and the fact material with zero stiffness cannot support shear waves. If code developers prefer a single site coefficient value for a given seismic site class, the functional forms can be used to determine that value. For example, the largest or the middle-range median value within a site class could be used for design code applications.

2.6.2 Application

The procedure for constructing an acceleration design response spectrum (ADRS) outlined in AASHTO (2011a), can be summarized in the following four steps: First, the NEHRP site class is determined. Second, $PGA_{B\text{-}C}$, S_S and S_1 are obtained from probabilistic seismic hazard maps. Third, the site class, $PGA_{B\text{-}C}$, S_S and S_1 are used to select F_{PGA}, F_a and F_v that account for the effect of local site conditions. Fourth, three points of the ADRS are obtained as follows

$$PGA = F_{PGA} PGA_{B-C} \tag{2.5}$$

$$S_{DS} = F_a S_S \tag{2.6}$$

$$S_{D1} = F_v S_1 \tag{2.7}$$

where S_{DS} is the design short-period (0.2 s) spectral response acceleration at the ground surface; and S_{D1} is the design long-period (1.0 s) spectral response acceleration at the ground surface.

Illustrated in Figure 2.16 is the AASHTO (2011a) procedure for constructing what is called the 3-point ADRS. The procedure implicitly assumes: (1) all significant peaks occur at $T < 1.0$ s or close to 1.0 s; (2) the plateau defined by S_{DS} provides a conservative bound for these peaks; and (3) spectral acceleration descends proportionally with $1/T$, when $T > T_s$ ($T_s = S_{D1}/S_{DS}$). However, as presented below, we observed that (1) significant peaks may not always occur at shorter periods ($T < 1.0$ s), especially when $V_{S100ft} < 656$ ft/s; and (2) the plateau cannot always be defined as S_{DS}, unless $T_s \leq 1.0$ s ($S_{D1} \leq S_{DS}$).

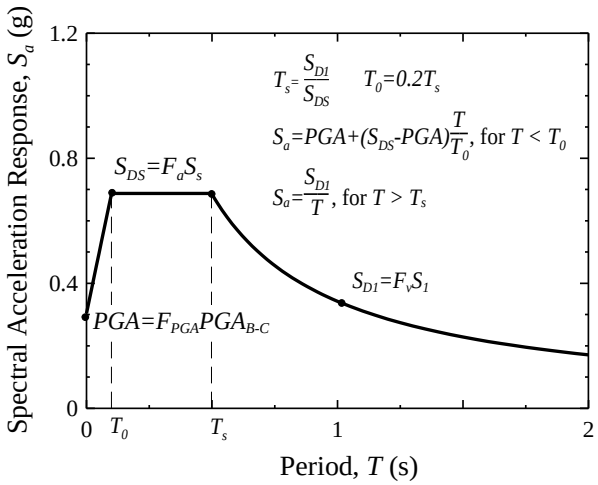

Figure 2.16 Construction of the 3-point acceleration design response spectrum based on AASHTO (2011a).

Presented in Figures 2.17a-2.17d are sample response spectra for four profiles with V_{S100ft} = 1,404, 968, 560 and 453 ft/s, respectively, and $PGA_{B\text{-}C}$ = 0.2 g. Plotted in each figure are the site-specific response spectrum and the soft rock outcrop response spectrum. Also plotted are the 3-point ADRS curves constructed based on the AASHTO LRFD guideline, and median F_{PGA}, F_a and F_v values derived in this study. It can be seen that the AASHTO 3-point curves are unconservative when $0.2 \leq T \leq 0.5$ s for the profiles with V_{S100ft} = 1,404 and 968 ft/s; and excessively over conservative when $T < 1.0$ s for the profiles with V_{S100ft} = 560 and 453 ft/s. The 3-point ADRS curves based on coefficients derived in this study provide better approximations of the site-specific spectra, except for the V_{S100ft} = 453 ft/s profile and $1.1 \leq T \leq 1.8$ s.

Because the 3-point ADRS method implicitly assumes that all significant peaks occur below T = 1.0 s, the 3-point ADRS curve based on site coefficients derived in this study under-predicts the site-specific curve for the V_{S100ft} = 453 ft/s profile, when $1.1 \leq T \leq 1.8$ s (Figure 2.17d). Additional comparisons made by the authors, but not shown here, indicate that the 3-point ADRS method may be unconservative when $T > 1.0$ s, $V_{S100ft} < 660$ ft/s, and $PGA_{B\text{-}C} > 0.1$ g. This finding agrees with Power et al. (1998) who showed that the 3-point method can be unconservative in the Central and Eastern United States for spectral periods between 1 and 3 s. Therefore, a multi-point ADRS method is also shown in Figure 2.17d based on SCDOT (2008a).

The multi-point ADRS for the V_{S100ft} = 453 ft/s shown in Figure 2.17d is constructed by determining $S_{outcrop}$ for several spectral periods (i.e., 0.0, 0.08, 0.15, 0.2, 0.3, 0.5, 1.0, 2.0 and 3.0 s) and applying the median F value for the corresponding spectral period (i.e., F_{PGA}, F_a, $F_{0.6}$, F_v, $F_{1.6}$, *and* F_3, respectively*).* Connecting the resulting points with straight line segments provides a reasonable fit to the site-specific spectrum, as shown in Figure 2.17d.

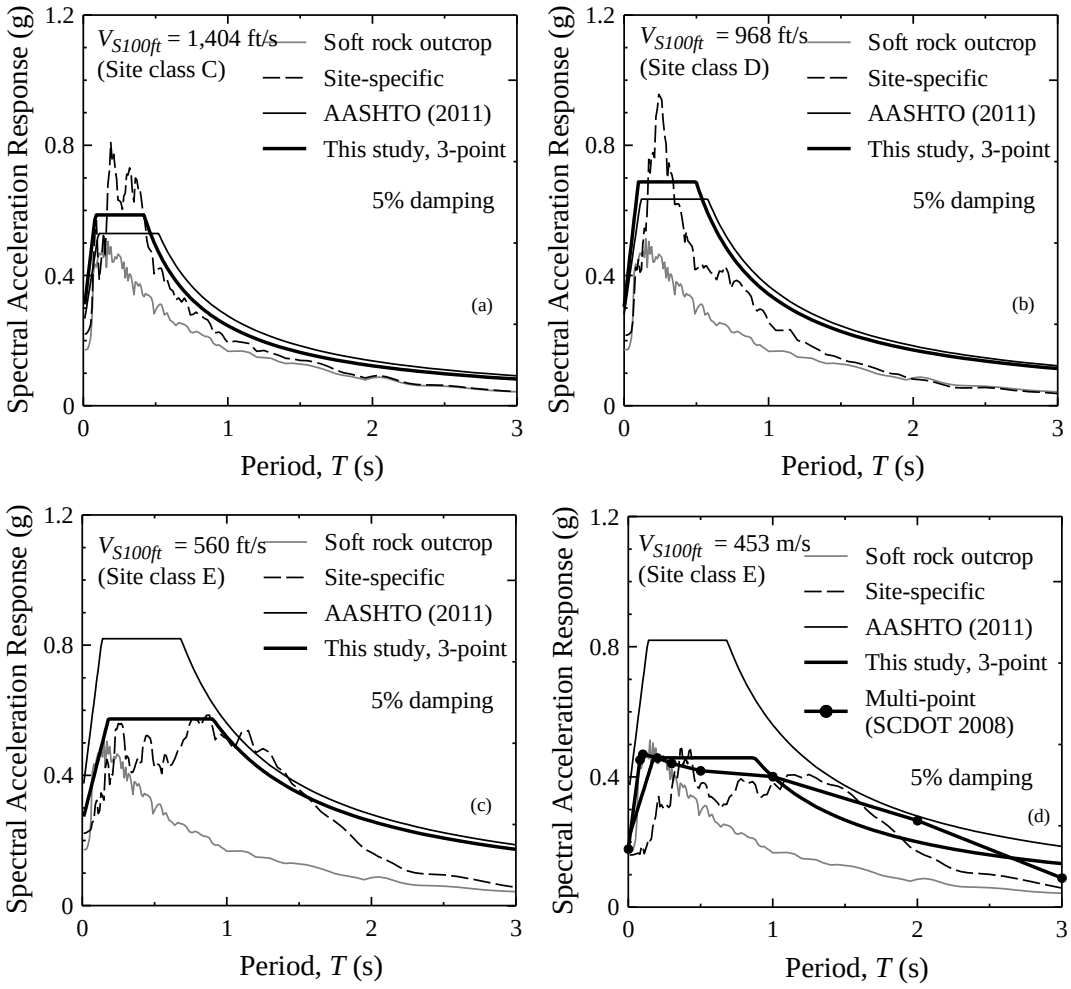

Figure 2.17 Sample acceleration response spectra for profiles with V_{S100ft} equal to (a) 1,404 ft/s, (b) 968 ft/s, (c) 558 ft/s, and (d) 453 ft/s.

In practice, when V_{S100ft} < 660 ft/s, it is recommended that both 3-point and multi-point ADRS curves be constructed. The values of $S_{outcrop}$ for B-C boundary material are obtained from Scenario_PC. If any point of the multi-point ADRS exceeds the 3-point ADRS, the multi-point ADRS (or a modified 3-point ADRS) should be used.

2.6.3 Comparison of Results based on Two Rock Models

Computed surface spectral accelerations at T = 0.0, 0.2, 0.6, 1.0, 1.6, 3.0 s based on the geologic realistic model and the hard rock model are compared in Figure 2.18. The comparison is made such that each data point plotted in Figure 2.18 has the same V_S profile above 450 ft for both models. The spectral accelerations based on the hard rock model are, on average, slightly greater than the spectral accelerations based on the geologic realistic model for T < 0.2 s. For T ≥ 0.2 s, the spectral accelerations based on the hard rock model are, on average, less than accelerations based on the geologic realistic model. The average difference in computed accelerations is most significant for T = 3.0 s.

Thus, the overall effect of the deeper soil stacks in the hard rock model, not captured by Scenario_PC and the assumed material properties, is to filter the low frequency amplitudes and slightly amplify the high frequency amplitudes. This observation is in good agreement with a ground response study of Columbia, South Carolina by Lester and Chapman (2005). Given that the average spectral surface accelerations for the soft and hard rock models are generally within 20% and also given that the material property information below 450 ft is severely limited, the results presented in Figure 2.18 justify the use of the geologic realistic model for this study.

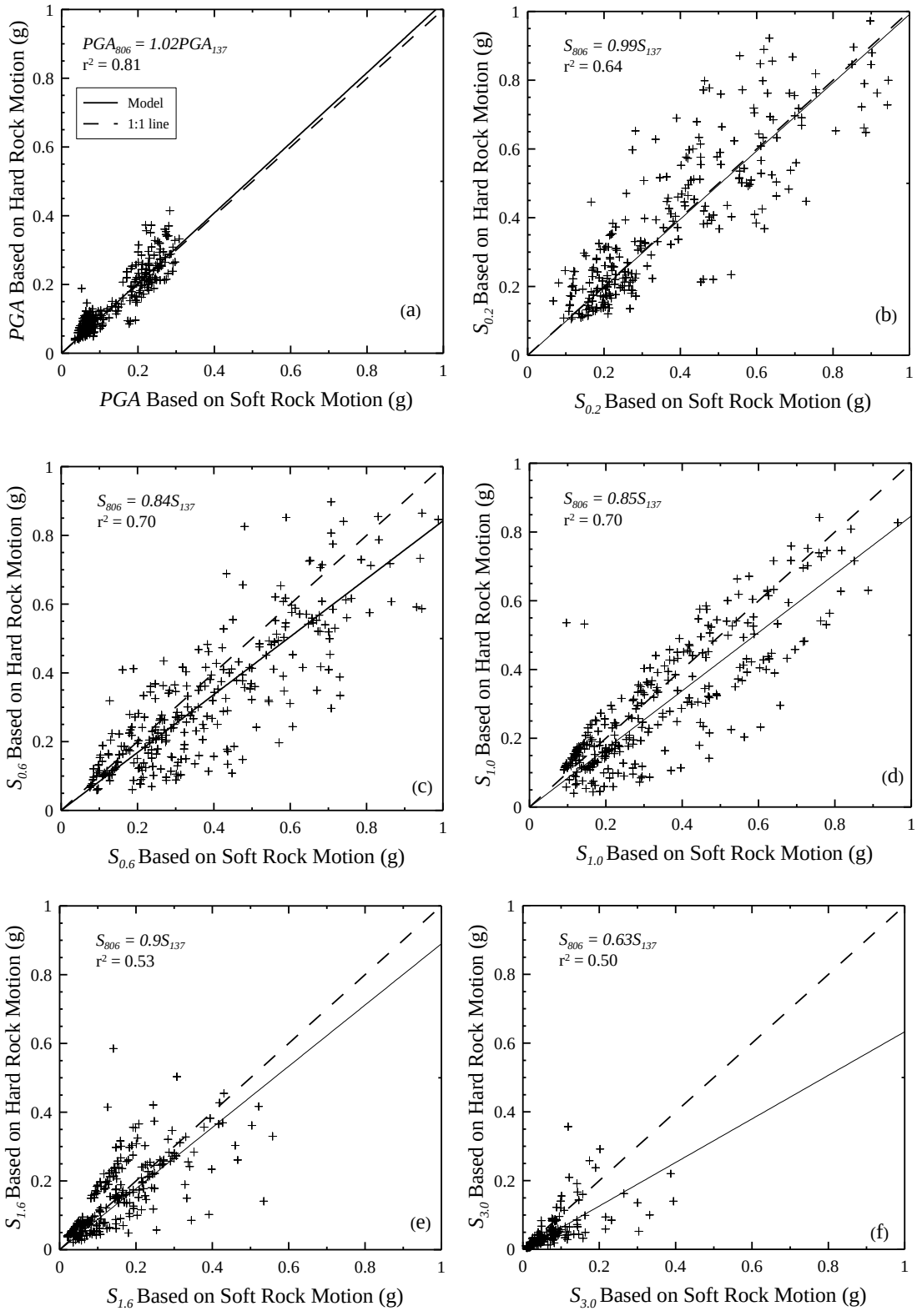

Figure 2.18 Comparison of surface accelerations obtained using hard rock motions with V_S = 11,500 ft/s half-space located at 2,644 ft and soft rock motions with V_S = 2,300 ft/s half-space located at 450 ft for (a) 0.0 s, (b) 0.2 s, (c), 0.6 s, (d) 1.0 s, (e) 1.6 s, and (f) 3.0 s spectral periods.

2.6.4 Limitations

There are several limitations concerning the results that should be noted. Although the V_S profiles shown in Figure 2.2 represent a realistic range at each depth, they are not generated assuming a correlation structure between layers. More realistic models can be generated using data-driven correlation models (Toro 1995). Calculation of accurate correlation coefficients requires (a) information about the correlation between layers, (b) accurate upper and lower bound values, and (c) a large number of generated profiles. Even if reasonable assumptions on (a) and (b) are made, a much larger number of generated profiles would require considerable computational time, especially with the non-linear code. Further work is needed to implement realistic random generation V_S models.

Similar to the NEHRP F_a and F_v values, the site coefficients calculated are amplitude dependent and return period independent. The intrinsic discrepancy between the probabilistic nature of rock accelerations and the deterministic nature of the NEHRP F_a and F_v values is not dealt in this paper. However, Hashash et al. (2008) and Park et al. (2012) have shown that this discrepancy may be significant in future studies and recommendations.

The effect of depth to V_S = 2,300 ft/s material is not considered in this chapter. Studies have shown that the depth to soft rock (or depth to hard rock) can produce significant variability in ground response results that is dependent on spectral period (Silva et al. 2000; Hashash et al. 2008). Presented in Chapter 3 are results of additional analyses that considered the effect of depth to soft rock.

Finally, the results presented in this chapter are most appropriate for the Charleston area, where the area is relatively flat to support the application of 1-D ground response analysis. The assumptions made do not take into account the actual topography of the bed rock and earthquake directivity effects. The results may be appropriate for other areas, but additional ground response analysis is needed to verify this conclusion.

2.7 Summary

Seismic site coefficients at average spectral periods of 0.0, 0.2, 0.6, 1.0, 1.6 and 3.0 s were calculated for conditions typical of Charleston based on over 13,000 ground response simulations. The site coefficients were grouped by spectral acceleration and plotted versus V_{S100ft}. From the plotted V_{S100ft}-site coefficient data pairs, median relationships were developed. Each relationship exhibited a peak value somewhere between V_{S100ft} of 260 and 1,050 ft/s, depending on spectral acceleration and period. The relationships were expressed by a linear model for $V_{S100ft} < V_{S100ftP}$ and a linear or exponential model for $V_{S100ft} \geq V_{S100ftP}$. The amount of uncertainty that can be expected with estimating site coefficients using V_{S100ft} was represented by 95% upper bound and 5% lower bound relationships.

The computed relationships for periods of 0.0, 0.2 and 1.0 s were compared with the 1994 NEHRP F_a and F_v values. The computed median F_{PGA} and F_a values typically plotted slightly above the NEHRP F_a values for $V_{S100ft} > 600$ ft/s. The computed median F_v values typically plotted above the NEHRP F_v values by as much as about 1.5 times for $600 \leq V_{S100ft} \leq 980$ ft/s. For $V_{S100ft} < 600$ ft/s, the computed values plotted significantly below the NEHRP values. Because the computed site coefficients are based on regional conditions, they were recommended for the Charleston area.

The 3-point procedure for constructing ADRS curves was shown to be generally adequate when $V_{S100ft} > 660$ ft/s. When $V_{S100ft} \leq 660$ ft/s, peaks exceeding the 3-point ADRS can occur at $T > 1.0$ s. For this reason, it was suggested that a multi-point ADRS curve also be plotted to check if long-period accelerations are under predicted. Models to calculate site coefficients at long periods ($T = 1.6$ and 3.0 s) were provided to check predicted surface accelerations at long periods. The objective of the multi-point ADRS is not to replace the design code philosophy, but to provide a check to make sure that longer period accelerations are not excessively under predicted by the 3-point ADRS curve.

CHAPTER THREE

SEISMIC SITE COEFFICIENT MODEL BASED ON CONDITIONS IN THE COASTAL PLAIN[2]

3.1 Geology and Seismology

Presented in Figure 3.1 is the geologic map of South Carolina published by the South Carolina Department of Natural Resources (SCDNR 2005). Highlighted on the map are the Fall Line, which marks the boundary between the Coastal Plain and the Piedmont physiographic provinces; the Brevard Fault, which marks the boundary between the Piedmont and the Blue Ridge Mountains; and ten locations selected for ground response analysis (solid squares). In the Coastal Plain, relatively undeformed sediments of mainly Quaternary, Tertiary and Cretaceous ages lie on top of Mesozoic/Paleozoic folded, faulted and recrystallized basement rocks (Wheeler and Cramer 2000; Odum et al. 2003). In the Piedmont, road-cut exposures of residual soil and highly weathered crystalline rock are common. The basement rock includes granite, schist, and gneiss (Weems and Lewis 2002).

Based on geology and available V_S profiles presented later, the South Carolina Coastal Plain (SCCP) is divided for this study into the following four general areas: (1) Charleston-Savannah, (2) Myrtle Beach, (3) Columbia-Florence-Lake Marion, and (4) Aiken. These four areas match the general geographic division made by Silva et al. (2003). The Charleston-Savannah area lies in the southeastern part of the SCCP. Quaternary geology of the Charleston-Savannah area consists of beach/barrier ridges representing former stands of sea level, as well as fluvial and backbarrier deposits. Underlying Cretaceous and Tertiary sediments consist of marine deposits of marl, cemented sand and limestone, which were incised to varying degrees by stream activity prior to the deposition of the Quaternary sediments.

[2] A similar version of this chapter is published in the *Bulletin of Seismological Society of America*. Aboye, S.A., Andrus, R.D., Ravichandran, N., Bhuiyan, A.H., Harman, N., and Martin, J.R. II, "A New Seismic Site Coefficient Model Based on Conditions in the South Carolina Coastal Plain", 2014, Vol. 104, Issue 6, doi: 10.1785/0120140005, in press.

The Myrtle Beach area lies in the northeastern part of the SCCP. Near-surface sediments in the Myrtle Beach area are generally older and stiffer than sediments in Charleston-Savannah at the same depths. Tertiary and Cretaceous strata in the Myrtle Beach area gently dip both to the south and to the north forming what is called the Cape Fear Arch (DuBar 1987; Owens 1989; Moses 2002). The Cape Fear arch is a main structural feature in the SCCP and is characterize with an east-west trending axis located between the mouth of the Cape Fear River and the North Carolina-South Carolina state line.

The Columbia-Florence-Lake Marion area lies in the central and northwestern parts of the SCCP. Extending east from Columbia and the Fall Line, near-surface weathered crystalline rock gently dips to the south-east beneath thickening deposits of Pleistocene, Pliocene and upper Cretaceous sediments. These overlying sediments are dominated by interbeds of floodplain clay and channel fill sand (Maybin and Nystrom 1995; Odum et al. 2003).

The Aiken area lies in the southwestern part of the SCCP. Prowell (1996) indicated that Paleocene, Eocene and Miocene sediments form the majority of surface exposures in the Aiken area. These sediments typically reflect marine and fluvial depositional environments dominated by delta sedimentation. Paleocene deposits consist of clayey and silty quartz sand, and kaolinitic clay and silt. Eocene deposits consist of silty micaceous sand, silt, silty sand and clay. Miocene deposits are dominated by sand resulting from uplift and erosion of the Piedmont.

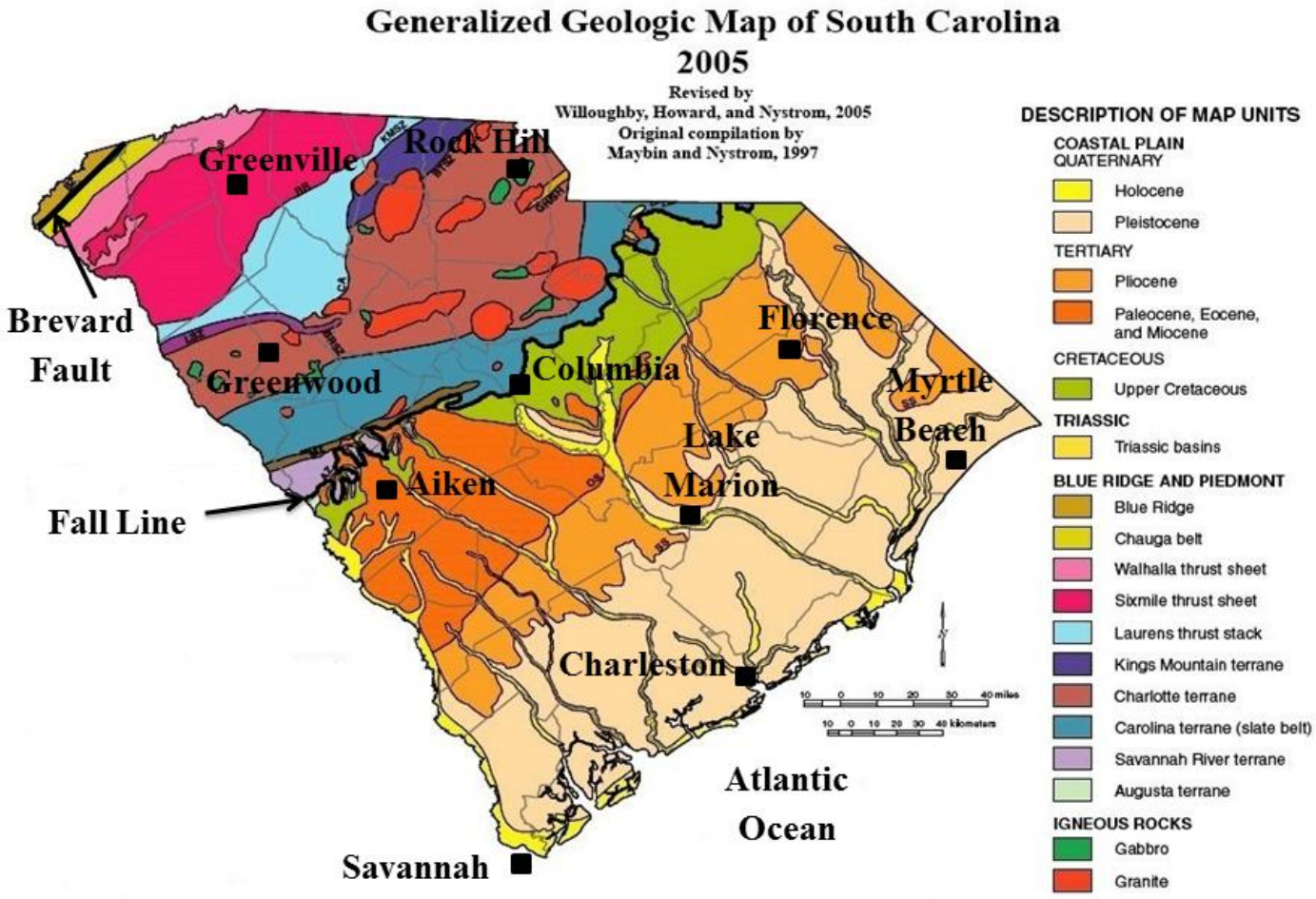

Figure 3.1 Geologic map of South Carolina (SCDNR 2005) showing the Fall Line and sites considered in ground response analysis.

Presented in Figure 3.2 is an isopach map of the Coastal Plain sediment thickness by Chapman and Talwani (2002). As illustrated in Figure 3.2, the thicknesses of sediments are 1,970-3,940 ft in the Charleston-Savannah area; 985-1,970 ft in the Myrtle Beach area; 0-2,300 ft in the Columbia-Florence-Lake Marion area; and 0-2,300 ft in the Aiken area. These sediment thicknesses roughly correspond to the depths to weathered crystalline rock.

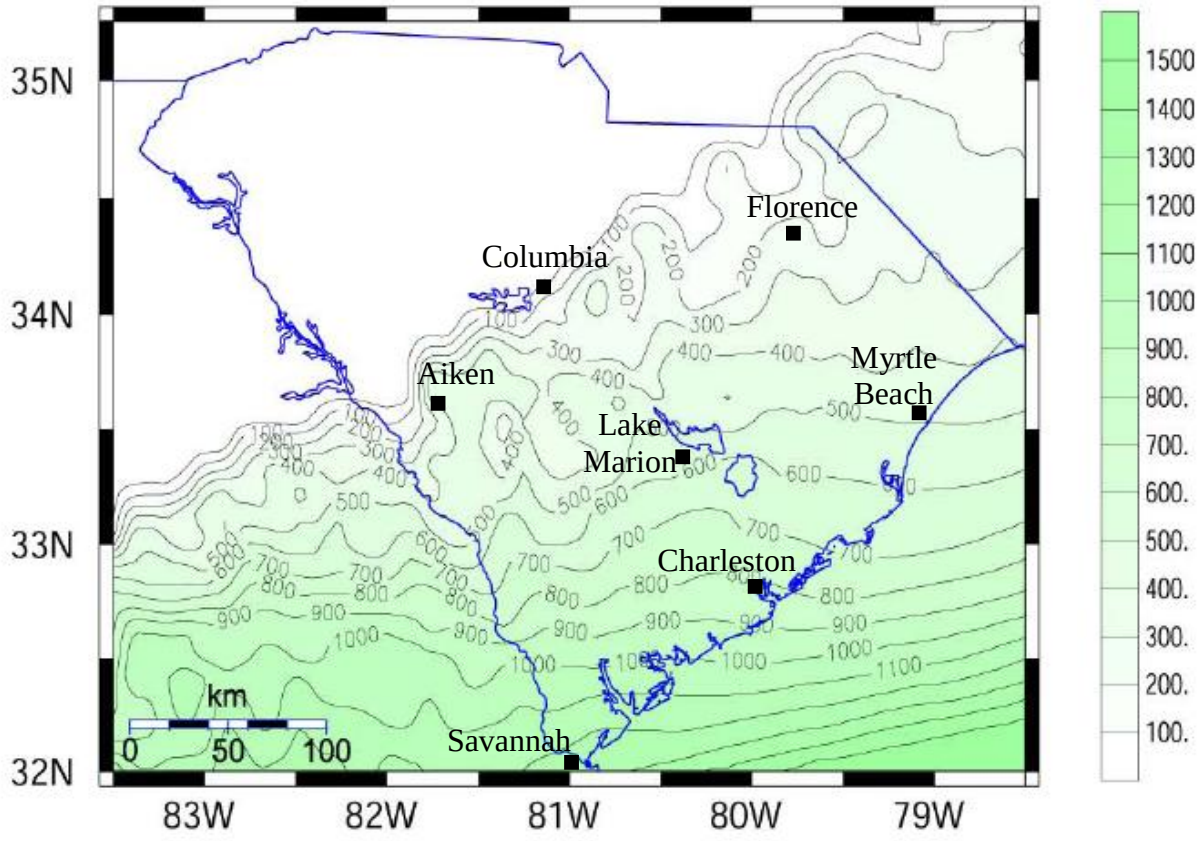

Figure 3.2 Isopach map of the Coastal Plain sediment thickness, in meters (Chapman and Talwani 2002).

Seismicity of the SCCP is dominated by the Charleston Seismic Zone located about 19 miles northwest of downtown Charleston. Several major earthquakes have occurred in the Charleston Seismic Zone during the past 6,000 years (Talwani and Schaeffer 2001). The most recent of which was the August 31, 1886 Charleston earthquake with estimates of moment magnitude (M_w) ranging from 6.9 ± 0.3 (Bollinger 1977; Bakun and Hopper 2004; Talwani and Gassman 2008; Heidari and Andrus 2010; Cramer and Boyd 2011) to 7.3 ± 0.3 (Martin and Clough 1994;

Johnston 1996). Damage caused by the 1886 Charleston earthquake included severe lateral and vertical displacement along more than 50 miles of railroad track, as well as numerous other ground and building failures (Dutton 1889). The maximum damage intensity is estimated to be X on the Modified Mercalli Intensity scale. Seismic events like the 1886 Charleston earthquake occur in the SCCP, on average, every 500 years (Talwani and Schaffer 2001).

3.2 Dynamic Soil/Rock Model

Four reference V_S profiles and 108 other V_S profiles are used in this chapter to represent the variations in small-strain soil/rock stiffness in the SCCP. Presented in Figures 3.3a-d are the V_S profiles assumed for the Charleston-Savannah, Myrtle Beach, Columbia-Florence-Lake Marion and Aiken areas, respectively. The dynamic soil/rock model (including the V_S profiles) described in Chapter 2 is used for Charleston-Savannah.

For Myrtle Beach, the reference V_S profile shown in Figure 3.3b is based on averages of profiles presented in Silva et al. (2003) and Odum et al. (2003). Values of V_S in the reference profile vary from 660 to 990 ft/s in the top 33 ft; and from 990 to 2,130 ft/s between the depths of 33 and 490 ft. Below the depth of 490 ft in Figure 3.3b, a soft rock half space with V_S of 2,300 ft/s is assumed.

For Columbia-Florence-Lake Marion, the reference V_S profile shown in Figure 3.3c is derived from information presented in Silva et al. (2003), Odum et al. (2003), Chapman and Lester (2005) and Andrus et al. (2006). Values of V_S in this reference profile vary between 660 and 1,310 ft/s in the top 100 ft; and from 1,310 to 2,300 ft/s between the depths of 100 ft and 450 ft. Additional profiles presented in Appendix H (Figures H.1-H.6) are assumed to account for the likely possibility of shallower soft rock (i.e., V_S = 2,300 ft/s) in the middle and upper parts of the SCCP. The profiles shown in Figures H.1-H.6 are generated by varying the depth to the V_S = 2,300 ft/s half space shown in Figure 3.3c (i.e., depth to half space = 1.6, 4.9, 16.4, 33, 66, 100, 165, 330 and 450 ft).

For Aiken, the reference V_S profile shown in Figure 3.3d is the average profile presented in Silva et al. (2003) and is based on measurements made at several locations at the Savannah River Site. Values of V_S in this reference profile vary between 1,150 and 1,310 ft/s above the depth of

165 ft; and increase from 1,310 to 1,970 ft/s between the depths of 165 and 475 ft. Below the depth of 475 ft, a soft rock half space with V_S of 2,300 ft/s is assumed.

The other one hundred eight V_S profiles shown in Figures 3.3a-d are derived from the reference profiles assuming estimates of standard deviation (σ) based on the study by Andrus et al. (2006). Respective histograms of V_{S100ft} for the V_S profiles shown in Figures 3.3a-d are presented in Figures 3.4a-d. The lognormal mean V_{S100ft} values for the profiles in Figures 3.3a-d are 680, 720, 885, and 850 ft/s, respectively.

Predictive relationships of G/G_{max}-γ and D-γ derived by Zhang et al. (2005) for Quaternary sediments and Tertiary and older sediments are used to describe the nonlinear behavior of each layer above the soft rock half space. The Zhang et al. (2005) G/G_{max}-γ relationships are defined as functions of mean effective stress (σ_m') and plasticity index (PI). The D-γ relationships are defined as functions of G/G_{max}, $\sigma_m'$and PI. For the calculation of σ_m', the coefficients of at-rest lateral earth pressure are assumed to be 0.5 for the Quaternary sediments and 1.0 for the Tertiary and older sediments; and the groundwater table depth is assumed to be 5 ft. These assumptions are justified because they are only used to estimate mean effective stress. An estimation of the mean effective stresses within ±50% of the actual value is considered sufficient for the estimation of normalized shear modulus and damping versus shearing strain relationships. Presented in Figure 3.5 are sample mean G/G_{max}-γ and D-γ relationships assumed for the Quaternary and Tertiary layers. The uncertainty associated with the relationships of G/G_{max}-γ and D-γ is considered using ± 1σ G/G_{max}-γ and D-γ relationships (Zhang et al. 2008).

For the soft rock half spaces in Figures 3.3a-d, linear or constant relationships of G/G_{max}-γ and D-γ are assumed. This is done by entering G/G_{max} = 1 and D = 0.5% for all γ values. A damping ratio of 0.5% was assumed for soft rock in the ground motion modeling study by Chapman (2006).

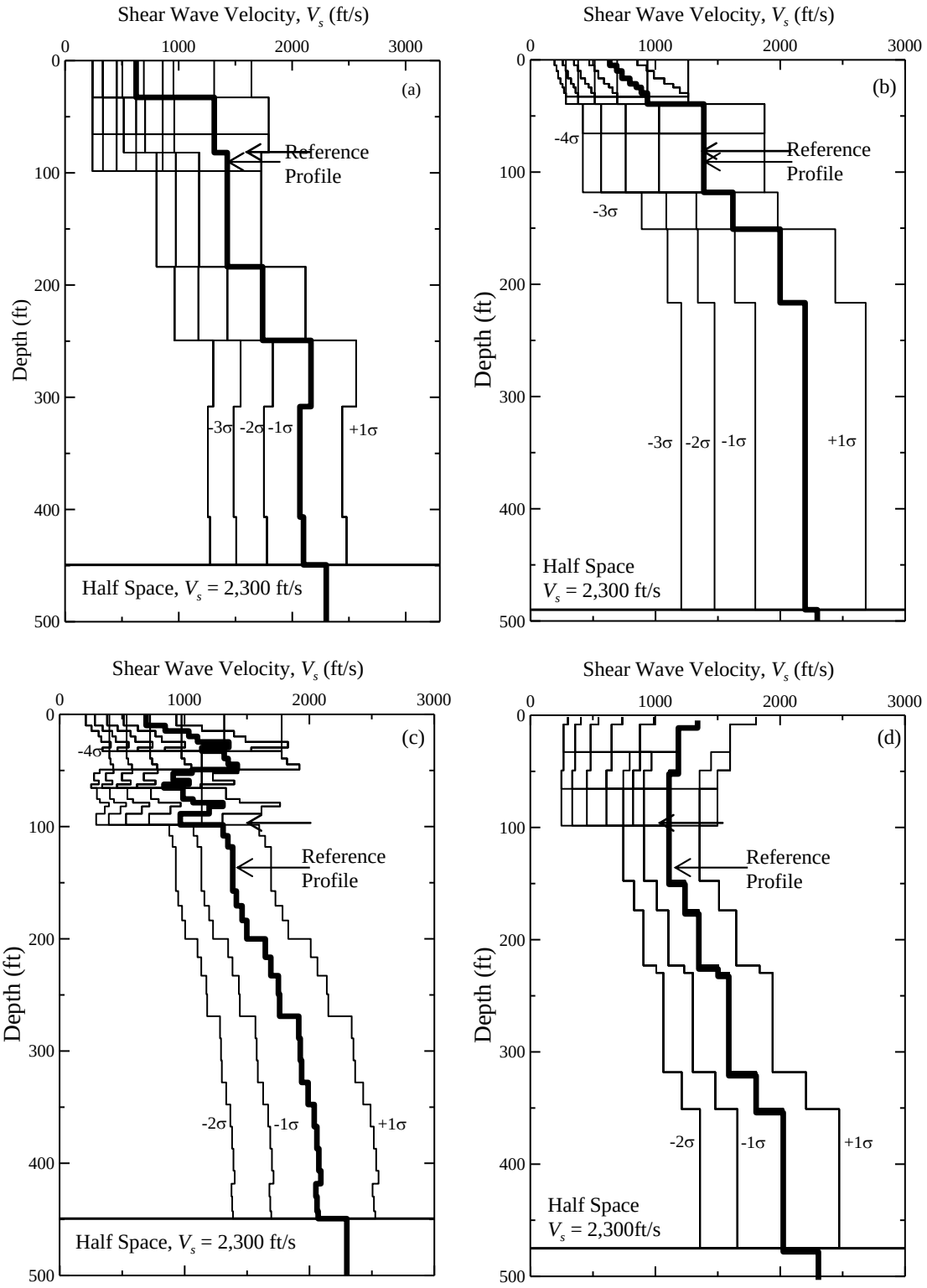

Figure 3.3 Shear wave velocity profiles considered for (a) Charleston-Savannah, (b) Myrtle Beach, (c) Columbia-Florence-Lake Marion, and (d) Aiken.

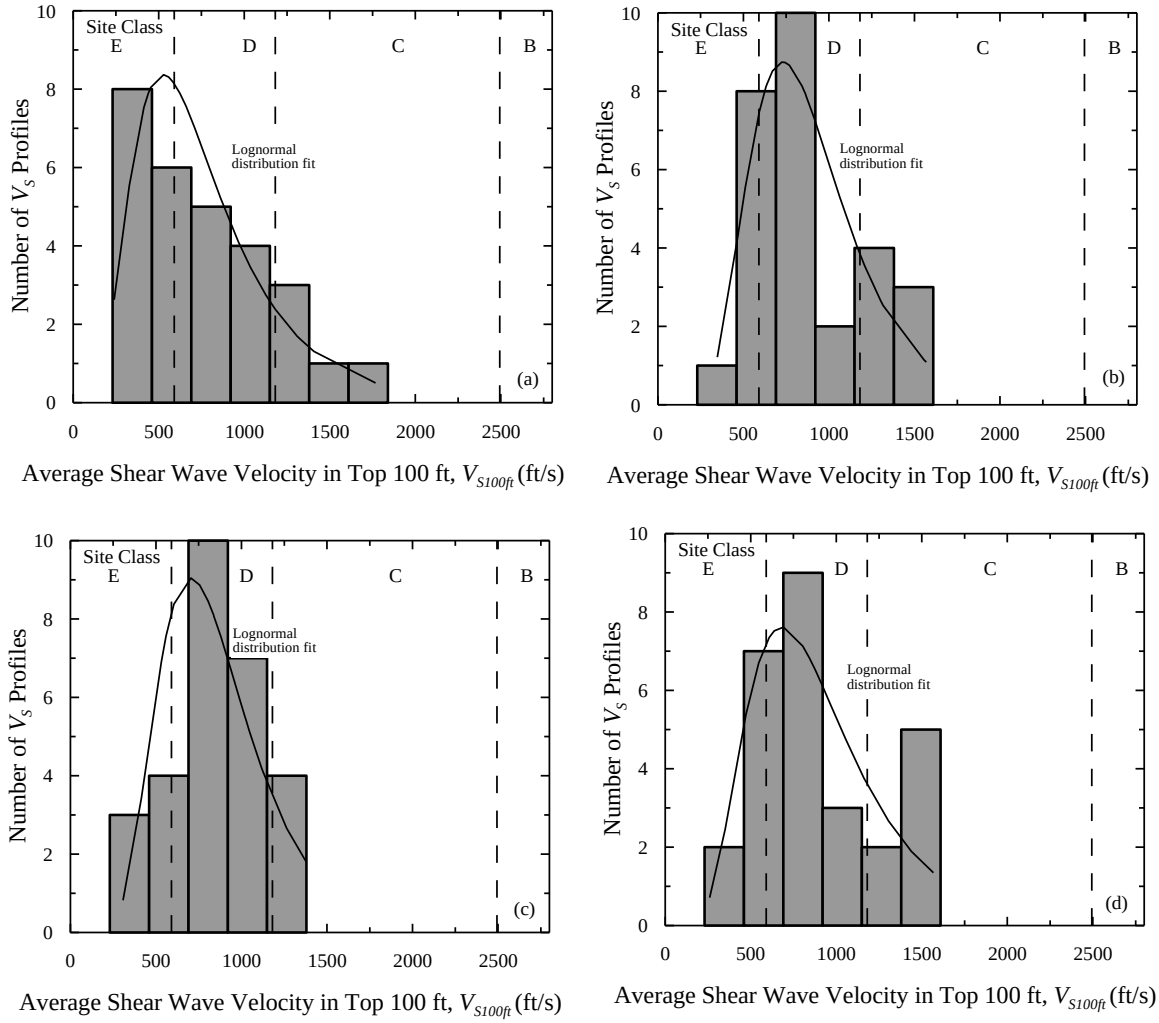

Figure 3.4 Histograms of V_{S100ft} for profiles assumed for (a) Charleston-Savannah, (b) Myrtle Beach, (c) Columbia-Florence-Lake Marion, and (d) Aiken.

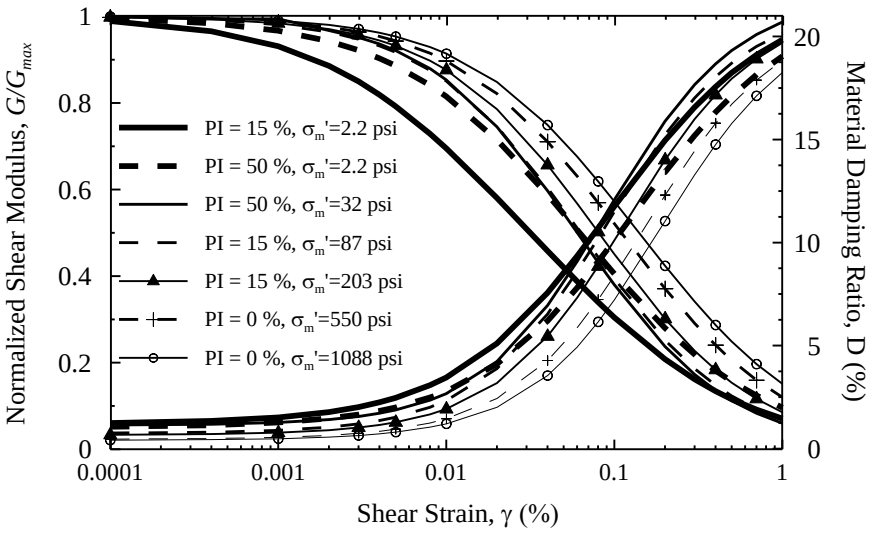

Figure 3.5 Sample mean G/G_{max}-γ and D-γ relationships used in ground response analysis.

3.3 Input Ground Motions

Input ground motions are generated using a program called Scenario_PC (Chapman 2006), because there are no real strong motion recording available for South Carolina. Scenario_PC uses a point-source stochastic model. The rationale for using stochastic methods is the resemblance of ground motion time histories to transient stochastic processes (Seed and Idriss 1969). The four inputs needed for generating synthetic acceleration-time histories with Scenario_PC are: (1) the deaggregated seismic hazard parameters, including earthquake magnitude and site-to-source distance; (2) the earthquake return period; (3) the target frequencies to be matched; and (4) the generalized rock model.

The deaggregated seismic hazard parameters at six oscillator frequencies (i.e., 0 Hz or free-field, 1, 2, 3.3, 5 and 10 Hz) are computed using the USGS deaggregation website (http://eqint.cr.usgs.gov/deaggint/2002/) for the centers of the 12, 4, 4, 4, 4, 4 and 15 quadrangles (1:24,000 scale) nearest Charleston, Savannah, Myrtle Beach, Columbia, Florence, Lake Marion and Aiken, respectively. Return periods considered are 475 and 2,475 years (or 10% and 2% probabilities of exceedance in 50 years, respectively). The former return period is sometimes referred to as the Functional Evaluation Earthquake (FEE); and the latter return period is sometimes referred to as the Safety Evaluation Earthquake (SEE).

The modal M_w obtained for all locations, oscillator frequencies and both return periods is ~7.3, because the seismic hazard in the SCCP is dominated by the Charleston Seismic Zone (Chapman 2006). The modal site-to-source distance is also practically the same for a given site. Thus, the generation of input motions matching the entire target uniform hazard spectrum is justified, and an earthquake acceleration-time history representing the predominant scenario is adequate for the six oscillator frequencies.

The rock model selected in Scenario_PC is the geologic realistic model, which consists of an outcropping soft rock (V_S = 2,300 ft/s) layer over weathered hard rock. The thickness of the soft rock layer at any one location is equal to the combined thickness of Quaternary, Tertiary and Cretaceous sediments. Two distinct advantages of assuming the geologic realistic model are (1) the input V_S profiles need only extend to the top of soft rock, and (2) the computed seismic site coefficients can be directly applied to the soft-rock accelerations available in the USGS and SCDOT seismic hazard maps.

A total of ninety-four synthetic input motions are used in the ground response analyses for the SCCP sites. Presented in Figure 3.6 are sample FEE and SEE input motions generated for the centers of the Charleston, Myrtle Beach, Columbia, and Aiken quadrangles. Values of $PGA_{outcrop}$ for the sample motions in Figure 3.6 range from 0.05 to 0.14 g for the FEE condition, and from 0.19 to 0.51 g for the SEE condition. Presented in Figure 3.7 are Fourier amplitude plots of the motions in Figure 3.6a and 3.6b.

One proxy variable that has been suggested for representing the general frequency (or period) content of a ground motion is mean predominant period (T_m) defined by (Rathje et al. 1998; Stewart et al. 2001):

$$T_m = \frac{\sum_{i=1}^{m} C_i^2 \left(1 / f_i \right)}{\sum_{i=1}^{n} C_i^2} \tag{3.1}$$

where, f_i is the i^{th} discrete Fourier frequency between 0.25 and 20 Hz; C_i is the corresponding Fourier amplitude; and m is the number of frequency points between 0.25 and 20 Hz. The computed values of T_m range from 0.24-0.43 s for the 47 FEE motions considered; and from

0.23-0.37 s for the 47 SEE motions. They exhibit similar ranges because M_w = 7.3 is assumed in the generation of both the FEE and SEE motions.

Because T_m characterizes the frequency (or period) content of the input time histories, it is dependent upon the site-to-source distance (R) and the depth to the top of hard rock (H_{HR}). Plotted in Figure 3.8 are values of T_m versus H_{HR} and R for the 94 synthetic soft rock motions generated by Scenario_PC and used in this chapter. Values of T_m are computed from the motions using Equation 3.1. Values of R are obtained from the USGS deaggregated seismic hazard information. Values of H_{HR} are obtained from outputs provided by Scenario_PC, which are based on the isopach map by Chapman and Talwani (2002). It can be seen from Figure 3.8 that T_m increases with increasing R and H_{HR}, due to attenuation of high frequency amplitudes with increasing distance from the source.

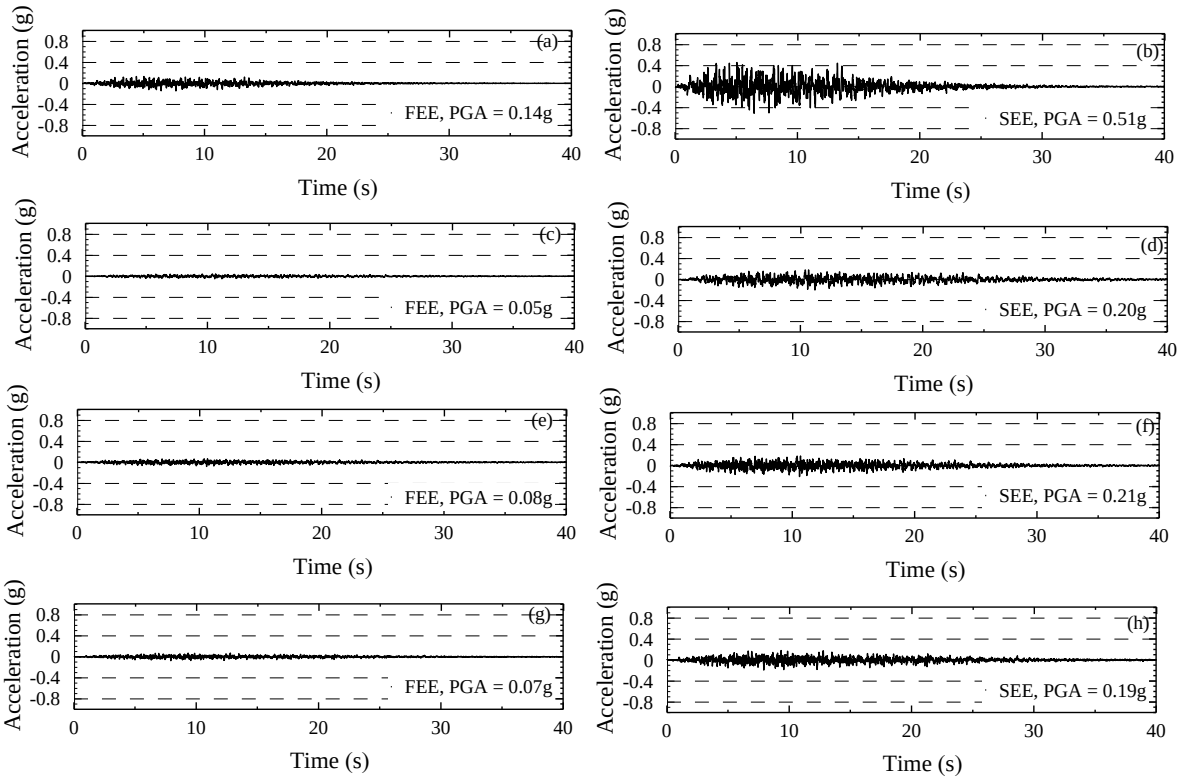

Figure 3.6 Sample synthetic soft rock outcrop motions generated by Scenario_PC for 10% and 2% probability of exceedance in 50 years for the (a-b) Charleston, (c-d) Myrtle Beach, (e-f) Columbia, and (g-h) Aiken quadrangles.

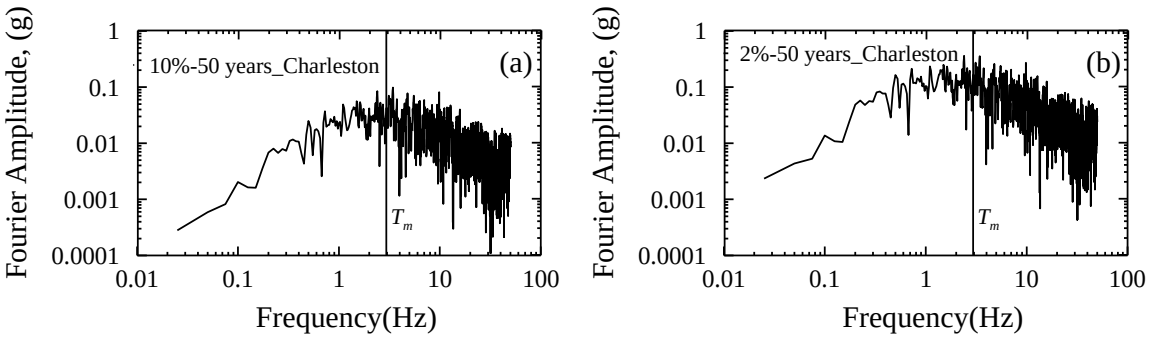

Figure 3.7 Fourier amplitude plots for (a) FEE and (b) SEE motions generated for the Charleston quadrangle.

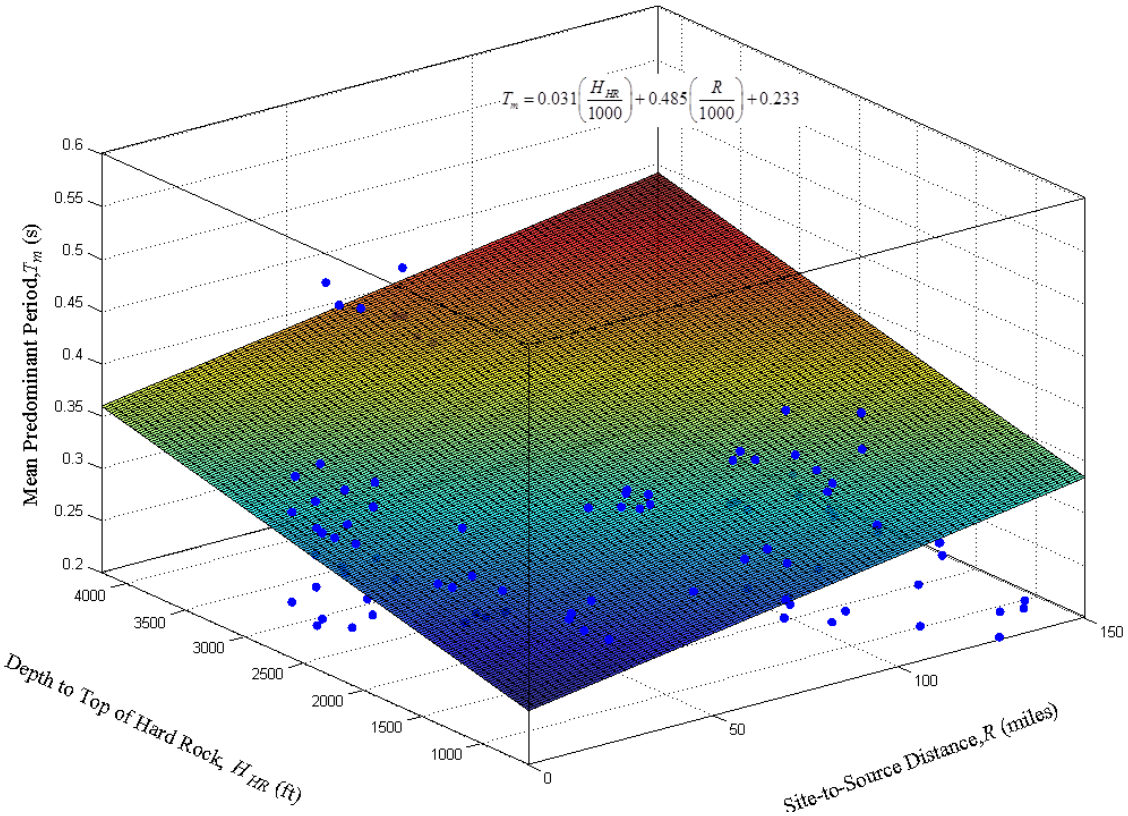

Figure 3.8 Plot of T_m versus depth to top of hard rock and site-to-source distance.

The best-fit planar surface shown in Figure 3.8 relating T_m, R and H_{HR} is defined by:

$$T_m = 0.031\left(\frac{H_{HR}}{1000}\right) + 0.485\left(\frac{R}{1000}\right) + 0.233 \tag{3.2}$$

where H_{HR} is in feet, R is in miles, and T_m is in seconds. It can be seen from Equation 3.2 that T_m values computed for the synthetic motions generated by Scenario_PC increase with increasing distance from the source.

Presented in Figure 3.9 are residual plots of T_m versus the predicting variables, H_{HR} and R. The residual, ε, is defined here as T_m of the plotted data minus T_m obtained from Equation 3.2. The mean values of ε are computed to be zero, suggesting a central tendency of the predicting equation. Equation 3.2 gives an unbiased prediction of T_m, because the ε data do not exhibit a systematic pattern with H_{HR} and R. Thus, Equation 3.2 can be used for predicting T_m in the SCCP.

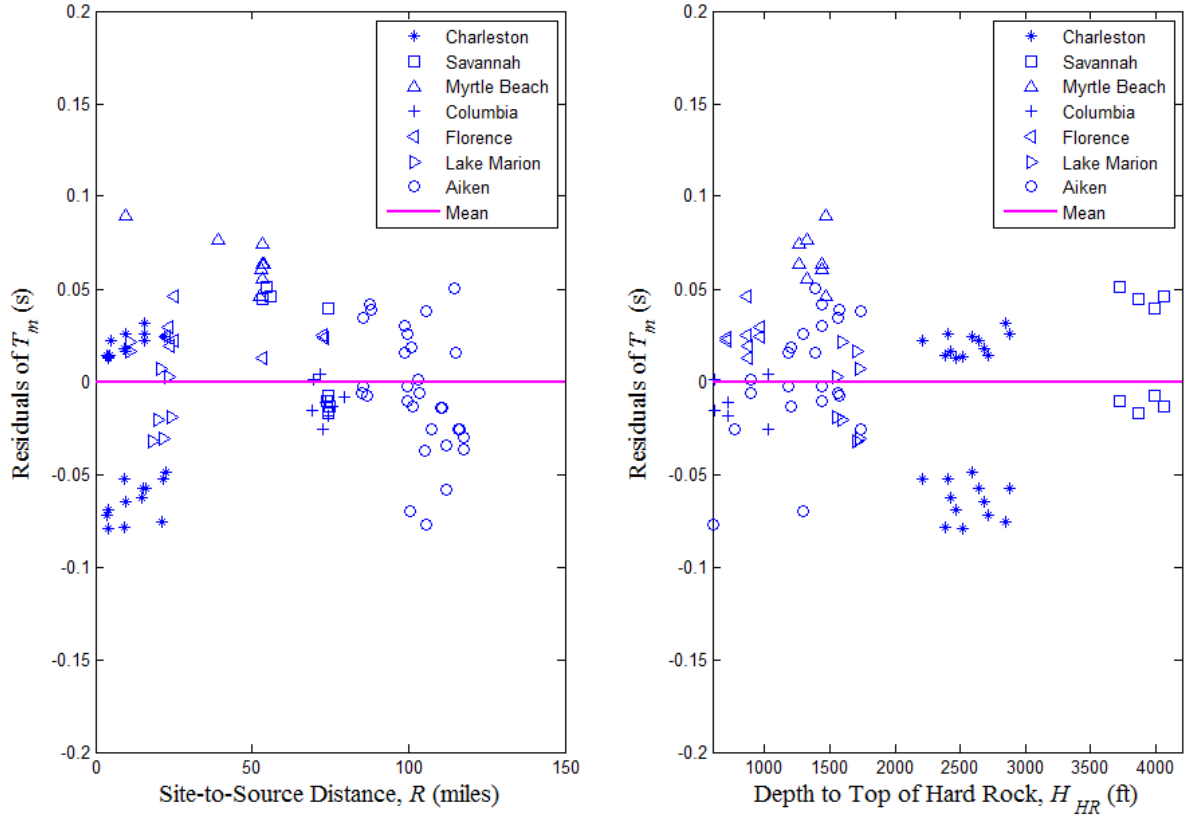

Figure 3.9 Residual plots of T_m versus R and H_{HR}.

Presented in Figures 3.10a and 3.10b are plots of $PGA_{outcrop}$ of the input motions with respect to H_{HR} and R. The anomaly in $PGA_{outcrop}$ values plotted in Figure 3.10a between H_{HR} 1,640 and 2,950 ft is due to the close proximity of the Charleston Seismic Hazard Zone. This can be seen in Figure 3.10b where $PGA_{outcrop}$ values are plotted versus site-to-source distance.

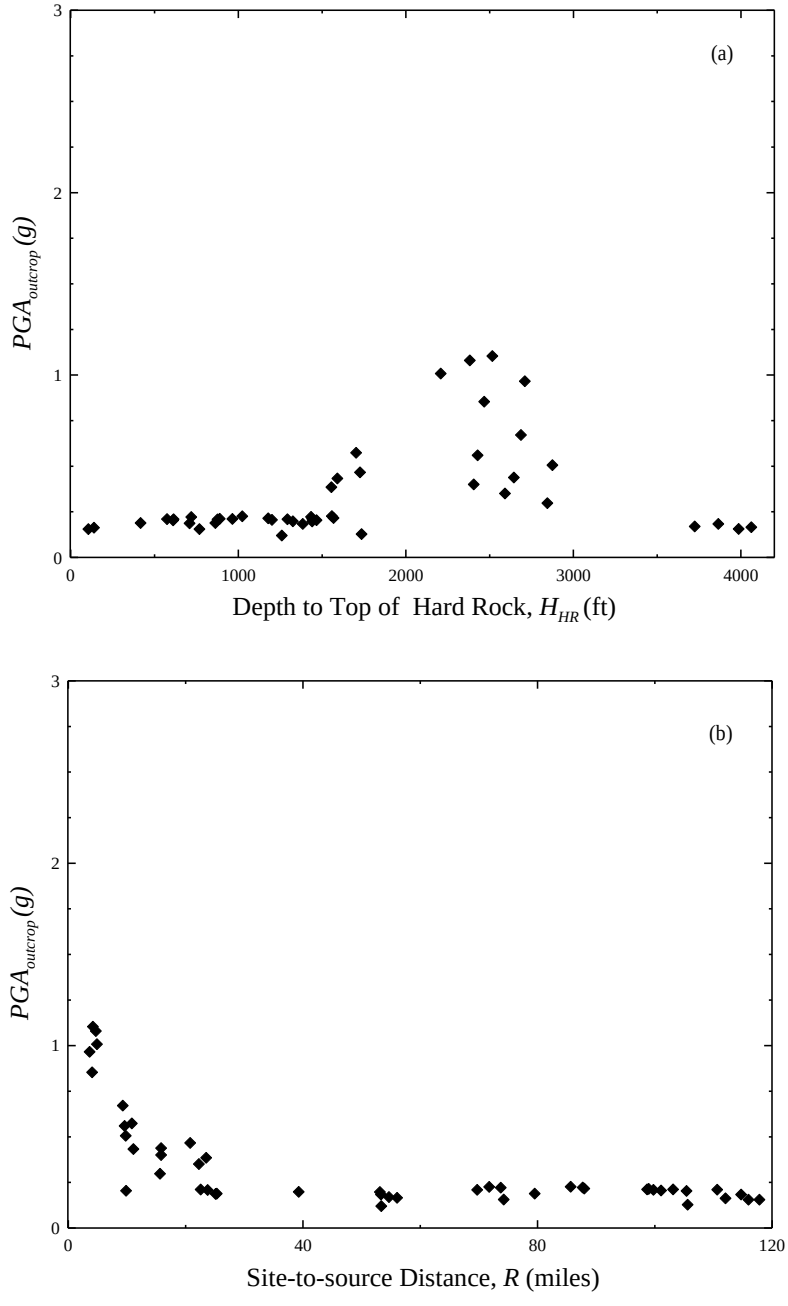

Figure 3.10 $PGA_{outcrop}$ of input motions used versus (a) H_{HR}, and (b) R.

3.4 Results

3.4.1 Generalized Model

Results of the ground response analysis using the V_S profiles shown in Figures 3.3a-3.3d are compiled into over two hundred fifty plots of computed seismic site coefficients versus V_{S100ft} grouped by spectral period (i.e., T: $\leq$ 0.01, 0.01-0.4, 0.41-0.8, 0.81-1.2, 1.21-2.0 and 2.01-4.0 s), spectral acceleration, and site location. Seismic site coefficients are referred to herein by their middle-range periods, and denoted as $F_{0.0}$ (or F_{PGA}), $F_{0.2}$ (or F_a), $F_{0.6}$, F_1 (or F_v), $F_{1.6}$ and F_3, respectively. Presented in Figures 3.11-3.13 are eighteen sample plots for Myrtle Beach corresponding to F_{PGA}, F_a, and F_v. The other plots are given in Appendices A-G. Each data point plotted in Figures 3.11-3.13 and Appendices A-G are determined by averaging the results of simulations with either FEE or SEE motions generated for the quadrangles of a given study region (e.g., Myrtle Beach, Aiken, etc.) over the corresponding period range. The data plotted in Figures 3.11-3.13 and Appendices A-G are sampled from over 36,000 SHAKE and 12,000 DMOD simulations.

In Figures 3.11-3.13, each data point representing either the FEE or SEE motions is determined by averaging the results of simulations for the respective motions over the corresponding period range. Averaging F over a spectral period range (e.g., T = 0.01-0.4 s) is consistent with the development of the NEHRP F_a and F_v values. The NEHRP F_a values were determined by averaging over the period ranges of 0.1-0.5 s; and the NEHRP F_v values were determined by averaging over the period ranges of 0.4-2.0 s. Because F can vary significantly within a period range, narrower ranges are assumed in this study for better estimates.

The plotted V_{S100ft}-F data pairs in Figures 3.11-3.13, as well as in Appendices A-G, exhibit three distinct features—(1) an increasing trend in F as V_{S100ft} increases from zero; (2) a zone of peak values of F; and (3) a decreasing trend in F as V_{S100ft} increases beyond the zone of peak F values. Similar features can be observed in data reported by other investigators (Silva et al. 2000; Chapman et al. 2006; Fairbanks et al. 2008). Because a simple continuous function to accurately models these features was not found, a piecewise function of F is developed beginning with the estimation of the peak seismic site coefficient within a given plot and the corresponding average shear wave velocity.

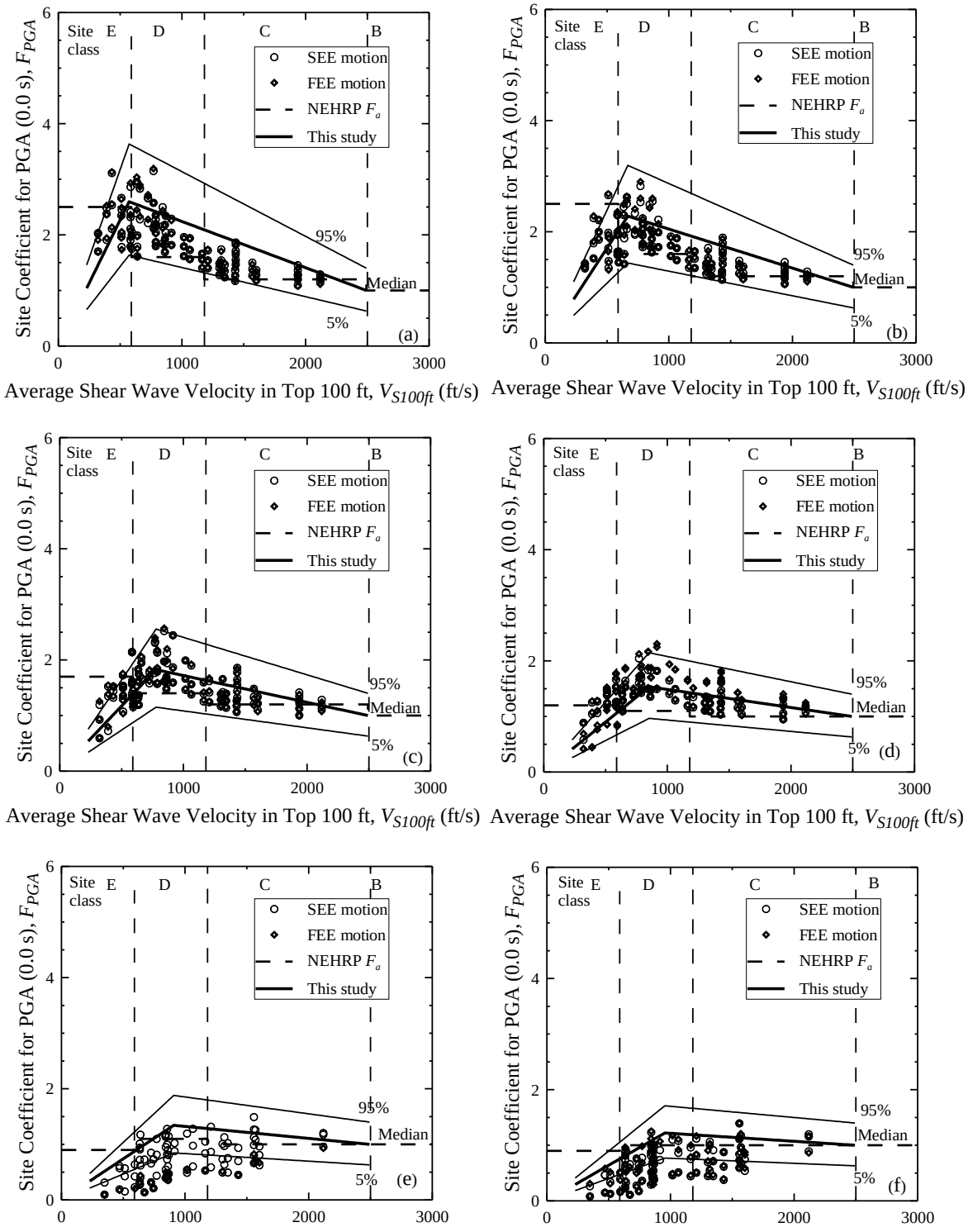

Figure 3.11 Site coefficients for 0.0 s spectral period (free-field) with PGA_{oucrop} equal to (a) 0.05 g, (b) 0.1 g, (c) 0.2 g, (d) 0.3 g, (e) 0.4 g, and (f) 0.5 g based on V_S profiles shown in Figure 3.3b for Myrtle Beach.

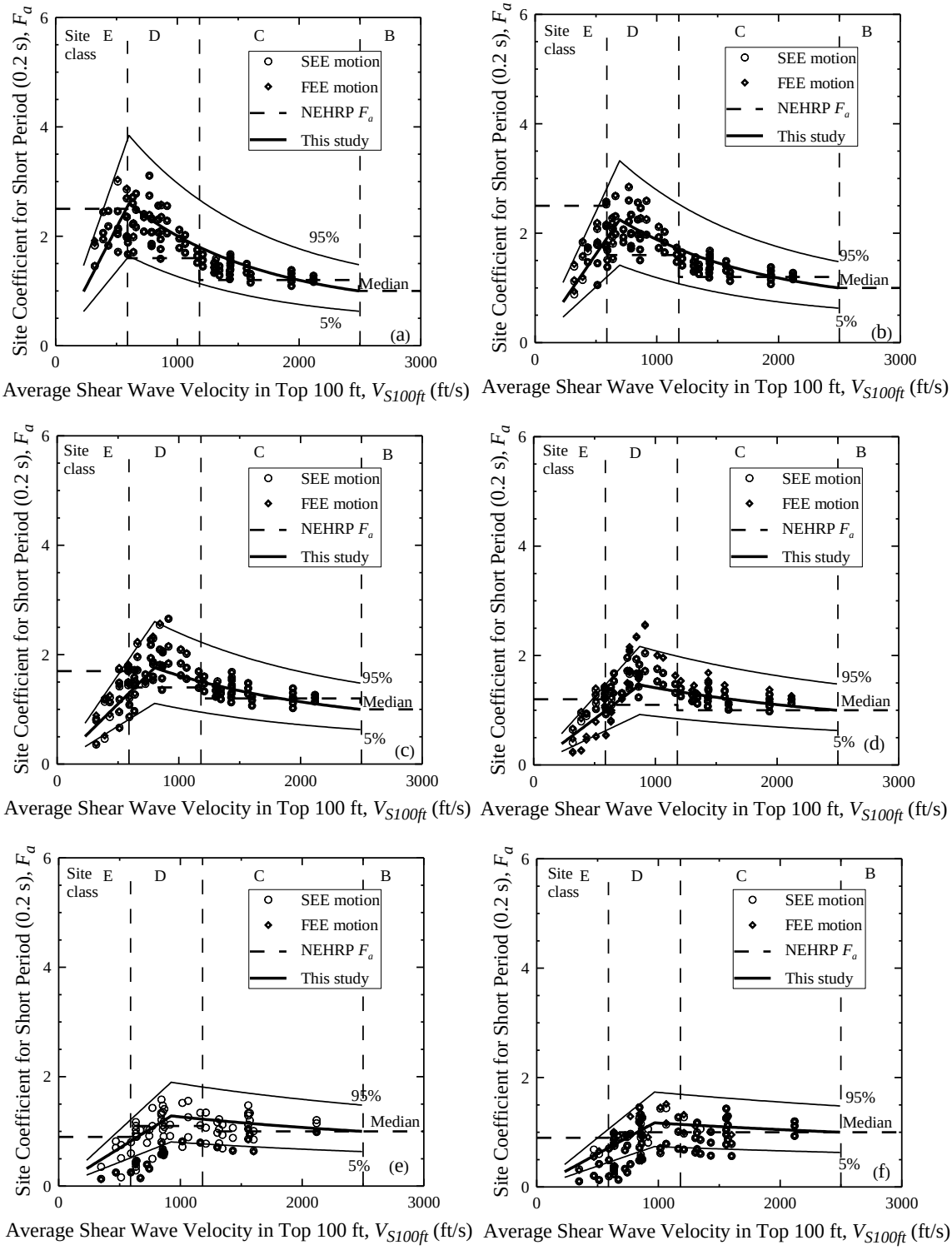

Figure 3.12 Site coefficients for 0.2 s (short) spectral period with S_S equal to (a) 0.125 g, (b) 0.25 g, (c) 0.50 g, (d) 0.75 g, (e) 1.0 g, and (f) 1.25 g based on V_S profiles shown in Figure 3.3b for Myrtle Beach.

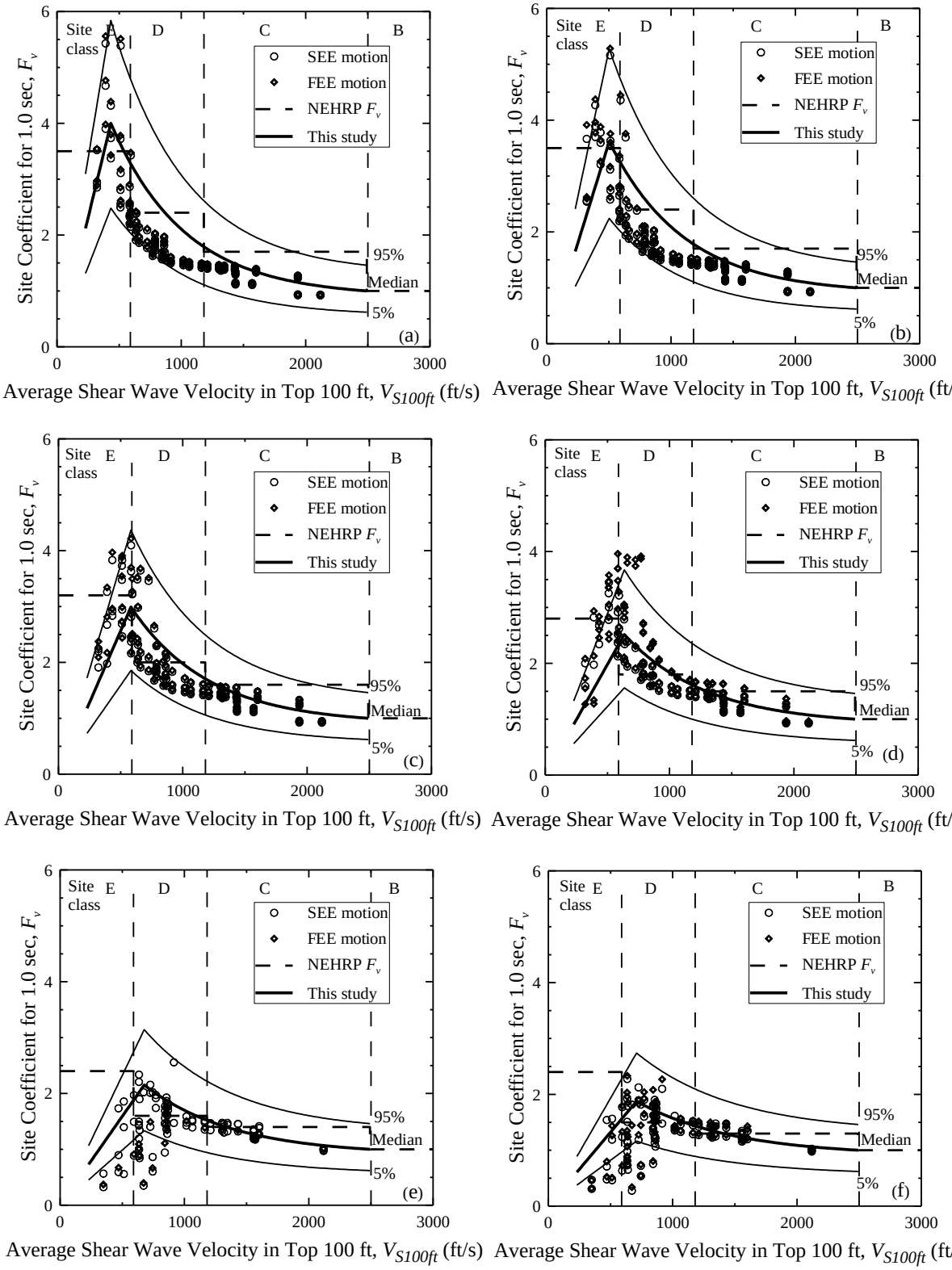

Figure 3.13 Site coefficients for 1.0 s (long) spectral period with S_1 equal to (a) 0.05 g, (b) 0.1 g, (c) 0.2 g, (d) 0.3 g, (e) 0.4 g, and (f) 0.5 g based on V_S profiles shown in Figure 3.3b for Myrtle Beach.

3.4.1.1 Estimating the Peak Site Coefficient

Extending the site coefficient model developed in Chapter 2, the peak site coefficient within a given plot (F_P) and the corresponding average shear wave velocity in the top 100 ft ($V_{S100ftP}$) can be estimated by:

$$F_P = \left[d_1 \exp\left(\frac{d_2 S_{outcrop}}{1g} \right) \left(\frac{T_m}{T_{330ft}} \right)^{d_3} + 1 \right] K_{H1} \tag{3.3a}$$

$$V_{S100ftP} = d_4 \left(\frac{S_{outcrop}}{1g} \right)^{d_5} \left(\frac{T_m}{1s} \right)^{d_6} K_{H2} \tag{3.3b}$$

where d_1, d_2, d_3, d_4, d_5 *and* d_6 are regression coefficients given in Table 3.1; $S_{outcrop}$ is in units of g; g is the acceleration of gravity; T_{330ft} is a proxy variable for the site fundamental period; s is one second to normalize T_m; and K_{H1} and K_{H2} are dimensionless adjustment coefficients to account for the influence of shallow soft rock. Although linear F_P-$S_{outcrop}$ and $V_{S100ftP}$-$S_{outcrop}$ relationships were assumed to model the simulation results for Charleston in Chapter 2, the results for all seven site locations in the SCCP indicate slightly nonlinear relationships. For this reason, the $S_{outcrop}$ terms in Equations 3.3a and 3.3b are expressed as exponential and power functions, respectively, based on a rigorous analysis of model residuals.

The proxy variable for site fundamental period in Equation 3.3a is defined as:

$$T_{330ft} = 4(330) \Big/ V_{S330ft} \tag{3.4}$$

where V_{S330ft} is the averaged shear wave velocity in the top 330 ft and is calculated similar to V_{S100ft}. The depth of 330 ft is selected because it provides just as good of model fits, if not better, as the depth to half-space. Range and reference profile values of V_{S330ft} for the profiles shown in Figures 3.3a-3.3d are listed in Table 3.2. Also listed in Table 3.2 are range and reference profile values of T_{330ft} and T_m for the seven locations in the SCCP.

Table 3.1 Regression coefficients for estimating seismic site coefficients in the SCCP.

$S_{outcrop}$	d_1	d_2	d_3	d_4 (ft/s)	d_5	d_6	a	$Z_{0.05}$	$Z_{0.95}$
$PGA_{outcrop}$	7.510	-4.394	1.614	846	0.222	-0.276	-*	0.63	1.40
S_S	7.305	-1.980	1.546	804	0.206	-0.141	0.65	0.63	1.48
$S_{0.6}$	10.691	-3.382	1.487	466	0.181	-0.721	0.85	0.63	1.50
S_1	4.929	-2.734	0.437	344	0.214	-0.876	0.90	0.62	1.46
$S_{1.6}$	3.477	-2.555	0.185	420	0.228	-0.647	0.99	0.68	1.40
$S_{3.0}$	0.720	-5.638	-0.860	692	0.208	-0.036	0.99	0.65	1.30

*T < 0.2 s, use Equation 3.6a.

Table 3.2 Typical values of V_{S330ft}, T_{330ft}, and T_m for seven locations in the SCCP.

Site	V_{S330ft} (ft/s)		T_{330ft} (s)		T_m (s)		$\frac{\text{Average } T_m}{\text{Reference } T_{330ft}}$
	Range	Reference Profile	Range	Reference Profile	Range	Average	
Charleston	518-2063	1237	0.64-2.53	1.06	0.24-0.35	0.29	0.27
Savannah	518-2063	1237	0.64-2.53	1.06	0.37-0.43	0.40	0.38
Myrtle Beach	718-2230	1555	0.59-1.83	0.84	0.35-0.38	0.37	0.44
Columbia	659-2247	1381	0.58-1.96	0.95	0.27-0.31	0.29	0.30
Florence	659-2247	1381	0.58-1.96	0.95	0.29-0.31	0.30	0.32
Lake Marion	659-2247	1381	0.58-1.96	0.95	0.26-0.31	0.28	0.29
Aiken	604-2109	1299	0.62-2.17	1.01	0.24-0.38	0.31	0.31

Presented in Figures 3.14a-f are F_p values plotted versus $S_{outcrop}$ and T_m/T_{330ft} for spectral periods of 0.0, 0.2, 0.6, 1.0, 1.6, and 3.0 s, respectively. As expected, F_p decreases with increasing $S_{outcrop}$ at all spectral periods. This is due to increased damping and nonlinear effects at higher $S_{outcrop}$. Maximum amplification is expected when the resonance frequency of a soil column matches with the frequency content of the motion. In Figures 3.14a-f, it can be seen that F_p tends to increase with increasing T_m/T_{330ft} for all values of T, except T =3.0 s. This increasing trend in F_p as T_m/T_{330ft} increases in reflected in the positive values of d_3 (see Table 3.1). Presented in Figures 3.15a-f are values of $V_{S100ftP}$, corresponding to F_P, plotted versus $S_{outcrop}$ and T_m/T_{330ft} for spectral periods of 0.0, 0.2, 0.6, 1.0, 1.6, and 3.0 s, respectively. At smaller $S_{outcrop}$, maximum amplification occurs in soft soils; and at higher $S_{outcrop}$ maximum amplification occurs in stiff soils.

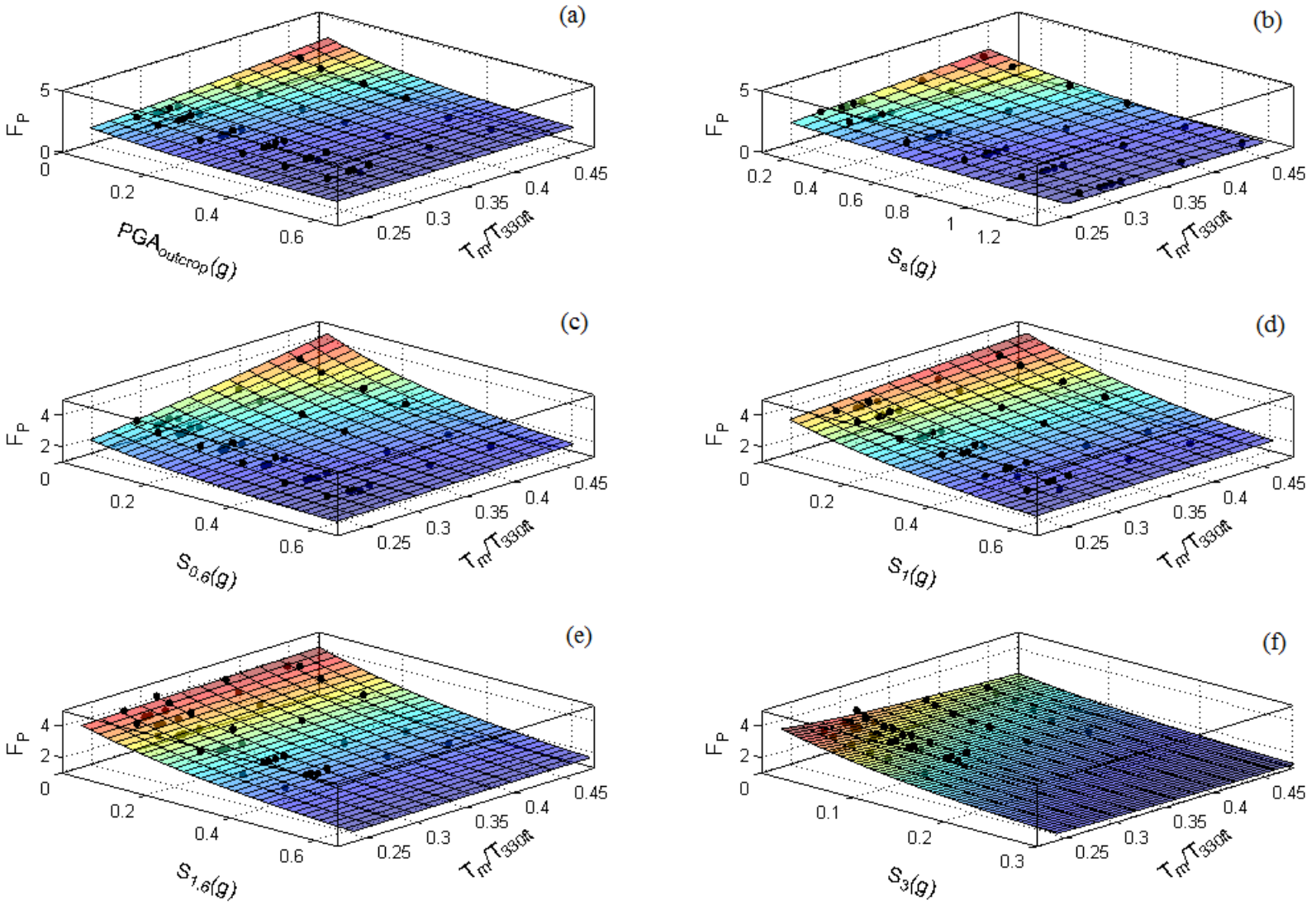

Figure 3.14 Effect of T_m/T_{330ft} and $S_{outcrop}$ on F_P for (a) 0.0 s, (b) 0.2 s, (c) 0.6 s, (d) 1.0 s, (e) 1.6 s, and (f) 3.0 s spectral periods.

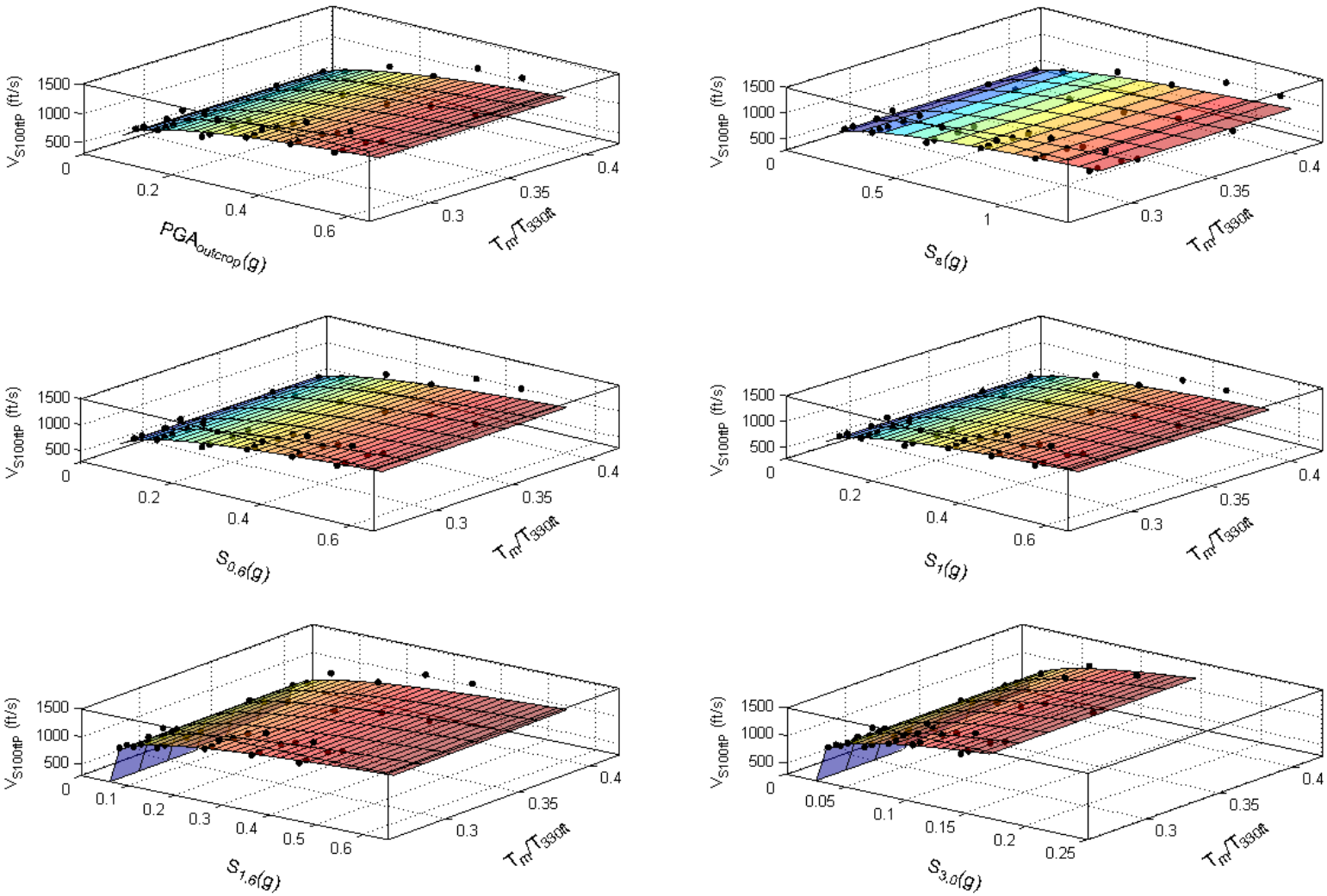

Figure 3.15 Effect of T_m/T_{330ft} and $S_{outcrop}$ on $V_{S100ftP}$ for (a) 0.0 s, (b) 0.2 s, (c) 0.6 s, (d) 1.0 s, (e) 1.6 s, and (f) 3.0 s spectral periods.

Plotted in Figure 3.16a-3.16b, and tabulated in Table 3.3, are computed values of K_{H1} and K_{H2}, respectively, based on the results of site response analysis preformed using the motions from five quadrangles near Columbia and the V_S profiles from Figure 3.3c modified such that the depths to the soft rock ($H_{B\text{-}C}$) are 1.6, 4.9, 16.5, 33, 66, 100, 165, 330 and 450 ft. A summary of inputs and outputs of these ground response analyses is presented in Appendix H. It can be seen in Figure 3.16a that values of F_P for $PGA_{outcrop}$ and S_S can be as much as 60 % higher at sites where $H_{B\text{-}C} < 330$ ft than at sites where $H_{B\text{-}C} \geq 330$ ft. On the other hand, values of F_P for $S_{0.6}$, S_1, $S_{1.6}$, and S_3 can range from about the same to much lower at sites where $H_{B\text{-}C} < 330$ ft than at sites where $H_{B\text{-}C} \geq 330$ ft. In Figure 3.16b, it can be seen that $V_{S100ftP}$ increases as $H_{B\text{-}C}$ decreases for all spectral periods. More work is needed to extend the analysis to sites other than Columbia, and to develop functional forms of K_{H1} and K_{H2}.

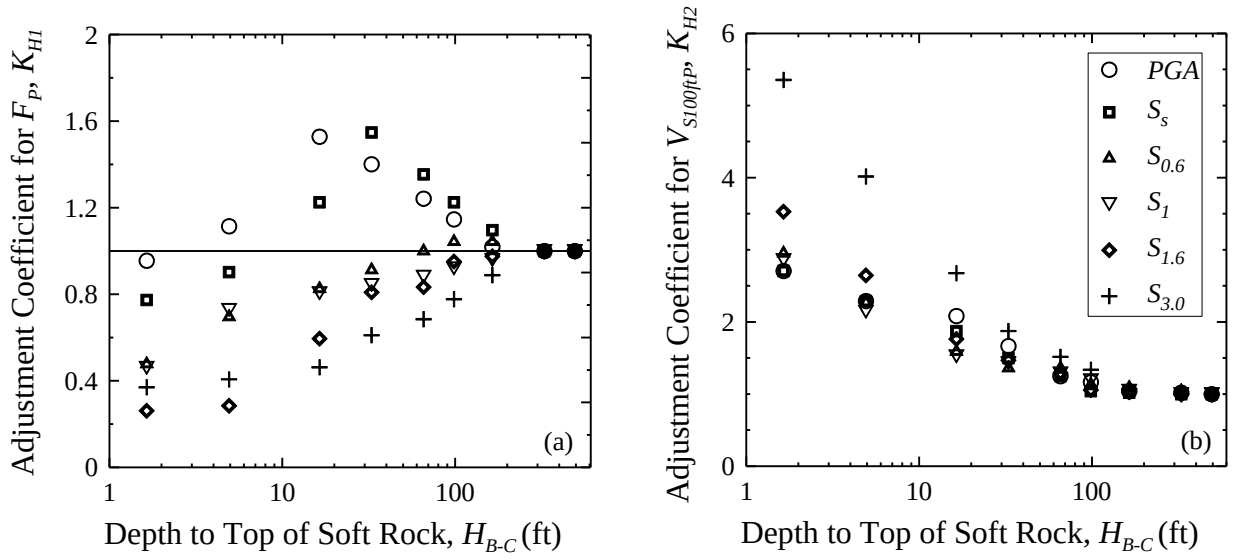

Figure 3.16 Depth-to-top of soft rock adjustment coefficients, K_{H1} and K_{H2}.

Table 3.3 Recommended depth-to-top of soft rock adjustment coefficients.

$S_{outcrop}$	Adjustment coefficient	Depth to soft rock, $H_{B\text{-}C}$ (ft)							
		1.5	5	16.5	33	66	100	165	≥ 330
$PGA_{outcrop}$	K_{H1}	0.96	1.11	1.53	1.40	1.24	1.15	1.02	1.00
	K_{H2}	2.71	2.29	2.08	1.67	1.25	1.17	1.04	1.00
Ss	K_{H1}	0.77	0.90	1.23	1.55	1.35	1.23	1.10	1.00
	K_{H2}	2.71	2.29	1.88	1.50	1.25	1.04	1.02	1.00
$S_{0.6}$	K_{H1}	0.48	0.70	0.83	0.91	1.00	1.04	1.04	1.00
	K_{H2}	2.95	2.27	1.59	1.36	1.36	1.14	1.09	1.00
S_1	K_{H1}	0.46	0.73	0.80	0.84	0.88	0.92	0.96	1.00
	K_{H2}	2.86	2.14	1.52	1.43	1.29	1.19	1.05	1.00
$S_{1.6}$	K_{H1}	0.26	0.29	0.60	0.81	0.83	0.95	0.98	1.00
	K_{H2}	3.53	2.65	1.76	1.47	1.29	1.06	1.03	1.00
S_3	K_{H1}	0.37	0.41	0.46	0.61	0.69	0.78	0.89	1.00
	K_{H2}	5.36	4.02	2.68	1.88	1.52	1.34	1.07	1.00

Presented in Figures 3.17a-3.17c are sample plots of computed site coefficients for $H_{B\text{-}C}$ = 33 ft for a site near Columbia. Also plotted in Figures 3.17a-3.17c are the median recommended F_P-$V_{S100ftP}$ relationships for $H_{B\text{-}C}$ = 33 and 450 ft. The dashed median relationships for $H_{B\text{-}C}$ = 33 ft exhibit fair to good fits of the plotted data and considerably better predictions than the relationships for $H_{B\text{-}C}$ = 450 ft. One reason why the median relationships for $H_{B\text{-}C}$ = 33 ft are not more accurate is because the data are based on ratios of computed seismic site coefficient whereas the dashed median relationships are based on Equations 3.3a and 3.3b with depth to

shallow rock adjustment coefficients from Table 3.3. Hashash et al. (2008) also observed depth-dependency in seismic site coefficients computed for the Mississippi Embayment.

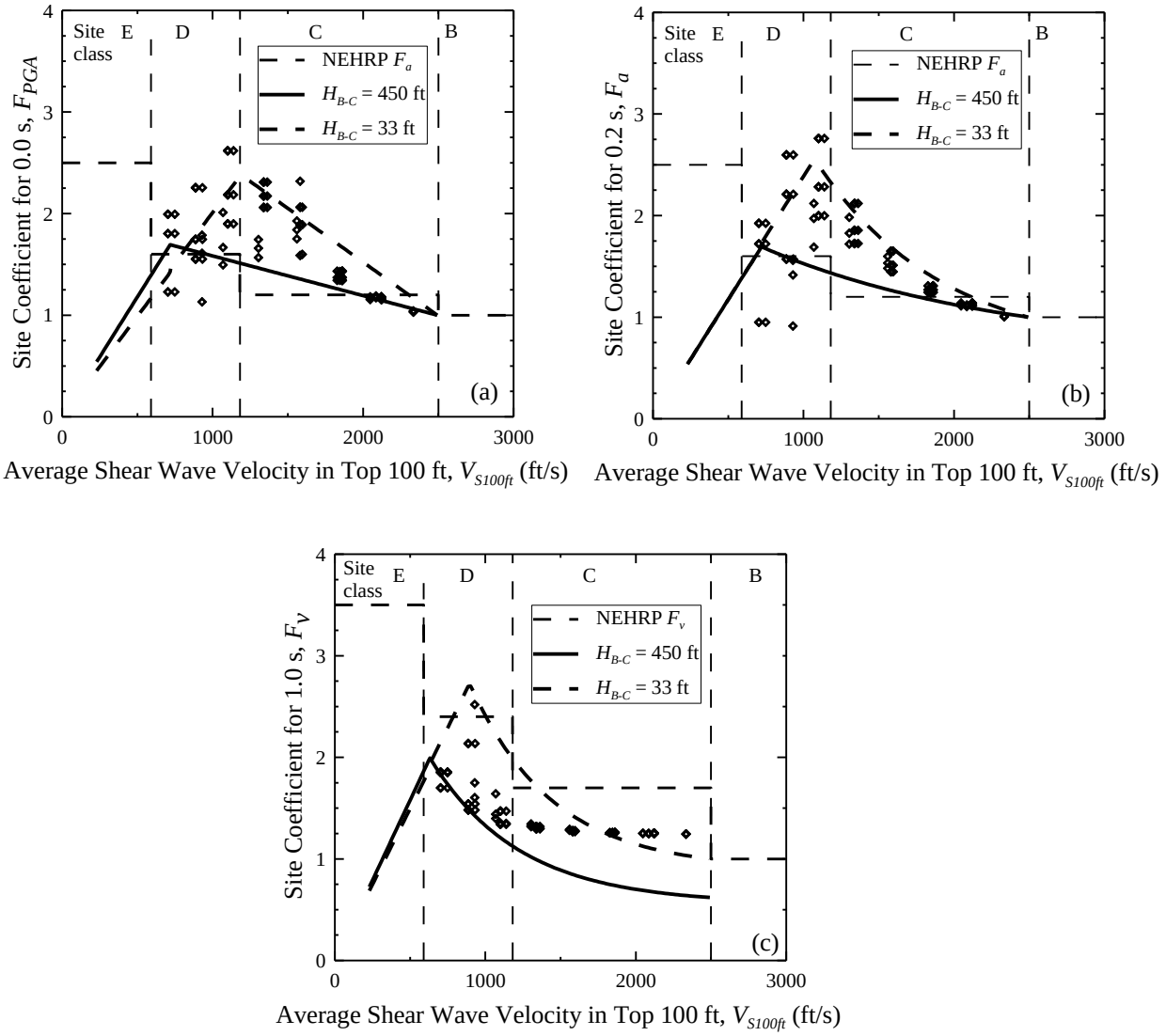

Figure 3.17 Sample median F-V_{S100ft} relationship for H_{B-C} = 450 and 33 ft and (a) $PGA_{outcrop}$ = 0.1 g, (b) S_S = 0.25 g, and (c) S_1 = 0.1 g with computed values for H_{B-C} = 33 ft.

3.4.1.2 Development of Relationship between F and V_{S100ft}

With the estimates of F_P and $V_{S100ftP}$, the median V_{S100ft}-F relationships of the eighteen plots shown in Figures 3.11-3.13 (as well as Appendices A-G) can be expressed as follows (Aboye et al. 2015):

$$F = \left(\frac{F_P}{V_{S100ftP}} \right) V_{S100ft} \qquad \text{for } V_{S100ft} < V_{S100ftP} \text{ and all spectral periods } T \tag{3.5}$$

$$F = \frac{(F_P - 1)(2500 - V_{S100ft})}{2500 - V_{S100ftP}} + 1 \qquad \text{for } V_{S100ft} \geq V_{S100ftP} \text{ and } T < 0.2 \text{ s} \tag{3.6a}$$

$$F = a + b\, e^{cV_{S100ft}} \qquad \text{for } V_{S100ft} \geq V_{S100ftP} \text{ and } T \geq 0.2 \text{ s} \tag{3.6b}$$

where a is a regression coefficient given in Table 3.1; and b and c are coefficients calculated from:

$$b = \frac{1 - a}{\exp^{2500c}} \tag{3.7}$$

$$c = \left(\frac{1}{2500 - V_{S100ftP}} \right) \ln \left(\frac{1 - a}{F_P - a} \right) \tag{3.8}$$

Equations 3.5 and 3.6 provide the same value of F at $V_{S100ftP}$. Equation 3.5 is a linear relationship that satisfies the condition of no amplification for a material with zero stiffness. The assumption that F = 0 when V_{S100ft} = 0 ft/s agrees with the fact that material with zero stiffness cannot support shear waves and, for this reason, F should be zero regardless of $S_{outcrop}$. Equations 3.6a and 3.6b satisfy the assumed reference soft rock outcrop condition of F = 1.0 when V_{S100ft} = 2,500 ft/s, which is the reference rock condition assumed in the USGS national hazard maps. When $V_{S100ft} > V_{S100ftP}$ and $T \geq 0.2$ s, the computed amplification coefficients are better fitted by an exponential function (Equation 3.6b) than by a linear function (Equation 3.6a).

Following the approach of Aboye et al. (2015), the development of Equations 3.5 and 3.6 involves a three-step procedure. First, median curves are derived by studying the residuals of the individual data subsets grouped by geologic area and spectral period. The residual, ε, is defined here as F of the computed data divided by F of the median relationship. Based on the probability plotting method, ε is shown to follow a lognormal distribution. The second step involves

obtaining least-squared regression approximations of F_p and $V_{S100ftP}$ as a function of $S_{outcrop}$ and T_m/T_{330ft}. Finally, based on F_P, $V_{S100ftP}$, K_{H1} and $K_{H2,}$ Equations 3.5 and 3.6 are established. The predictor variables V_{S100ft}, $S_{outcrop}$, T_m/T_{330ft} and $H_{B\text{-}C}$ are shown to have little or no bias in the median relationships expressed by Equations 3.5 and 3.6, because plots of variables-ε do not show any systematic structure.

The upper and lower curves shown in Figures 3.11-3.13 are drawn to bound 95% and 5%, respectively, of all the data points for a given F. They are drawn by multiplying Equations 3.5 and 3.6 by the average standard Z-scores (i.e., $Z_{0.95}$ or $Z_{0.05}$) listed in Table 3.1. The Z-scores are obtained from lognormal cumulative distribution of computed F divided by predicted F for each set of data.

3.4.2 Recommended Site Coefficients

Presented in Appendices A-G are computed site coefficients for Charleston, Savannah, Myrtle Beach, Columbia, Florence, Lake Marion, and Aiken, respectively. In decreasing order, the computed site coefficients were generally found to be greater in Myrtle Beach, Savannah, Charleston, Florence, Columbia, Lake Marion and Aiken. More closely matching values of T_m and T_{330ft} (i.e., T_m = 0.37 and T_{330ft} = 0.84 for the Myrtle Beach reference profile may explain the higher site coefficients obtained for Myrtle Beach and Savannah.

Plotted in Figures 3.11, 3.12, and 3.13 are F_{PGA}, F_a, and F_v values computed for Myrtle Beach, respectively. Also plotted for comparison are the NEHRP F_a and F_v values. Maximum computed median F_{PGA} values range from 1.2 to 2.6, as shown in Figure 3.11. The computed median F_{PGA} values are generally greater than the NEHRP F_a values for all values of $S_{outcrop}$. The difference is most significant for Site Class D, and can be greater by as much as 75%. As shown in Figure 3.12, maximum computed median F_a values range from 1.25 to 2.6. The computed median F_a values are greater than the NEHRP F_a values by as much as 80%. For the Site Class E, the NEHRP F_a is found to be conservative compared to the computed median F_{PGA} and F_a values from this study. This finding generally agrees with Silva et al. (2000), Rodriguez-Marek et al. (2001), Borcherdt (2002), Stewart et al. (2003), Seyhan and Stewart (2012) and the NGA-GMPEs (http://peer.berkeley.edu/ngaeast/) whose computed F_a values are greater for Site Class D and smaller for Site Class E compared to the NEHRP.

Presented in Figure 3.13 are F_v values computed for Myrtle Beach. It can be seen in Figure 3.13 that the computed median F_v values range from 2.0 to 3.7. The computed maximum median F_v values plot generally below the NEHRP F_v values for Site Class E and C. For Site Class D, the computed median F_v values are sometimes greater than the NEHRP values. Figure 3.13 shows that long-period amplification is critical when V_{S100ft} is between 590-990 ft/s. This observation generally agrees with Silva et al. (2000), Borcherdt (2002), Stewart et al. (2003) and Choi and Stewart (2005) who also obtained F_v values greater than the NEHRP for Site Class D.

The new seismic site coefficient model defined by Equations 3.3, 3.5 and 3.6 is recommended for the SCCP because it provides better matches to the computed values than do the NEHRP coefficients for all values of V_{S100ft}. A flowchart of the procedure for obtaining the recommended site coefficients from soft rock spectral accelerations is presented in Figure 3.18. The procedure begins with (1) determining four key site variables (i.e., V_{S100ft}; V_{S330ft} or T_{330ft}; H_{HR}; and $H_{B\text{-}C}$) from in situ test results and available geologic information; and (2) obtaining three key ground motion variables (i.e., $S_{outcrop} = PGA_{outcrop}$, $S_{0.2}$, $S_{0.6}$, S_1, $S_{1.6}$, S_3; R; and T_m) from hazard maps or computer programs like Scenario_PC. With these inputs, the values of F_P and $V_{S100ftP}$ are calculated from Equations 3.3a and 3.3b, respectively; and the site coefficients corresponding to each value of $S_{outcrop}$ needed are calculated using Equation 3.5 or 3.6.

It is worth noting that the recommended site coefficients are based on motions generated by Scenario_PC assuming the modal M_w of 7.3 and scaling to different values of $PGA_{outcrop}$. Additional analyses are performed with soft rock motions generated by assuming M_w of 5, 6, 7 and 8 and scaling the motions to different values of $PGA_{outcrop}$ (see Appendix I). Although the motions exhibit varying frequency contents and durations depending on M_w, there is < 5% difference, on average, between the computed site coefficients as shown in Figure 3.19. This finding indicates that the influence of frequency content on F is captured by the T_m terms in Equations 3.3a and 3.3b; and the influence of ground motion duration on F is comparatively small compared to the influence of $PGA_{outcrop}$. Thus, the site coefficients described by Equations 3.3a, 3.3b, 3.5 and 3.6 can be applied to soft rock spectra accelerations for all earthquake magnitudes.

Additional analyses are performed as part of this study to investigate the influence of H_{HR} versus $H_{B\text{-}C}$ on the site coefficients. It is found that much, if not all, of the variations in computed site coefficients at a given location due to the depth to top of rock can be explained by $H_{B\text{-}C}$. Thus, the adjustment coefficients K_{H1} and K_{H2} are sufficient to capture the influence of soft rock at shallow depths (< 330 ft).

Additional analyses are performed to compare the results of SHAKE2000 and DMOD2000 for a wide range of $PGA_{outcrop}$ (0.05-5 g) and V_{S100ft} (240-1,780 ft/s) values considering conditions in Charleston. The results of these additional analyses are presented in Appendix K. It is found that the site coefficients based on SHAKE2000 can be as much as (or more) 20 % higher than that of DMOD2000 for softer profiles (low V_{S100ft}) due to nonlinear behavior even at low $PGA_{outcrop}$. This finding further supports the use of the recommended site coefficient model for Site Class E locations, instead of the overly conservative NEHRP site coefficients.

A partial field validation of the recommended site coefficient model for the SCCP is presented in Appendix L using data from the 1989 Loma Prieta earthquake. As can be seen in Figure L.1, the site coefficient model developed for Charleston better predicts the plotted Loma Prieta F_a values, than do the NEHRP F_a values. This partial field validation provides additional strong support for the use of the recommended site coefficient model.

3.5 Summary

The model for predicting site coefficients developed in Chapter 2 was extended to a generalized seismic site coefficient model for the SCCP in this chapter. Soil/rock and seismic conditions typical of sites in the SCCP (i.e., Charleston, Savannah, Myrtle Beach, Columbia, Florence, Lake Marion, and Aiken) were considered. Input ground motions were scaled to obtain good coverage over the spectral acceleration range that is provided in codes and guidelines. It was shown that scaling of input motions is justified because the SCCP is dominated by a single seismic source zone. The generalized model was based on over 48,000 total stress, one-dimensional equivalent linear and nonlinear ground response analyses, and derived at spectral periods of 0.0, 0.2, 0.6, 1.0, 1.6 and 3.0 s. The respective site coefficients were referred to as F_{PGA}, F_a, $F_{0.6}$, F_1, $F_{1.6}$, and F_3, and were calculated as averages over period ranges of $\leq$ 0.1, 0.1-0.4, 0.4-0.8, 0.8-1.2, 1.2-2.0, 2.0-4.0 s.

The most important variables identified in developing the seismic site coefficient model are: V_{S100ft}, spectral acceleration (amplitude), mean predominant period of the input motion (T_m), approximate fundamental frequency of soil/rock column in the top 330 ft (T_{330ft}), and depth to soft rock ($H_{B\text{-}C}$). A relationship to compute T_m based on depth to hard rock (H_{HR}) and site-to-source distance (R) was suggested for the SCCP. In decreasing order, the computed site coefficients were found to be greater in Myrtle Beach, Savannah, Charleston, Florence, Columbia, Lake Marion and Aiken. More closely matching values of T_m and T_{330ft} (i.e., T_m = 0.37 and T_{330ft} = 0.84 for the Myrtle Beach reference profile) may explain the higher site coefficients found for Myrtle Beach.

The computed site coefficients for each of the seven areas in the SCCP were grouped by spectral acceleration and plotted versus V_{S100ft}. The site coefficient model was expressed by a linear model for $V_{S100ft} < V_{S100ftP}$ and a linear or exponential model for $V_{S100ft} \geq V_{S100ftP}$. Each set of data exhibited a peak value for V_{S100ft} values between 240 and 1,050 ft/s, depending on soft rock-outcrop acceleration ($S_{outcrop}$) and spectral period. Site coefficients were found to decrease with increasing $S_{outcrop}$ and the rate of decrease is higher when V_{S100ft} < 660 ft/s. As $S_{outcrop}$ increases, the induced shear strains were observed to increase, causing higher hysteretic damping in the soil. The increased hysteretic damping dissipates the wave energy. Because softer sediments develop larger strains than stiffer sediments, this effect is more pronounced when V_{S100ft} < 660 ft/s. It is also noted that F_{PGA} and F_a attenuate more rapidly with increasing $S_{outcrop}$ than F_v. The variability in computed site coefficients for sites with similar V_{S100ft} was characterized by 5% lower bound and 95% upper bound curves.

The computed relationships for periods of 0.0, 0.2 and 1.0 s for Myrtle Beach were compared with the NEHRP F_a and F_v values. It was observed that the computed median F_{PGA} values are greater than the NEHRP F_a values by as much as 70%. The computed median F_a values also plotted above the NEHRP F_a values for V_{S100ft} > 590 ft/s. The computed median F_v values plotted above the NEHRP F_v values by as much as about 40% for 590 ≤ V_{S100ft} ≤ 1,150 ft/s. The computed median F_v values agreed with the NEHRP F_v values for $V_{S100ft} \geq$ 1,180 ft/s. For V_{S100ft} < 590 ft/s, the NEHRP F_a and F_v were greater than the computed median values.

The effect of $H_{B\text{-}C}$ was considered by using hypothetical $H_{B\text{-}C}$ values of 1.6, 4.9, 16.5, 33, 66, 100, 165, 330 and 450 ft in the V_S profiles for Columbia. Higher amplifications were found at lower values of $H_{B\text{-}C}$ when $T \leq 0.6$ s. When $T > 0.6$ s, higher amplifications were found at higher values of $H_{B\text{-}C}$. Factors were introduced to adjust the site coefficient estimates for different depths to the B-C boundary. The procedure for applying the seismic site coefficient model is summarized in the flow chart presented in Figure 3.18.

The computed F_{PGA}, F_a and F_v median relationships were recommended for the SCCP because they are: (1) based on regional conditions; (2) continuous with V_{S100ft}, (3) consider depth to rock, and (4) consider the frequency content of the design motion.

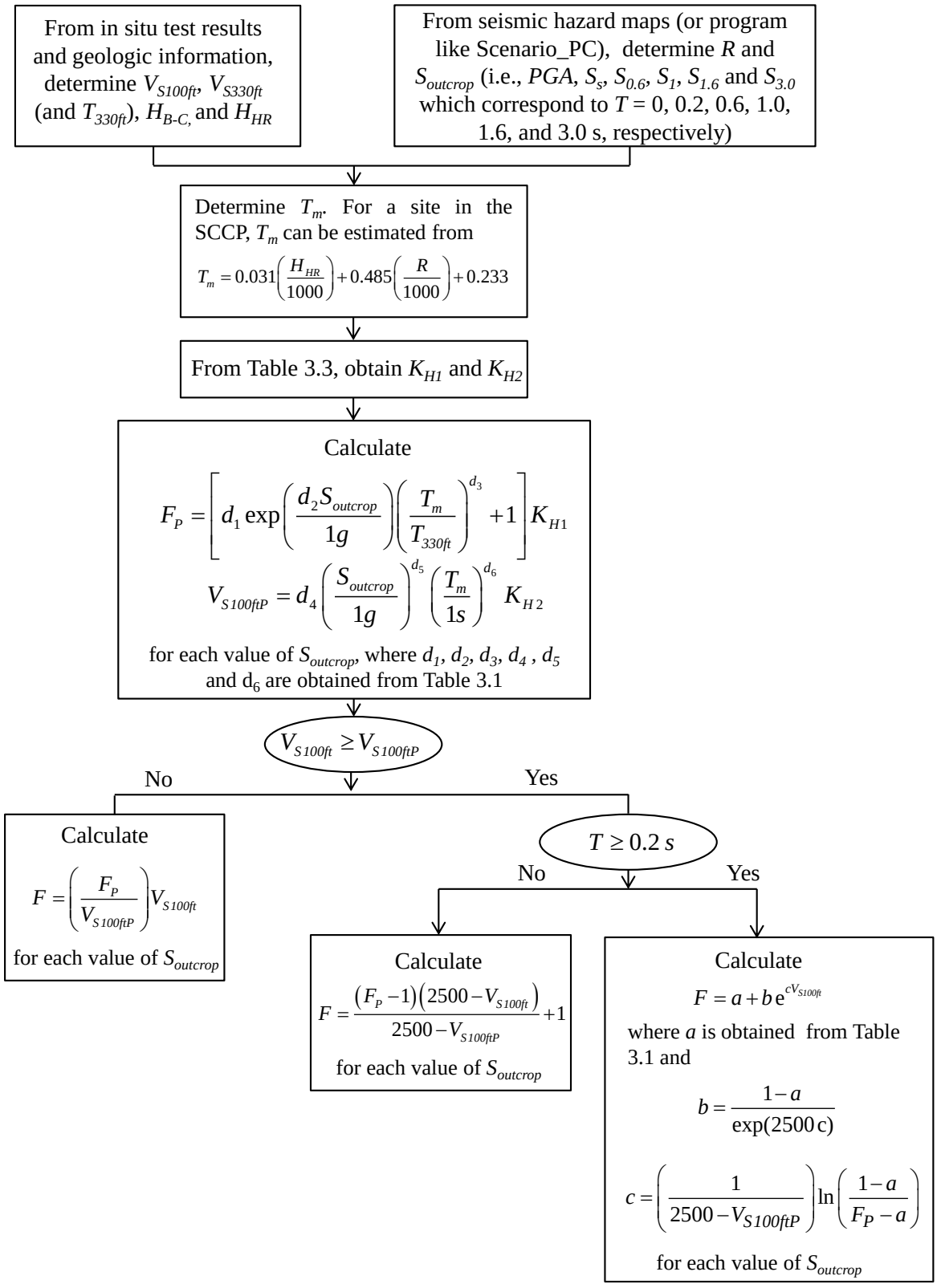

Figure 3.18 Flow chart of obtaining site coefficients for conditions in the SCCP.

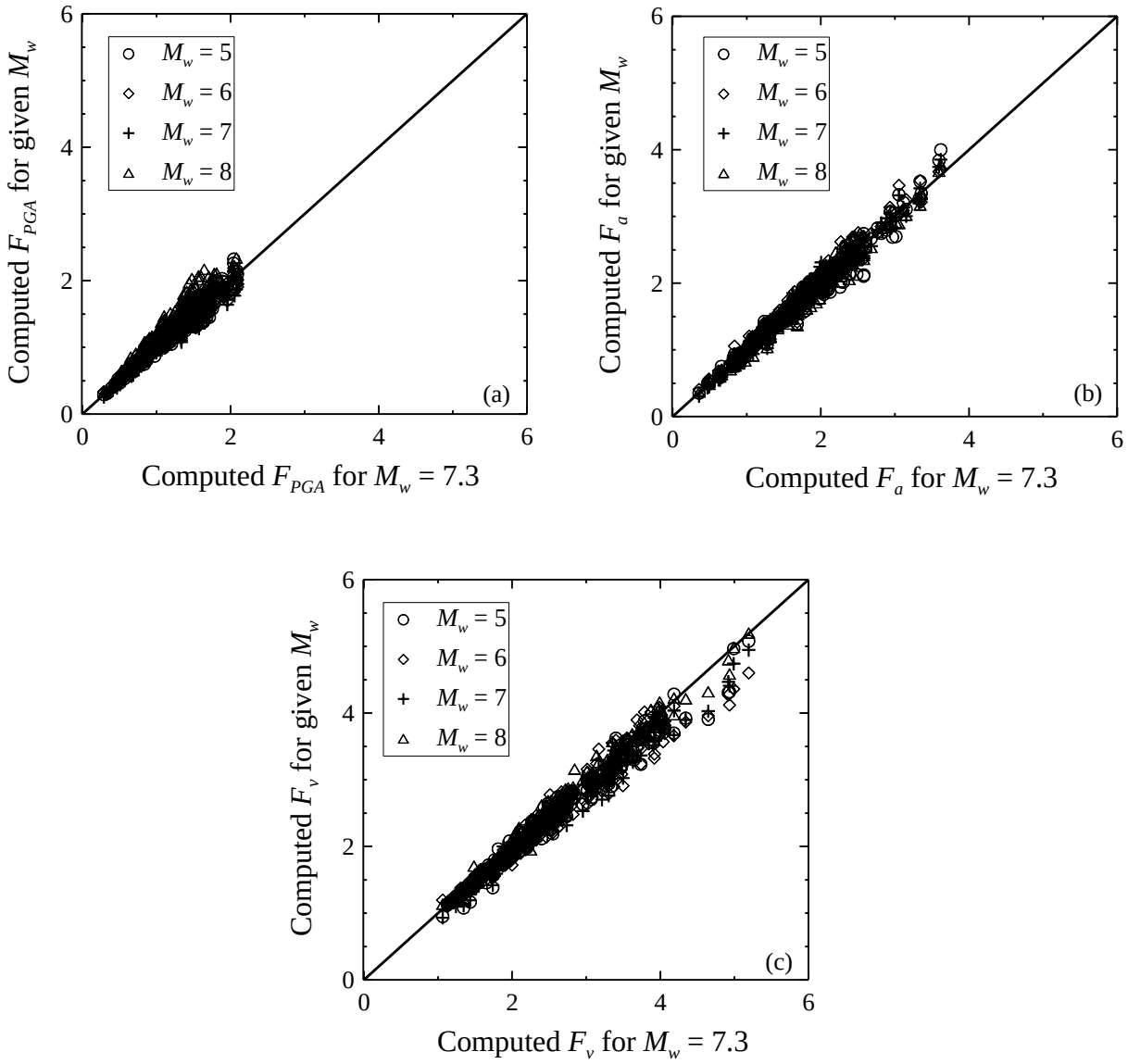

Figure 3.19 Comparison of computed (a) F_{PGA}, (b) F_a, and (c) F_v based on input motions for different earthquake magnitudes scaled to the same $PGA_{outcrop}$.

CHAPTER FOUR

SEISMIC SITE COEFFICIENT MODEL BASED ON CONDITIONS IN THE PIEDMONT

4.1 Geology and Seismology

The South Carolina Piedmont (SCP) is an area of rolling hills that lies between the Fall Line and the Brevard fault, as shown on the geologic map presented in Figure 4.1. The Fall Line marks the boundary between the Piedmont and the Coastal Plain physiographic provinces. The Brevard fault is a major topographic and structural feature in South Carolina which marks the boundary between the Piedmont and the Blue Ridge Mountains. The rolling hills of the SCP are erosional remains of an ancient mountain chain that today range in elevation from 330 to 1,640 ft above sea level.

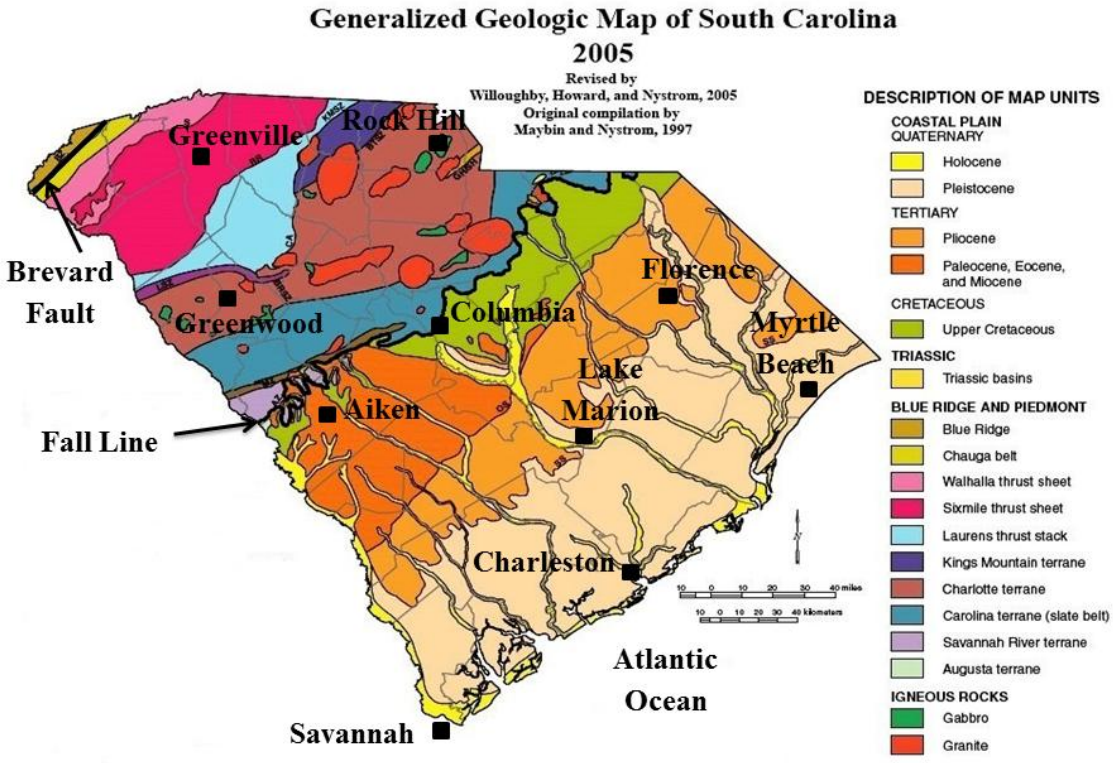

Figure 4.1 Geologic map of South Carolina (SCDNR 2005) showing the Fall Line and the Brevard Fault, which mark the boundaries of the South Carolina Piedmont, as well as the sites considered in ground response analyses.

Based on rock type and geologic structures, the SCP can be divided into several physiographic units (or belts). Among these are included the Brevard fault unit and the inner Piedmont unit. As described by Krinitzsky and Dunbar (1990), the Brevard fault unit is characterized by cataclystic rocks produced by crushing and fracturing from fault movements. Other rock types existing in the Brevard fault unit are phyllites, schists (chlorite, graphite, and mica), gneiss, amphibolite quartizites and carbonates. The age of these rocks is Paleozoic or older. The inner Piedmont contains rocks of the highest metamorphic grade found in the SCP. These include volcanic and sedimentary rocks metamorphosed to the almandine-amphibolite facies (amphibolite, granitic gneiss, paragneiss, metasandstone, and schist).

The typical vertical stratigraphic sequence in the SCP consists of 0 to 70 ft of residual soils at the surface underlain by extremely weathered rock (called saprolites) and less weathered hard rock (SCDOT 2008a). Residual soils consist of clayey materials near the surface, followed by sandy silts and silty sands. Saprolites are physically and chemically weathered rocks that can be soft/loose to very hard/dense, and typically retain the structure of the parent rock.

There are four major fault zones in the SCP that have been identified as potentially active seismic sources (Hatcher et al. 1977). These fault zones are called the Brevard, the Towaliga-Middleton-Lowndesville-Kings Mountain, the Goat Rock-Modoc, and the Augusta Shear Zones. The Towaliga-Middleton-Lowndesville-Kings Mountain fault is located between Greenville and Greeenwood. The Goat Rock-Modoc and the Augusta Shear Zones are located near the Fall Line. Most of these faults zones are thrust faults with strike-slip components, which were mainly formed and active during the Palezoic Era, prior to the opening of the Atlantic Ocean (Krinitzsky and Dunbar 1992). Due to the absence of any active faults and a high compressional stress regime, the seismicity in the SCP is believed to be due to the interaction of an ambient stress field on pre-existing zones of weakness. The predominant zones of weakness are networks of joints, thus limiting the size of the largest earthquake in the SCP (Talwani 1986).

Based on Bollinger (1975), the largest historic earthquake within the SCP occurred in Union County on January 1, 1913, on the Kings Mountain shear zone. This earthquake had a maximum Modified Mercalli Intensity Index (MMI) of VII to VIII and an estimated magnitude between 5.0 and 5.5. Other smaller historic earthquakes have occurred in the SCP, including the 1971 Oconee County earthquake (MMI = VI), the 1971 Lake Jocasse earthquake (MMI = VI), and the 2014 Edgefield County earthquake (MMI = V; moment magnitude of 4.1).

4.2 Seismic Hazard Assessment

The seismic hazard at the centers of sixteen quadrangles making up the four areas selected for ground response analyses in the SCP (i.e., Columbia, Greenville, Greenwood, and Rock Hill) is assessed based on the 2008 USGS deaggregation hazard mapping (http://eqint.cr.usgs.gov/deaggint/2008/index.php, accessed December 15, 2012). The seismic hazard in these areas, except Greenville and the western half of Greenwood, is dominated by earthquakes with modal moment magnitudes (M_w) of about 7.3 in the Charleston Seismic Hazard Source Zone for both the FEE and SEE conditions. The seismic hazard for the Greenville area and the western half of the Greenwood area is dominated by earthquakes with modal M_w of 4.8 and 7.3 for the SEE and FEE conditions, respectively. This indicates that, unlike the SCCP, the seismic hazard in the SCP is significantly influenced by other sources, in addition to the Charleston Seismic Hazard Source Zone.

Presented in Figures 4.2 is a sample deaggregated seismic hazard output from the Greenville quadrangle. It can be observed that the seismic hazard includes nearer small earthquakes (M_w = 4.5 to 6.0), and farther large earthquakes (M_w = 7.0 to 7.5). Thus, the justification of a single dominant seismic source, as assumed for the SCCP in Chapters 2 and 3, does not apply in the western half of the SCP. To account for multiple seismic source zones, input motions are generated by matching the seismic hazard at target frequency values, as will be discussed in Section 4.3.

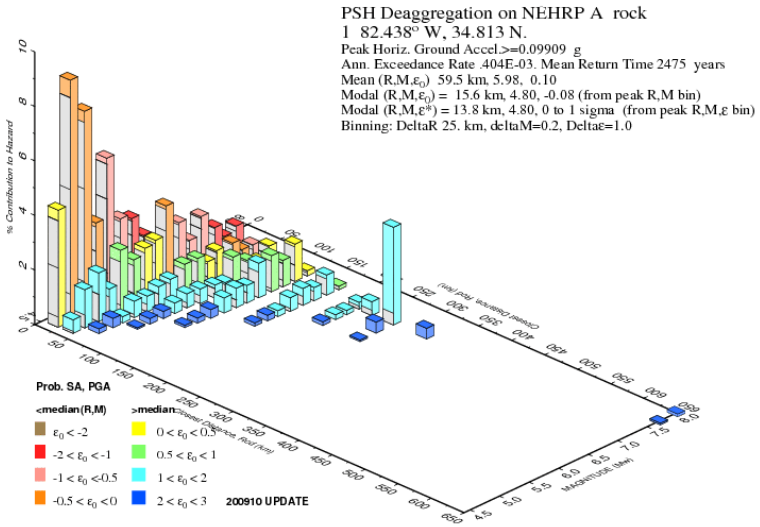

Figure 4.2 Deaggregated seismic hazard on NEHRP Site Class A rock for the Greenville quadrangle (http://eqint.cr.usgs.gov/deaggint/2008/index.php, accessed July 25, 2014).

4.3 Dynamic Soil/Rock Model

Presented in Figure 4.3 are representative V_S profiles assumed in the ground response analyses for the SCP. The reference V_S profile shown in Figure 4.3a is derived by combining V_S profiles measured by (or for) different consulting companies (e.g., WPC, S&ME and URS) with the V_S profile assumed by Silva et al. (2003). Most of the V_S measurements were made by the seismic cone penetration test method. Some were determined by the seismic downhole and spectral-analysis-of-surface-waves methods. Mean V_S values of the reference profile range from 895 to 985 ft/s in the top 33 ft; from 985 to 2,500 ft/s between depths of 33 and 66 ft; and from 2,500 to 8,200 ft/s between the depths of 66 and 100 ft. A V_S value of 8,200 ft/s is the assumed representative value for the weathered hard rock in the SCP.

Fifty-one other V_S profiles are also shown in Figure 4.3. These other profiles are derived by applying ±1, -2 and -3 standard deviations (σ) of ln(V_S) to the reference profile above the weathered hard rock (V_S = 8,200 ft/s) half space and by varying the depth to weather hard rock. The average value of σ of ln(V_S) assumed was either 0.30 or 0.32, depending on whether residual soil and saprolites or Quaternary sediment, respectively, is modeled. Assumed depths to the top of weathered hard rock are 165, 100, 66 and 33 ft, as indicated in Figures 4.3a, 4.3b, 4.3c and 4.3d, respectively.

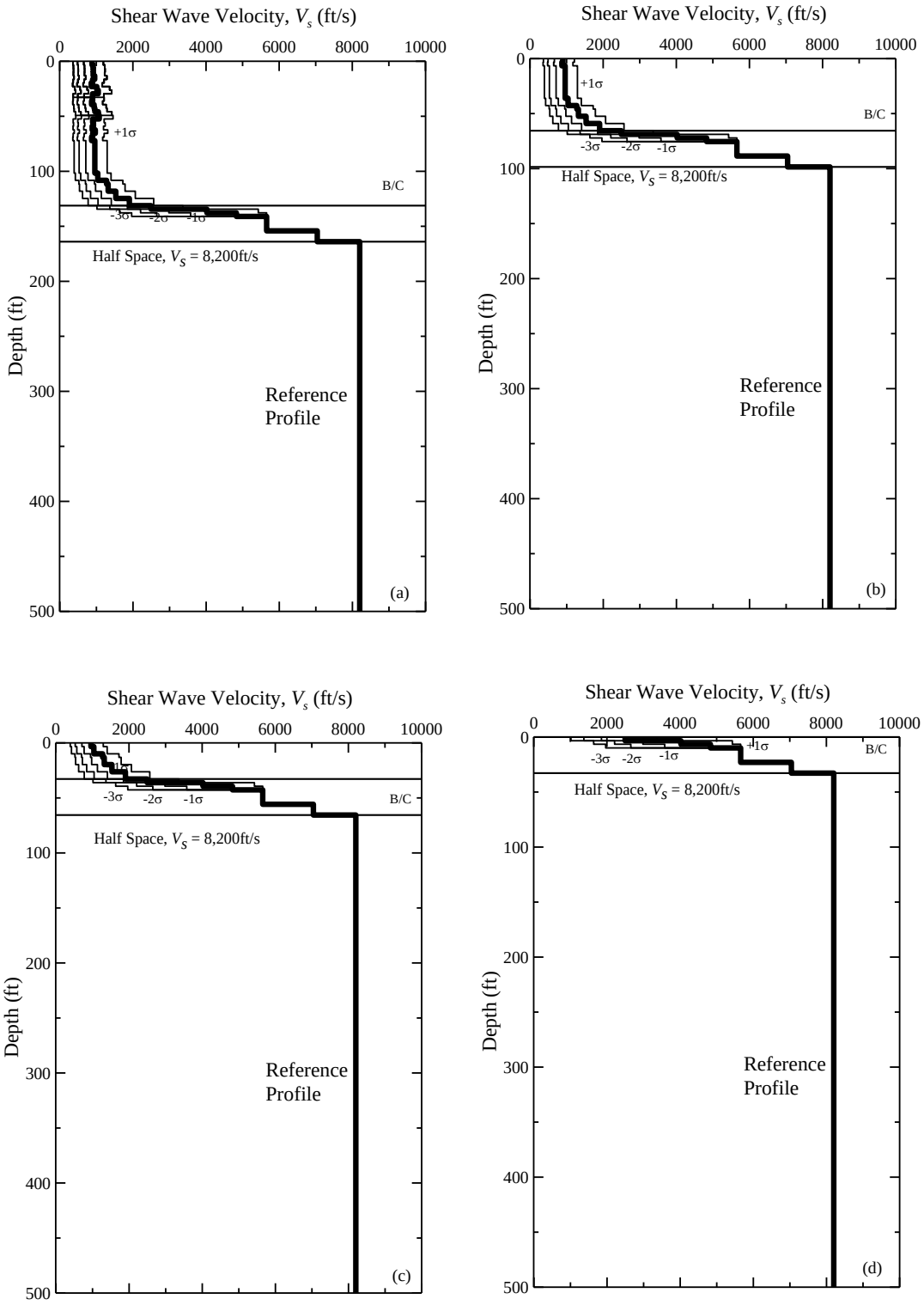

Figure 4.3 Representative profiles of V_S for the SCP with the top of V_S = 8,200 ft/s material at depths of (a) 165 ft, (b) 100 ft, (c) 66 ft and (d) 33 ft.

Presented in Figure 4.4 and 4.5 are two general soil/rock models assumed for selecting the variation of normalized shear modulus (G/G_{max}) and material damping ratio (D) with shearing strain amplitude. The soil/rock model presented in Figure 4.4 consists of a 33-ft thick residual soil on top of saprolite. Under lying the saprolite is a weathered hard rock half space with V_S = 8,200 ft/s. The soil/rock model presented in Figure 4.5 is identical to Figure 4.4 below the depth of 33 ft. Above the depth of 33 ft in Figure 4.5, properties typical of Quaternary flood plain material are assumed. The ground water depth is assumed to be 16 ft in both models.

Similar to Chapters 2 and 3, the Zhang et al. (2005) relationships are used to represent the variations in G/G_{max} and D with shearing strain amplitude (γ) in terms of geologic age, mean effective confining pressure, and soil plasticity index. Displayed in Figure 4.6 are sample G/G_{max}-γ and D-γ relationships for the Quaternary, the residual soil, and the saprolite layers shown in Figures 4.4 and 4.5. Also used in the ground response analysis are the $\pm 1\sigma$ G/G_{max}-γ and D-γ relationships according to Zhang et al. (2008). For the half space with V_S = 8,200 ft/s, linear or constant relationships of G/G_{max}-γ and D-γ are assumed. This is done by entering G/G_{max} = 1 and D = 0.1% for all γ values. A value of D = 0.1% is taken to be representative for the weathered hard rock (SCDOT 2008a).

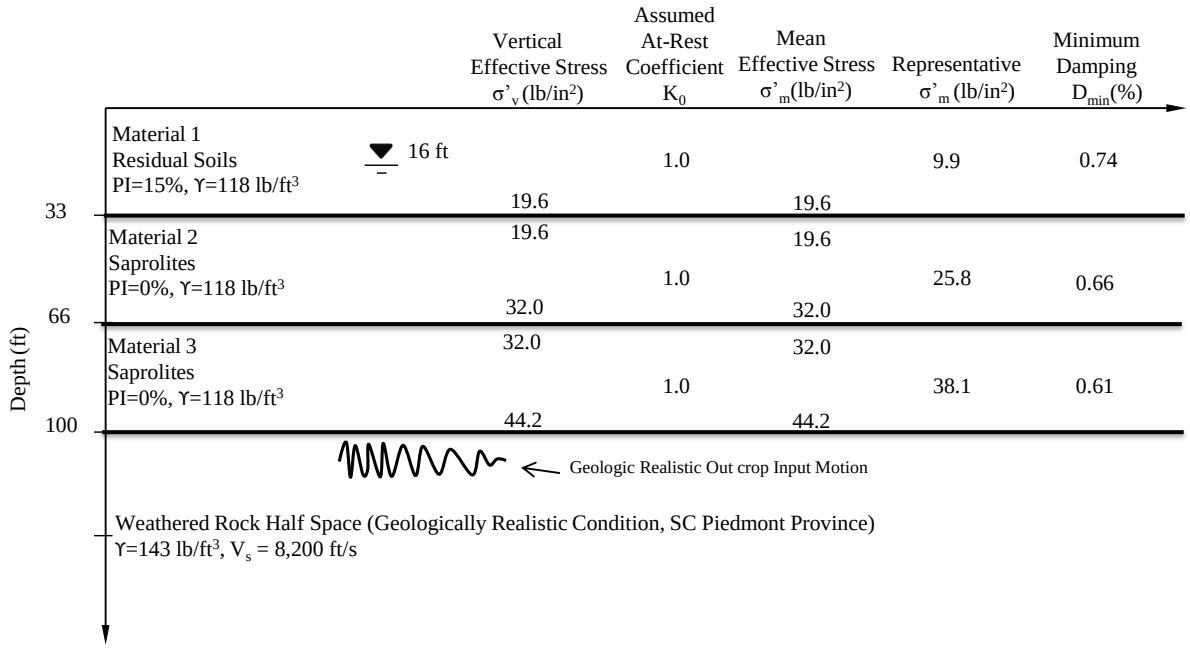

Figure 4.4 Soil/rock model for the Piedmont assuming residual soils over saprolites.

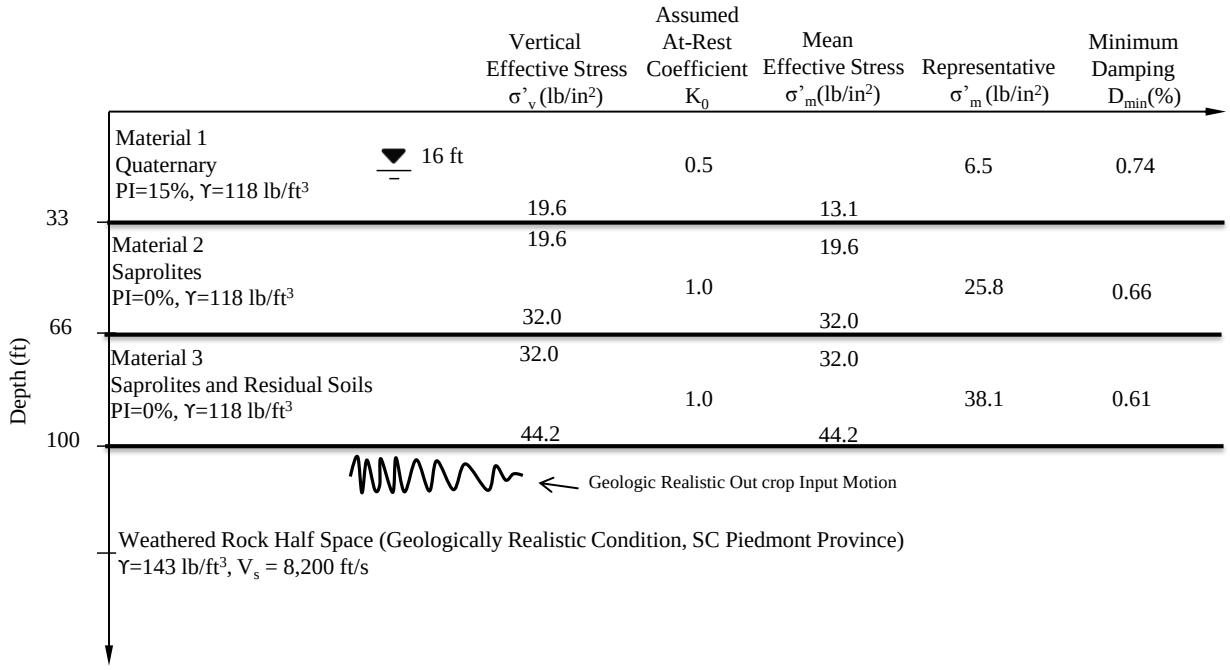

Figure 4.5 Soil/rock model for the Piedmont assuming Quaternary soils over saprolites.

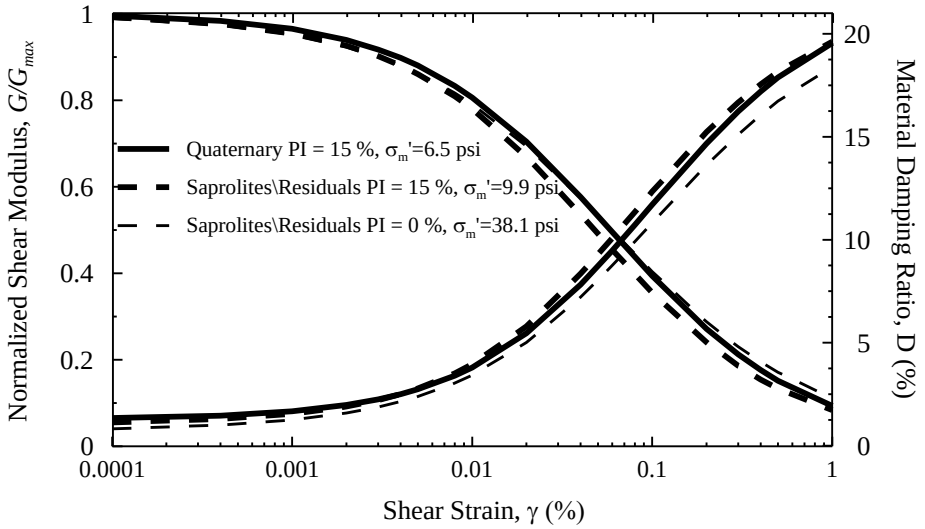

Figure 4.6 Sample mean G/G_{max}-γ and D-γ relationships used in ground response analysis based on Zhang et al. (2005).

4.4 Input Ground Motions

Synthetic ground motions for the SCP are generated using the program Scenario_PC (Chapman 2006) similar to the motions used for the SCCP in Chapters 2 and 3. However, two different assumptions are made for the SCP. First, the ‘‘geologic realistic’’ condition defined in Scenario_PC for the SCP consists of an 820 ft thick layer of weathered hard rock (V_S = 8,200 ft/s) over a half-space of unweathered hard rock (V_S = 11,480 ft/s). Second, ground motions are generated by matching (a) the seismic hazard with the uniform hazard spectrum (UHS) points, and (b) the seismic hazard at target spectral frequency (or periods) points. The latter matching is needed to account for contribution of the seismic hazard from multiple sources. The target spectral periods (T) used in the matching are 0.0, 0.2 and 1.0 s.

Presented in Figures 4.7-4.10 are sample ground motions for the Rock Hill West, Kirksey, and Irmo North East quadrangles for 2 % and 10 % probability of exceedance in 50 years. Kirksey and Irmo North East are quadrangles within the Greenwood and Columbia areas, respectively. The motions in Figure 4.7 were generated to match with the UHS points. The motions in Figures 4.8-4.10 were generated to match with the seismic hazard at 0.0, 0.2 and 1.0 s spectral periods.

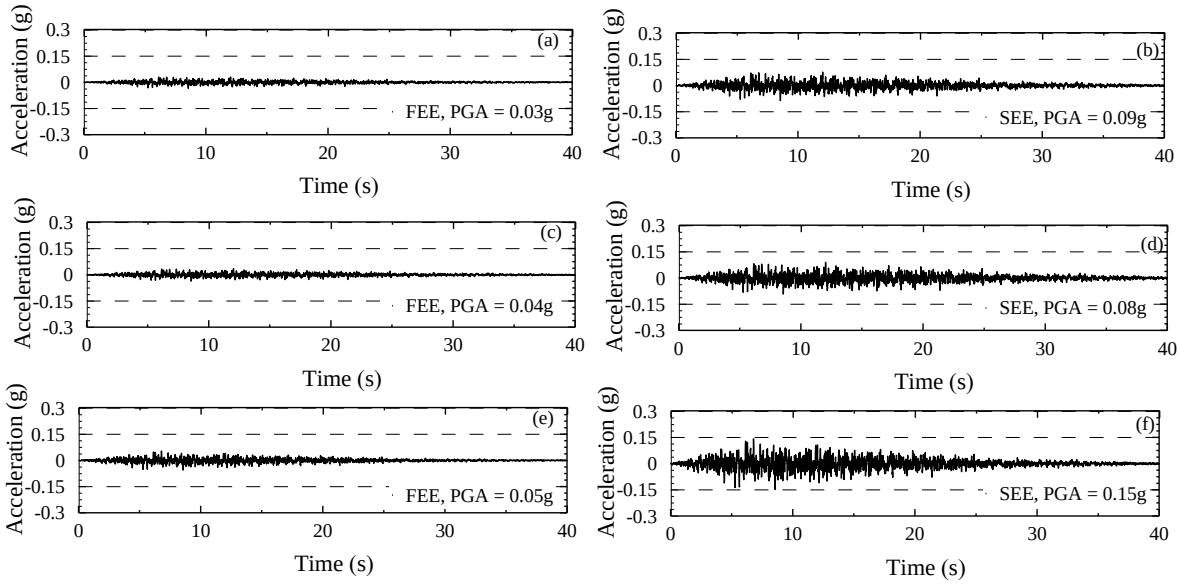

Figure 4.7 Sample synthetic weathered hard rock outcrop motions matching the UHS for 10% and 2% probability of exceedance in 50 years for (a-b) Rock Hill West, (c-d) Kirksey, and (e-f) Irmo North East quadrangles.

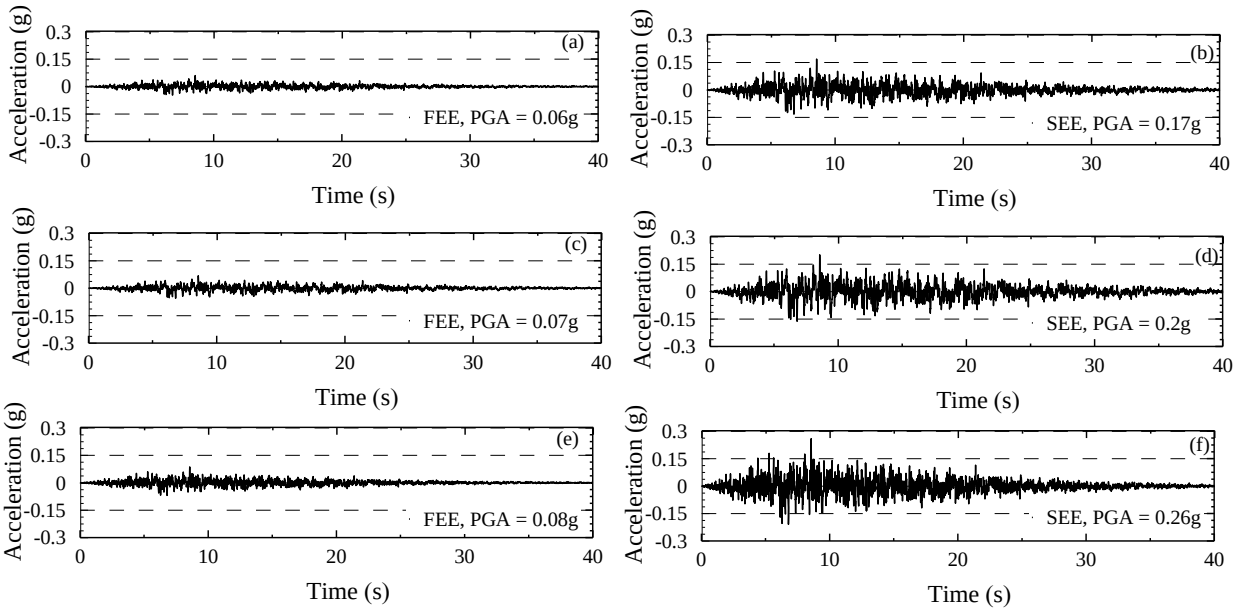

Figure 4.8 Sample synthetic weathered hard rock outcrop motions matching the seismic hazard at the *PGA* or 0.0 s for 10% and 2% probability of exceedance in 50 years for (a-b) Rock Hill West, (c-d) Kirksey, and (e-f) Irmo North East quadrangles.

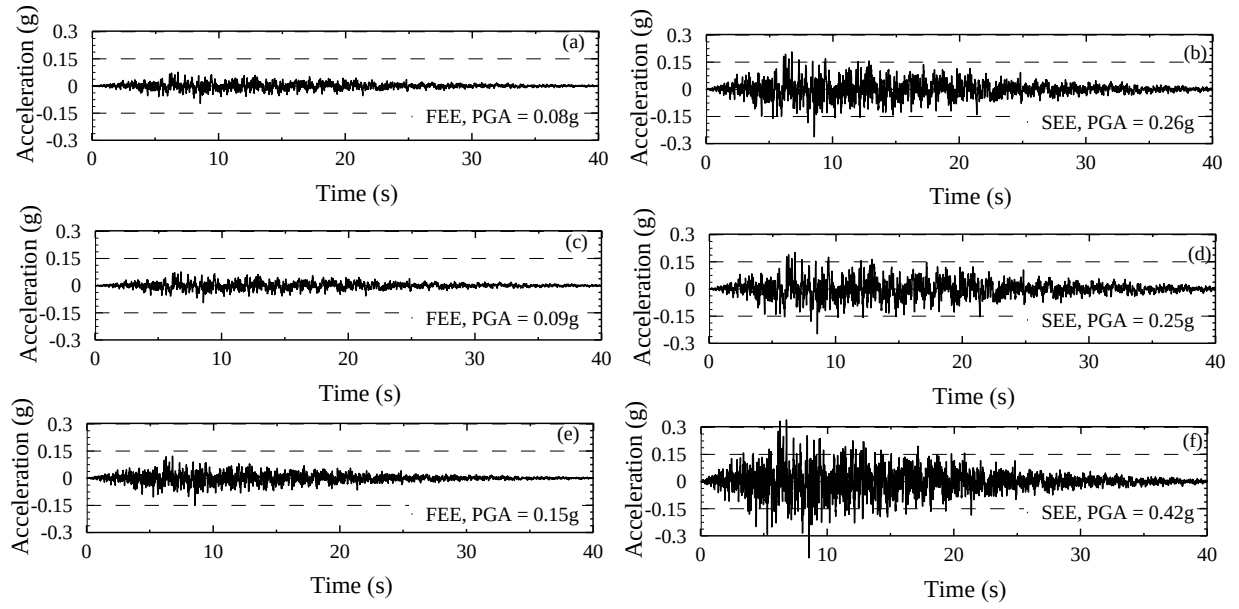

Figure 4.9 Sample synthetic weathered hard rock outcrop motions matching the seismic hazard at 0.2 s for 10% and 2% probability of exceedance in 50 years for (a-b) Rock Hill West, (c-d) Kirksey, and (e-f) Irmo North East quadrangles.

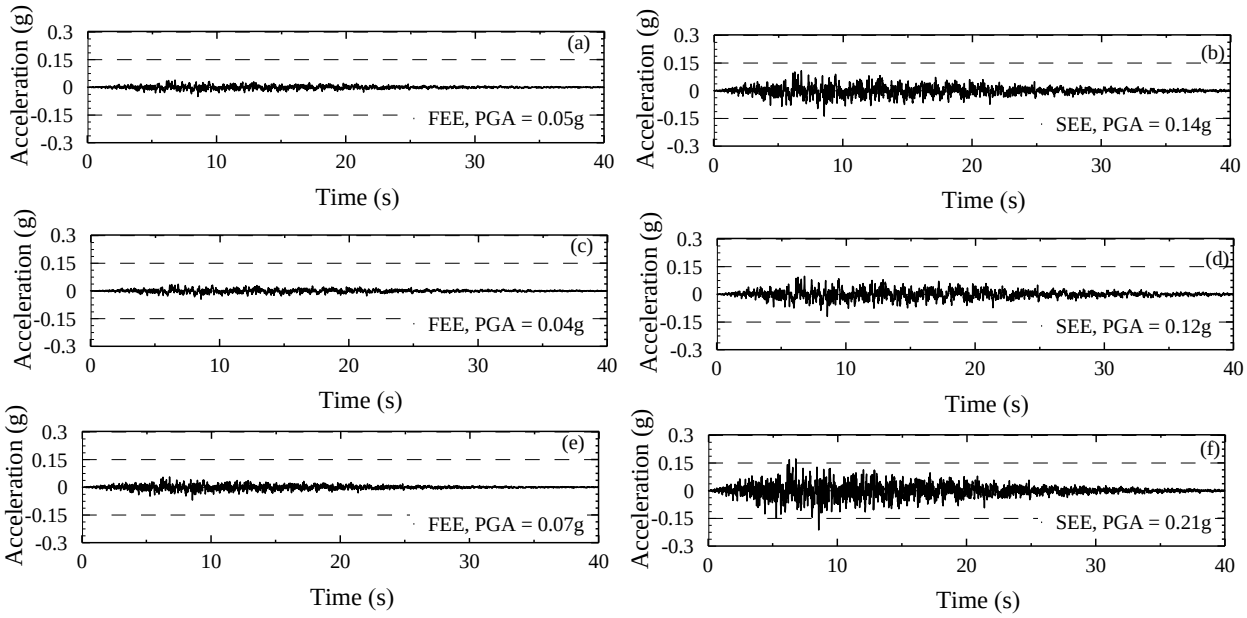

Figure 4.10 Sample synthetic weathered hard rock outcrop motions matching the seismic hazard at 1.0 s for 10% and 2% probability of exceedance in 50 years for (a-b) Rock Hill West, (c-d) Kirksey, and (e-f) Irmo North East quadrangles.

Compared to the UHS matched motions in Figures 4.7, the peak ground accelerations ($PGA_{outcrop}$) of the motions in Figures 4.8 and 4.9 are greater by as much as 220%. This is because the motions in Figures 4.8 and 4.9 are stronger, on average, at periods closer to the matching spectral periods (0.0 and 0.2 s, respectively). The difference in $PGA_{outcrop}$ values is small for the Columbia area and the 1.0 s spectral period matched motions (Figure 4.10).

A similar observation is made from weathered hard rock outcrop and computed spectral acceleration values obtained for the Kirksey (West Greenwood) quadrangle, as presented in Figures 4.11a and 4.11b. It can be seen from Figures 4.11a and 4.11b that spectral accelerations are higher when target frequency matched motions (especially at T = 0.0 s and 0.2 s) are used compared to UHS matched motions. In decreasing order, the spectral accelerations are higher when T = 0.2 s, T = 0.0 s, T = 1.0 s, and UHS matched motions are used. This observation indicates that for site-specific ground response analysis in the SCP, time-histories need to be generated at periods of structural significance (target frequencies).

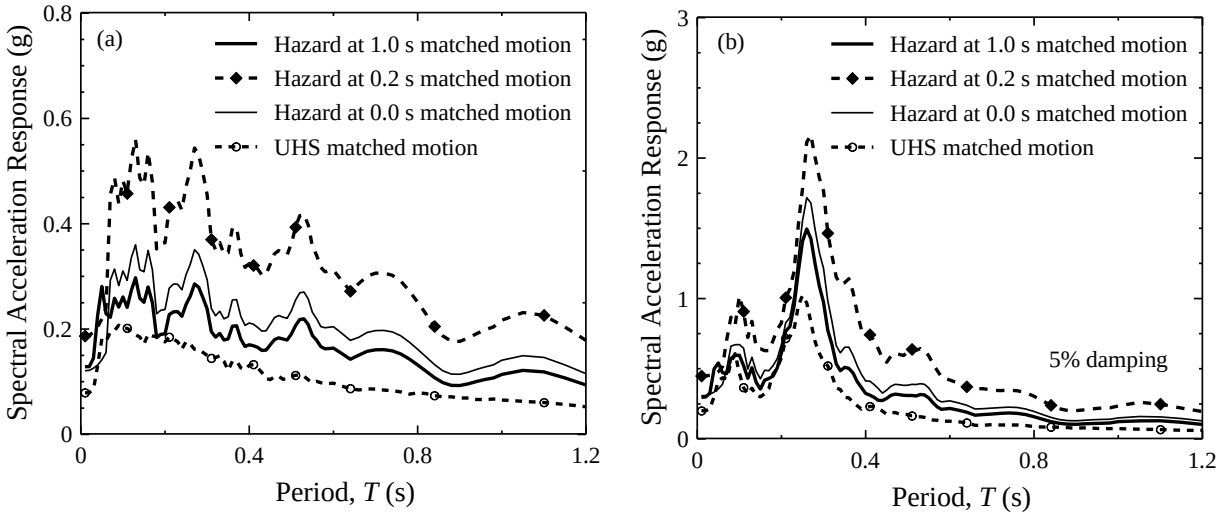

Figure 4.11 Sample (a) weathered hard rock outcrop and (b) site-specific spectral acceleration curves obtained by using motions generated to matched the UHS at 0.0, 0.2 and 1.0 s.

The effect of the different assumptions made in generating the input motions is further analyzed in Figure 4.12 by considering SEE and FEE motions. The analysis is based on the reference V_S profile in Figure 4.3b, and motions in Figures 4.7-4.10 for the Kirksey quadrangle. It can be seen from Figure 4.12a that the peak spectral acceleration predicted by the SEE and FEE motions occur at about the same spectral periods. As displayed in Figure 4.12b, the T = 0.0 s matched motion predicts higher accelerations at $T < 0.15$ s, and lower accelerations at $T \geq 0.15$ s for the SEE condition. Computed spectral acceleration using the T = 0.0 s matched FEE motion is higher than UHS matched FEE motion by as much as 90% at T = 0.2 s, as shown in Figure 4.12c. This is because the T = 0.0 s matched motion is rich in amplitudes closer to T = 0.0 s. Compared to the UHS matched motions, the T = 0.2 s matched motions predict significantly greater spectral acceleration as shown in Figures 4.12d and 4.12e. The difference can be as much as 160% and 110% at T = 0.2 s and 0.0 s, respectively. As shown in Figure 4.12f the predicted spectral acceleration is greater by as much as 50% for the T = 1.0 s matched motions compared to the UHS matched motions. These findings indicate that there is little (or no) difference between the period contents of the SEE and FEE motions generated by Scenario_PC for the west Greenwood area.

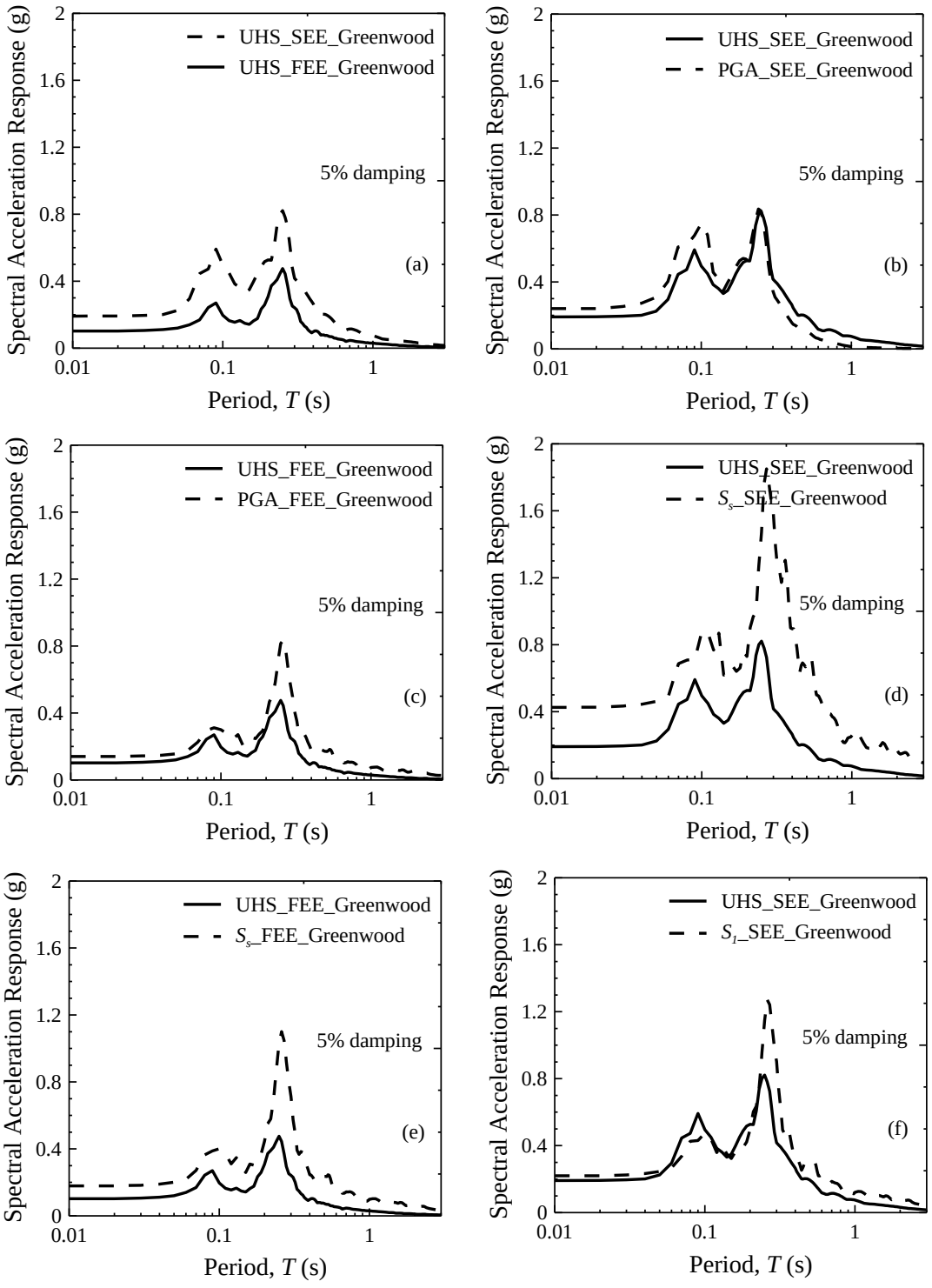

Figure 4.12 Sample plots showing sensitivity of spectral acceleration to the assumption made in input motion generation for the west Greenwood area.

Presented in Figures 4.13 is a plot of T_m of the input motions generated by Scenario_PC with respect to R. The anomaly of T_m at R = 9.3 miles corresponds to the Greenville area and western half of the Greenwood area for the SEE condition (open circles). Lower T_m values are expected for the SEE condition in the Greenville area and western half of the Greenwood area, because these areas are dominated by modal M_w of about 4.8. However, this is not the case in Figure 4.13, which indicates that the seismic hazard of the western half of the SCP is more complex than the SCCP.

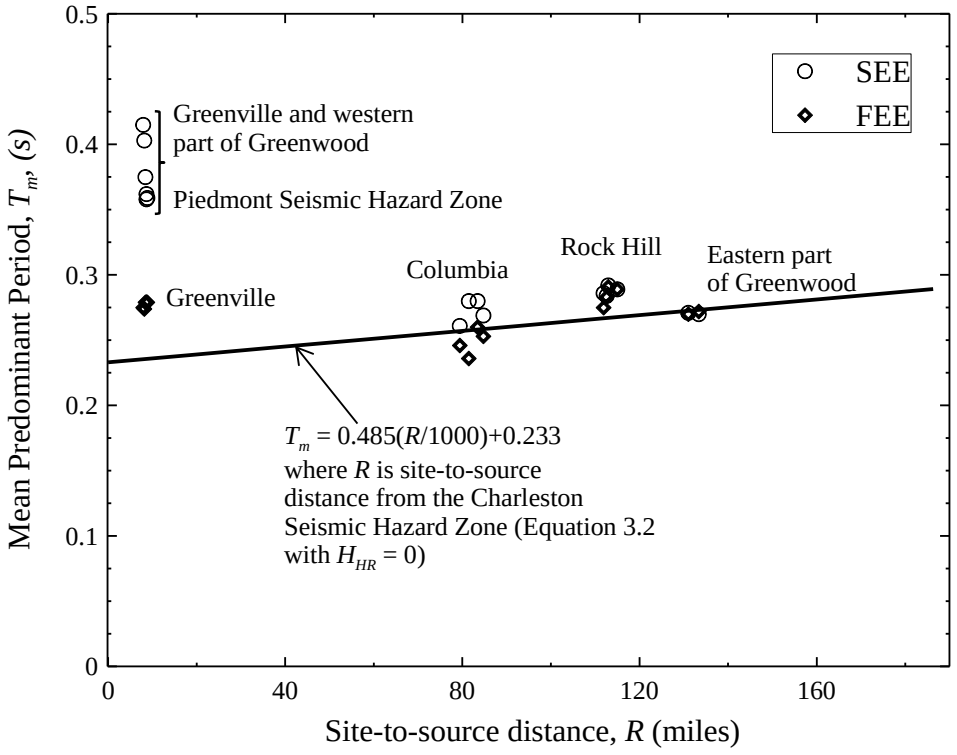

Figure 4.13 T_m of the input motions generated by Scenario_PC versus R.

4.5 Ground Response Analysis

One-dimensional, total stress ground response analyses are performed using the equivalent linear (SHAKE2000) and nonlinear (DMOD2000) ground response tools. The rationale behind the one-dimensional assumption is that the response of the soil is predominantly caused by horizontally polarized shear-waves propagating in nearly vertical path from the underlying bedrock. As discussed in Section 2.4, in SHAKE2000, the actual hysteretic stress-strain behavior is represented by the normalized shear modulus and the material damping ratio. An

iterative procedure is used until strain compatible properties are attained in all layers. In contrast, DMOD2000 uses direct numerical integration in the time domain and an assumed hysteretic stress-strain model to analyze the nonlinear response of soils. Stiffness-proportional Rayleigh coefficients are determined using the MKZ cyclic stress-strain model (Matasović and Ordóñez 2011).

Similar to Chapters 2 and 3, ground response analyses for the SCP are performed with SHAKE20000 when $PGA_{outcrop} \leq 0.3$ g and with DMOD2000 when $PGA_{outcrop} > 0.3$ g.

4.6 Results

Presented in Figures 4.14-4.19 are the site coefficients (i.e., F_{PGA}, F_a, $F_{0.6}$, F_v, $F_{1.6}$ and F_3, respectively) derived from ground response analyses plotted versus V_{S100ft} assuming the V_S profiles in Figure 4.3b with the top of weathered hard rock at 100 ft. Each data point plotted in Figures 4.14-4.19 is the average site coefficient obtained for either the SEE or FEE motions and for a given V_S profile. Also presented in Figures 4.14-4.19 are median, 95% upper bound and 5% lower bound relationships for the plotted data. Similar to the SCCP, the plotted V_{S100ft}-F data pairs in Figures 4.14-4.19 exhibit three general features—(1) an increasing trend in F as V_{S100ft} increases from zero; (2) a zone of peak F values; and (3) a decreasing trend in F as V_{S100ft} increases beyond the zone of peak F values.

The derivation of the seismic site coefficient model for the SCP is somewhat different from what was proposed for the SCCP in Chapter 3. The difference is due to the assumed reference rock outcrop site. The site coefficients derived in this chapter are meant to adjust weathered hard rock accelerations, instead of soft rock accelerations in the SCCP. Modifying the model developed for the SCCP, the peak site coefficient within a given plot (F_P) and the corresponding average shear wave velocity in the top 100 ft ($V_{S100ftP}$) can be estimated by:

$$F_P = \left[d_7 \exp\left(\frac{d_8 S_{outcrop}}{1g} \right) + 1 \right] K_{H3} \tag{4.1a}$$

$$V_{S100ftP} = \left[d_9 \left(\frac{S_{outcrop}}{1g} \right)^{d_{10}} \left(\frac{T_m}{1s} \right)^{d_{11}} \right] K_{H4} \tag{4.1b}$$

where d_7, d_8, d_9, d_{10}, and d_{11} are regression coefficients given in Table 4.1; $S_{outcrop}$ is in units of g; g is the acceleration of gravity; 1s is one second to normalize T_m; and K_{H3} and K_{H4} are dimensionless adjustment coefficients to account for the influence of depth to weathered hard rock. Unlike Equations 3.3a for the SCCP, the term of T_m/T_{330ft} has been omitted from Equation 4.1a because of the limited number of T_{330ft} values considered for the SCP. Presented in Table 4.2 are range and average values of T_m determined from hard rock outcrop motions generated by Scenario_PC for the four selected areas in the SCP. Presented in Table 4.3 are computed values of K_{H3} and K_{H4}.

Table 4.1 Regression coefficients for estimating site coefficients in the SCP.

$S_{outcrop}$	d_7	d_8	d_9 (ft/s)	d_{10}	d_{11}	a	$Z_{0.05}$	$Z_{0.95}$
$PGA_{outcrop}$	2.589	-3.772	1916	0.162	0.198	-	0.69	1.37
S_s	2.430	-0.934	1765	0.180	0.184	0.70	0.67	1.38
$S_{0.6}$	2.940	-2.653	1765	0.162	0.228	0.99	0.66	1.40
S_1	1.489	-0.896	1227	0.090	0.333	0.99	0.60	1.50
$S_{1.6}$	1.159	-1.423	1230	0.204	0.427	0.99	0.66	1.35
$S_{3.0}$	1.093	-4.480	695	0.208	-0.036	0.99	0.66	1.30

*For $T < 0.2$ s, use Equation 4.3a.

Table 4.2 Typical values of T_m for the SCP.

Site	T_m (s)	
	Range	Average
Columbia	0.25-0.28	0.27
Rock Hill	0.27-0.29	0.28
Greenwood	0.27-0.42	0.35
Greenville	0.28-0.38	0.33

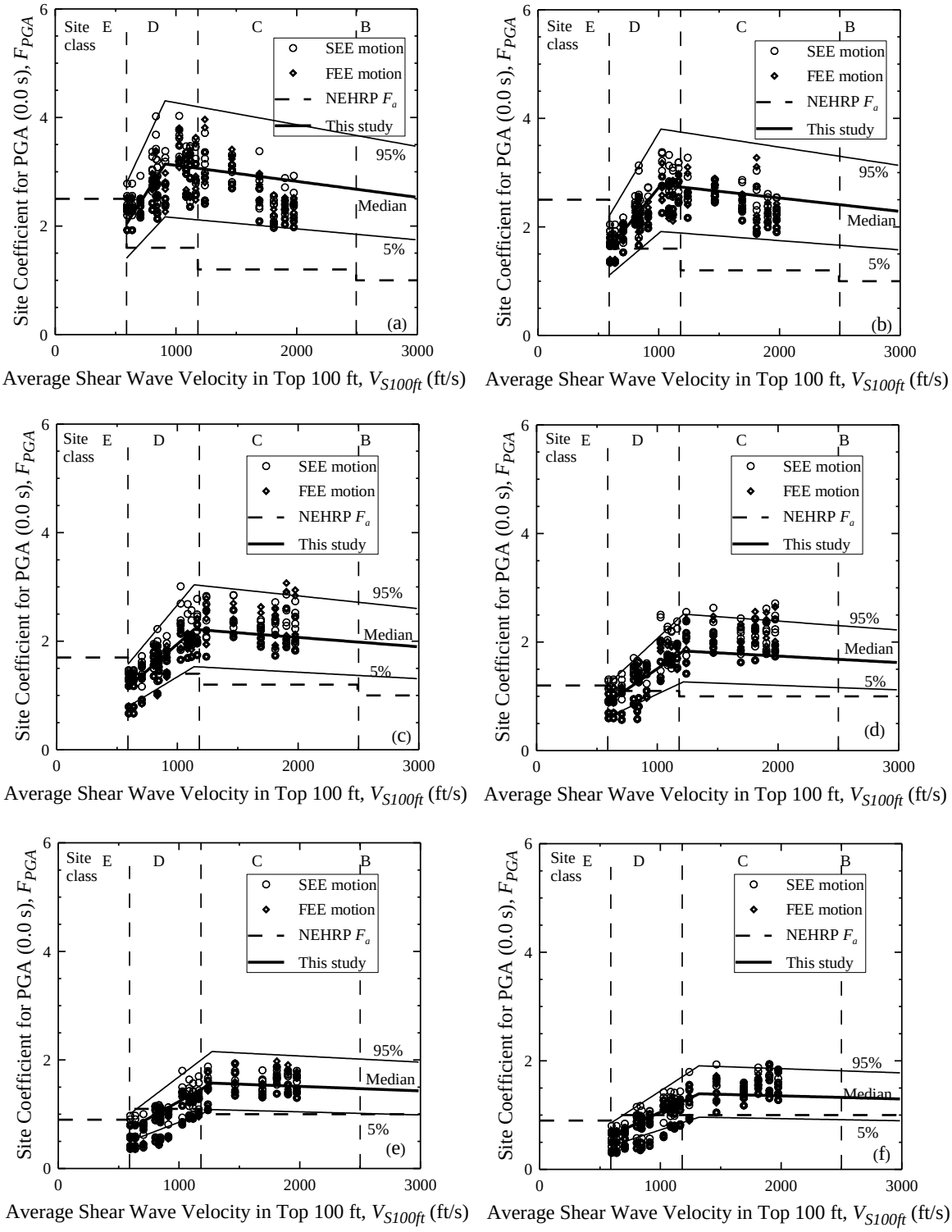

Figure 4.14 Site coefficient for 0.0 s spectral period (free-field) with $PGA_{outcrop}$ equal to (a) 0.05 g, (b) 0.1 g, (c) 0.2 g, (d) 0.3 g, (e) 0.4 g, and (f) 0.5 g for the SCP with top of V_S = 8,200 ft/s at depth of 100 ft.

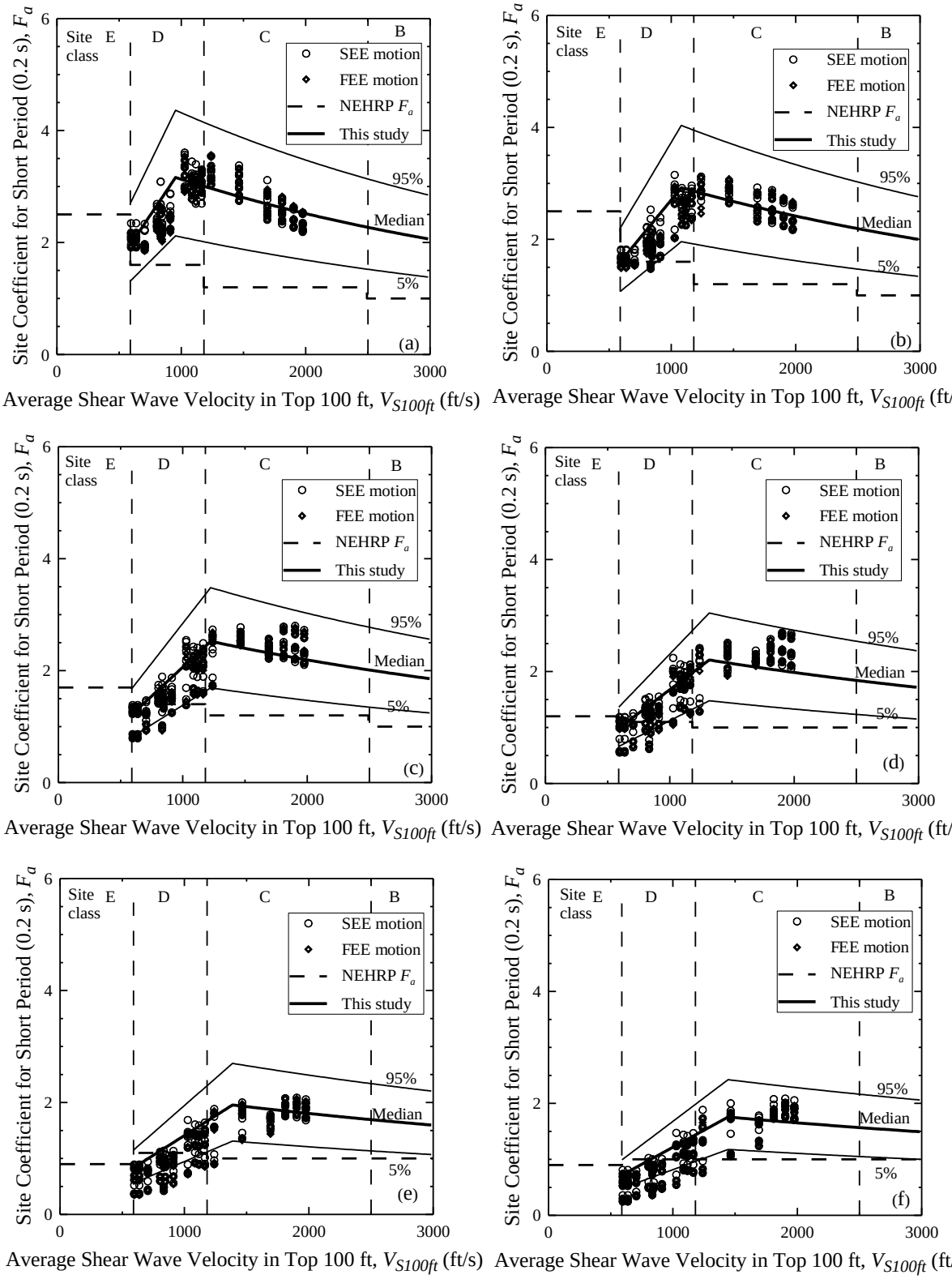

Figure 4.15 Site coefficient for 0.2 s (short) spectral period with S_S equal to (a) 0.125 g, (b) 0.25 g, (c) 0.5 g, (d) 0.75 g, (e) 1.0 g, and (f) 1.25 g for the SCP with top of V_S = 8,200 ft/s at depth of 100 ft.

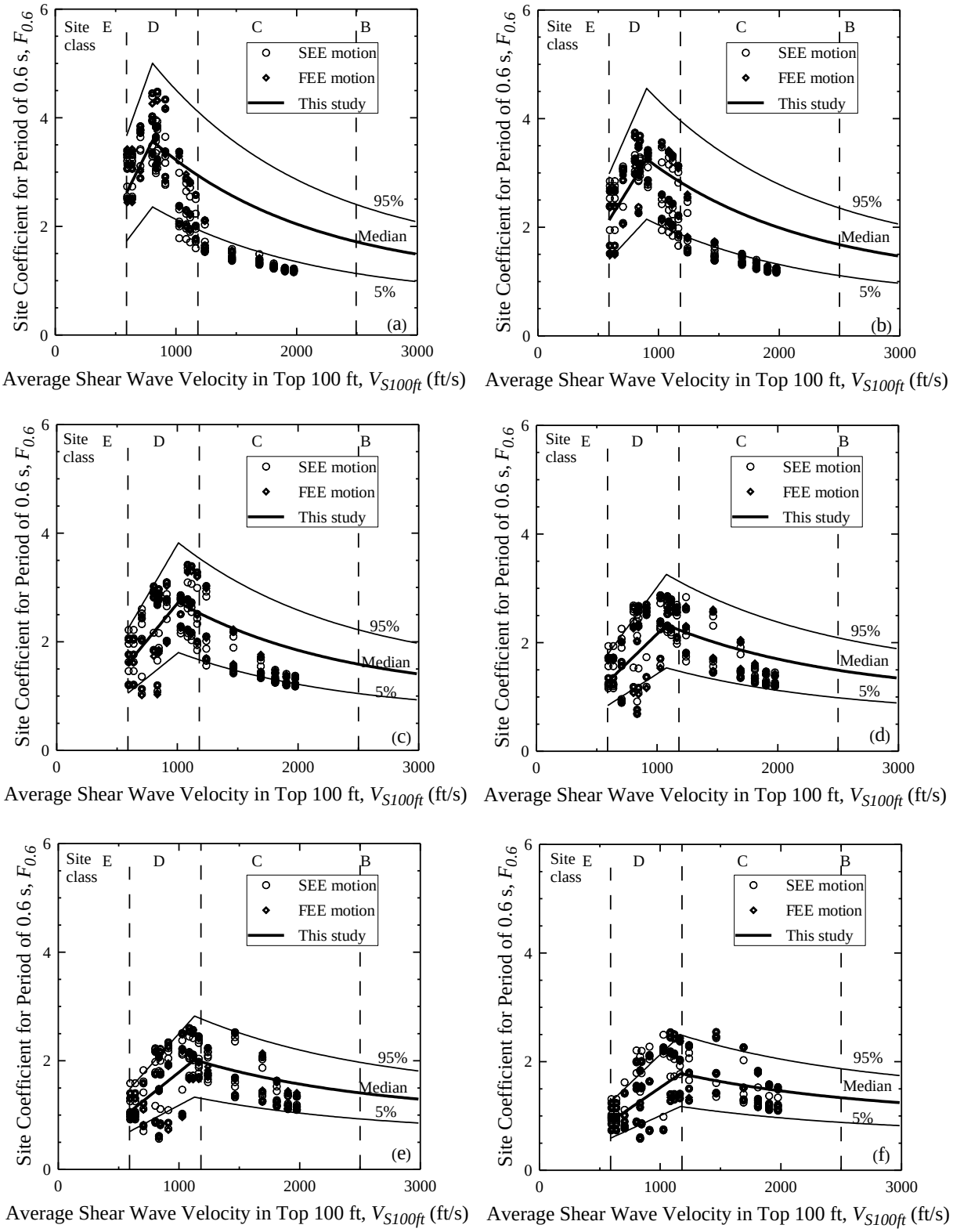

Figure 4.16 Site coefficient for 0.6 s spectral period with $S_{0.6}$ equal to (a) 0.05 g, (b) 0.1 g, (c) 0.2 g, (d) 0.3 g, (e) 0.4 g, and (f) 0.5 g for the SCP with top of V_S = 8,200 ft/s at depth of 100 ft.

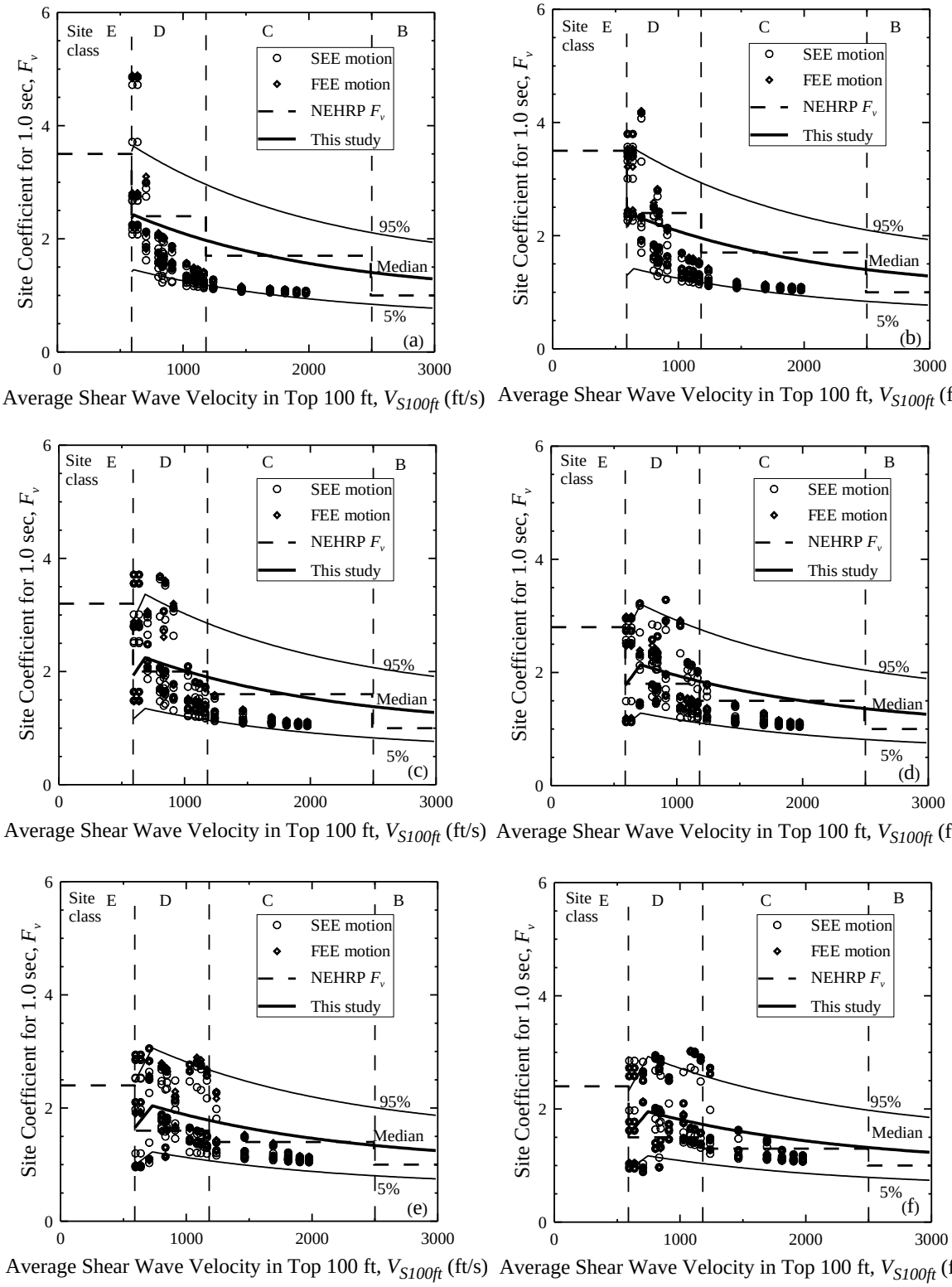

Figure 4.17 Site coefficient for 1.0 s (long) spectral period with S_1 equal to (a) 0.05 g, (b) 0.1 g, (c) 0.2 g, (d) 0.3 g, (e) 0.4 g, and (f) 0.5 g for the SCP with top of V_S = 8,200 ft/s at depth of 100 ft.

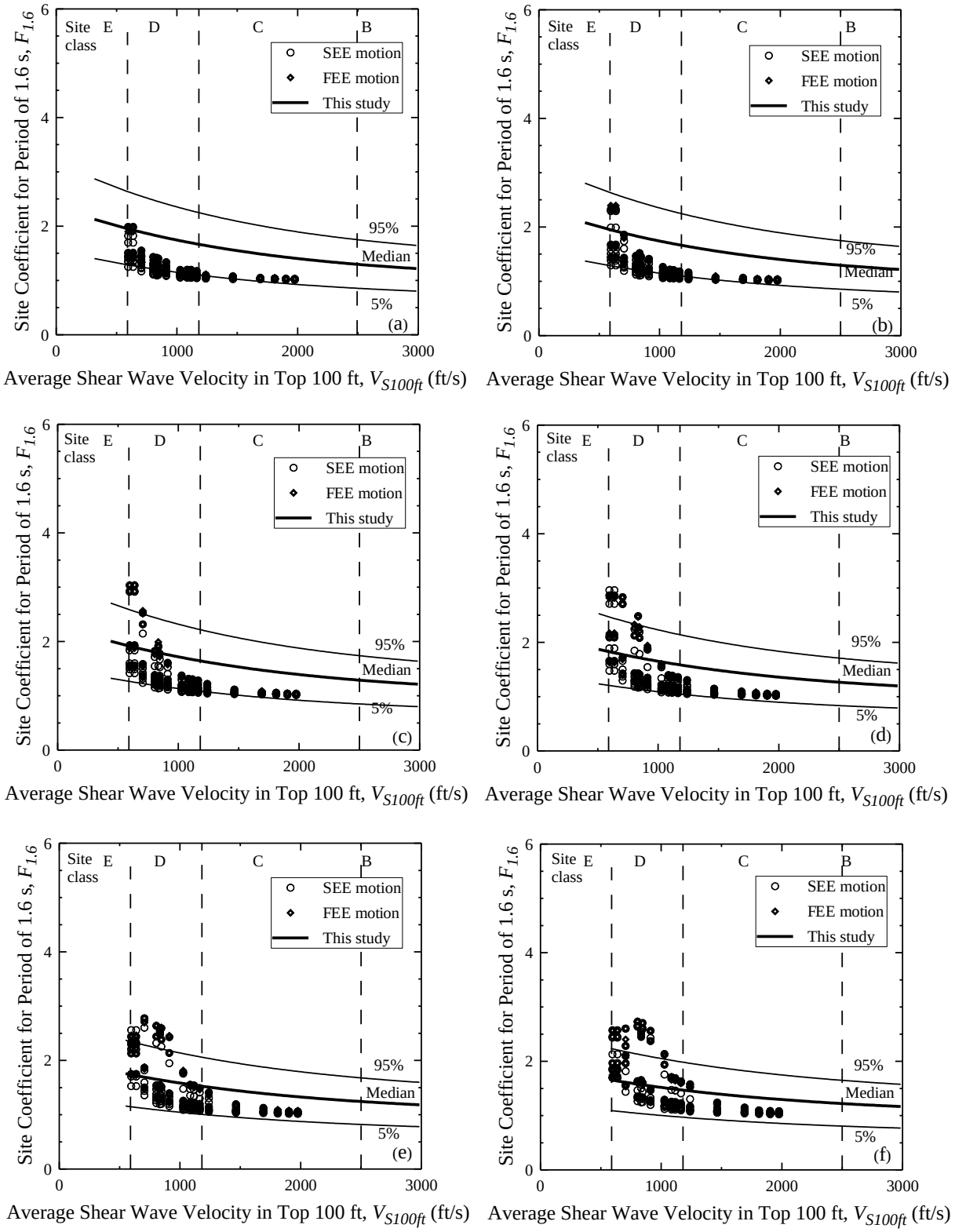

Figure 4.18 Site coefficient for 1.6 s spectral period with $S_{1.6}$ equal to (a) 0.02 g, (b) 0.05 g, (c) 0.1 g, (d) 0.15 g, (e) 0.2 g, and (f) 0.4 g for the SCP with top of V_S = 8,200 ft/s at depth of 100 ft.

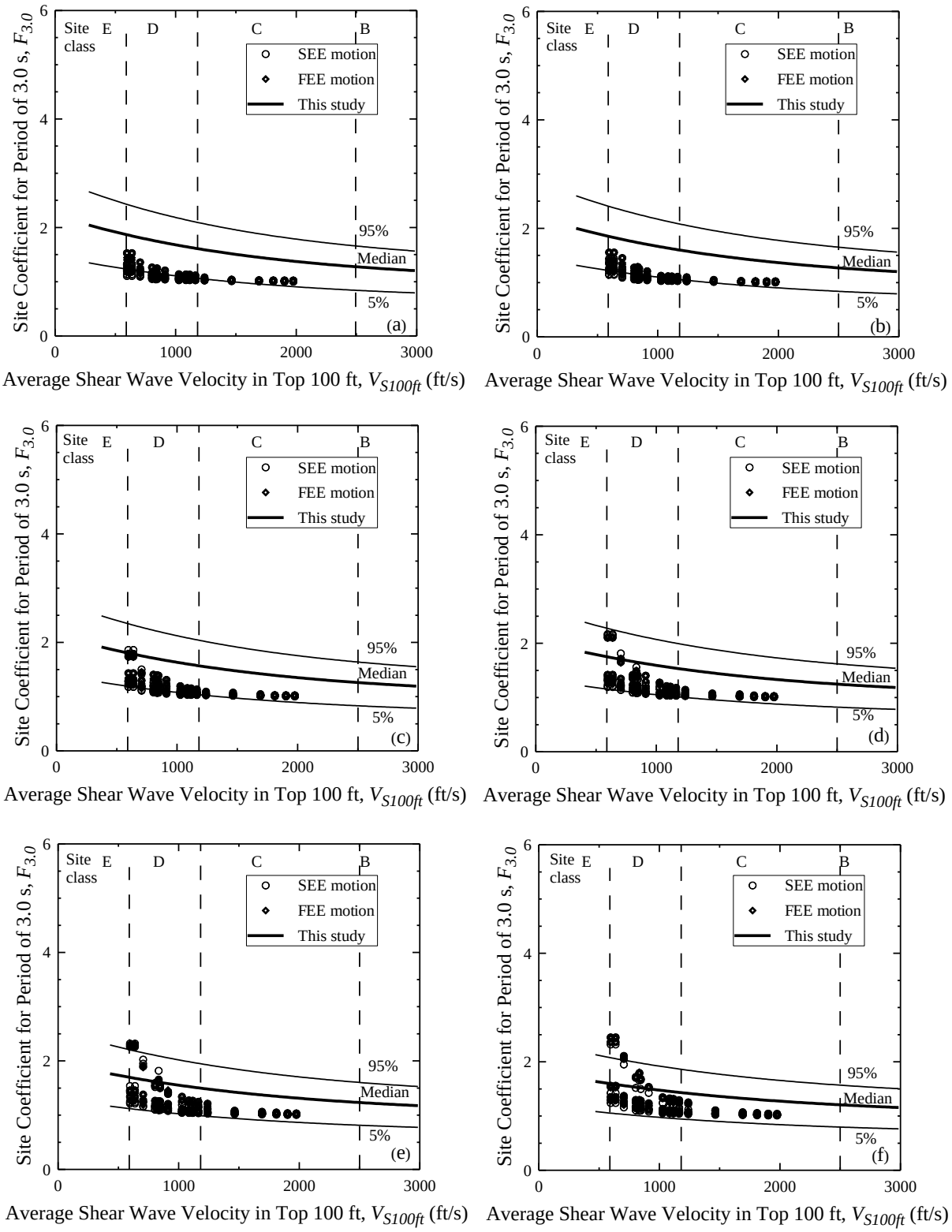

Figure 4.19 Site coefficient for 3.0 s spectral period with $S_{3.0}$ equal to (a) 0.01 g, (b) 0.02 g, (c) 0.04 g, (d) 0.06 g, (e) 0.08 g, and (f) 0.12 g for the SCP with top of V_S = 8,200 ft/s at depth of 100 ft.

Table 4.3 Depth-to-weathered hard rock adjustment coefficients.

$S_{outcrop}$	Adjustment coefficient	Depth to weathered hard rock, H_{HR} (ft)						
		16.5	33	66	100	131	165	330
$PGA_{outcrop}$	K_{H3}	0.35	0.37	1.00	1.00	0.96	0.89	0.78
	K_{H4}	7.83	7.33	1.67	1.00	0.97	0.93	0.77
Ss	K_{H3}	0.34	0.37	1.13	1.00	0.94	0.87	0.79
	K_{H4}	7.03	6.25	1.41	1.00	0.97	0.94	0.78
$S_{0.6}$	K_{H3}	0.30	0.32	0.62	1.00	1.04	1.05	1.18
	K_{H4}	9.69	9.39	2.86	1.00	0.97	0.94	0.79
S_1	K_{H3}	0.35	0.36	0.45	1.00	1.15	1.19	1.25
	K_{H4}	12.63	12.11	3.79	1.00	0.95	0.89	0.63
$S_{1.6}$	K_{H3}	0.59	0.61	0.77	1.00	1.03	1.03	1.10
	K_{H4}	12.00	11.00	3.60	1.00	0.95	0.90	0.65
S_3	K_{H3}	0.78	0.78	0.91	1.00	1.03	1.03	1.11
	K_{H4}	13.16	11.58	3.79	1.00	0.89	0.79	0.26

It should be noted that the median relationships shown in Figures 4.14-4.19 are based on regression of all computed F values for a given spectral period (e.g., Figures 4.14a-4.14f). For this reason, the median relationships provide fair to very good fits of the plotted data. Excellent fits can be obtained with Equations 4.1a and 4.1b for a given plot (e.g., Figure 4.14a). However, the desired objective is to develop relationships that are continuous with V_{S100ft} and $S_{outcrop}$.

Presented in Figure 4.20 is a sample residual plot of F_P versus the predicting variable in Equation 4.1a (i.e., $S_{outcrop}$) for short-period spectral acceleration and depth to weathered hard rock equal to 100 ft. The residual, ε, is defined here as F_P of the plotted data minus F_P obtained from Equation 4.1a. The computed mean of the plotted ε values is near zero, indicating the central tendency of the predicting Equation 4.1a. Thus, Equation 4.1a gives an overall unbiased prediction of F_P, because the ε data do not exhibit an increasing or decreasing with $S_{outcrop}$. On the other hand, the data points for a given site maintain the same relative position suggesting an influence of frequency (or period content) of the input motions.

Plotted in Figure 4.21 is a sample residual plot of $V_{S100ftP}$ versus the predicting variables in Equation 4.1b (i.e., $S_{outcrop}$ and T_m) for short-period spectral acceleration and depth to weathered hard rock equal to 100 ft. The residual, ε, is defined here as $V_{S100ftP}$ of the plotted data minus

$V_{S100ftP}$ obtained from Equation 4.1b. Similar to the plots in Figure 4.20, the mean values of ε plotted in Figure 4.21 are scattered about zero, and the ε data do not exhibit a systematic pattern with $S_{outcrop}$ and T_m.

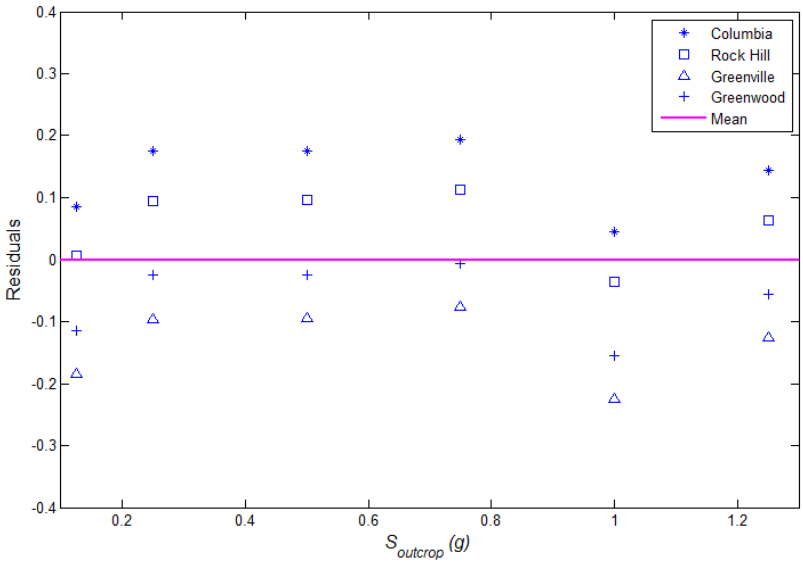

Figure 4.20 Residual plots of F_P versus $S_{outcrop}$.

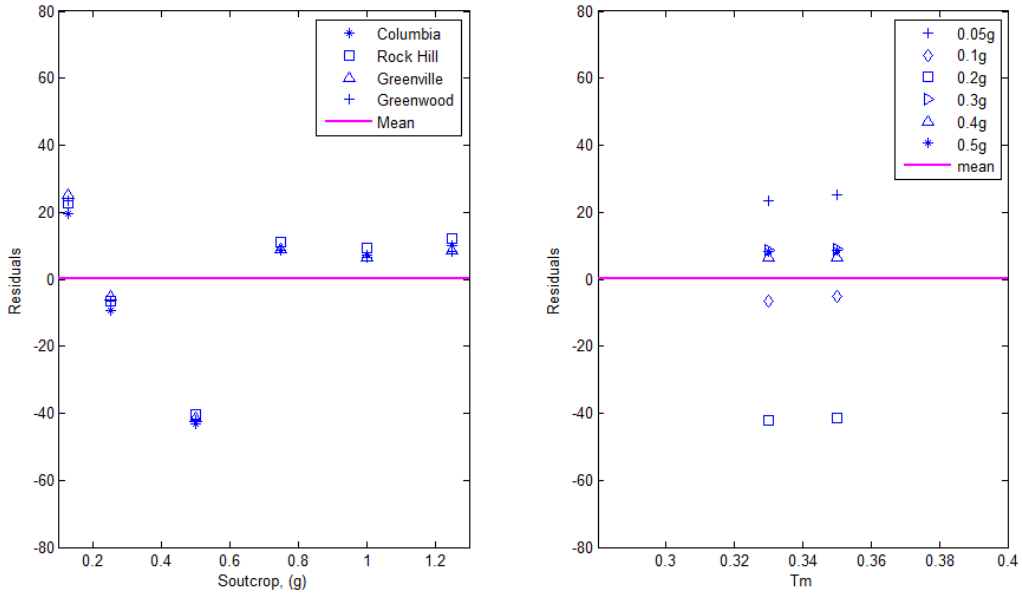

Figure 4.21 Residual plots of $V_{S100ftP}$ versus $S_{outcrop}$ and T_m.

Plotted in Figure 4.22 are computed values of F_{PGA} for $PGA_{outcrop}$ = 0.05 g and H_{HR} = 165, 100, 66 and 33 ft. It can be seen in Figure 4.22 that values of V_{S100ft} corresponding to the peak values of F_{PGA} increase with decreasing H_{HR}, and maximum amplification occurs where H_{HR} is around 100 ft. The T_m/T_{330ft} values for the four cases shown in Figures 4.22a-4.22d are 0.49, 1.18, 1.21 and 1.44, respectively.

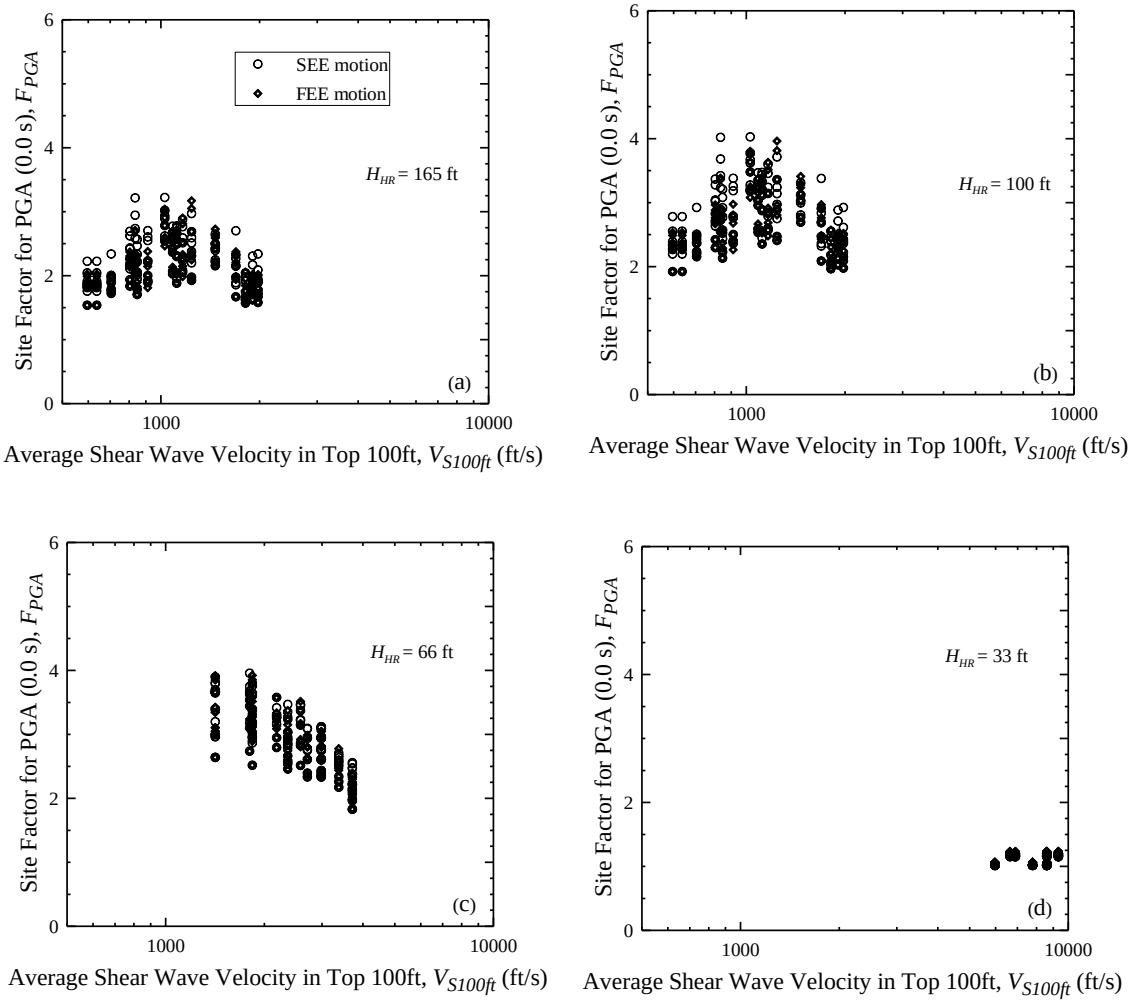

Figure 4.22 Computed F_{PGA} for $PGA_{outcrop}$ = 0.05 g and depth to weathered hard rock (H_{HR}) of (a) 165 ft, (b) 100 ft, and (c) 33 ft.

With the estimates of F_P and $V_{S100ftP}$ from Equation 4.1a and 4.1b, the median V_{S100ft}-F relationships of the plots shown in Figures 4.14-4.19 can be expressed as follows:

$$F = \left(\frac{F_P}{V_{S100ftP}} \right) V_{S100ft} \qquad \text{for } V_{S100ft} < V_{S100ftP} \text{ and all spectral periods } T \tag{4.2}$$

$$F = \frac{(F_P - 1)(8200 - V_{S100ft})}{8200 - V_{S100ftP}} + 1 \qquad \text{for } V_{S100ft} \geq V_{S100ftP} \text{ and } T < 0.2 \text{ s} \tag{4.3a}$$

$$F = a + b\, e^{cV_{S100ft}} \qquad \text{for } V_{S100ft} \geq V_{S100ftP} \text{ and } T \geq 0.2 \text{ s} \tag{4.3b}$$

where a is a regression coefficient given in Table 4.1; and b and c are coefficients calculated from:

$$b = \frac{1 - a}{e^{8200c}} \tag{4.4}$$

$$c = \left(\frac{1}{8200 - V_{S100ftP}} \right) \ln \left(\frac{1 - a}{F_P - a} \right) \tag{4.5}$$

Both Equations 4.2 and 4.3 provide the same value of F at $V_{S100ftP}$. Equation 4.2 is a linear relationship, which implicitly assumes F = 0 when V_{S100ft} = 0 ft/s. Equations 4.3a and 4.3b are linear and exponential relationships, respectively, and satisfy the assumed reference weathered hard rock outcrop condition of F = 1.0 when V_{S100ft} = 8,200 ft/s.

4.7 Discussion

Based on the computed site coefficients, peak computed median F_{PGA} values range from 1.5 to 3.3 in Figure 4.14. The peak computed median F_a and F_v values range from 1.5 to 3.25, and 1.8 and 2.6, respectively, in Figures 4.15 and 4.17. These peak values of F_{PGA}, F_a and F_v computed for the SCP are higher than values computed in Chapter 3 for the SCCP, because weathered hard rock is assumed as the reference site and because impedance contrast is higher in the SCP. Impedance contrast refers to the difference in stiffness and density between rock and the overlying soil. Impedance contrast (ζ) is defined as (Kramer 1996):

$$\zeta = \frac{\rho_2 V_{S2}}{\rho_1 V_{S1}} \tag{4.6}$$

where ρ_1 is soil layer density; V_{S1} is soil shear wave velocity; ρ_2 is density of rock; and V_{S2} is shear wave velocity of rock. Higher ζ between hard rock and overlying soil can cause higher amplification.

Three example comparisons between ADRS curves predicted by the site coefficient model derived in this chapter for the SCP and ADRS curves predicted by the model derived in Chapter 3 for the SCCP are presented in Figures 4.23-4.25. For the comparisons, the centers of Irmo and Columbia quadrangles are selected because of their proximity to the Fall Line. From the map by Chapman and Talwani (2002), H_{HR} at the center of Irmo and Columbia quadrangles are 164 ft and 420 ft, respectively. Two different input motions generated by Scenario_PC for the geologic realistic conditions in the SCCP and the SCP are used. The geologic realistic condition for the SCCP consists of a very thick outcropping soft rock layer over a weathered hard rock layer, which is underlain by un-weathered hard rock (V_S = 11,500 ft/s). The geologic realistic condition for the SCP consists of an 820 ft thick weathered hard rock layer over a hard rock half space.

Presented in Figures 4.23a and 4.23b are V_S profiles with $H_{B\text{-}C}$ = 420 ft for the SCCP and SCP, respectively. A soft rock half space is assumed for the SCCP; and a weathered hard rock half space is assumed for the SCP. The rock motions are applied at the top of the half space in each profile. The resulting site-specific and 3-point ADRS curves based on SEE and FEE motions are displayed in Figures 4.23c and 4.23d, respectively. It can be seen in Figures 4.23c and 4.23d that the SCCP- and 1994 NEHRP-based ADRS curves provide the better "average" predictions of the site-specific curves.

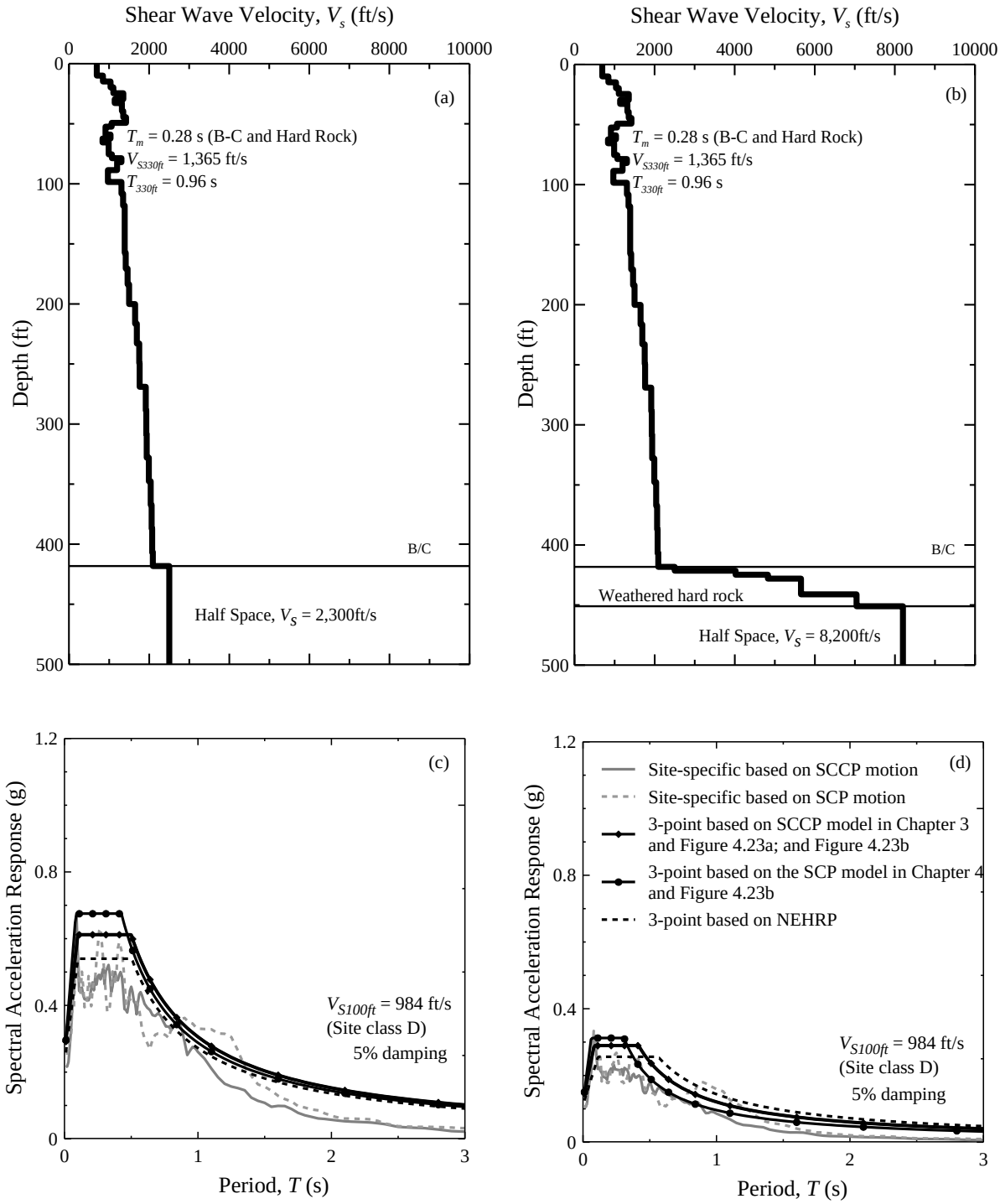

Figure 4.23 Assumed V_S profiles for the Columbia area representing the (a) SCCP and (b) SCP conditions with $H_{B\text{-}C}$ = 420 ft; and resulting site-specific and ADRS curves based on (c) SEE and (d) FEE motions.

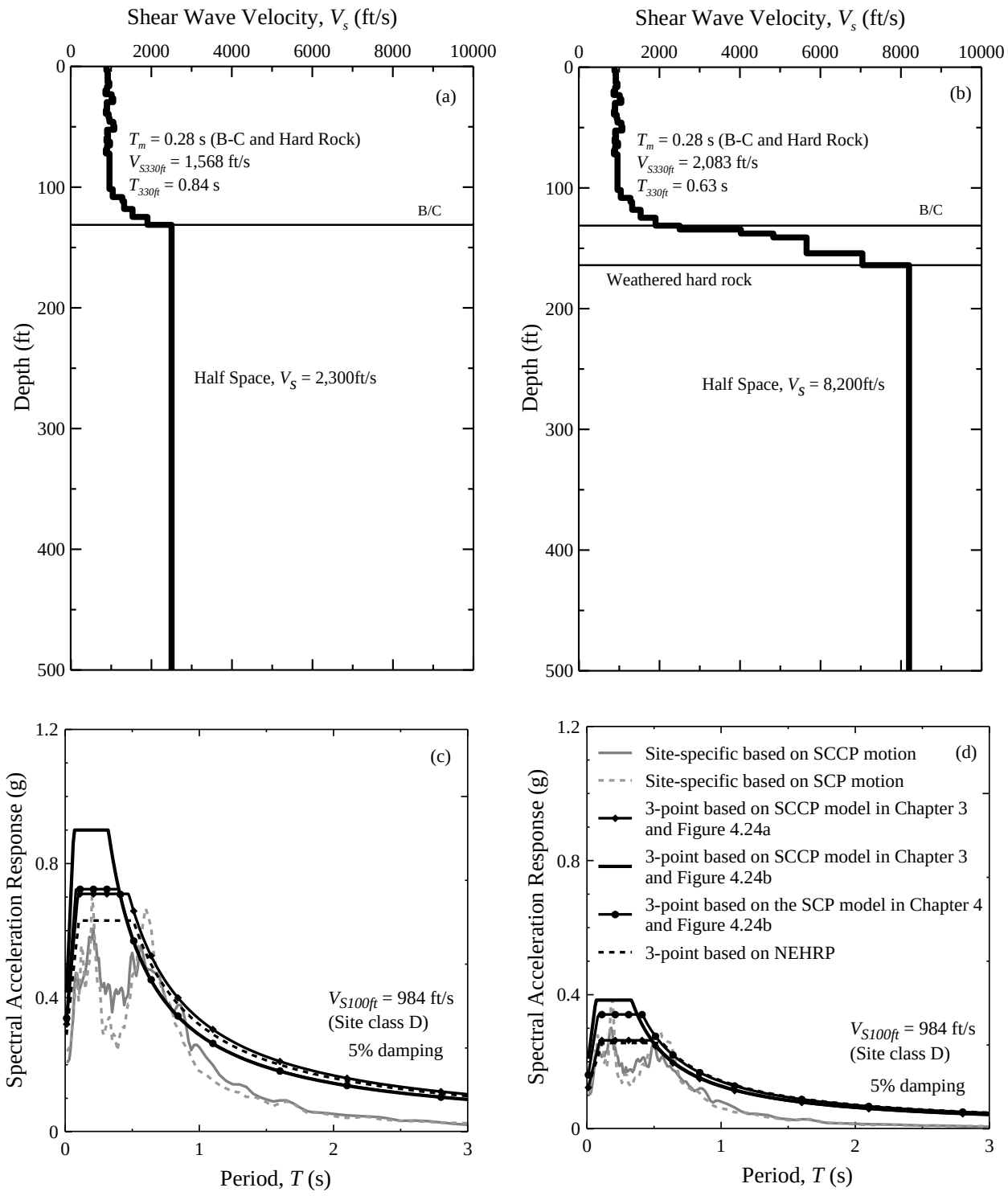

Figure 4.24 Assumed V_S profiles for the Columbia area representing the (a) SCCP and (b) SCP conditions with $H_{B\text{-}C}$ = 131 ft; and resulting site-specific and ADRS curves based on (c) SEE and (d) FEE motions.

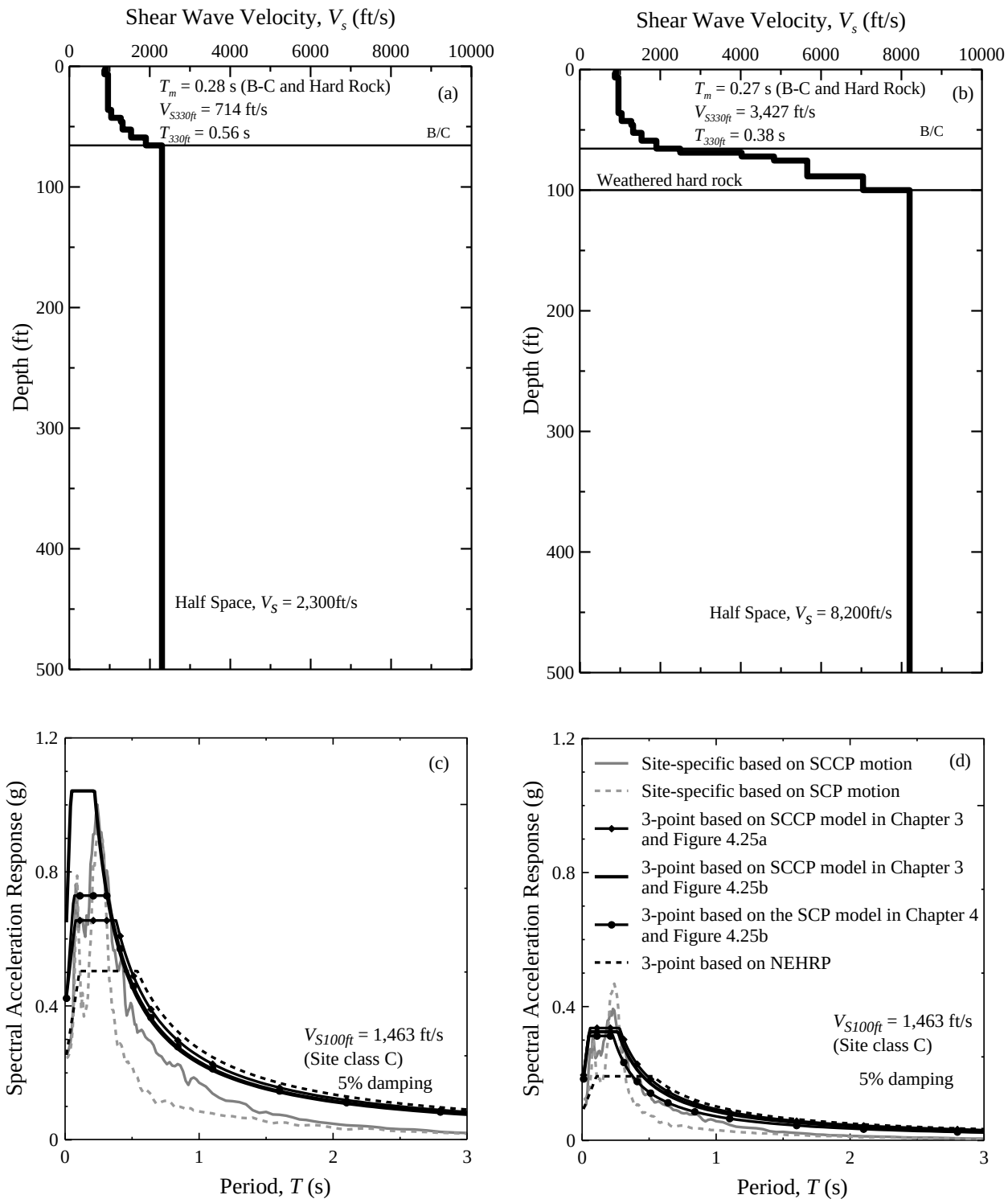

Figure 4.25 Assumed V_S profiles for the Columbia area representing the (a) SCCP and (b) SCP conditions with $H_{B\text{-}C}$ = 66 ft; and resulting site-specific and ADRS curves based on (c) SEE and (d) FEE motions.

Presented in Figures 4.24a and 4.24b are V_S profiles with $H_{B\text{-}C}$ = 131 ft for the SCCP and SCP, respectively. Similar to the previous example, a soft rock half space is assumed for the SCCP; and a weathered hard rock half space is assumed for the SCP. Rock motions are applied at the top of the half space in each profile. It can be seen in Figures 4.24c and 4.24d that the SCCP-, SCP- and NEHRP-based ADRS curves provide similar "average" predictions of the site-specific curves.

Presented in Figures 4.25a and 4.25b are V_S profiles with $H_{B\text{-}C}$ = 66 ft for the SCCP and SCP, respectively. Similar to the previous two examples, a soft rock half space is assumed for the SCCP; and a weathered hard rock half space is assumed for the SCP. The rock motions are applied at the top of the half space in each profile. It can be seen in Figures 4.25c and 4.25d that the SCP-based ADRS curves based on the appropriate V_S profiles provide the better "average" predictions of the site-specific curves at short periods.

Also shown in Figures 4.23-4.25 are ADRS curves based on the SCCP-based site coefficient model (developed in Chapter 3) applied to the V_S profile for the SCP. It can be seen in Figures 4.24c, 4.24d and 4.25c, that this approach provides overly conservative ADRS curves. Thus, the site coefficient model used should be appropriate for the given soil/rock condition.

Because the SCP model developed in this chapter provide somewhat better "average" ADRS curves in Figures 4.24 and 4.25, it is recommended that it be used in the SCP and in areas of the SCCP near the Fall line where $H_{HR} < 330$.

4.8 Limitations of the SCP Site Coefficient Model

The variations in small-strain stiffness of soil/rock conditions in the SCP are represented by the V_S profiles shown in Figure 4.3. These V_S profiles are derived from rather limited field measurements and assuming equal correlation between layers. Additional field V_S measurements from the SCP at all depths should be gathered to ensure that all variations are represented. Additional ground response analyses also should be conducted to investigate the influence of layer correlation (Toro 1995) on the site coefficient model.

The recommendations in this study are exclusively based on numerical simulations assuming laterally-constant horizontal layering. This assumption does not consider 3-dimensional heterogeneity (i.e., basin geometry and topographic effects). Because the SCP is an area of

rolling hills, the effect of basin geometry can be significant at weak and moderate excitations. Additional two- and three-dimensional ground response analyses should be conducted to quantify the effects of lateral heterogeneity and sloping ground. Actual ground motion recordings at rock and soils sites in the Piedmont are needed to validate the recommended model.

4.9 Summary

A seismic ground response study based on conditions in the SCP was presented in this chapter. Target-frequency matched motions were used in the ground response analyses, because they resulted in greater spectral acceleration compared to the UHS matched motions, especially at periods close to the matching frequencies. Based on the results of over 10,000 total stress, one-dimensional equivalent linear and nonlinear ground response analyses, a model for estimating seismic site coefficients in the SCP was developed. Model input variables included: V_{S100ft}, spectral acceleration (amplitude), mean predominant period of the input motion (T_m), and depth to weathered hard rock (H_{HR}). The model was expressed by a linear relationship for $V_{S100ft} < V_{S100ftP}$ and a linear or exponential relationship for $V_{S100ft} \geq V_{S100ftP}$.

The procedure for applying the site coefficient model for the SCP is summarized in the flow chart presented in Figure 4.26. Unlike the relationship for F_P developed for the SCCP, the relationship for F_P developed for the SCP does not include the term of T_m/T_{330ft} because of the limited number of T_{330ft} values considered. Additional analyses are needed to justify the inclusion of the term T_m/T_{330ft} in the F_P relationship for the SCP.

Comparisons between 3-point ADRS curves created by the site coefficient model developed in this chapter and the model developed in Chapter 3 for the SCCP were made based on possible conditions near the Fall Line, where hard rock is located at shallow depths. There is good general agreement between ADRS curves created with the SCCP and the SCP site factor models. Because there is some differences between ADRS curves, the SCP model is recommended for sites in the SCP and areas of the SCCP near the Fall Line where $H_{HR} < 330$ ft. The SCP site coefficient model should be used exclusively for adjusting outcropping weathered hard rock (V_S = 8,200 ft/s) spectral accelerations.

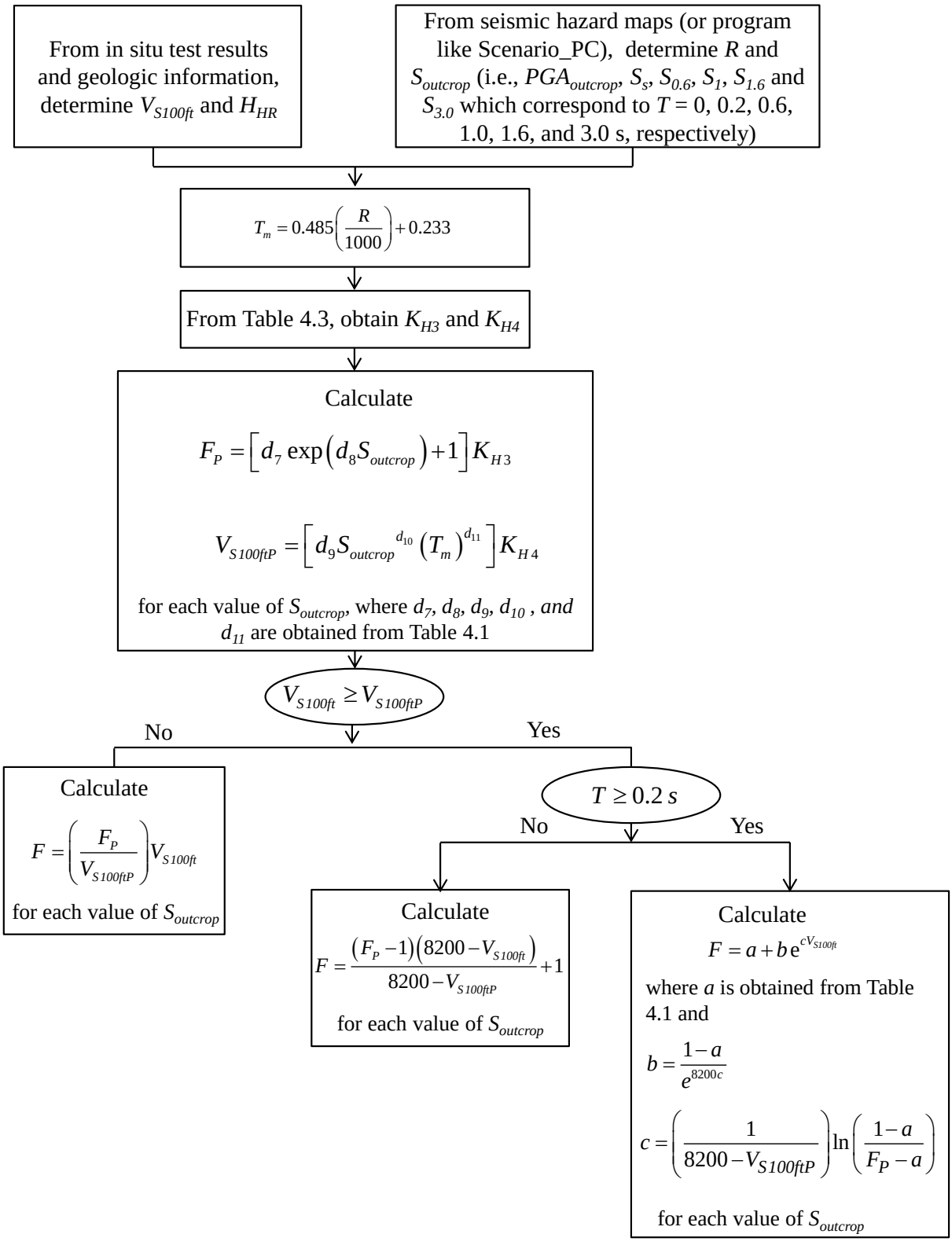

Figure 4.26 Flow chart of obtaining site coefficients for conditions in the SCP and areas in the SCCP near the Fall Line where H_{HR} < 330 ft.

CHAPTER FIVE

DISCUSSION OF THE 2008 SCDOT GEOTECHNICAL DESIGN MANUAL PROCEDURE FOR CONSTRUCTING ACCELERATION DESIGN RESPONSE SPECTRA

5.1 Introduction

Presented in this chapter is a discussion of the SCDOT Geotechnical Design Manual procedure for constructing acceleration design response spectra (SCDOT 2008a, Chapter 12). The discussion is mainly based on results presented in Chapters 3 and 4 of this report. Presented in Chapter 3 are results of ground response analyses assuming conditions in seven areas of the SCCP (i.e., Charleston, South Carolina side of Savannah, Myrtle Beach, Columbia, Florence, Lake Marion, and Aiken). Presented in Chapter 4 are results of ground response analyses assuming conditions in four areas in the SCP (i.e., Columbia, Greenwood, Rock Hill, and Greenville). Tabulated site coefficients recommended in SCDOT (2008a) and AASHTO (2011a) are compared with the maximum median site coefficients within a seismic site class derived for the SCCP and SCP.

5.2 Local Site Effect on PGA

In SCDOT (2008a), the local site peak horizontal ground surface acceleration (i.e., free-field or spectral period T = 0 s) is determined by adjusting the mapped rock peak horizontal ground surface acceleration using the following equation:

$$PGA = F_{PGA}PGA_{outcrop} \tag{5.1}$$

where PGA is the peak horizontal ground acceleration at the site ground surface adjusted for local conditions; $PGA_{outcrop}$ is the mapped rock peak horizontal ground acceleration obtained from the SC Seismic Hazard maps for the appropriate design earthquake (i.e., Functional Evaluation Earthquake, FEE, or Safety Evaluation Earthquake, SEE); and F_{PGA} is the site coefficient based on the site class and the mapped $PGA_{outcrop}$.

Presented in Table 5.1 are the F_{PGA} values recommended in SCDOT (2008a). The selection of these F_{PGA} values for design is based solely on NEHRP Site Class (i.e., A, B, C, D, E, and F) and $PGA_{outcrop}$ (or $PGA_{B\text{-}C}$ because the site coefficients are referenced to the B-C boundary condition with V_S = 2,500 ft/s).

Presented in Tables 5.2-5.5 are computed maximum median F_{PGA} values within a site class derived in Chapter 3 for four selected areas in the SCCP: (1) Charleston (2) Myrtle Beach, (3) Columbia, and (4) Aiken, respectively. The tabulated site coefficients for Site Class C, D and E in the SCCP are for six different depths to the B-C boundary ($H_{B\text{-}C}$ = 16, 33, 66, 100, 165, and ≥ 330 ft). Comparing Table 5.1 with Tables 5.2-5.5, it can be seen that the median F_{PGA} values derived in Chapter 3 are sometimes much greater than the values recommended in SCDOT (2008a).

Presented in Table 5.6 are computed maximum median F_{PGA} values within a site class derived in Chapter 4 for the SCP. The tabulated site coefficients for Site Class C, D and E in the SCP are for six different depths to weathered hard rock with V_S = 8,200 ft/s (i.e., H_{HR} = 16, 33, 50, 66, 100, and ≥ 165 ft). It is important to note that the coefficients in Table 5.6 should be only applied to $PGA_{outcrop}$ for the weathered hard rock condition (PGA_{HR}).

Table 5.1 F_{PGA} as a function of site class and mapped $PGA_{B\text{-}C}$ recommended in SCDOT (2008a).

Site Class	Peak Horizontal Ground Acceleration[(1)], $PGA_{B\text{-}C}$ (Period = 0.0 s)				
	≤ 0.10 g	0.20 g	0.30 g	0.40 g	≥ 0.50 g
A	0.8	0.8	0.8	0.8	0.8
B	1.0	1.0	1.0	1.0	1.0
C	1.2	1.2	1.1	1.0	1.0
D	1.6	1.4	1.2	1.1	1.0
E	2.5	1.7	1.2	0.9	0.9
F[(2)]	N/A	N/A	N/A	N/A	N/A

[(1)]Use linear interpolation for intermediate values of $PGA_{B\text{-}C}$.
[(2)]Site-specific response analysis shall be performed.

Table 5.2 Maximum median F_{PGA} as a function of site class and $PGA_{B\text{-}C}$ derived in Chapter 3 for Charleston.

Site Class	$H_{B\text{-}C}$, ft	Peak Ground Acceleration[1] $PGA_{B\text{-}C}$ (Period = 0.0 s)					
		≤ 0.05 g	0.1 g	0.2 g	0.3 g	0.4 g	≥ 0.5 g
A[2]	-	-	-	-	-	-	-
B	0	1.0	1.0	1.0	1.0	1.0	1.0
C	16	3.2	2.9	2.4	2.1	1.9	1.8
	33	2.7	2.6	2.2	1.9	1.7	1.6
	66	2.2	2.1	1.8	1.7	1.5	1.4
	100	2.0	1.9	1.7	1.5	1.4	1.3
	165	1.8	1.7	1.5	1.3	1.2	1.2
	≥330	1.8	1.7	1.4	1.3	1.2	1.1
D	16	3.1	2.4	1.7	1.3	1.1	1.0
	33	2.9	2.6	1.9	1.5	1.3	1.1
	66	2.6	2.3	2.0	1.7	1.5	1.4
	100	2.4	2.2	1.8	1.6	1.4	1.3
	165	2.1	1.9	1.6	1.4	1.3	1.2
	≥330	2.1	1.9	1.6	1.4	1.2	1.2
E	16	1.5	1.2	0.8	0.7	0.6	0.5
	33	1.7	1.3	1.0	0.8	0.6	0.6
	66	2.1	1.6	1.1	0.9	0.8	0.7
	100	2.1	1.6	1.1	0.9	0.8	0.7
	165	2.0	1.6	1.1	0.9	0.8	0.7
	≥330	2.1	1.6	1.1	0.9	0.8	0.7
F[3]	N/A	N/A	N/A	N/A	N/A	N/A	N/A

[1]Use linear interpolation for intermediate values of $PGA_{B\text{-}C}$.
[2]Site Class A not present in the Charleston area. No response analysis performed.
[3]Site-specific response analysis shall be performed.

Table 5.3 Maximum median F_{PGA} as a function of site class and $PGA_{B\text{-}C}$ derived in Chapter 3 for Myrtle Beach.

Site Class	$H_{B\text{-}C}$, ft	Peak Ground Acceleration[1] $PGA_{B\text{-}C}$ (Period = 0.0 s)					
		≤ 0.05 g	0.1 g	0.2 g	0.3 g	0.4 g	≥ 0.5 g
A[2]	-	-	-	-	-	-	-
B	0	1.0	1.0	1.0	1.0	1.0	1.0
C	16	4.0	3.5	2.8	2.3	2.1	1.9
	33	3.3	3.1	2.6	2.1	1.9	1.7
	66	2.7	2.5	2.1	1.8	1.7	1.5
	100	2.4	2.3	1.9	1.7	1.5	1.4
	165	2.2	2.0	1.7	1.5	1.3	1.2
	≥330	2.1	1.9	1.6	1.4	1.3	1.2
D	16	3.9	2.9	2.0	1.5	1.3	1.1
	33	3.6	3.2	2.3	1.8	1.5	1.3
	66	3.2	2.8	2.3	1.9	1.7	1.5
	100	3.0	2.6	2.1	1.8	1.5	1.4
	165	2.7	2.3	1.9	1.6	1.4	1.2
	≥330	2.6	2.3	1.8	1.5	1.3	1.2
E	16	2.0	1.5	1.0	0.8	0.6	0.6
	33	2.2	1.7	1.2	0.9	0.7	0.6
	66	2.6	2.0	1.4	1.0	0.9	0.7
	100	2.6	2.0	1.4	1.0	0.9	0.7
	165	2.6	2.0	1.3	1.0	0.8	0.7
	≥330	2.6	2.0	1.4	1.1	0.9	0.7
F[3]	N/A	N/A	N/A	N/A	N/A	N/A	N/A

[1]Use linear interpolation for intermediate values of $PGA_{B\text{-}C}$.
[2]Site Class A not present in the Myrtle Beach area. No response analysis performed.
[3]Site-specific response analysis shall be performed.

Table 5.4 Maximum median F_{PGA} as a function of site class and $PGA_{B\text{-}C}$ derived in Chapter 3 for Columbia in the SCCP.

Site Class	$H_{B\text{-}C}$, ft	Peak Ground Acceleration[1] $PGA_{B\text{-}C}$ (Period = 0.0 s)					
		≤ 0.05 g	0.1 g	0.2 g	0.3 g	0.4 g	≥ 0.5 g
A[2]	-	-	-	-	-	-	-
B	0	1.0	1.0	1.0	1.0	1.0	1.0
C	16	3.0	2.7	2.3	2.0	1.8	1.7
	33	2.6	2.5	2.1	1.8	1.7	1.6
	66	2.1	2.0	1.8	1.6	1.5	1.4
	100	1.9	1.8	1.6	1.5	1.4	1.3
	165	1.7	1.6	1.4	1.3	1.2	1.1
	≥330	1.7	1.6	1.4	1.3	1.2	1.1
D	16	2.8	2.2	1.6	1.3	1.1	1.0
	33	2.7	2.5	1.8	1.4	1.2	1.1
	66	2.4	2.2	1.8	1.6	1.5	1.3
	100	2.2	2.0	1.7	1.5	1.4	1.3
	165	2.0	1.8	1.5	1.3	1.2	1.2
	≥330	2.0	1.8	1.5	1.3	1.2	1.1
E	16	1.4	1.1	0.8	0.6	0.5	0.5
	33	1.6	1.2	0.9	0.7	0.6	0.5
	66	1.9	1.5	1.1	0.8	0.7	0.6
	100	1.9	1.4	1.0	0.8	0.7	0.6
	165	1.9	1.4	1.0	0.8	0.7	0.6
	≥330	1.9	1.5	1.1	0.9	0.7	0.7
F[3]	N/A	N/A	N/A	N/A	N/A	N/A	N/A

[1]Use linear interpolation for intermediate values of $PGA_{B\text{-}C}$.
[2]Site Class A not present in the Columbia area of the SCCP. No response analysis performed.
[3]Site-specific response analysis shall be performed.

Table 5.5 Maximum median F_{PGA} as a function of site class and $PGA_{B\text{-}C}$ derived in Chapter 3 for Aiken.

Site Class	$H_{B\text{-}C}$, ft	Peak Ground Acceleration[1] $PGA_{B\text{-}C}$ (Period = 0.0 s)					
		≤ 0.05 g	0.1 g	0.2 g	0.3 g	0.4 g	≥ 0.5 g
A[2]	-	-	-	-	-	-	-
B	0	1.0	1.0	1.0	1.0	1.0	1.0
C	16	2.9	2.6	2.2	2.0	1.8	1.7
	33	2.5	2.4	2.1	1.8	1.7	1.6
	66	2.0	1.9	1.7	1.6	1.5	1.4
	100	1.9	1.8	1.6	1.5	1.4	1.3
	165	1.7	1.6	1.4	1.3	1.2	1.1
	≥330	1.6	1.5	1.4	1.2	1.2	1.1
D	16	2.8	2.1	1.6	1.3	1.1	1.0
	33	2.7	2.4	1.8	1.4	1.2	1.1
	66	2.4	2.1	1.8	1.6	1.5	1.3
	100	2.2	2.0	1.7	1.5	1.4	1.3
	165	1.9	1.8	1.5	1.3	1.2	1.1
	≥330	1.9	1.7	1.5	1.3	1.2	1.1
E	16	1.4	1.1	0.8	0.6	0.5	0.5
	33	1.6	1.2	0.9	0.7	0.6	0.6
	66	1.9	1.4	1.1	0.9	0.7	0.7
	100	1.8	1.4	1.0	0.8	0.7	0.7
	165	1.8	1.4	1.0	0.8	0.7	0.7
	≥330	1.9	1.5	1.1	0.9	0.7	0.7
F[3]	N/A	N/A	N/A	N/A	N/A	N/A	N/A

[1]Use linear interpolation for intermediate values of $PGA_{B\text{-}C}$.
[2]Site Class A not present in the Aiken area. No response analysis performed.
[3]Site-specific response analysis shall be performed.

Table 5.6 Maximum median F_{PGA} as a function of site class and PGA_{HR} derived in Chapter 4 for Columbia in the SCP.

Site Class	H_{HR}, ft	Peak Ground Acceleration[(1)] PGA_{HR} (Period = 0.0 s)					
		≤ 0.05 g	0.10 g	0.20 g	0.30 g	0.40 g	≥ 0.50 g
A	0	1.0	1.0	1.0	1.0	1.0	1.0
B	16	1.0	1.0	0.8	0.8	0.7	0.6
	33	1.1	1.0	0.9	0.8	0.7	0.7
	66	2.6	2.3	1.9	1.6	1.4	1.3
	100	2.5	2.3	1.9	1.6	1.4	1.3
	165	2.3	2.0	1.7	1.4	1.3	1.2
	330	2.0	1.8	1.5	1.3	1.2	1.1
C	16	1.0	1.0	1.0	1.0	1.0	1.0
	33	1.1	1.0	1.0	1.0	1.0	1.0
	66	2.9	2.6	2.1	1.8	1.5	1.4
	100	2.9	2.6	2.1	1.7	1.5	1.4
	165	2.6	2.3	1.8	1.5	1.3	1.2
	330	2.3	2.0	1.6	1.4	1.2	1.1
D	16	0.6	0.4	0.3	0.2	0.2	0.2
	33	0.6	0.5	0.4	0.3	0.2	0.2
	66	3.1	2.8	2.2	1.8	1.6	1.4
	100	3.1	2.7	2.2	1.8	1.6	1.4
	165	2.7	2.4	1.9	1.6	1.4	1.2
	330	2.4	2.1	1.7	1.4	1.2	1.1
E	16	-	-	-	-	-	-
	33	-	-	-	-	-	-
	66	3.1	2.8	2.2	1.7	1.4	1.2
	100	3.1	2.8	2.2	1.8	1.6	1.4
	165	2.8	2.4	2.0	1.6	1.4	1.2
	330	2.5	2.2	1.7	1.4	1.2	1.1
F[(2)]	N/A	N/A	N/A	N/A	N/A	N/A	N/A

[(1)]Use linear interpolation for intermediate values of $PGA_{B\text{-}C}$.
[(2)]Site-specific response analysis shall be performed.

5.3 Local Site Effects on Short- and Long-Period Spectral Accelerations

The local site short-period (T = 0.2 s) and long-period (T = 1.0 s) horizontal spectral response accelerations are determined by adjusting mapped rock spectral values using the following equations:

$$S_{DS} = F_a S_S \tag{5.2}$$

$$S_{D1} = F_v S_1 \tag{5.3}$$

where S_{DS} is the design short-period horizontal spectral response acceleration adjusted for local site conditions; S_{D1} is the design long-period horizontal spectral response acceleration adjusted for local site conditions; F_a is the short-period site coefficient; F_v is the long-period site coefficient; S_S is the mapped short-period horizontal spectral response acceleration, and S_1 is the mapped long-period horizontal spectral response acceleration.

Presented in Tables 5.7 and 5.8 are respective F_a and F_v values recommended in SCDOT (2008a). Presented in Tables 5.9-5.12 and 5.14-5.17 are computed F_a and F_v values, respectively, for the SCCP. Presented in Tables 5.13 and 5.18 are respective F_a and F_v values for the SCP. It should be noted that $PGA_{outcrop}$ is for the B-C boundary condition ($PGA_{B\text{-}C}$) when using Tables 5.9-5.12 and 5.14-5.17; and $PGA_{outcrop}$ is for the weathered hard rock condition (PGA_{HR}) when using Tables 5.13 and 5.18.

Table 5.7 F_a as a function of site class and S_S recommended in SCDOT (2008a) for B-C boundary mapped soft rock acceleration.

Site Class	Mapped Horizontal Spectral Acceleration at Period of 0.2 s[(1)], S_S				
	≤ 0.25 g	0.50 g	0.75 g	1.00 g	≥ 1.25 g
A	0.8	0.8	0.8	0.8	0.8
B	1.0	1.0	1.0	1.0	1.0
C	1.2	1.2	1.1	1.0	1.0
D	1.6	1.4	1.2	1.1	1.0
E	2.5	1.7	1.2	0.9	0.9
F[(2)]	N/A	N/A	N/A	N/A	N/A

[(1)]Use linear interpolation for intermediate values of S_S.
[(2)]Site-specific response analysis shall be performed.

Table 5.8 F_v as a function of site class and S_1 recommended in SCDOT (2008a) for B-C boundary condition mapped soft rock acceleration.

Site Class	Mapped Horizontal Spectral Acceleration at Period of 1.0 s[(1)], S_1				
	≤ 0.10 g	0.20 g	0.30 g	0.40 g	≥ 0.50 g
A	0.8	0.8	0.8	0.8	0.8
B	1.0	1.0	1.0	1.0	1.0
C	1.7	1.6	1.5	1.4	1.3
D	2.4	2.0	1.8	1.6	1.5
E	3.5	3.2	2.8	2.4	2.4
F[(2)]	N/A	N/A	N/A	N/A	N/A

[(1)]Use linear interpolation for intermediate values of S_1.
[(2)]Site-specific response analysis shall be performed.

Table 5.9 Maximum median F_a as a function of site class and mapped S_S for the B-C boundary condition derived in Chapter 3 for Charleston.

Site Class	$H_{B\text{-}C}$, ft	Mapped Spectral Acceleration at Short-Period[(1)] for the B-C Condition (Period = 0.2 sec)					
		≤ 0.15 g	0.25 g	0.50 g	0.75 g	1.00 g	1.25 g
A[(2)]	-	-	-	-	-	-	-
B	0	1.0	1.0	1.0	1.0	1.0	1.0
C	16	2.5	2.3	1.9	1.6	1.5	1.4
	33	2.5	2.6	2.4	2.1	1.9	1.7
	66	2.1	2.0	1.9	1.7	1.6	1.5
	100	1.8	1.8	1.6	1.5	1.4	1.3
	165	1.7	1.6	1.5	1.3	1.3	1.2
	≥330	1.6	1.5	1.4	1.2	1.2	1.1
D	16	2.6	2.1	1.5	1.2	1.0	0.9
	33	3.3	2.9	2.3	1.8	1.6	1.4
	66	2.9	2.5	2.1	1.8	1.6	1.5
	100	2.6	2.3	1.9	1.6	1.5	1.4
	165	2.3	2.1	1.7	1.5	1.3	1.2
	≥330	2.1	1.9	1.5	1.3	1.2	1.1
E	16	1.3	1.0	0.7	0.6	0.5	0.4
	33	2.1	1.6	1.2	0.9	0.8	0.7
	66	2.2	1.7	1.2	1.0	0.8	0.7
	100	2.4	1.9	1.3	1.0	0.9	0.8
	165	2.2	1.7	1.2	1.0	0.8	0.7
	≥330	2.0	1.6	1.1	0.9	0.8	0.7
F[(3)]	N/A	N/A	N/A	N/A	N/A	N/A	N/A

[(1)]Use linear interpolation for intermediate values of S_S.
[(2)]Site Class A not present in Charleston. No response analysis performed.
[(3)]Site-specific response analysis shall be performed.

Table 5.10 Maximum median F_a as a function of site class and mapped S_S for the B-C boundary condition derived in Chapter 3 for Myrtle Beach.

Site Class	$H_{B\text{-}C}$, ft	Mapped Spectral Acceleration at Short-Period[1] for the B-C Condition (Period = 0.2 sec)					
		≤ 0.15 g	≤ 0.15 g	≤ 0.15 g	≤ 0.15 g	≤ 0.15 g	≤ 0.15 g
A[2]	-	-	-	-	-	-	-
B	0	1.0	1.0	1.0	1.0	1.0	1.0
C	16	3.1	2.8	2.2	1.8	1.6	1.4
	33	3.0	3.0	2.7	2.3	2.0	1.8
	66	2.4	2.3	2.1	1.9	1.7	1.6
	100	2.1	2.0	1.8	1.6	1.5	1.4
	165	1.9	1.8	1.6	1.5	1.3	1.2
	≥330	1.8	1.7	1.5	1.3	1.2	1.1
D	16	3.2	2.5	1.7	1.3	1.1	0.9
	33	4.0	3.5	2.7	2.0	1.7	1.5
	66	3.5	3.0	2.4	2.0	1.7	1.5
	100	3.2	2.8	2.2	1.8	1.6	1.4
	165	2.9	2.5	1.9	1.6	1.4	1.3
	≥330	2.6	2.2	1.8	1.5	1.3	1.2
E	16	1.7	1.2	0.8	0.6	0.5	0.5
	33	2.6	2.0	1.3	1.0	0.8	0.7
	66	2.7	2.0	1.4	1.1	0.9	0.8
	100	3.0	2.2	1.5	1.2	1.0	0.8
	165	2.7	2.0	1.4	1.1	0.9	0.8
	≥330	2.5	1.9	1.3	1.0	0.8	0.7
F[3]	N/A	N/A	N/A	N/A	N/A	N/A	N/A

[1]Use linear interpolation for intermediate values of S_S.
[2]Site Class A not present in Myrtle Beach. No response analysis performed.
[3]Site-specific response analysis shall be performed.

Table 5.11 Maximum median F_a as a function of site class and mapped S_S for the B-C boundary condition derived in Chapter 3 for Columbia in the SCCP.

Site Class	$H_{B\text{-}C}$, ft	Mapped Spectral Acceleration at Short-Period[1] for the B-C Condition (Period = 0.2 sec)					
		≤ 0.15 g	≤ 0.15 g	≤ 0.15 g	≤ 0.15 g	≤ 0.15 g	≤ 0.15 g
A[2]	-	-	-	-	-	-	-
B	0	1.0	1.0	1.0	1.0	1.0	1.0
C	16	2.4	2.2	1.8	1.6	1.4	1.4
	33	2.5	2.5	2.3	2.0	1.8	1.7
	66	2.0	2.0	1.8	1.7	1.6	1.5
	100	1.8	1.7	1.6	1.5	1.4	1.3
	165	1.7	1.6	1.4	1.3	1.2	1.2
	≥330	1.6	1.5	1.3	1.2	1.1	1.1
D	16	2.4	1.9	1.4	1.1	0.9	0.8
	33	3.1	2.7	2.1	1.7	1.5	1.3
	66	2.7	2.4	2.0	1.7	1.5	1.4
	100	2.4	2.2	1.8	1.6	1.4	1.4
	165	2.2	1.9	1.6	1.4	1.3	1.2
	≥330	2.0	1.8	1.5	1.3	1.2	1.1
E	16	1.2	0.9	0.7	0.5	0.5	0.4
	33	1.9	1.5	1.1	0.9	0.7	0.7
	66	2.0	1.6	1.1	0.9	0.8	0.7
	100	2.2	1.7	1.2	1.0	0.8	0.8
	165	2.0	1.5	1.1	0.9	0.8	0.7
	≥330	1.9	1.4	1.0	0.8	0.7	0.6
F[3]	N/A	N/A	N/A	N/A	N/A	N/A	N/A

[1]Use linear interpolation for intermediate values of S_S.
[2]Site Class A not present in the Columbia area of the SCCP. No response analysis performed.
[3]Site-specific response analysis shall be performed.

Table 5.12 Maximum median F_a as a function of site class and mapped S_S for the B-C boundary condition derived in Chapter 3 for Aiken.

Site Class	$H_{B\text{-}C}$, ft	Mapped Spectral Acceleration at Short-Period[1] for the B-C Condition (Period = 0.2 sec)					
		≤ 0.15 g	≤ 0.15 g	≤ 0.15 g	≤ 0.15 g	≤ 0.15 g	≤ 0.15 g
A[2]	-	-	-	-	-	-	-
B	0	1.0	1.0	1.0	1.0	1.0	1.0
C	16	2.3	2.1	1.8	1.6	1.4	1.4
	33	2.4	2.4	2.2	2.0	1.8	1.7
	66	2.0	1.9	1.8	1.7	1.6	1.5
	100	1.7	1.7	1.5	1.4	1.4	1.3
	165	1.6	1.6	1.4	1.3	1.2	1.2
	≥330	1.5	1.5	1.3	1.2	1.1	1.1
D	16	2.4	1.9	1.4	1.1	0.9	0.9
	33	3.0	2.7	2.1	1.7	1.5	1.4
	66	2.6	2.3	1.9	1.7	1.6	1.4
	100	2.4	2.1	1.8	1.6	1.4	1.4
	165	2.1	1.9	1.6	1.4	1.3	1.2
	≥330	1.9	1.7	1.4	1.3	1.2	1.1
E	16	1.2	0.9	0.7	0.5	0.5	0.4
	33	1.9	1.5	1.1	0.9	0.7	0.7
	66	2.0	1.5	1.1	0.9	0.8	0.7
	100	2.2	1.7	1.2	1.0	0.9	0.8
	165	2.0	1.5	1.1	0.9	0.8	0.7
	≥330	1.8	1.4	1.0	0.8	0.7	0.7
F[3]	N/A	N/A	N/A	N/A	N/A	N/A	N/A

[1]Use linear interpolation for intermediate values of S_S.
[2]Site Class A not present in Aiken. No response analysis performed.
[3]Site-specific response analysis shall be performed.

Table 5.13 Maximum median F_a as a function of site class and mapped S_S for the weathered hard rock condition derived in Chapter 4 for Columbia in the SCP.

Site Class	H_{HR}, ft	Mapped Spectral Acceleration at Short-Period [(1)] for the Weathered Hard Rock Condition (Period = 0.2 sec)					
		≤ 0.15 g	0.25 g	0.50 g	0.75 g	1.00 g	≥ 1.25 g
A	0	1.0	0.6	0.6	0.6	0.6	0.6
B	16	1.1	0.6	0.6	0.6	0.6	0.6
	33	2.3	2.2	2.0	1.8	1.7	1.6
	66	2.1	2.0	1.8	1.7	1.6	1.5
	100	1.9	1.8	1.7	1.5	1.4	1.3
	165	1.8	1.7	1.5	1.4	1.3	1.2
	330	1.2	1.2	1.2	1.2	1.2	1.2
C	16	1.2	1.2	1.2	1.2	1.2	1.2
	33	3.0	2.8	2.5	2.3	2.0	1.9
	66	2.6	2.5	2.2	2.0	1.8	1.6
	100	2.3	2.2	2.0	1.8	1.6	1.4
	165	2.1	2.0	1.8	1.6	1.4	1.3
	330	1.1	1.1	1.1	1.1	1.1	1.1
D	16	1.1	1.1	1.1	1.1	1.1	1.1
	33	3.4	3.2	2.8	2.5	2.2	2.0
	66	3.0	2.8	2.4	2.1	1.9	1.7
	100	2.6	2.4	2.1	1.9	1.7	1.5
	165	2.3	2.2	1.9	1.7	1.5	1.4
	330	1.3	1.3	1.3	1.3	1.3	1.3
E	16	-	-	-	-	-	-
	33	-	-	-	-	-	-
	66	3.2	2.9	2.5	2.2	2.0	1.8
	100	2.7	2.5	2.2	1.9	1.7	1.5
	165	2.5	2.3	2.0	1.7	1.5	1.4
	330	1.0	0.6	0.6	0.6	0.6	0.6
F[(2)]	N/A	N/A	N/A	N/A	N/A	N/A	N/A

[(1)]Use linear interpolation for intermediate values of S_S.
[(2)]Site-specific response analysis shall be performed.

Table 5.14 Maximum median F_v as a function of site class and mapped S_1 for the B-C boundary condition derived in Chapter 3 for Charleston.

Site Class	$H_{B\text{-}C}$, ft	Mapped Horizontal Spectral Acceleration at Period of 1.0 s[(1)] for the B-C Boundary Condition					
		≤ 0.05 g	0.1 g	0.2 g	0.3 g	0.4 g	≥ 0.5 g
A[(2)]	-	-	-	-	-	-	-
B	0	1.0	1.0	1.0	1.0	1.0	1.0
C	16	1.9	1.9	1.9	1.7	1.6	1.4
	33	1.9	1.9	1.9	1.7	1.6	1.5
	66	1.8	1.9	1.8	1.7	1.6	1.5
	100	1.8	1.8	1.8	1.7	1.6	1.5
	165	1.8	1.8	1.7	1.6	1.5	1.4
	≥330	1.8	1.8	1.7	1.6	1.5	1.4
D	16	3.0	2.7	2.2	1.9	1.6	1.4
	33	3.1	2.8	2.3	2.0	1.7	1.5
	66	3.3	3.0	2.4	2.1	1.8	1.6
	100	3.4	3.1	2.6	2.2	1.9	1.6
	165	3.2	3.2	2.7	2.3	1.9	1.7
	≥330	3.3	3.3	2.8	2.4	2.0	1.8
E	16	2.4	1.9	1.3	1.0	0.8	0.7
	33	2.7	2.1	1.5	1.2	0.9	0.8
	66	3.1	2.4	1.7	1.3	1.1	0.9
	100	3.4	2.7	2.0	1.5	1.2	1.0
	165	3.5	3.2	2.3	1.8	1.5	1.2
	≥330	3.7	3.4	2.5	2.0	1.6	1.3
F[(3)]	N/A	N/A	N/A	N/A	N/A	N/A	N/A

[(1)]Use linear interpolation for intermediate values of S_1.
[(2)]Site Class A not present in Charleston. No response analysis performed.
[(3)]Site-specific response analysis shall be performed.

Table 5.15 Maximum median F_v as a function of site class and mapped S_1 for the B-C boundary condition derived in Chapter 3 for Myrtle Beach.

Site Class	$H_{B\text{-}C}$, ft	Mapped Horizontal Spectral Acceleration at Period of 1.0 s[(1)] for the B-C Boundary Condition					
		≤ 0.05 g	0.1 g	0.2 g	0.3 g	0.4 g	≥ 0.5 g
A[(2)]	-	-	-	-	-	-	-
B	0	1.8	1.9	1.8	1.7	1.6	1.4
C	16	1.9	1.9	1.8	1.7	1.6	1.4
	33	1.9	1.9	1.8	1.7	1.6	1.5
	66	1.8	1.8	1.8	1.7	1.6	1.4
	100	1.8	1.8	1.8	1.7	1.5	1.4
	165	1.8	1.8	1.7	1.6	1.5	1.4
	≥330	1.8	1.8	1.7	1.6	1.5	1.4
D	16	3.2	2.9	2.4	2.0	1.7	1.5
	33	3.3	3.0	2.5	2.1	1.8	1.6
	66	3.4	3.2	2.6	2.2	1.9	1.7
	100	3.4	3.3	2.7	2.3	2.0	1.7
	165	3.3	3.2	2.9	2.4	2.1	1.8
	≥330	3.3	3.3	3.0	2.5	2.1	1.9
E	16	2.8	2.2	1.6	1.2	1.0	0.8
	33	3.2	2.5	1.8	1.4	1.1	0.9
	66	3.5	2.9	2.0	1.6	1.3	1.1
	100	3.6	3.3	2.3	1.8	1.4	1.2
	165	3.8	3.5	2.7	2.1	1.7	1.4
	≥330	4.0	3.6	3.0	2.3	1.9	1.5
F[(3)]	N/A	N/A	N/A	N/A	N/A	N/A	N/A

[(1)]Use linear interpolation for intermediate values of S_1.
[(2)]Site Class A not present in Myrtle Beach. No response analysis performed.
[(3)]Site-specific response analysis shall be performed.

Table 5.16 Maximum median F_v as a function of site class and mapped S_1 for the B-C boundary condition derived in Chapter 3 for Columbia in the SCCP.

Site Class	$H_{B\text{-}C}$, ft	Mapped Horizontal Spectral Acceleration at Period of 1.0 s[(1)] for the B-C Boundary Condition					
		≤ 0.05 g	0.1 g	0.2 g	0.3 g	0.4 g	≥ 0.5 g
A[(2)]	-	-	-	-	-	-	-
B	0	1.9	2.0	2.0	1.9	1.6	1.4
C	16	2.0	2.0	2.0	1.8	1.6	1.4
	33	1.9	2.0	2.0	1.9	1.7	1.5
	66	1.9	1.9	1.9	1.8	1.7	1.5
	100	1.9	1.9	1.9	1.7	1.6	1.5
	165	1.8	1.8	1.8	1.7	1.6	1.5
	≥330	1.8	1.8	1.8	1.7	1.6	1.5
D	16	2.9	2.6	2.2	1.8	1.5	1.2
	33	3.0	2.7	2.3	1.9	1.6	1.4
	66	3.2	2.9	2.4	2.0	1.8	1.5
	100	3.3	3.0	2.5	2.1	1.8	1.6
	165	3.4	3.1	2.6	2.2	1.9	1.7
	≥330	3.4	3.2	2.7	2.3	2.0	1.8
E	16	2.1	1.6	1.2	0.9	0.7	0.6
	33	2.3	1.8	1.3	1.0	0.8	0.7
	66	2.7	2.1	1.5	1.2	1.0	0.8
	100	3.0	2.4	1.7	1.3	1.1	0.9
	165	3.4	2.8	2.0	1.6	1.3	1.1
	≥330	3.6	3.1	2.2	1.7	1.4	1.2
F[(3)]	N/A	N/A	N/A	N/A	N/A	N/A	N/A

[(1)]Use linear interpolation for intermediate values of S_1.
[(2)]Site Class A not present for Columbia area in the SCCP. No response analysis performed.
[(3)]Site-specific response analysis shall be performed.

Table 5.17 Maximum median F_v as a function of site class and mapped S_1 for the B-C boundary condition derived in Chapter 3 for Aiken.

Site Class	$H_{B\text{-}C}$, ft	Mapped Horizontal Spectral Acceleration at Period of 1.0 s[(1)] for the B-C Boundary Condition					
		≤ 0.05 g	0.1 g	0.2 g	0.3 g	0.4 g	≥ 0.5 g
A[(2)]	-	-	-	-	-	-	-
B	0	1.0	1.0	1.0	1.0	1.0	1.0
C	16	1.9	1.9	1.9	1.8	1.6	1.4
	33	1.9	1.9	1.9	1.8	1.6	1.5
	66	1.8	1.8	1.8	1.7	1.6	1.5
	100	1.8	1.8	1.8	1.7	1.6	1.5
	165	1.8	1.8	1.7	1.6	1.5	1.4
	≥330	1.8	1.8	1.7	1.6	1.5	1.4
D	16	2.9	2.6	2.2	1.8	1.6	1.3
	33	3.0	2.7	2.3	1.9	1.7	1.5
	66	3.1	2.8	2.4	2.0	1.7	1.5
	100	3.3	3.0	2.5	2.1	1.8	1.6
	165	3.2	3.1	2.6	2.2	1.9	1.7
	≥330	3.2	3.2	2.7	2.3	2.0	1.7
E	16	2.2	1.7	1.2	1.0	0.8	0.7
	33	2.5	1.9	1.4	1.1	0.9	0.7
	66	2.8	2.2	1.6	1.2	1.0	0.9
	100	3.2	2.5	1.8	1.4	1.2	1.0
	165	3.4	3.0	2.1	1.7	1.4	1.1
	≥330	3.6	3.2	2.4	1.8	1.5	1.2
F[(3)]	N/A	N/A	N/A	N/A	N/A	N/A	N/A

[(1)]Use linear interpolation for intermediate values of S_1.
[(2)]Site Class A not present in Aiken. No response analysis performed.
[(3)]Site-specific response analysis shall be performed.

Table 5.18 Maximum median F_v as a function of site class and mapped S_1 for the weathered hard rock condition derived in Chapter 4 for Columbia in the SCP.

Site Class	H_{HR}, ft	Mapped Horizontal Spectral Acceleration at Period of 1.0 s[(1)] for the Weathered Hard Rock Condition					
		≤ 0.05 g	0.1 g	0.2 g	0.3 g	0.4 g	≥ 0.5 g
A	0	1.0	1.0	1.0	1.0	1.0	1.0
B	16	1.1	1.0	0.6	0.6	0.6	0.6
	33	1.0	0.6	0.6	0.6	0.6	0.6
	66	1.3	1.2	1.1	0.6	0.6	0.6
	100	2.1	2.0	1.8	1.7	1.6	1.5
	165	2.3	2.2	2.0	1.8	1.7	1.6
	330	2.3	2.2	2.1	1.9	1.8	1.7
C	16	1.4	1.4	1.4	1.4	1.4	1.4
	33	1.4	1.4	1.4	1.4	1.4	1.4
	66	1.4	1.4	1.4	1.4	1.4	1.4
	100	2.6	2.5	2.2	2.0	1.8	1.6
	165	3.0	2.8	2.5	2.3	2.0	1.9
	330	3.1	2.9	2.6	2.3	2.1	1.9
D	16	1.4	1.4	1.4	1.4	1.4	1.4
	33	1.4	1.4	1.4	1.4	1.4	1.4
	66	1.4	1.4	1.4	1.4	1.4	1.4
	100	3.0	2.8	2.4	2.1	1.9	1.7
	165	3.4	3.2	2.8	2.5	2.2	2.0
	330	3.6	3.3	2.9	2.6	2.3	2.1
E	16	-	-	-	-	-	-
	33	-	-	-	-	-	-
	66	2.0	2.0	2.0	2.0	2.0	2.0
	100	3.2	2.9	2.5	2.2	2.0	2.0
	165	3.7	3.4	2.9	2.6	2.3	2.1
	330	3.9	3.7	3.2	2.8	2.4	2.2
F[(2]		NA	NA	NA	NA	NA	NA

[(1)] Use linear interpolation for intermediate values of S_S.

[(2)]Site-specific response analysis shall be performed.

5.4 Three-Point Acceleration Design Response Spectrum

The 3-point procedure for constructing an acceleration design response spectrum (ADRS) recommended in SCDOT (2008a) and AASHTO (2011a) can be summarized in five steps. First, the site V_{S100ft} is determined. Second, $PGA_{outcrop}$, S_S and S_1 are obtained from probabilistic seismic hazard maps. Third, the V_{S100ft}, $PGA_{outcrop}$, S_S and S_1 are used to obtain site coefficients F_{PGA}, F_a and F_v. Fourth, the three points of the ADRS are obtained as follows:

$$PGA = F_{PGA} PGA_{outcrop} \tag{5.4}$$

$$S_{DS} = F_a S_S \tag{5.5}$$

$$S_{D1} = F_v S_1 \tag{5.6}$$

where PGA is the design peak ground acceleration, S_{DS} is the short-period (0.2 s) spectral response acceleration, and S_{D1} is the long-period (1.0 s) spectral response acceleration at the site. Finally the ADRS is constructed as illustrated in Figure 5.1.

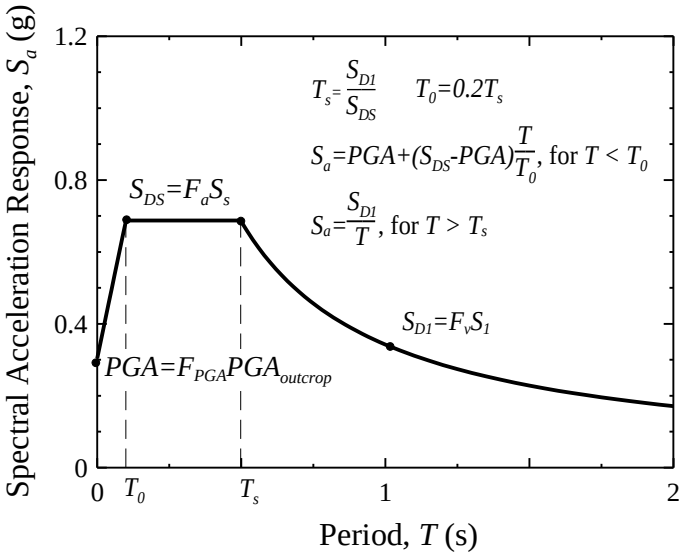

Figure 5.1 Three-point ADRS curve (SCDOT 2008a).

The procedure illustrated in Figure 5.1 implicitly assumes: (1) all significant peaks are expected to occur at $T \leq 1.0$ s; (2) the plateau defined by S_{DS} provides a reasonable average for the peaks of the site-specific response spectrum; and (3) spectral acceleration descends proportionally with $1/T$, when $T > T_s$ ($T_s = S_{D1}/S_{DS}$). However, it was shown in Chapter 2 that significant peaks may not always occur at shorter periods ($T \leq 1.0$ s), especially when $V_{S100ft} <$ 660 ft/s; and the plateau cannot always be defined as S_{DS}, unless $T_s \leq 1.0$ s ($S_{D1} \leq S_{DS}$).

The 3-point procedure for constructing ADRS curves was shown in Chapter 2 to be generally valid when $V_{S100ft} > 660$ ft/s. However, when $V_{S100ft} \leq 660$ ft/s, significant peaks may occur at $T > 1.0$ s. For this reason, it was suggested that a multi-point ADRS curve be plotted in addition to the 3-point curve, to check if long-period accelerations are under predicted. Procedures to calculate site coefficients at long periods ($T = 1.6$ and 3.0 s) are provided in Chapters 3 and 4.

5.5 Multi-Point Acceleration Design Response Spectrum

The objective of the multi-point ADRS is to provide a check to make sure that longer period accelerations are not under-predicted by the 3-point ADRS design curve. The multi-point ADRS is drawn by first constructing the 3-point ADRS curve and then overlaying on the same graph the multi-point ADRS values as illustrated in Figure 5.2.

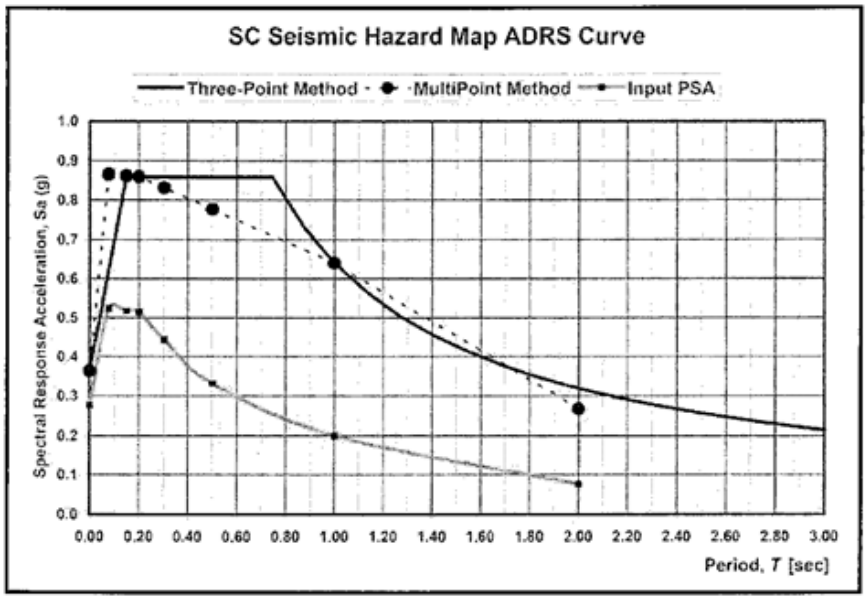

Figure 5.2 Example of 3-point and multi-point ADRS curves for a Site Class C location (SCDOT 2008a).

After the multi-point horizontal ADRS curve has been constructed, the 3-point ADRS is checked to see if it is underestimating spectral accelerations or if it is not representative of the acceleration response spectrum. In certain circumstances there may be a shift that is not captured by the 3-point ADRS. This is particularly true in the Eastern United States where the soil column is deep and V_{S100ft} < 660 ft/s (SCDOT 2008a). The result is a shift in the acceleration response spectrum towards the 1.0 s period.

The ADRS curves shown in Figure 5.3 provide an example where discrepancies between the 3-point and the multi-point methods indicate spectral accelerations significantly underestimated at the 1.0 s period and significantly dissimilar acceleration response spectrum shape. For this particular example, the site class is E and the difference at spectral period of 1.0 s is important because the fundamental period of the bridge being designed was 1.0 s (SCDOT 2008a).

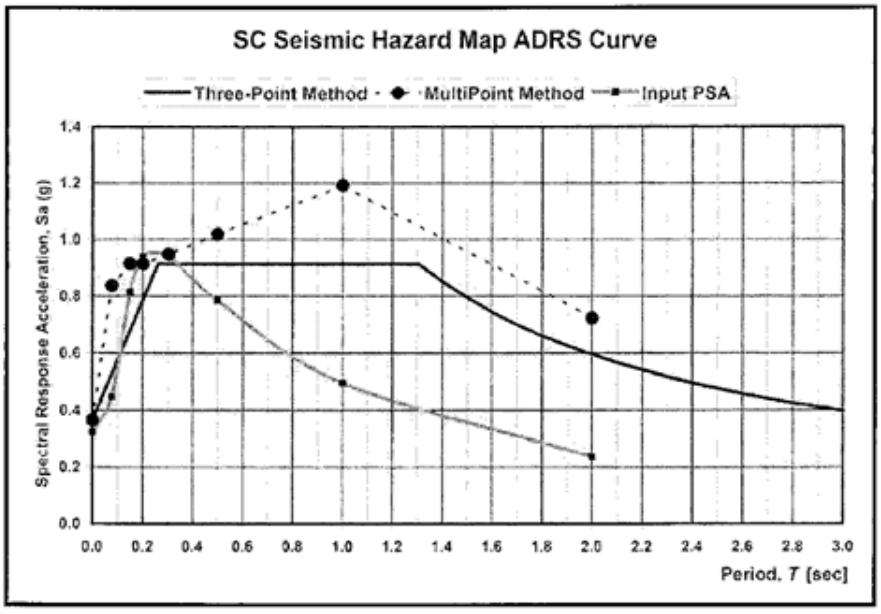

Figure 5.3 Example of 3-point and multi-point ADRS curves for a Site Class E location (SCDOT 2008a).

It should be noted that the multi-point method currently described in SCDOT (2008a) can give ambiguous results (Power and Chiou 2000), because F_a is used for all T less than or equal to 0.2 s and F_v is used for all T greater than or equal to 1.0 s to compute the response spectrum. To improve the current multi-point method, additional site coefficients $F_{0.6}$, $F_{1.6}$ and F_3 were developed in Chapters 3 and 4 for T values of 0.6, 1.6 and 3.0 s, respectively.

5.6 Comparison of Maximum Median Site Coefficients

Presented in Figures 5.4-5.6 are bar charts showing maximum median values of F_{PGA}, F_a, and F_v, respectively, grouped by the NEHRP site classes for Charleston, Myrtle Beach, Columbia and Aiken. Also plotted are the NEHRP F_{PGA}, F_a, and F_v values for comparison. It can be seen in Figure 5.4 that the maximum median F_{PGA} values for the four selected areas are within 20%. The maximum median F_{PGA} values decrease by area in the following order: Myrtle Beach, Charleston, Columbia, and Aiken. For Site Class C and D, the NEHRP F_{PGA} can be exceeded by as much as 70%.

As shown in Figure 5.5, the computed maximum median F_a values are the highest for Myrtle Beach. For Site Class D, the computed maximum median F_a in Myrtle Beach, Charleston, Columbia, and Aiken can be as much as 60%, 40%, 30%, and 20% greater than the NEHRP F_a, respectively. For Site Class E, the NEHRP F_a is found to be greater than nearly all the computed maximum median values.

Presented in Figure 5.6 are bar charts comparing maximum median F_v values for the four selected SCCP sites and the NEHRP F_v. It can be seen that the computed F_v values for all four SCCP sites are close for Site Class C and only slightly greater than the NERHP F_v. For Site Class D, the computed F_v in Myrtle Beach, Charleston, Columbia, and Aiken can be as much as 50%, 40%, 40% and 40% greater than the NEHRP F_v.

Presented in Figures 5.7-5.9 are sample depth-to-rock dependent F_{PGA}, F_a, and F_v values grouped by amplitude and site class for Charleston. Also plotted are the corresponding depth-to-rock independent NEHRP values. The plots show the sensitivity of site amplification at shallow depths to soft rock ($H_{B\text{-}C} \leq 165$ ft).

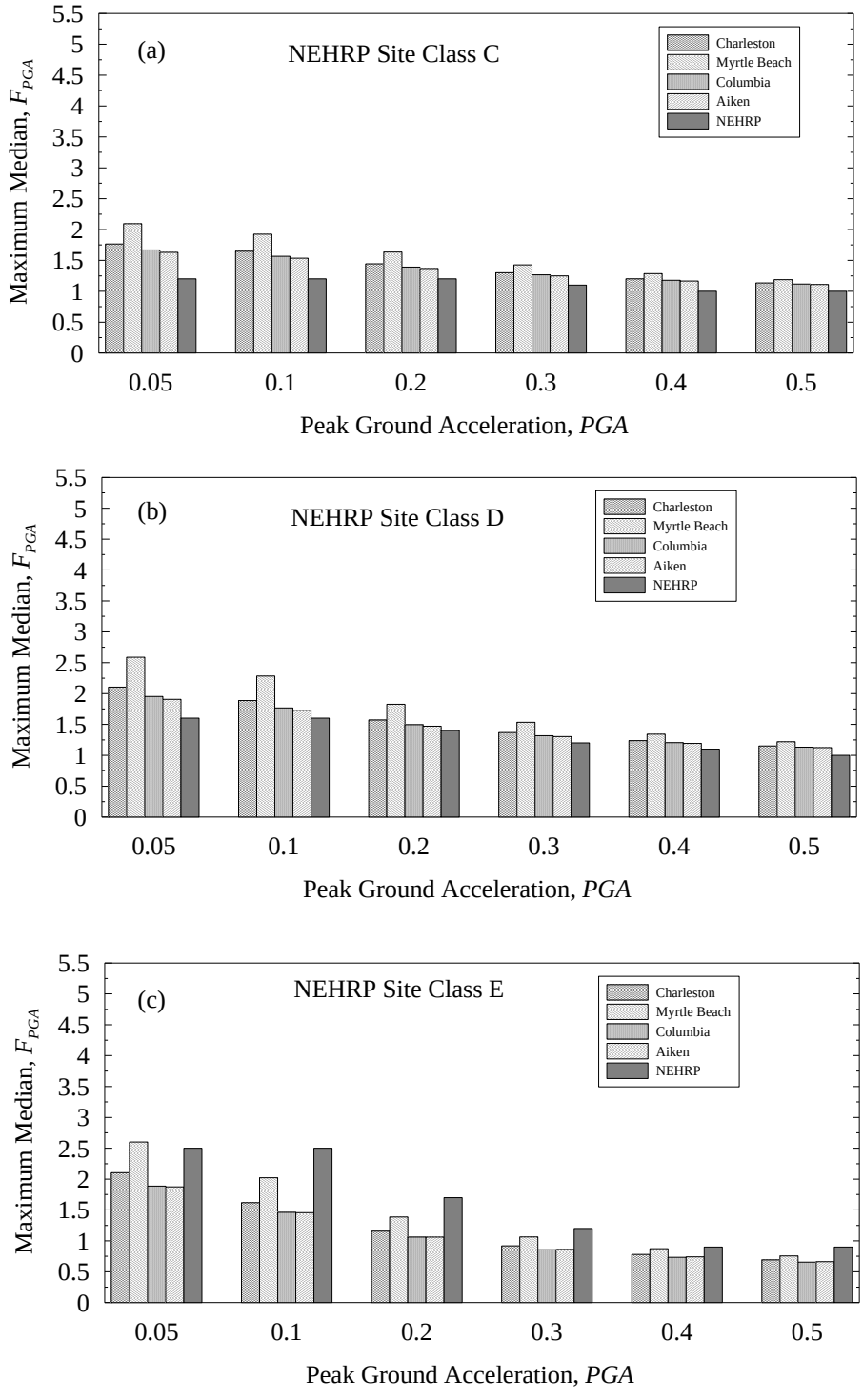

Figure 5.4 Maximum median F_{PGA} within site classes for four areas in the SCCP with $H_{B\text{-}C}$ > 330 ft compared with the NEHRP F_{PGA}.

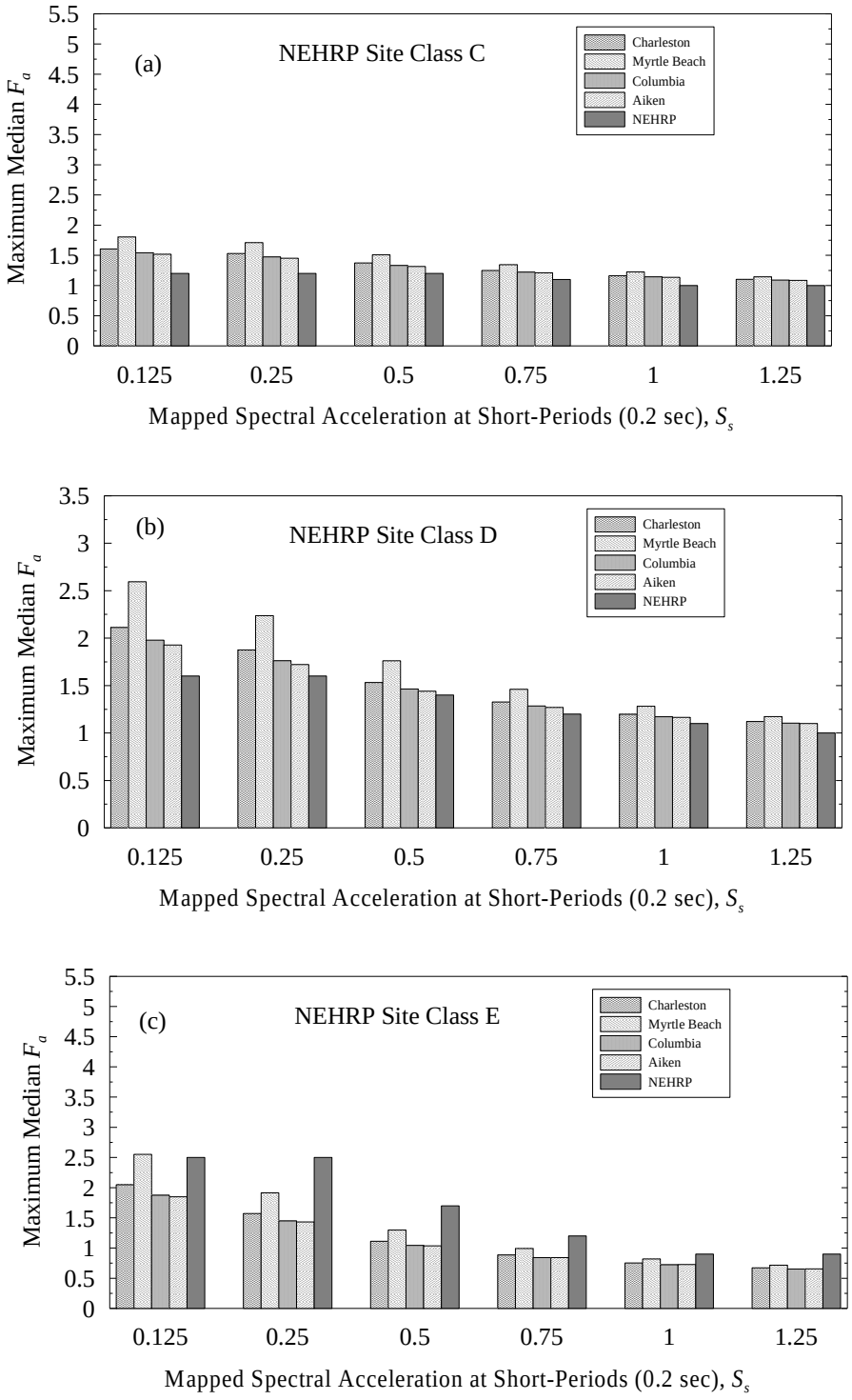

Figure 5.5 Maximum median F_a within site classes for four areas in the SCCP compared with the NEHRP F_a.

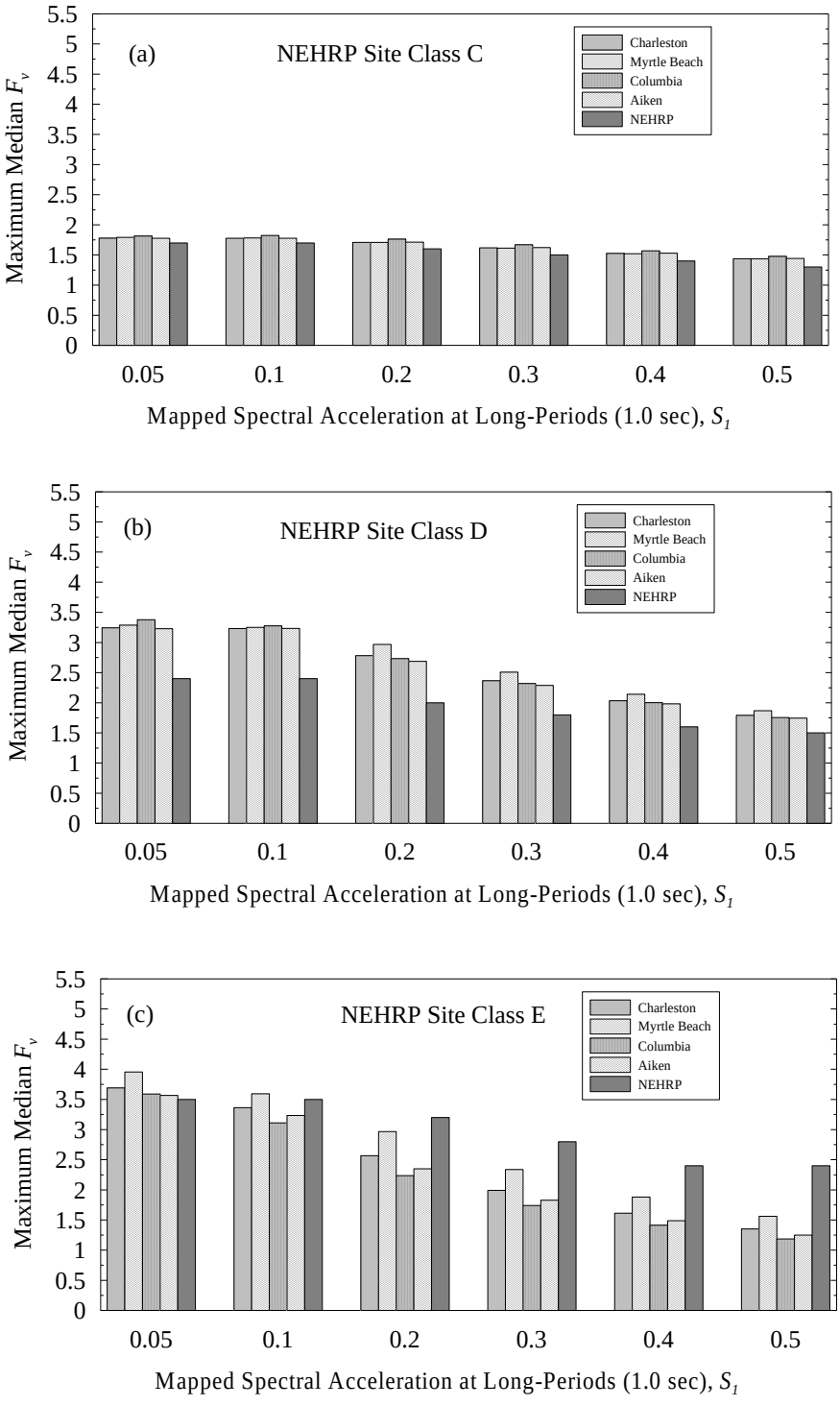

Figure 5.6 Maximum median F_v within site classes for four areas in the SCCP compared with the NEHRP F_v.

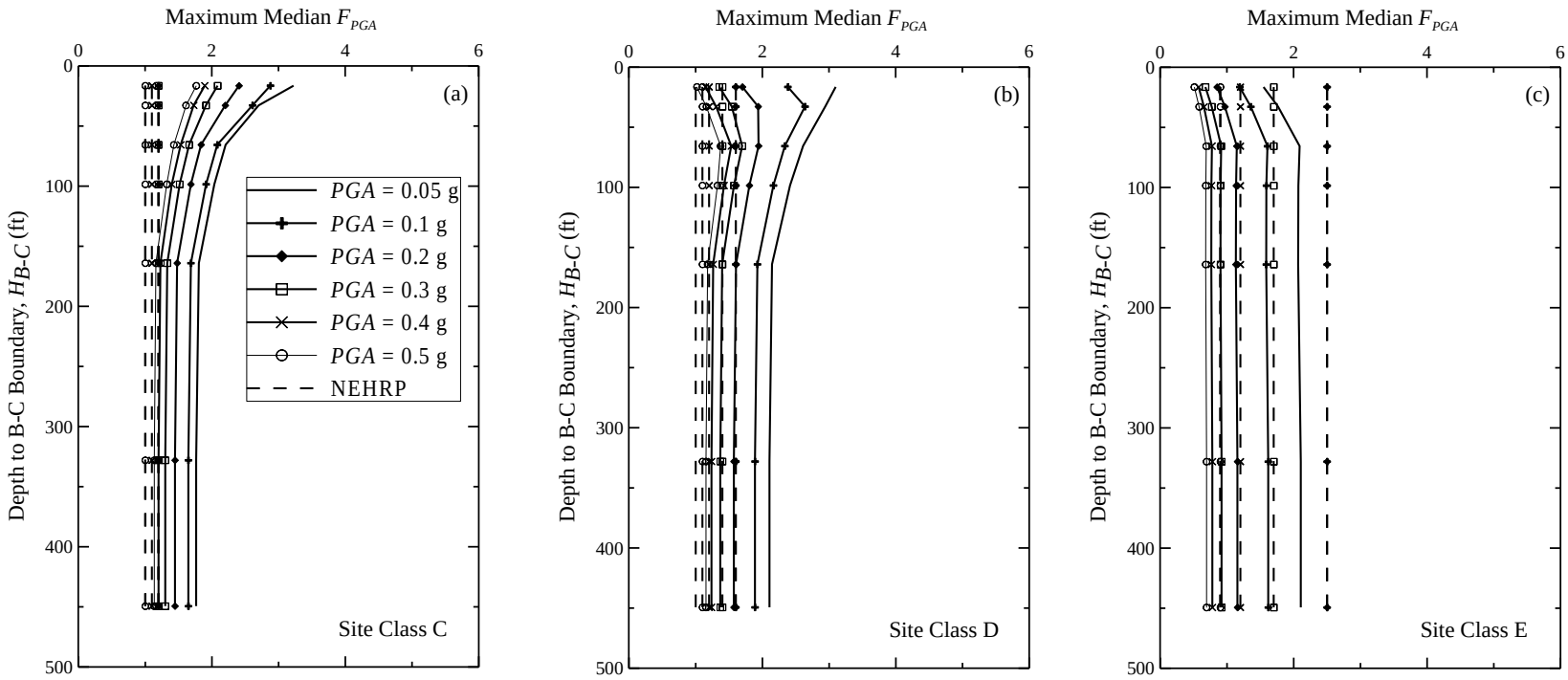

Figure 5.7 Sample depth-to-rock dependent maximum median F_{PGA} for Charleston.

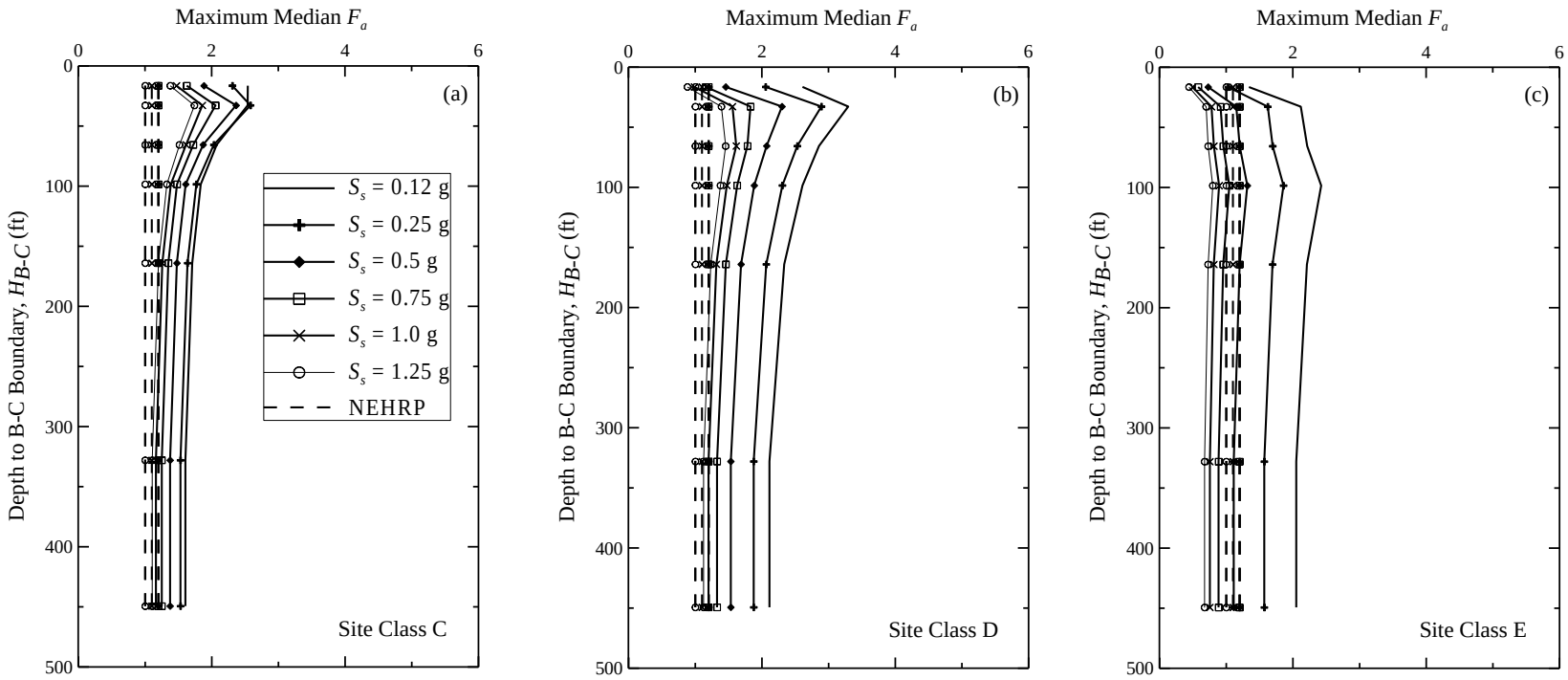

Figure 5.8 Sample depth-to-rock dependent maximum median F_a for Charleston.

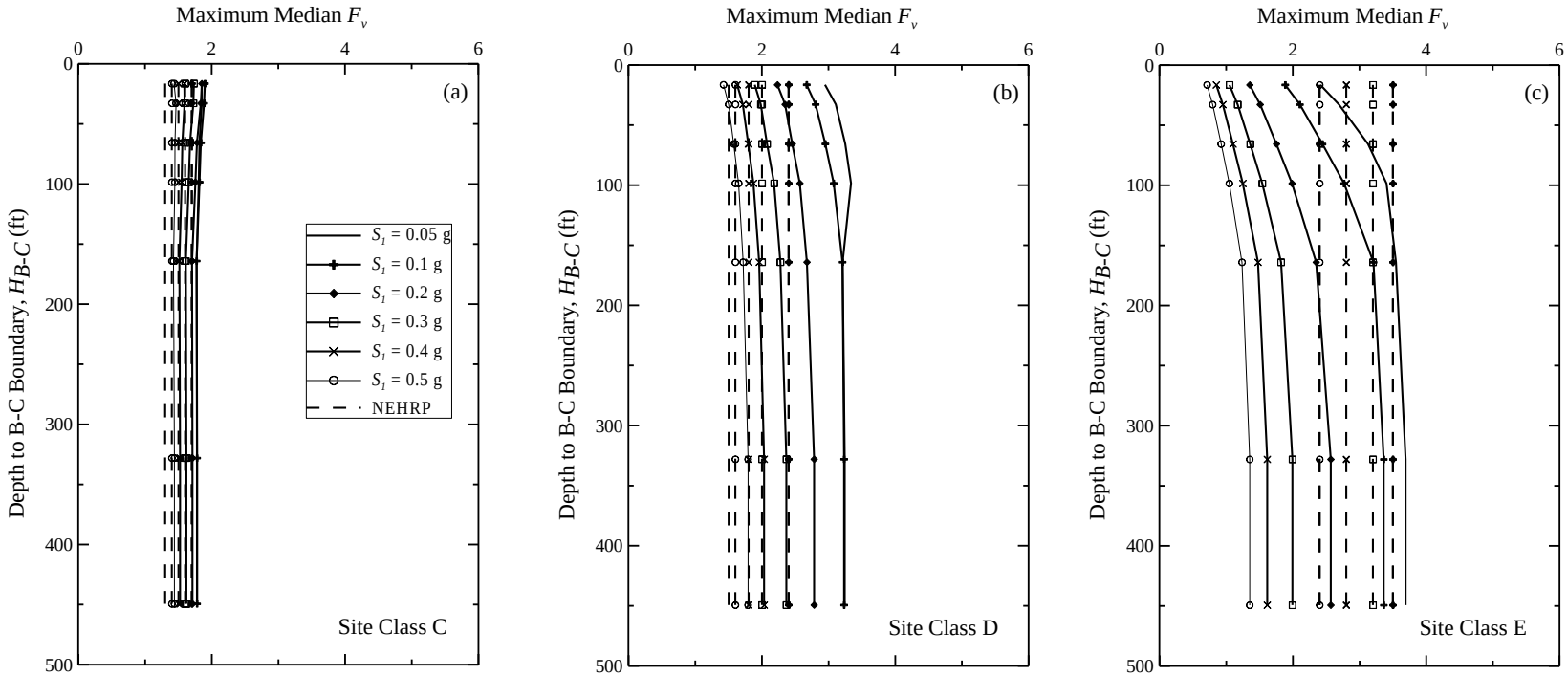

Figure 5.9 Sample depth-to-rock dependent maximum median F_v for Charleston.

As shown in Figure 5.7, F_{PGA} and F_a generally increase with decreasing $H_{B\text{-}C}$, for Site Class C and D. For Site Class E, however, F_{PGA} and F_a slightly decrease with decreasing $H_{B\text{-}C}$. Concerning F_v, the computed depth-dependent coefficients do not differ much for Site Class C. For Site Class D and E, F_v decreases with decreasing $H_{B\text{-}C}$. These observations agree well with a depth-to-rock dependent site response study for the Mississippi Embayment (Hashash et al. 2008). Hashash et al. (2008) obtained increasing F_a and decreasing F_v with decreasing depth for Site Class D.

5.7 Summary

In this chapter, seismic site coefficients recommended in SCDOT (2008a) were compared with site coefficients computed in Chapters 3 and 4. It was shown that the computed F_{PGA} for all areas in the SCCP are within 20% of each other. For Site Class C and D, the NEHRP F_{PGA} can be exceeded by as much as 70% in the SCCP. The computed maximum median F_a in Myrtle Beach, Charleston, Columbia, and Aiken can be as much as 60%, 40%, 30% and 20% greater than the NEHRP F_a, respectively. Similarly, the computed maximum median F_v in Myrtle Beach, Charleston, Columbia, and Aiken can be as much as 50%, 40%, 40% and 40% greater than the NEHRP $F_{v.}$

Unlike the NEHRP coefficients, the coefficients derived in Chapters 3 and 4 are depth-to-rock dependent. F_{PGA} and F_a generally increase with decreasing $H_{B\text{-}C}$ for Site Class C and D; where as F_v decreases with decreasing $H_{B\text{-}C}$ for Site Class D and E. For Site Class E, F_{PGA}, F_a and F_v slightly decrease with decreasing $H_{B\text{-}C}$.

It was shown that multiple tables will be needed to accurately represent the new site coefficients and to account for all significant conditions. Thus, the use of the continuous relationships of site coefficients with V_{S100ft} presented in Chapters 3 and 4 is a more efficient approach to defining the recommended site coefficients for seismic design in South Carolina.

CHAPTER SIX

REPERCUSSIONS OF NEW SEISMIC SITE COEFFICIENTS AND ADRS CURVES

6.1 Introduction

The development of models for site coefficients for the South Carolina Coastal Plain (SCCP) was described in earlier chapters (Chapters 2 and 3) in detail. It was observed that the newly recommended site coefficients are different from the site coefficients currently used by SCDOT (2008a) and the difference varies with the site class. The Acceleration Design Response Spectrum (ADRS) generated based on these new site coefficients are expected to be different than the ones generated using the current (AASHTO 2011a and SCDOT 2008a) site coefficients used by SCDOT. This could greatly impact the seismic demand of existing and to-be-built highway structures (i.e. bridges) which will consequently impact the industry from an economic standpoint.

On this view, an attempt was made to apply the ADRS curves generated from AASHTO (2011a) and the new site coefficients presented in Chapter 3), on actual highway structures to observe the differences in responses of interest. Thus the goal of this chapter is to implement ADRS curves from both the current (also referred to as "AASHTO 2011a" in this report) and the recommended methods as one of the inputs on typical highway bridge structures and compare the responses to better understand the effect of the newly developed site coefficients on structural analysis outcomes.

Two sample highway bridges are used in this study as listed in Table 6.1. They are: (1) the "LRFD Example Bridge", a Cast in Place (CIP) concrete box-girder bridge which is design example no. 8 in "Design examples: Recommended LRFD guidelines for the seismic design of highway bridges" (ATC/MCEER 2003a); and (2) the "Russell Creek Bridge", a to-be-built concrete deck-girder bridge over the Russell Creek River in Charleston County, SC. The LRFD Example Bridge was analyzed using SAP2000 version 14.2.2 (CSI 2009) for NEHRP Site Class C, D and E. For Site Class D and E, the site coefficients corresponding to Charleston are used because these two site classes are the most frequently encountered in that area. For Site Class C, site coefficients corresponding to Columbia are used. On the other hand, the Russell Creek

Bridge is analyzed using CSiBridge version 15 (CSI 2011) for Site Class D (site coefficients corresponding to Charleston), following the original design consideration. First, ADRS curves corresponding to each site class are generated using the AASHTO (2011a) and the recommended site coefficients. Then, multi-modal response spectrum (MMRS) analysis results obtained by applying the AASHTO (2011a) and recommended ADRS curves on these two bridges were compared at intermediate bents. For the LRFD Example Bridge, forces, moments and displacements are compared at the top and bottom of all four intermediate bent columns. For the Russell Creek Bridge, forces, moments and displacements are compared at the top of the piles of all nine intermediate bents. Two different load combinations are used for each bridge. Finally, a parametric study is conducted for the LRFD Example Bridge to investigate the effect of fixity of the foundations (fixed and springs) because the original LRFD Design Example uses foundation springs, whereas SCDOT (2008b) suggests the application of fixed-base for pile foundations. Details are provided in subsequent sections.

Table 6.1 List of sample highway bridges considered.

Sample No.	Bridge name	Location	Number of spans	Deck type	Pier type	Abutment type	Foundation type	Site Class
1	LRFD Example Bridge	Puget Sound region of Washington State	5	Concrete box girder	Two column integral bent	Stub type	Concrete piles	Analyzed for Site Classes C, D and E
2	Russell Creek Bridge	Charleston County, SC	10	Concrete I-girder	Pile bent	Pile bent	Concrete piles	Site Class D

6.2 Generation of ADRS Curves for LRFD Example Bridge Analysis

As mentioned before, site coefficients for Charleston are selected for Site Class D and E and site coefficients for Columbia are selected for Site Class C. The depth to the B-C boundary is assumed as 450 ft for Charleston (see reference profile for Charleston in Chapter 2) and 100 ft for Columbia. The depth to the B-C boundary is one of the parameters to be used in the recommended site coefficient model.

Seven different ADRS curves were used in this chapter. The first three ADRS curves (I, II and III) were generated based on AASHTO (2011a) for Site Class C, D and E, respectively. ADRS-IV, V, VI and VII were generated based on the newly recommended model for the SCCP (Chapter 3). ADRS-IV is for Site Class C with V_{S100ft} of 1,263 ft/s, and depth to soft-rock equal to 100 ft, which was assumed for Columbia in Chapter 3 (thus both K_{H1} and K_{H2} are equal to 1.0). ADRS-V is for Site Class D with V_{S100ft} of 961 ft/s, and depth to soft-rock equal to 450 ft which was assumed for Charleston in Chapter 2. ADRS-VI is the maximum possible ADRS curve in Site Class D using the recommended model and also for the location (i.e. the input motion). This ADRS curve was developed by using the site coefficient model developed in Chapter 3 and calculating the maximum possible site coefficients for spectral periods of 0, 0.2 and 1.0 s. The maximum ADRS was used to produce the maximum difference between the recommended and AASHTO (2011a) ADRS curves and observe its impact on the structural response. ADRS-VII is for Site Class E with V_{S100ft} of 600 ft/s which is the highest V_{S100ft} within Site Class E. Based on the simulations conducted in this study, site coefficients were found to generally decrease with decreasing V_{S100ft} within Site Class E. In contrast, the AASHTO (2011a) and SCDOT (2008a) site coefficients are constants considering the middle range values within each site class. Thus by selecting 600 ft/s as V_{S100ft}, the recommended model is expected to produce the highest response (i.e., ADRS curve and also the structural responses) within Site Class E. Then by comparing that with the corresponding similarly generated AASHTO (2011a) ADRS curve outcome should produce the maximum plausible difference scenario with respect to the structural response.

The ADRS curves (IV, V, VI and VII) generated using the newly recommended site coefficients for SCCP (Chapters 3) are compared with the ADRS curves (I, II and III) based on the AASHTO (2011a) site coefficients (AASHTO 2011a and SCDOT 2008a) in Figure 6.1. Noticeably, in Figure 6.1 ADRS curves II and V fall very close to each other while ADRS curves II and VI and ADRS curves III and VII show larger differences. The amplitude of ADRS-I is greater than ADRS-IV for spectral periods <0.5 s (0-0.5 s) and lesser for periods beyond 0.5 s. Similar inter-relationships are also expected to be reflected on the respective bridge responses presented in later sections.

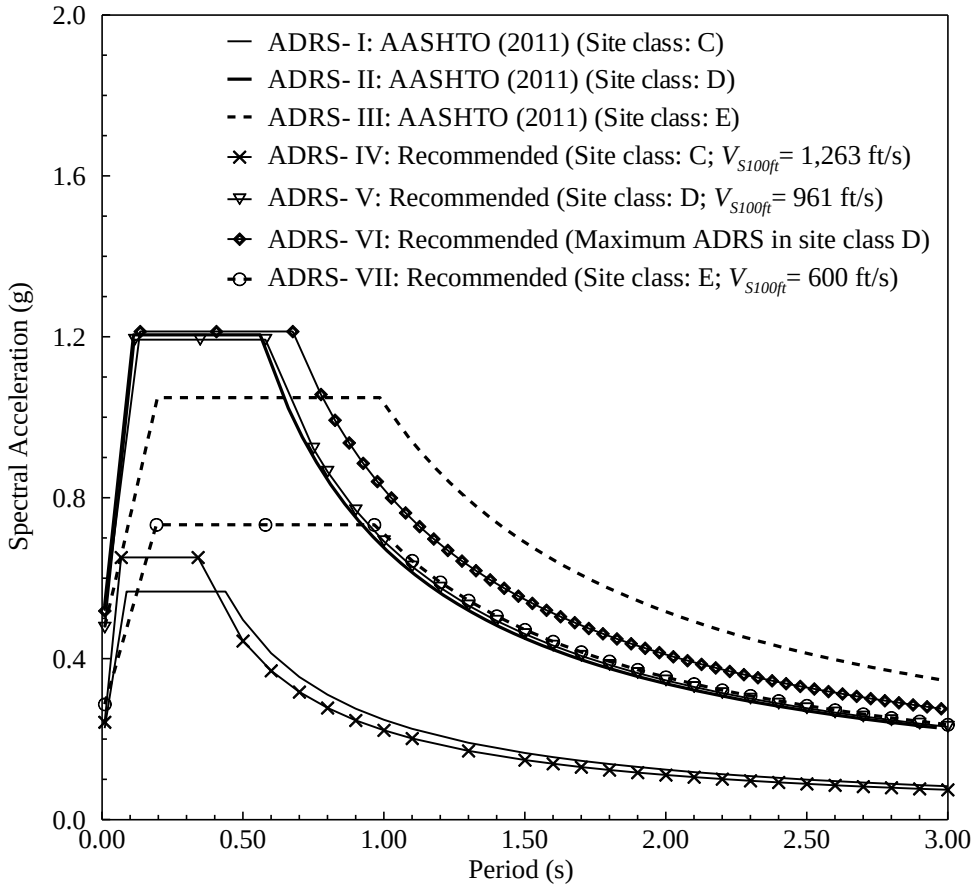

Figure 6.1 ADRS curves used in this chapter based on an SEE motion for Charleston generated by Scenario_PC.

Table 6.2 presents the site coefficients based on the seven ADRS curves generated. The spectral accelerations listed in the Table 6.2, $PGA_{B\text{-}C}$, S_S and S_1, and respective site coefficients, F_{PGA}, F_a and F_v, corresponding to periods of 0, 0.2 and 1.0 s, respectively. Charleston SEE ground motion (2% probability of exceedance in 50 years) with moment magnitude of 7.3 was generated by Scenerio_PC (Chapman 2006). This motion was then used to compute the acceleration response at the B-C boundary i.e. $S_{B\text{-}C}$, which are then multiplied by the corresponding site coefficients to calculate the surface spectral acceleration (i.e., S_{site}) for different periods. S_{site} values are then used for ADRS curves generation following procedures defined in SCDOT (2008a) and AASHTO (2011a). Figure 6.2 presents the procedure followed to develop 3-point ADRS curves. For detailed step-by-step procedures, readers are suggested to visit SCDOT (2008a), from where the figure was originally adopted.

Table 6.2 Site coefficients corresponding to the seven ADRS curves considered.

ADRS curve	Spectral accelerations at B-C boundary			Site Coefficient		
	PGA_{B-C}	S_S	S_1	F_{PGA}	F_a	F_v
I	0.190	0.472	0.151	1.200	1.200	1.650
II	0.532	1.165	0.431	1.000	1.034	1.569
III	0.532	1.165	0.431	0.900	0.900	2.400
IV	0.190	0.472	0.151	1.278	1.380	1.475
V	0.532	1.165	0.431	0.877	1.024	1.607
VI	0.532	1.165	0.431	0.975	1.041	1.910
VII	0.532	1.165	0.431	0.539	0.629	1.644

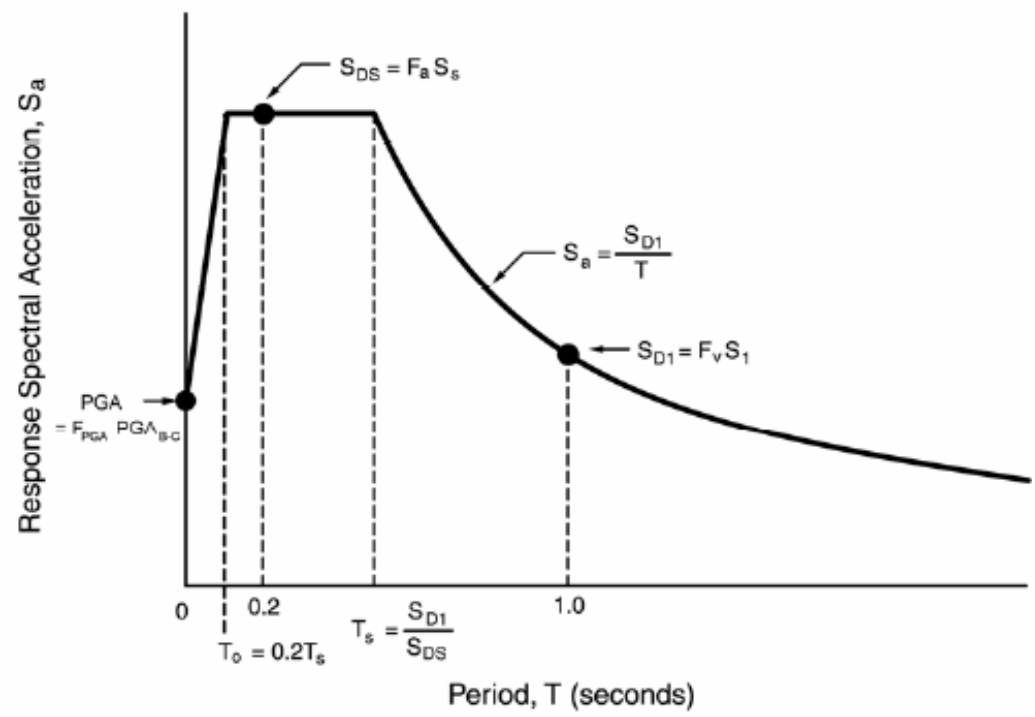

Figure 6.2 Three-point ADRS curve development methodology (SCDOT, 2008a).

6.3 LRFD Example Bridge and Modeling Procedure

6.3.1 Problem Description

The bridge is a five-span CIP concrete box-girder with two-column bents and no skew. Each span is about 100 ft long, totaling a 500 ft long structure (abutment to abutment). A schematic diagram of the bridge is shown in Figure 6.3 and Table 6.3 presents the column and foundation

seal height. The four bents are attached to the box-girder superstructure with integrated cross-beams. On the other end, the two circular columns of each bent are integrated with pile caps. Figure 6.4 shows a cross-section of the bridge superstructure-bent system. Stub-type abutment with an assumption of free longitudinal (in global X direction) translation is assumed on both sides of the bridge.

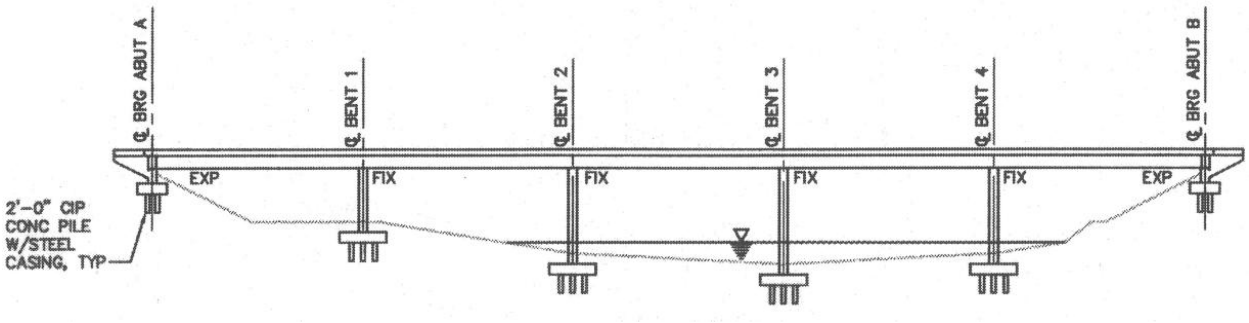

Figure 6.3 Schematic diagram of the LRFD Example Bridge (ATC/MCEER 2003a).

Table 6.3 Bent details of LRFD Example Bridge.

Bents	Column Height (ft)	Pile Cap Seal Depth (ft)
1	30	3
2	45	4
3	50	6
4	45	4

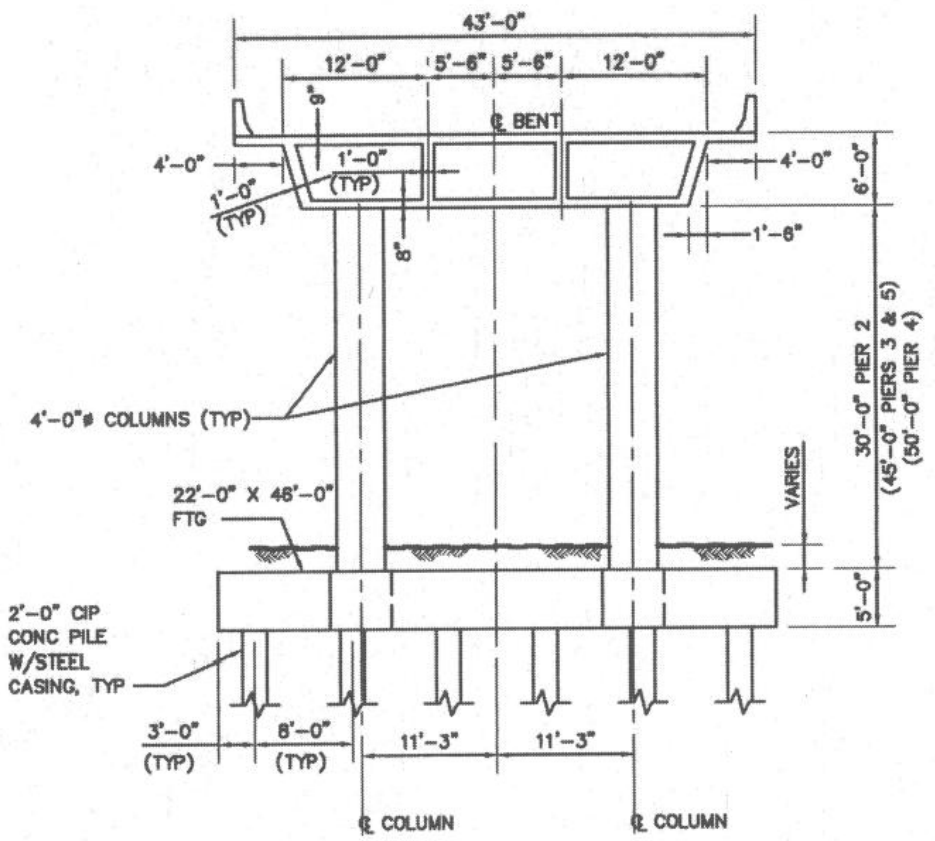

Figure 6.4 LRFD Example Bridge cross-section at an intermediate pier (ATC/MCEER 2003a).

6.3.2 Analysis Tool

The three dimensional bridge analysis model of the LRFD Example Bridge is generated with the widely used structural analysis program SAP2000 (CSI 2009). SAP2000 is capable of performing elastic response spectrum analysis of three dimensional structures, which is the requirement for this study. SAP2000 version 14.2.2 uses object-based-modeling technique. This particular modeling technique involves development of the object based geometry of the structure through an intuitive graphical interface and automatic conversion of the object-based model into the analysis model (i.e., finite element model consisting of the traditional elements and nodes). Smart graphical environment, helpful object-based modeling option and MMRS analysis capability on three dimensional structures –all together helped make the decision to use SAP2000 for this study.

6.3.3 Modeling in SAP2000

In this sub-section, modeling of the three dimensional bridge system in SAP2000 is described. The numerical model is developed following the procedure described in the design example (Example 8) from the LRFD guidelines (ATC/MCEER 2003a). In the guidelines, foundation springs are used to represent the pile. However, for this analysis, fixed column bases were used because: (i) SCDOT (2008b) suggests the use of fixed base in the case of deep foundations; (ii) it is a widely accepted procedure among practitioners; and (iii) the use of fixed column base makes the bridge response independent of soil-pile interaction. Therefore, ADRS curves generated for South Carolina conditions could be used for a bridge model that has been borrowed from the West Coast of US without misrepresenting the subsurface soil-pile conditions. In a later part of this chapter, the same bridge was modeled with foundation springs to evaluate the effect of using foundation springs instead of fixed supports. Thus addressing both of the 'with' and 'without' spring modeling approaches helps covering the interest of a wide range of practicing community. However, in this sub-section, discussion is limited to the modeling of the bridge using fixed support. Modeling with foundation springs will be discussed under a parametric study section (Section 6.7.1) to show the effect of support conditions in the computed responses.

Figure 6.5 presents the details of an interior bent including all its frame elements assumed for the SAP2000 model used in the LRFD example (ATC/MCEER 2003a). This configuration was used to develop the actual bridge model for this study. The model used for this study is presented in Figures 6.6 and 6.7. Figure 6.6 presents a similar bent as drawn in Figure 6.5 modeled in SAP2000, showing the elements and node numbers referred to in this study. Figure 6.7 presents the 3-D frame or 'spine' model of the bridge developed in SAP2000 using fixed base condition.

As is seen in the Figures 6.5, 6.6 and 6.7, the bridge deck section is represented with a straight line consisting of frame elements and individual elements are assigned for the other components of the structure (i.e., cross-beams and columns). For the deck, four elements per span are provided while for the columns, three elements which covers the entire length as required by SCDOT (2008b) are used. Both the column tops are connected to the cap beam element using rigid links. The bottom nodes of the seal elements are connected to the node with

springs by using the rigid link elements again. The only difference from the bent model presented in Figure 6.5 to the model in Figure 6.6 are: the model in Figure 6.6 skips the elements representing the pile cap, the seal element, the rigid link connecting the two columns with the foundation springs and obviously the foundation springs. Rather, the column bases are restrained for displacements at all directions (fixed base) as shown in Figure 6.6.

Necessary frame member properties (i.e. cross-sectional area, density and inertias) in all three directions are listed in Table 6.4 which was directly adopted from the LRFD guideline's design example. Also adopted from the example were the total dead load including the self-weight, which was 2.35 kips per linear foot of superstructure, and a foundation spring stiffness of 375 kips/ft, which was used to model the backfill at each of the abutments.

Table 6.4 Section properties for the LRFD Example Bridge model (ATC/MCEER 2003a).

Properties	Structural Elements				
	Bridge Deck	Bent Cap Beam	Bent Columns	Pile Caps	Seals
Cross sectional area (ft^2)	72	27	12.57	506	196
Moment of inertia in Global X direction, I_X (ft^4)	1,177	10,000	5	109,634	6,403
Moment of inertia in Global Y direction, I_Y (ft^4)	401	10,000	5	89225	89225
Moment of inertia in Global Z direction, I_Z (ft^4)	9,697	10,000	10	20,409	20,409
Density (lb/ft^3)	180	150	150	150	140

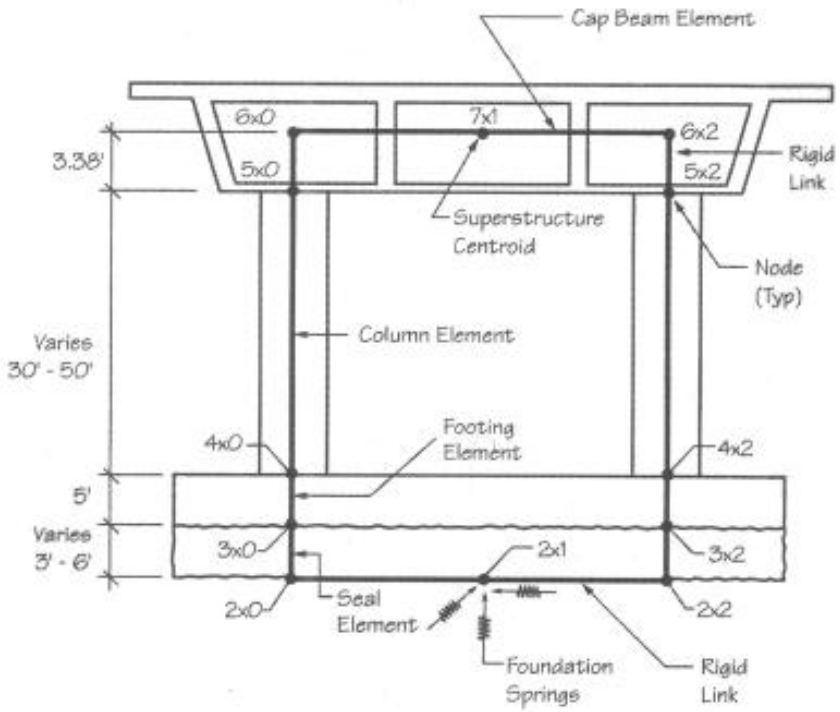

Figure 6.5 Intermediate bent details in the model with foundation springs of LRFD Example Bridge (ATC/MCEER 2003a).

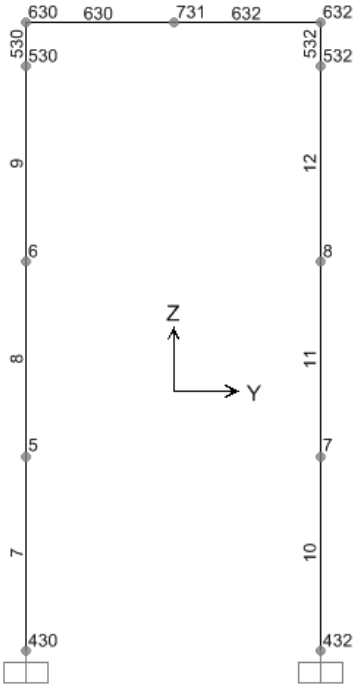

Figure 6.6 Intermediate bent details with frame elements and joint numbers in the case of fixed column base for a sample bent of LRFD Example Bridge (screen capture of SAP2000 model).

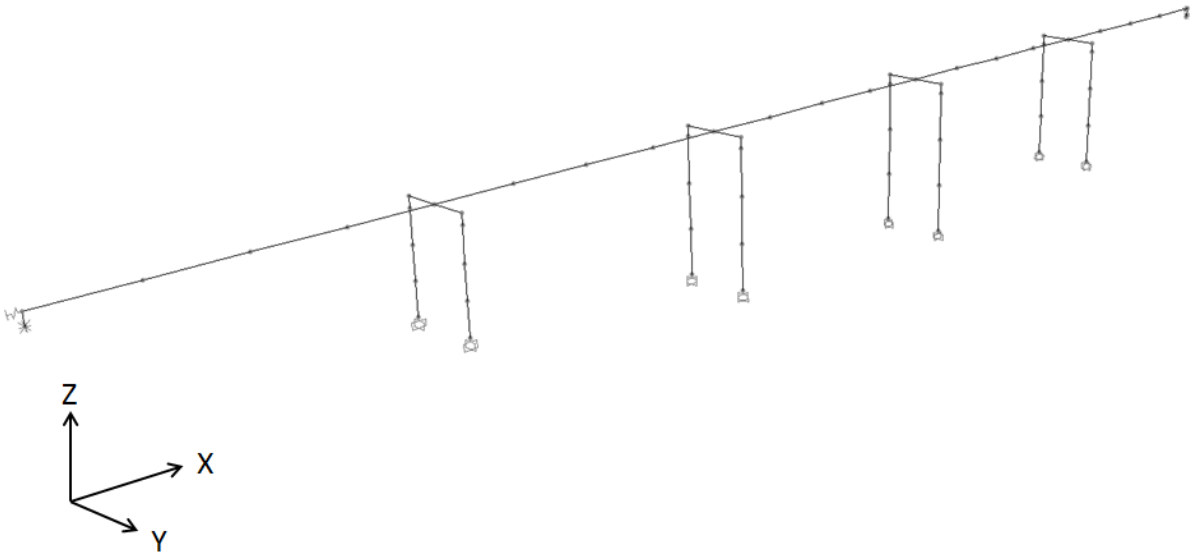

Figure 6.7 Three-dimensional 'spine' model of the bridge in the case of fixed column base of LRFD Example Bridge (screen capture of SAP2000 model).

Readers are suggested to visit the original design example in the LRFD guidelines (ATC/MCEER 2003a) for further information about the bridge system and the modeling technique.

6.4 LRFD Example Bridge Analysis Procedure

Multi-Modal Response Spectral (MMRS) analysis is selected for this study. The analysis is performed according to the procedure described in LRFD bridge design specification (ATC/MCEER 2003b) and also meets the requirements defined in the SCDOT Seismic Design Specification of Highway Bridges (SCDOT 2008b). Because this method considers a wide band of spectral period by producing different structural modes with different periods, the effect of using different ADRS curves will be determined for a broad range of spectral periods.

The major steps of the MMRS analysis procedure are presented below.

Step 1: By performing modal analysis of the entire structure, the mode shapes, corresponding periods and the mass participations are determined. The total mass participation should be above

90% for the considered number of modes. From this requirement, the required number of modes for modal analysis is determined.

Step 2: Using the periods obtained from previous step, corresponding spectral acceleration values are obtained using the ADRS curve that were defined for this analysis. These accelerations are then multiplied with the corresponding mass contributions to calculate the base shears of the different modes.

Step 3: Base shears from all the modes are then combined using several statistical sums and applied at the base of the structure for the seismic analysis of the structure which is a static type analysis in this case.

In MMRS analysis, structural modes of vibrations are estimated in two directions: longitudinal (global X direction) and transverse (global Y direction). Then the Complete Quadratic Combination (CQC) rule was applied to combine the different modal responses and to estimate the 'enveloping' response of the structural components: EQ_{LONG} (for longitudinal direction) and EQ_{TRANS} (for transverse direction). Responses from these two directions are then further combined using the 100%-30% rule (SCDOT 2008b) to generate the load or displacement combinations to aid in estimating seismic design demands over the structure. The 100%-30% combination rule is defined as:

Table 6.5 Cases considered for the comparison between the AASHTO (2011a) model and the recommended model.

Case #	Foundation Type	ADRS curve generation	
		ADRS curve used	Site class considered
1	Fixed	I and IV	C[(1)] with V_{S100ft}= 1263 ft/s
2	Fixed	II and V	D[(2)] with V_{S100ft}= 962 ft/s
3	Fixed	II and VI	Maximum possible ADRS curve within Site Class D
4	Fixed	III and VII	E[(3)] with V_{S100ft}= 600 ft/s

(1) Site Class C is ranging from 1,200 to 2,500 ft/s
(2) Site Class D is ranging from 600 to 1,200 ft/s
(3) Site Class E is ranging from 0 to 600 ft/s

Load Case 1 or LC1= 100% of EQ_{LONG}+ 30% of EQ_{TRANS}

Load Case 2 or LC2= 30% of EQ_{LONG}+ 100% of EQ_{TRANS}

These LC1 and LC2 are calculated and compared between desired cases for all the intermediate bent columns at the top and bottom positions. This entire process (from model generation to the calculation of LC1 and LC2) is done through a single run with SAP2000.

Table 6.5 presents the cases considered in estimating the repercussions of the new site coefficient model. The bridge model developed in Section 6.3.3 with fixed column base-type is selected as was discussed earlier (Section 6.3.3). The recommended site coefficient model used to generate ADRS curves IV, V, VI and VII were applied on the structure and the analysis outcomes are compared with those from the respective AASHTO (2011a) ADRS curves I, II and III.

6.5 LRFD Example Bridge Analysis Results

The complete analysis results in terms of forces, moments and displacements at all the columns for cases 1-4 are presented in tabular and graphical formats in the Appendix J. In this section, selected structural responses are reported and compared.

Tables J.1 and J.2 in Appendix J present the natural periods of vibrations and the corresponding mass participations for the first 40 modes (including longitudinal and transverse vibration) for the bridge model with the fixed base and with foundation springs, respectively. For both models, the cumulative mass participation attained above 90% in both directions which is the minimum requirement according to both ATC/MCEER (2003b) and SCDOT (2008b).

Column forces, moments and displacements in longitudinal (global X direction) and transverse (global Y direction) directions are obtained for the load and displacement combinations LC1 and LC2. The AASHTO and the recommended cases are compared in terms of percentage differences in structural response for LC1 and LC2 at the column top and bottom positions and at all the bents and are presented both graphically and tabular format. This section and Appendix J jointly present all the tables and necessary figures oriented to all of these analyses cases this study involved.

Now the analyses outcomes from the four cases (listed in Table 6.5) oriented to the comparison between the AASHTO (2011a) and the recommended model will be presented. For Case#1, all the analysis outcomes and comparisons are presented in tabular format in the Appendix J in Tables J.3 through J.8. Table J.3 presents analyses results for a case when the

seismic loading was applied in the longitudinal direction (EQ_{LONG}) which includes the forces -Shear X, -Shear Y (Shear in Global X and Y directions, respectively), axial, moments -Moment X, -Moment Y (Moments with respect to the Global X and Y axes, respectively) at all the column tops and bottoms. Table J.4 presents analyses results for transverse (global Y direction) directional loading (EQ_{TRANS}) and Table J.5 presents displacements (both global X and Y directional) for both of the EQ_{LONG} and EQ_{TRANS} loadings. Tables J.6 and J.7 present the comparison between analyses results (forces and moments) estimated from AASHTO (2011a) and recommended models with respect to the load combinations LC1 and LC2 and their percentage differences for all the column tops and bottoms, respectively. In Tables J.8, the comparison between displacements from AASHTO (2011a) and recommended models with respect to the load combinations LC1 and LC2 (and also by stating their percentage differences) for all the column top positions are presented.

Presented in the Figure J.1 is the comparison between AASHTO (2011a) and recommended model outcomes such as axial force, shear force, and bending moment in the form of percentage difference for load combinations LC1 and LC2 (in the sub-figures – (a) and (b)). Since the observed differences in the forces and moments (as reported in Tables J.6 and J.7) at the column top and bottom are identical, so only the differences at the column top are presented in Figure J.1 in Appendix J. Similarly, comparison with respect to the difference in computed displacements at the column top of all four bents for load combinations LC1 and LC2 is compared in Figure 6.8. Displacement is a better parameter than force or moment to illustrate the difference in structural responses estimated by two different ADRS curves. A summary table (Table 6.6) for Case #1 showing the estimated forces and moments and their percentage differences at the column top for load combinations LC1 and LC2 is included in this chapter for discussion purposes. As is seen, the difference is -11 to -9% (negative percentage denotes higher AASHTO 2011a outcome) for Site Class C between the AASHTO (2011a) and recommended model.

Similar tables and figures comparing the analysis results for Case #2 (Tables J.9-J.14 and Figure J.2), #3 (Tables J.15-J.20 and Figure J.3) and #4 (Tables J.21-J.26) and Figure J.4) are included in Appendix J. Figures showing the percentage difference in displacements at the column top of all four bents for load combinations LC1 and LC2 are presented in Figures 6.9, 6.10 and 6.11 for Case #2, #3 and #4, respectively.

Table 6.6 Sample analyses results from Case#1 with two directional combinations of the forces and moments: the LC1 and LC2- at the column tops of all the bents.

		FORCES AND MOMENTS- COLUMN TOPS														
		Longitudinal (Global X direction)						Transverse (Global Y direction)						Axial (kips)		
		Shear X (kips)			Moment Y (kips-ft)			Shear Z (kips)			Moment X (kips-ft)					
Support/ Location	Load Case	AASHTO (2011a)	Rec.	Difference (%)*	AASHTO (2011a)	Rec.	Difference (%)*	AASHTO (2011a)	Rec.	Difference (%)*	AASHTO (2011a)	Rec.	Difference (%)*	AASHTO (2011a)	Rec.	Difference (%)*
Bent 1 Col	LC1	345	308	-10.56	5183	4636	-10.56	44	40	-10.53	668	597	-10.55	90	81	-10.44
	LC2	123	110	-10.47	1848	1655	-10.45	148	132	-10.56	2225	1990	-10.56	236	211	-10.55
Bent 2 Col	LC1	102	91	-10.37	2326	2081	-10.53	31	28	-10.35	699	625	-10.53	100	90	-10.39
	LC2	40	36	-10.33	917	820	-10.50	103	92	-10.36	2330	2084	-10.53	241	216	-10.51
Bent 3 Col	LC1	72	65	-10.08	1843	1650	-10.49	33	29	-10.46	837	748	-10.55	86	77	-10.30
	LC2	25	22	-9.48	628	563	-10.37	110	98	-10.46	2789	2495	-10.55	271	242	-10.53
Bent 4 Col	LC1	102	91	-10.33	2328	2083	-10.52	33	30	-10.36	760	680	-10.53	86	77	-10.25
	LC2	40	36	-10.01	908	813	-10.43	111	100	-10.37	2532	2265	-10.54	246	220	-10.50

* % Difference (in column Forces, Moments or Displacement combinations: LC1 and LC2) = [Recommended- AASHTO (2011a)] X 100/ AASHTO (2011a). A negative value represents greater AASHTO (2011a) outcomes.

Rec.: Based on ADRS curves developed using the recommended site coefficients.

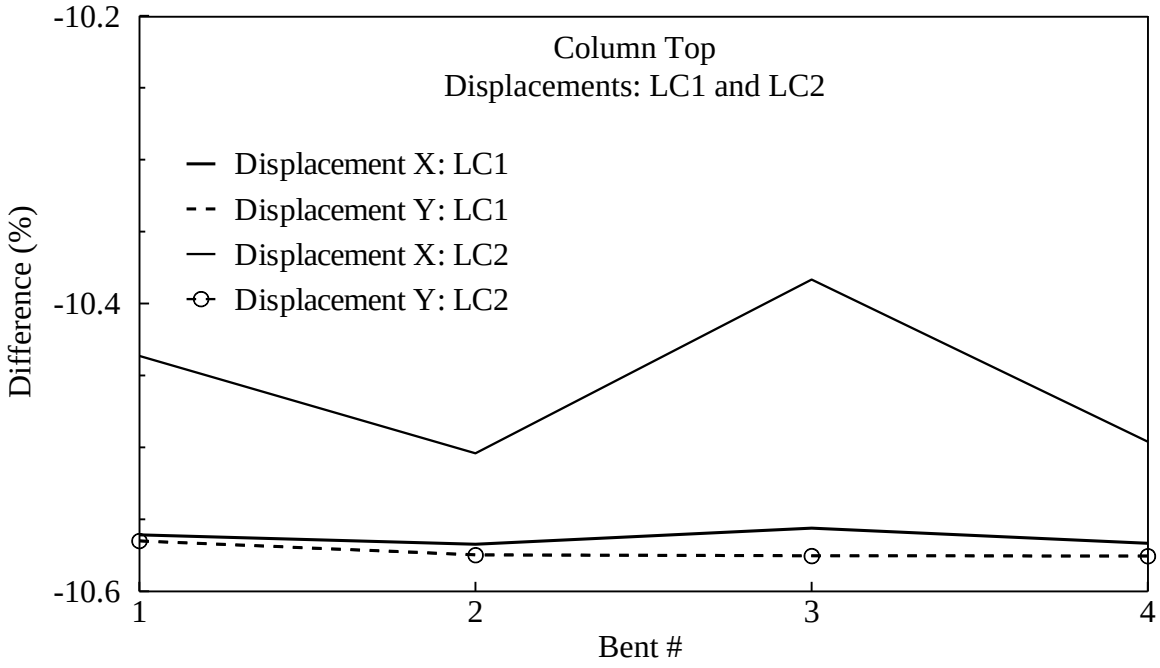

Figure 6.8 Comparison (% difference between AASHTO 2011a and recommended) of displacements (Disp. -X and Disp. -Y) from Case#1 in all four bent columns at the top position with load cases LC1 and LC2.

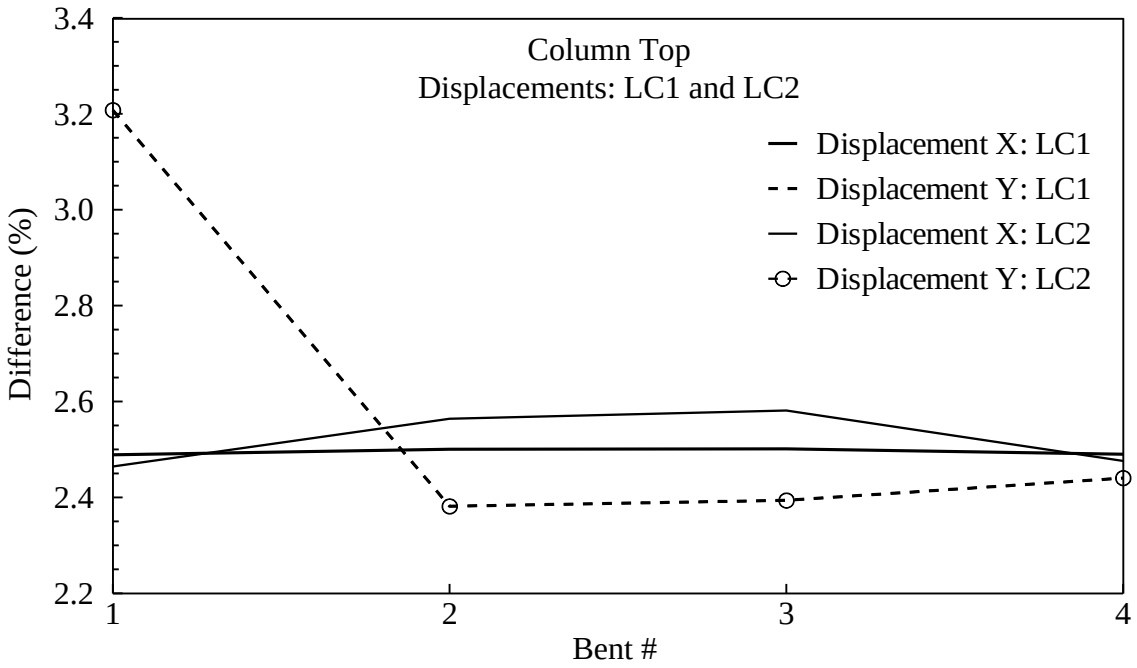

Figure 6.9 Comparison (% difference between AASHTO 2011a and recommended) of displacements (Disp. -X and Disp. -Y) from Case#2 in all four bent columns at the top position with LC1 and LC2 load cases.

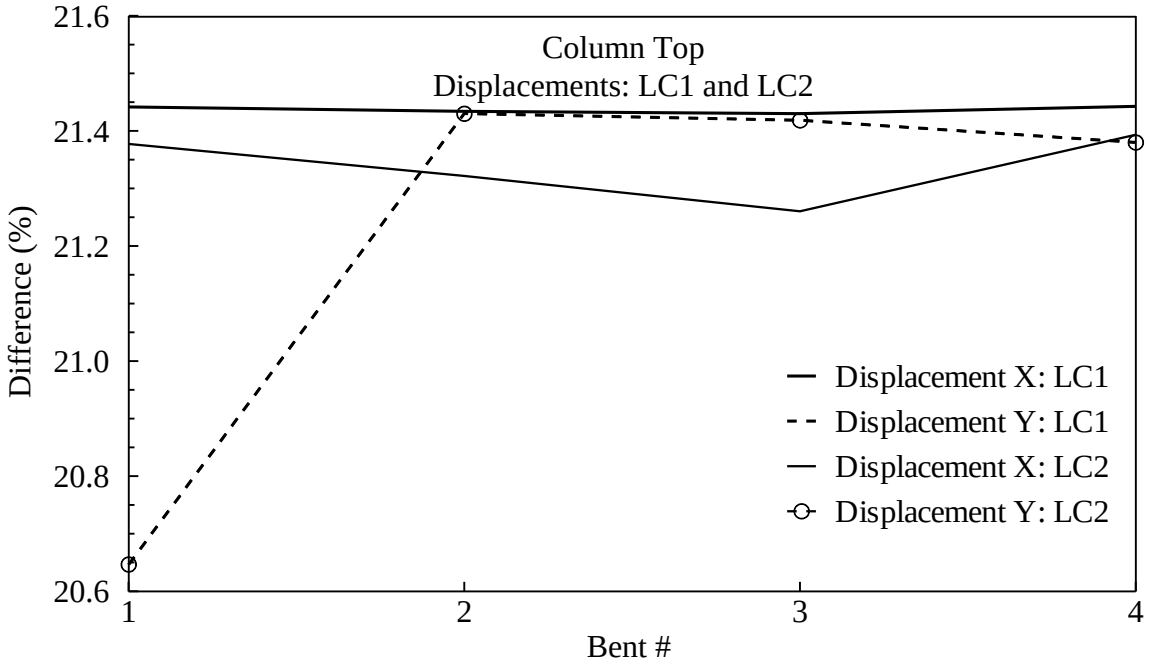

Figure 6.10 Comparison (% difference between AASHTO 2011a and recommended) of displacements (Disp. -X and Disp. -Y) from Case#3 in all four bent columns at the top position with LC1 and LC2 load cases.

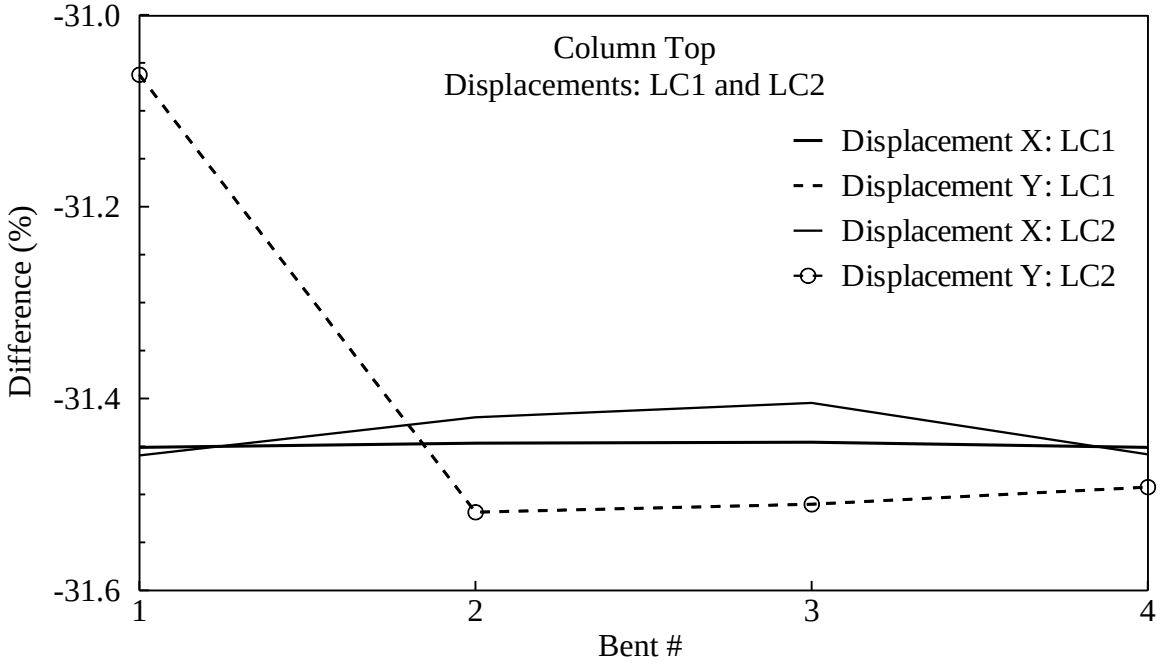

Figure 6.11 Comparison (% difference between AASHTO 2011a and recommended) of displacements (Disp. -X and Disp. -Y) from Case#4 in all four bent columns at the top position with LC1 and LC2 load cases.

6.6 Discussion

The overall percentage differences (for LC1 and LC2) between the AASHTO (2011a) and the recommended model obtained from the results presented in Section 6.5 are summarized in Table 6.7 for deriving the general conclusion. For Case#1, the differences in the column outcomes predicted with the recommended and the AASHTO (2011a) ADRS curves are between 9 and 11%; with AASHTO (2011a) predicting conservative design (e.g. see displacement differences in Figure 6.8). The AASHTO (2011a) ADRS curve fall above the recommended ADRS curve at periods higher than approximately 0.5 s, as reported earlier (see Figure 6.1). Since the first few modes of vibration of the LRFD design bridge have frequencies greater than 0.5 s and those modes cover the largest share in mass participation in the analysis (see Table J.1), the AASHTO (2011a) outcomes are higher than that of the recommended outcomes. For Case#2, all the column outcomes predicted with the recommended ADRS curve are only 2-3% higher than that predicted from the AASHTO (2011a) ADRS curve (e.g. see displacement differences in Figure 6.9). Such an observation is expected since the recommended and the AASHTO (2011a) ADRS curves corresponding to the profile with V_{S100ft} of 961 ft/s (Site Class D) are nearly identical (see Figure 6.1). In Case#3, which compares the maximum possible recommended ADRS curve within Site Class D with the AASHTO (2011a) Site Class D curve, the difference is 20-22% (e.g. see displacement differences in Figure 6.10). This comparison suggests that the design forces/displacements computed using the recommended curves can be up to 22% higher than the forces/displacements computed using the AASHTO (2011a) curves for similar transportation structures in SCCP (e.g., Charleston).

For Case#4, the AASHTO (2011a) and the recommended ADRS curves for Site Class E are compared. Because the design spectral acceleration for Site Class E is much higher for the AASHTO ADRS than that of the recommended, the predicted column outcomes are about 31% lower for the recommended ADRS curve (e.g. see displacement differences in Figure 6.11). Thus more economical design is expected in Site Class E for SCCP locations using the recommended site coefficient models.

Table 6.7 Generalized comparison results between the AASHTO (2011a) model and the recommended model based on column forces, moments or displacement combinations LC1 and LC2.

Case #	Foundation Type	ADRS curve generation		% Difference[4] with AASHTO (2011a) (Approximate)
		ADRS curve used	Site class considered	
1	Fixed	I and IV	C[1] with V_{S100ft}= 1,263 ft/s	-11 to -9%
2	Fixed	II and V	D[2] with V_{S100ft}= 962 ft/s	2 to 3%
3	Fixed	II and VI	Maximum possible ADRS curve within Site Class D	20 to 22%
4	Fixed	III and VII	E[3] with V_{S100ft}= 600 ft/s	-31%

(1) Site Class C is ranging from 1200 to 2,500 ft/s
(2) Site Class D is ranging from 600 to 1,200 ft/s
(3) Site Class E is ranging from 0 to 600 ft/s
(4) % Difference (in column Forces, Moments or Displacement combinations: LC1 and LC2) = [Recommended- AASHTO (2011a)] X 100/ AASHTO (2011a). A negative value represents greater AASHTO (2011a) outcomes.

6.7 Parametric Study

Parametric studies are performed in this section to investigate the effect of different techniques that can be used to model the bridge foundation in SAP2000. Discussed in this section are: adjustments made to the previous bridge model to convert the foundation system to springs; development of a set of parametric test cases; and finally presented are the parametric study outcomes and related discussions.

6.7.1 Addition of Foundation Springs

This time the same bridge (developed in Section 6.3.3) is taken and the fixed column bases are modified to include the foundations springs. This modeling modification of the same three dimensional bridge system in SAP2000 is described in this sub-section.

To include spring elements in the bridge model, the procedure described in the LRFD example (ATC/MCEER 2003a) is followed. As discussed in the Section 6.3.3 and also presented in Figure 6.5, all the required elements are added to the existing SAP2000 model systematically. First, all the restraints at the foundation base nodes are removed, then the elements representing the pile cap and foundation seal are introduced, and finally the seal elements are connected by rigid links to a node to which all the foundation springs are then attached. The foundation springs consist of three translational and three rotational springs. Figure 6.12 presents an interior bent modeled in SAP2000 environment with foundation springs and Figure 6.13 shows the whole 3-D frame or 'spine' model of the bridge including the foundation springs with their directions. The frame member properties (for the added frame member also) are presented in Tables 6.3 and 6.4 while the foundation spring stiffness properties are listed in Table 6.8, which were directly adopted from the LRFD guideline's design example (ATC/MCEER 2003a). Readers are suggested to visit the original design example in the LRFD guidelines (ATC/MCEER 2003a) for further information about the bridge system and modeling technique.

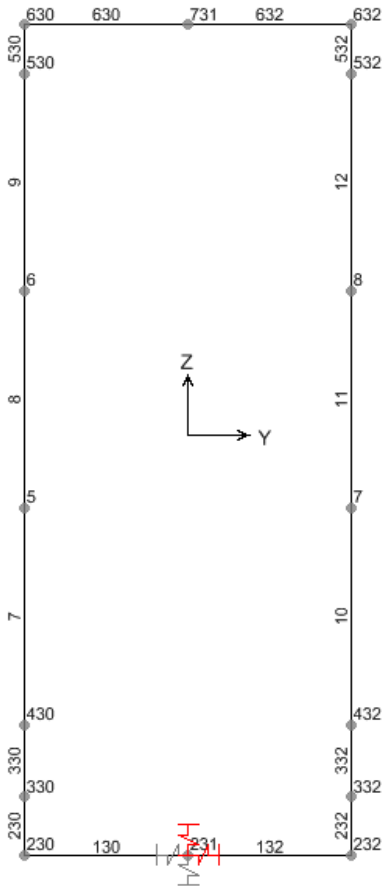

Figure 6.12 Intermediate bent details with frame elements and joint numbers with foundation springs for a sample bent (screen capture of SAP2000 model).

Table 6.8 Foundation spring stiffness.

	Translational stiffness			Rotational stiffness		
	Axial	Longitudinal	Lateral	Axial	Longitudinal	Lateral
Global	UY	UX	UZ	RY	RX	RZ
Pier #	K_{11} (k/ft)	K_{22} (k/ft)	K_{33} (k/ft)	K_{44} (k-ft/rad)	K_{55} (k-ft/rad)	K_{66} (k-ft/rad)
1	7.30E+04	0.00E+00	1.60E+05	0.00E+00	2.99E+07	0.00E+00
2	3.21E+05	3.33E+05	2.47E+05	1.19E+07	4.74E+07	1.19E+09
3	3.31E+05	3.43E+05	2.73E+05	1.31E+07	5.24E+07	1.23E+09
4	4.47E+05	4.59E+05	2.86E+05	1.37E+07	5.50E+07	1.68E+09
5	3.31E+05	3.43E+05	2.73E+05	1.31E+07	5.24E+07	1.23E+09
6	7.30E+04	0.00E+00	1.60E+05	0.00E+00	2.99E+07	0.00E+00

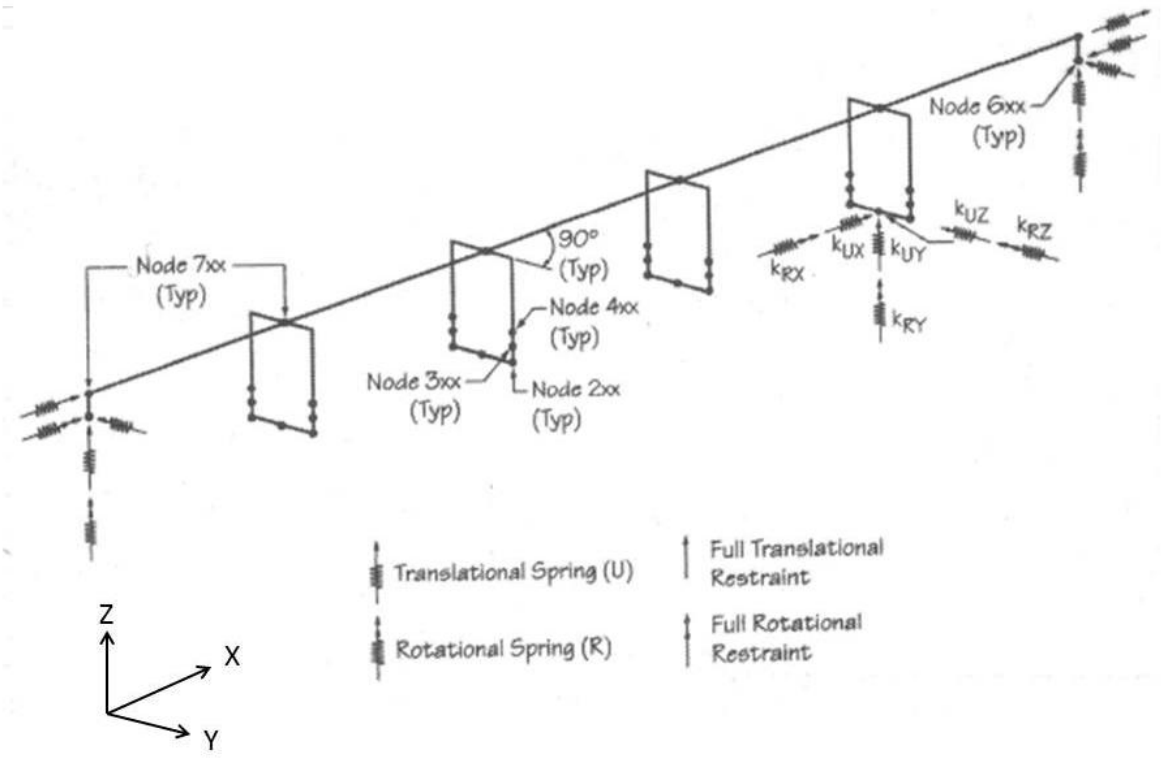

Figure 6.13 Three-dimensional 'spine' model of the bridge in the case of model with foundation spring directions (ATC/MCEER 2003a).

6.7.2 Test Cases Considered

The numerical test cases considered in this section are presented in Table 6.9. The objective of these tests was to study the effect of using foundation springs instead of fixed base in the analysis. The ADRS curves used for the parametric studies are: IV, V, VI and VII. These ADRS curves are applied on both bridge models (with fixed support and with foundation springs) and the responses are compared. The numerical tests corresponding to these four ADRS curves are referred to as Test # 1, 2, 3 and 4, respectively. The site class and the V_{S100ft} used for developing corresponding ADRS curves are shown in Table 6.9. It is worth noting that: (i) both 'with' and 'without' spring bridge models are subjected to the ADRS curves developed considering typical V_{S100ft} values for corresponding site classes and (ii) the foundation springs are adopted from the LRFD guideline's design example (ATC/MCEER 2003a) which are developed for a different site (the Puget Sound region of Washington State). Therefore, the conclusions made based on the responses computed 'with' spring bridge model in this study are expected to have a bias.

Table 6.9 Parametric study test cases.

Test #	Parameters considered in the compared cases					
	Case #1			Case #2		
	Foundation Type	ADRS curve generation		Foundation Type	ADRS curve generation	
		ADRS curve used	Site class considered		ADRS curve used	Site class considered
1	Fixed	IV	C[(1)] with V_{S100ft}= 1,263 ft/s	Foundation Springs	IV	C[(1)] with V_{S100ft}= 1,263 ft/s
2	Fixed	V	D[(2)] with V_{S100ft}= 962 ft/s	Foundation Springs	V	D[(2)] with V_{S100ft}= 962 ft/s
3	Fixed	VI	Maximum possible ADRS curve within Site Class D	Foundation Springs	VI	Maximum possible ADRS curve within Site Class D
4	Fixed	VII	E[(3)] with V_{S100ft}= 600 ft/s	Foundation Springs	VII	E[(3)] with V_{S100ft}= 600 ft/s

(1) Site Class C is ranging from 1,200 to 2,500 ft/s
(2) Site Class D is ranging from 600 to 1,200 ft/s
(3) Site Class E is ranging from 0 to 600 ft/s

6.7.3 Parametric Study Results

This sub-section presents the parametric study (test cases presented in Table 6.9) outcomes. The natural periods of vibrations and the corresponding mass participations for the first 40 modes (including longitudinal and transverse vibration) for the bridge model described in Section 6.7.1 is presented in Table J.2 in Appendix J. The cumulative mass participation attained is above 90% in both directions which is the minimum requirement according to both ATC/MCEER (2003b) and SCDOT (2008b).

For each analysis, column forces (Shear X, Shear Y and Axial), moments (Moments X and Moment Y) and displacements in longitudinal (global X-direction) and transverse (global Y-direction) directions are obtained with the load and displacement combinations LC1 and LC2. The foundation spring model is compared to the fixed support model in terms of the percentage difference in the column forces and moments at the column top and bottom positions and the displacement at the column top position only, at each bent and for each of the load cases LC1 and LC2. Typical results are presented in Figures 6.14 and 6.15 which show the percentage difference in displacements at the column tops at all four bents for load combinations LC1 and LC2 for numerical Tests #1 and #2, respectively. The complete results from this parametric study are presented in Tables J.27-J32 and Figure J.5 for Test#1, in Tables J.33-J.38 and Figures J.6 and J.7 for Test#2, in Tables J.39-J.44 and Figures J.8 and J.9 for Test #3, and Tables J.45-J.50 and Figures J.10 and J.11 for Test #4 of Appendix J.

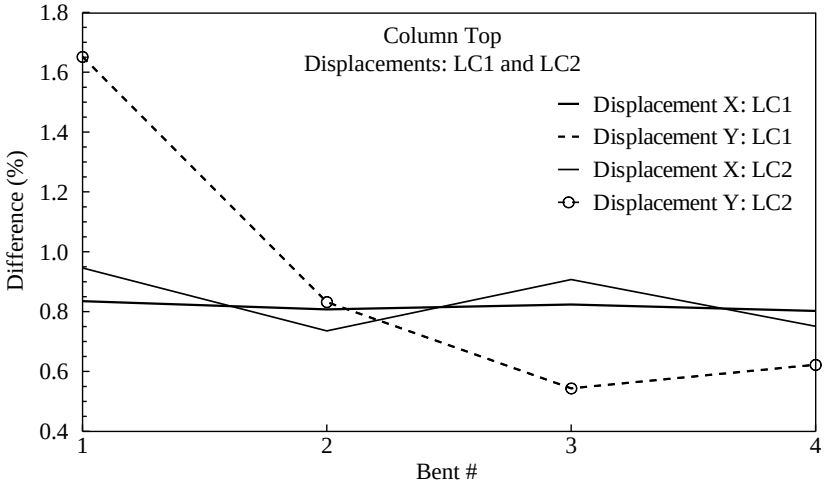

Figure 6.14 Comparison (% difference between 'Fixed base' and 'Foundation springs' conditions) of displacements (Disp. -X and Disp. -Y) from Test#1 in all four bent columns at the top locations with LC1 and LC2 load cases.

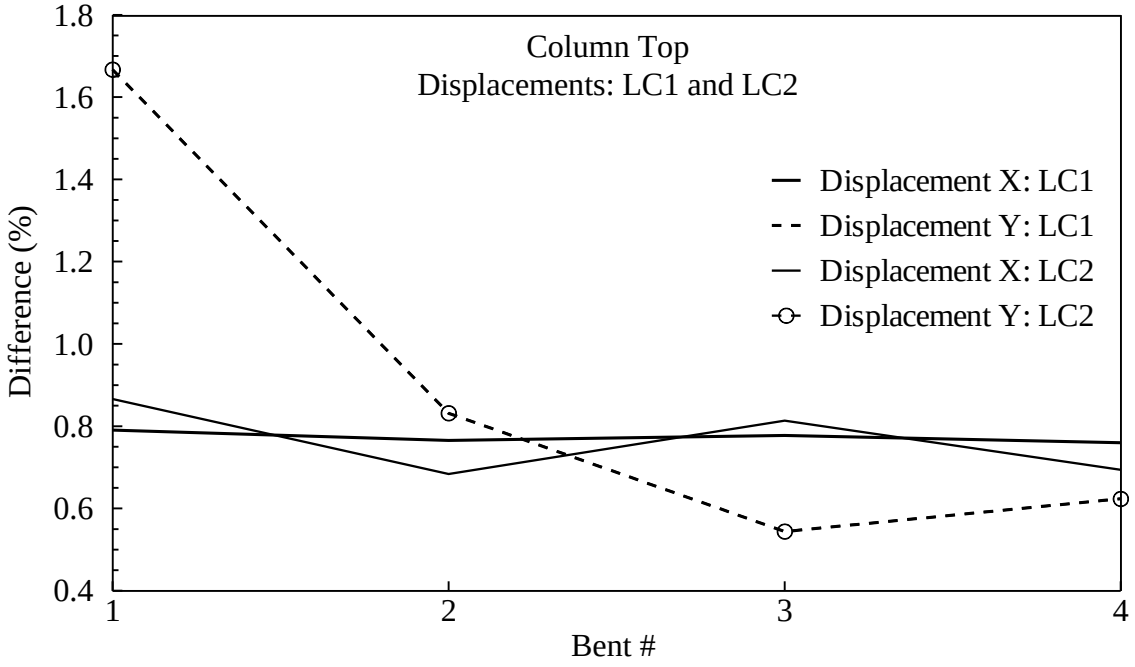

Figure 6.15 Comparison (% difference between 'Fixed base' and 'Foundation springs' conditions) of displacements (Disp. -X and Disp. -Y) from Test#2 in all four bent columns at the top locations with LC1 and LC2 load cases.

6.7.4 Discussion on Parametric Study

Summarized in Table 6.10 are the approximate ranges of percentage difference in column response (force, moment and displacement) for all four numerical tests. The percentage difference values indicate the sensitivity of the MMRS analysis outcomes to the foundation type and support condition (i.e., comparison between the cases with fixed column bases and the cases with foundation springs). For the Tests #1- #4, the differences in the computed outcomes are between -6.0 and 7.5% for the combinations LC1 and LC2 which indicates that the computed responses are less sensitive to the support condition of the columns for the loading and soil conditions considered in this study. Therefore, the simplified approach (fixed column base) used in this study gives reasonable results.

Table 6.10 Parametric study results. Comparison was done based on column forces, moments or displacement combinations i.e. LC1 and LC2.

Test #	Parameters considered in the compared cases						% Difference[3] between Case #1 and Case #2 (Approx.)
	Case #1			Case #2			
	Foundation Type	ADRS curve generation		Foundation Type	ADRS curve generation		
		ADRS curve used	Site class considered		ADRS curve used	Site class considered	
1	Fixed	IV	C[1] with V_{S100ft}= 1,263 ft/s	Foundation Springs	IV	C[1] with V_{S100ft}= 1,263 ft/s	-5.5 to 7.5%
2	Fixed	V	D[2] with V_{S100ft}= 962 ft/s	Foundation Springs	V	D[2] with V_{S100ft}= 962 ft/s	-6 to 6%
3	Fixed	VI	Maximum possible ADRS curve within Site Class D	Foundation Springs	VI	Maximum possible ADRS curve within Site Class D	-6 to 4%
4	Fixed	VII	E[3] with V_{S100ft}= 600 ft/s	Foundation Springs	VII	E[3] with V_{S100ft}= 600 ft/s	-6 to 2%

(1) Site Class C is ranging from 1,200 to 2,500 ft/s
(2) Site Class D is ranging from 600 to 1,200 ft/s
(3) Site Class E is ranging from 0 to 600 ft/s
(4) % Difference (in column Forces, Moments or Displacement combinations: LC1 and LC2) = [Case #2- Case #1] X 100/ Case #1. A negative value represents greater Case #2 outcomes.

6.8 Russell Creek Bridge Analysis

This section covers the analysis of a 510 ft long concrete I-Girder bridge, the Russell Creek Bridge, in Charleston County. This to-be-built highway structure on SC 174 will be constructed over the Russell Creek River. A CSiBridge model of Russell Creek Bridge developed by SCDOT engineers during its design phase was adopted in this study to perform MMRS analysis. The analysis results obtained by applying the ADRS curves generated using the AASHTO (2011a) and the recommended coefficients are compared.

6.8.1 Generation of ADRS Curves for Russell Creek Bridge Analysis

During the design phase of the Russell Creek Bridge, the ADRS curves corresponding to the FEE and SEE motions based on AASHTO (2011a) site coefficients were generated and used. Figure 6.16 presents the 'Design' (AASHTO 2011a coefficients) and recommended (based on Chapter 3) ADRS curves based on factors for both FEE and SEE cases and used in this study (Figure 6.16). Table 6.11 presents the spectral accelerations ($PGA_{B\text{-}C}$, S_S and S_1) and the site coefficients (F_{PGA}, F_a and F_v) corresponding to 0, 0.2 and 1.0 s periods, respectively, from which ADRS curves were generated. This bridge site has a measured average shear wave velocity in the upper 100ft (V_{S100ft}) of 715 ft/s which indicates the bridge site is in Site Class D (SCDOT 2008a). Point to be noted, the site coefficients from the recommended model were generated based on the equations (corresponding to the site V_{S100ft}) presented in Chapter 3 rather than using the tabulated values from Chapter 5 (Tables 5.2, 5.9 and 5.14). As is seen in Figure 6.16, in the case of FEE motions, the both the 'Design' and recommended lines are close to each other over the entire period range. On the other hand, in the case of SEE motions, the 'Design' line is much higher than the recommended counterpart.

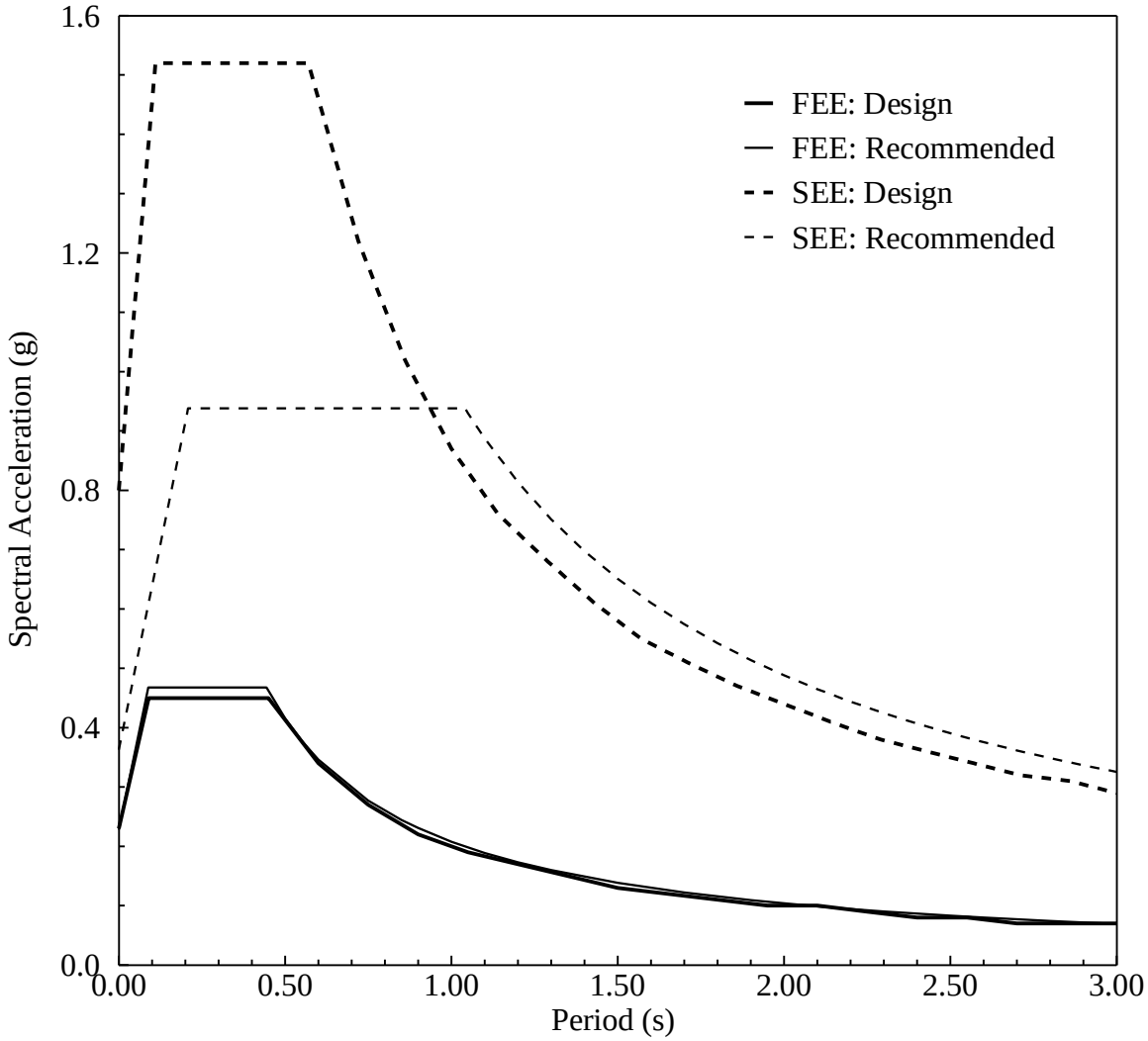

Figure 6.16 ADRS curves used for Russell Creek Bridge.

Table 6.11 Required parameters to generate site coefficients.

ADRS #	Type	V_{S100ft} (Site Class)	Spectral accelerations at B-C boundary			Site coefficients		
			PGA_{B-C}	S_S	S_1	F_{PGA}	F_a	F_v
1	FEE: Design	715 ft/s (Site Class: D)	0.152	0.288	0.084	1.515	1.560	2.400
2	FEE: Recommended					1.503	1.622	2.474
3	SEE: Design		0.803	1.522	0.581	1.000	1.000	1.500
4	SEE: Recommended					0.452	0.616	1.681

6.8.2 Problem Description

A schematic diagram and cross section of the Russell Creek Bridge are shown in Figures 6.17 and 6.18, respectively. The bridge is a concrete I-Girder bridge with 10 spans supported on 9 intermediate bents and pile-bent type abutments at both ends. Span length varies from 45 ft to 55 ft. The bents consist of 3 to 7 concrete piles. Bents #1 through #8 have 7 piles made of 24 inch (square) pre-stressed concrete while Bent #9 and the abutments are supported by 3 drilled shafts of 42 inch diameter. Table 6.12 presents the interior bent details including the pile lengths. Bridge I-Girders are integrated with the deck slab above. The super-structure dead load is transmitted to the piles through the bent cap beams on which the I-Girders are supported through the bearings. These elastomeric type bearings are assigned fixity for translations and rotations in all directions at the abutments while at the interior bents only rotations are allowed.

Table 6.12 Bent details of Russell Creek Bridge.

Bent #	Pile length (ft)	Number of Piles in the bent
1	32.0	7
2	31.9	7
3	32.9	7
4	33.3	7
5	33.8	7
6	33.8	7
7	33.0	7
8	32.3	7
9	46.5	3 (Drilled shaft)

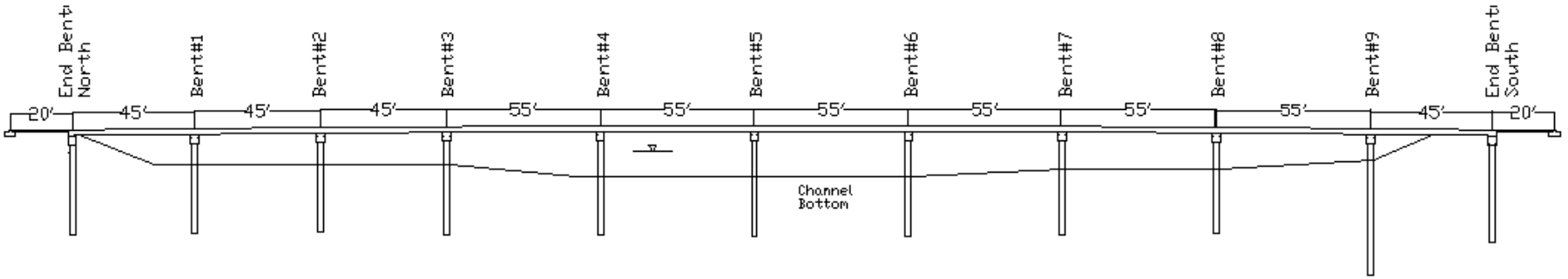

Figure 6.17 Schematic diagram of Russell Creek Bridge.

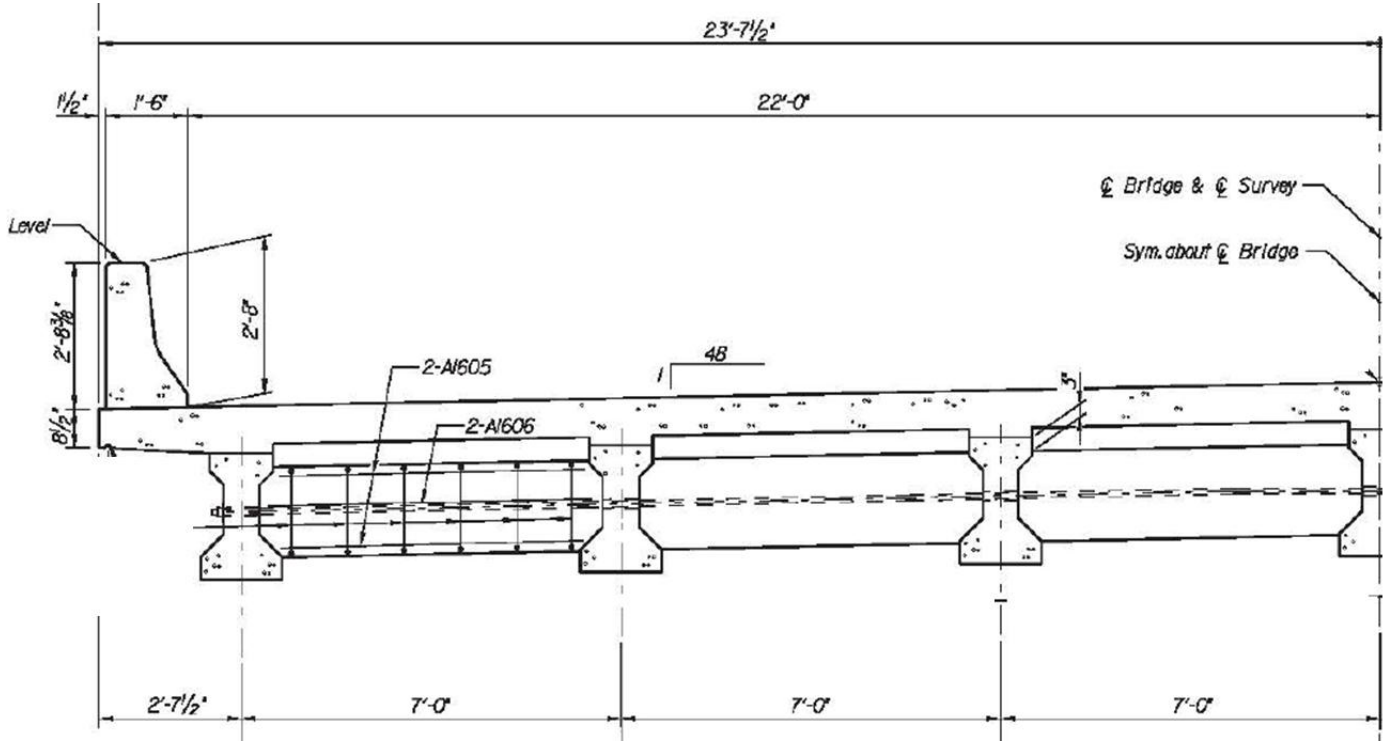

Figure 6.18 Russell Creek Bridge deck cross-section at an interior bent.

6.8.3 Analysis Tool and Model Generation

CSiBridge, a special purpose software for modeling, analysis, and design of bridges, is used to analyze the Russell Creek Bridge as the original analyses of this bridge is also conducted using CSiBridge before constructing it. This software is widely used by practicing engineers, including the SCDOT.

Figures 6.19 and 6.20 present the intermediate bent details and 3-D model of the bridge in CSiBridge, respectively. In the 3-D spine model in Figure 6.20, the bridge deck including the I-Girders are represented by the bridge layout line (layout lines define the bridge alignments in CSiBridge) made of frame elements which extend longitudinally in the global X direction. As shown in Figure 6.19, the girder bottom is resting on the bearings placed on top of the bent cap beams (see Figure 6.19). The cap beam is represented by frame elements and is connected to the bearings by rigid links. At the bents, piles are represented with frame elements with fixed bases. All the frame member properties such as cross-sectional area, density and inertias in all three directions of the girder, cap, beam and the pile sections are listed in Table 6.13.

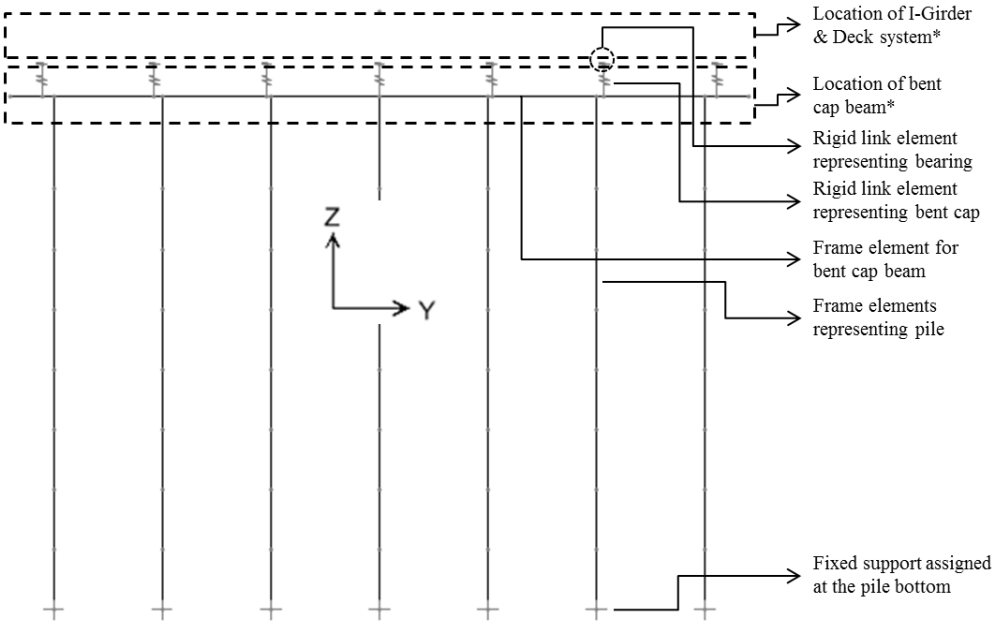

*Broken lines are drawn externally (outside of CSiBridge environment) to locate the specific bridge elements.

Figure 6.19 Intermediate bent details of Russell Creek Bridge (screen capture from CSiBridge model).

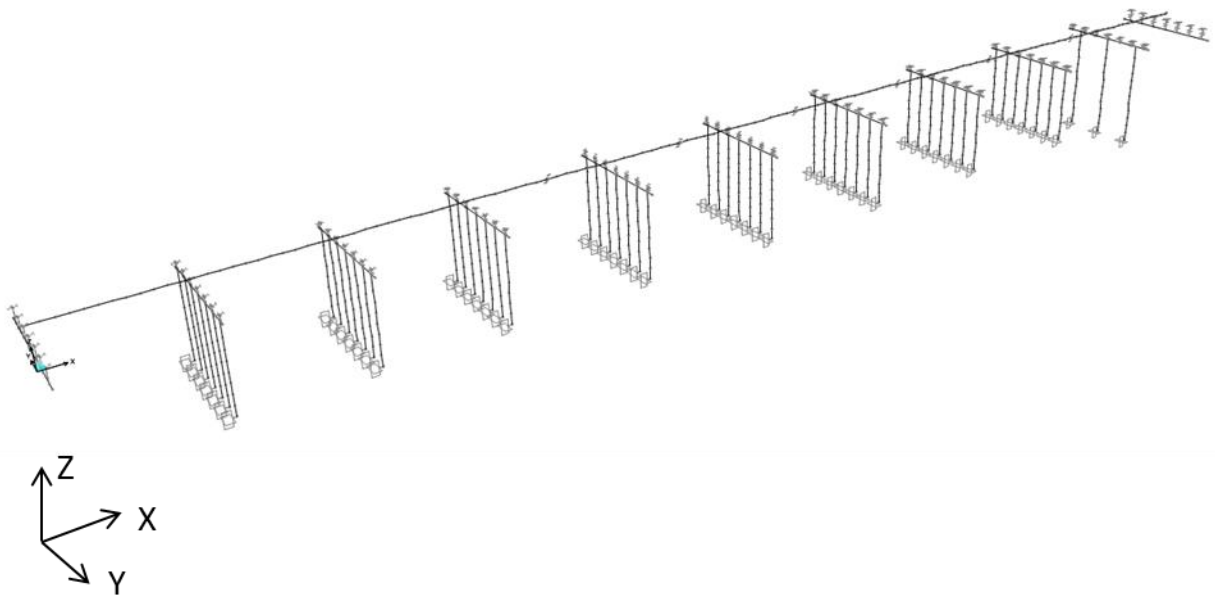

Figure 6.20 Three-dimensional 'spine' model of Russell Creek Bridge (screen capture from CSiBridge model).

Table 6.13 Section properties used for Russell Creek Bridge model.

Properties	Structural Elements			
	I-Girder (Each)	Bent Cap Beam	Pile details	
			24" (square section) Pre-stressed Concrete Pile	42" Dia. Drilled Shaft
Cross sectional area (ft^2)	2.31	14.00	3.99	8.67
Moment of inertia in Global X direction, I_X (ft^4)	0.37	18.67	2.25	23.93
Moment of inertia in Global Y direction, I_Y (ft^4)	1.28	27.19	1.33	5.98
Moment of inertia in Global Z direction, I_Z (ft^4)	0.25	14.29	1.33	5.98
Density (lb/ft^3)	150.00	150.00	150.00	150.00

6.8.4 Analysis and Results

Similar to the LRFD Example Bridge, MMRS analysis is performed for the Russell Creek Bridge. In the modal analyses, cracked section stiffness properties are used for the concrete section.

The bridge responses (forces, moments and displacements) at the top of the middle pile for all nine bents were computed by applying both 'Design' and recommended FEE and SEE ADRS curves in the longitudinal and transverse directions. The analyzed results from the 'Design' and recommended cases are compared (with respect to both FEE and SEE) to understand the effect of new site coefficients on the to-be-built bridge. Table J.51 in Appendix J presents the natural periods of vibration and the corresponding mass participations for the first 60 modes (longitudinal and transverse) of vibration. It was confirmed that the cumulative mass participation attained was above 90% in both directions (translation in Global X and Y).

Similar to the LRFD Example Bridge study, the forces, moments, and displacements in both longitudinal (global X direction) and transverse (global Y direction) directions are obtained for load and displacement combinations LC1 and LC2. These recordings are taken at each intermediate bent at the middle piles where the pile and cap beam connects to each-other. The percentage differences in forces and displacements are calculated for all the cases and compared (Appendix J).

The results corresponding to the FEE motion are tabulated in Tables J.52 through J.56 in format similar to Section 6.5. Tables J.52 and J.53 present analyses results for longitudinal (global X direction) directional loading (EQ_{LONG}) and transverse (global Y direction) directional loading (EQ_{TRANS}), respectively. Table J.54 presents displacements (both global X and Y directions) for both of the EQ_{LONG} and EQ_{TRANS} loadings. Table J.55 present the comparison between analyses results (forces and moments) from the 'Design' and the recommended FEE cases with respect to the load combinations LC1 and LC2 and also by stating their percentage differences for all the column tops and bottoms. Similarly, presented in Table J.56 are the displacements from the 'Design' and the recommended FEE cases with respect to the load combinations LC1 and LC2 and also their percentage differences for all the column top positions. Presented in the Figure 6.21 are the differences in computed axial force, shear force, and bending moment for the 'Design' and the recommended FEE cases and load combinations LC1 and LC2. Similarly, the computed percentage difference in displacement at the column top of all the bents are shown in Figure 6.22.

The results for the SEE motion are shown in similar tables (Tables J.57 through J.61 in Appendix J) and Figures 6.23 and 6.24.

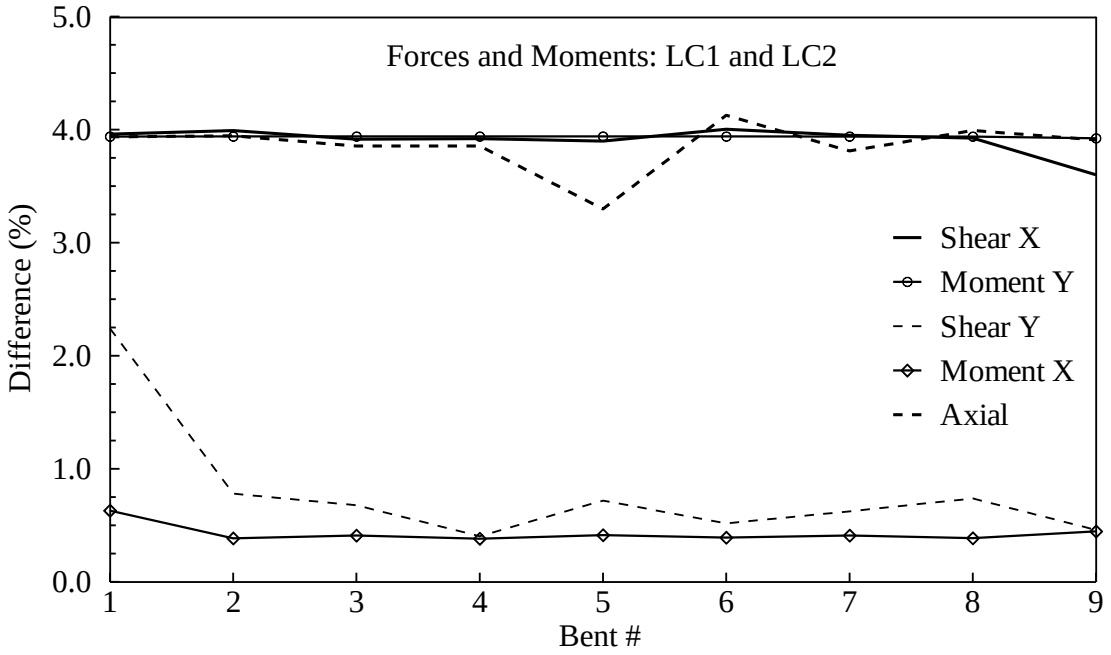

Figure 6.21 Comparison (% difference between 'Design' and recommended) of forces and moments (Shear X, Shear Y, Moment X, Moment Y and Axial) for FEE in the middle pile of each bent at the top for LC1 and LC2 load cases.

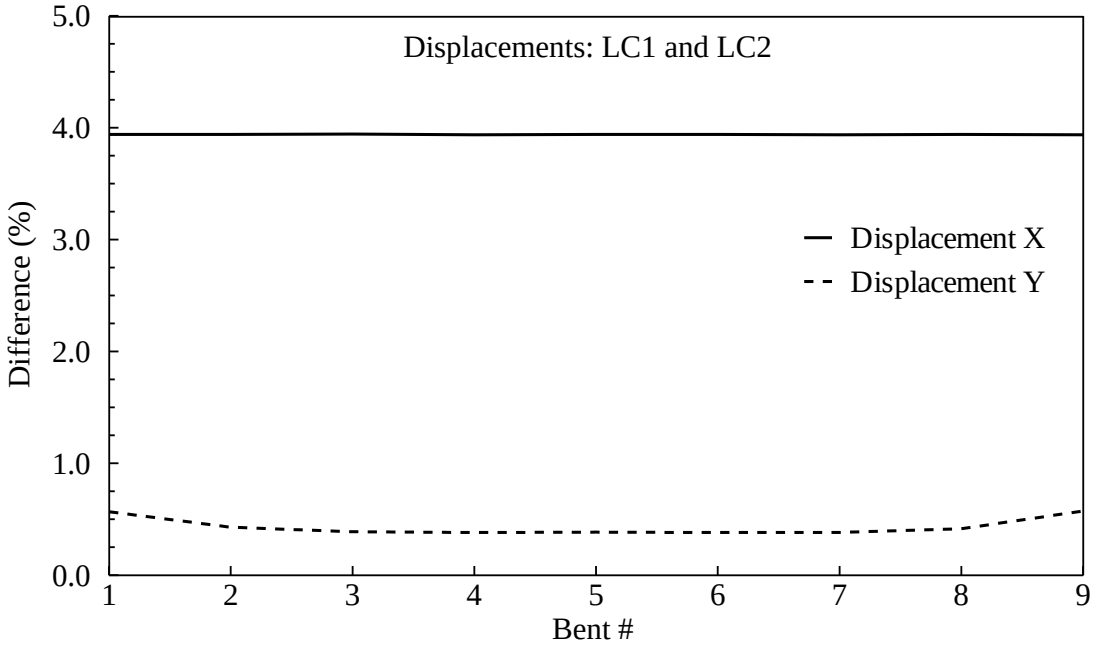

Figure 6.22 Comparison (% difference between 'Design' and recommended) of displacements (Disp. -X and Disp. -Y) for FEE in the middle pile of each bent at the top for LC1 and LC2 load cases.

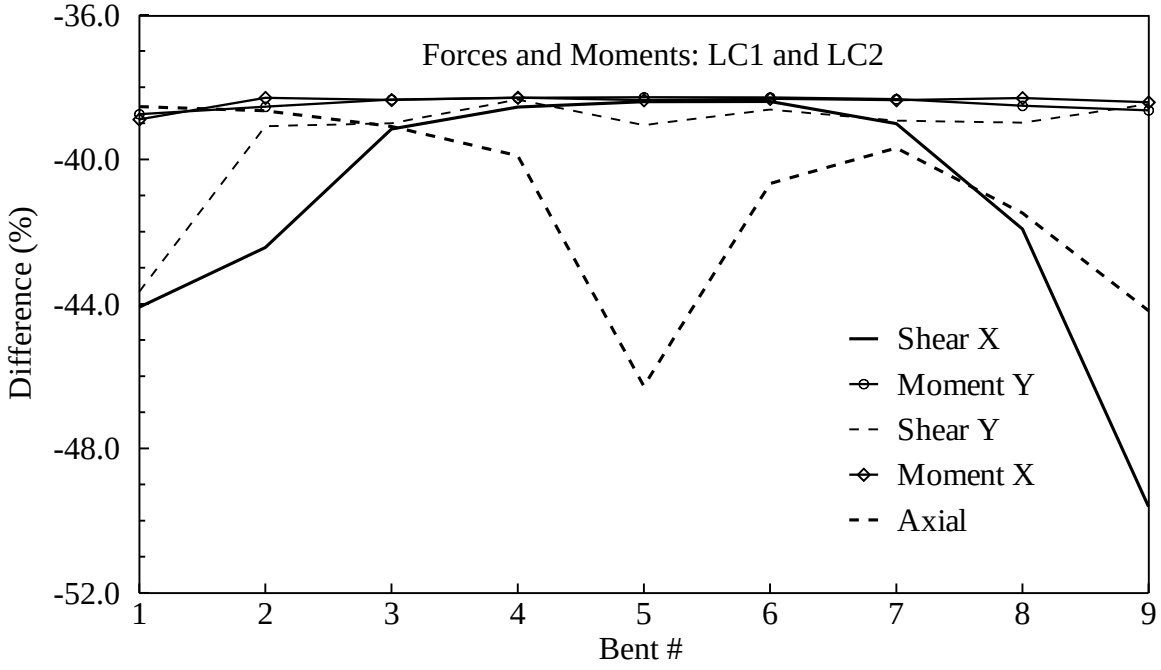

Figure 6.23 Comparison (% difference between 'Design' and recommended) of forces and moments (Shear X, Shear Y, Moment X, Moment Y and Axial) for SEE in the middle pile of each bent at the top for LC1 and LC2 load cases.

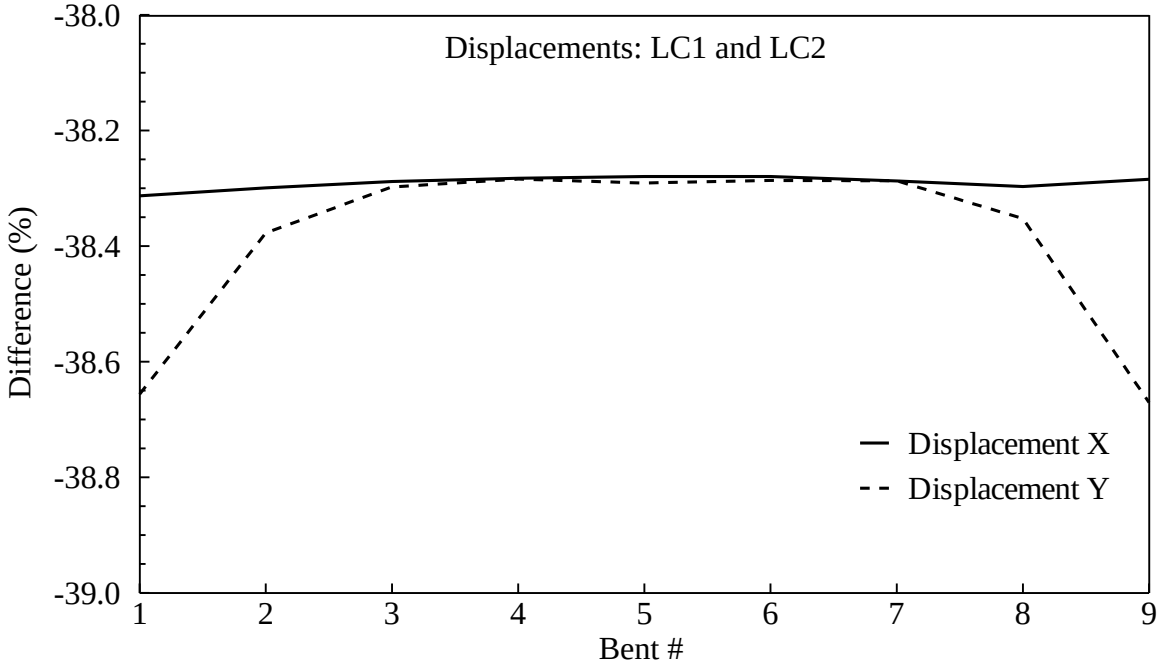

Figure 6.24 Comparison (% difference between 'Design' and recommended) of displacements (Disp.-X and Disp.-Y) for SEE in the middle pile of each bent at the top for LC1 and LC2 load cases.

6.8.5 Discussion

In the case of FEE motion, the ADRS curves with 'Design' and recommended coefficients produced almost identical results with a margin of 1-4% with respect to the percentage difference in forces, moments and displacements. On the other hand, the results for 'Design' are found to be conservative with a large margin of 38-50% than that of the recommended for the SEE cases. As the FEE based 'Design' and recommended ADRS curves are similar (Figure 6.16), it was expected that MMRS analysis would also produce similar responses. In contrast, the SEE based 'Design' and recommended ADRS curves showed significant difference and that is also seen in the MMRS analysis outcomes.

Therefore with respect to FEE motion, the demand estimated through the 'Design' curve satisfied the demand estimated using the recommended model. The recommended model would have produced a considerably smaller design demand in the case of SEE motion for this site condition, and therefore a more economic design.

6.9 Summary

The LRFD Example Bridge and Russell Creek Bridge were analyzed for seismic performance using SAP2000 and CSiBridge, respectively, by applying the ADRS curves generated based on the recommended and the current (AASHTO 2011a) site coefficients. Based on the computed results, the following observations were made:

LRFD Example Bridge:

- For Site Class C (in Columbia using V_{S100ft} of 1263 ft/s), the AASHTO (2011a) produced conservative results compared to the recommended model. This indicates further cost reduction is possible if the recommended coefficients are used.
- For Site Class D (in Charleston), the recommended model is expected to generate more conservative design forces/moments and displacements of the structural components than the AASHTO (2011a) would have. Two different cases modeled based on the recommended coefficients produced seismic demands from 2 to 3% (using V_{S100ft} of 961 ft/s) to 20-22% (for maximum ADRS within Site Class D) more than the respective cases modeled with AASHTO (2011a) ADRS curves.

- For Site Class E (in Charleston using V_{S100ft} of 600 ft/s), the cases based on recommended coefficients predicted approximately 31% less design forces/moments and displacements of the structural components than the AASHTO (2011a) would have required, possibility for a more economical design option for the softer sites in SCCP.
- A sensitivity study was performed to investigate the effect of fixed versus spring foundation types. Results from both the approaches fell within a close range proving no practical bias on the analysis outcomes. Thus this sensitivity study confirmed that the MMRS analysis outcomes using fixed column base are valid.

Russell Creek Bridge:

- In the case of Russell Creek Bridge, a Site Class D site, the analysis with the recommended site coefficients produced slightly higher (1-4%) results (forces, moments and displacement) compared to that of the AASHTO (2011a) site coefficients in the case of FEE motion. This indicates that the original design is satisfactory with respect to the new site coefficients. However, in the case of SEE motion, the analysis with the recommended coefficients produced significantly lower (38-50%) results. Based on these results, the use of recommended site coefficients has the potential to significantly reduce the project cost for bridges similar to the Russell Creek Bridge in Site Class D.

CHAPTER SEVEN

SUMMARY AND RECOMMENDATIONS

7.1 Summary

New generalized models for estimating site coefficients for seismic design in the South Carolina Coastal Plain (SCCP) and the South Carolina Piedmont (SCP) were developed in this report based on over 60,000 total stress, one-dimensional equivalent linear (SHAKE2000) and nonlinear (DMOD2000) ground response analyses. Development of the models involved assuming geologic and seismic conditions typical of seven sites in the Coastal Plain (i.e., Charleston, the South Carolina side of Savannah, Myrtle Beach, Columbia, Florence, Lake Marion, and Aiken) and four sites in the SCP (i.e., Columbia, Greenwood, Rock Hill, and Greenville). Over 130 synthetic ground motions generated using the computer program Scenario_PC were scaled to different peak accelerations and used as inputs for the ground response analyses.

A model for estimating site coefficients in the Charleston area was first developed in Chapter 2. The site coefficients were calculated as averages over spectral period ranges of ≤ 0.1, 0.1-0.4, 0.4-0.8, 0.8-1.2, 1.2-2.0, and 2.0-4.0 s and were referred to as F_{PGA}, F_a, $F_{0.6}$, F_v, $F_{1.6}$, and F_3, respectively. The site coefficients were then grouped by spectral acceleration and plotted versus V_{S100ft}. From the plotted V_{S100ft}-site coefficient data pairs, overall median relationships were developed. Each relationship exhibited a peak site coefficient somewhere between V_{S100ft} of 260 and 1050 ft/s, depending on spectral acceleration and period. The V_{S100ft}-site coefficient relationships were expressed by a linear equation for $V_{S100ft} < V_{S100ftP}$, and a linear or exponential equation for $V_{S100ft} \geq V_{S100ftP}$. The variability in computed coefficients was characterized by 5% lower bound and 95% upper bound relationships.

The computed relationships for spectral periods of 0.0, 0.2 and 1.0 s were compared with the 1994 NEHRP F_a and F_v values, which are currently widely used in seismic design practice. The computed median F_{PGA} and F_a values typically plotted above the NEHRP F_a values for V_{S100ft} >

590 ft/s. The computed median F_v values also typically plotted above the NEHRP F_v values by as much as about 1.5 times for $590 \leq V_{S100ft} \leq 980$ ft/s. For $V_{S100ft} < 590$ ft/s, the computed F_a and F_v values typically plotted below the NEHRP values. Because the computed site coefficients in Chapter 2 are based on local geologic and seismic conditions, they were recommended for use in the Charleston area.

Also in Chapter 2, the 3-point procedure for constructing ADRS curves (based on F_{PGA}, F_a, and F_v) was shown to be generally valid when $V_{S100ft} > 650$ ft/s. When $V_{S100ft} \leq 650$ ft/s, peaks exceeding the 3-point ADRS curves were shown to sometimes occur at $T > 1.0$ s. For this reason, it was recommended that multi-point ADRS curves (based on F_{PGA}, F_a, $F_{0.6}$, F_v, $F_{1.6}$, and F_3) also be plotted to check if long-period accelerations are under predicted.

In Chapter 3, the model for estimating site coefficients developed in Chapter 2 was modified to accommodate geologic and seismic variations in the entire SCCP. The most important variables identified in the modified site coefficient model were: V_{S100ft}, spectral acceleration, mean predominant period (T_m), approximate fundamental period of soil/rock column in the top 330 ft (T_{330ft}), and depth to soft rock ($H_{B\text{-}C}$). A relationship to compute T_m based on depth to weathered hard rock (H_{HR}) and site-to-source distance (R) was suggested. In decreasing order, the computed site coefficients were found to be greatest in Myrtle Beach, Savannah, Charleston, Florence, Columbia, Lake Marion and Aiken. More closely matching values of T_m and T_{330ft} (e.g., $T_m = 0.37$ and $T_{330ft} = 0.84$ for the Myrtle Beach reference profile) may explain the higher site coefficients obtained for Myrtle Beach.

The computed site coefficients for Myrtle Beach were compared with the 1994 NEHRP site coefficients. The computed F_a and F_v values for Myrtle Beach were found to be significantly greater than the NEHRP F_a and F_v when the depth to soft rock was less than 330 ft, particularly for F_a. The results clearly indicated that the assumption of a single value of F_a and F_v for a wide range of V_{S100ft} values (e.g., a NEHRP Site Class) is an overly simplified approach.

In Chapter 4, the model for estimating site coefficients in the SCCP was extended to the SCP. Because there were limited available V_S data, a single dynamic soil/rock model was assumed for the entire SCP and adjusted to account for variations in stiffness and depth to weathered hard

rock (V_S = 8,200 ft/s). It is found that both the FEE and SEE conditions in the SCP were dominated by earthquakes with modal M_w = 7.3, except in the western half of the SCP where the SEE condition was dominated by earthquakes with modal M_w = 4.8. Because the seismic hazard in the SCP can be dominated by multiple sources, generation of input motions matching the uniform hazard points was shown to give unconservative results. Therefore, input motions matching target frequencies were used. The computed site coefficients for the SCP were found to be higher than the computed site coefficients for the SCCP, because weathered hard rock was assumed as reference outcrop condition in the SCP and because soil-rock impedance contrasts are higher in the SCP.

Site coefficients developed for the SCP in Chapter 4 should only be used to modify hard rock outcropping accelerations. For this reason, the site coefficients are not comparable with the 1994 NEHRP F_a and F_v values, which are referenced to B-C boundary rock accelerations. For sites close to the Fall Line, predicted 3-point ADRS curves using the SCP and SCCP models were shown to be similar, but can differ due to the different rock models assumed. For SCCP sites close to the Fall Line where H_{HR} < 330 ft, the ADRS based on the SCP model was recommended for design. For SCCP sites close to the Fall Line and where $H_{HR} \geq$ 330 ft, the ADRS based on the SCCP model was recommended for design.

In Chapter 5, the site coefficient models developed in Chapters 3 and 4 were used to calculate maximum median site coefficients within a site class (i.e., A, B, C, D, E). Multiple tables were needed for the new site coefficients to account for differences between sites and depths to rock. Thus, it was concluded that use of the continuous models presented in Chapters 3 and 4 would be more efficient in defining the recommended site coefficients.

The median site coefficient relationships derived in Chapters 3 and 4 were recommended for seismic design in South Carolina because they are: (1) based on regional conditions; (2) continuous with V_{S100ft}; (3) dependent on depth to top of rock; and (4) dependent on the period content of the design motion. Because the recommended site coefficient models are based on a very broad range of soil/rock and rock motion properties, they can be directly applied to other areas with similar geologic and seismic conditions. In areas outside of South Carolina, modification of model variables may be required.

In Chapter 6, repercussions of the new site coefficients were investigated. ADRS curves generated based on the 1994 NEHRP (or current practice) and the new site coefficients were applied to two sample bridges (CIP concrete box girder and I-Girder) and multi-modal response spectrum analysis was performed with using SAP2000 or CSiBridge software. The analyzed results (forces, moments and displacements) were compared to distinguish the difference imposed by the new site coefficient model over the current practice. For the cases studied, significant variations were observed including both conservativeness and un-conservativeness with respect to the current practice. In the case of Site Class D, an increase of structural demand was observed in general and that increase reached up to 20-22%. Moreover, for the I-Girder Bridge it was found the bridge was adequately designed for FEE but significantly over designed (38-50% less demand by the application of the recommended than the current ADRS curve) for SEE. In the case of Site Class E, approximately 31% less demand in terms of design forces/moments and displacements was observed with the recommended site coefficients compared to the current practice. Because the above mentioned findings were based on the analysis of two sample bridges, it was recommended to analyze other typical South Carolina bridges to accurately estimate the repercussions of the new model with respect to cost instead of joint forces or displacements, inauguration of soil-structure interaction at the bridge foundation, etc.

7.2 Recommendations for Future Studies

The following future studies are recommended:

1. Field V_S measurements available for this study below the depth of 100 ft in the SCCP and at all depths in the SCP were limited to relatively few locations. Additional field measurements are needed to completely and accurately characterize the V_S model of South Carolina.
2. Because only synthetic ground motions were used in this study, the results are limited to the assumptions (e.g., rock model) made in Scenario_PC. Real earthquake recordings at soil and rock sites are needed to validate the recommended site coefficient models.

3. Additional work is needed to investigate the influence of layer correlation on the site coefficient models and to make refinements to models as needed. In the ground response analyses conducted in this study, reasonable ranges of V_S profiles for the SCCP and the SCP were considered by assuming a reference profile and applying reasonable standard deviation values.

4. Two- and three-dimensional ground response analyses are needed to quantify the effects of lateral heterogeneity and sloping ground in the SCP.

5. Additional work is needed to extend the new site coefficient models to areas outside of South Carolina.

6. In the current study, multi-modal response analyses were conducted on two example bridges with the 1994 NEHRP and the new site coefficients using SAP2000 or CSiBridge software to evaluate the repercussions of ADRS curves based on the new site coefficients. Full-scale numerical models using CSiBridge software of other typical South Carolina highway bridges covering the Seismic Design Categories B, C and D for each area in South Carolina should be developed. After completion of seismic analysis and design, estimated material costs resulting from the 1994 NEHRP and the new site coefficients could be compared, which will provide useful information for decision making and fund allocation.

7. Investigate the influence of the interaction between soil and structural system including abutments (end bents) subjected to representative ground motions by performing analysis of a sample fully-coupled soil-foundation-bridge (SFB) system. Such complex but necessary analyses can reveal further insights into the overall soil-structure response subjected to acceleration-time history. The analysis could be performed using the open source finite element software platform OpenSees.

APPENDIX A

SUMMARY OF INPUTS AND OUTPUTS OF SITE RESPONSE ANALYSIS FOR THE CHARLESTON AREA

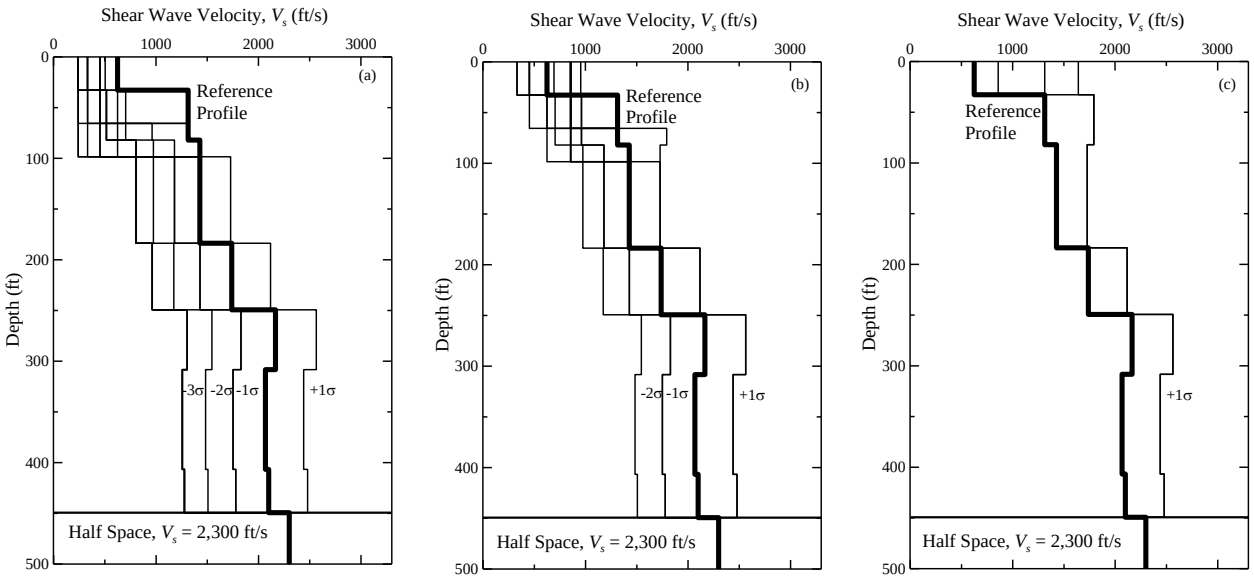

Figure A.1 Shear wave velocity profiles considered for Charleston without a low velocity layer at depth = 410-440 ft and soft rock half space at depth = 450 ft grouped by NEHRP Site Class (a) E, (b) D, and (c) C. The reference profile and standard deviation values are based on Andrus et al. (2006).

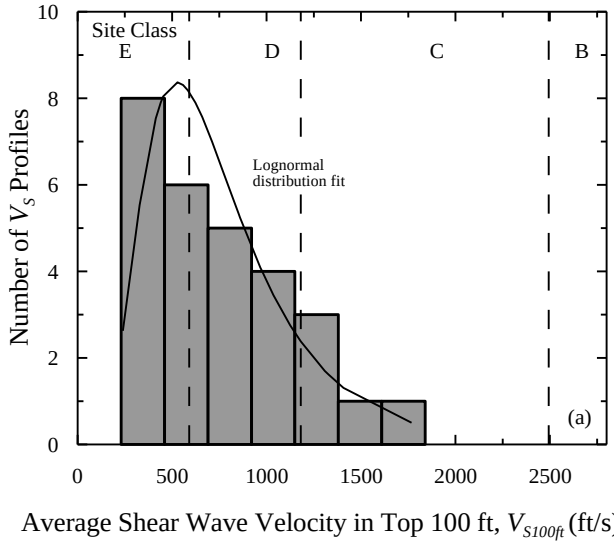

Figure A.2 V_{S100ft} histogram of shear wave velocity profiles in Figure A.1.

Table A.1 Table of best fit values of F_P and $V_{S100ftP}$.

Figure	F_p	$V_{S100ftP}$	a
A.3a	2.0	499	-
A.3b	1.8	586	-
A.3c	1.5	736	-
A.3d	1.4	841	-
A.3e	1.0	1050	-
A.3f	1.0	1148	-
A.4a	2.0	525	0.63
A.4b	1.7	590	0.63
A.4c	1.5	820	0.65
A.4d	1.4	951	0.65
A.4e	1.1	1017	0.67
A.4f	1.0	1082	0.67
A.5a	3.0	525	0.84
A.5b	2.6	558	0.86
A.5c	2.5	701	0.85
A.5d	2.1	713	0.85
A.5e	1.5	805	0.85
A.5f	1.4	820	0.84
A.6a	3.7	524	0.98
A.6b	3.3	540	0.96
A.6c	2.9	599	0.88
A.6d	2.7	633	0.70
A.6e	1.9	678	0.80
A.6f	1.8	705	0.71
A.7a	4.1	374	1.00
A.7b	3.5	441	1.00
A.7c	3.1	489	0.99
A.7d	2.8	521	0.98
A.7e	2.0	605	0.93
A.7f	1.9	641	0.91
A.8a	1.9	328	0.99
A.8b	2.0	394	0.99
A.8c	2.3	476	0.99
A.8d	2.3	492	1.00
A.8e	1.7	508	0.97
A.8f	1.6	525	0.85

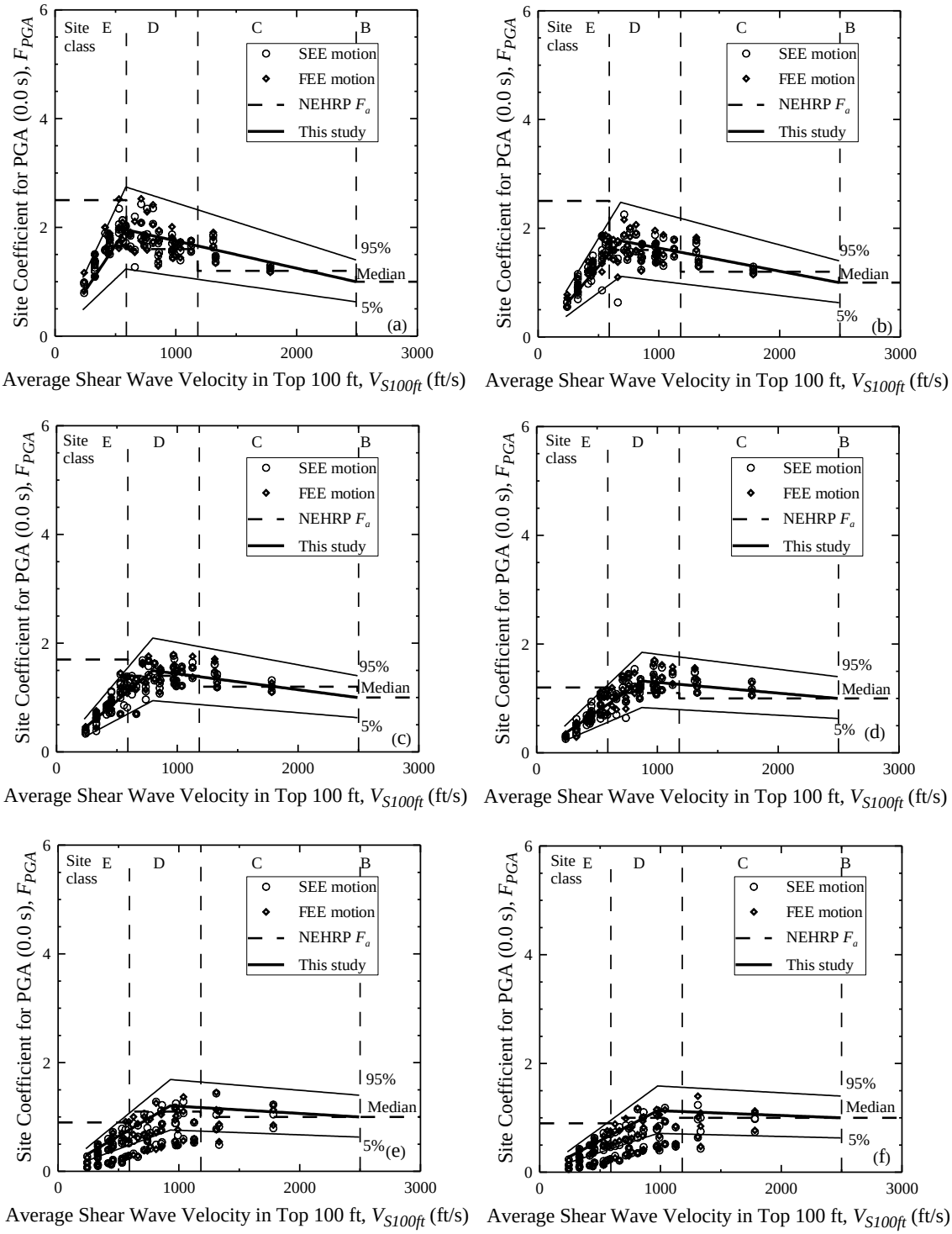

Figure A.3 Site coefficients for 0.0 s spectral period (free-field) with *PGA* equal to (a) 0.05 g, (b) 0.1 g, (c) 0.2 g, (d) 0.3 g, (e) 0.4 g, and (f) 0.5 g based on V_S profiles shown in Figure A.1 for Charleston.

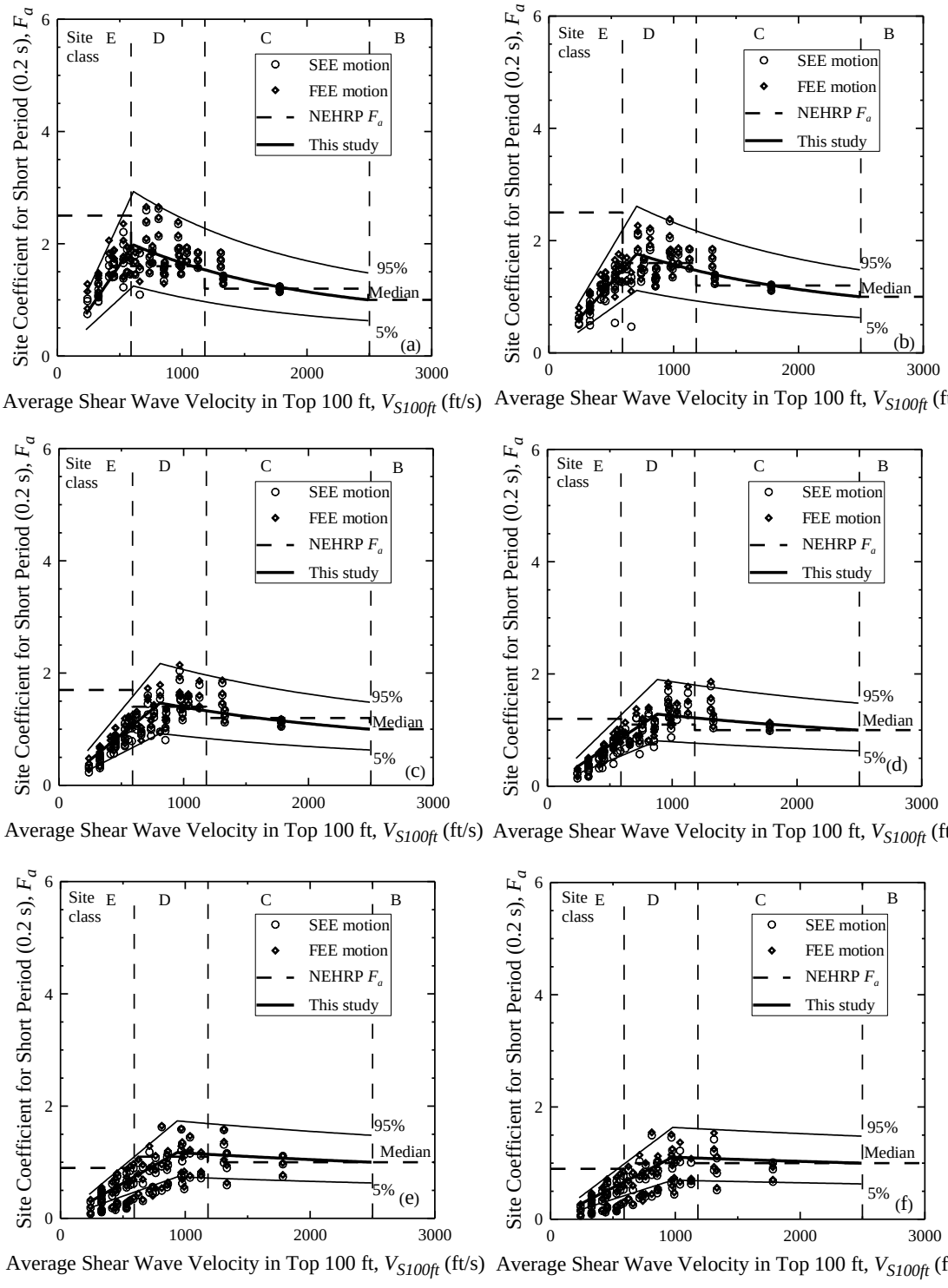

Figure A.4 Site coefficients for 0.2 s (short) spectral period with S_S equal to (a) 0.125 g, (b) 0.25 g, (c) 0.50 g, (d) 0.75 g, (e) 1.0 g, and (f) 1.25 g based on V_S profiles shown in Figure A.1 for Charleston.

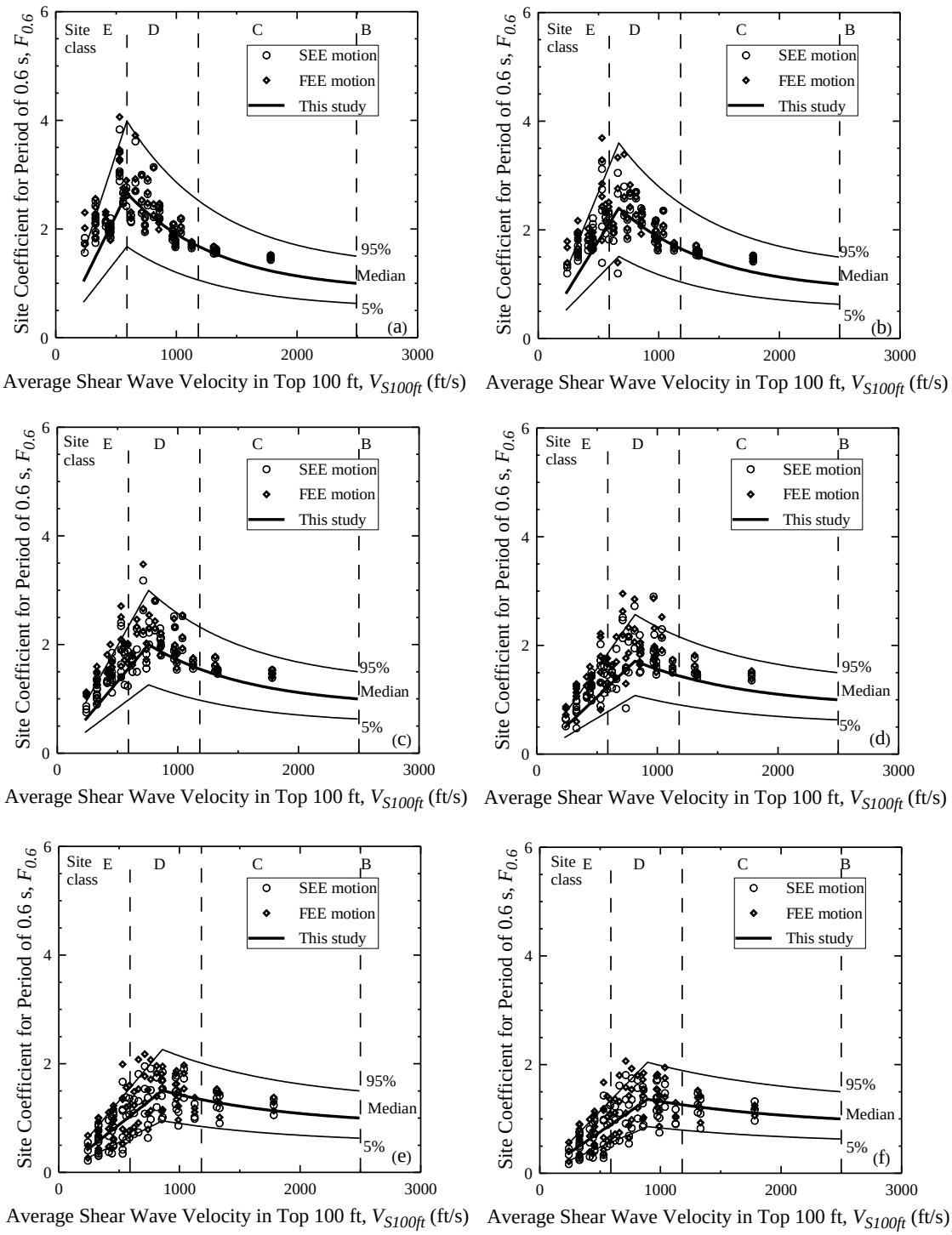

Figure A.5 Site coefficients for 0.6 s spectral period with $S_{0.6}$ equal to (a) 0.05 g, (b) 0.1 g, (c) 0.2 g, (d) 0.3 g, (e) 0.4 g, and (f) 0.5 g based on V_S profiles shown in Figure A.1 for Charleston.

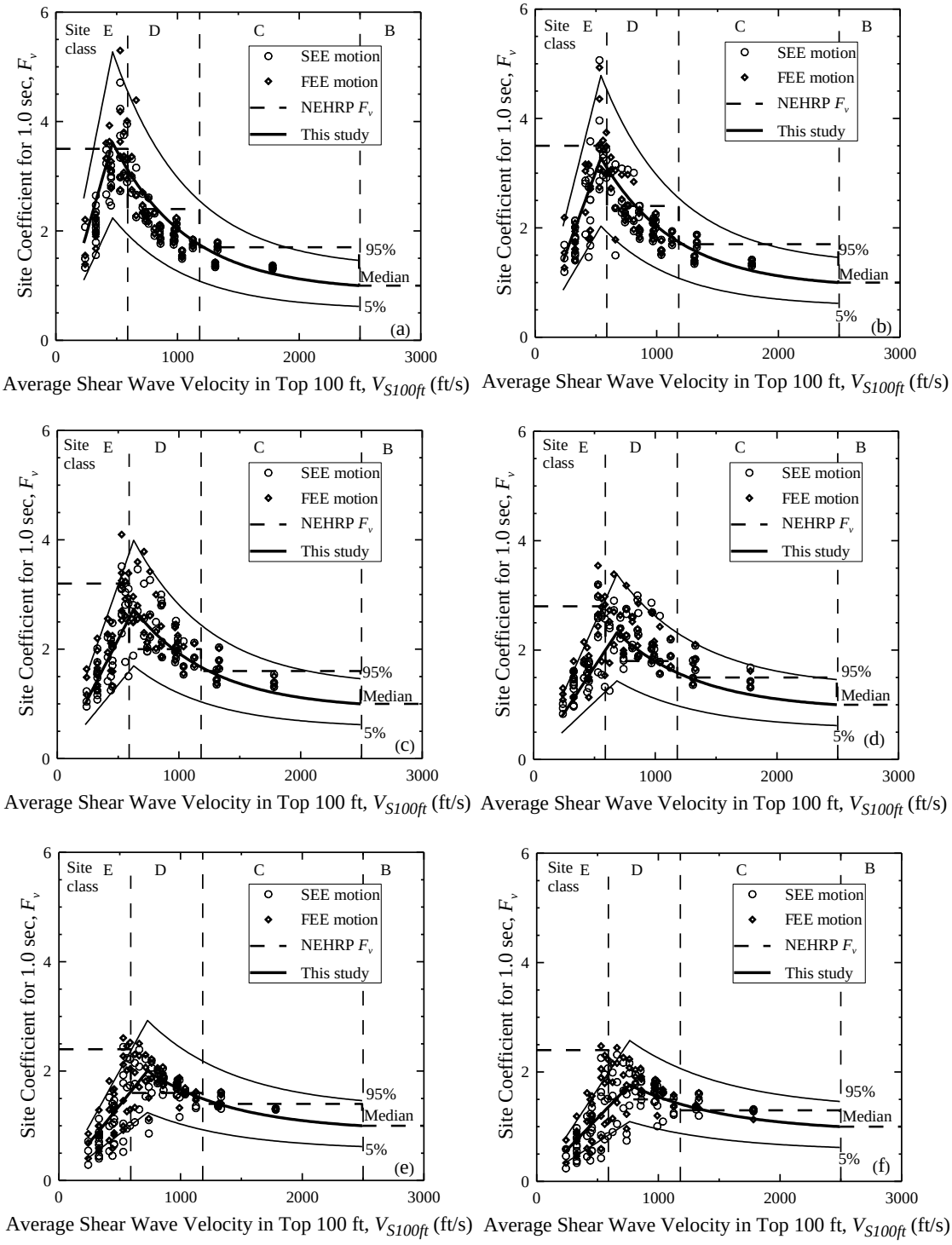

Figure A.6 Site coefficients for 1.0 s (long) spectral period with S_1 equal to (a) 0.05 g, (b) 0.1 g, (c) 0.2 g, (d) 0.3 g, (e) 0.4 g, and (f) 0.5 g based on V_S profiles shown in Figure A.1 for Charleston.

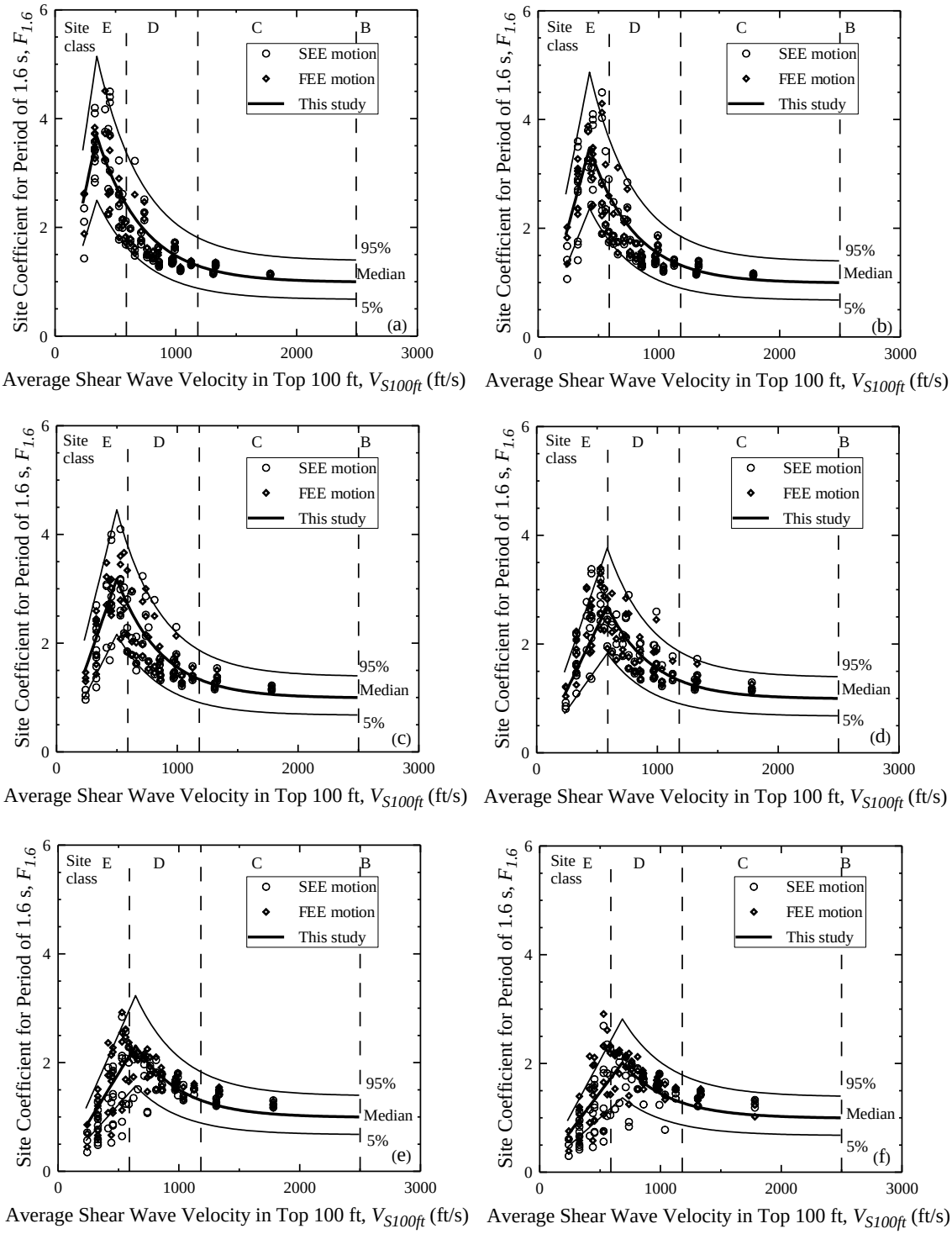

Figure A.7 Site coefficients for 1.6 s spectral period with $S_{1.6}$ equal to (a) 0.02 g, (b) 0.05 g, (c) 0.1 g, (d) 0.2 g, (e) 0.3 g, and (f) 0.4 g based on V_S profiles shown in Figure A.1 for Charleston.

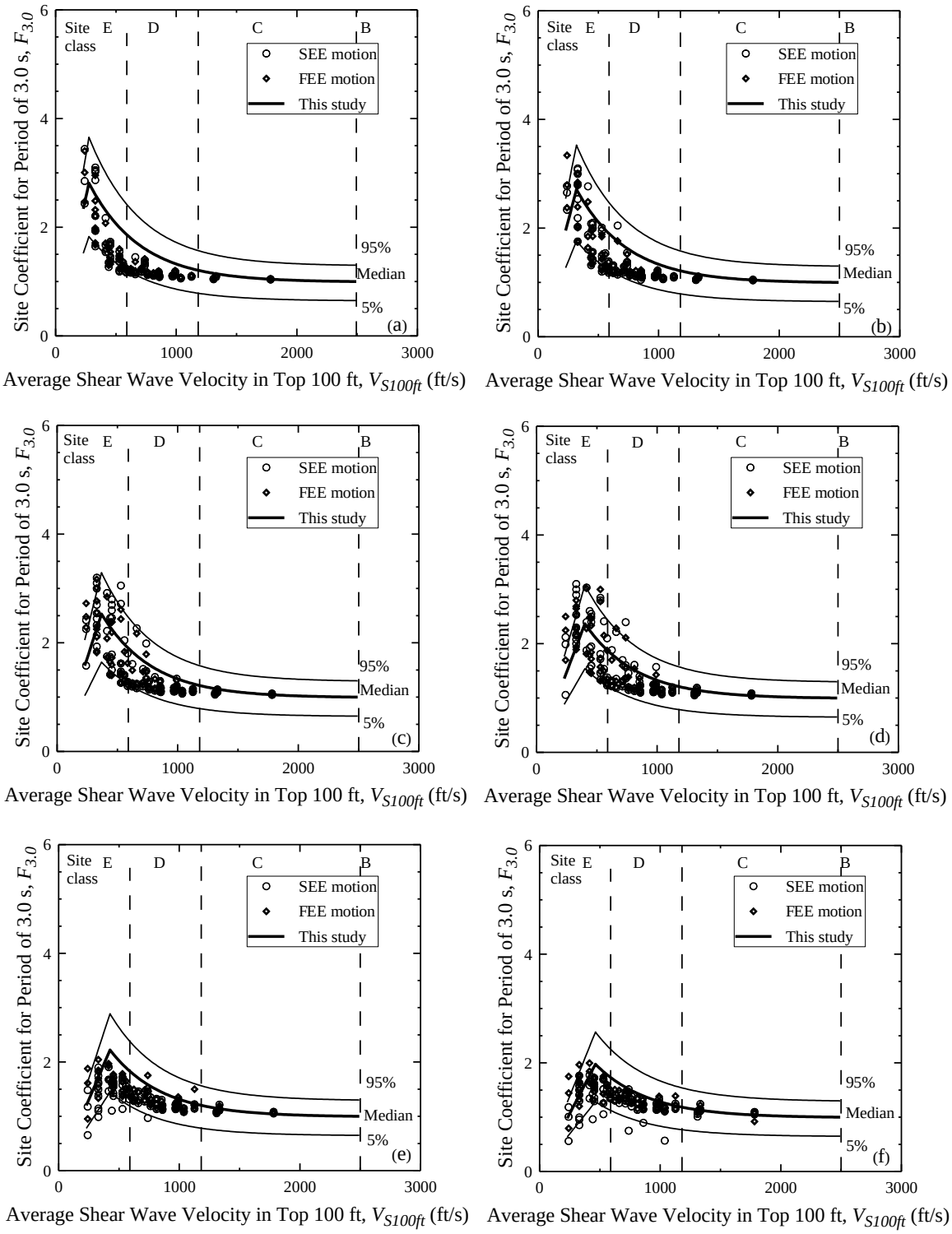

Figure A.8 Site coefficients for 3.0 s spectral period with $S_{3.0}$ equal to (a) 0.01 g, (b) 0.02 g, (c) 0.04 g, (d) 0.06 g, (e) 0.08 g and (f) 0.12 g based on V_S profiles shown in Figure A.1 for Charleston.

APPENDIX B

SUMMARY OF INPUTS AND OUTPUTS OF SITE RESPONSE ANALYSIS FOR THE MYRTLE BEACH AREA

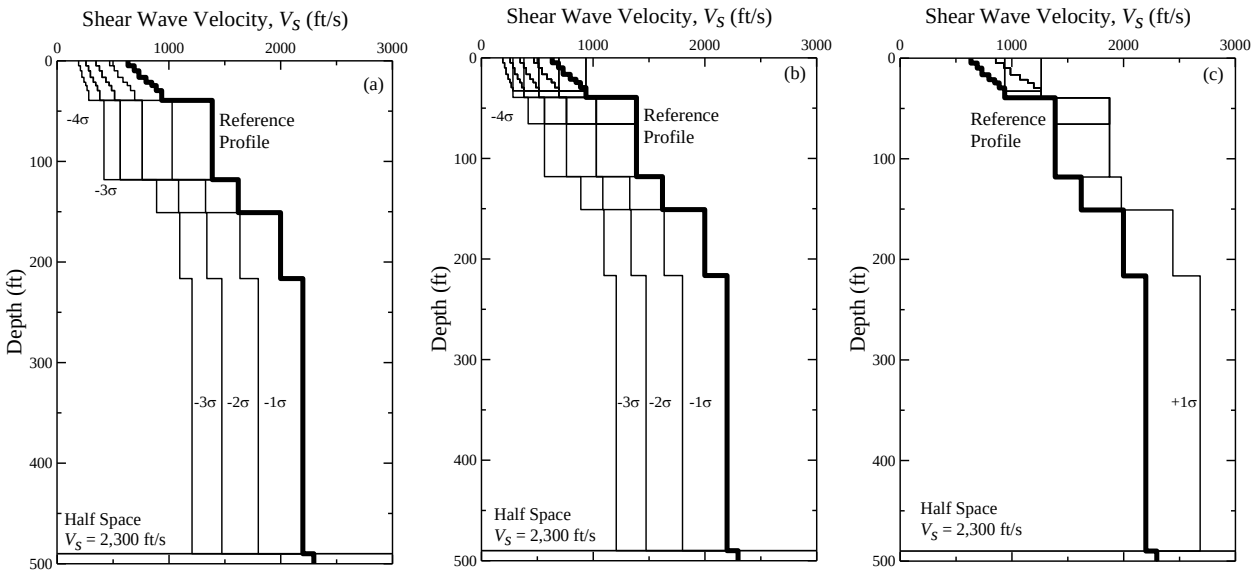

Figure B.1 Shear wave velocity profiles considered for Myrtle Beach with soft rock half space at depth = 490 ft grouped by NEHRP Site Class (a) E, (b) D, and (c) C. The reference profile is from Silva et al. (2003), and the standard deviation values are based on a study by Andrus et al. (2006).

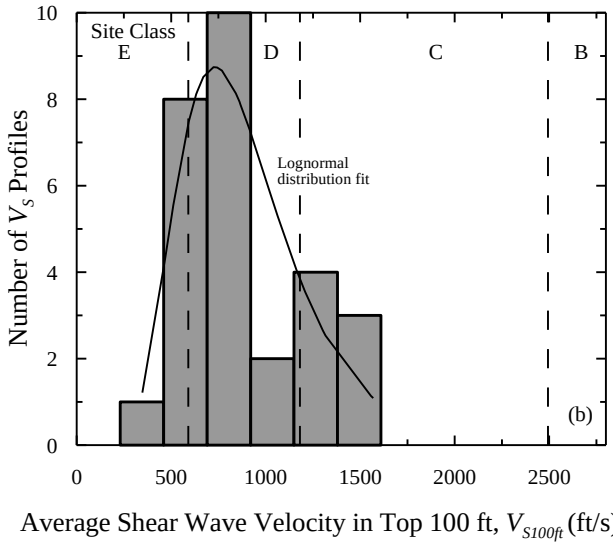

Figure B.2 V_{S100ft} histogram of shear wave velocity profiles in Figure B.1.

Table B.1 Table of best fit values of F_P and $V_{S100ftP}$.

Figure	F_p	$V_{S100ftP}$	a
B.3a	2.8	499	-
B.3b	2.4	586	-
B.3c	2.0	736	-
B.3d	1.8	841	-
B.3e	1.0	1181	-
B.3f	1.0	1246	-
B.4a	2.7	525	0.80
B.4b	2.3	656	0.85
B.4c	2.0	820	0.91
B.4d	1.9	886	0.95
B.4e	1.0	984	0.99
B.4f	1.0	1050	0.99
B.5a	3.7	525	0.97
B.5b	3.2	558	0.92
B.5c	2.9	701	0.95
B.5d	2.7	713	0.93
B.5e	1.4	805	0.94
B.5f	1.4	820	0.96
B.6a	3.9	459	0.99
B.6b	3.7	492	0.99
B.6c	3.4	558	0.99
B.6d	3.2	623	0.99
B.6e	1.6	689	0.65
B.6f	1.6	722	0.60
B.7a	4.0	374	1.00
B.7b	3.9	441	1.00
B.7c	3.4	489	1.00
B.7d	3.2	521	1.00
B.7e	1.6	605	0.99
B.7f	1.5	641	0.99
B.8a	1.7	239	0.99
B.8b	1.7	262	0.99
B.8c	1.7	426	0.96
B.8d	1.6	525	1.00
B.8e	1.5	590	0.97
B.8f	1.4	689	0.85

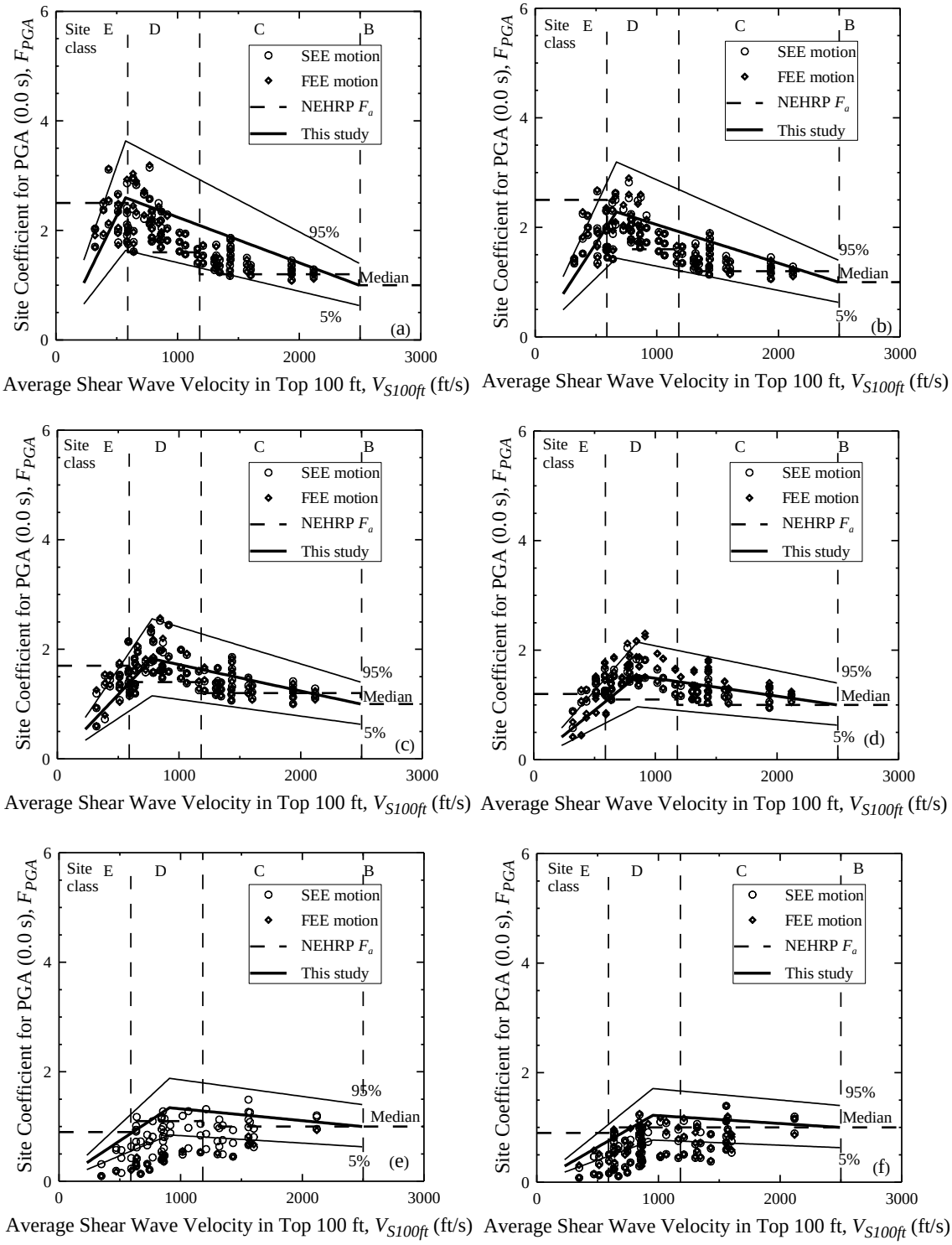

Figure B.3 Site coefficients for 0.0 s spectral period (free-field) with *PGA* equal to (a) 0.05 g, (b) 0.1 g, (c) 0.2 g, (d) 0.3 g, (e) 0.4 g, and (f) 0.5 g based on V_S profiles shown in Figure B.1 for Myrtle Beach.

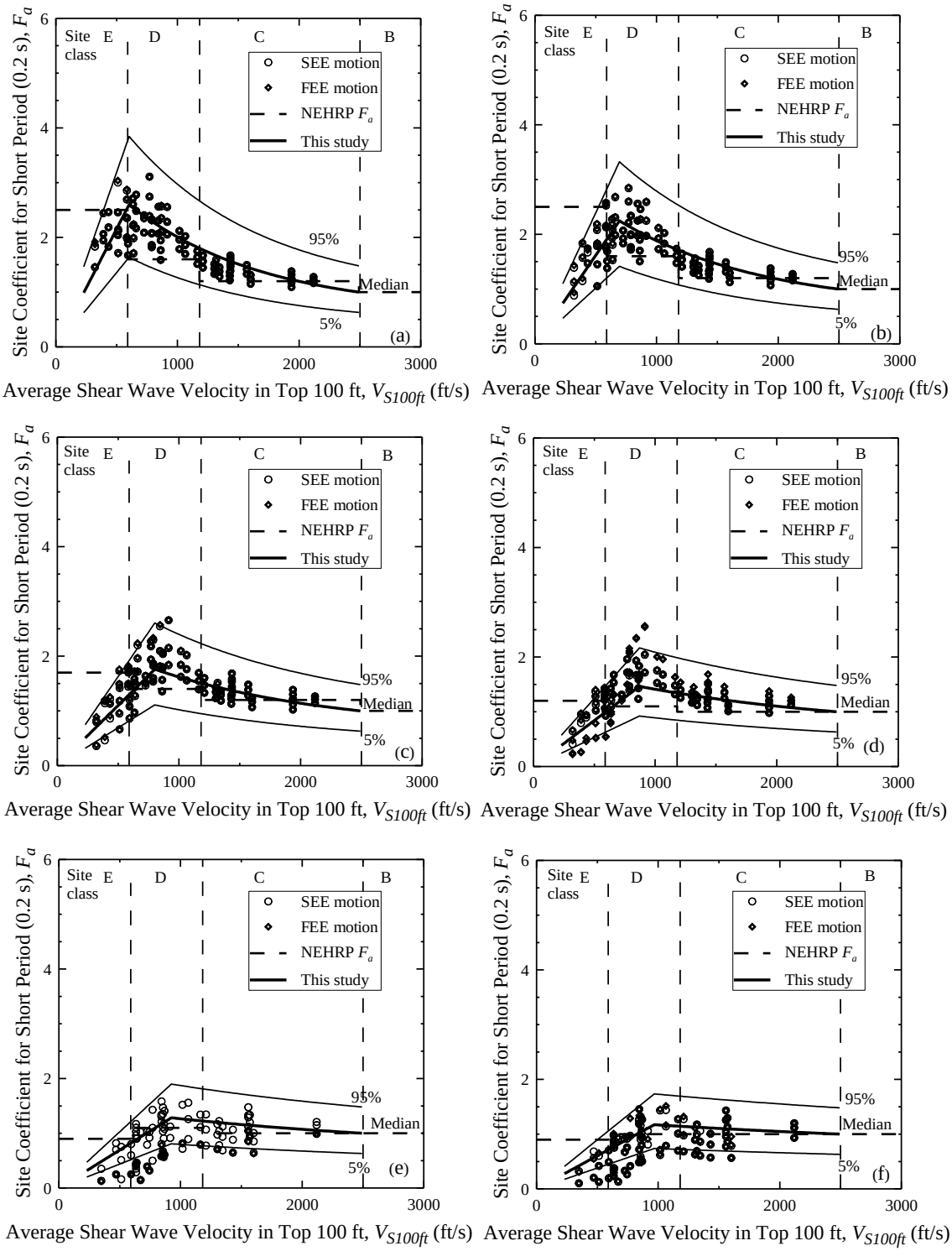

Figure B.4 Site coefficients for 0.2 s (short) spectral period with S_S equal to (a) 0.125 g, (b) 0.25 g, (c) 0.50 g, (d) 0.75 g, (e) 1.0 g, and (f) 1.25 g based on V_S profiles shown in Figure B.1 for Myrtle Beach.

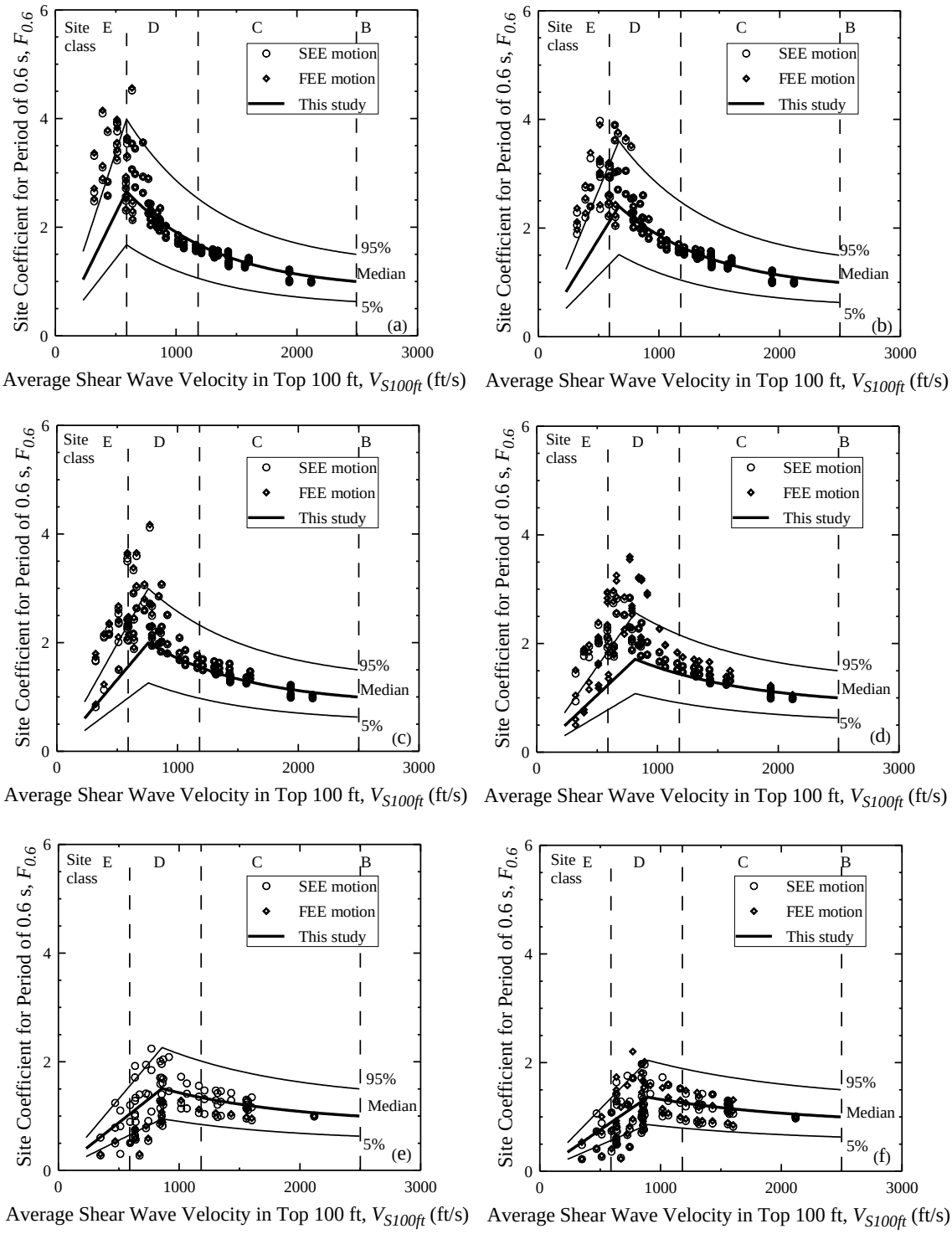

Figure B.5 Site coefficients for 0.6 s spectral period with $S_{0.6}$ equal to (a) 0.05 g, (b) 0.1 g, (c) 0.2 g, (d) 0.3 g, (e) 0.4 g, and (f) 0.5 g based on V_S profiles shown in Figure B.1 for Myrtle Beach.

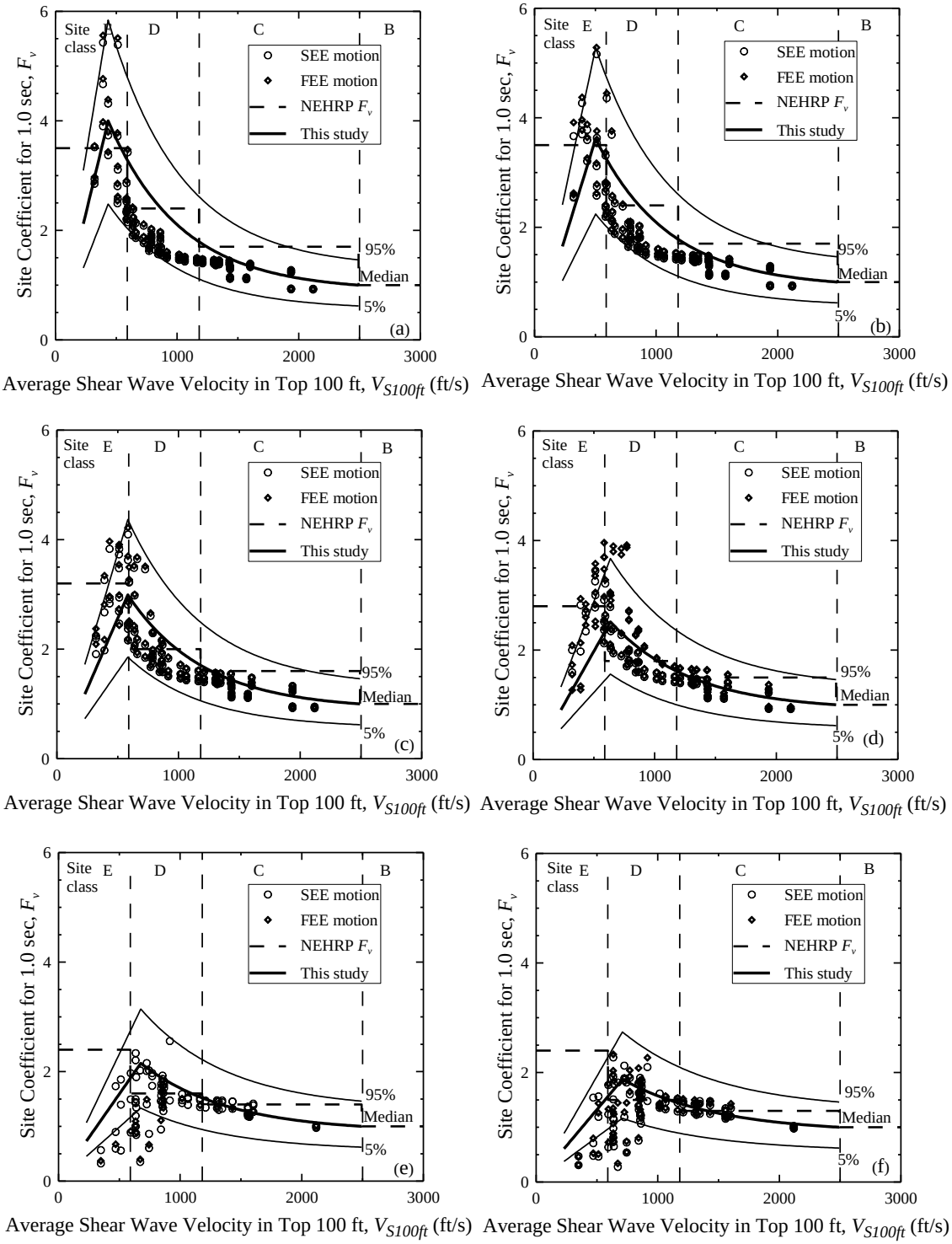

Figure B.6 Site coefficients for 1.0 s (long) spectral period with S_1 equal to (a) 0.05 g, (b) 0.1 g, (c) 0.2 g, (d) 0.3 g, (e) 0.4 g, and (f) 0.5 g based on V_S profiles shown in Figure B.1 for Myrtle Beach.

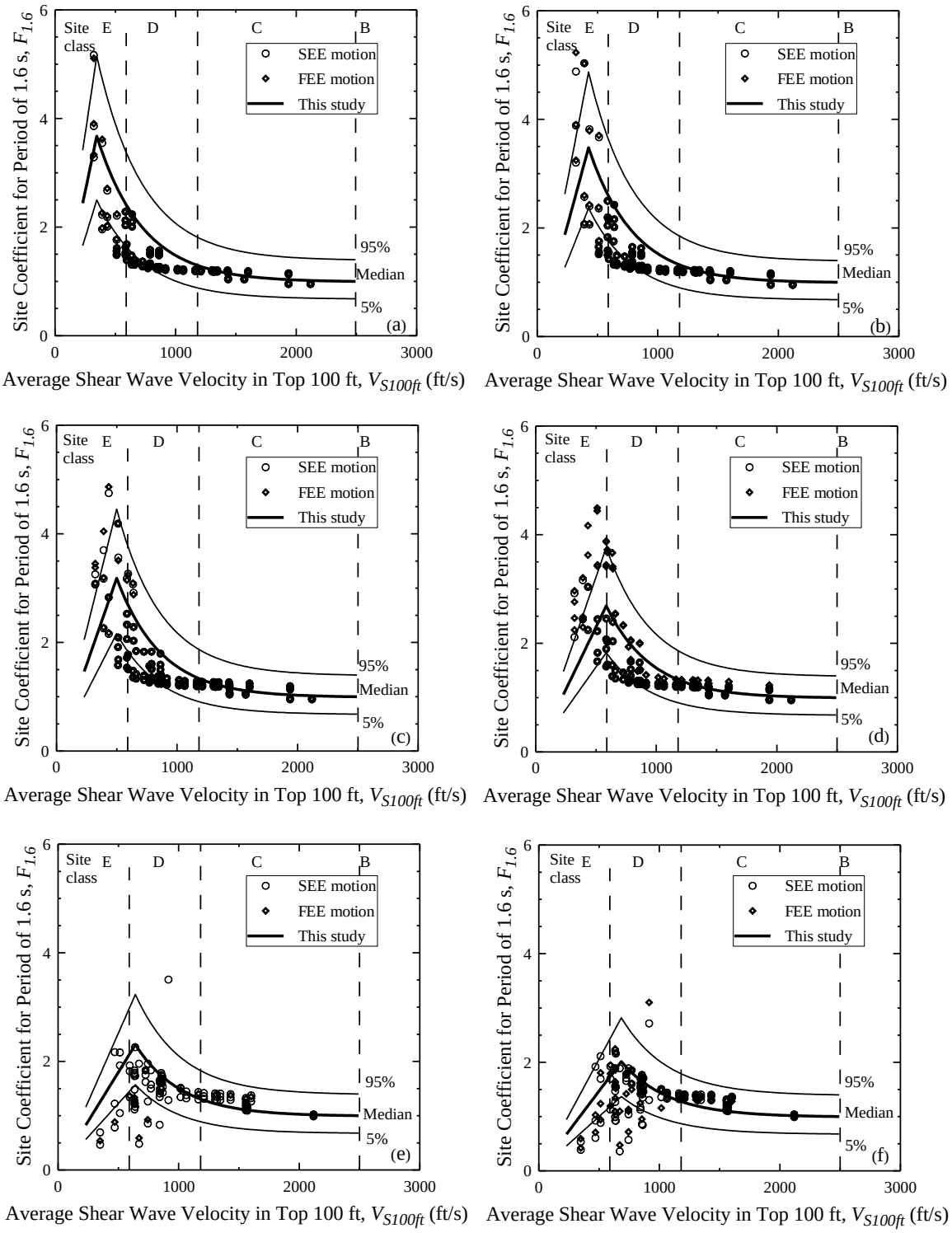

Figure B.7 Site coefficients for 1.6 s spectral period with $S_{1.6}$ equal to (a) 0.02 g, (b) 0.05 g, (c) 0.1 g, (d) 0.2 g, (e) 0.3 g, and (f) 0.4 g based on V_S profiles shown in Figure B.1 for Myrtle Beach.

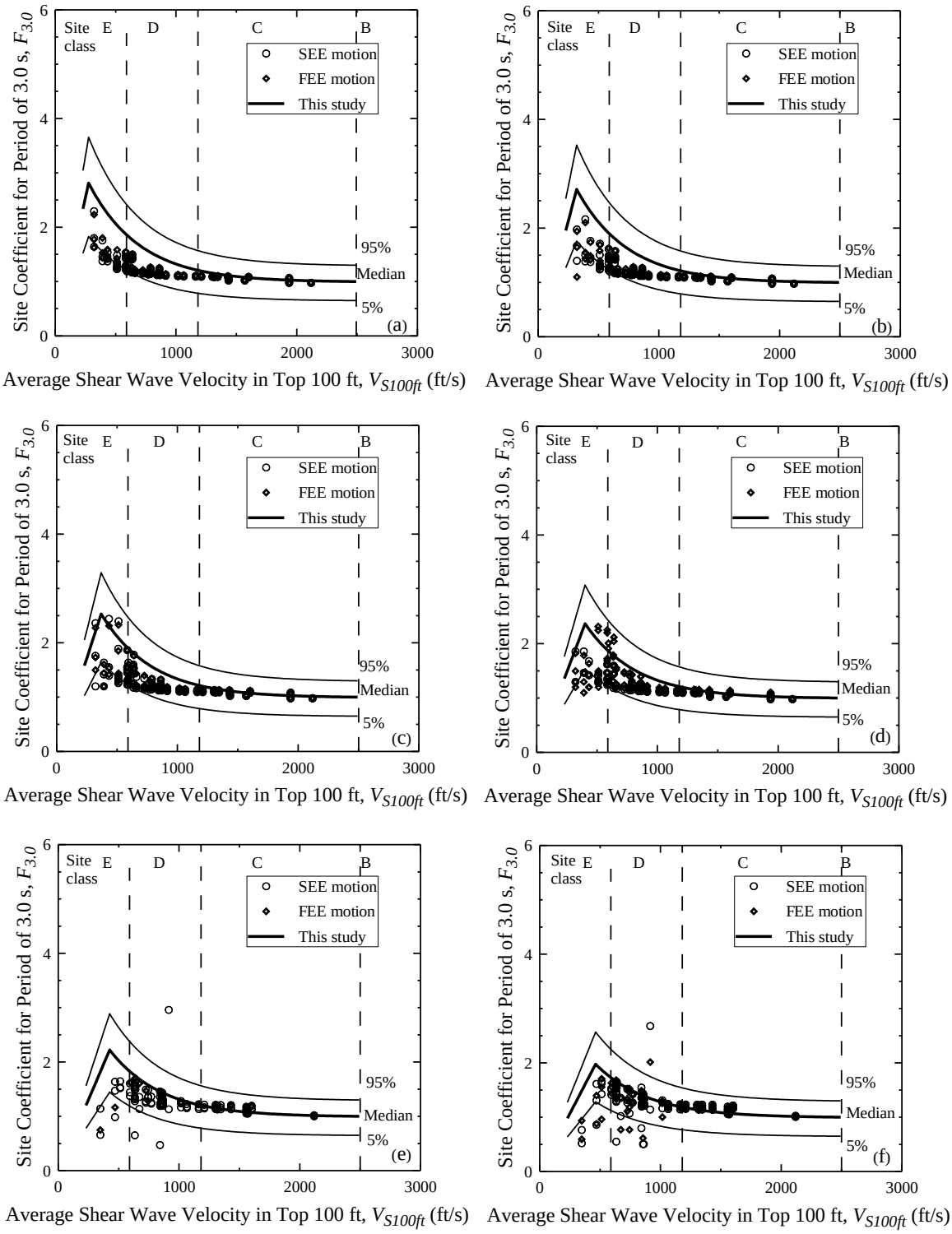

Figure B.8 Site coefficients for 3.0 s spectral period with $S_{3.0}$ equal to (a) 0.01 g, (b) 0.02 g, (c) 0.04 g, (d) 0.06 g, (e) 0.08 g and (f) 0.12 g based on V_S profiles shown in Figure B.1 for Myrtle Beach.

APPENDIX C

SUMMARY OF INPUTS AND OUTPUTS OF SITE RESPONSE ANALYSIS FOR THE COLUMBIA AREA

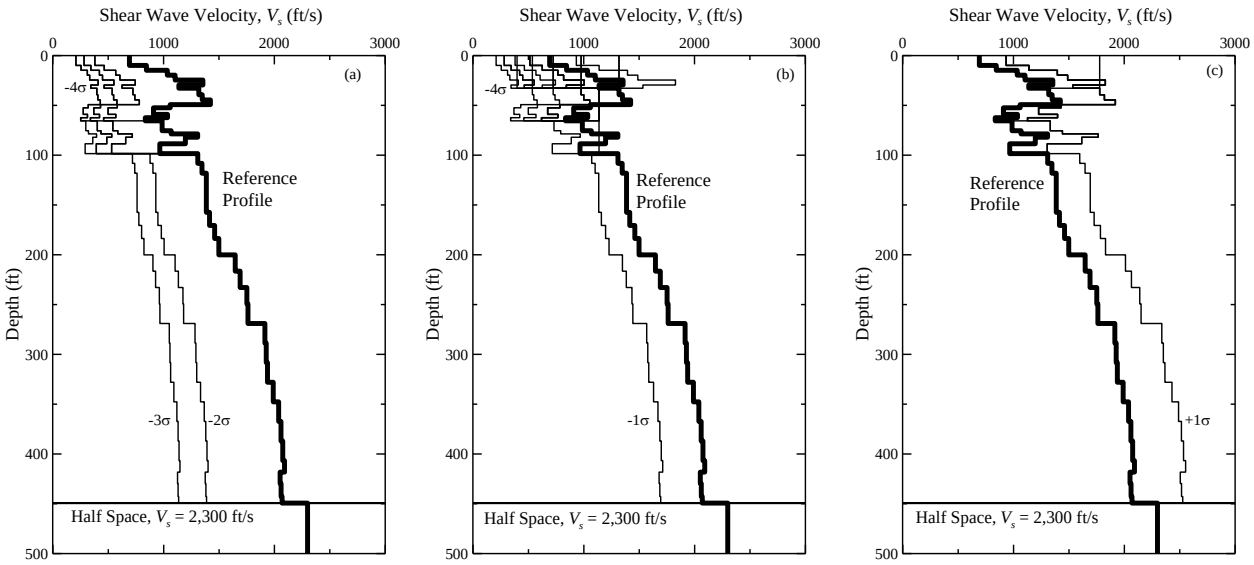

Figure C.1 Shear wave velocity profiles considered for Columbia-Florence-Lake Marion with soft rock half space at depth = 450 ft grouped by NEHRP Site Class (a) E, (b) D, and (c) C. The reference profile is compiled from Odum et al. (2003), Silva et al. (2003), Chapman et al. (2006) and Andrus et al. (2006), and the standard deviation values are based on Andrus et al. (2006).

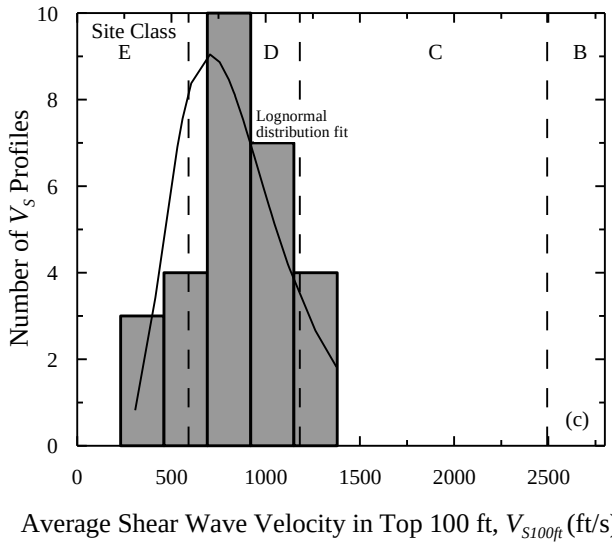

Figure C.2 V_{S100ft} histogram of shear wave velocity profiles in Figure C.1.

Table C.1 Table of best fit values of F_P and $V_{S100ftP}$.

Figure	F_P	$V_{S100ftP}$	a
C.3a	2.0	648	-
C.3b	1.6	787	-
C.3c	1.1	886	-
C.3d	1.1	1148	-
C.3e	1.0	984	-
C.3f	1.0	1017	-
C.4a	2.2	459	0.99
C.4b	1.5	722	0.99
C.4c	1.1	984	0.70
C.4d	1.0	1181	0.70
C.4e	1.0	820	0.70
C.4f	1.0	918	0.70
C.5a	2.4	722	0.72
C.5b	2.0	754	0.46
C.5c	1.8	787	0.99
C.5d	1.4	853	0.99
C.5e	1.4	853	0.99
C.5f	1.3	951	0.99
C.6a	2.8	568	0.83
C.6b	2.6	650	0.83
C.6c	2.3	825	0.83
C.6d	2.0	911	0.83
C.6e	2.0	918	0.83
C.6f	1.9	984	0.83
C.7a	3.0	410	0.98
C.7b	2.6	492	0.94
C.7c	2.3	558	0.59
C.7d	2.2	656	0.31
C.7e	2.4	722	0.73
C.7f	2.4	820	0.75
C.8a	2.3	295	0.99
C.8b	2.2	361	0.99
C.8c	2.0	426	0.96
C.8d	2.4	492	1.00
C.8e	2.4	623	0.75
C.8f	2.4	722	0.80

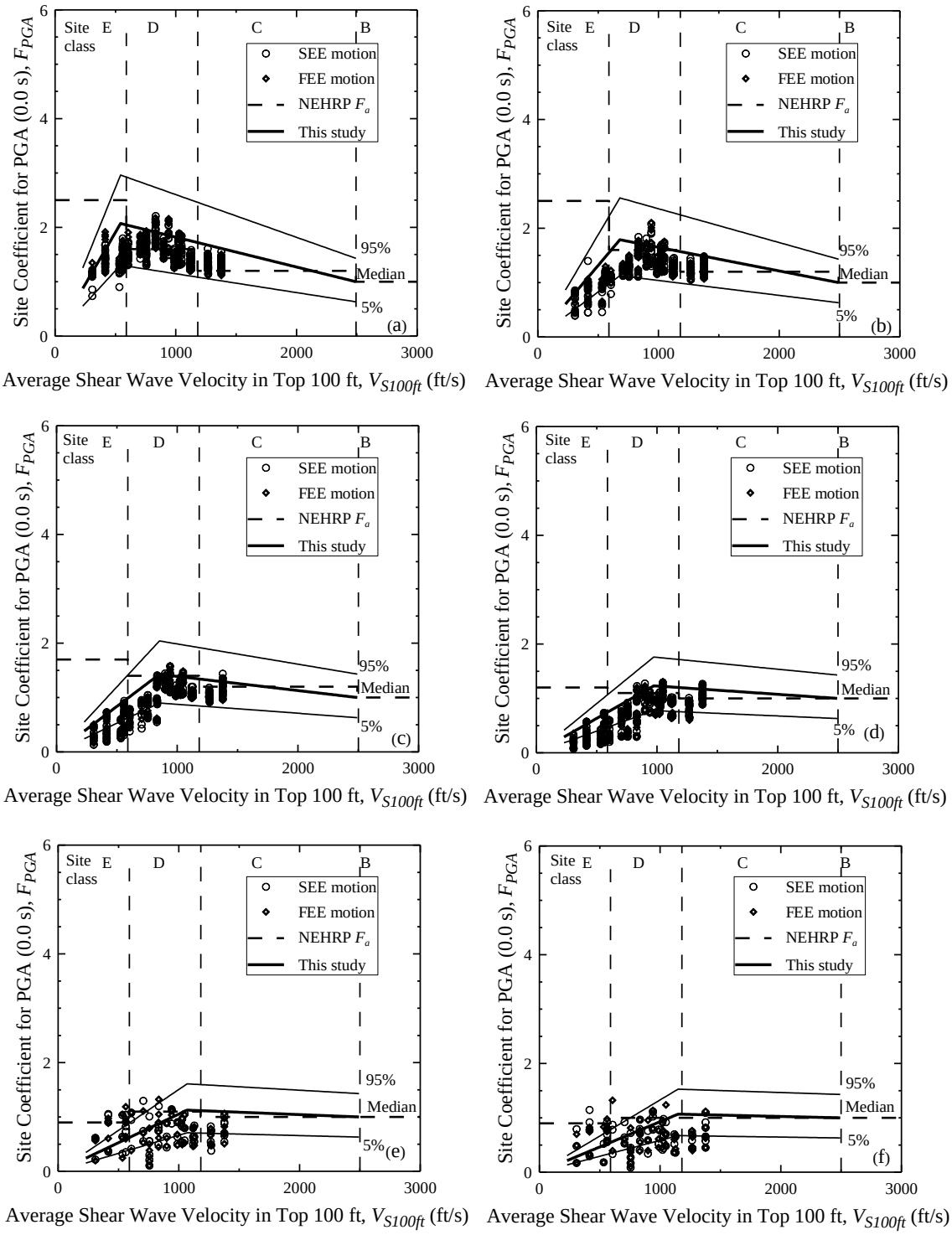

Figure C.3 Site coefficients for 0.0 s spectral period (free-field) with *PGA* equal to (a) 0.05 g, (b) 0.1 g, (c) 0.2 g, (d) 0.3 g, (e) 0.4 g, and (f) 0.5 g based on V_S profiles shown in Figure C.1 for Columbia.

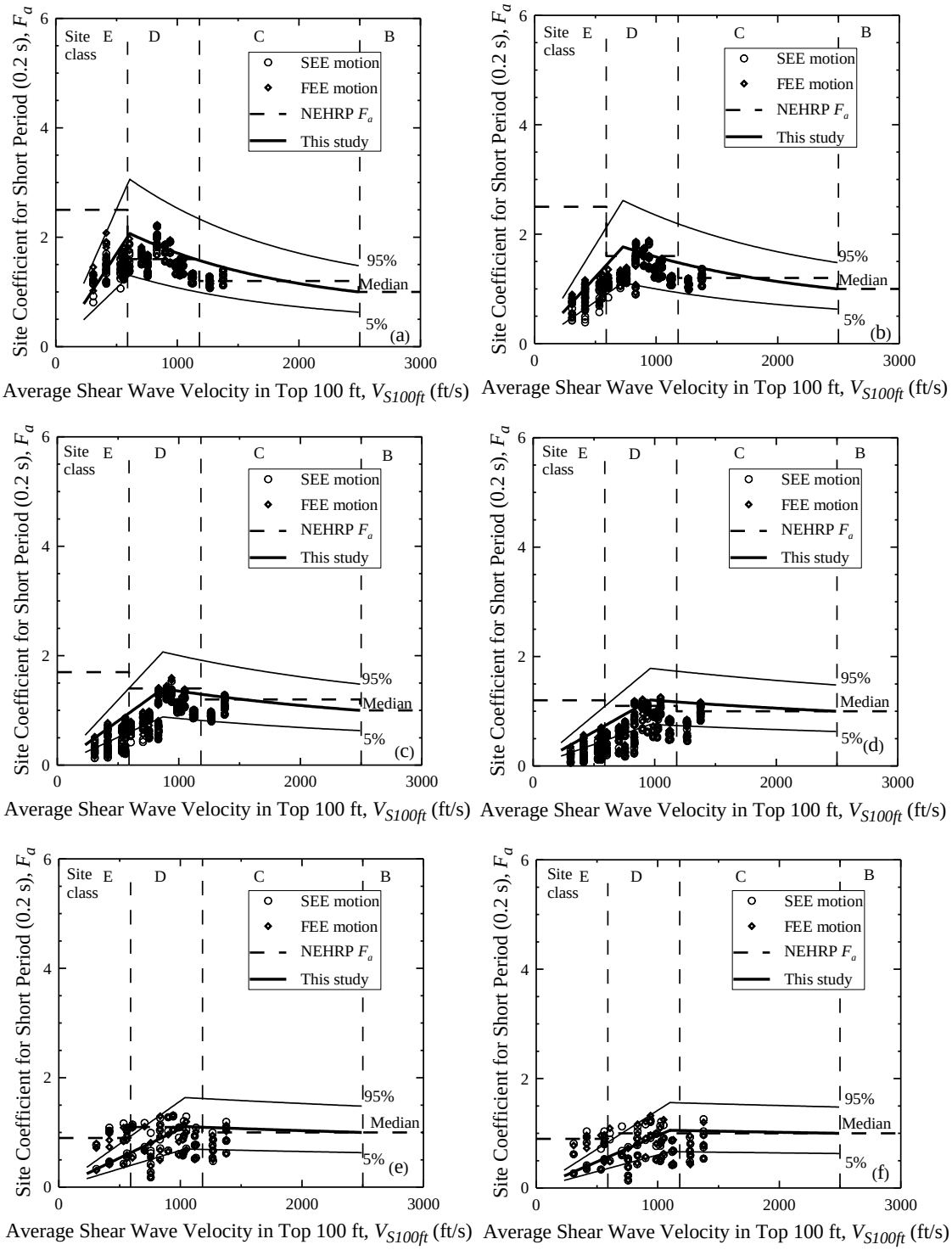

Figure C.4 Site coefficients for 0.2 s (short) spectral period with S_S equal to (a) 0.125 g, (b) 0.25 g, (c) 0.50 g, (d) 0.75 g, (e) 1.0 g, and (f) 1.25 g based on V_S profiles shown in Figure C.1 for Columbia.

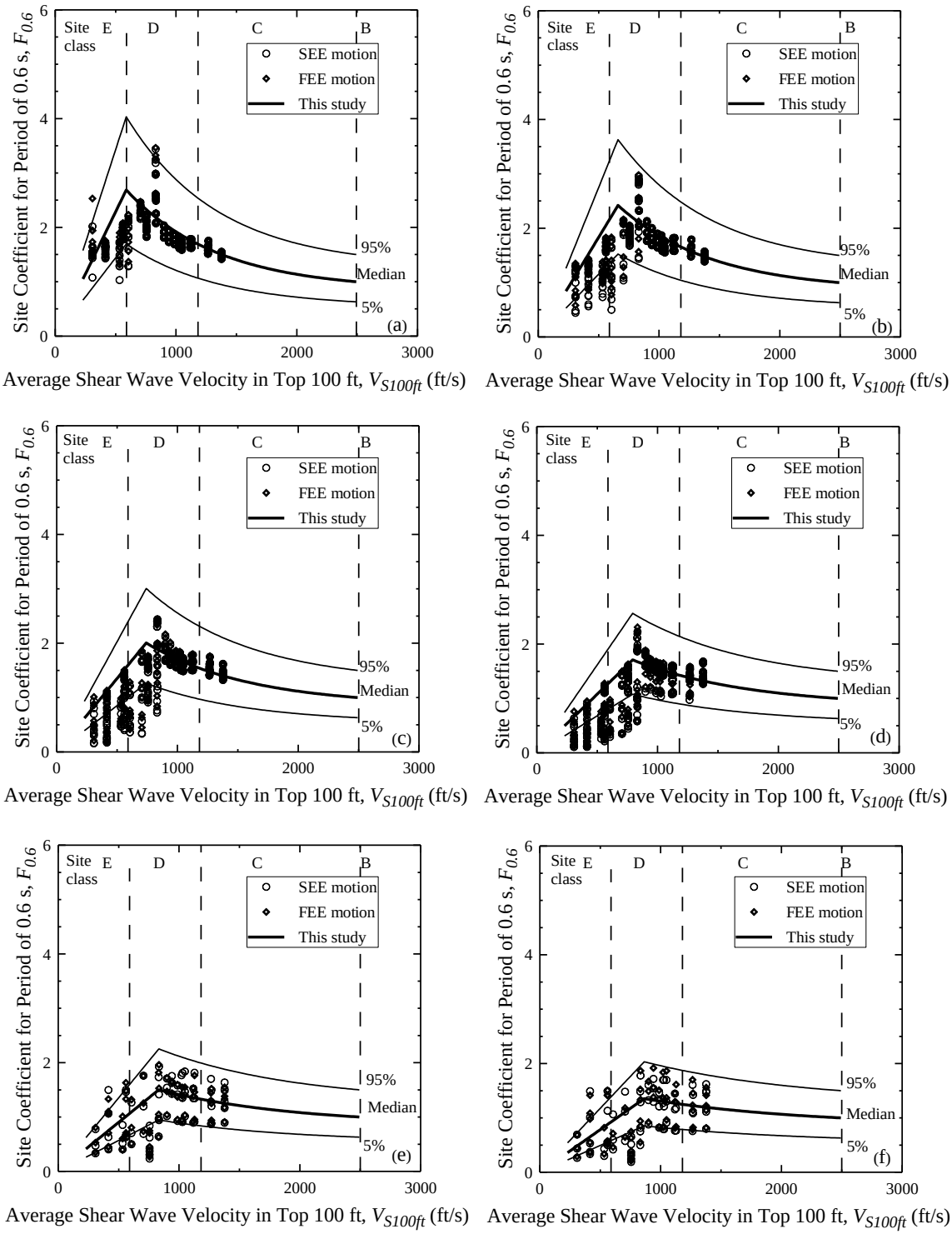

Figure C.5 Site coefficients for 0.6 s spectral period with $S_{0.6}$ equal to (a) 0.05 g, (b) 0.1 g, (c) 0.2 g, (d) 0.3 g, (e) 0.4 g, and (f) 0.5 g based on V_S profiles shown in Figure C.1 for Columbia.

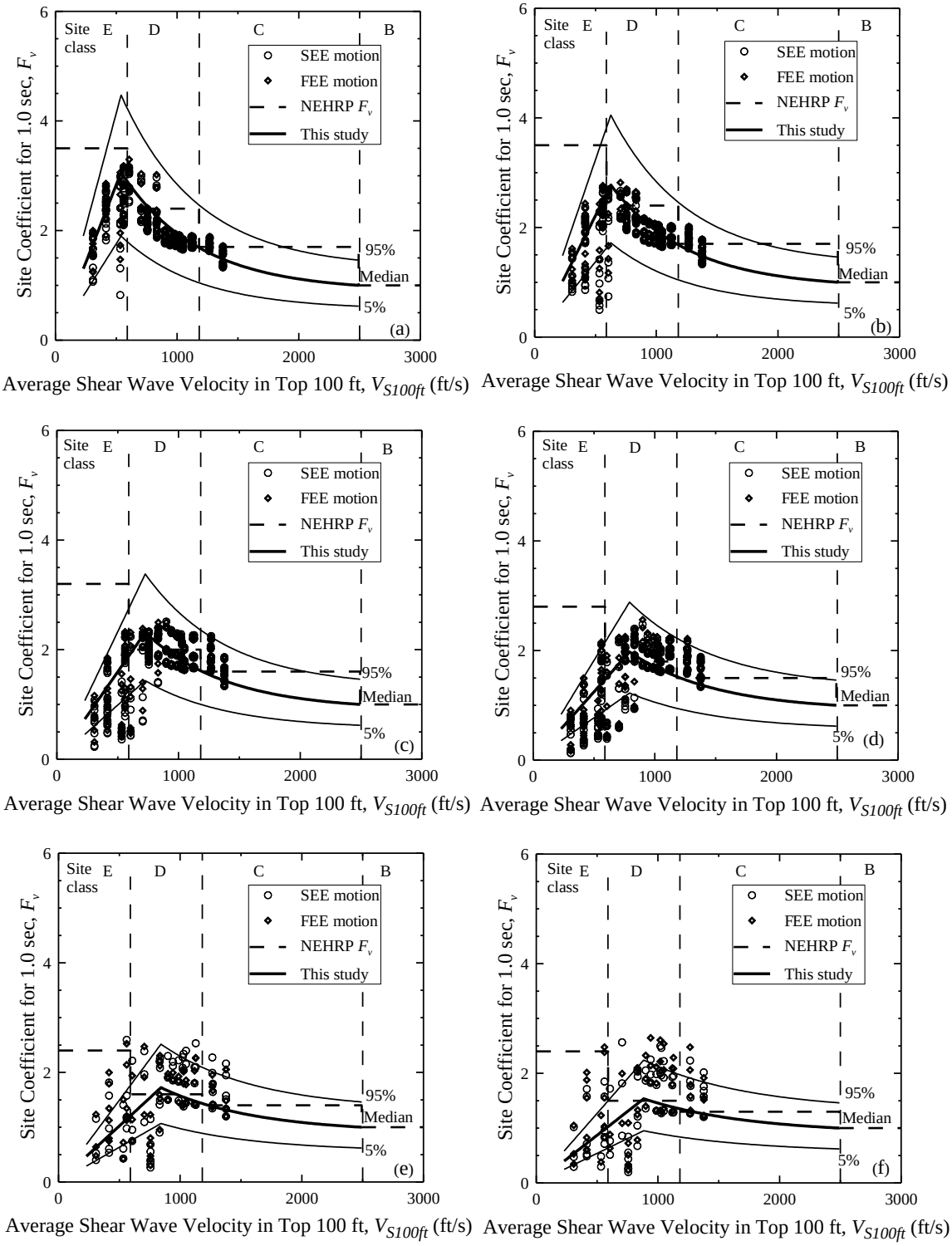

Figure C.6 Site coefficients for 1.0 s (long) spectral period with S_1 equal to (a) 0.05 g, (b) 0.1 g, (c) 0.2 g, (d) 0.3 g, (e) 0.4 g, and (f) 0.5 g based on V_S profiles shown in Figure C.1 for Columbia.

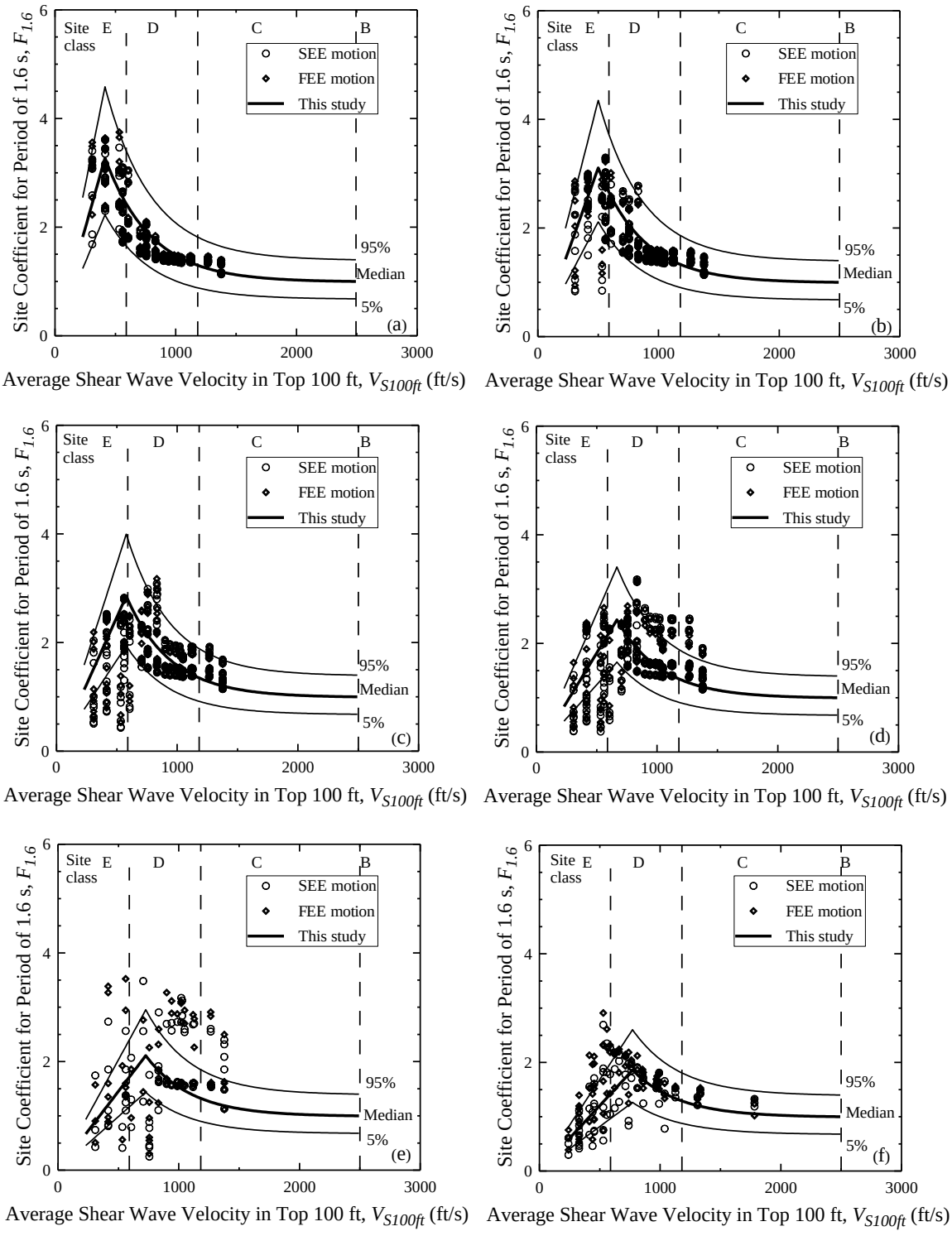

Figure C.7 Site coefficients for 1.6 s spectral period with $S_{1.6}$ equal to (a) 0.02 g, (b) 0.05 g, (c) 0.1 g, (d) 0.2 g, (e) 0.3 g, and (f) 0.4 g based on V_S profiles shown in Figure C.1 for Columbia.

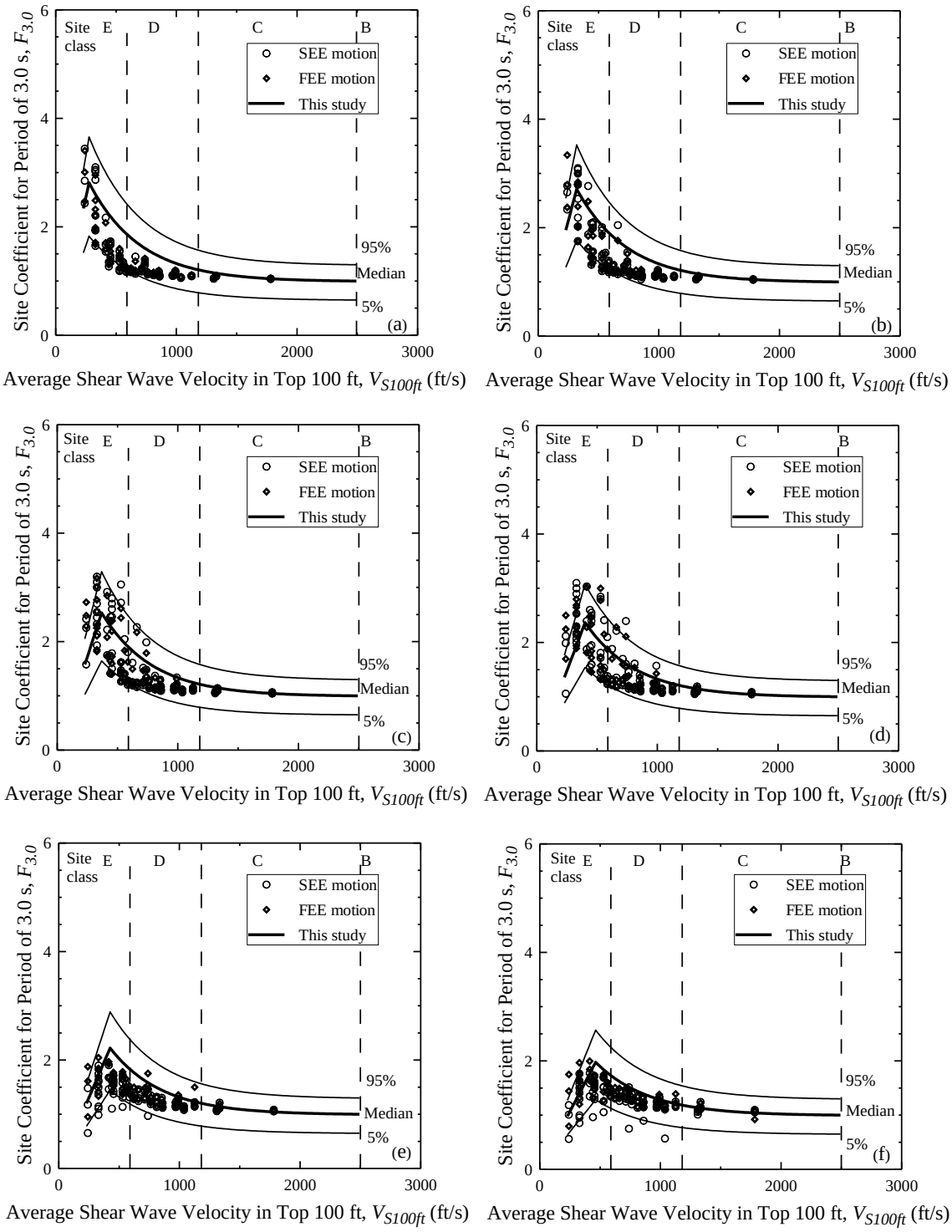

Figure C.8 Site coefficients for 3.0 s spectral period with $S_{3.0}$ equal to (a) 0.01 g, (b) 0.02 g, (c) 0.04 g, (d) 0.06 g, (e) 0.08 g and (f) 0.12 g based on V_S profiles shown in Figure C.1 for Columbia.

APPENDIX D

SUMMARY OF INPUTS AND OUTPUTS OF SITE RESPONSE ANALYSIS FOR THE AIKEN AREA

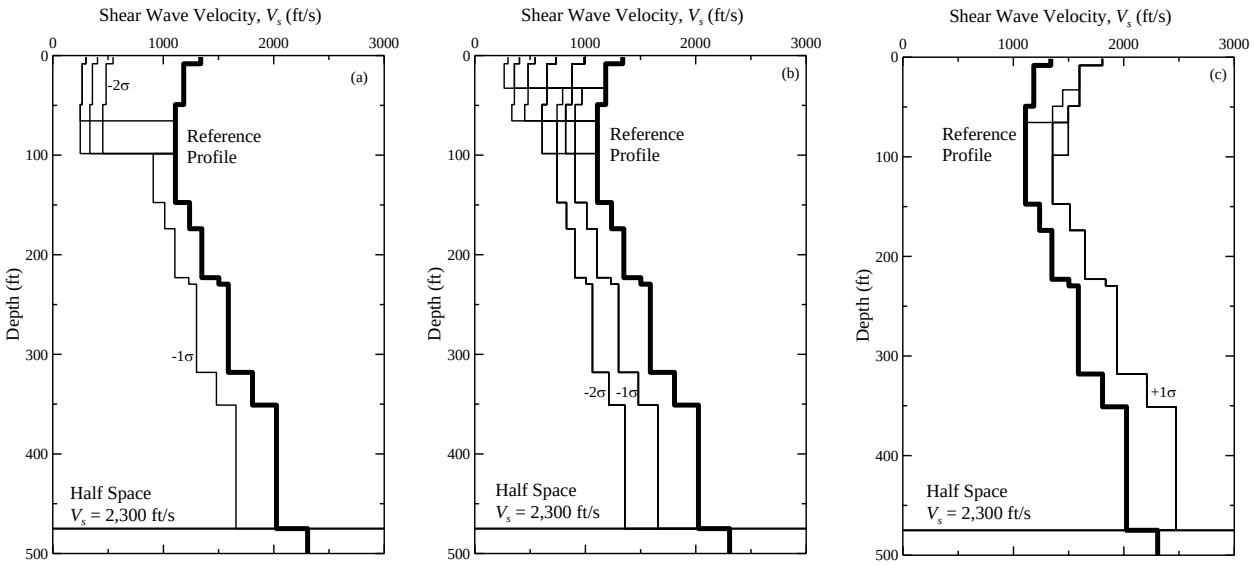

Figure D.1 Shear wave velocity profiles considered for Aiken with soft rock half space at depth = 475 ft grouped by NEHRP Site Class (a) E, (b) D, and (c) C. The reference profile is from Silva et al. (2003), and the standard deviation values are based on a study by Andrus et al. (2006).

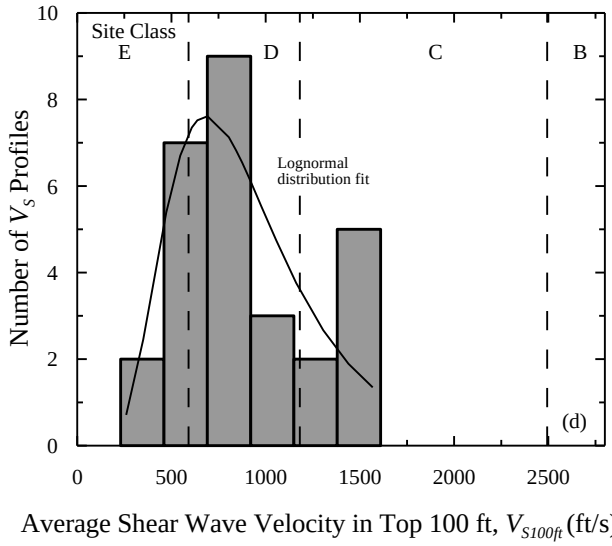

Figure D.2 V_{S100ft} histogram of shear wave velocity profiles in Figure D.1.

Table D.1 Table of best fit values of F_P and $V_{S100ftP}$.

Figure	F_P	$V_{S100ftP}$	a
D.3a	2.3	525	-
D.3b	1.8	607	-
D.3c	1.7	754	-
D.3d	1.3	853	-
D.3e	1.0	1476	-
D.3f	1.0	1509	-
D.4a	2.1	590	0.98
D.4b	1.8	722	0.98
D.4c	1.4	820	0.99
D.4d	1.2	886	0.99
D.4e	1.0	1345	0.99
D.4f	1.0	1443	0.99
D.5a	2.6	590	0.72
D.5b	2.3	623	0.46
D.5c	2.2	701	0.90
D.5d	1.8	853	0.70
D.5e	1.1	1050	0.99
D.5f	1.0	1050	0.99
D.6a	3.2	590	0.85
D.6b	3.0	623	0.85
D.6c	2.8	656	0.85
D.6d	2.5	722	0.85
D.6e	1.1	951	0.85
D.6f	1.1	984	0.85
D.7a	3.5	374	0.85
D.7b	3.3	441	0.85
D.7c	3.0	489	0.83
D.7d	2.9	656	0.85
D.7e	1.4	886	0.85
D.7f	1.4	918	0.85
D.8a	2.4	239	0.90
D.8b	2.3	295	0.90
D.8c	2.2	590	0.90
D.8d	2.1	656	0.90
D.8e	1.7	689	0.90
D.8f	1.6	918	0.90

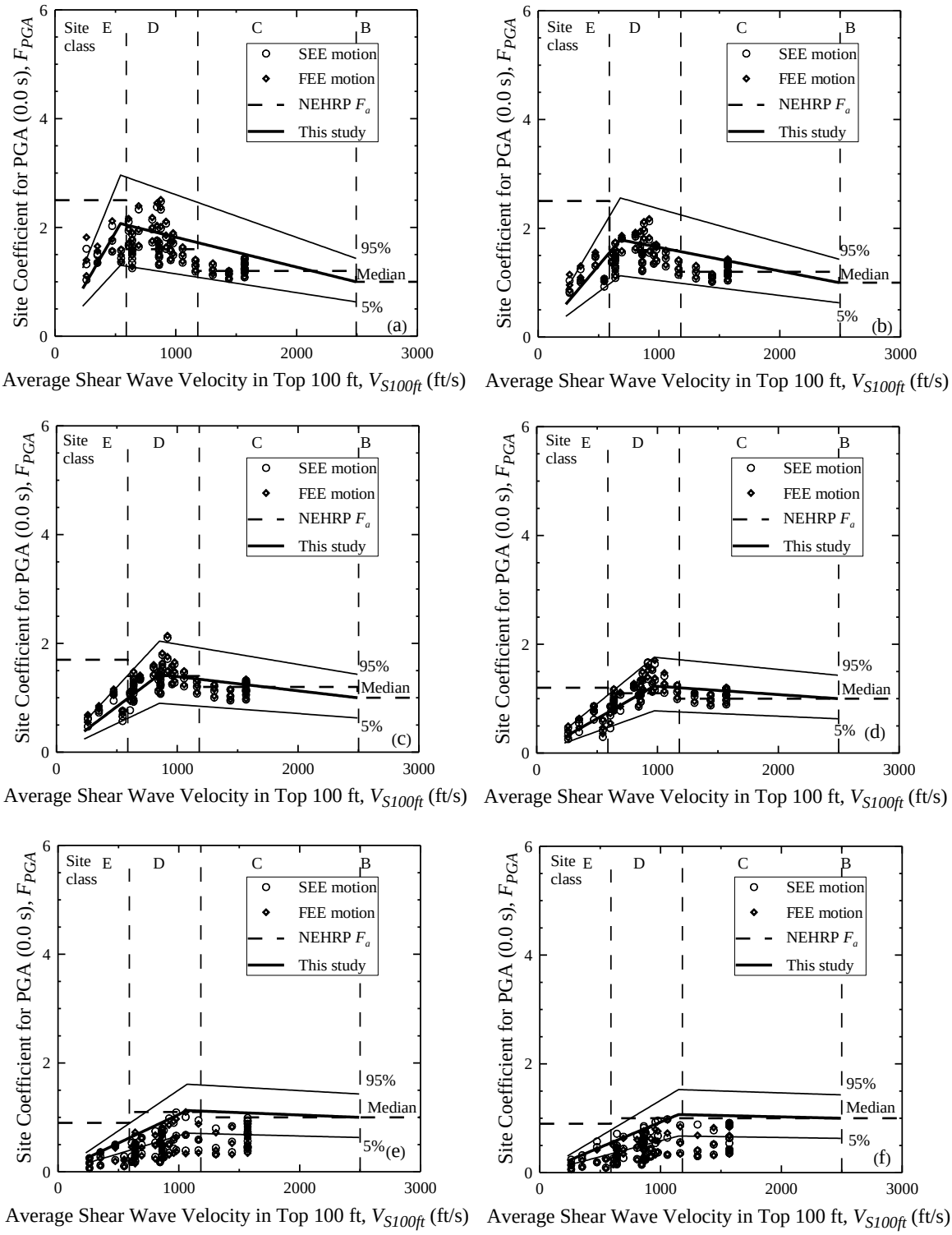

Figure D.3 Site coefficients for 0.0 s spectral period (free-field) with *PGA* equal to (a) 0.05 g, (b) 0.1 g, (c) 0.2 g, (d) 0.3 g, (e) 0.4 g, and (f) 0.5 g based on V_S profiles shown in Figure D.1 for Aiken.

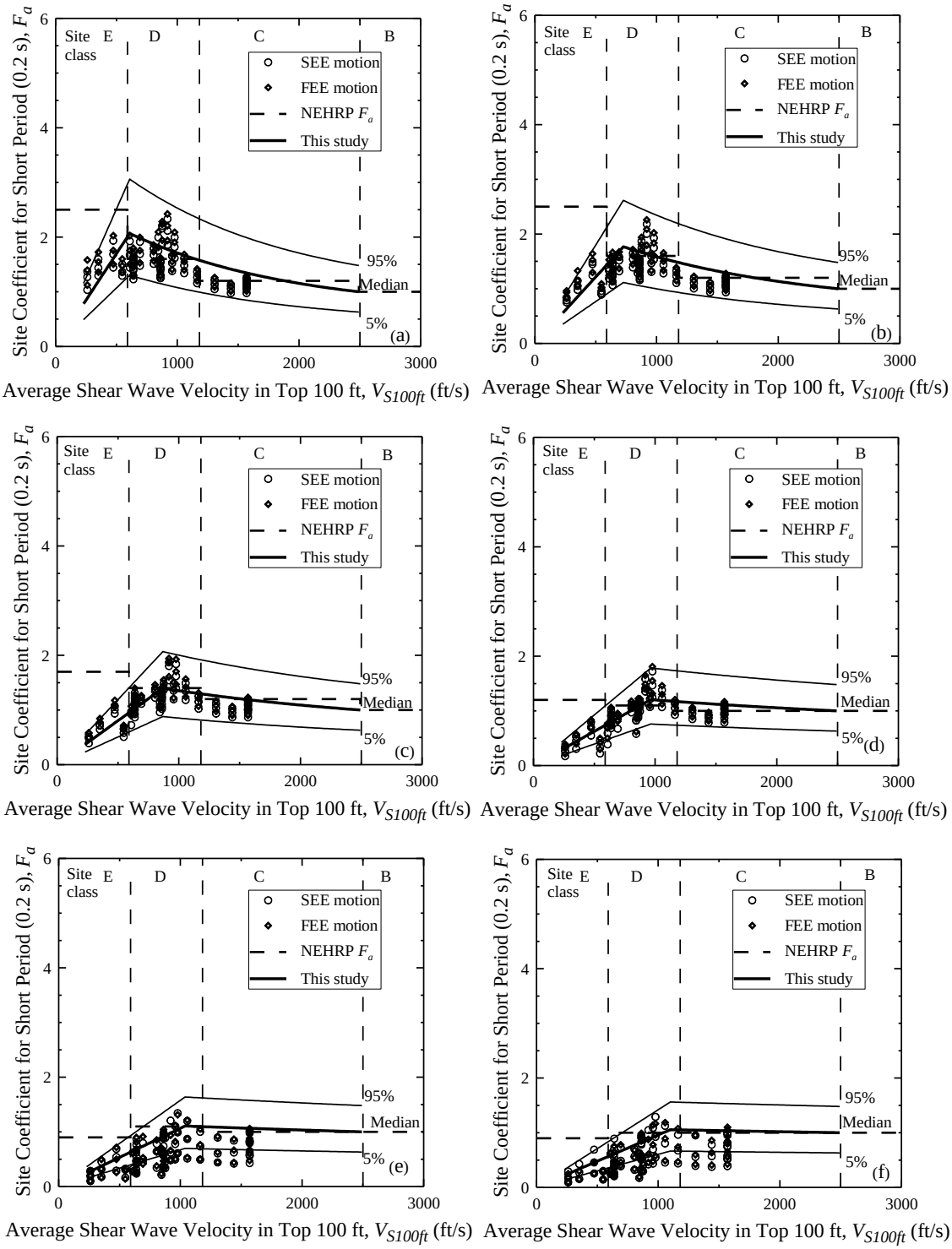

Figure D.4 Site coefficients for 0.2 s (short) spectral period with S_S equal to (a) 0.125 g, (b) 0.25 g, (c) 0.50 g, (d) 0.75 g, (e) 1.0 g, and (f) 1.25 g based on V_S profiles shown in Figure D.1 for Aiken.

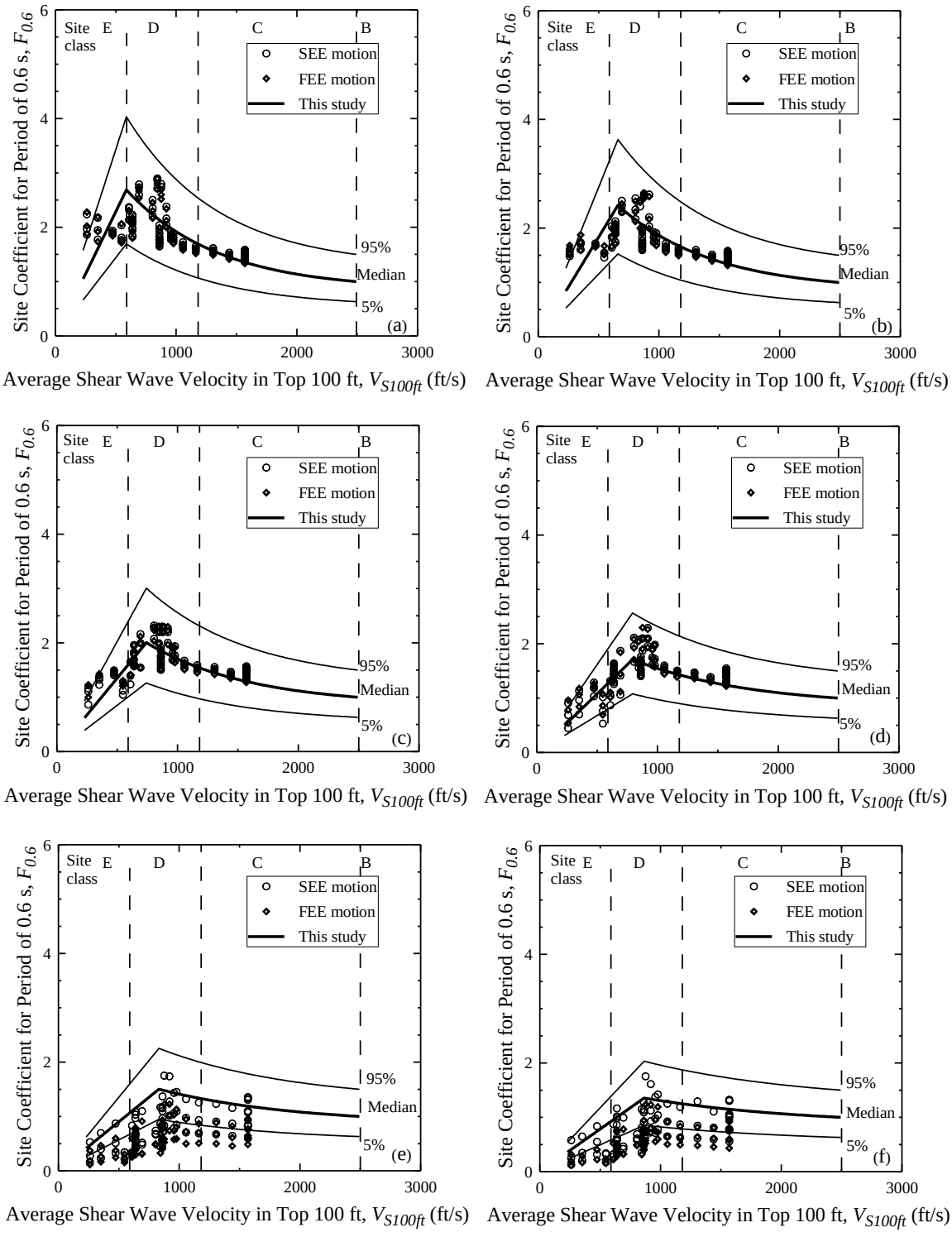

Figure D.5 Site coefficients for 0.6 s spectral period with $S_{0.6}$ equal to (a) 0.05 g, (b) 0.1 g, (c) 0.2 g, (d) 0.3 g, (e) 0.4 g, and (f) 0.5 g based on V_S profiles shown in Figure D.1 for Aiken.

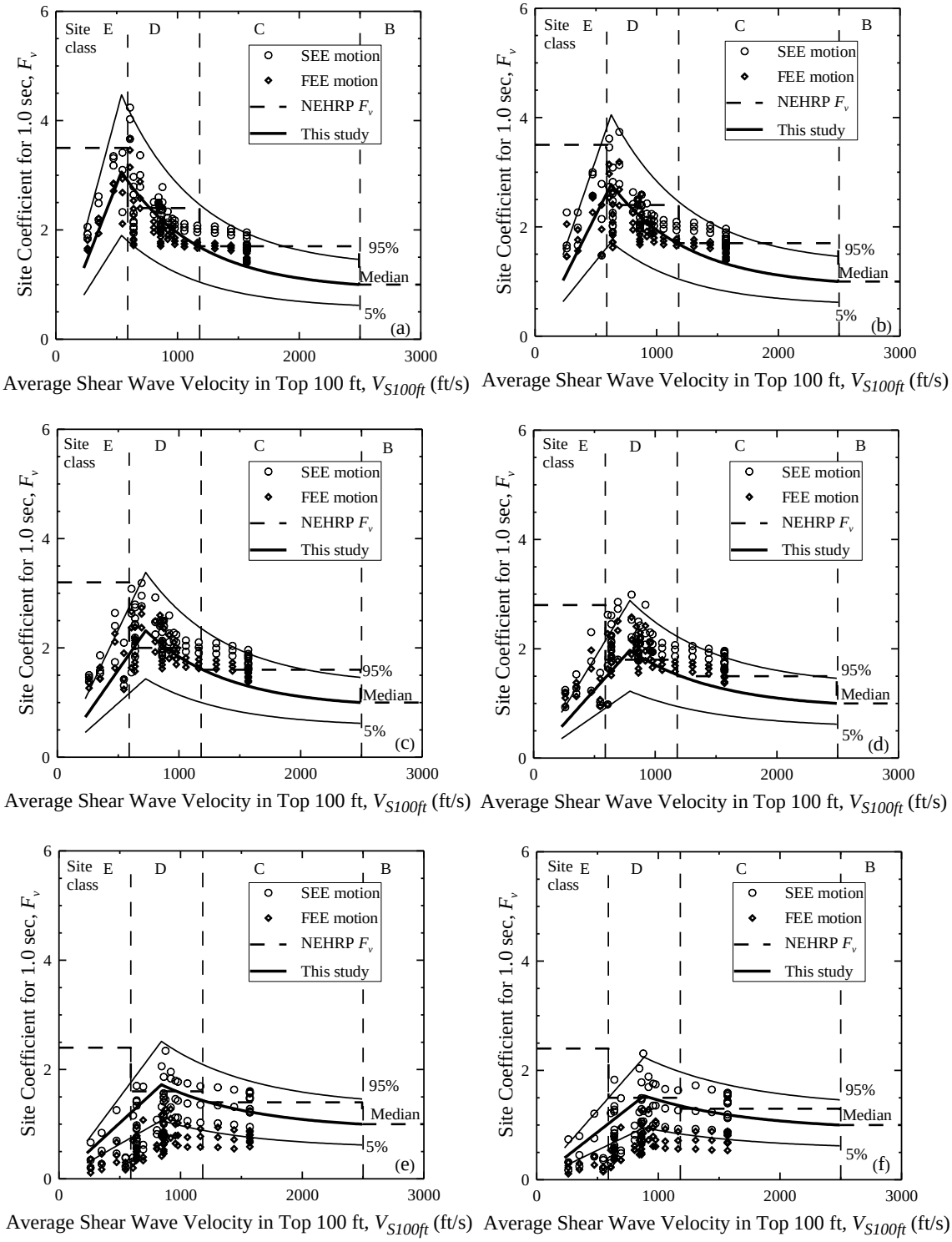

Figure D.6 Site coefficients for 1.0 s (long) spectral period with S_1 equal to (a) 0.05 g, (b) 0.1 g, (c) 0.2 g, (d) 0.3 g, (e) 0.4 g, and (f) 0.5 g based on V_S profiles shown in Figure D.1 for Aiken.

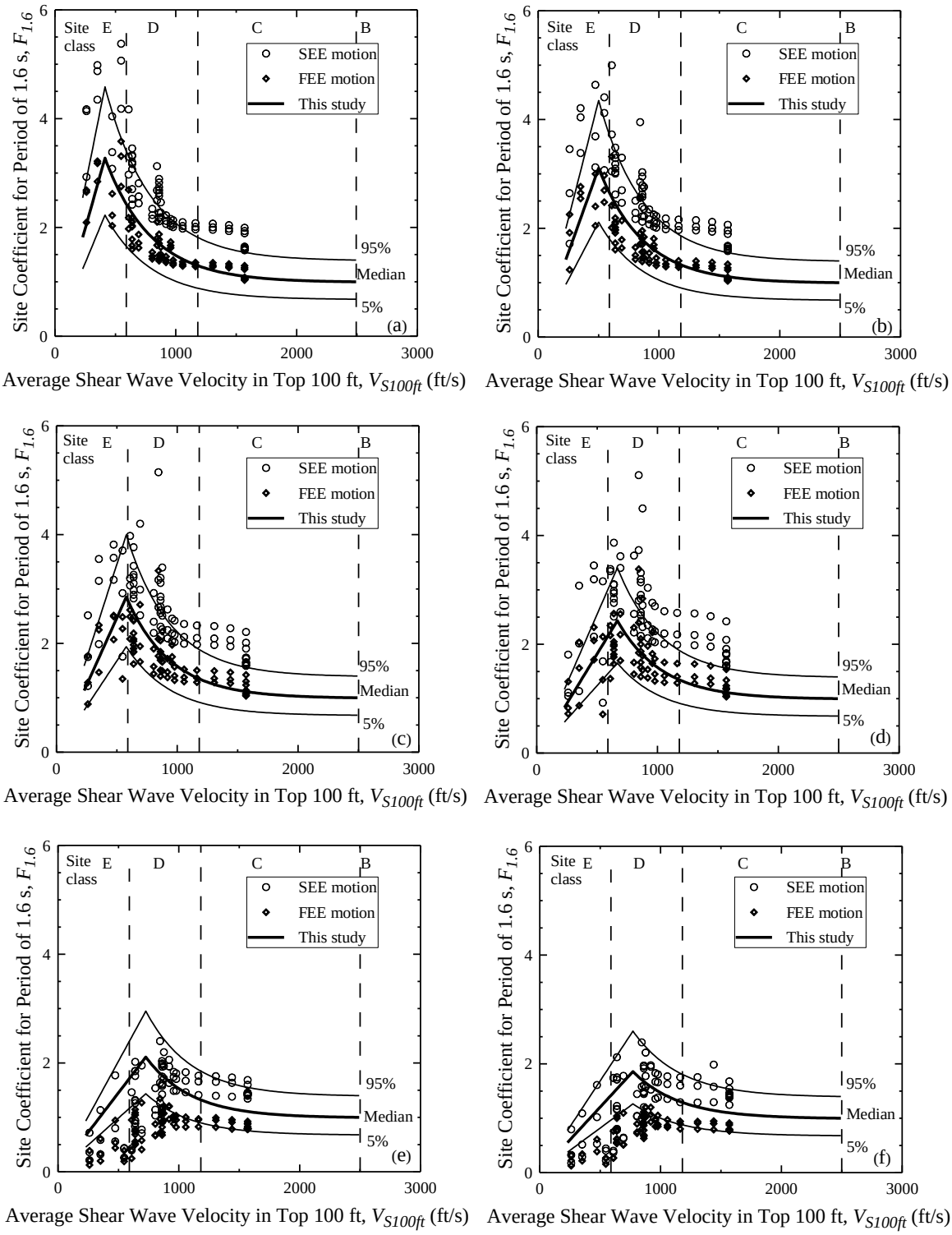

Figure D.7 Site coefficient for 1.6 s spectral period with $S_{1.6}$ equal to (a) 0.02 g, (b) 0.05 g, (c) 0.1 g, (d) 0.2 g, (e) 0.3 g, and (f) 0.4 g based on V_S profiles shown in Figure D.1 for Aiken.

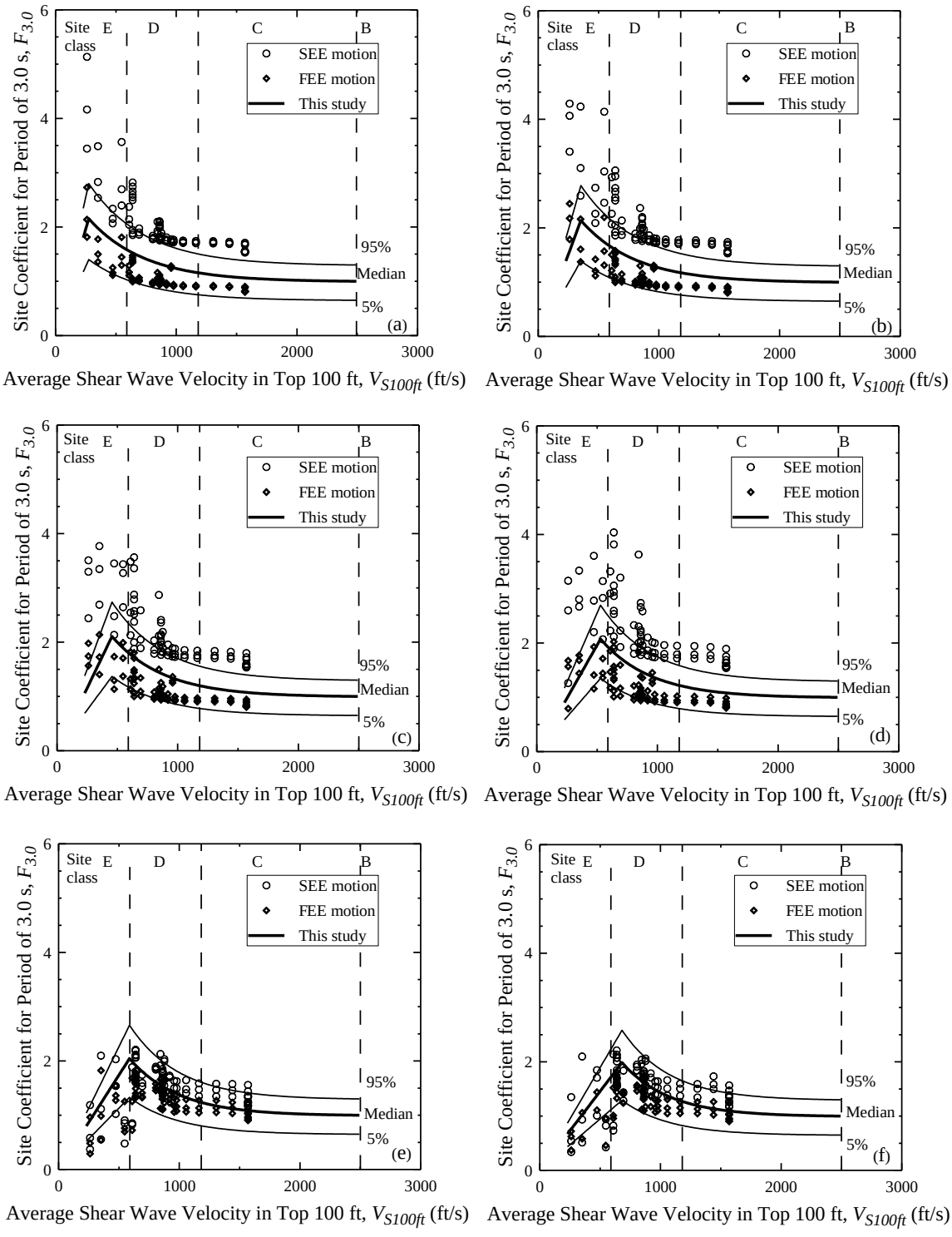

Figure D.8 Site coefficient for 3.0 s spectral period with $S_{3.0}$ equal to (a) 0.01 g, (b) 0.02 g, (c) 0.04 g, (d) 0.06 g, (e) 0.08 g and (f) 0.12 g based on V_S profiles shown in Figure D.1 for Aiken.

APPENDIX E

SUMMARY OF INPUTS AND OUTPUTS OF SITE RESPONSE ANALYSIS FOR THE SAVANNAH AREA

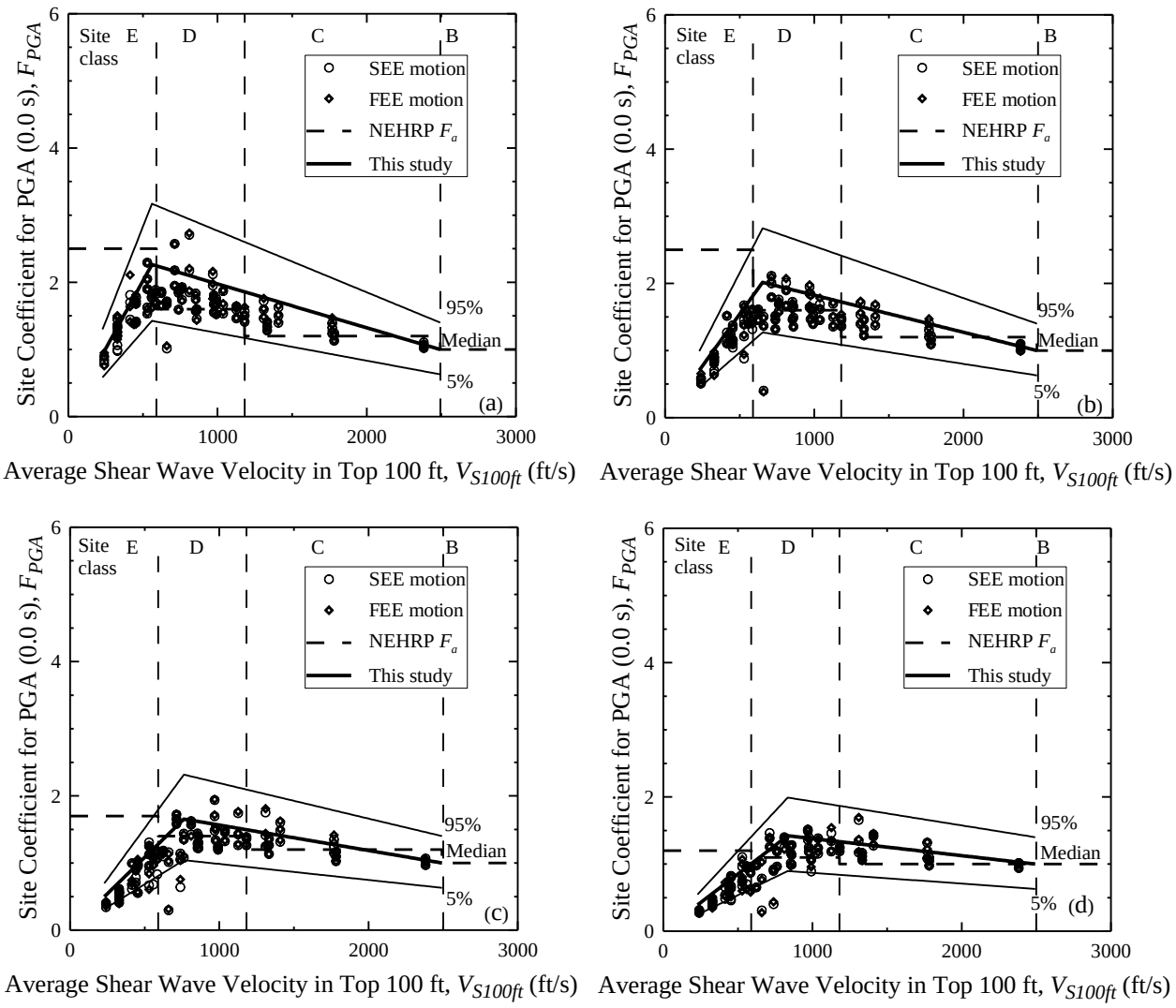

Figure E.1 Site coefficients for 0.0 s spectral period (free-field) with *PGA* equal to (a) 0.05 g, (b) 0.1 g, (c) 0.2 g, (d) 0.3 g, and (e) 0.4 g for Savannah.

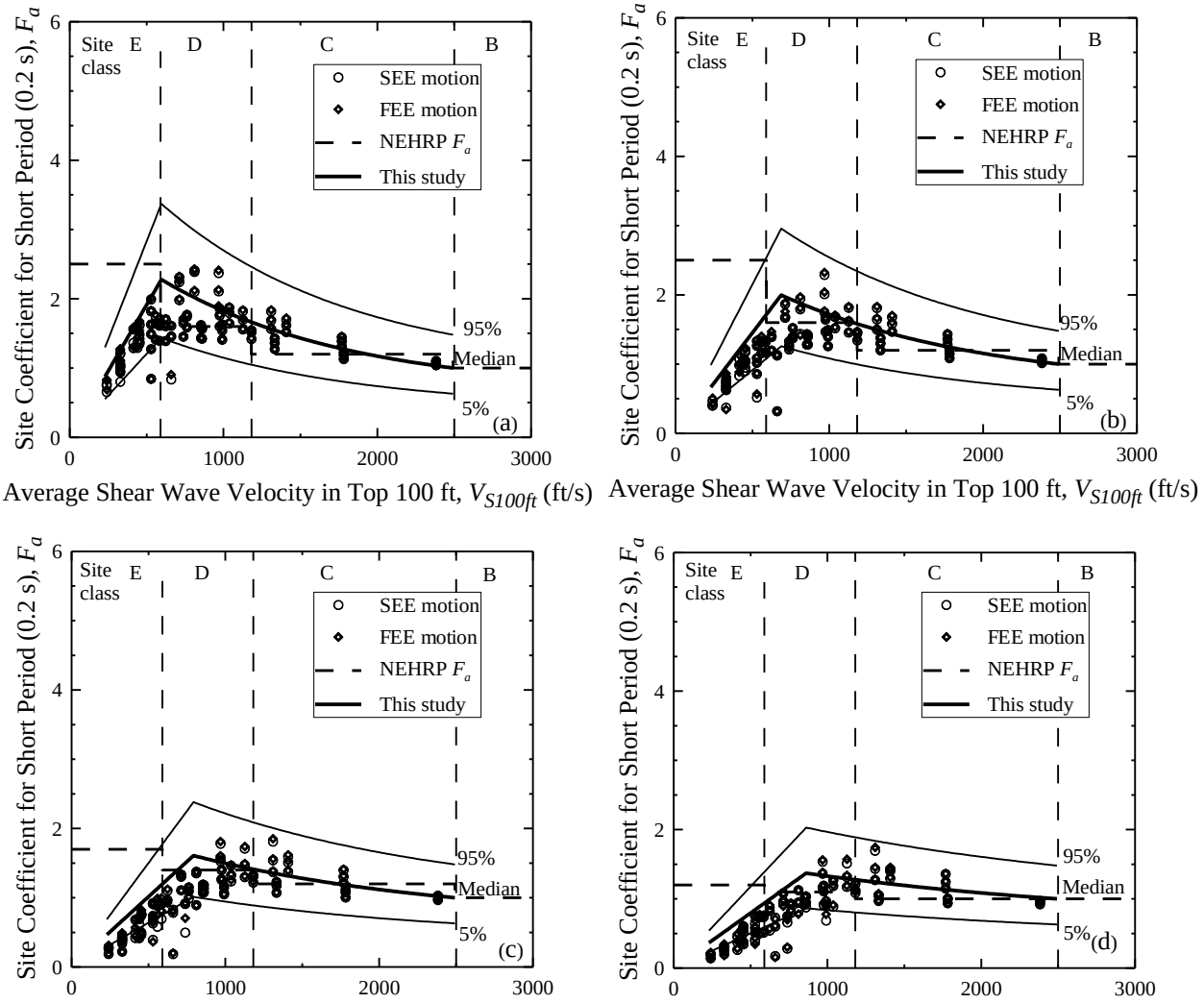

Figure E.2 Site coefficients for 0.2 s (short) spectral period with S_S equal to (a) 0.125 g, (b) 0.25 g, (c) 0.50 g, and (d) 0.75 g for Savannah.

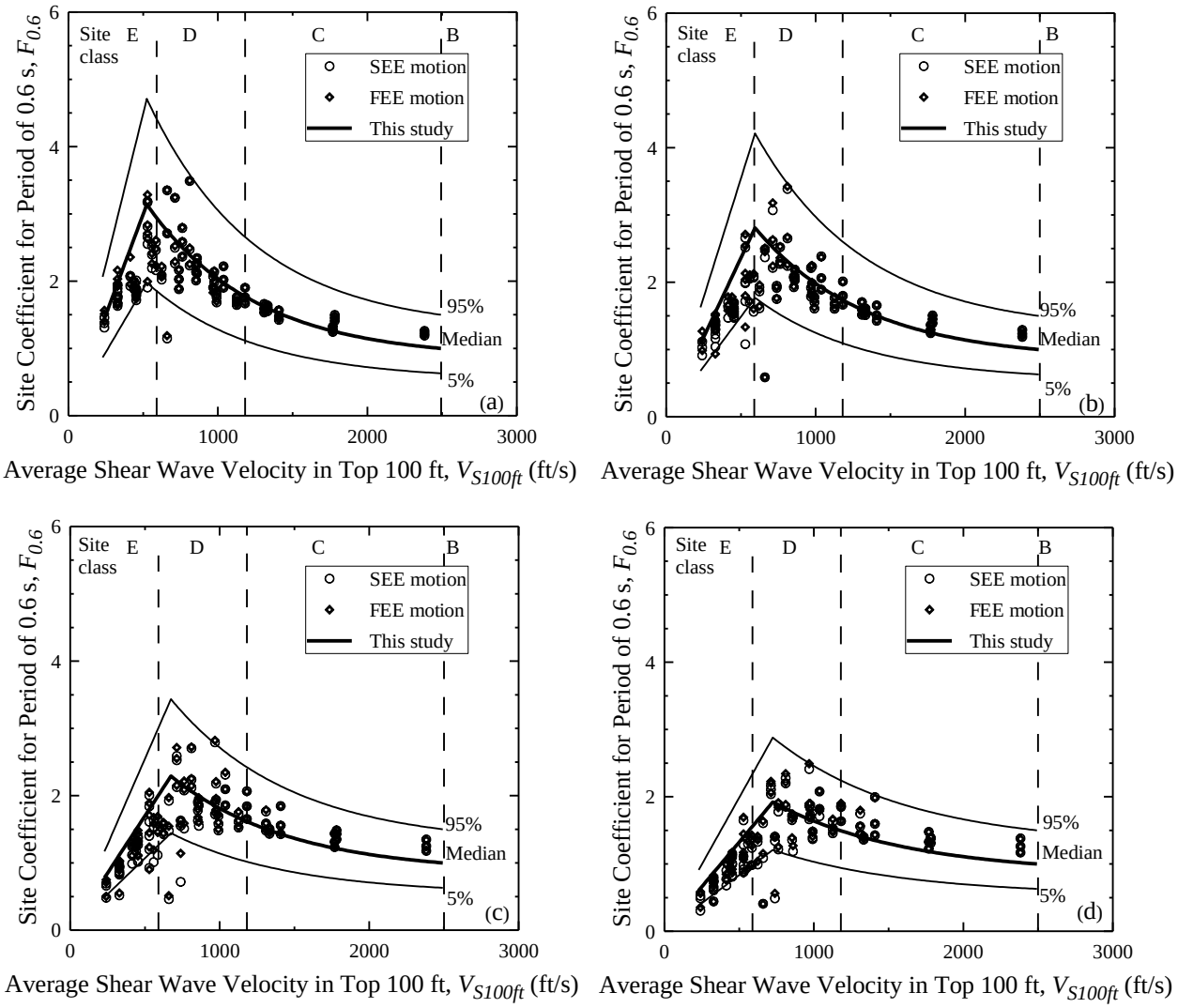

Figure E.3 Site coefficients for 0.6 s spectral period with $S_{0.6}$ equal to (a) 0.05 g, (b) 0.1 g, (c) 0.2 g, and (d) 0.3 g for Savannah.

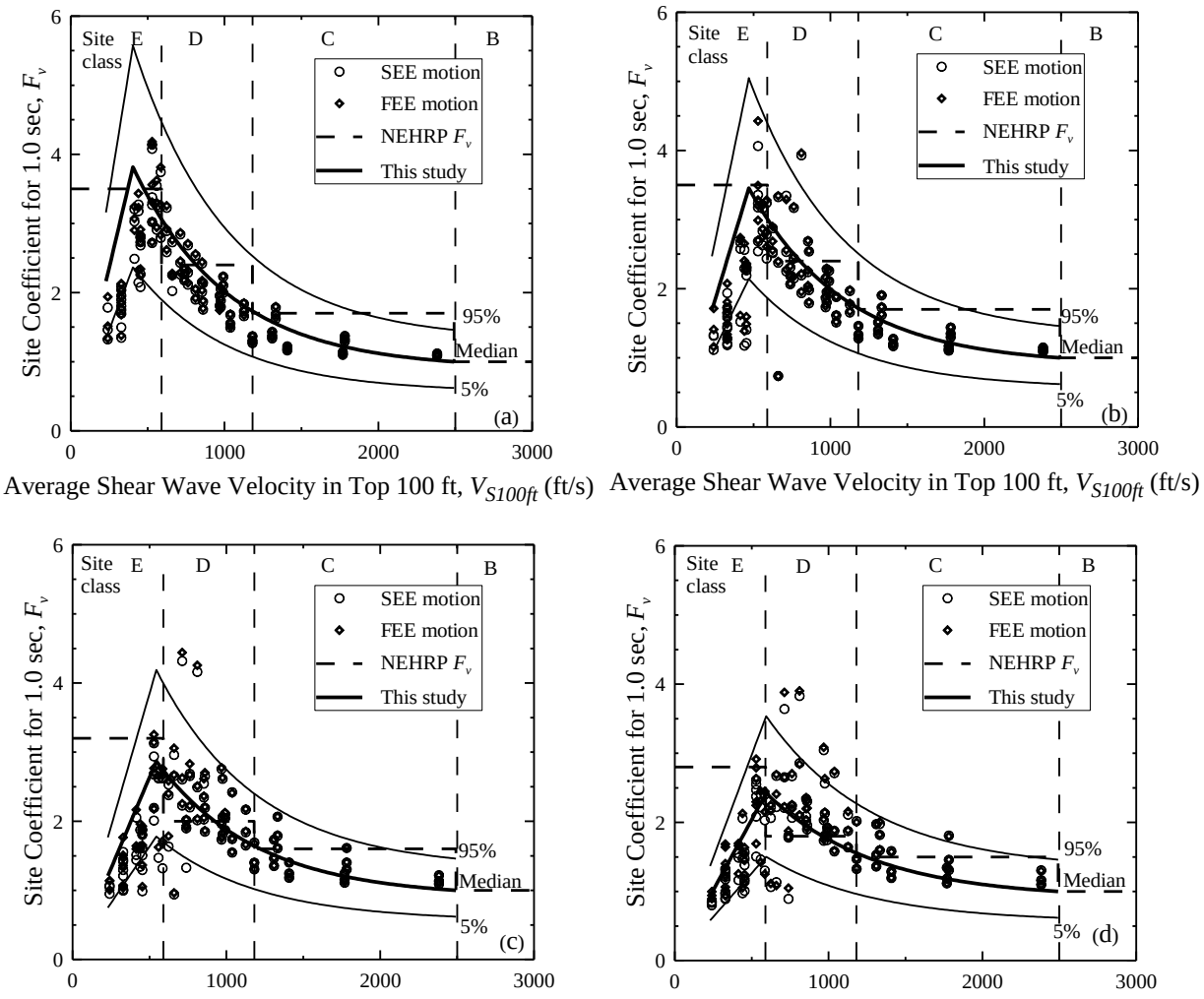

Figure E.4 Site coefficients for 1.0 s (long) spectral period with S_1 equal to (a) 0.05 g, (b) 0.1 g, (c) 0.2 g, and (d) 0.3 g for Savannah.

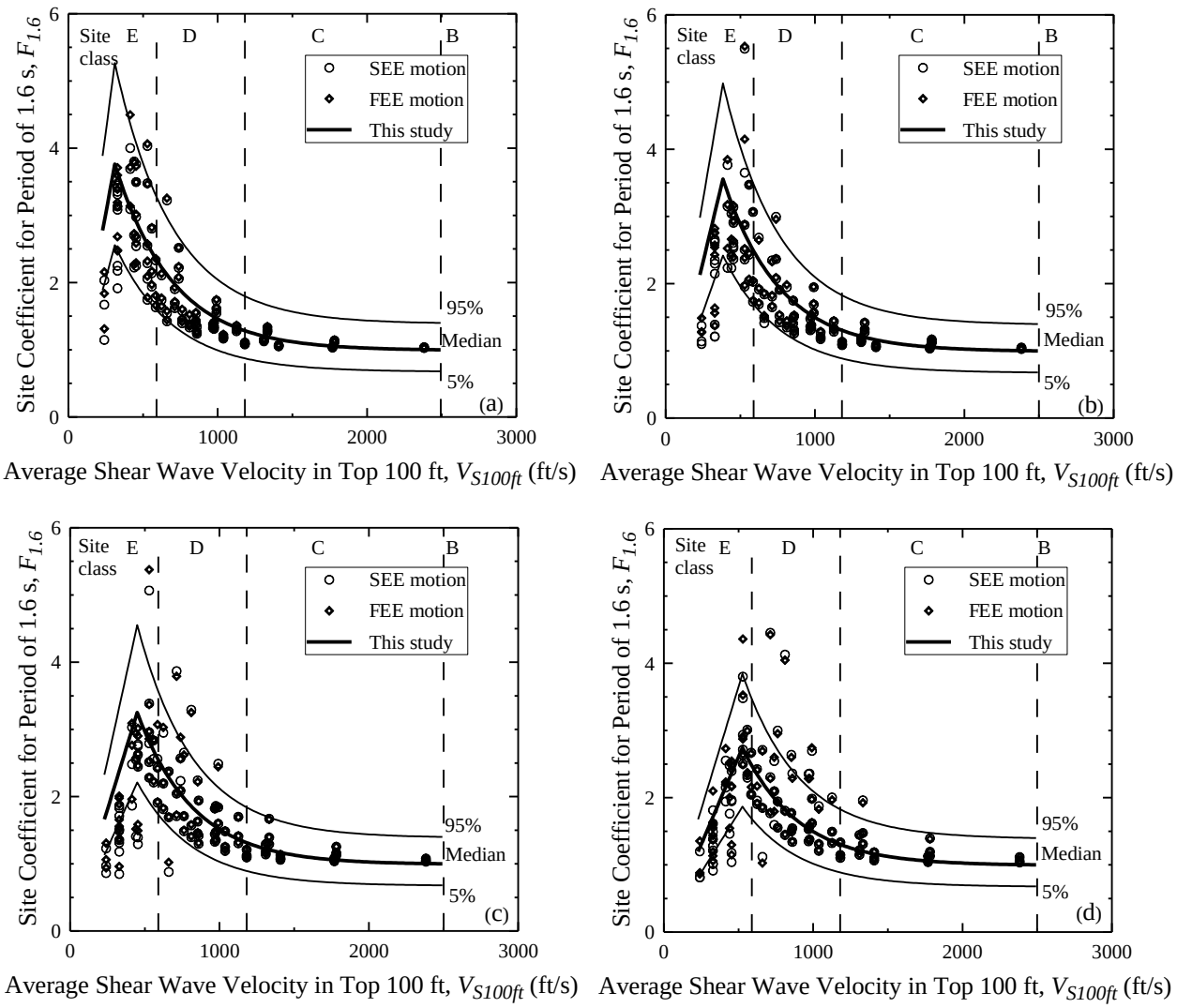

Figure E.5 Site coefficient for 1.6 s spectral period with $S_{1.6}$ equal to (a) 0.02 g, (b) 0.05 g, (c) 0.1 g, and (d) 0.2 g for Savannah.

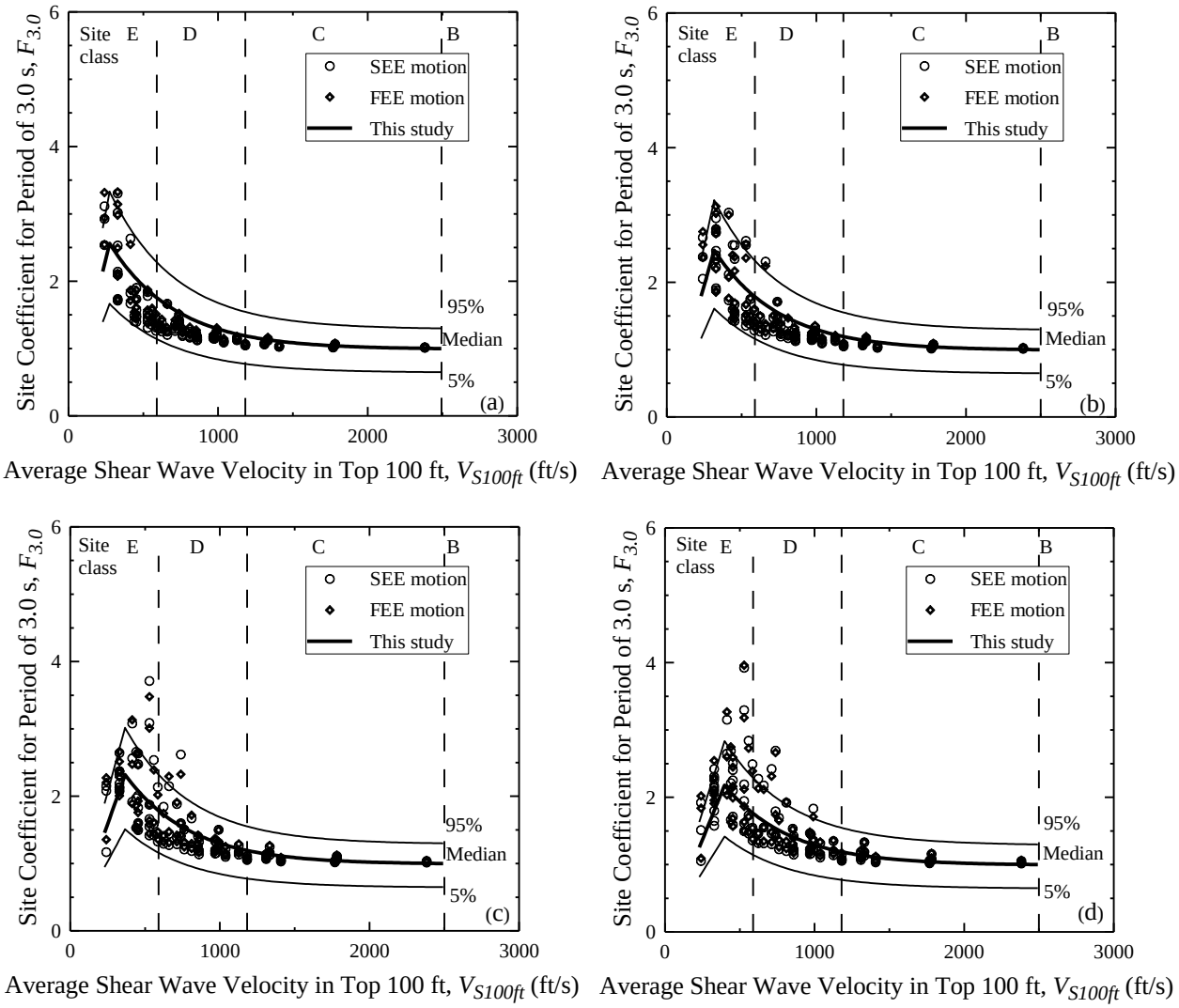

Figure E.6 Site coefficient for 3.0 s spectral period with $S_{3.0}$ equal to (a) 0.01 g, (b) 0.02 g, (c) 0.04 g, and (d) 0.06 g for Savannah.

APPENDIX F

SUMMARY OF INPUTS AND OUTPUTS OF SITE RESPONSE ANALYSIS FOR THE FLORENCE AREA

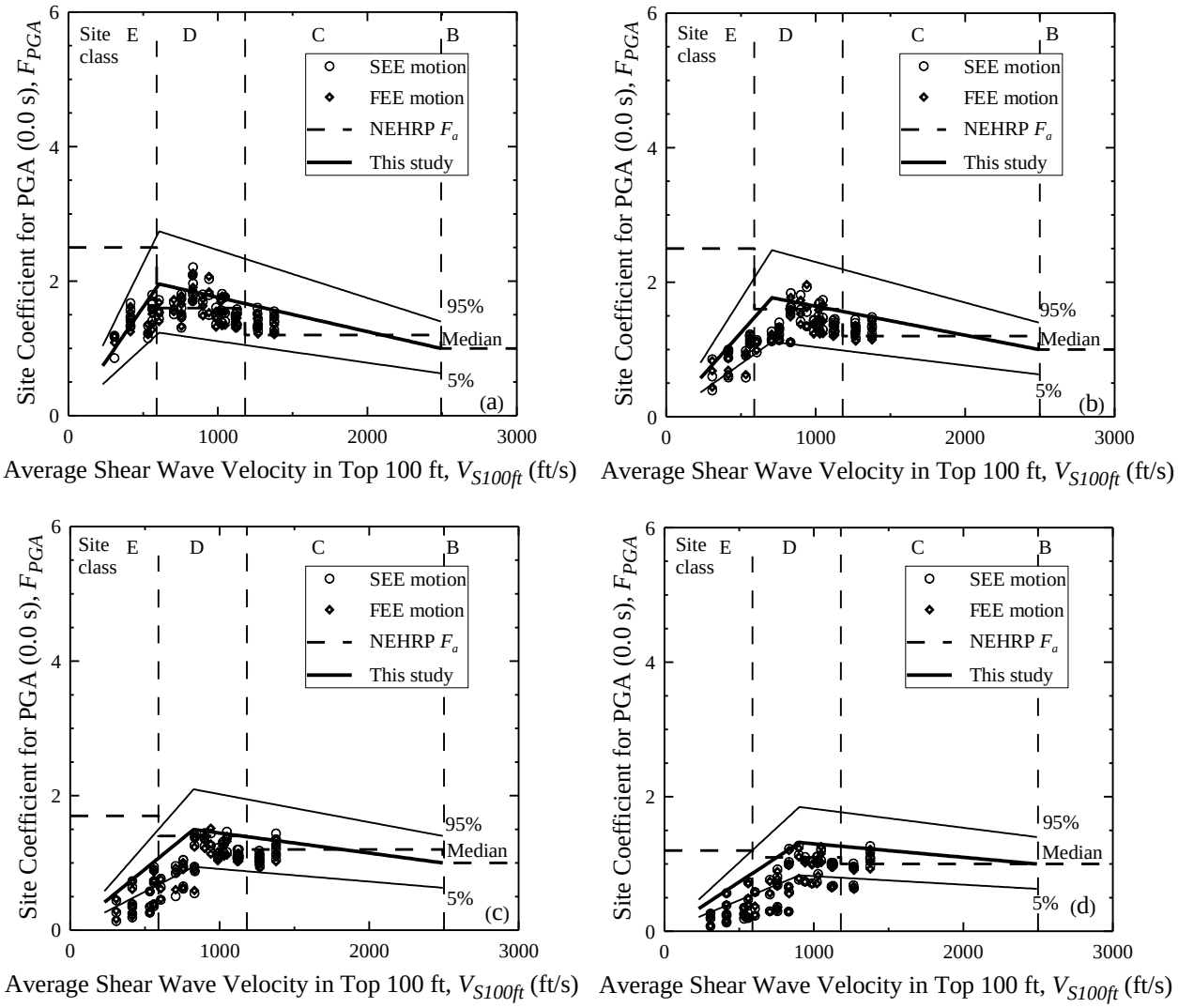

Figure F.1 Site coefficients for 0.0 s spectral period (free-field) with *PGA* equal to (a) 0.05 g, (b) 0.1 g, (c) 0.2 g, and (d) 0.3 g for Florence.

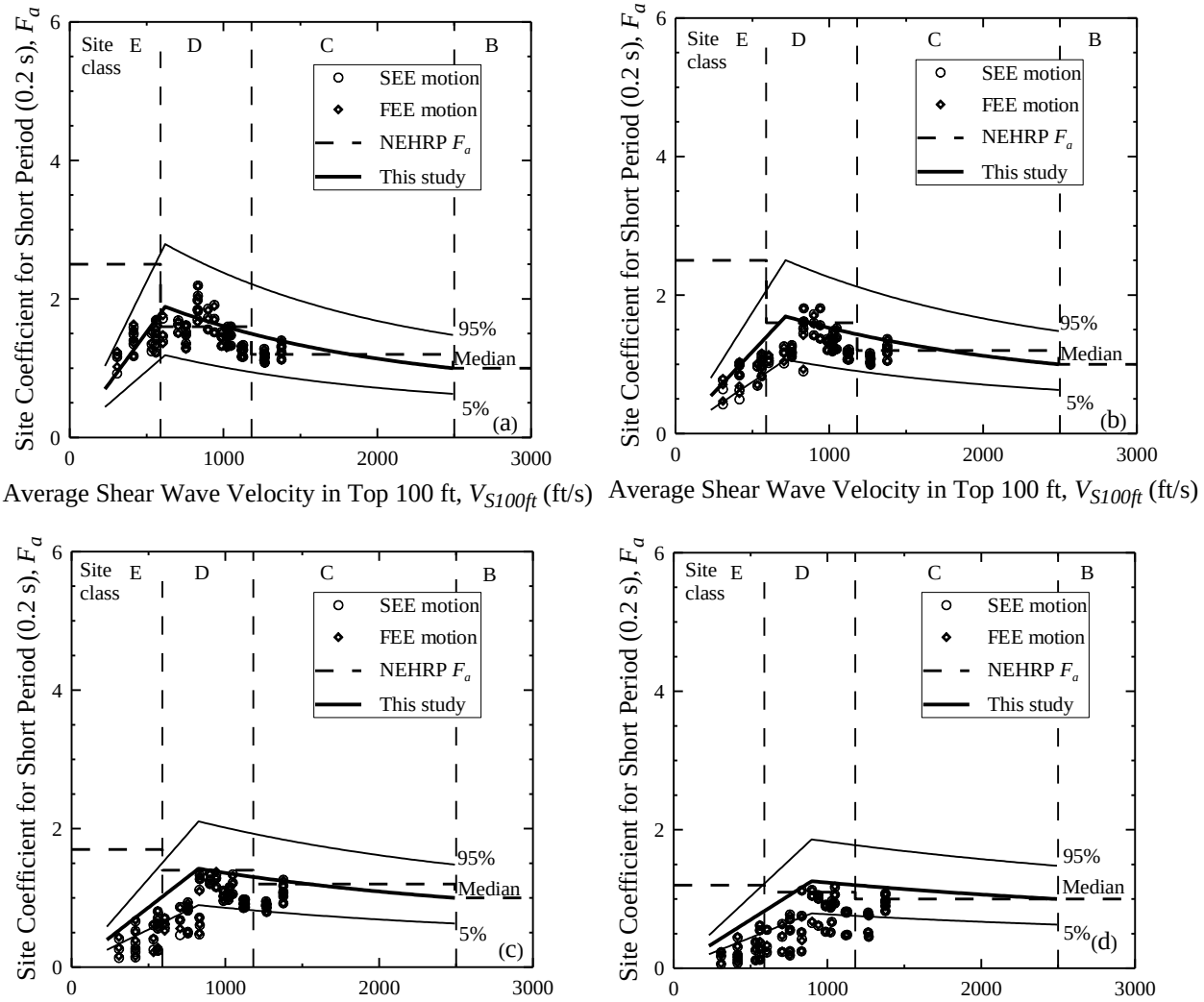

Figure F.2 Site coefficients for 0.2 s (short) spectral period with S_S equal to (a) 0.125 g, (b) 0.25 g, (c) 0.50 g, and (d) 0.75 g for Florence.

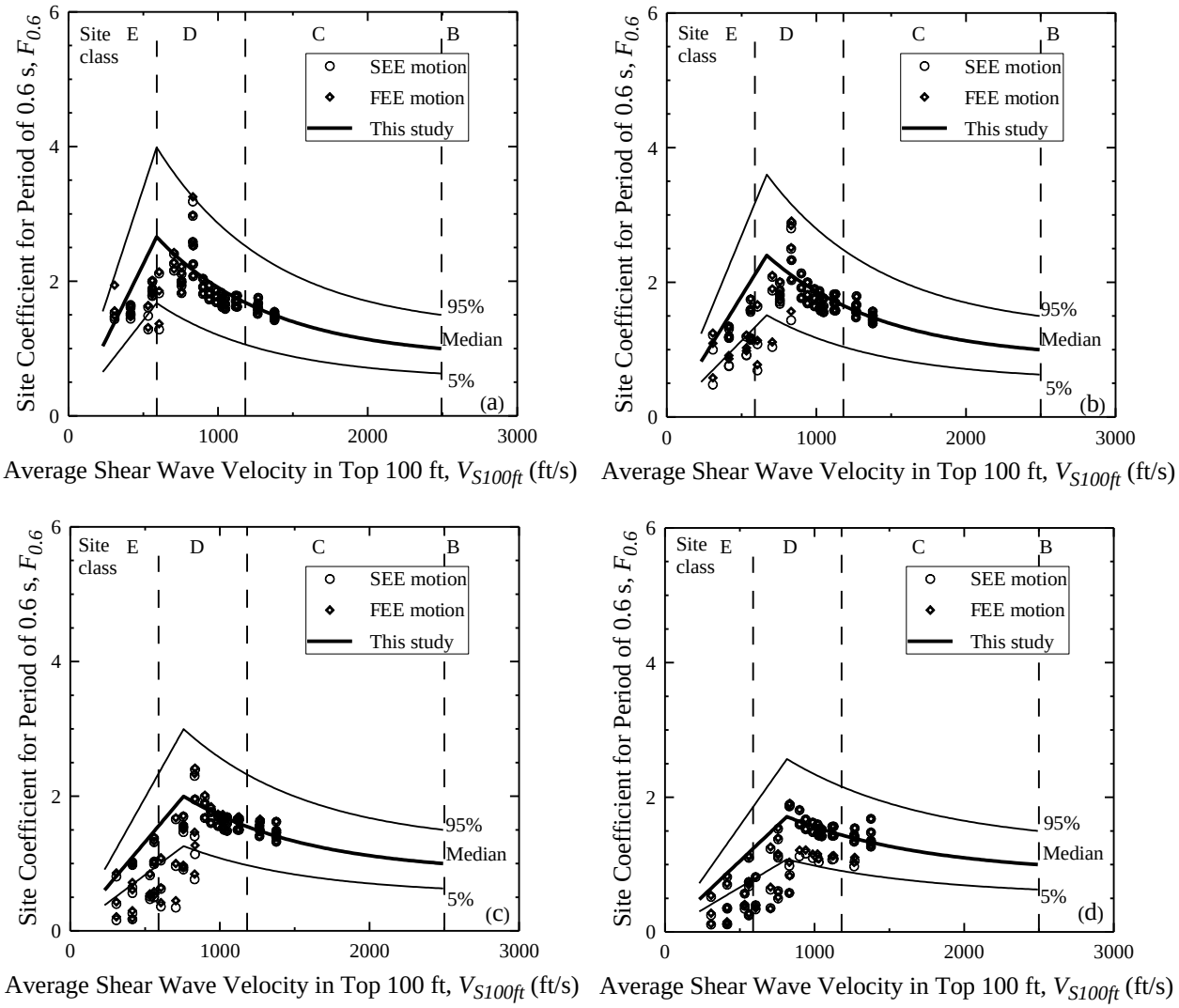

Figure F.3 Site coefficients for 0.6 s spectral period with $S_{0.6}$ equal to (a) 0.05 g, (b) 0.1 g, (c) 0.2 g, and (d) 0.3 g for Florence.

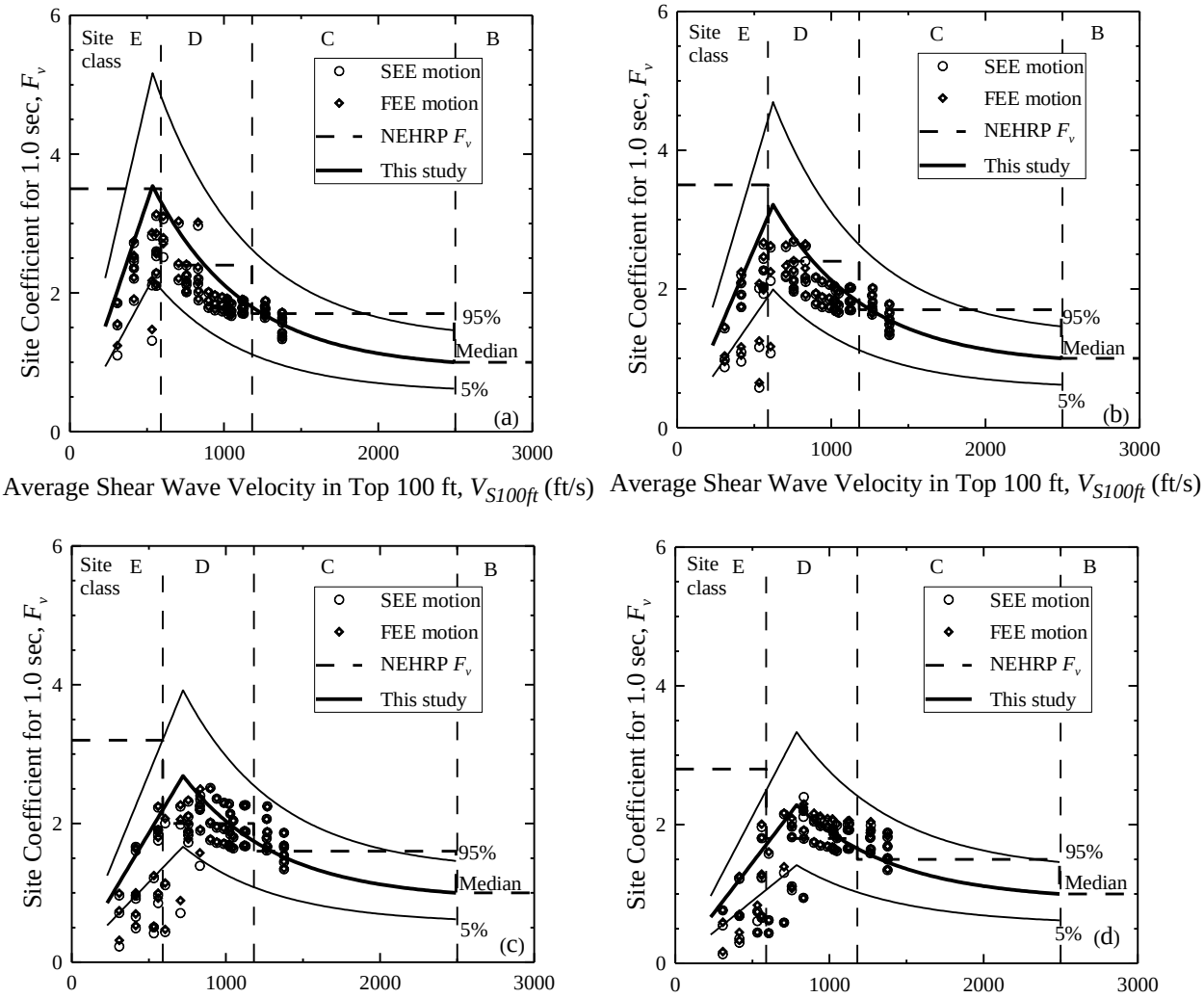

Figure F.4 Site coefficients for 1.0 s (long) spectral period with S_1 equal to (a) 0.05 g, (b) 0.1 g, (c) 0.2 g, and (d) 0.3 g for Florence.

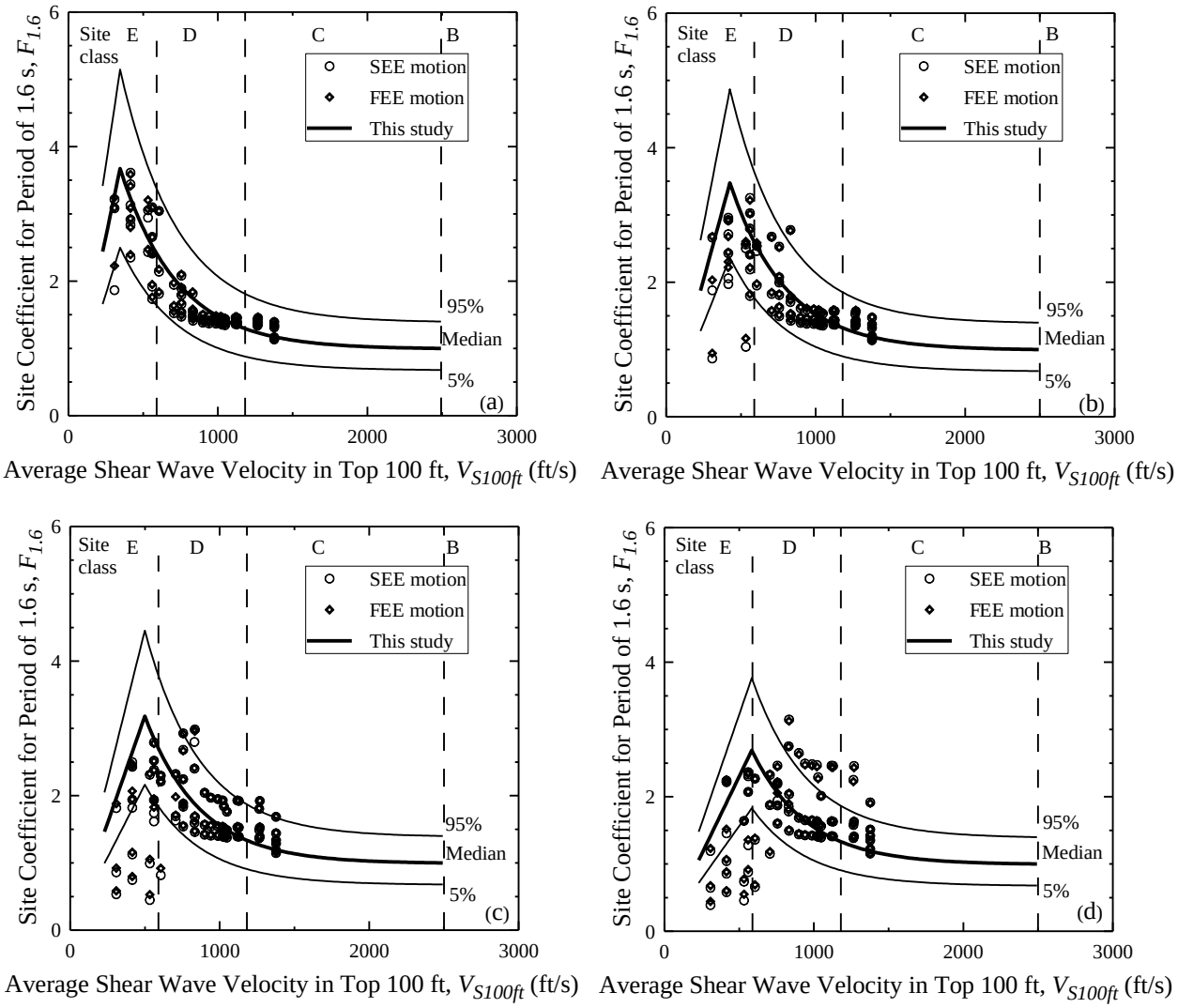

Figure F.5 Site coefficient for 1.6 s spectral period with $S_{1.6}$ equal to (a) 0.02 g, (b) 0.05 g, (c) 0.1 g, and (d) 0.2 g for Florence.

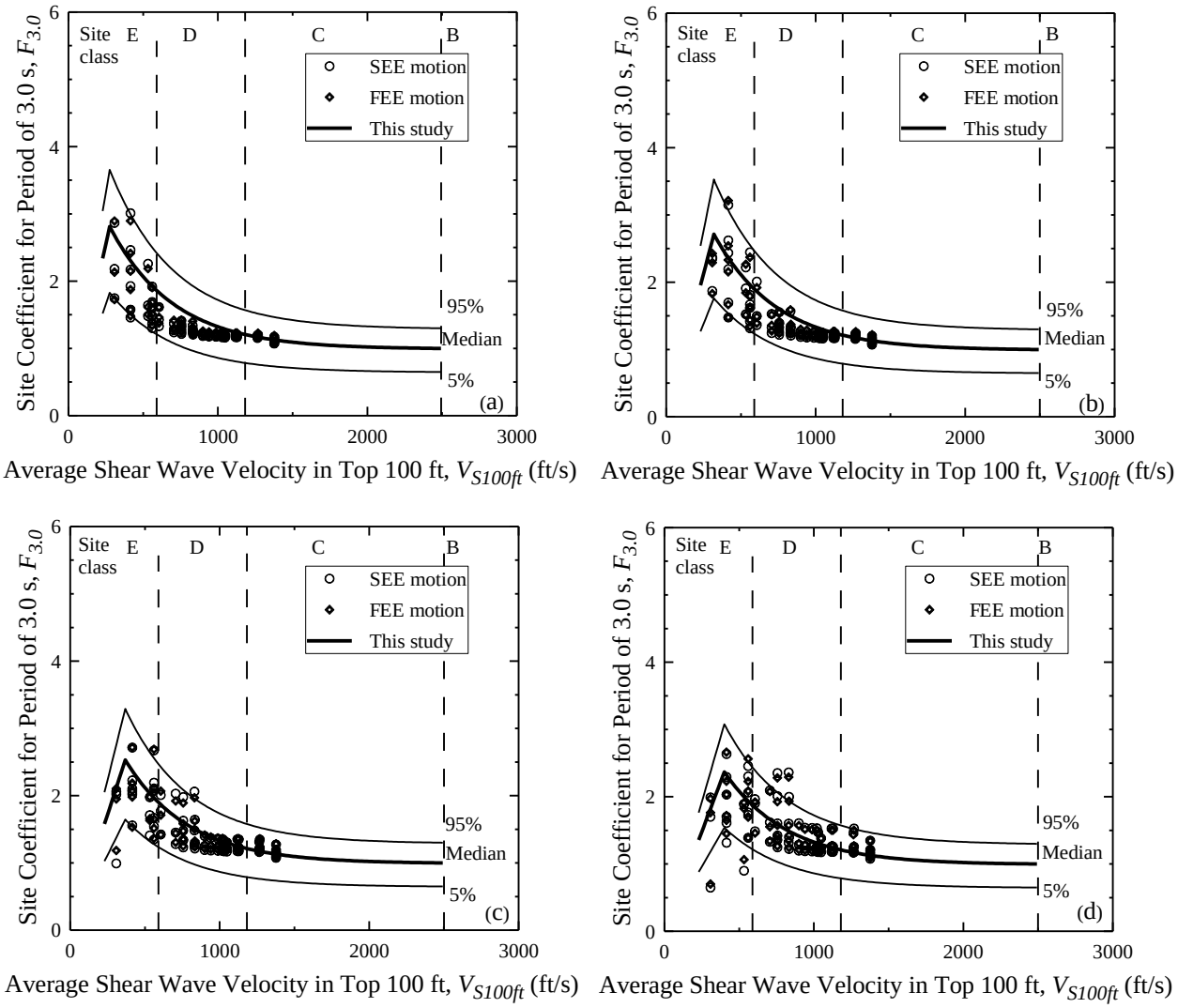

Figure F.6 Site coefficient for 3.0 s spectral period with $S_{3.0}$ equal to (a) 0.01 g, (b) 0.02 g, (c) 0.04 g, and (d) 0.06 g for Florence.

APPENDIX G

SUMMARY OF INPUTS AND OUTPUTS OF SITE RESPONSE ANALYSIS FOR THE LAKE MARION AREA

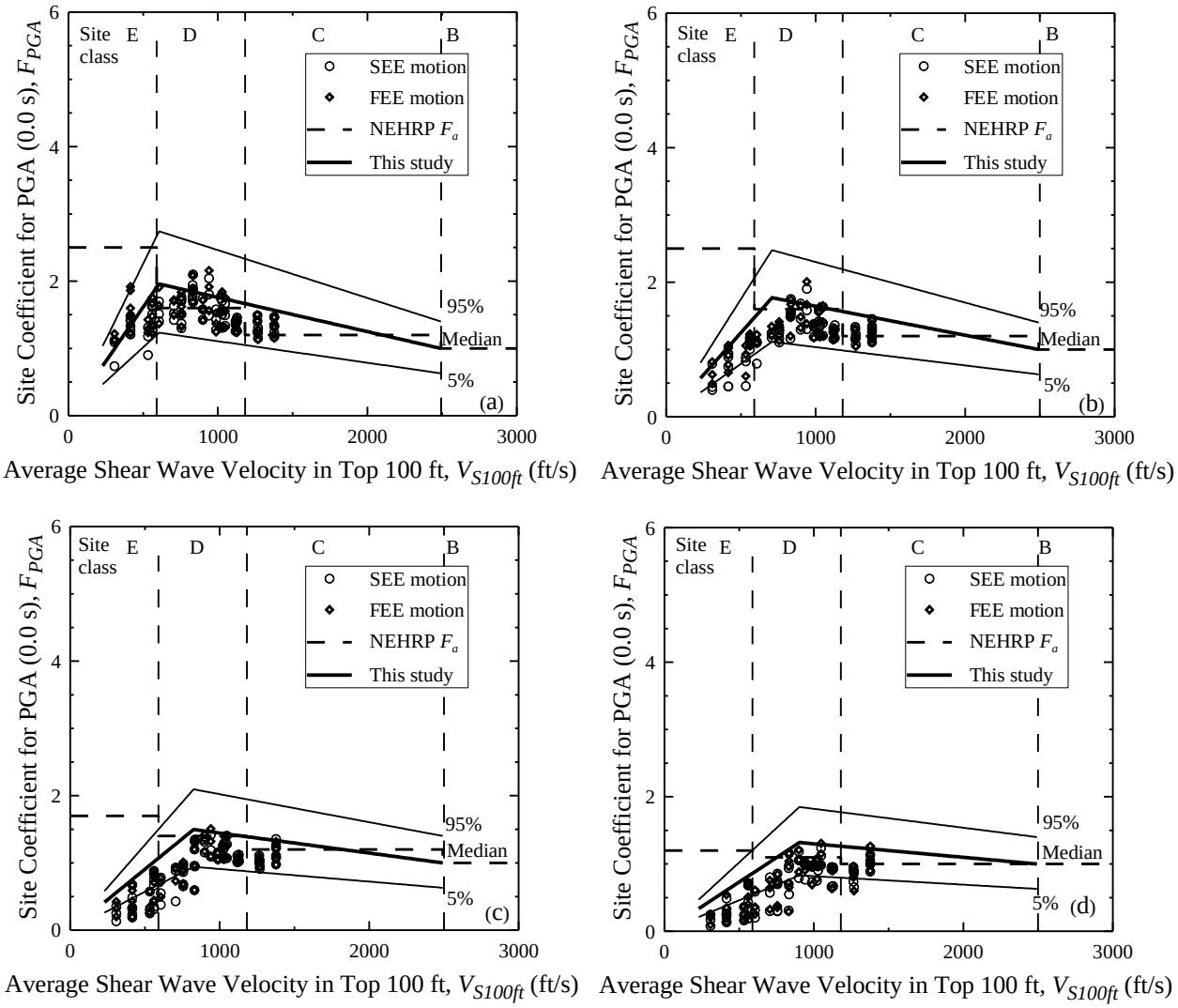

Figure G.1 Site coefficients for 0.0 s spectral period (free-field) with *PGA* equal to (a) 0.05 g, (b) 0.1 g, (c) 0.2 g, (d) 0.3 g, and (e) 0.4 g for Lake Marion.

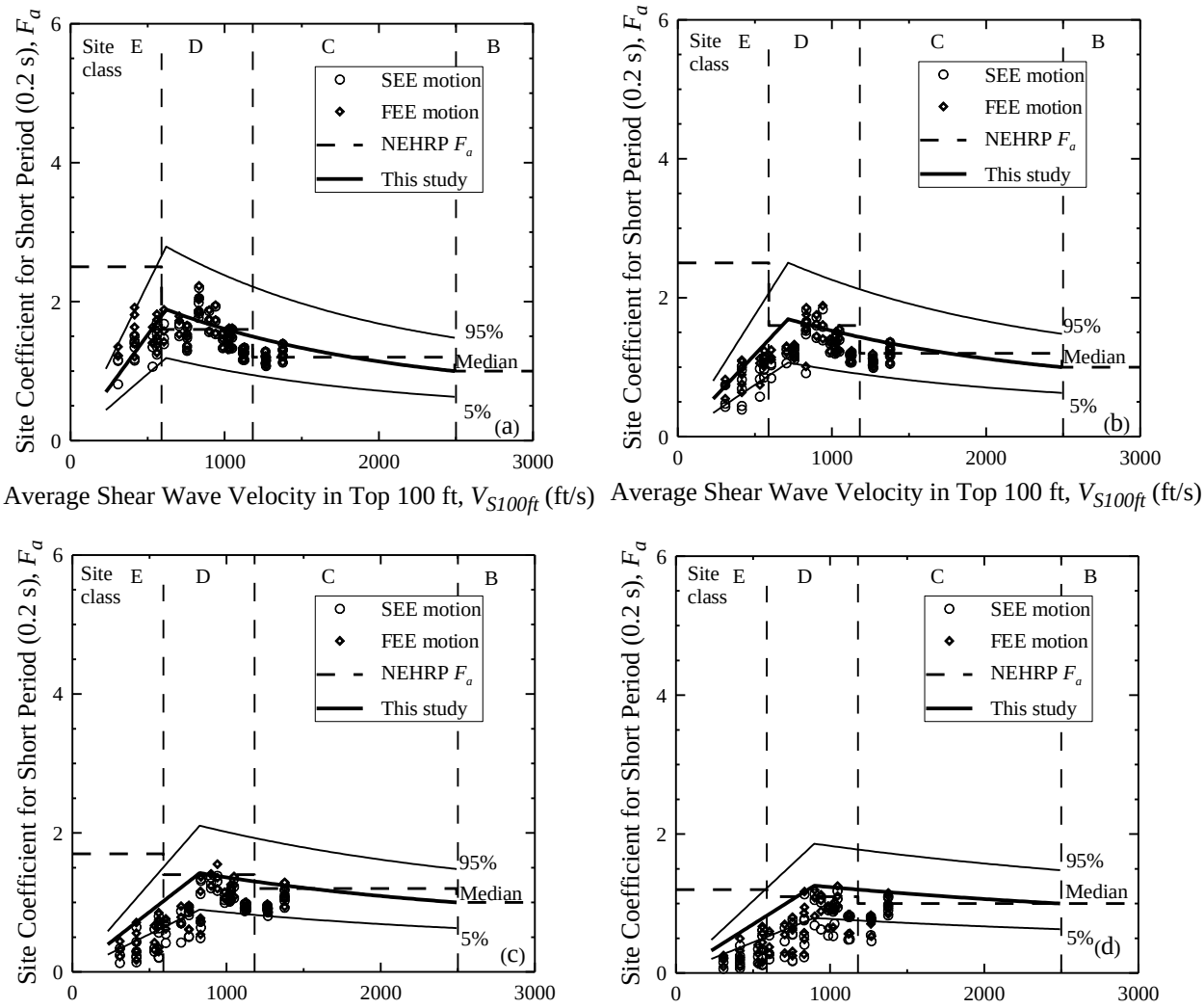

Figure G.2 Site coefficients for 0.2 s (short) spectral period with S_S equal to (a) 0.125 g, (b) 0.25 g, (c) 0.50 g, and (d) 0.75 g for Lake Marion.

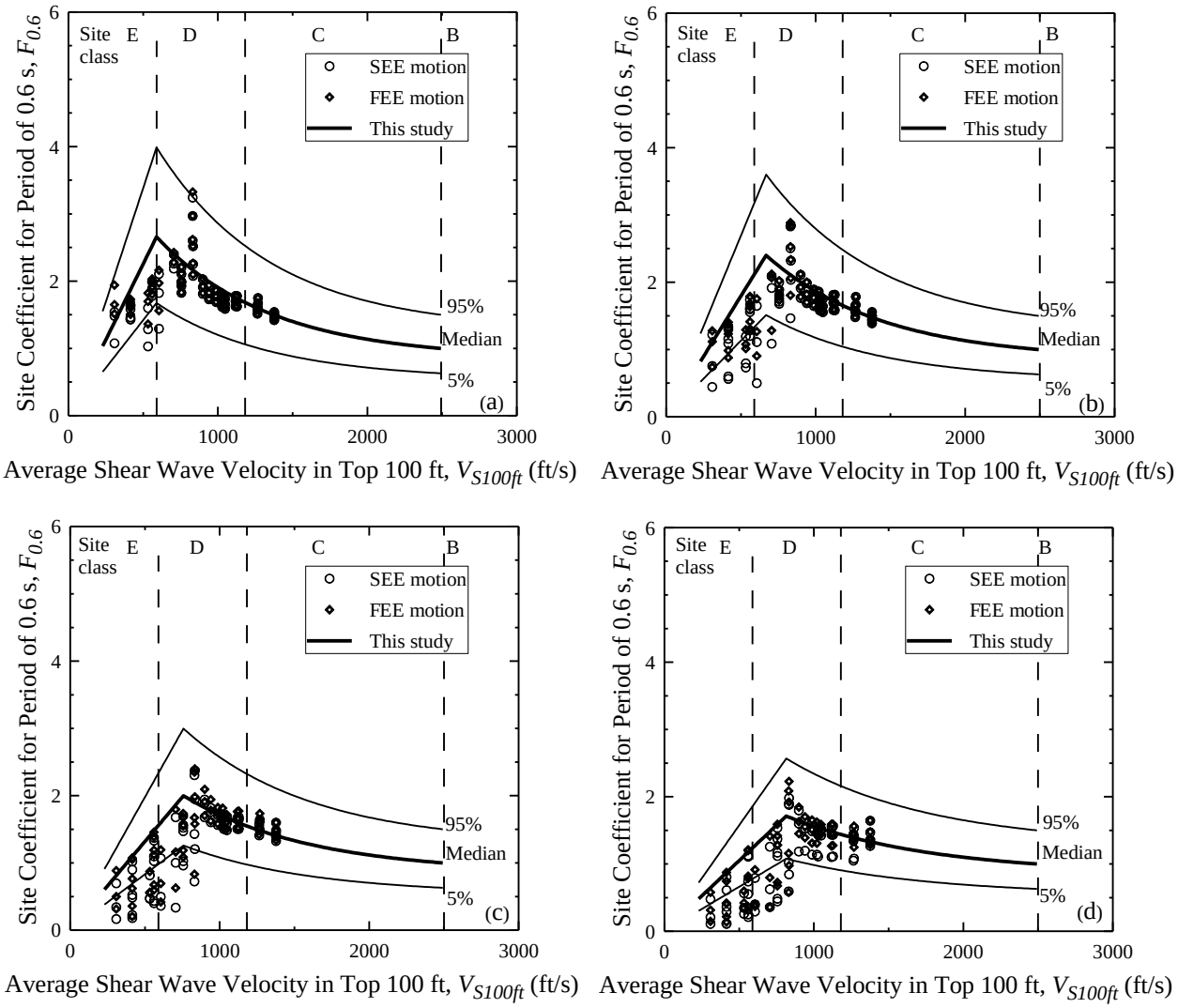

Figure G.3 Site coefficients for 0.6 s spectral period with $S_{0.6}$ equal to (a) 0.05 g, (b) 0.1 g, (c) 0.2 g, and (d) 0.3 g for Lake Marion.

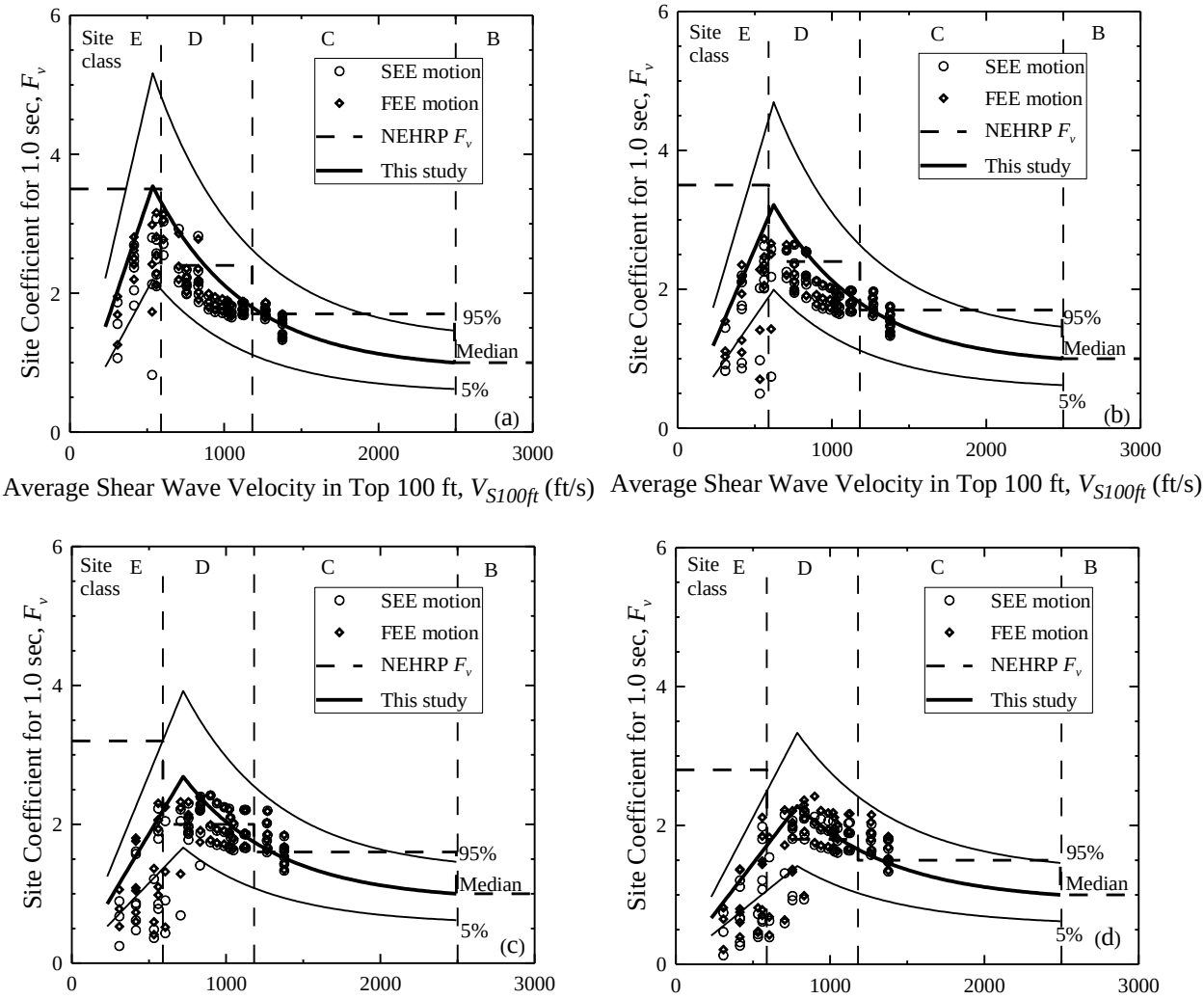

Figure G.4 Site coefficients for 1.0 s (long) spectral period with S_1 equal to (a) 0.05 g, (b) 0.1 g, (c) 0.2 g, and (d) 0.3 g for Lake Marion.

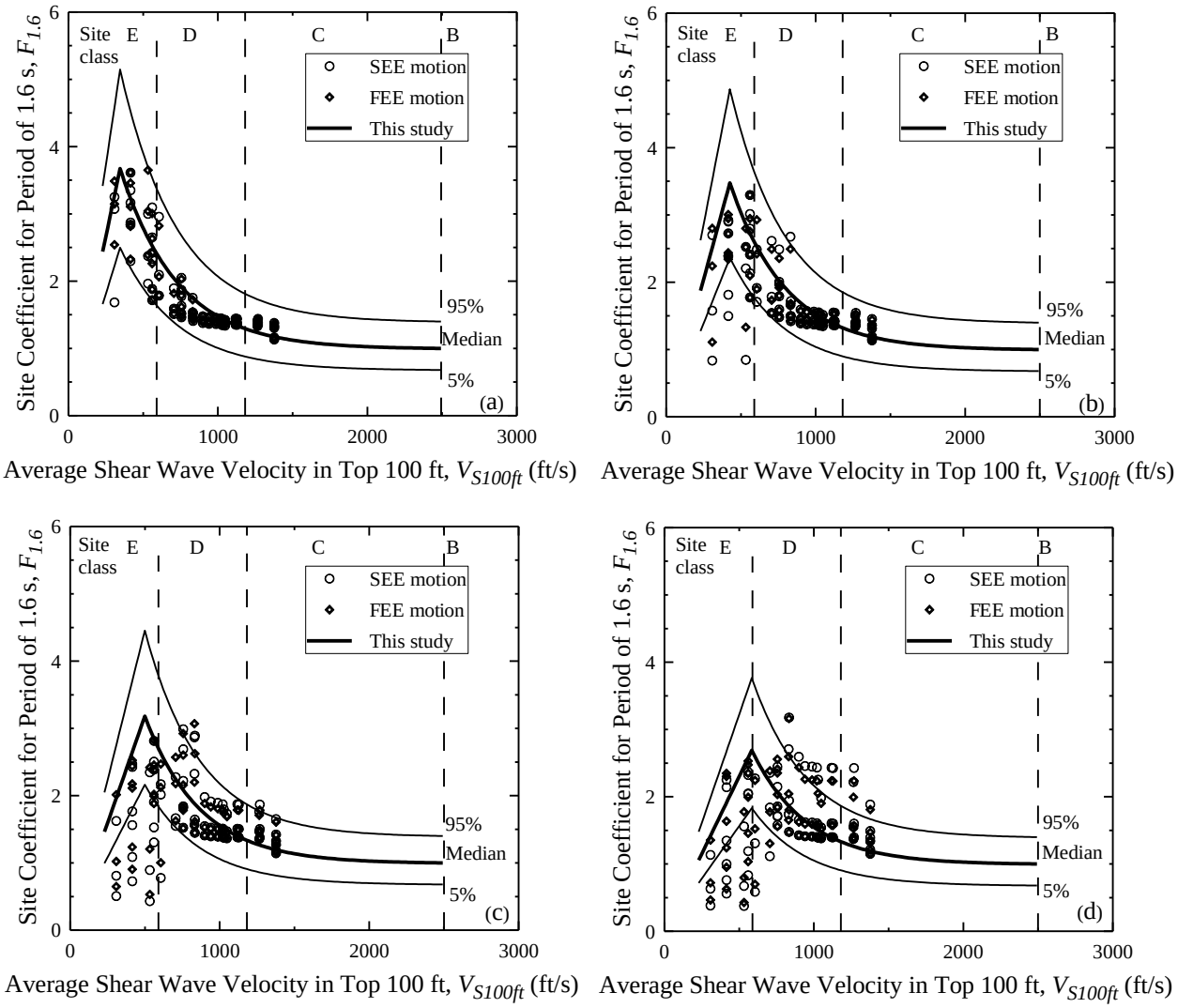

Figure G.5 Site coefficient for 1.6 s spectral period with $S_{1.6}$ equal to (a) 0.02 g, (b) 0.05 g, (c) 0.1 g, and (d) 0.2 g for Lake Marion.

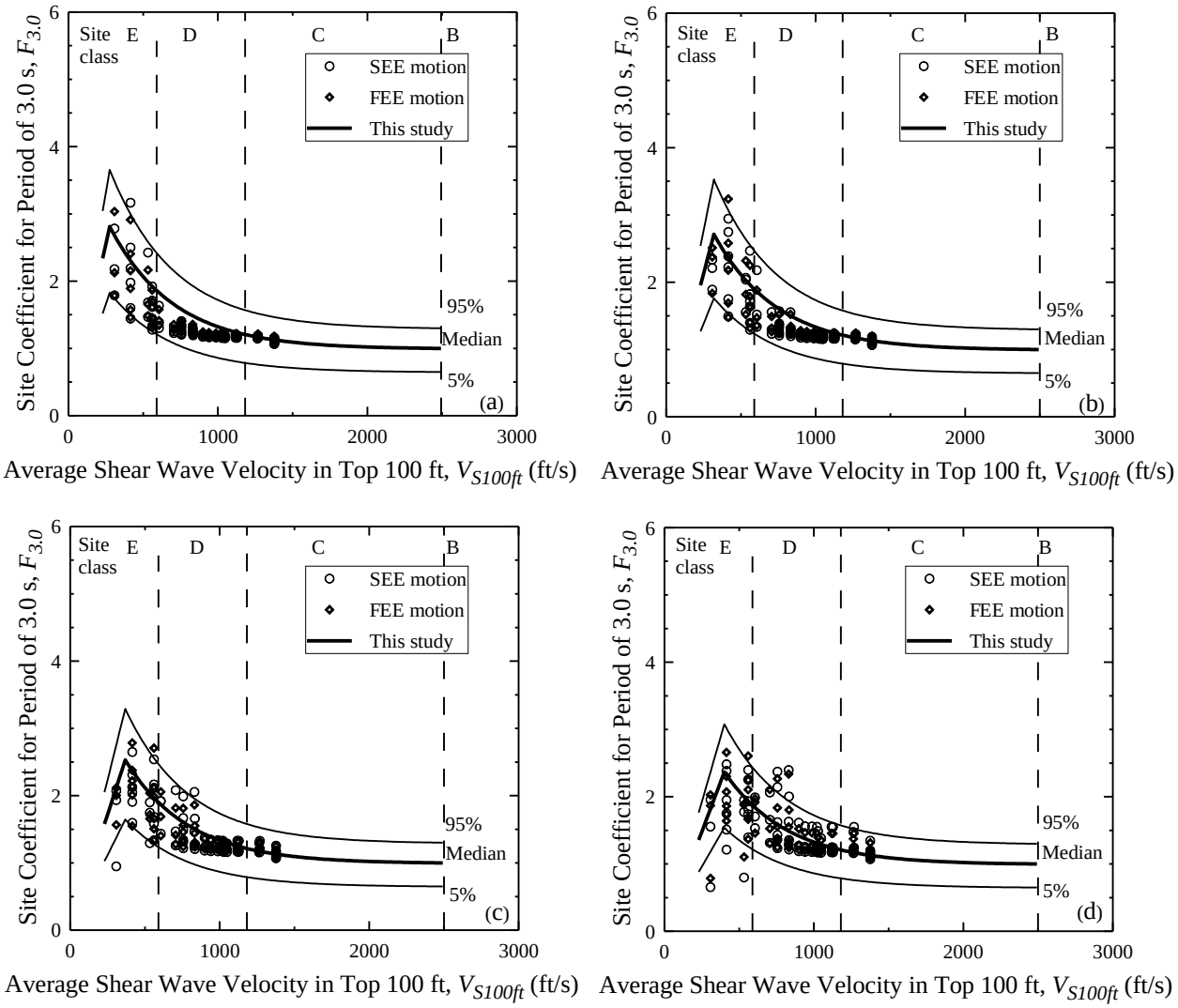

Figure G.6 Site coefficient for 3.0 s spectral period with $S_{3.0}$ equal to (a) 0.01 g, (b) 0.02 g, (c) 0.04 g, and (d) 0.06 g for Lake Marion.

APPENDIX H

SUMMARY OF INPUTS AND OUTPUTS OF SITE RESPONSE ANALYSIS FOR DIFFERENT B-C BOUNDARY DEPTHS FOR THE COLUMBIA AREA

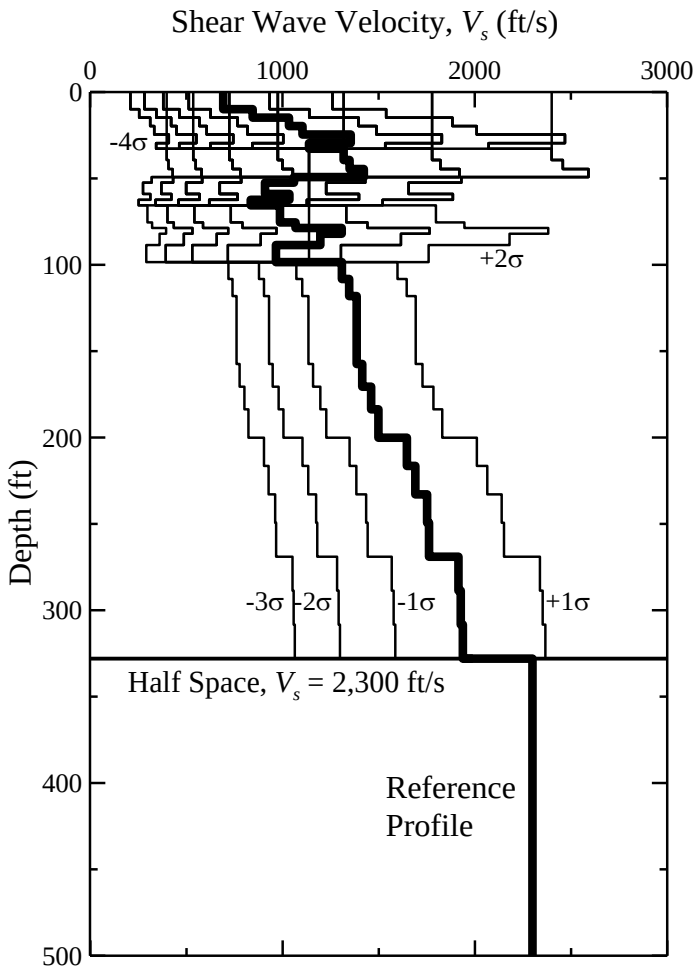

Figure H.1 Shear wave velocity profiles considered for Columbia with soft rock half space at depth = 328 ft. The reference profile is compiled from Odum et al. (2003), Silva et al. (2003), Chapman et al. (2006) and Andrus et al. (2006), and the standard deviation values are based on Andrus et al. (2006).

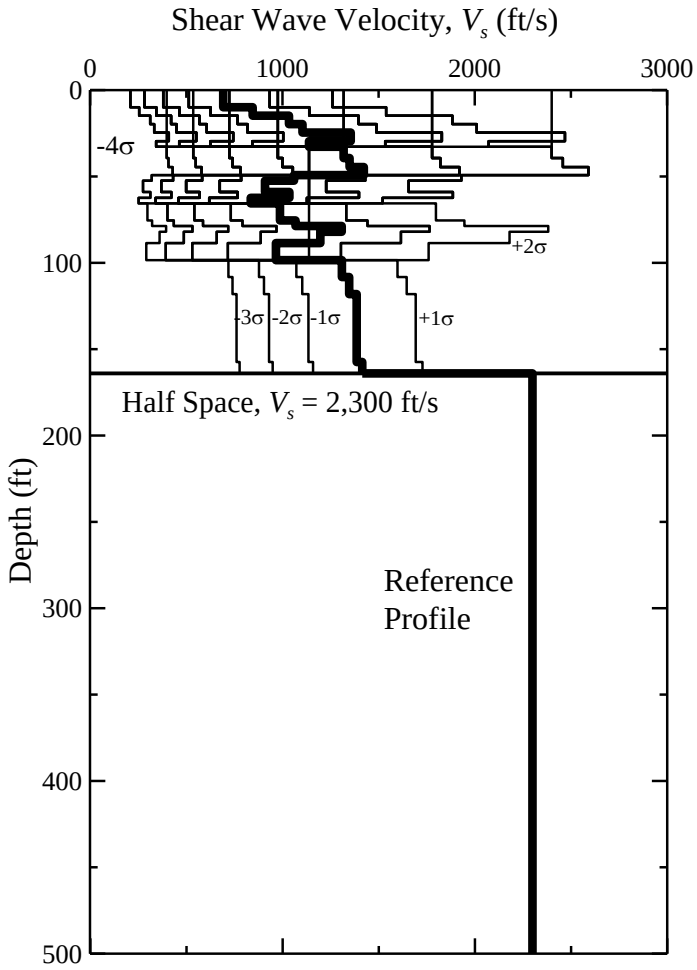

Figure H.2 Shear wave velocity profiles considered for Columbia with soft rock half space at depth = 164 ft. The reference profile is compiled from Odum et al. (2003), Silva et al. (2003), Chapman et al. (2006) and Andrus et al. (2006), and the standard deviation values are based on Andrus et al. (2006).

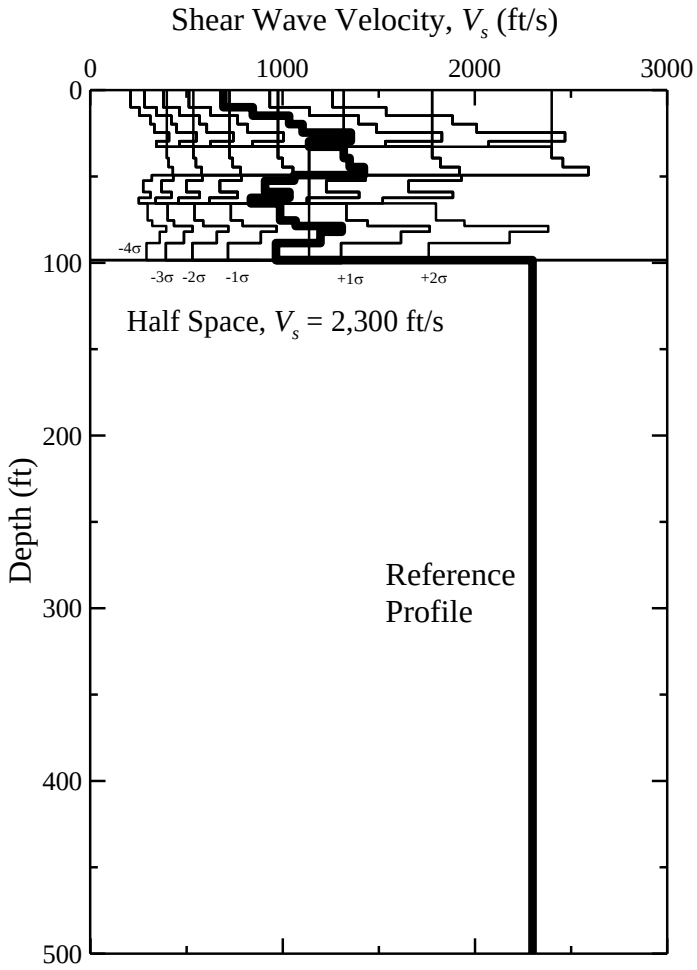

Figure H.3 Shear wave velocity profiles considered for Columbia with soft rock half space at depth = 100 ft. The reference profile is compiled from Odum et al. (2003), Silva et al. (2003), Chapman et al. (2006) and Andrus et al. (2006), and the standard deviation values are based on Andrus et al. (2006).

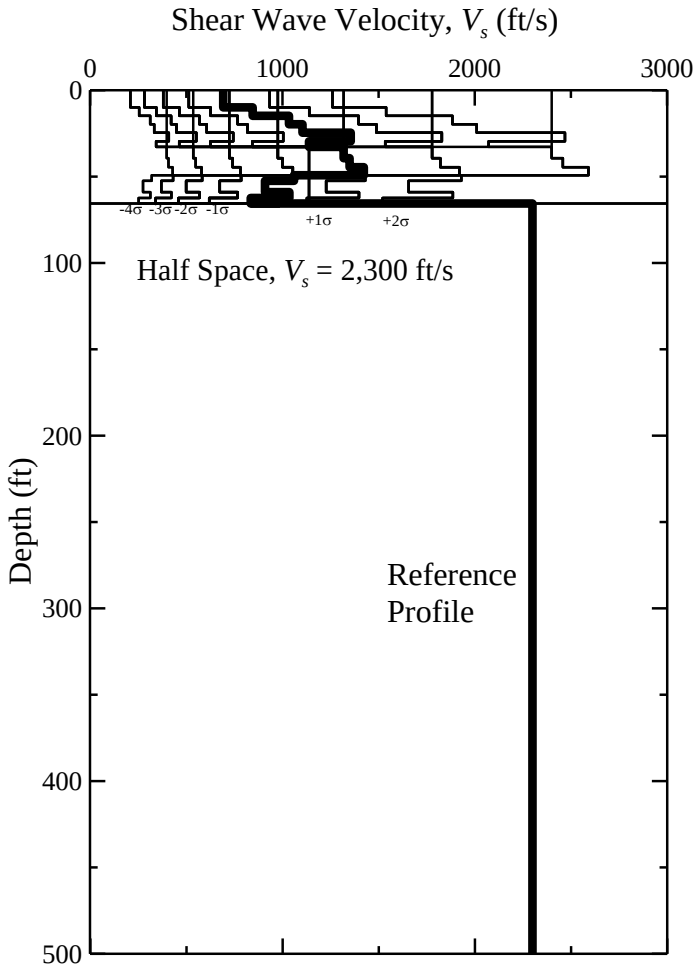

Figure H.4 Shear wave velocity profiles considered for Columbia with soft rock half space at depth = 65.6 ft. The reference profile is compiled from Odum et al. (2003), Silva et al. (2003), Chapman et al. (2006) and Andrus et al. (2006), and the standard deviation values are based on Andrus et al. (2006).

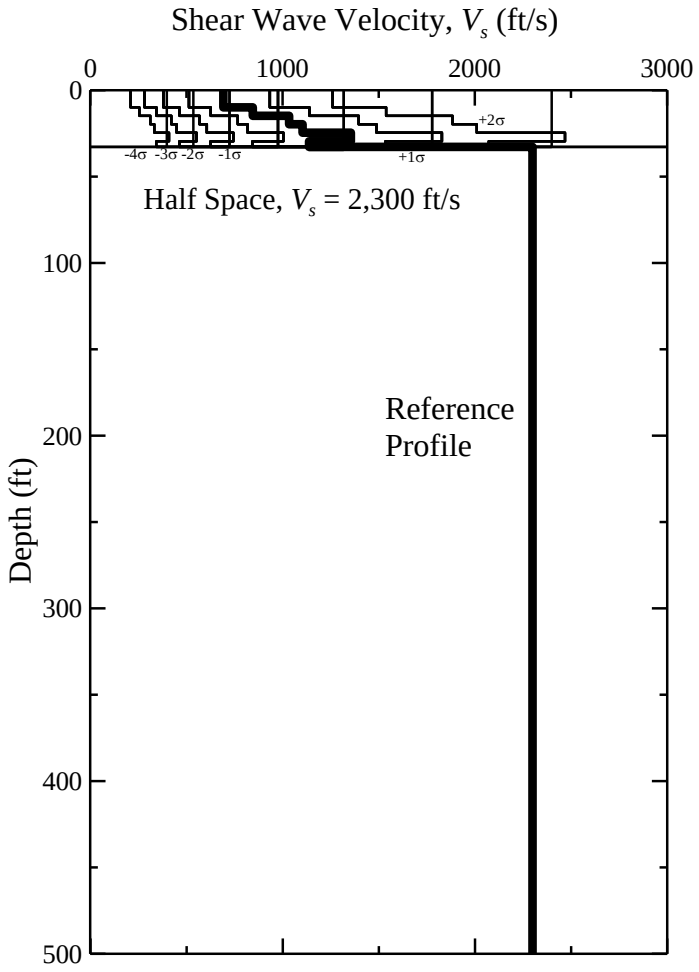

Figure H.5 Shear wave velocity profiles considered for Columbia with soft rock half space at depth = 32.8 ft. The reference profile is compiled from Odum et al. (2003), Silva et al. (2003), Chapman et al. (2006) and Andrus et al. (2006), and the standard deviation values are based on Andrus et al. (2006).

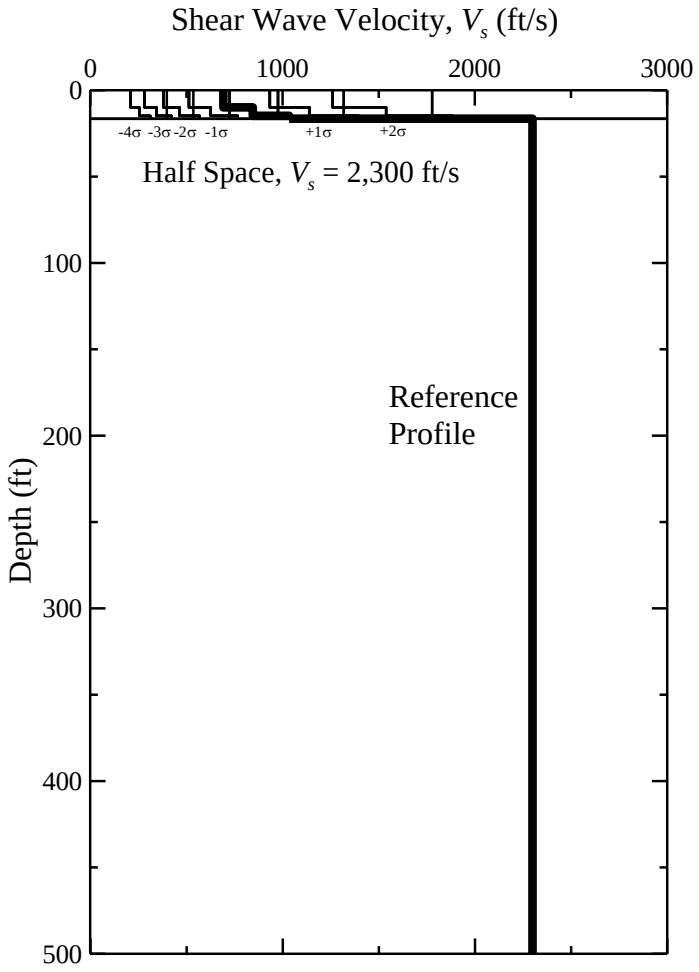

Figure H.6 Shear wave velocity profiles considered for Columbia with soft rock half space at depth = 16.4 ft. The reference profile is compiled from Odum et al. (2003), Silva et al. (2003), Chapman et al. (2006) and Andrus et al. (2006), and the standard deviation values are based on Andrus et al. (2006).

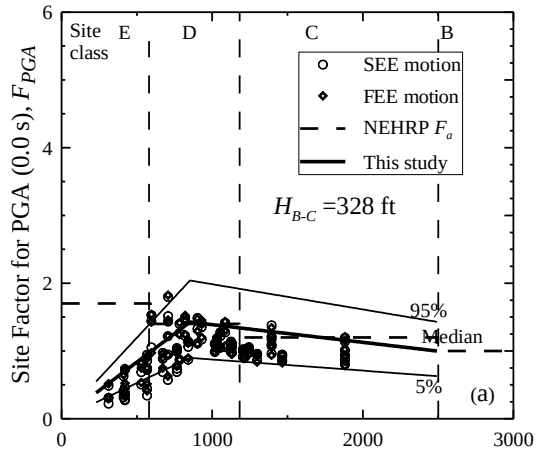
Site class
E
D
C
B
SEE motion
FEE motion
NEHRP F_a
This study
H_{B-C} =328 ft
95%
Median
5%
(a)
Site Factor for PGA (0.0 s), F_{PGA}
Average Shear Wave Velocity in Top 100 ft, V_{S100ft} (ft/s)

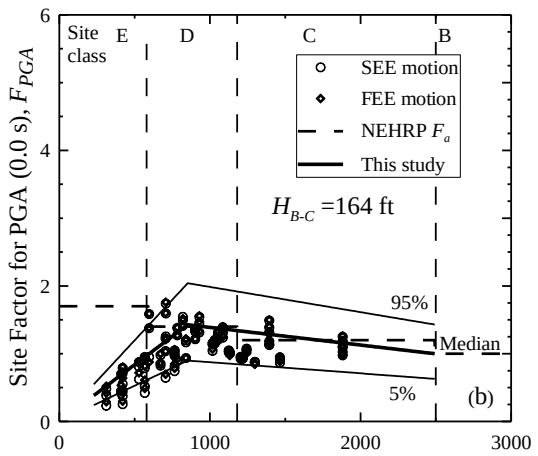
Site class
E
D
C
B
SEE motion
FEE motion
NEHRP F_a
This study
H_{B-C} =164 ft
95%
Median
5%
(b)
Site Factor for PGA (0.0 s), F_{PGA}
Average Shear Wave Velocity in Top 100 ft, V_{S100ft} (ft/s)

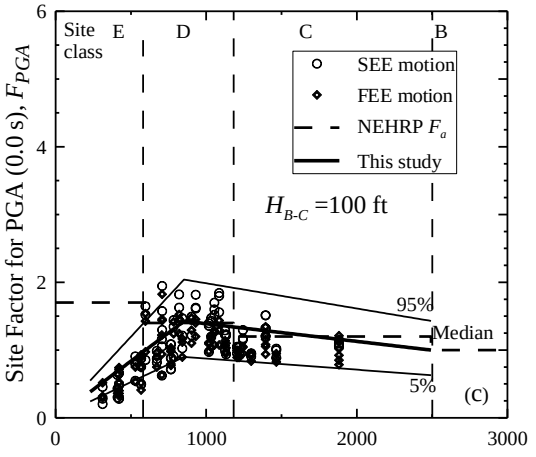
Site class
E
D
C
B
SEE motion
FEE motion
NEHRP F_a
This study
H_{B-C} =100 ft
95%
Median
5%
(c)
Site Factor for PGA (0.0 s), F_{PGA}
Average Shear Wave Velocity in Top 100 ft, V_{S100ft} (ft/s)

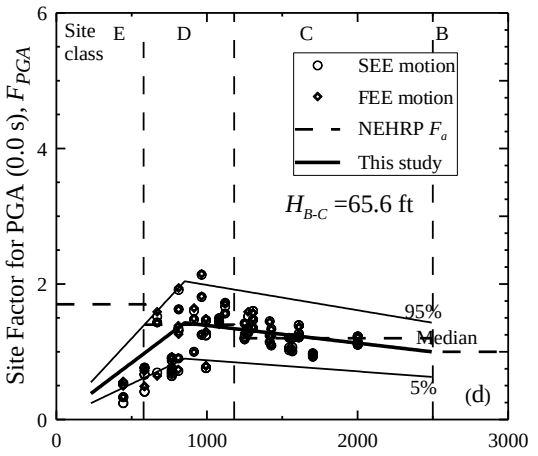
Site class
E
D
C
B
SEE motion
FEE motion
NEHRP F_a
This study
H_{B-C} =65.6 ft
95%
Median
5%
(d)
Site Factor for PGA (0.0 s), F_{PGA}
Average Shear Wave Velocity in Top 100 ft, V_{S100ft} (ft/s)

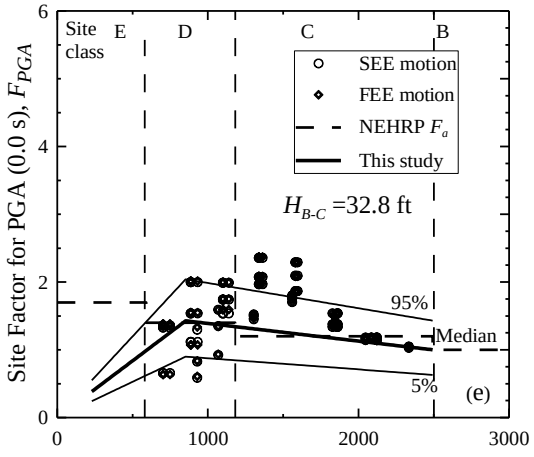
Site class
E
D
C
B
SEE motion
FEE motion
NEHRP F_a
This study
H_{B-C} =32.8 ft
95%
Median
5%
(e)
Site Factor for PGA (0.0 s), F_{PGA}
Average Shear Wave Velocity in Top 100 ft, V_{S100ft} (ft/s)

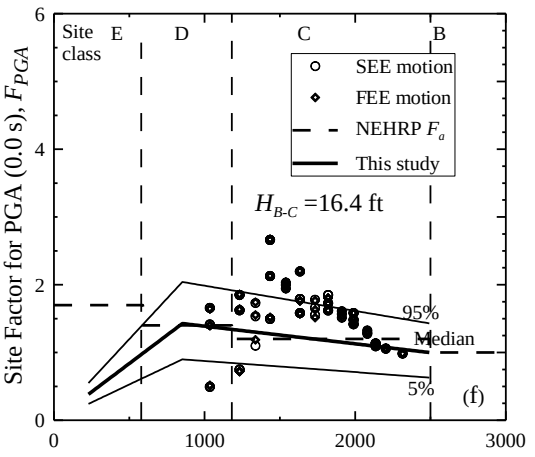
Site class
E
D
C
B
SEE motion
FEE motion
NEHRP F_a
This study
H_{B-C} =16.4 ft
95%
Median
5%
(f)
Site Factor for PGA (0.0 s), F_{PGA}
Average Shear Wave Velocity in Top 100 ft, V_{S100ft} (ft/s)

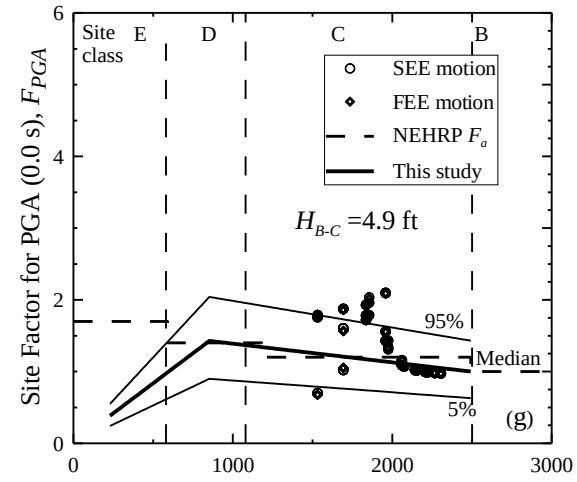

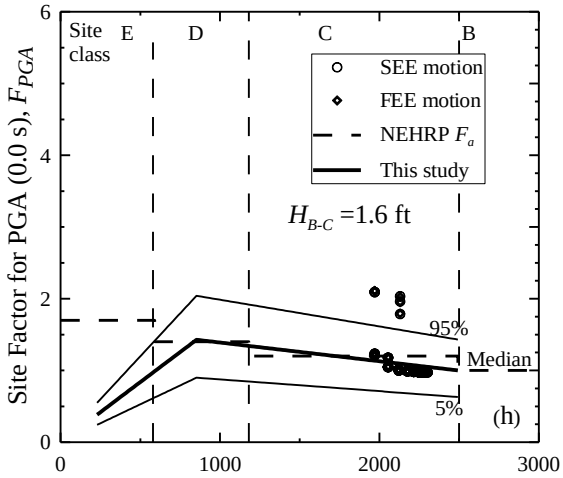

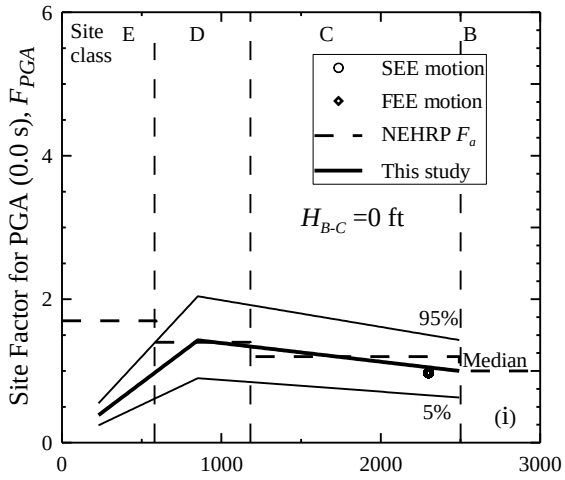

Figure H.7 Site coefficients for 0.0 s spectral period (free-field) with *PGA* equal to 0.2 g and soft rock half space at depth equal to (a) 328 ft, (b) 164 ft, (c) 100 ft, (d) 65.6 ft, (e) 32.8 ft, (f) 16.4 ft, (g) 4.9 ft, (h) 1.6 ft, and (i) 0.0 ft based on V_S profiles shown in Figures H.1-H.6 for Columbia.

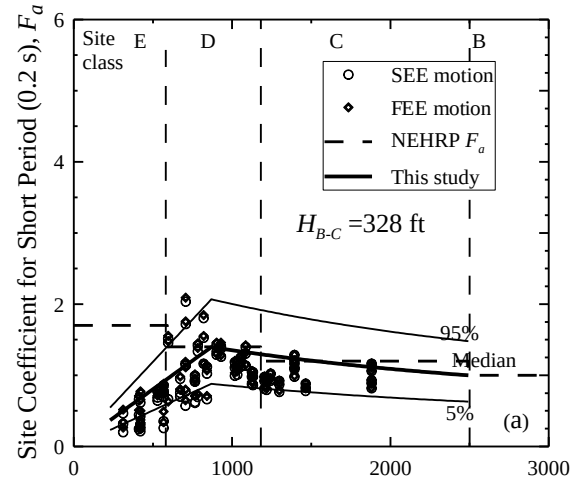
Site class
E
D
C
B
SEE motion
FEE motion
NEHRP F_a
This study
$H_{B\text{-}C}$ =328 ft
95%
Median
5%
(a)
Site Coefficient for Short Period (0.2 s), F_a
Average Shear Wave Velocity in Top 100 ft, V_{S100ft} (ft/s)

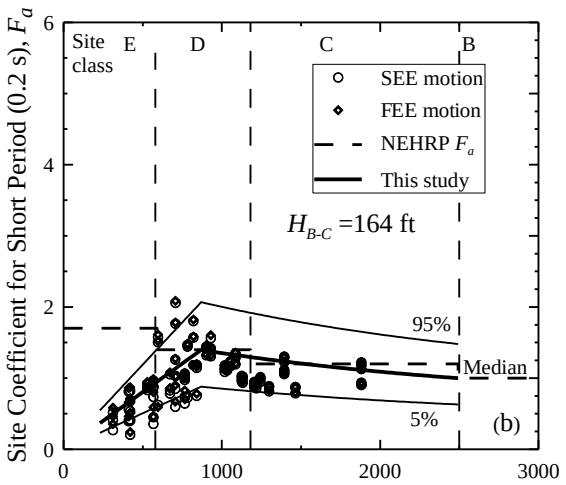
Site class
E
D
C
B
SEE motion
FEE motion
NEHRP F_a
This study
$H_{B\text{-}C}$ =164 ft
95%
Median
5%
(b)
Site Coefficient for Short Period (0.2 s), F_a
Average Shear Wave Velocity in Top 100 ft, V_{S100ft} (ft/s)

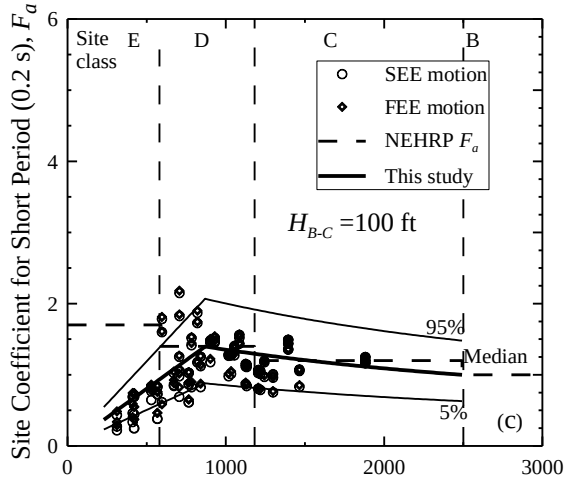
Site class
E
D
C
B
SEE motion
FEE motion
NEHRP F_a
This study
$H_{B\text{-}C}$ =100 ft
95%
Median
5%
(c)
Site Coefficient for Short Period (0.2 s), F_a
Average Shear Wave Velocity in Top 100 ft, V_{S100ft} (ft/s)

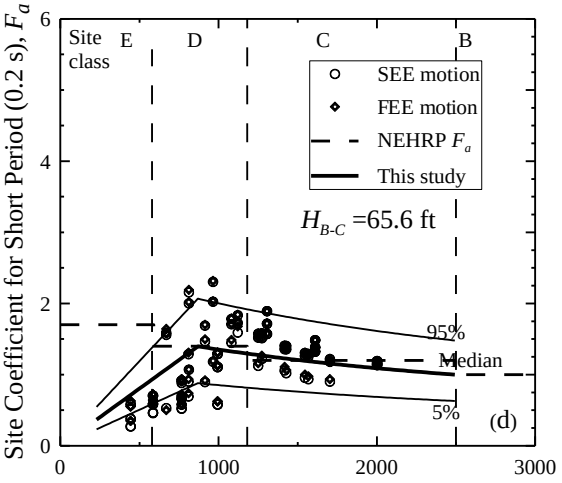
Site class
E
D
C
B
SEE motion
FEE motion
NEHRP F_a
This study
$H_{B\text{-}C}$ =65.6 ft
95%
Median
5%
(d)
Site Coefficient for Short Period (0.2 s), F_a
Average Shear Wave Velocity in Top 100 ft, V_{S100ft} (ft/s)

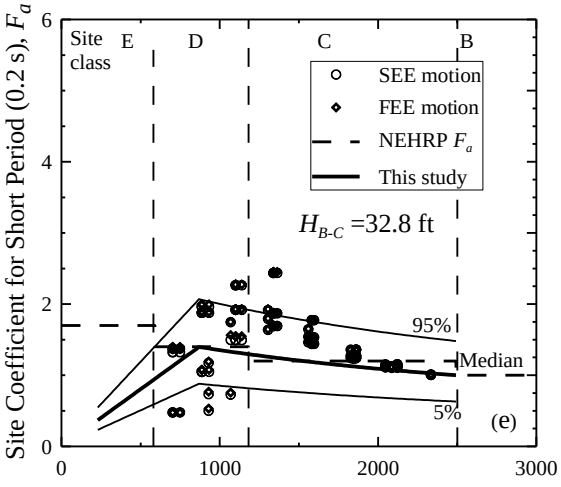
Site class
E
D
C
B
SEE motion
FEE motion
NEHRP F_a
This study
$H_{B\text{-}C}$ =32.8 ft
95%
Median
5%
(e)
Site Coefficient for Short Period (0.2 s), F_a
Average Shear Wave Velocity in Top 100 ft, V_{S100ft} (ft/s)

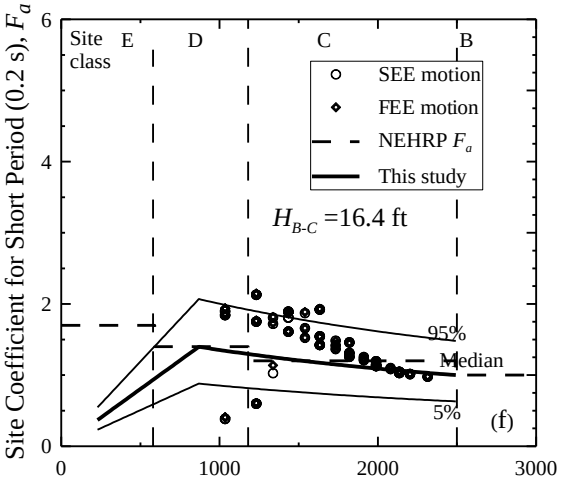
Site class
E
D
C
B
SEE motion
FEE motion
NEHRP F_a
This study
$H_{B\text{-}C}$ =16.4 ft
95%
Median
5%
(f)
Site Coefficient for Short Period (0.2 s), F_a
Average Shear Wave Velocity in Top 100 ft, V_{S100ft} (ft/s)

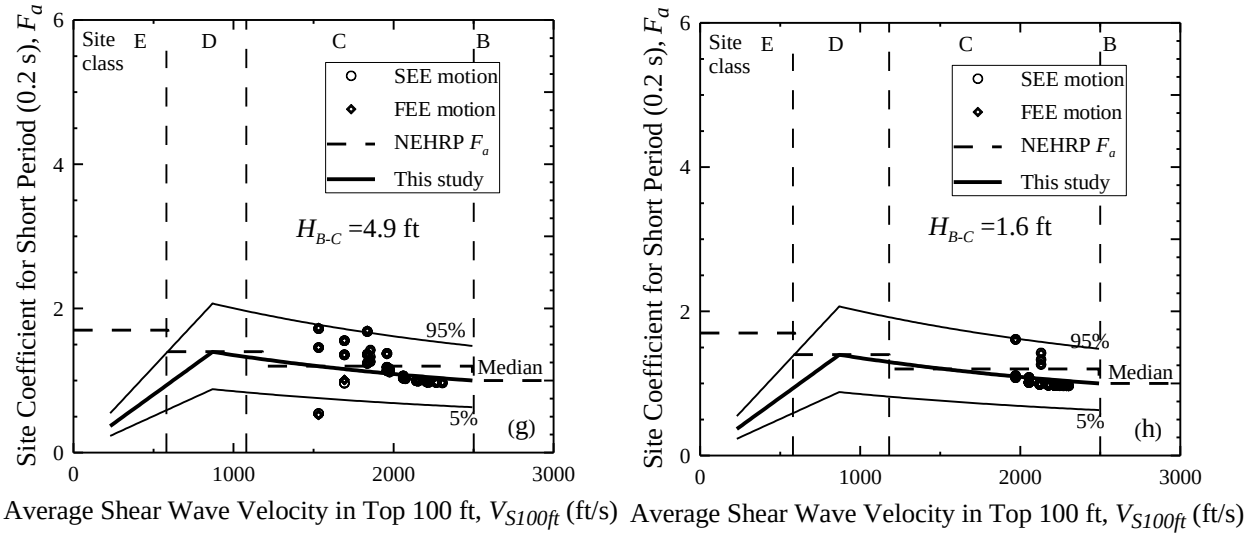

Figure H.8 Site coefficients for 0.2 s (short) spectral period with S_S equal to 0.5 g, and soft rock half space at depth equal to (a) 328 ft, (b) 164 ft, (c) 100 ft, (d) 65.6 ft, (e) 32.8 ft, (f) 16.4 ft, (g) 4.9 ft, and (h) 1.6 ft based on V_S profiles shown in Figures H.1-H.6 for Columbia.

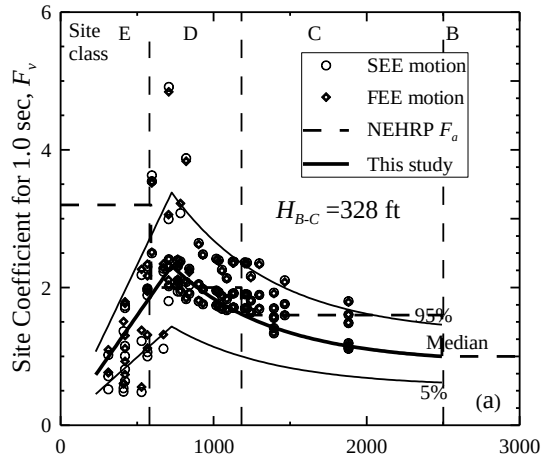
Site class
E
D
C
B
SEE motion
FEE motion
NEHRP F_a
This study
$H_{B\text{-}C}$ =328 ft
95%
Median
5%
(a)
Site Coefficient for 1.0 sec, F_v
Average Shear Wave Velocity in Top 100 ft, V_{S100ft} (ft/s)

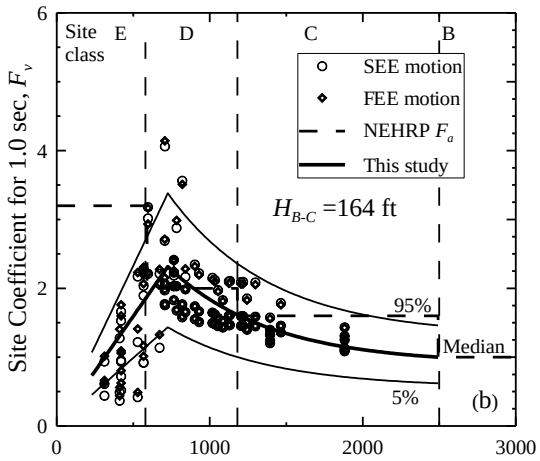
Site class
E
D
C
B
SEE motion
FEE motion
NEHRP F_a
This study
$H_{B\text{-}C}$ =164 ft
95%
Median
5%
(b)
Site Coefficient for 1.0 sec, F_v
Average Shear Wave Velocity in Top 100 ft, V_{S100ft} (ft/s)

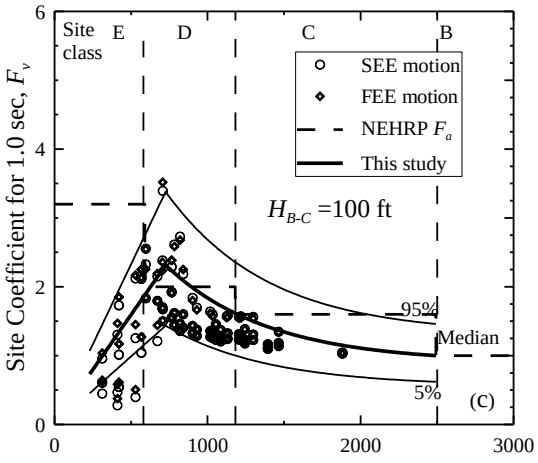
Site class
E
D
C
B
SEE motion
FEE motion
NEHRP F_a
This study
$H_{B\text{-}C}$ =100 ft
95%
Median
5%
(c)
Site Coefficient for 1.0 sec, F_v
Average Shear Wave Velocity in Top 100 ft, V_{S100ft} (ft/s)

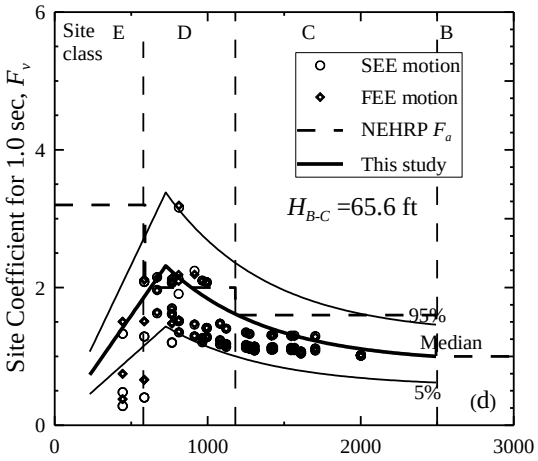
Site class
E
D
C
B
SEE motion
FEE motion
NEHRP F_a
This study
$H_{B\text{-}C}$ =65.6 ft
95%
Median
5%
(d)
Site Coefficient for 1.0 sec, F_v
Average Shear Wave Velocity in Top 100 ft, V_{S100ft} (ft/s)

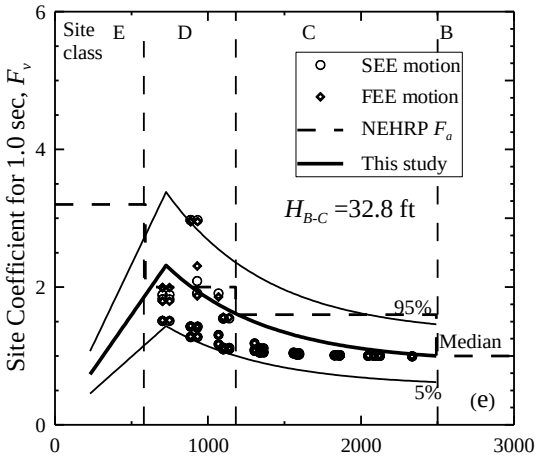
Site class
E
D
C
B
SEE motion
FEE motion
NEHRP F_a
This study
$H_{B\text{-}C}$ =32.8 ft
95%
Median
5%
(e)
Site Coefficient for 1.0 sec, F_v
Average Shear Wave Velocity in Top 100 ft, V_{S100ft} (ft/s)

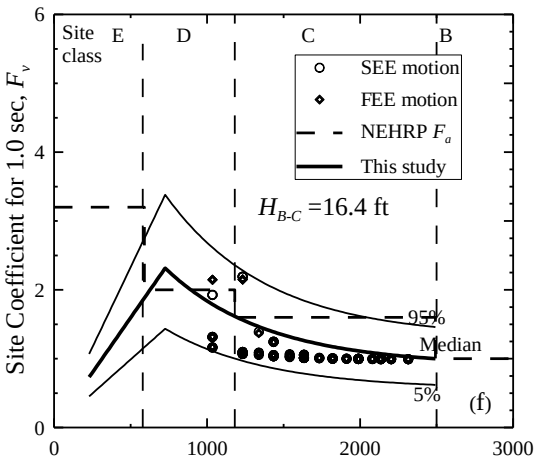
Site class
E
D
C
B
SEE motion
FEE motion
NEHRP F_a
This study
$H_{B\text{-}C}$ =16.4 ft
95%
Median
5%
(f)
Site Coefficient for 1.0 sec, F_v
Average Shear Wave Velocity in Top 100 ft, V_{S100ft} (ft/s)

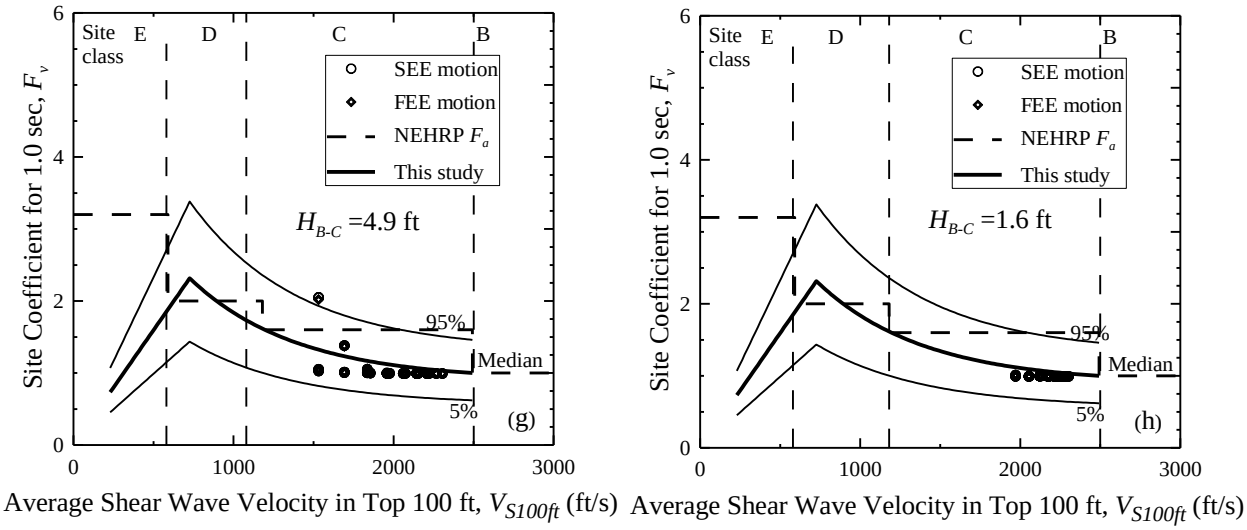

Figure H.9 Site coefficients for 1.0 s (long) spectral period with S_1 equal to 0.2 g, and soft rock half space at depth equal to (a) 328 ft, (b) 164 ft, (c) 100 ft, (d) 65.6 ft, (e) 32.8 ft, (f) 16.4 ft, (g) 4.9 ft, (h) 1.6 ft based on V_S profiles shown in Figures H.1-H.6 for Columbia.

APPENDIX I

EFFECT OF MAGNITUDE ON COMPUTED SITE COEFFICIENTS

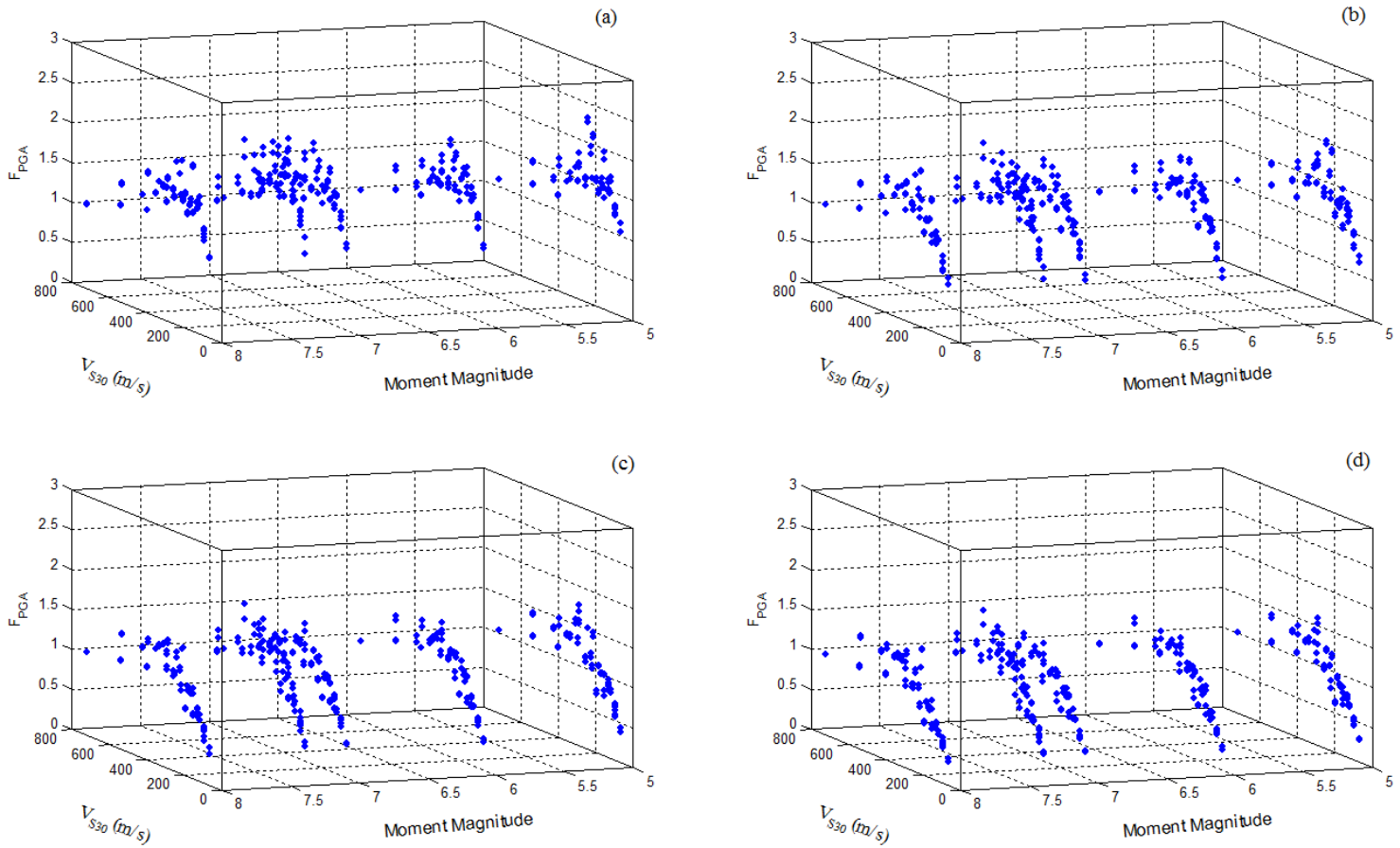

Figure I.1 F_{PGA} versus V_{S100ft} (or V_{S30} in m/s) and moment magnitude with *PGA* equal to (a) 0.05 g, (b) 0.1 g, (c) 0.2 g, and (d) 0.3 g.

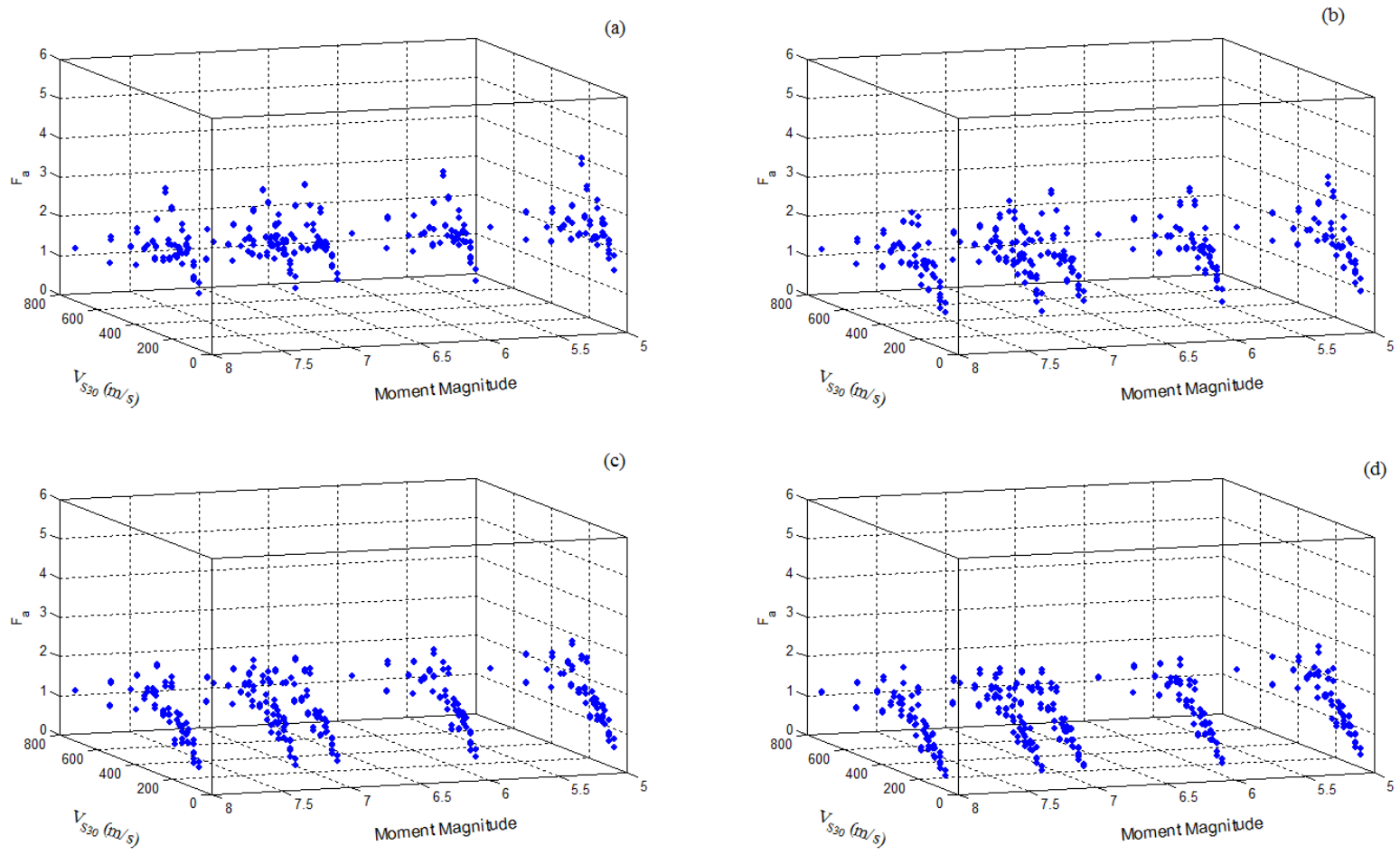

Figure I.2 F_a versus V_{S100ft} (or V_{S30} in m/s) and moment magnitude with S_S equal to (a) 0.125 g, (b) 0.25 g, (c) 0.50 g, and (d) 0.75 g.

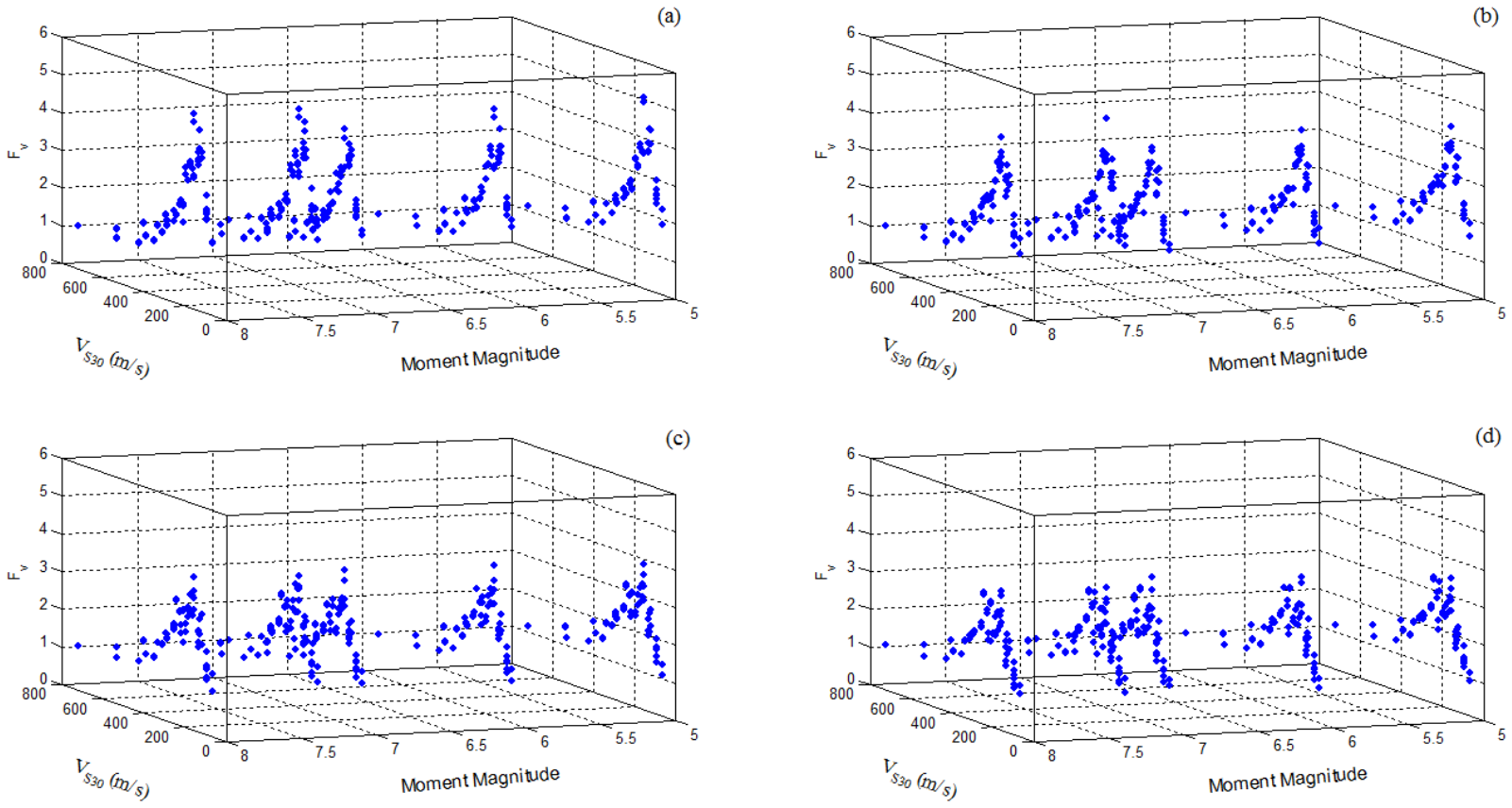

Figure I.3 F_v versus V_{S100ft} (or V_{S30} in m/s) and moment magnitude with S_1 equal to (a) 0.05 g, (b) 0.1 g, (c) 0.2 g, and (d) 0.3 g.

APPENDIX J

SUMMARY OF MODEL INFORMATION, ANALYSIS RESULTS, AND COMPARISON WITH AASHTO (2011a) FOR CHAPTER 6

Modal Information

Table J.1 Modal periods and participating mass with 'Fixed base'.

Modes	Period (sec)	Participating mass					
		Individual Mode (Percent)			Cumulative Sum (Percent)		
		UX	UY	UZ	UX	UY	UZ
1	1.605524	0.00%	68.17%	0.00%	0.00%	68.17%	0.00%
2	1.3625	98.40%	0.00%	0.00%	98.40%	68.17%	0.00%
3	1.030894	0.00%	3.48%	0.00%	98.40%	71.65%	0.00%
4	0.668836	0.00%	15.23%	0.00%	98.40%	86.89%	0.00%
5	0.442127	0.00%	0.21%	0.00%	98.40%	87.09%	0.00%
6	0.274762	0.00%	2.33%	0.00%	98.40%	89.42%	0.00%
7	0.203888	0.00%	0.00%	0.00%	98.40%	89.42%	0.00%
8	0.151085	0.00%	1.01%	0.00%	98.40%	90.43%	0.00%
9	0.117486	0.00%	0.01%	0.00%	98.40%	90.44%	0.00%
10	0.110662	0.02%	0.00%	0.00%	98.41%	90.44%	0.00%
11	0.104737	0.00%	0.08%	0.00%	98.41%	90.52%	0.00%
12	0.103904	0.00%	0.00%	0.00%	98.41%	90.52%	0.00%
13	0.10376	0.34%	0.00%	0.00%	98.75%	90.52%	0.00%
14	0.103604	0.00%	0.10%	0.00%	98.75%	90.62%	0.00%
15	0.093127	0.00%	0.17%	0.00%	98.75%	90.79%	0.00%
16	0.08709	0.00%	0.00%	54.27%	98.75%	90.79%	54.28%
17	0.085262	0.00%	0.02%	0.00%	98.75%	90.81%	54.28%
18	0.084654	0.00%	0.13%	0.00%	98.75%	90.94%	54.28%
19	0.084322	0.35%	0.00%	2.64%	99.10%	90.94%	56.92%
20	0.084193	0.00%	0.00%	0.00%	99.10%	90.94%	56.92%
21	0.084187	0.01%	0.00%	0.10%	99.11%	90.94%	57.02%
22	0.083777	0.35%	0.00%	1.64%	99.45%	90.94%	58.65%
23	0.083469	0.00%	0.03%	0.00%	99.45%	90.96%	58.65%
24	0.082231	0.00%	0.99%	0.00%	99.45%	91.96%	58.65%
25	0.081093	0.00%	0.00%	0.92%	99.46%	91.96%	59.57%
26	0.07255	0.00%	0.00%	26.39%	99.46%	91.96%	85.96%
27	0.069316	0.00%	0.00%	0.00%	99.46%	91.96%	85.96%
28	0.065467	0.00%	0.00%	2.88%	99.46%	91.96%	88.84%
29	0.060783	0.00%	0.29%	0.00%	99.46%	92.24%	88.84%
30	0.056545	0.00%	0.00%	2.23%	99.46%	92.24%	91.07%
31	0.055103	0.01%	0.00%	0.00%	99.47%	92.24%	91.07%
32	0.051975	0.00%	0.01%	0.00%	99.47%	92.25%	91.07%
33	0.045713	0.00%	0.22%	0.00%	99.47%	92.47%	91.07%
34	0.044889	0.00%	0.04%	0.00%	99.47%	92.52%	91.07%
35	0.044715	0.00%	0.00%	0.00%	99.47%	92.52%	91.07%
36	0.044692	0.08%	0.00%	0.00%	99.55%	92.52%	91.07%
37	0.04412	0.00%	0.05%	0.00%	99.55%	92.57%	91.07%
38	0.039936	0.00%	0.05%	0.00%	99.55%	92.62%	91.07%
39	0.038071	0.08%	0.00%	0.03%	99.63%	92.62%	91.10%
40	0.03803	0.00%	0.02%	0.00%	99.63%	92.64%	91.10%

* UX, UY and UZ represent respective mass participations in Global three directions

Table J.2 Modal periods and participating mass with 'Foundation springs'.

Modes	Period (sec)	Participating mass					
		Individual Mode (Percent)			Cumulative Sum (Percent)		
		UX	UY	UZ	UX	UY	UZ
1	1.610791	0.00%	45.67%	0.00%	0.00%	45.67%	0.00%
2	1.370173	65.80%	0.00%	0.00%	65.80%	45.67%	0.00%
3	1.035744	0.00%	2.34%	0.00%	65.80%	48.01%	0.00%
4	0.672964	0.00%	10.38%	0.00%	65.80%	58.38%	0.00%
5	0.445255	0.00%	0.14%	0.00%	65.80%	58.52%	0.00%
6	0.277953	0.00%	1.80%	0.00%	65.80%	60.32%	0.00%
7	0.20747	0.00%	0.00%	0.00%	65.80%	60.32%	0.00%
8	0.15439	0.00%	1.03%	0.00%	65.80%	61.35%	0.00%
9	0.132092	0.00%	0.00%	79.26%	65.80%	61.35%	79.26%
10	0.126357	0.00%	0.00%	2.77%	65.81%	61.35%	82.03%
11	0.120668	0.00%	0.01%	0.00%	65.81%	61.36%	82.03%
12	0.112764	0.01%	0.00%	9.46%	65.81%	61.36%	91.49%
13	0.11072	0.04%	0.00%	0.27%	65.85%	61.36%	91.76%
14	0.105942	0.00%	0.23%	0.00%	65.85%	61.59%	91.76%
15	0.104987	0.56%	0.00%	0.09%	66.41%	61.59%	91.85%
16	0.104272	0.00%	0.10%	0.00%	66.41%	61.69%	91.85%
17	0.104228	0.00%	0.00%	0.00%	66.41%	61.69%	91.85%
18	0.095921	0.00%	0.57%	0.00%	66.41%	62.26%	91.85%
19	0.091662	0.02%	0.00%	0.00%	66.43%	62.26%	91.85%
20	0.086596	0.00%	2.98%	0.00%	66.43%	65.24%	91.85%
21	0.086438	1.53%	0.00%	0.02%	67.96%	65.24%	91.87%
22	0.086064	0.00%	1.17%	0.00%	67.96%	66.41%	91.87%
23	0.085723	0.87%	0.00%	0.01%	68.83%	66.41%	91.87%
24	0.085625	0.00%	0.73%	0.00%	68.83%	67.13%	91.87%
25	0.084534	0.00%	0.00%	0.00%	68.83%	67.13%	91.87%
26	0.084534	0.00%	0.00%	0.00%	68.83%	67.13%	91.87%
27	0.084248	0.00%	1.35%	0.00%	68.83%	68.48%	91.87%
28	0.076822	0.00%	0.07%	0.00%	68.83%	68.55%	91.87%
29	0.07206	0.00%	0.22%	0.00%	68.83%	68.77%	91.87%
30	0.070286	0.00%	9.40%	0.00%	68.83%	78.17%	91.87%
31	0.069931	0.06%	0.00%	2.62%	68.88%	78.17%	94.49%
32	0.069319	0.00%	0.00%	0.00%	68.88%	78.17%	94.49%
33	0.069026	0.00%	11.40%	0.00%	68.88%	89.57%	94.49%
34	0.067641	0.00%	9.73%	0.00%	68.88%	99.30%	94.49%
35	0.062743	0.00%	0.03%	0.00%	68.88%	99.32%	94.49%
36	0.06215	6.39%	0.00%	0.00%	75.27%	99.32%	94.49%
37	0.06194	2.01%	0.00%	0.00%	77.28%	99.32%	94.49%
38	0.061681	4.60%	0.00%	0.00%	81.88%	99.32%	94.49%
39	0.061607	9.20%	0.00%	0.00%	91.08%	99.32%	94.50%
40	0.059434	8.33%	0.00%	0.00%	99.41%	99.32%	94.50%

* UX, UY and UZ represent respective mass participations in Global three directions

Comparison of shear force, axial force, bending moment and displacement computed with AASHTO (2011a) and the Recommended model

Case #1:

Table J.3 Analyses results from Case#1 at column top and bottom with seismic loading in longitudinal direction.

Support/ Location		FORCES AND MOMENTS- EQ_{LONG}									
		Longitudinal				Transverse				Axial (kips)	
		Shear X (kips)		Moment Y (kips-ft)		Shear Y (kips)		Moment X (kips-ft)			
		AASHTO (2011a)	Rec.	AASHTO (2011a)	Rec.	AASHTO (2011a)	Rec.	AASHTO (2011a)	Rec.	AASHTO (2011a)	Rec.
Bent 1 Col	Top	338	303	5087	4549	0	0	0	0	22	19
	Bottom	342	306	5122	4581	0	0	0	0	22	19
Bent 2 Col	Top	99	88	2254	2016	0	0	0	0	30	27
	Bottom	104	93	2308	2065	0	0	0	0	30	27
Bent 3 Col	Top	71	64	1818	1627	0	0	0	0	5	5
	Bottom	77	69	1885	1687	0	0	0	0	5	5
Bent 4 Col	Top	99	89	2259	2021	0	0	0	0	14	12
	Bottom	104	93	2315	2071	0	0	0	0	14	13

Rec.: Based on ADRS curves developed using the recommended site factors

Table J.4 Analyses results from Case#1 at column top and bottom with seismic loading in transverse direction.

Support/ Location		FORCES AND MOMENTS- EQ_{TRANS}									
		Longitudinal				Transverse				Axial (kips)	
		Shear X (kips)		Moment Y (kips-ft)		Shear Y (kips)		Moment X (kips-ft)			
		AASHTO (2011a)	Rec.	AASHTO (2011a)	Rec.	AASHTO (2011a)	Rec.	AASHTO (2011a)	Rec.	AASHTO (2011a)	Rec.
Bent 1 Col	Top	58	19	880	290	400	132	6041	1990	618	205
	Bottom	59	20	885	293	412	136	6165	2031	618	205
Bent 2 Col	Top	28	9	656	216	279	92	6351	2084	632	208
	Bottom	31	10	683	226	291	96	6515	2138	632	208
Bent 3 Col	Top	9	3	228	75	299	98	7601	2495	732	241
	Bottom	12	4	261	89	318	104	7865	2582	732	241
Bent 4 Col	Top	35	9	662	207	305	100	6900	2265	661	217
	Bottom	36	10	679	214	319	104	7093	2329	661	217

Rec.: Based on ADRS curves developed using the recommended site factors

Table J.5 Analyses results from Case#1 at column top with seismic loading in transverse direction.

Support/ Location	DISPLACEMENTS							
	EQ_{LONG}				EQ_{TRANS}			
	Global X (ft)		Global Y (ft)		Global X (ft)		Global Y (ft)	
	AASHTO (2011a)	Rec.	AASHTO (2011a)	Rec.	AASHTO (2011a)	Rec.	AASHTO (2011a)	Rec.
Bent 1 Col	0.2786	0.2491	0.0000	0.0000	0.0176	0.0159	0.1238	0.1108
Bent 2 Col	0.2796	0.2501	0.0000	0.0000	0.0302	0.0271	0.2922	0.2613
Bent 3 Col	0.2803	0.2507	0.0000	0.0000	0.0134	0.0122	0.4340	0.3881
Bent 4 Col	0.2806	0.2509	0.0000	0.0000	0.0285	0.0256	0.3178	0.2842

Rec.: Based on ADRS curves developed using the recommended site factors

Table J.6 Analyses results from Case#1 at column top with seismic loading in both longitudinal and transverse directions, LC1 and LC2.

		FORCES AND MOMENTS														
		Longitudinal						Transverse						Axial (kips)		
		Shear X (kips)			Moment Y (kips-ft)			Shear Z (kips)			Moment X (kips-ft)					
Support/ Location	Load Case	AASHTO (2011a)	Rec.**	Difference (%)*	AASHTO (2011a)	Rec.**	Difference (%)*	AASHTO (2011a)	Rec.**	Difference (%)*	AASHTO (2011a)	Rec.**	Difference (%)*	AASHTO (2011a)	Rec.**	Difference (%)*
Bent 1 Col	LC1	345	308	-10.56	5183	4636	-10.56	44	40	-10.53	668	597	-10.55	90	81	-10.44
	LC2	123	110	-10.47	1848	1655	-10.45	148	132	-10.56	2225	1990	-10.56	236	211	-10.55
Bent 2 Col	LC1	102	91	-10.37	2326	2081	-10.53	31	28	-10.35	699	625	-10.53	100	90	-10.39
	LC2	40	36	-10.33	917	820	-10.50	103	92	-10.36	2330	2084	-10.53	241	216	-10.51
Bent 3 Col	LC1	72	65	-10.08	1843	1650	-10.49	33	29	-10.46	837	748	-10.55	86	77	-10.30
	LC2	25	22	-9.48	628	563	-10.37	110	98	-10.46	2789	2495	-10.55	271	242	-10.53
Bent 4 Col	LC1	102	91	-10.33	2328	2083	-10.52	33	30	-10.36	760	680	-10.53	86	77	-10.25
	LC2	40	36	-10.01	908	813	-10.43	111	100	-10.37	2532	2265	-10.54	246	220	-10.50

* % Difference (in column Forces, Moments or Displacement combinations: LC1 and LC2) = [Recommended- AASHTO (2011a)] X 100/ AASHTO (2011a). A negative value represents greater AASHTO (2011a) outcomes.

**Rec.: Based on ADRS curves developed using the recommended site factors

Table J.7 Analyses results from Case#1 at column bottom with seismic loading in both longitudinal and transverse directions, LC1 and LC2.

		FORCES AND MOMENTS														
		Longitudinal						Transverse						Axial (kips)		
		Shear X (kips)			Moment Y (kips-ft)			Shear Z (kips)			Moment X (kips-ft)					
Support/ Location	Load Case	AASHTO (2011a)	Rec.**	Difference (%)*	AASHTO (2011a)	Rec.**	Difference (%)*	AASHTO (2011a)	Rec.**	Difference (%)*	AASHTO (2011a)	Rec.**	Difference (%)*	AASHTO (2011a)	Rec.**	Difference (%)*
Bent 1 Col	LC1	348	312	-10.56	5220	4669	-10.56	46	41	-10.52	682	610	-10.55	90	81	-10.43
	LC2	124	111	-10.40	1861	1667	-10.42	152	136	-10.56	2271	2031	-10.56	236	211	-10.55
Bent 2 Col	LC1	107	96	-10.37	2384	2133	-10.52	32	29	-10.36	717	642	-10.53	100	90	-10.37
	LC2	43	38	-10.18	944	846	-10.41	107	96	-10.36	2390	2138	-10.53	241	216	-10.50
Bent 3 Col	LC1	78	70	-10.10	1914	1714	-10.45	35	31	-10.46	866	775	-10.55	86	77	-10.19
	LC2	27	25	-9.24	662	595	-10.04	117	104	-10.46	2887	2582	-10.55	271	242	-10.51
Bent 4 Col	LC1	107	96	-10.33	2386	2135	-10.51	35	31	-10.37	781	699	-10.53	86	78	-10.22
	LC2	42	38	-9.88	931	835	-10.34	117	104	-10.38	2603	2329	-10.54	246	221	-10.49

* % Difference (in column Forces, Moments or Displacement combinations: LC1 and LC2) = [Recommended- AASHTO (2011a)] X 100/ AASHTO (2011a). A negative value represents greater AASHTO (2011a) outcomes.

**Rec.: Based on ADRS curves developed using the recommended site factors

Table J.8 Analyses results from Case#1 at column top with seismic loading in both longitudinal and transverse directions, LC1 and LC2.

		DISPLACEMENTS					
		Global X (ft)			Global Y (ft)		
Support/ Location	Load Case	AASHTO (2011a)	Recommended	Difference (%)*	AASHTO (2011a)	Recommended	Difference (%)*
Bent 1 Col	LC1	0.2838	0.2539	-10.5608	0.0372	0.0332	-10.5650
	LC2	0.1012	0.0906	-10.4364	0.1238	0.1108	-10.5650
Bent 2 Col	LC1	0.2887	0.2582	-10.5673	0.0877	0.0784	-10.5747
	LC2	0.1141	0.1021	-10.5041	0.2922	0.2613	-10.5749
Bent 3 Col	LC1	0.2844	0.2543	-10.5561	0.1302	0.1164	-10.5753
	LC2	0.0975	0.0874	-10.3833	0.4340	0.3881	-10.5755
Bent 4 Col	LC1	0.2891	0.2586	-10.5667	0.0953	0.0853	-10.5755
	LC2	0.1127	0.1008	-10.4960	0.3178	0.2842	-10.5756

* % Difference (in column Forces, Moments or Displacement combinations: LC1 and LC2) = [Recommended- AASHTO (2011a)] X 100/ AASHTO (2011a).
A negative value represents greater AASHTO (2011a) outcomes.

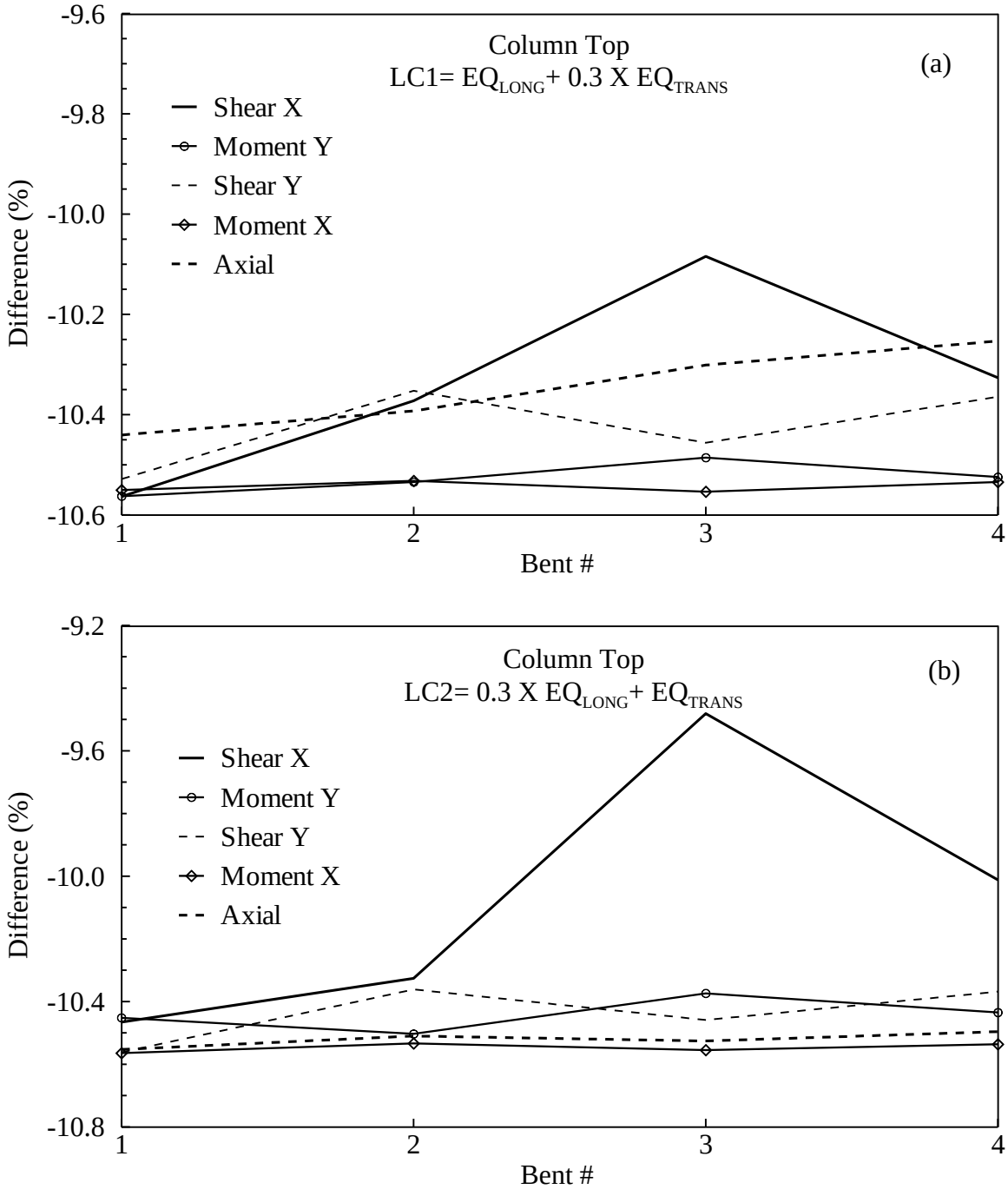

Figure J.1 Comparison (% difference between AASHTO 2011a and recommended) of forces and moments (Shear X, Shear Y, Moment X, Moment Y and Axial) from Case#1 in all four bent columns at the top with load cases: (a) LC1 and (b) LC2.

Case #2:

Table J.9 Analyses results from Case#2 at column top and bottom with seismic loading in longitudinal direction.

Support/ Location		FORCES AND MOMENTS- EQ_{LONG}									
		Longitudinal				Transverse				Axial (kips)	
		Shear X (kips)		Moment Y (kips-ft)		Shear Y (kips)		Moment X (kips-ft)			
		AASHTO (2011a)	Rec.	AASHTO (2011a)	Rec.	AASHTO (2011a)	Rec.	AASHTO (2011a)	Rec.	AASHTO (2011a)	Rec.
Bent 1 Col	Top	917	940	13791	14134	0	0	1	1	58	60
	Bottom	927	950	13887	14233	0	0	1	1	58	60
Bent 2 Col	Top	267	273	6108	6260	0	0	0	0	82	84
	Bottom	281	288	6256	6411	0	0	0	0	82	84
Bent 3 Col	Top	192	197	4926	5049	0	0	0	0	13	13
	Bottom	208	213	5107	5234	0	0	0	0	13	13
Bent 4 Col	Top	268	274	6122	6274	0	0	0	0	37	37
	Bottom	282	289	6274	6430	0	0	0	0	37	37

Rec.: Based on ADRS curves developed using the recommended site factors

Table J.10 Analyses results from Case#2 at column top and bottom with seismic loading in transverse direction.

Support/ Location		FORCES AND MOMENTS- EQ_{TRANS}									
		Longitudinal				Transverse				Axial (kips)	
		Shear X (kips)		Moment Y (kips-ft)		Shear Y (kips)		Moment X (kips-ft)			
		AASHTO (2011a)	Rec.	AASHTO (2011a)	Rec.	AASHTO (2011a)	Rec.	AASHTO (2011a)	Rec.	AASHTO (2011a)	Rec.
Bent 1 Col	Top	58	59	880	891	400	413	6041	6233	618	641
	Bottom	59	60	885	897	412	425	6165	6362	618	641
Bent 2 Col	Top	28	29	656	672	279	286	6351	6491	632	647
	Bottom	31	32	683	700	291	297	6515	6659	632	647
Bent 3 Col	Top	9	9	228	230	299	306	7601	7774	732	750
	Bottom	12	11	261	263	318	325	7865	8046	732	751
Bent 4 Col	Top	35	28	662	639	305	310	6900	7058	661	675
	Bottom	36	30	679	656	319	325	7093	7256	661	675

Rec.: Based on ADRS curves developed using the recommended site factors

Table J.11 Analyses results from Case#2 at column top with seismic loading in transverse direction.

Support/ Location	DISPLACEMENTS							
	EQ_{LONG}				EQ_{TRANS}			
	Global X (ft)		Global Y (ft)		Global X (ft)		Global Y (ft)	
	AASHTO (2011a)	Rec.	AASHTO (2011a)	Rec.	AASHTO (2011a)	Rec.	AASHTO (2011a)	Rec.
Bent 1 Col	0.7552	0.7740	0.0000	0.0000	0.0476	0.0487	0.3362	0.3469
Bent 2 Col	0.7581	0.7770	0.0000	0.0000	0.0819	0.0842	0.7954	0.8143
Bent 3 Col	0.7600	0.7789	0.0000	0.0000	0.0361	0.0373	1.1814	1.2097
Bent 4 Col	0.7607	0.7797	0.0000	0.0000	0.0774	0.0792	0.8650	0.8862

Rec.: Based on ADRS curves developed using the recommended site factors

Table J.12 Analyses results from Case#2 at column top with seismic loading in both longitudinal and transverse directions, LC1 and LC2.

		FORCES AND MOMENTS														
		Longitudinal						Transverse						Axial (kips)		
		Shear X (kips)			Moment Y (kips-ft)			Shear Z (kips)			Moment X (kips-ft)					
Support/ Location	Load Case	AASHTO (2011a)	Rec.**	Difference (%)*	AASHTO (2011a)	Rec.**	Difference (%)*	AASHTO (2011a)	Rec.**	Difference (%)*	AASHTO (2011a)	Rec.**	Difference (%)*	AASHTO (2011a)	Rec.**	Difference (%)*
Bent 1 Col	LC1	935	958	2.49	14052	14402	2.49	120	124	3.19	1813	1871	3.20	245	252	2.97
	LC2	333	341	2.47	5008	5132	2.47	400	413	3.19	6040	6233	3.20	639	659	3.11
Bent 2 Col	LC1	275	282	2.49	6304	6462	2.50	84	86	2.37	1902	1947	2.38	272	278	2.40
	LC2	108	111	2.53	2486	2550	2.56	279	286	2.37	6340	6491	2.38	656	672	2.38
Bent 3 Col	LC1	195	199	2.45	4993	5118	2.49	90	92	2.38	2278	2332	2.39	233	238	2.38
	LC2	66	68	2.48	1701	1745	2.57	298	306	2.38	7592	7774	2.39	737	754	2.38
Bent 4 Col	LC1	276	283	2.47	6309	6466	2.49	91	93	2.41	2067	2117	2.43	234	240	2.41
	LC2	108	110	2.44	2461	2522	2.47	303	310	2.41	6890	7058	2.43	670	686	2.42

* % Difference (in column Forces, Moments or Displacement combinations: LC1 and LC2) = [Recommended- AASHTO (2011a)] X 100/ AASHTO (2011a). A negative value represents greater AASHTO (2011a) outcomes.

** Rec.: Based on ADRS curves developed using the recommended site factors

Table J.13 Analyses results from Case#2 at column bottom with seismic loading in both longitudinal and transverse directions, LC1 and LC2.

		FORCES AND MOMENTS														
		Longitudinal						Transverse						Axial (kips)		
		Shear X (kips)			Moment Y (kips-ft)			Shear Z (kips)			Moment X (kips-ft)					
Support/ Location	Load Case	AASHTO (2011a)	Rec.**	Difference (%)*	AASHTO (2011a)	Rec.**	Difference (%)*	AASHTO (2011a)	Rec.**	Difference (%)*	AASHTO (2011a)	Rec.**	Difference (%)*	AASHTO (2011a)	Rec.**	Difference (%)*
Bent 1 Col	LC1	944	968	2.49	14151	14503	2.49	124	127	3.21	1850	1909	3.21	245	252	2.97
	LC2	337	345	2.46	5043	5168	2.46	411	425	3.22	6165	6363	3.21	640	659	3.11
Bent 2 Col	LC1	290	298	2.49	6460	6621	2.50	87	89	2.37	1952	1998	2.38	272	278	2.40
	LC2	115	118	2.55	2558	2624	2.56	291	297	2.37	6505	6659	2.38	656	672	2.38
Bent 3 Col	LC1	211	216	2.46	5184	5313	2.49	95	97	2.39	2357	2414	2.39	233	239	2.37
	LC2	74	75	2.49	1788	1833	2.56	317	325	2.39	7858	8046	2.39	737	755	2.38
Bent 4 Col	LC1	290	298	2.47	6466	6626	2.49	95	97	2.44	2125	2177	2.44	234	240	2.41
	LC2	114	116	2.43	2522	2585	2.47	317	325	2.44	7083	7256	2.44	670	686	2.42

* % Difference (in column Forces, Moments or Displacement combinations: LC1 and LC2) = [Recommended- AASHTO (2011a)] X 100/ AASHTO (2011a). A negative value represents greater AASHTO (2011a) outcomes.

** Rec.: Based on ADRS curves developed using the recommended site factors

Table J.14 Analyses results from Case#2 at column top with seismic loading in both longitudinal and transverse directions, LC1 and LC2.

		DISPLACEMENTS					
		Global X (ft)			Global Y (ft)		
Support/ Location	Load Case	AASHTO (2011a)	Recommended	Difference (%)*	AASHTO (2011a)	Recommended	Difference (%)*
Bent 1 Col	LC1	0.7695	0.7886	2.4889	0.1009	0.1041	3.2077
	LC2	0.2742	0.2809	2.4643	0.3362	0.3469	3.2076
Bent 2 Col	LC1	0.7827	0.8023	2.5004	0.2386	0.2443	2.3816
	LC2	0.3093	0.3173	2.5639	0.7954	0.8143	2.3815
Bent 3 Col	LC1	0.7708	0.7901	2.5011	0.3544	0.3629	2.3940
	LC2	0.2641	0.2710	2.5812	1.1814	1.2097	2.3938
Bent 4 Col	LC1	0.7839	0.8035	2.4900	0.2595	0.2658	2.4403
	LC2	0.3056	0.3131	2.4760	0.8650	0.8862	2.4405

* % Difference (in column Forces, Moments or Displacement combinations: LC1 and LC2) = [Recommended- AASHTO (2011a)] X 100/ AASHTO (2011a).
A negative value represents greater AASHTO (2011a) outcomes.

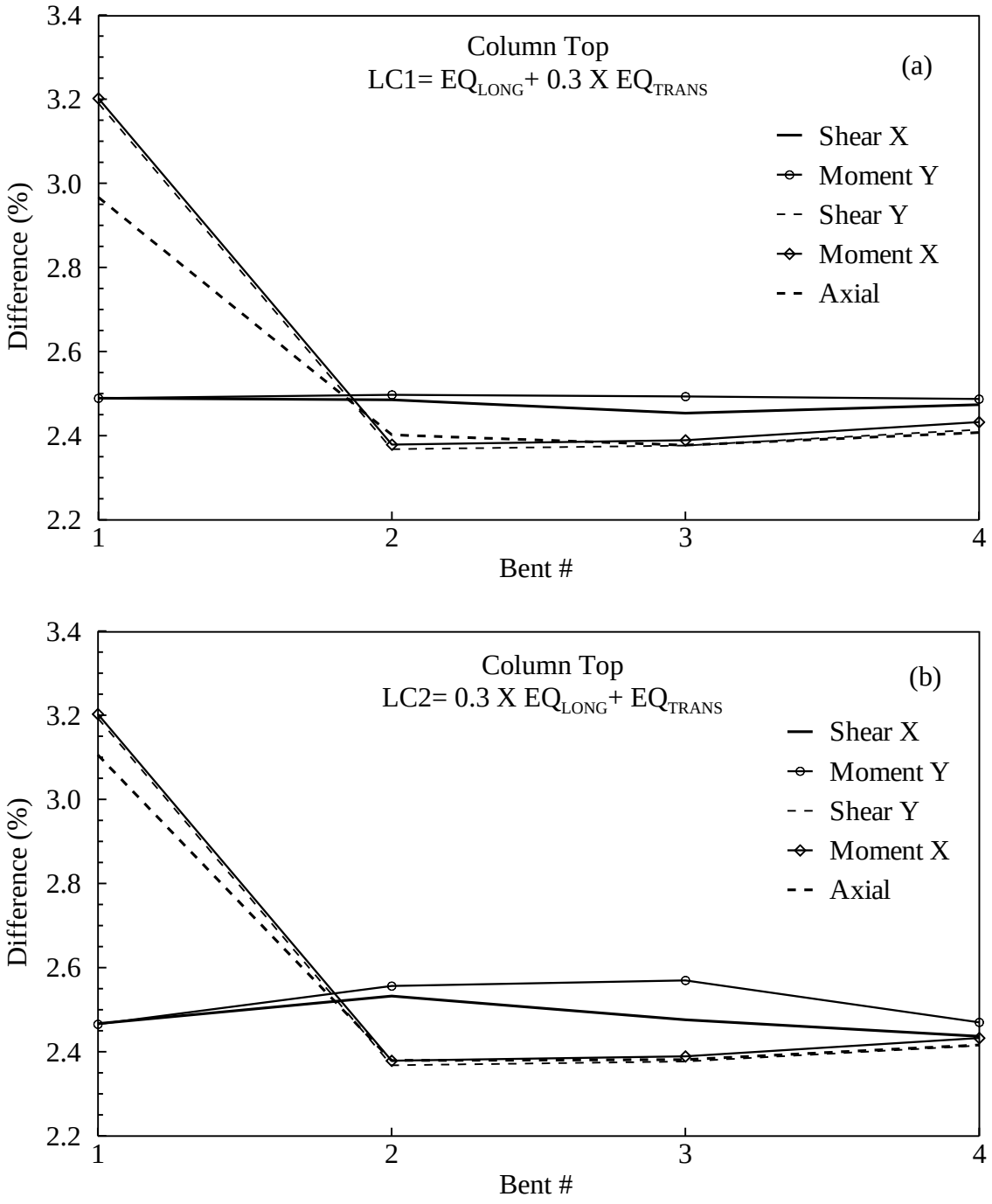

Figure J.2 Comparison (% difference between AASHTO 2011a and recommended) of forces and moments (Shear X, Shear Y, Moment X, Moment Y and Axial) from Case#2 in all four bent columns at the top with load cases: (a) LC1 and (b) LC2.

Case #3:

Table J.15 Analyses results from Case#3 at column top and bottom with seismic loading in longitudinal direction.

Support/ Location		FORCES AND MOMENTS- EQ_{LONG}									
		Longitudinal				Transverse				Axial (kips)	
		Shear X (kips)		Moment Y (kips-ft)		Shear Y (kips)		Moment X (kips-ft)			
		AASHTO (2011a)	Rec.	AASHTO (2011a)	Rec.	AASHTO (2011a)	Rec.	AASHTO (2011a)	Rec.	AASHTO (2011a)	Rec.
Bent 1 Col	Top	917	1114	13791	16749	0	0	1	1	58	71
	Bottom	927	1125	13887	16866	0	0	1	1	58	71
Bent 2 Col	Top	267	324	6108	7417	0	0	0	0	82	100
	Bottom	281	341	6256	7597	0	0	0	0	82	100
Bent 3 Col	Top	192	233	4926	5981	0	0	0	0	13	16
	Bottom	208	252	5107	6201	0	0	0	0	13	16
Bent 4 Col	Top	268	325	6122	7434	0	0	0	0	37	44
	Bottom	282	342	6274	7618	0	0	0	0	37	44

Rec.: Based on ADRS curves developed using the recommended site factors

Table J.16 Analyses results from Case#3 at column top and bottom with seismic loading in transverse direction.

Support/ Location		FORCES AND MOMENTS- EQ_{TRANS}									
		Longitudinal				Transverse				Axial (kips)	
		Shear X (kips)		Moment Y (kips-ft)		Shear Y (kips)		Moment X (kips-ft)			
		AASHTO (2011a)	Rec.	AASHTO (2011a)	Rec.	AASHTO (2011a)	Rec.	AASHTO (2011a)	Rec.	AASHTO (2011a)	Rec.
Bent 1 Col	Top	58	70	880	1054	400	483	6041	7287	618	751
	Bottom	59	71	885	1061	412	496	6165	7437	618	751
Bent 2 Col	Top	28	34	656	791	279	339	6351	7698	632	767
	Bottom	31	37	683	823	291	353	6515	7898	632	767
Bent 3 Col	Top	9	10	228	269	299	362	7601	9218	732	890
	Bottom	12	13	261	305	318	385	7865	9540	732	890
Bent 4 Col	Top	35	33	662	757	305	367	6900	8362	661	800
	Bottom	36	35	679	775	319	384	7093	8597	661	800

Rec.: Based on ADRS curves developed using the recommended site factors

Table J.17 Analyses results from Case#3 at column top with seismic loading in transverse direction.

Support/ Location	DISPLACEMENTS							
	EQ_{LONG}				EQ_{TRANS}			
	Global X (ft)		Global Y (ft)		Global X (ft)		Global Y (ft)	
	AASHTO (2011a)	Rec.	AASHTO (2011a)	Rec.	AASHTO (2011a)	Rec.	AASHTO (2011a)	Rec.
Bent 1 Col	0.7552	0.9172	0.0000	0.0000	0.0476	0.0576	0.3362	0.4056
Bent 2 Col	0.7581	0.9207	0.0000	0.0000	0.0819	0.0991	0.7954	0.9658
Bent 3 Col	0.7600	0.9230	0.0000	0.0000	0.0361	0.0434	1.1814	1.4345
Bent 4 Col	0.7607	0.9239	0.0000	0.0000	0.0774	0.0938	0.8650	1.0500

Rec.: Based on ADRS curves developed using the recommended site factors

Table J.18 Analyses results from Case#3 at column top with seismic loading in both longitudinal and transverse directions, LC1 and LC2.

		FORCES AND MOMENTS														
		Longitudinal						Transverse						Axial (kips)		
		Shear X (kips)			Moment Y (kips-ft)			Shear Z (kips)			Moment X (kips-ft)					
Support/ Location	Load Case	AASHTO (2011a)	Rec.**	Difference (%)*	AASHTO (2011a)	Rec.**	Difference (%)*	AASHTO (2011a)	Rec.**	Difference (%)*	AASHTO (2011a)	Rec.**	Difference (%)*	AASHTO (2011a)	Rec.**	Difference (%)*
Bent 1 Col	LC1	935	1135	21.44	14052	17065	21.44	120	145	20.64	1813	2187	20.65	245	296	20.86
	LC2	333	404	21.39	5008	6079	21.38	400	483	20.66	6040	7287	20.65	639	772	20.75
Bent 2 Col	LC1	275	334	21.36	6304	7655	21.42	84	102	21.36	1902	2310	21.42	272	330	21.37
	LC2	108	131	21.27	2486	3017	21.33	279	339	21.36	6340	7698	21.42	656	797	21.41
Bent 3 Col	LC1	195	236	21.19	4993	6061	21.39	90	109	21.37	2278	2765	21.41	233	282	21.34
	LC2	66	80	20.85	1701	2063	21.26	298	362	21.37	7592	9218	21.41	737	895	21.41
Bent 4 Col	LC1	276	335	21.35	6309	7661	21.43	91	110	21.32	2067	2509	21.37	234	284	21.27
	LC2	108	131	21.20	2461	2987	21.37	303	367	21.32	6890	8362	21.37	670	813	21.37

* % Difference (in column Forces, Moments or Displacement combinations: LC1 and LC2) = [Recommended- AASHTO (2011a)] X 100/ AASHTO (2011a). A negative value represents greater AASHTO (2011a) outcomes.

**Rec.: Based on ADRS curves developed using the recommended site factors

Table J.19 Analyses results from Case#3 at column bottom with seismic loading in both longitudinal and transverse directions, LC1 and LC2.

		FORCES AND MOMENTS														
		Longitudinal						Transverse						Axial (kips)		
		Shear X (kips)			Moment Y (kips-ft)			Shear Z (kips)			Moment X (kips-ft)					
Support/ Location	Load Case	AASHTO (2011a)	Rec.**	Difference (%)*	AASHTO (2011a)	Rec.**	Difference (%)*	AASHTO (2011a)	Rec.**	Difference (%)*	AASHTO (2011a)	Rec.**	Difference (%)*	AASHTO (2011a)	Rec.**	Difference (%)*
Bent 1 Col	LC1	944	1147	21.44	14151	17185	21.44	124	149	20.62	1850	2232	20.63	245	296	20.86
	LC2	337	408	21.36	5043	6121	21.37	411	496	20.63	6165	7437	20.64	640	772	20.74
Bent 2 Col	LC1	290	352	21.36	6460	7844	21.42	87	106	21.35	1952	2369	21.41	272	330	21.36
	LC2	115	140	21.19	2558	3102	21.28	291	353	21.35	6505	7898	21.41	656	797	21.41
Bent 3 Col	LC1	211	256	21.20	5184	6292	21.38	95	115	21.36	2357	2862	21.40	233	283	21.31
	LC2	74	89	20.71	1788	2165	21.10	317	385	21.36	7858	9540	21.41	737	895	21.40
Bent 4 Col	LC1	290	352	21.35	6466	7851	21.42	95	115	21.30	2125	2579	21.36	234	284	21.26
	LC2	114	138	21.14	2522	3060	21.33	317	384	21.30	7083	8597	21.36	670	813	21.37

* % Difference (in column Forces, Moments or Displacement combinations: LC1 and LC2) = [Recommended- AASHTO (2011a)] X 100/ AASHTO (2011a). A negative value represents greater AASHTO (2011a) outcomes.

** Rec.: Based on ADRS curves developed using the recommended site factors

Table J.20 Analyses results from Case#3 at column top with seismic loading in both longitudinal and transverse directions, LC1 and LC2.

		DISPLACEMENTS					
		Global X (ft)			Global Y (ft)		
Support/ Location	Load Case	AASHTO (2011a)	Recommended	Difference (%)*	AASHTO (2011a)	Recommended	Difference (%)*
Bent 1 Col	LC1	0.7695	0.9344	21.4416	0.1009	0.1217	20.6461
	LC2	0.2742	0.3328	21.3772	0.3362	0.4056	20.6466
Bent 2 Col	LC1	0.7827	0.9505	21.4341	0.2386	0.2898	21.4302
	LC2	0.3093	0.3753	21.3216	0.7954	0.9658	21.4300
Bent 3 Col	LC1	0.7708	0.9360	21.4300	0.3544	0.4304	21.4186
	LC2	0.2641	0.3203	21.2605	1.1814	1.4345	21.4184
Bent 4 Col	LC1	0.7839	0.9520	21.4428	0.2595	0.3150	21.3800
	LC2	0.3056	0.3709	21.3932	0.8650	1.0500	21.3800

* % Difference (in column Forces, Moments or Displacement combinations: LC1 and LC2) = [Recommended- AASHTO (2011a)] X 100/ AASHTO (2011a). A negative value represents greater AASHTO (2011a) outcomes.

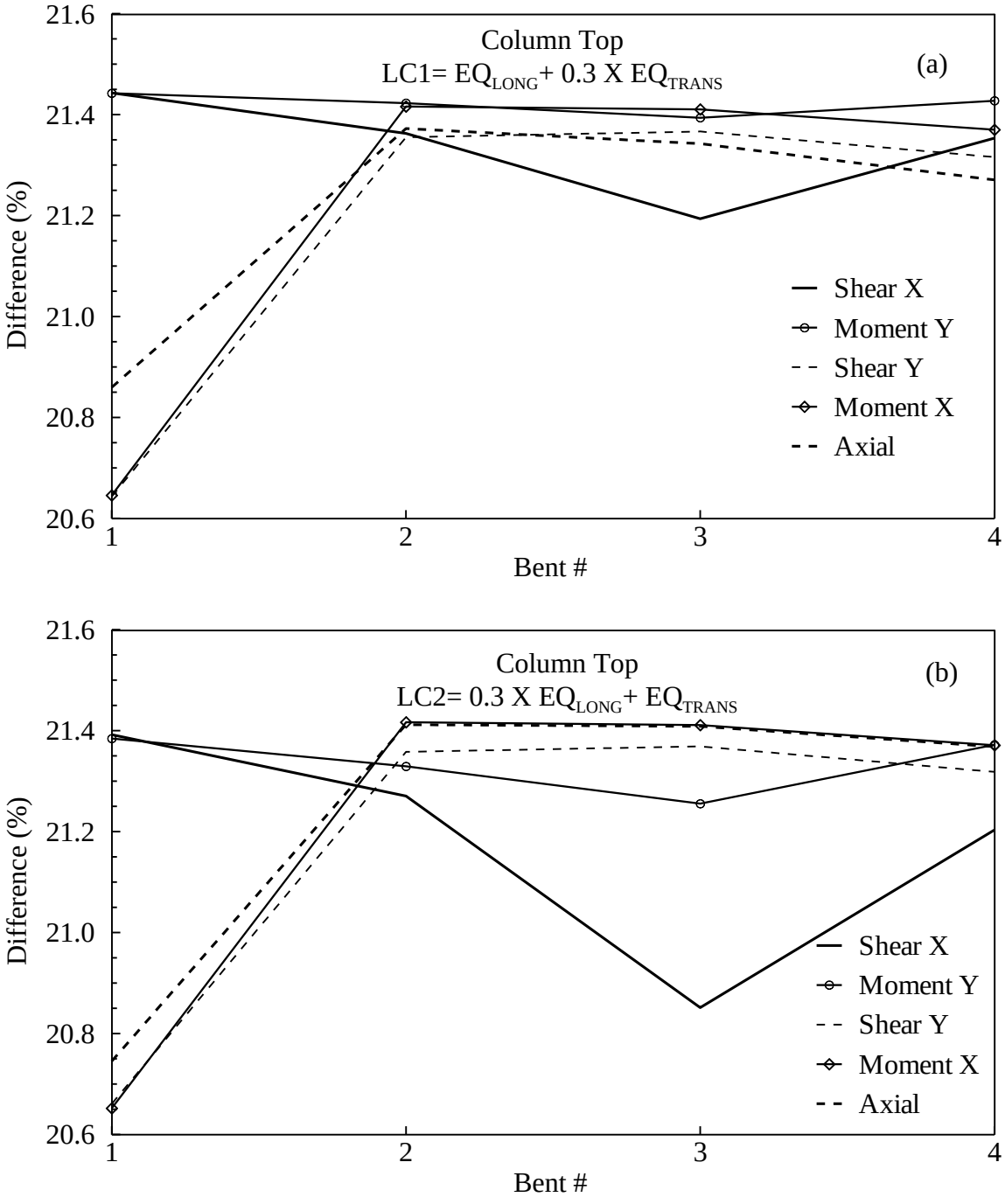

Figure J.3 Comparison (% difference between AASHTO 2011a and recommended) of forces and moments (Shear X, Shear Y, Moment X, Moment Y and Axial) from Case#3 in all four typical bent columns at the top with load cases: (a) LC1 and (b) LC2.

Case #4:

Table J.21 Analyses results from Case#4 at column top and bottom with seismic loading in longitudinal direction.

Support/ Location		FORCES AND MOMENTS- EQ_{LONG}									
		Longitudinal				Transverse				Axial (kips)	
		Shear X (kips)		Moment Y (kips-ft)		Shear Y (kips)		Moment X (kips-ft)			
		AASHTO (2011a)	Rec.	AASHTO (2011a)	Rec.	AASHTO (2011a)	Rec.	AASHTO (2011a)	Rec.	AASHTO (2011a)	Rec.
Bent 1 Col	Top	1403	962	21096	14461	0	0	1	0	89	61
	Bottom	1417	972	21244	14562	0	0	1	0	89	61
Bent 2 Col	Top	408	279	9341	6404	0	0	0	0	125	86
	Bottom	429	294	9567	6558	0	0	0	0	125	86
Bent 3 Col	Top	293	201	7531	5163	0	0	0	0	19	13
	Bottom	317	217	7808	5352	0	0	0	0	19	13
Bent 4 Col	Top	409	280	9363	6418	0	0	0	0	55	38
	Bottom	431	295	9595	6577	0	0	0	0	55	38

Rec.: Based on ADRS curves developed using the recommended site factors

Table J.22 Analyses results from Case#4 at column top and bottom with seismic loading in transverse direction.

Support/ Location		FORCES AND MOMENTS- EQ_{TRANS}									
		Longitudinal				Transverse				Axial (kips)	
		Shear X (kips)		Moment Y (kips-ft)		Shear Y (kips)		Moment X (kips-ft)			
		AASHTO (2011a)	Rec.	AASHTO (2011a)	Rec.	AASHTO (2011a)	Rec.	AASHTO (2011a)	Rec.	AASHTO (2011a)	Rec.
Bent 1 Col	Top	58	60	880	905	400	360	6041	5420	618	568
	Bottom	59	61	885	910	412	368	6165	5519	618	568
Bent 2 Col	Top	28	28	656	641	279	292	6351	6638	632	661
	Bottom	31	30	683	660	291	304	6515	6809	632	662
Bent 3 Col	Top	9	8	228	201	299	312	7601	7929	732	766
	Bottom	12	9	261	223	318	331	7865	8199	732	766
Bent 4 Col	Top	35	28	662	644	305	314	6900	7147	661	685
	Bottom	36	30	679	658	319	328	7093	7336	661	685

Rec.: Based on ADRS curves developed using the recommended site factors

Table J.23 Analyses results from Case#4 at column top with seismic loading in transverse direction.

Support/ Location	DISPLACEMENTS							
	EQ_{LONG}				EQ_{TRANS}			
	Global X (ft)		Global Y (ft)		Global X (ft)		Global Y (ft)	
	AASHTO (2011a)	Rec.	AASHTO (2011a)	Rec.	AASHTO (2011a)	Rec.	AASHTO (2011a)	Rec.
Bent 1 Col	1.1552	0.7919	0.0000	0.0000	0.0721	0.0494	0.4371	0.3013
Bent 2 Col	1.1597	0.7950	0.0000	0.0000	0.1162	0.0798	1.2162	0.8329
Bent 3 Col	1.1625	0.7969	0.0000	0.0000	0.0466	0.0321	1.8010	1.2335
Bent 4 Col	1.1637	0.7977	0.0000	0.0000	0.1164	0.0798	1.3089	0.8967

Rec.: Based on ADRS curves developed using the recommended site factors

Table J.24 Analyses results from Case#4 at column top with seismic loading in both longitudinal and transverse directions, LC1 and LC2.

		FORCES AND MOMENTS														
		Longitudinal						Transverse						Axial (kips)		
		Shear X (kips)			Moment Y (kips-ft)			Shear Z (kips)			Moment X (kips-ft)					
Support/ Location	Load Case	AASHTO (2011a)	Rec.**	Difference (%)*	AASHTO (2011a)	Rec.**	Difference (%)*	AASHTO (2011a)	Rec.**	Difference (%)*	AASHTO (2011a)	Rec.**	Difference (%)*	AASHTO (2011a)	Rec.**	Difference (%)*
Bent 1 Col	LC1	1429	980	-31.45	21492	14732	-31.45	157	108	-31.07	2359	1626	-31.07	336	231	-31.21
	LC2	509	349	-31.46	7649	5243	-31.46	523	360	-31.07	7863	5420	-31.07	851	586	-31.14
Bent 2 Col	LC1	420	288	-31.45	9622	6596	-31.45	128	88	-31.52	2908	1992	-31.52	415	284	-31.50
	LC2	163	112	-31.43	3736	2562	-31.42	426	292	-31.52	9693	6638	-31.52	1003	687	-31.52
Bent 3 Col	LC1	296	203	-31.45	7618	5223	-31.45	137	94	-31.51	3473	2379	-31.51	355	243	-31.51
	LC2	99	68	-31.42	2551	1750	-31.41	455	312	-31.51	11577	7929	-31.51	1125	770	-31.51
Bent 4 Col	LC1	421	289	-31.45	9645	6612	-31.45	138	94	-31.50	3130	2144	-31.49	355	243	-31.49
	LC2	164	112	-31.46	3749	2570	-31.46	459	314	-31.50	10432	7147	-31.49	1017	697	-31.50

* % Difference (in column Forces, Moments or Displacement combinations: LC1 and LC2) = [Recommended- AASHTO (2011a)] X 100/ AASHTO (2011a). A negative value represents greater AASHTO (2011a) outcomes.

** Rec.: Based on ADRS curves developed using the recommended site factors

Table J.25 Analyses results from Case#4 at column bottom with seismic loading in both longitudinal and transverse directions, LC1 and LC2.

		FORCES AND MOMENTS														
		Longitudinal						Transverse						Axial (kips)		
		Shear X (kips)			Moment Y (kips-ft)			Shear Z (kips)			Moment X (kips-ft)					
Support/ Location	Load Case	AASHTO (2011a)	Rec.**	Difference (%)*	AASHTO (2011a)	Rec.**	Difference (%)*	AASHTO (2011a)	Rec.**	Difference (%)*	AASHTO (2011a)	Rec.**	Difference (%)*	AASHTO (2011a)	Rec.**	Difference (%)*
Bent 1 Col	LC1	1444	990	-31.45	21642	14835	-31.45	160	110	-31.06	2402	1656	-31.06	336	231	-31.21
	LC2	514	352	-31.46	7701	5278	-31.46	534	368	-31.05	8005	5519	-31.06	851	586	-31.14
Bent 2 Col	LC1	442	303	-31.45	9856	6756	-31.45	133	91	-31.52	2983	2043	-31.52	415	284	-31.50
	LC2	172	118	-31.41	3832	2628	-31.42	444	304	-31.52	9943	6809	-31.52	1004	687	-31.52
Bent 3 Col	LC1	321	220	-31.44	7905	5419	-31.44	145	99	-31.51	3591	2460	-31.51	355	243	-31.51
	LC2	109	75	-31.39	2665	1828	-31.40	483	331	-31.51	11972	8199	-31.51	1125	770	-31.51
Bent 4 Col	LC1	443	304	-31.45	9883	6774	-31.45	143	98	-31.49	3212	2201	-31.49	355	244	-31.49
	LC2	172	118	-31.46	3838	2631	-31.46	478	328	-31.49	10708	7336	-31.49	1017	697	-31.50

* % Difference (in column Forces, Moments or Displacement combinations: LC1 and LC2) = [Recommended- AASHTO (2011a)] X 100/ AASHTO (2011a). A negative value represents greater AASHTO (2011a) outcomes.

** Rec.: Based on ADRS curves developed using the recommended site factors

Table J.26 Analyses results from Case#4 at column top with seismic loading in both longitudinal and transverse directions, LC1 and LC2.

		DISPLACEMENTS					
		Global X (ft)			Global Y (ft)		
Support/ Location	Load Case	AASHTO (2011a)	Recommended	Difference (%)*	AASHTO (2011a)	Recommended	Difference (%)*
Bent 1 Col	LC1	1.1768	0.8067	-31.4510	0.1311	0.0904	-31.0624
	LC2	0.4187	0.2870	-31.4594	0.4371	0.3013	-31.0623
Bent 2 Col	LC1	1.1946	0.8189	-31.4465	0.3649	0.2499	-31.5185
	LC2	0.4641	0.3183	-31.4197	1.2162	0.8329	-31.5185
Bent 3 Col	LC1	1.1765	0.8066	-31.4455	0.5403	0.3700	-31.5102
	LC2	0.3953	0.2712	-31.4046	1.8010	1.2335	-31.5102
Bent 4 Col	LC1	1.1986	0.8216	-31.4510	0.3927	0.2690	-31.4924
	LC2	0.4655	0.3191	-31.4581	1.3089	0.8967	-31.4923

* % Difference (in column Forces, Moments or Displacement combinations: LC1 and LC2) = [Recommended- AASHTO (2011a)] X 100/ AASHTO (2011a). A negative value represents greater AASHTO (2011a) outcomes.

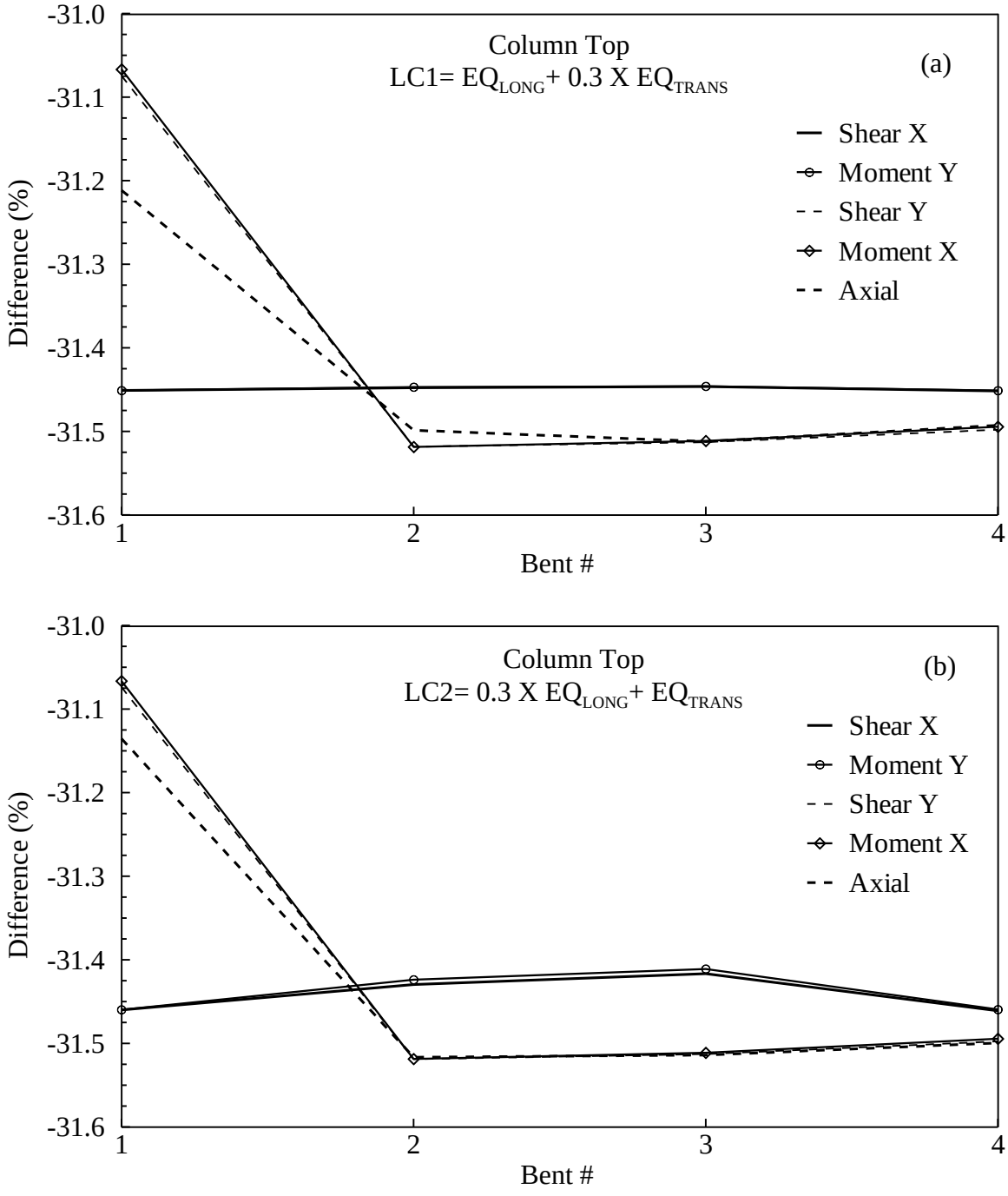

Figure J.4 Comparison (% difference between AASHTO 2011a and recommended) of forces and moments (Shear X, Shear Y, Moment X, Moment Y and Axial) from Case#4 in all four bent columns at the top with load cases: (a) LC1 and (b) LC2.

Parametric study

Test #1:

Table J.27 Analyses results from Test#1 at column top and bottom with seismic loading in longitudinal direction.

Support/ Location		FORCES AND MOMENTS- EQ_{LONG}									
		Longitudinal				Transverse				Axial (kips)	
		Shear X (kips)		Moment Y (kips-ft)		Shear Y (kips)		Moment X (kips-ft)			
		Case#1	Case#2	Case#1	Case#2	Case#1	Case#2	Case#1	Case#2	Case#1	Case#2
Bent 1 Col	Top	303	300	4549	4516	0	0	0	0	19	17
	Bottom	306	303	4581	4527	0	0	0	0	19	17
Bent 2 Col	Top	88	91	2016	2030	0	0	0	0	27	22
	Bottom	93	95	2065	2072	0	0	0	0	27	22
Bent 3 Col	Top	64	66	1627	1640	0	0	0	1	5	3
	Bottom	69	70	1687	1693	0	0	0	1	5	3
Bent 4 Col	Top	89	91	2021	2035	0	0	0	0	12	11
	Bottom	93	95	2071	2079	0	0	0	0	13	12

Table J.28 Analyses results from Test#1 at column top and bottom with seismic loading in transverse direction.

Support/ Location		FORCES AND MOMENTS- EQ_{TRANS}									
		Longitudinal				Transverse				Axial (kips)	
		Shear X (kips)		Moment Y (kips-ft)		Shear Y (kips)		Moment X (kips-ft)			
		Case#1	Case#2	Case#1	Case#2	Case#1	Case#2	Case#1	Case#2	Case#1	Case#2
Bent 1 Col	Top	58	19	880	293	400	132	6041	1990	618	204
	Bottom	59	20	885	296	412	136	6165	2029	618	204
Bent 2 Col	Top	28	10	656	218	279	96	6351	2105	632	210
	Bottom	31	11	683	229	291	100	6515	2159	632	210
Bent 3 Col	Top	9	4	228	78	299	99	7601	2500	732	241
	Bottom	12	5	261	93	318	105	7865	2586	732	241
Bent 4 Col	Top	35	11	662	216	305	104	6900	2281	661	219
	Bottom	36	12	679	223	319	108	7093	2344	661	219

Table J.29 Analyses results from Test#1 at column top with seismic loading in transverse direction.

Support/ Location	DISPLACEMENTS							
	EQ_{LONG}				EQ_{TRANS}			
	Global X (ft)		Global Y (ft)		Global X (ft)		Global Y (ft)	
	Case#1	Case#2	Case#1	Case#2	Case#1	Case#2	Case#1	Case#2
Bent 1 Col	0.2491	0.2511	0.0000	0.0000	0.0159	0.0161	0.1108	0.1126
Bent 2 Col	0.2501	0.2521	0.0000	0.0000	0.0271	0.0272	0.2613	0.2635
Bent 3 Col	0.2507	0.2527	0.0000	0.0000	0.0122	0.0124	0.3881	0.3902
Bent 4 Col	0.2509	0.2530	0.0000	0.0000	0.0256	0.0257	0.2842	0.2859

Table J.30 Analyses results from Test#1 at column top with seismic loading in both longitudinal and transverse directions, LC1 and LC2.

		FORCES AND MOMENTS														
		Longitudinal						Transverse						Axial (kips)		
		Shear X (kips)			Moment Y (kips-ft)			Shear Z (kips)			Moment X (kips-ft)					
Support/ Location	Load Test	Case#1	Case#2	Difference (%)*	Case#1	Case#2	Difference (%)*	Case#1	Case#2	Difference (%)*	Case#1	Case#2	Difference (%)*	Case#1	Case#2	Difference (%)*
Bent 1 Col	LC1	308	306	-0.87	4636	4604	-0.69	40	40	0.11	597	597	-0.02	81	78	-4.00
	LC2	110	109	-0.58	1655	1648	-0.40	132	132	0.20	1990	1990	0.02	211	209	-1.02
Bent 2 Col	LC1	91	94	2.84	2081	2095	0.68	28	29	4.79	625	632	1.04	90	85	-5.28
	LC2	36	37	3.37	820	827	0.80	92	96	4.74	2084	2105	1.02	216	216	0.29
Bent 3 Col	LC1	65	67	3.23	1650	1663	0.82	29	30	1.34	748	750	0.27	77	75	-2.65
	LC2	22	23	4.72	563	570	1.22	98	99	1.20	2495	2500	0.20	242	242	-0.27
Bent 4 Col	LC1	91	95	3.43	2083	2100	0.80	30	31	4.01	680	684	0.71	77	77	-0.40
	LC2	36	39	7.45	813	827	1.69	100	104	3.96	2265	2281	0.69	220	223	0.91

* % Difference (in column Forces, Moments or Displacement combinations: LC1 and LC2) = [Case#2- Case#1] X 100/ Case#1. A negative value represents greater Case#1 outcomes.

Table J.31 Analyses results from Test#1 at column bottom with seismic loading in both longitudinal and transverse directions, LC1 and LC2.

		FORCES AND MOMENTS														
		Longitudinal						Transverse						Axial (kips)		
		Shear X (kips)			Moment Y (kips-ft)			Shear Z (kips)			Moment X (kips-ft)					
Support/ Location	Load Test	Case#1	Case#2	Difference (%)*	Case#1	Case#2	Difference (%)*	Case#1	Case#2	Difference (%)*	Case#1	Case#2	Difference (%)*	Case#1	Case#2	Difference (%)*
Bent 1 Col	LC1	312	309	-0.87	4669	4616	-1.13	41	41	-0.03	610	609	-0.16	81	78	-4.00
	LC2	111	111	-0.53	1667	1654	-0.77	136	136	0.06	2031	2029	-0.12	211	209	-1.03
Bent 2 Col	LC1	96	98	2.17	2133	2141	0.38	29	30	4.29	642	648	0.98	90	85	-5.15
	LC2	38	39	2.77	846	850	0.58	96	100	4.25	2138	2159	0.96	216	217	0.40
Bent 3 Col	LC1	70	72	1.79	1714	1721	0.43	31	32	0.86	775	776	0.22	77	75	-2.29
	LC2	25	26	3.16	595	601	0.94	104	105	0.71	2582	2586	0.15	242	242	-0.17
Bent 4 Col	LC1	96	99	2.72	2135	2146	0.50	31	32	3.54	699	703	0.66	78	77	-0.19
	LC2	38	40	6.41	835	847	1.44	104	108	3.50	2329	2344	0.64	221	223	1.03

* % Difference (in column Forces, Moments or Displacement combinations: LC1 and LC2) = [Case#2- Case#1] X 100/ Case#1. A negative value represents greater Case#1 outcomes.

Table J.32 Analyses results from Test#1 at column top with seismic loading in both longitudinal and transverse directions, LC1 and LC2.

		DISPLACEMENTS					
		Global X (ft)			Global Y (ft)		
Support/ Location	Load Test	Case#1	Case#2	Difference (%)*	Case#1	Case#2	Difference (%)*
Bent 1 Col	LC1	0.2539	0.2560	0.8351	0.0332	0.0338	1.6523
	LC2	0.0906	0.0915	0.9458	0.1108	0.1126	1.6515
Bent 2 Col	LC1	0.2582	0.2603	0.8072	0.0784	0.0790	0.8318
	LC2	0.1021	0.1028	0.7357	0.2613	0.2635	0.8321
Bent 3 Col	LC1	0.2543	0.2564	0.8237	0.1164	0.1171	0.5437
	LC2	0.0874	0.0882	0.9072	0.3881	0.3902	0.5435
Bent 4 Col	LC1	0.2586	0.2607	0.8020	0.0853	0.0858	0.6229
	LC2	0.1008	0.1016	0.7507	0.2842	0.2859	0.6222

* % Difference (in column Forces, Moments or Displacement combinations: LC1 and LC2) = [Case#2- Case#1] X 100/ Case#1.
A negative value represents greater Case#1 outcomes.

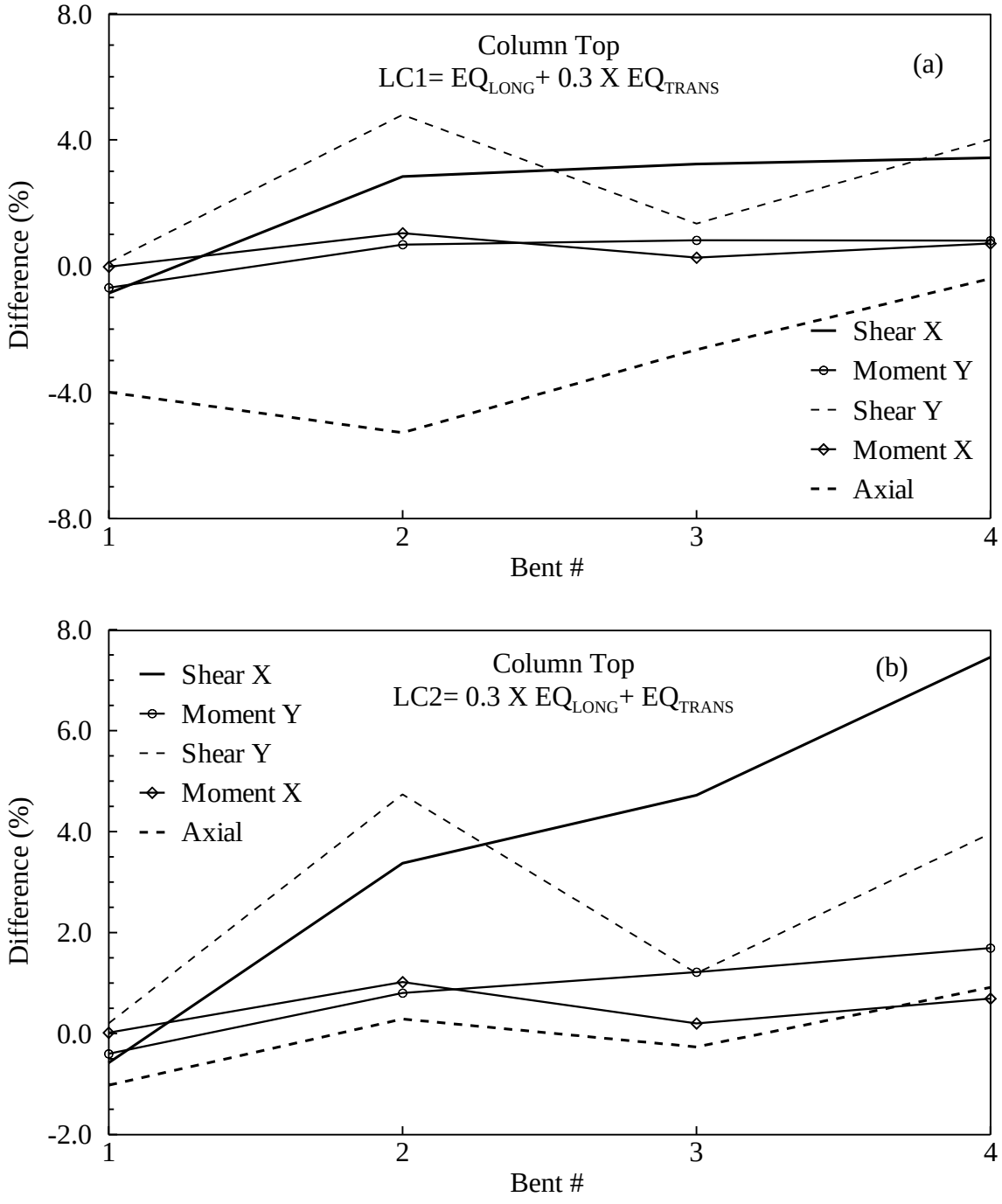

Figure J.5 Comparison (% difference between 'Fixed base' and 'Foundation springs' conditions) of forces and moments (Shear X, Shear Y, Moment X, Moment Y and Axial) from Test#1 in all four typical bent columns at the top with load cases: (a) LC1 and (b) LC2.

Test #2:

Table J.33 Analyses results from Test#2 at column top and bottom with seismic loading in longitudinal direction.

Support/ Location		FORCES AND MOMENTS- EQ_{LONG}									
		Longitudinal				Transverse				Axial (kips)	
		Shear X (kips)		Moment Y (kips-ft)		Shear Y (kips)		Moment X (kips-ft)			
		Case#1	Case#2	Case#1	Case#2	Case#1	Case#2	Case#1	Case#2	Case#1	Case#2
Bent 1 Col	Top	940	931	14134	14024	0	0	1	0	60	51
	Bottom	950	940	14233	14061	0	0	1	0	60	51
Bent 2 Col	Top	273	273	6260	6267	0	0	0	1	84	67
	Bottom	288	288	6411	6402	0	0	0	1	84	68
Bent 3 Col	Top	197	198	5049	5067	0	0	0	1	13	5
	Bottom	213	214	5234	5240	0	0	0	1	13	6
Bent 4 Col	Top	274	274	6274	6281	0	0	0	0	37	34
	Bottom	289	288	6430	6420	0	0	0	0	37	34

Table J.34 Analyses results from Test#2 at column top and bottom with seismic loading in transverse direction.

Support/ Location		FORCES AND MOMENTS- EQ_{TRANS}									
		Longitudinal				Transverse				Axial (kips)	
		Shear X (kips)		Moment Y (kips-ft)		Shear Y (kips)		Moment X (kips-ft)			
		Case#1	Case#2	Case#1	Case#2	Case#1	Case#2	Case#1	Case#2	Case#1	Case#2
Bent 1 Col	Top	58	60	880	899	400	413	6041	6227	618	637
	Bottom	59	60	885	905	412	424	6165	6356	618	637
Bent 2 Col	Top	28	29	656	673	279	286	6351	6497	632	646
	Bottom	31	32	683	702	291	298	6515	6665	632	646
Bent 3 Col	Top	9	9	228	234	299	306	7601	7776	732	748
	Bottom	12	12	261	268	318	325	7865	8048	732	748
Bent 4 Col	Top	35	35	662	674	305	312	6900	7061	661	676
	Bottom	36	36	679	690	319	327	7093	7259	661	677

Table J.35 Analyses results from Test#2 at column top with seismic loading in transverse direction.

Support/ Location	DISPLACEMENTS							
	EQ_{LONG}				EQ_{TRANS}			
	Global X (ft)		Global Y (ft)		Global X (ft)		Global Y (ft)	
	Case#1	Case#2	Case#1	Case#2	Case#1	Case#2	Case#1	Case#2
Bent 1 Col	0.7740	0.7800	0.0000	0.0000	0.0487	0.0493	0.3469	0.3527
Bent 2 Col	0.7770	0.7831	0.0000	0.0000	0.0842	0.0845	0.8143	0.8211
Bent 3 Col	0.7789	0.7849	0.0000	0.0000	0.0373	0.0377	1.2097	1.2163
Bent 4 Col	0.7797	0.7857	0.0000	0.0000	0.0792	0.0796	0.8862	0.8917

Table J.36 Analyses results from Test#2 at column top with seismic loading in both longitudinal and transverse directions, LC1 and LC2.

		FORCES AND MOMENTS														
		Longitudinal						Transverse						Axial (kips)		
		Shear X (kips)			Moment Y (kips-ft)			Shear Z (kips)			Moment X (kips-ft)					
Support/ Location	Load Test	Case#1	Case#2	Difference (%)*	Case#1	Case#2	Difference (%)*	Case#1	Case#2	Difference (%)*	Case#1	Case#2	Difference (%)*	Case#1	Case#2	Difference (%)*
Bent 1 Col	LC1	958	948	-0.97	14402	14293	-0.75	124	124	-0.18	1871	1868	-0.12	252	242	-4.09
	LC2	341	339	-0.69	5132	5107	-0.49	413	413	-0.12	6233	6227	-0.09	659	652	-1.12
Bent 2 Col	LC1	282	282	-0.11	6462	6469	0.11	86	86	0.05	1947	1950	0.12	278	261	-6.06
	LC2	111	111	-0.01	2550	2553	0.14	286	286	0.01	6491	6497	0.10	672	666	-0.81
Bent 3 Col	LC1	199	201	0.75	5118	5138	0.39	92	92	0.26	2332	2334	0.07	238	229	-3.78
	LC2	68	69	1.37	1745	1755	0.55	306	306	0.19	7774	7777	0.04	754	750	-0.61
Bent 4 Col	LC1	283	284	0.62	6466	6483	0.26	93	94	0.63	2117	2119	0.06	240	237	-1.35
	LC2	110	117	6.31	2522	2558	1.43	310	312	0.61	7058	7062	0.06	686	687	0.04

* % Difference (in column Forces, Moments or Displacement combinations: LC1 and LC2) = [Case#2- Case#1] X 100/ Case#1. A negative value represents greater Case#1 outcomes.

Table J.37 Analyses results from Test#2 at column bottom with seismic loading in both longitudinal and transverse directions, LC1 and LC2.

		FORCES AND MOMENTS														
		Longitudinal						Transverse						Axial (kips)		
		Shear X (kips)			Moment Y (kips-ft)			Shear Z (kips)			Moment X (kips-ft)					
Support/ Location	Load Test	Case#1	Case#2	Difference (%)*	Case#1	Case#2	Difference (%)*	Case#1	Case#2	Difference (%)*	Case#1	Case#2	Difference (%)*	Case#1	Case#2	Difference (%)*
Bent 1 Col	LC1	968	958	-0.95	14503	14333	-1.17	127	127	-0.14	1909	1907	-0.13	252	242	-4.07
	LC2	345	343	-0.67	5168	5123	-0.86	425	424	-0.08	6363	6356	-0.11	659	652	-1.12
Bent 2 Col	LC1	298	297	-0.09	6621	6613	-0.13	89	89	0.06	1998	2000	0.11	278	262	-6.02
	LC2	118	118	0.02	2624	2622	-0.05	297	298	0.02	6659	6666	0.09	672	667	-0.80
Bent 3 Col	LC1	216	218	0.66	5313	5320	0.14	97	98	0.27	2414	2415	0.06	239	230	-3.45
	LC2	75	76	1.17	1833	1840	0.35	325	325	0.19	8046	8048	0.03	755	750	-0.58
Bent 4 Col	LC1	298	299	0.55	6626	6627	0.01	97	98	0.63	2177	2178	0.05	240	237	-1.29
	LC2	116	123	5.60	2585	2616	1.23	325	327	0.61	7256	7259	0.04	686	687	0.06

* % Difference (in column Forces, Moments or Displacement combinations: LC1 and LC2) = [Case#2- Case#1] X 100/ Case#1. A negative value represents greater Case#1 outcomes.

Table J.38 Analyses results from Test#2 at column top with seismic loading in both longitudinal and transverse directions, LC1 and LC2.

		DISPLACEMENTS					
		Global X (ft)			Global Y (ft)		
Support/ Location	Load Test	Case#1	Case#2	Difference (%)*	Case#1	Case#2	Difference (%)*
Bent 1 Col	LC1	0.7886	0.7948	0.7905	0.1041	0.1058	1.6669
	LC2	0.2809	0.2833	0.8661	0.3469	0.3527	1.6671
Bent 2 Col	LC1	0.8023	0.8084	0.7653	0.2443	0.2463	0.8313
	LC2	0.3173	0.3194	0.6836	0.8143	0.8211	0.8317
Bent 3 Col	LC1	0.7901	0.7962	0.7774	0.3629	0.3649	0.5439
	LC2	0.2710	0.2732	0.8134	1.2097	1.2163	0.5441
Bent 4 Col	LC1	0.8035	0.8096	0.7596	0.2658	0.2675	0.6237
	LC2	0.3131	0.3153	0.6939	0.8862	0.8917	0.6234

* % Difference (in column Forces, Moments or Displacement combinations: LC1 and LC2) = [Case#2- Case#1] X 100/ Case#1.
A negative value represents greater Case#1 outcomes.

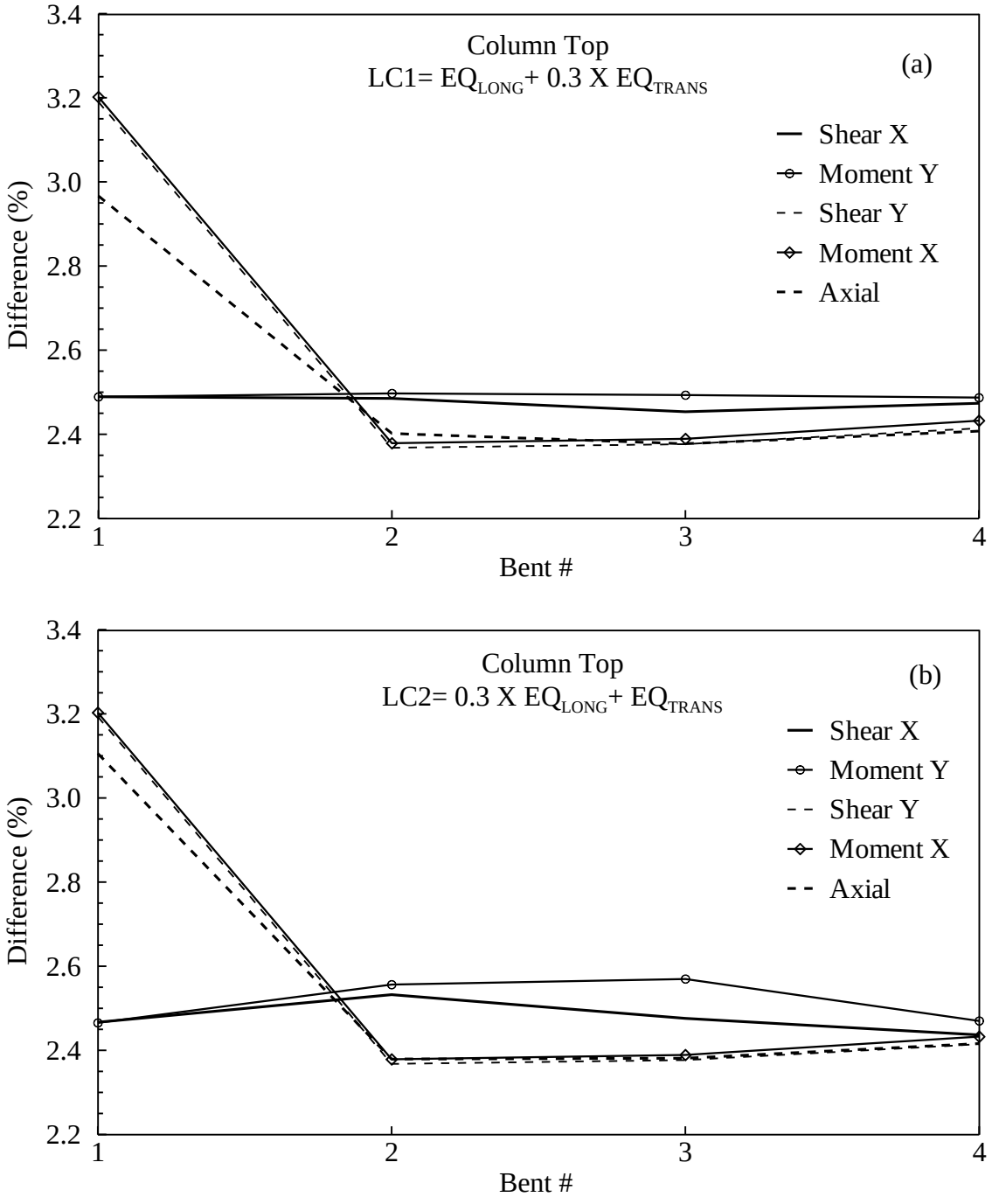

Figure J.6 Comparison (% difference between 'Fixed base' and Foundation springs' conditions) of forces and moments (Shear X, Shear Y, Moment X, Moment Y and Axial) from Test#2 in all four typical bent columns at the top with load cases: (a) LC1 and (b) LC2.

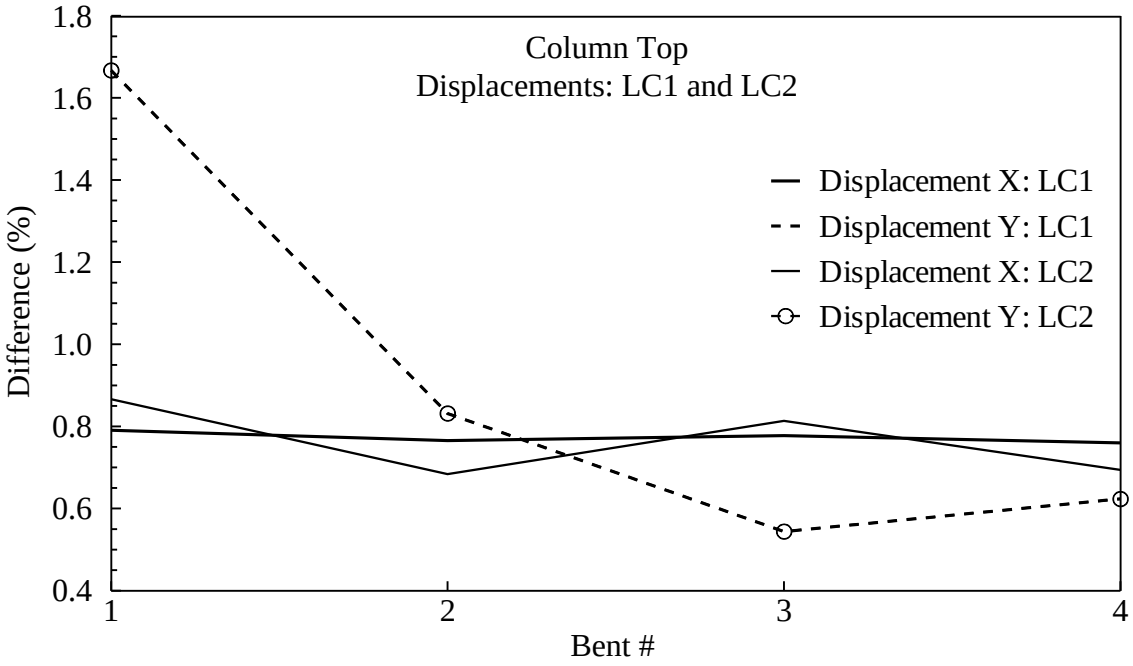

Figure J.7 Comparison (% difference between 'Fixed base' and 'Foundation springs' conditions) displacements (Disp. -X and Disp. -Y) from Test#2 in all four bent columns at the top with LC1 and LC2 load cases.

Test #3:

Table J.39 Analyses results from Test#3 at column top and bottom with seismic loading in longitudinal direction.

Support/ Location		FORCES AND MOMENTS- EQ_{LONG}									
		Longitudinal				Transverse				Axial (kips)	
		Shear X (kips)		Moment Y (kips-ft)		Shear Y (kips)		Moment X (kips-ft)			
		Case#1	Case#2	Case#1	Case#2	Case#1	Case#2	Case#1	Case#2	Case#1	Case#2
Bent 1 Col	Top	1114	1103	16749	16618	0	0	1	0	71	60
	Bottom	1125	1114	16866	16662	0	0	1	0	71	60
Bent 2 Col	Top	324	324	7417	7426	0	0	0	1	100	80
	Bottom	341	341	7597	7586	0	0	0	1	100	80
Bent 3 Col	Top	233	234	5981	6001	0	0	0	1	16	5
	Bottom	252	253	6201	6206	0	0	0	1	16	5
Bent 4 Col	Top	325	324	7434	7442	0	0	0	0	44	40
	Bottom	342	342	7618	7607	0	0	0	0	44	40

Table J.40 Analyses results from Test#3 at column top and bottom with seismic loading in transverse direction.

Support/ Location		FORCES AND MOMENTS- EQ_{TRANS}									
		Longitudinal				Transverse				Axial (kips)	
		Shear X (kips)		Moment Y (kips-ft)		Shear Y (kips)		Moment X (kips-ft)			
		Case#1	Case#2	Case#1	Case#2	Case#1	Case#2	Case#1	Case#2	Case#1	Case#2
Bent 1 Col	Top	58	71	880	1064	400	484	6041	7303	618	747
	Bottom	59	71	885	1069	412	498	6165	7452	618	748
Bent 2 Col	Top	28	34	656	794	279	339	6351	7705	632	766
	Bottom	31	37	683	826	291	353	6515	7904	632	766
Bent 3 Col	Top	9	11	228	273	299	363	7601	9219	732	887
	Bottom	12	14	261	310	318	385	7865	9539	732	887
Bent 4 Col	Top	35	39	662	783	305	369	6900	8363	661	801
	Bottom	36	40	679	801	319	386	7093	8596	661	801

Table J.41 Analyses results from Test#3 at column top with seismic loading in transverse direction.

Support/ Location	DISPLACEMENTS							
	EQ_{LONG}				EQ_{TRANS}			
	Global X (ft)		Global Y (ft)		Global X (ft)		Global Y (ft)	
	Case#1	Case#2	Case#1	Case#2	Case#1	Case#2	Case#1	Case#2
Bent 1 Col	0.9172	0.9243	0.0000	0.0000	0.0576	0.0583	0.4056	0.4136
Bent 2 Col	0.9207	0.9279	0.0000	0.0000	0.0991	0.0996	0.9658	0.9737
Bent 3 Col	0.9230	0.9301	0.0000	0.0000	0.0434	0.0440	1.4345	1.4421
Bent 4 Col	0.9239	0.9310	0.0000	0.0000	0.0938	0.0942	1.0500	1.0566

Table J.42 Analyses results from Test#3 at column top with seismic loading in both longitudinal and transverse directions, LC1 and LC2.

		FORCES AND MOMENTS														
		Longitudinal						Transverse						Axial (kips)		
		Shear X (kips)			Moment Y (kips-ft)			Shear Z (kips)			Moment X (kips-ft)					
Support/ Location	Load Test	Case#1	Case#2	Difference (%)*	Case#1	Case#2	Difference (%)*	Case#1	Case#2	Difference (%)*	Case#1	Case#2	Difference (%)*	Case#1	Case#2	Difference (%)*
Bent 1 Col	LC1	1135	1124	-0.97	17065	16937	-0.75	145	145	0.14	2187	2191	0.20	296	284	-3.93
	LC2	404	401	-0.70	6079	6049	-0.49	483	484	0.19	7287	7303	0.22	772	765	-0.86
Bent 2 Col	LC1	334	334	-0.06	7655	7664	0.13	102	102	0.06	2310	2312	0.10	330	310	-6.08
	LC2	131	131	0.04	3017	3022	0.18	339	339	0.03	7698	7705	0.09	797	790	-0.82
Bent 3 Col	LC1	236	237	0.53	6061	6083	0.35	109	109	0.16	2765	2766	0.04	282	271	-4.18
	LC2	80	81	0.99	2063	2073	0.50	362	363	0.10	9218	9219	0.01	895	889	-0.68
Bent 4 Col	LC1	335	336	0.41	7661	7677	0.21	110	111	0.35	2509	2509	0.01	284	280	-1.46
	LC2	131	136	4.11	2987	3016	0.96	367	369	0.34	8362	8363	0.01	813	813	-0.04

* % Difference (in column Forces, Moments or Displacement combinations: LC1 and LC2) = [Case#2- Case#1] X 100/ Case#1. A negative value represents greater Case#1 outcomes.

Table J.43 Analyses results from Test#3 at column bottom with seismic loading in both longitudinal and transverse directions, LC1 and LC2.

		FORCES AND MOMENTS														
		Longitudinal						Transverse						Axial (kips)		
		Shear X (kips)			Moment Y (kips-ft)			Shear Z (kips)			Moment X (kips-ft)					
Support/ Location	Load Test	Case#1	Case#2	Difference (%)*	Case#1	Case#2	Difference (%)*	Case#1	Case#2	Difference (%)*	Case#1	Case#2	Difference (%)*	Case#1	Case#2	Difference (%)*
Bent 1 Col	LC1	1147	1136	-0.95	17185	16983	-1.17	149	149	0.19	2232	2236	0.19	296	284	-3.91
	LC2	408	406	-0.67	6121	6068	-0.87	496	498	0.24	7437	7452	0.21	772	766	-0.85
Bent 2 Col	LC1	352	352	-0.04	7844	7834	-0.12	106	106	0.07	2369	2372	0.09	330	310	-6.05
	LC2	140	140	0.08	3102	3102	-0.02	353	353	0.05	7898	7904	0.08	797	790	-0.81
Bent 3 Col	LC1	256	257	0.48	6292	6298	0.10	115	116	0.17	2862	2863	0.03	283	272	-3.91
	LC2	89	90	0.88	2165	2171	0.31	385	385	0.11	9540	9540	0.00	895	889	-0.65
Bent 4 Col	LC1	352	354	0.37	7851	7848	-0.04	115	116	0.37	2579	2579	0.00	284	280	-1.42
	LC2	138	143	3.65	3060	3083	0.75	384	386	0.36	8597	8596	0.00	813	813	-0.02

* % Difference (in column Forces, Moments or Displacement combinations: LC1 and LC2) = [Case#2- Case#1] X 100/ Case#1. A negative value represents greater Case#1 outcomes.

Table J.44 Analyses results from Test#3 at column top with seismic loading in both longitudinal and transverse directions, LC1 and LC2.

		DISPLACEMENTS					
		Global X (ft)			Global Y (ft)		
Support/ Location	Load Test	Case#1	Case#2	Difference (%)*	Case#1	Case#2	Difference (%)*
Bent 1 Col	LC1	0.9344	0.9418	0.7908	0.1217	0.1241	1.9873
	LC2	0.3328	0.3356	0.8586	0.4056	0.4136	1.9868
Bent 2 Col	LC1	0.9505	0.9578	0.7706	0.2898	0.2921	0.8138
	LC2	0.3753	0.3780	0.7173	0.9658	0.9737	0.8140
Bent 3 Col	LC1	0.9360	0.9433	0.7820	0.4304	0.4326	0.5324
	LC2	0.3203	0.3230	0.8483	1.4345	1.4421	0.5325
Bent 4 Col	LC1	0.9520	0.9593	0.7606	0.3150	0.3170	0.6286
	LC2	0.3709	0.3735	0.6928	1.0500	1.0566	0.6285

* % Difference (in column Forces, Moments or Displacement combinations: LC1 and LC2) = [Case#2- Case#1] X 100/ Case#1.
A negative value represents greater Case#1 outcomes.

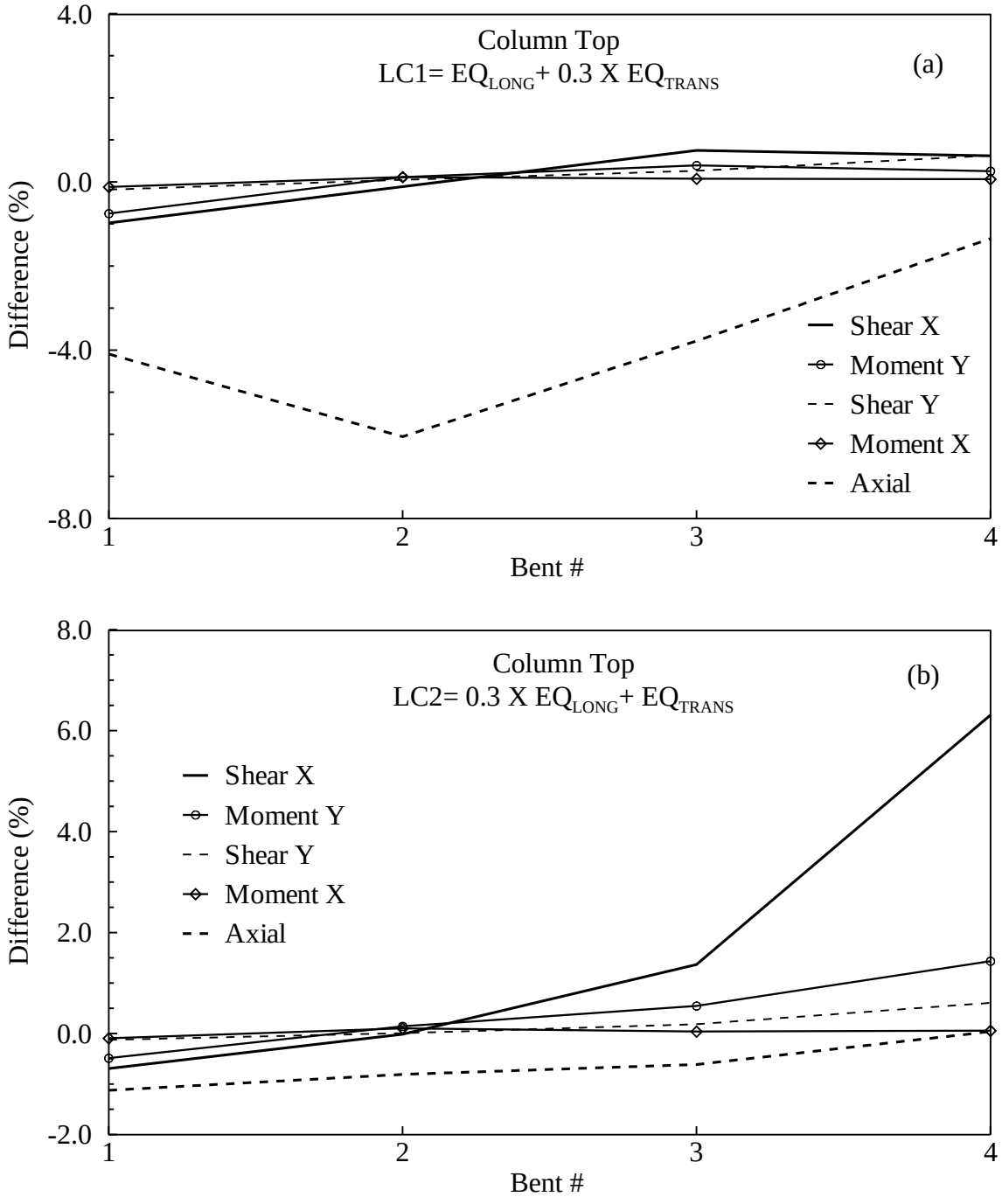

Figure J.8 Comparison (% difference between 'Fixed base' and 'Foundation springs' conditions) of forces and moments (Shear X, Shear Y, Moment X, Moment Y and Axial) from Test#3 in all four typical bent columns at the top with load cases: (a) LC1 and (b) LC2.

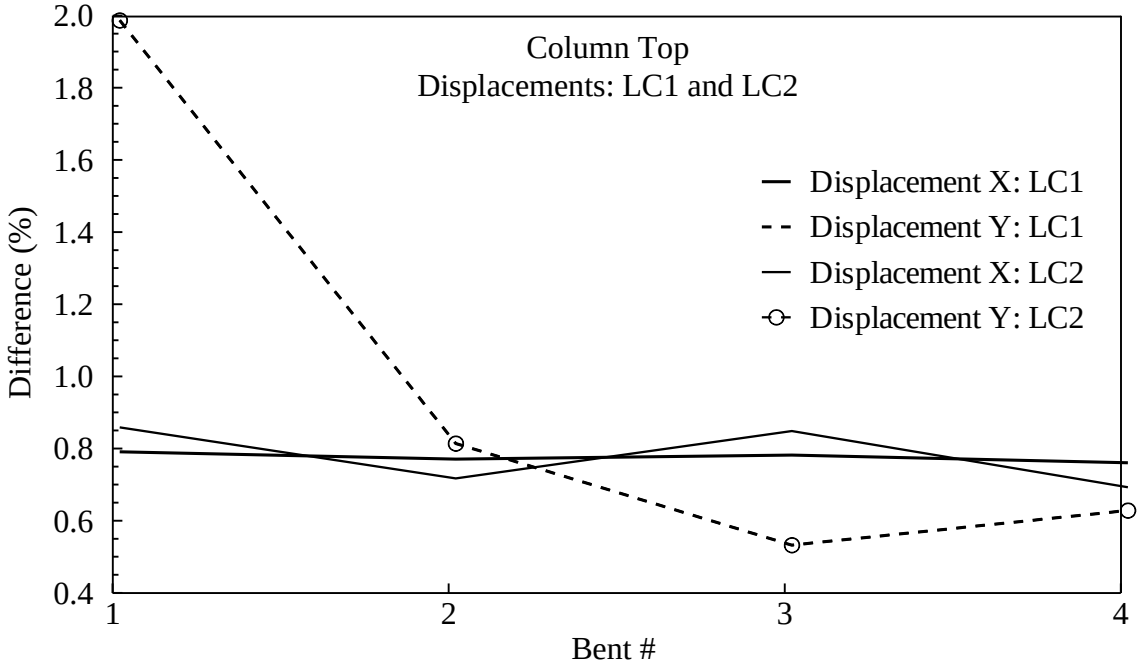

Figure J.9 Comparison (% difference between 'Fixed base' and 'Foundation springs' conditions) of displacement (Disp. -X and Disp. -Y) from Test#3 in all four bent columns at the top with LC1 and LC2 load cases.

Test #4:

Table J.45 Analyses results from Test#4 at column top and bottom with seismic loading in longitudinal direction.

Support/ Location		FORCES AND MOMENTS- EQ_{LONG}									
		Longitudinal				Transverse				Axial (kips)	
		Shear X (kips)		Moment Y (kips-ft)		Shear Y (kips)		Moment X (kips-ft)			
		Case#1	Case#2	Case#1	Case#2	Case#1	Case#2	Case#1	Case#2	Case#1	Case#2
Bent 1 Col	Top	962	952	14461	14348	0	0	0	0	61	52
	Bottom	972	962	14562	14386	0	0	0	0	61	52
Bent 2 Col	Top	279	279	6404	6412	0	0	0	0	86	69
	Bottom	294	294	6558	6550	0	0	0	0	86	69
Bent 3 Col	Top	201	201	5163	5178	0	0	0	0	13	2
	Bottom	217	218	5352	5355	0	0	0	0	13	3
Bent 4 Col	Top	280	280	6418	6426	0	0	0	0	38	34
	Bottom	295	295	6577	6568	0	0	0	0	38	34

Table J.46 Analyses results from Test#4 at column top and bottom with seismic loading in transverse direction.

Support/ Location		FORCES AND MOMENTS- EQ_{TRANS}									
		Longitudinal				Transverse				Axial (kips)	
		Shear X (kips)		Moment Y (kips-ft)		Shear Y (kips)		Moment X (kips-ft)			
		Case#1	Case#2	Case#1	Case#2	Case#1	Case#2	Case#1	Case#2	Case#1	Case#2
Bent 1 Col	Top	58	61	880	912	400	361	6041	5431	618	565
	Bottom	59	61	885	915	412	369	6165	5529	618	566
Bent 2 Col	Top	28	28	656	642	279	292	6351	6645	632	661
	Bottom	31	30	683	661	291	304	6515	6816	632	661
Bent 3 Col	Top	9	8	228	203	299	312	7601	7929	732	764
	Bottom	12	10	261	225	318	331	7865	8199	732	764
Bent 4 Col	Top	35	30	662	653	305	314	6900	7143	661	686
	Bottom	36	31	679	666	319	328	7093	7331	661	686

Table J.47 Analyses results from Test#4 at column top with seismic loading in transverse direction.

Support/ Location	DISPLACEMENTS							
	EQ_{LONG}				EQ_{TRANS}			
	Global X (ft)		Global Y (ft)		Global X (ft)		Global Y (ft)	
	Case#1	Case#2	Case#1	Case#2	Case#1	Case#2	Case#1	Case#2
Bent 1 Col	0.7919	0.7981	0.0000	0.0000	0.0494	0.0500	0.3013	0.3072
Bent 2 Col	0.7950	0.8012	0.0000	0.0000	0.0798	0.0801	0.8329	0.8398
Bent 3 Col	0.7969	0.8031	0.0000	0.0000	0.0321	0.0324	1.2335	1.2402
Bent 4 Col	0.7977	0.8038	0.0000	0.0000	0.0798	0.0801	0.8967	0.9022

Table J.48 Analyses results from Test#4 at column top with seismic loading in both longitudinal and transverse directions, LC1 and LC2.

		FORCES AND MOMENTS														
		Longitudinal						Transverse						Axial (kips)		
		Shear X (kips)			Moment Y (kips-ft)			Shear Z (kips)			Moment X (kips-ft)					
Support/ Location	Load Test	Case#1	Case#2	Difference (%)*	Case#1	Case#2	Difference (%)*	Case#1	Case#2	Difference (%)*	Case#1	Case#2	Difference (%)*	Case#1	Case#2	Difference (%)*
Bent 1 Col	LC1	980	970	-0.98	14732	14621	-0.75	108	108	0.12	1626	1629	0.17	231	221	-4.30
	LC2	349	346	-0.71	5243	5216	-0.51	360	361	0.16	5420	5431	0.19	586	581	-0.90
Bent 2 Col	LC1	288	288	-0.02	6596	6604	0.13	88	88	0.10	1992	1994	0.12	284	267	-6.08
	LC2	112	112	0.03	2562	2566	0.15	292	292	0.08	6638	6645	0.11	687	682	-0.79
Bent 3 Col	LC1	203	204	0.29	5223	5239	0.30	94	94	0.07	2379	2379	0.02	243	232	-4.78
	LC2	68	68	0.50	1750	1756	0.37	312	312	0.03	7929	7929	0.01	770	765	-0.73
Bent 4 Col	LC1	289	289	0.15	6612	6622	0.16	94	94	0.06	2144	2143	-0.06	243	240	-1.62
	LC2	112	114	1.58	2570	2581	0.43	314	314	0.06	7147	7143	-0.06	697	696	-0.13

* % Difference (in column Forces, Moments or Displacement combinations: LC1 and LC2) = [Case#2- Case#1] X 100/ Case#1. A negative value represents greater Case#1 outcomes.

Table J.49 Analyses results from Test#4 at column bottom with seismic loading in both longitudinal and transverse directions, LC1 and LC2.

		FORCES AND MOMENTS														
		Longitudinal						Transverse						Axial (kips)		
		Shear X (kips)			Moment Y (kips-ft)			Shear Z (kips)			Moment X (kips-ft)					
Support/ Location	Load Test	Case#1	Case#2	Difference (%)*	Case#1	Case#2	Difference (%)*	Case#1	Case#2	Difference (%)*	Case#1	Case#2	Difference (%)*	Case#1	Case#2	Difference (%)*
Bent 1 Col	LC1	990	980	-0.96	14835	14661	-1.18	110	111	0.17	1656	1659	0.17	231	221	-4.29
	LC2	352	350	-0.69	5278	5231	-0.89	368	369	0.20	5519	5529	0.18	586	581	-0.89
Bent 2 Col	LC1	303	303	-0.01	6756	6748	-0.12	91	91	0.11	2043	2045	0.11	284	267	-6.07
	LC2	118	118	0.05	2628	2626	-0.06	304	304	0.10	6809	6816	0.10	687	682	-0.79
Bent 3 Col	LC1	220	221	0.27	5419	5422	0.05	99	99	0.08	2460	2460	0.01	243	232	-4.61
	LC2	75	75	0.47	1828	1831	0.16	331	331	0.04	8199	8199	-0.01	770	765	-0.71
Bent 4 Col	LC1	304	304	0.14	6774	6768	-0.09	98	98	0.08	2201	2199	-0.06	244	240	-1.60
	LC2	118	120	1.42	2631	2637	0.22	328	328	0.08	7336	7331	-0.07	697	696	-0.12

* % Difference (in column Forces, Moments or Displacement combinations: LC1 and LC2) = [Case#2- Case#1] X 100/ Case#1. A negative value represents greater Case#1 outcomes.

Table J.50 Analyses results from Test#4 at column top with seismic loading in both longitudinal and transverse directions, LC1 and LC2.

		DISPLACEMENTS					
		Global X (ft)			Global Y (ft)		
Support/ Location	Load Test	Case#1	Case#2	Difference (%)*	Case#1	Case#2	Difference (%)*
Bent 1 Col	LC1	0.8067	0.8131	0.7879	0.0904	0.0922	1.9569
	LC2	0.2870	0.2894	0.8412	0.3013	0.3072	1.9570
Bent 2 Col	LC1	0.8189	0.8252	0.7651	0.2499	0.2519	0.8276
	LC2	0.3183	0.3205	0.6795	0.8329	0.8398	0.8279
Bent 3 Col	LC1	0.8066	0.8128	0.7754	0.3700	0.3721	0.5421
	LC2	0.2712	0.2733	0.7943	1.2335	1.2402	0.5420
Bent 4 Col	LC1	0.8216	0.8279	0.7571	0.2690	0.2707	0.6186
	LC2	0.3191	0.3212	0.6722	0.8967	0.9022	0.6185

* % Difference (in column Forces, Moments or Displacement combinations: LC1 and LC2) = [Case#2- Case#1] X 100/ Case#1.
A negative value represents greater Case#1 outcomes.

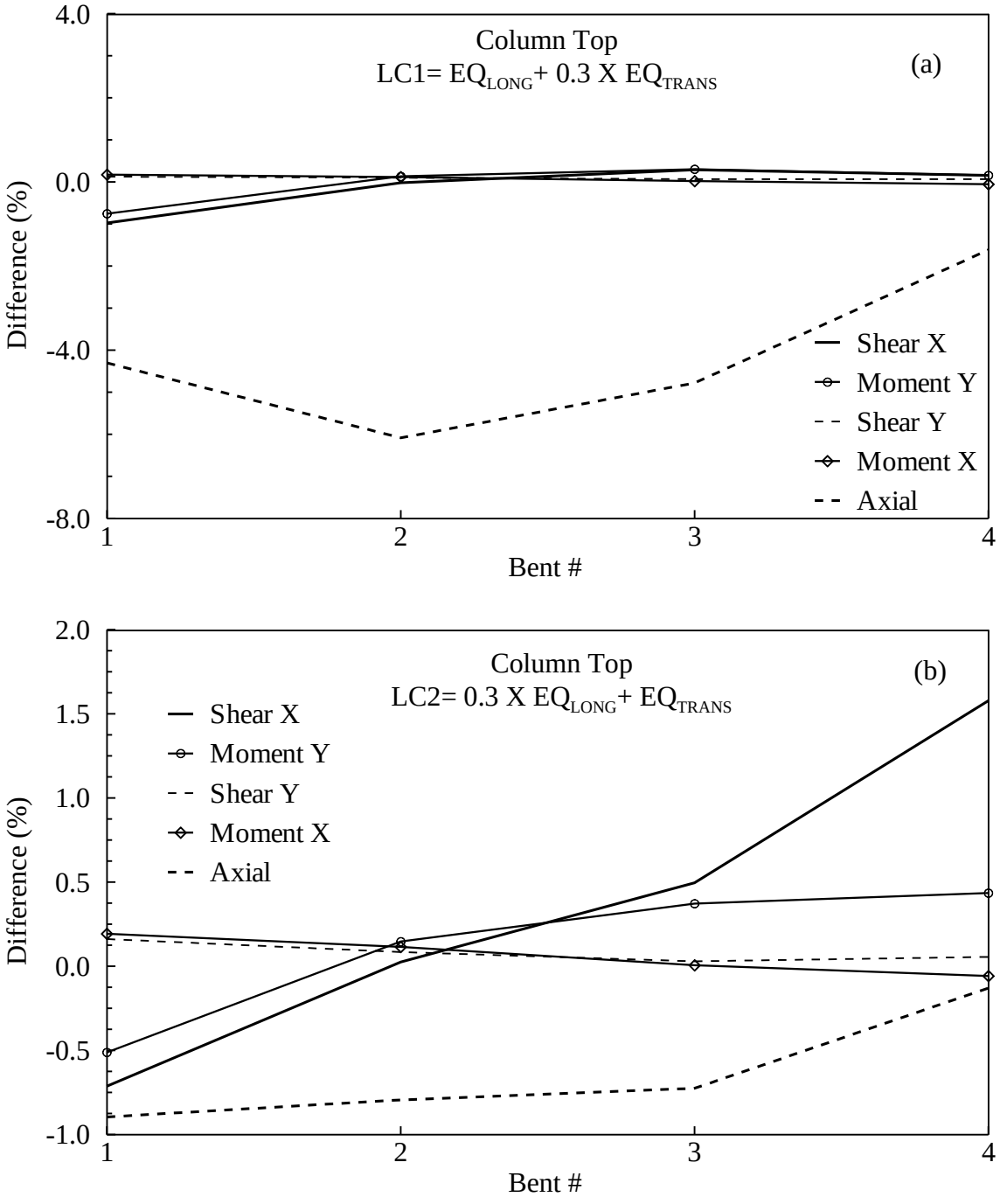

Figure J.10 Comparison (% difference between 'Fixed base' and 'Foundation springs' conditions) of forces and moments (Shear X, Shear Y, Moment X, Moment Y and Axial) from Test#4 in all four bent columns at the top with load cases: (a) LC1 and (b) LC2.

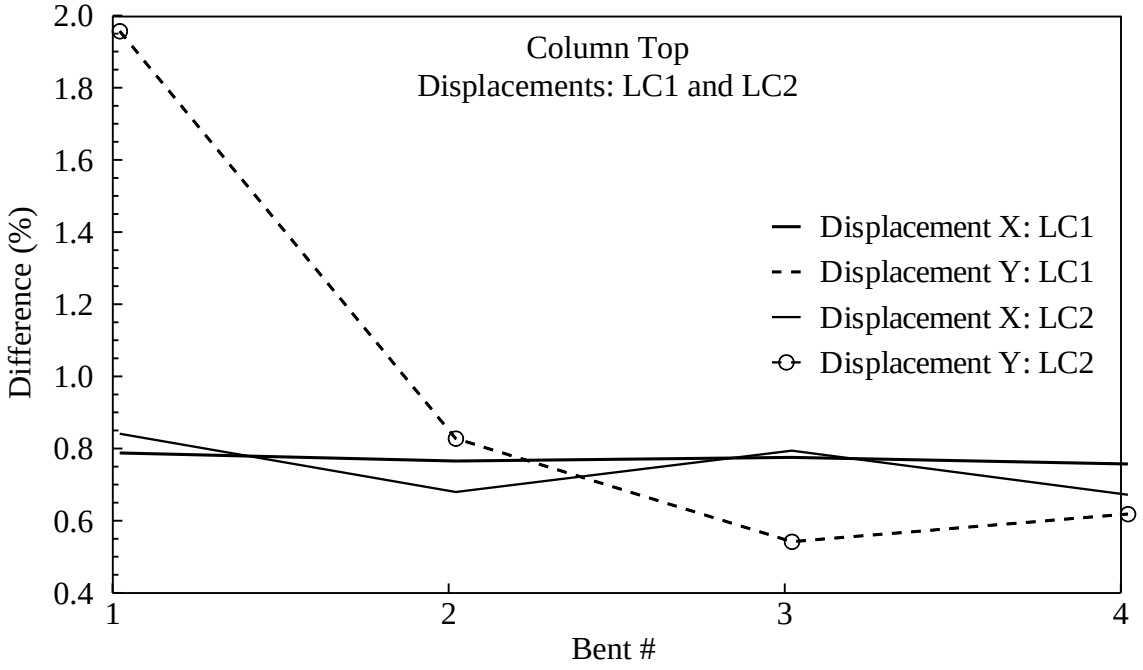

Figure J.11 Comparison (% difference between 'Fixed base' and 'Foundation springs' conditions) displacements (Disp. -X and Disp. -Y) from Test#4 in all four bent columns at the top with LC1 and LC2 load cases.

Modal Information (Russell Creek Bridge)

Table J.51 Modal periods and participating mass.

Modes	Period (sec)	Participating mass					
		Individual Mode (Percent)			Cumulative Sum (Percent)		
		UX	UY	UZ	UX	UY	UZ
1	0.535865	1.064E-19	0.68604	8.063E-18	1.064E-19	0.68604	8.063E-18
2	0.24793	4.214E-18	0.00001769	5.897E-17	4.321E-18	0.68606	6.704E-17
3	0.215441	0.94503	1.607E-16	0.000000169	0.94503	0.68606	0.000000169
4	0.172805	0.000001627	1.769E-14	0.00002019	0.94503	0.68606	0.00002036
5	0.160199	8.539E-07	1.415E-14	0.00338	0.94503	0.68606	0.0034
6	0.151785	5.053E-16	0.1945	1.423E-14	0.94503	0.88056	0.0034
7	0.146294	9.508E-09	5.485E-13	0.00005753	0.94503	0.88056	0.00346
8	0.14293	0.00006324	2.443E-14	0.00047	0.94509	0.88056	0.00393
9	0.142318	0.00007235	6.992E-14	0.00001237	0.94517	0.88056	0.00394
10	0.139284	0.00001039	1.127E-15	0.00006948	0.94518	0.88056	0.00401
11	0.137672	0.00001807	6.979E-14	2.777E-07	0.94519	0.88056	0.00401
12	0.136094	0.000003261	1.687E-15	0.00217	0.9452	0.88056	0.00618
13	0.132799	0.00002533	3.855E-13	0.00207	0.94522	0.88056	0.00826
14	0.13198	0.0001	3.896E-14	0.01661	0.94532	0.88056	0.02487
15	0.130891	0.00017	5.657E-17	0.00569	0.94549	0.88056	0.03056
16	0.128469	0.004	3.038E-14	0.00035	0.94949	0.88056	0.03091
17	0.123114	0.00001656	5.042E-14	0.00000141	0.94951	0.88056	0.03091
18	0.117701	0.000002602	8.883E-13	0.34615	0.94951	0.88056	0.37706
19	0.109126	5.83E-14	5.607E-07	2.332E-12	0.94951	0.88056	0.37706
20	0.107872	1.086E-08	1.949E-15	0.00642	0.94951	0.88056	0.38348
21	0.097127	7.219E-07	6.994E-15	0.13491	0.94951	0.88056	0.51839
22	0.091965	3.802E-14	0.00097	2.256E-11	0.94951	0.88152	0.51839
23	0.091833	1.2E-13	0.00001931	1.597E-12	0.94951	0.88154	0.51839
24	0.089486	6.824E-15	0.00213	2.58E-11	0.94951	0.88368	0.51839
25	0.088176	8.845E-14	0.00044	1.076E-11	0.94951	0.88412	0.51839
26	0.087722	1.624E-16	0.00045	6.447E-11	0.94951	0.88457	0.51839
27	0.086453	2.46E-16	0.03297	3E-13	0.94951	0.91754	0.51839
28	0.085525	0.00236	1.051E-13	0.01447	0.95188	0.91754	0.53286
29	0.084296	1.459E-15	0.00214	1.258E-11	0.95188	0.91968	0.53286
30	0.083704	1.33E-13	0.00046	5.282E-12	0.95188	0.92014	0.53286
31	0.083064	0.00014	5.027E-13	0.05461	0.95201	0.92014	0.58747
32	0.08299	8.055E-14	0.00157	1.788E-13	0.95201	0.92172	0.58747
33	0.08201	2.181E-09	2.176E-13	1.115E-10	0.95201	0.92172	0.58747
34	0.082002	6.769E-09	2.43E-13	6.399E-09	0.95201	0.92172	0.58747
35	0.081623	2.277E-14	0.00166	1.821E-14	0.95201	0.92338	0.58747
36	0.081455	0.000006467	4.02E-14	0.08397	0.95202	0.92338	0.67143
37	0.081405	2.02E-14	0.000000181	5.528E-13	0.95202	0.92338	0.67143
38	0.081383	7.127E-13	0.000001006	1.331E-11	0.95202	0.92338	0.67143
39	0.081155	3.967E-12	2.292E-12	3.642E-10	0.95202	0.92338	0.67143
40	0.081147	9.633E-15	4.505E-13	6.573E-13	0.95202	0.92338	0.67143

(Continued)

Modes	Period (sec)	Participating mass					
		Individual Mode (Percent)			Cumulative Sum (Percent)		
		UX	UY	UZ	UX	UY	UZ
41	0.081072	4.675E-13	5.084E-09	2.063E-16	0.95202	0.92338	0.67143
42	0.081045	3.081E-13	2.085E-08	8.122E-19	0.95202	0.92338	0.67143
43	0.081011	2.708E-11	3.204E-12	5.193E-12	0.95202	0.92338	0.67143
44	0.08098	1.739E-11	4.909E-14	1.186E-10	0.95202	0.92338	0.67143
45	0.08074	8.501E-14	1.566E-12	5.488E-12	0.95202	0.92338	0.67143
46	0.080737	2.564E-13	2.029E-10	3.618E-12	0.95202	0.92338	0.67143
47	0.080718	3.65E-14	2.112E-08	6.044E-13	0.95202	0.92338	0.67143
48	0.080698	8.771E-13	4.1E-13	5.267E-13	0.95202	0.92338	0.67143
49	0.080697	1.514E-13	9.528E-13	7.444E-12	0.95202	0.92338	0.67143
50	0.080694	4.753E-13	2.037E-08	3.93E-12	0.95202	0.92338	0.67143
51	0.080689	6.918E-13	1.461E-12	7.424E-14	0.95202	0.92338	0.67143
52	0.080687	3.198E-14	4.769E-09	2.096E-12	0.95202	0.92338	0.67143
53	0.080687	4.098E-14	5.374E-09	5.713E-12	0.95202	0.92338	0.67143
54	0.080684	8.8E-14	8.188E-09	1.703E-12	0.95202	0.92338	0.67143
55	0.080683	6.916E-14	1.368E-12	5.859E-12	0.95202	0.92338	0.67143
56	0.080679	2.652E-13	2.891E-14	1.373E-11	0.95202	0.92338	0.67143
57	0.079821	1.12E-13	0.00008122	5.859E-13	0.95202	0.92346	0.67143
58	0.079548	1.04E-09	1.982E-13	1.233E-09	0.95202	0.92346	0.67143
59	0.078941	2.652E-14	9.681E-07	5.015E-14	0.95202	0.92346	0.67143
60	0.078689	1.142E-12	2.741E-14	2.497E-12	0.95202	0.92346	0.67143

* UX, UY and UZ represent respective mass participations in Global three directions

Analysis case: FEE

Table J.52 Analyses results in case of FEE at central pile top and bottom with seismic loading in longitudinal direction.

Bent #	FORCES AND MOMENTS- EQ_{LONG}									
	Longitudinal				Transverse				Axial (kips)	
	Shear X (kips)		Moment Y (kips-ft)		Shear Y (kips)		Moment X (kips-ft)			
	Design	Rec.	Design	Rec.	Design	Rec.	Design	Rec.	Design	Rec.
1	1	1	15	16	0	0	0	0	1	1
2	1	1	16	17	0	0	0	0	1	1
3	1	1	18	19	0	0	0	0	0	0
4	1	1	19	20	0	0	0	0	0	0
5	2	2	20	21	0	0	0	0	0	0
6	2	2	20	21	0	0	0	0	0	0
7	1	1	18	19	0	0	0	0	1	1
8	1	1	17	17	0	0	0	0	1	1
9	1	1	32	33	0	0	0	0	3	3

Rec.: Based on ADRS curves developed using the recommended site factors

Table J.53 Analyses results in case of FEE at central pile top and bottom with seismic loading in transverse direction.

Bent #	FORCES AND MOMENTS- EQ_{TRANS}									
	Longitudinal				Transverse				Axial (kips)	
	Shear X (kips)		Moment Y (kips-ft)		Shear Y (kips)		Moment X (kips-ft)			
	Design	Rec.	Design	Rec.	Design	Rec.	Design	Rec.	Design	Rec.
1	0	0	0	0	2	2	32	32	0	0
2	0	0	0	0	4	4	73	73	0	0
3	0	0	0	0	6	6	114	115	0	0
4	0	0	0	0	7	7	156	157	0	0
5	0	0	0	0	8	8	171	172	0	0
6	0	0	0	0	8	8	161	162	0	0
7	0	0	0	0	7	7	132	132	0	0
8	0	0	0	0	4	4	82	82	0	0
9	0	0	0	0	14	14	355	357	0	0

Rec.: Based on ADRS curves developed using the recommended site factors

Table J.54 Analyses results in case of FEE at central pile top with seismic loading in transverse direction.

Bent #	DISPLACEMENTS							
	EQ_{LONG}				EQ_{TRANS}			
	Global X (ft)		Global Y (ft)		Global X (ft)		Global Y (ft)	
	Design	Recommended	Design	Recommended	Design	Recommended	Design	Recommended
1	0.0157	0.0163	0.0000	0.0000	0.0000	0.0000	0.0201	0.0202
2	0.0170	0.0177	0.0000	0.0000	0.0000	0.0000	0.0467	0.0469
3	0.0184	0.0191	0.0000	0.0000	0.0000	0.0000	0.0773	0.0776
4	0.0194	0.0201	0.0000	0.0000	0.0000	0.0000	0.1087	0.1091
5	0.0199	0.0207	0.0000	0.0000	0.0000	0.0000	0.1234	0.1238
6	0.0197	0.0205	0.0000	0.0000	0.0000	0.0000	0.1162	0.1167
7	0.0187	0.0195	0.0000	0.0000	0.0000	0.0000	0.0898	0.0901
8	0.0173	0.0180	0.0000	0.0000	0.0000	0.0000	0.0530	0.0532
9	0.0146	0.0152	0.0000	0.0000	0.0000	0.0000	0.0195	0.0197

Table J.55 Analyses results in case of FEE at central pile top with seismic loading in both longitudinal and transverse directions, LC1 and LC2.

		FORCES AND MOMENTS														
		Longitudinal						Transverse						Axial (kips)		
		Shear X (kips)			Moment Y (kips-ft)			Shear Y (kips)			Moment X (kips-ft)					
Bent #	Load Case	Design	Rec.	Difference (%)	Design	Rec.	Difference (%)	Design	Rec.	Difference (%)	Design	Rec.	Difference (%)	Design	Rec.	Difference (%)
1	LC1	1	1	3.96	15	16	3.94	1	1	2.24	10	10	0.63	1	1	3.94
	LC2	0	0	3.96	5	5	3.94	2	2	2.24	32	32	0.63	0	0	3.94
2	LC1	1	1	3.99	16	17	3.94	1	1	0.78	22	22	0.39	1	1	3.95
	LC2	0	0	3.99	5	5	3.94	4	4	0.78	73	73	0.39	0	0	3.95
3	LC1	1	1	3.92	18	19	3.94	2	2	0.68	34	34	0.41	0	0	3.85
	LC2	0	0	3.92	5	6	3.94	6	6	0.68	114	115	0.41	0	0	3.85
4	LC1	1	1	3.92	19	20	3.94	2	2	0.40	47	47	0.38	0	0	3.85
	LC2	0	0	3.92	6	6	3.94	7	7	0.40	156	157	0.38	0	0	3.85
5	LC3	2	2	3.90	20	21	3.94	2	2	0.72	51	52	0.41	0	0	3.30
	LC4	0	0	3.90	6	6	3.94	8	8	0.72	171	172	0.41	0	0	3.30
6	LC5	2	2	4.00	20	21	3.94	2	2	0.52	48	49	0.39	0	0	4.13
	LC6	0	0	4.00	6	6	3.94	8	8	0.52	161	162	0.39	0	0	4.13
7	LC7	1	1	3.95	18	19	3.94	2	2	0.62	40	40	0.41	1	1	3.81
	LC8	0	0	3.95	6	6	3.94	7	7	0.62	132	132	0.41	0	0	3.81
8	LC9	1	1	3.93	17	17	3.94	1	1	0.74	25	25	0.39	1	1	3.99
	LC10	0	0	3.93	5	5	3.94	4	4	0.74	82	82	0.39	0	0	3.99
9	LC11	1	1	3.60	32	33	3.92	4	4	0.46	107	107	0.45	3	3	3.91
	LC12	0	0	3.60	10	10	3.92	14	14	0.46	355	357	0.45	1	1	3.91

Rec.: Based on ADRS curves developed using the recommended site factors

Table J.56 Analyses results in case of FEE at central pile top with seismic loading in both longitudinal and transverse directions, LC1 and LC2.

		DISPLACEMENTS					
		Global X (ft)			Global Y (ft)		
Bent #	Load Case	Design	Rec.	Difference (%)	Design	Rec.	Difference (%)
1	LC1	0.0157	0.0163	3.9406	0.0060	0.0061	0.5669
	LC2	0.0047	0.0049	3.9406	0.0201	0.0202	0.5669
2	LC1	0.0170	0.0177	3.9408	0.0140	0.0141	0.4282
	LC2	0.0051	0.0053	3.9408	0.0467	0.0469	0.4282
3	LC1	0.0184	0.0191	3.9432	0.0232	0.0233	0.3879
	LC2	0.0055	0.0057	3.9432	0.0773	0.0776	0.3879
4	LC1	0.0194	0.0201	3.9375	0.0326	0.0327	0.3808
	LC2	0.0058	0.0060	3.9375	0.1087	0.1091	0.3808
5	LC3	0.0199	0.0207	3.9394	0.0370	0.0371	0.3843
	LC4	0.0060	0.0062	3.9394	0.1234	0.1238	0.3843
6	LC5	0.0197	0.0205	3.9406	0.0349	0.0350	0.3811
	LC6	0.0059	0.0062	3.9406	0.1162	0.1167	0.3811
7	LC7	0.0187	0.0195	3.9370	0.0269	0.0270	0.3821
	LC8	0.0056	0.0058	3.9370	0.0898	0.0901	0.3821
8	LC9	0.0173	0.0180	3.9406	0.0159	0.0160	0.4149
	LC10	0.0052	0.0054	3.9406	0.0530	0.0532	0.4149
9	LC11	0.0146	0.0152	3.9361	0.0059	0.0059	0.5731
	LC12	0.0044	0.0045	3.9361	0.0195	0.0197	0.5731

Rec.: Based on ADRS curves developed using the recommended site factors

Analysis case: SEE

Table J.57 Analyses results in case of SEE at central pile top and bottom with seismic loading in longitudinal direction.

Bent #	FORCES AND MOMENTS- EQ_{LONG}									
	Longitudinal				Transverse				Axial (kips)	
	Shear X (kips)		Moment Y (kips-ft)		Shear Y (kips)		Moment X (kips-ft)			
	Design	Rec.	Design	Rec.	Design	Rec.	Design	Rec.	Design	Rec.
1	4	2	52	32	0	0	0	0	3	2
2	4	2	55	34	0	0	0	0	2	1
3	4	3	61	38	0	0	0	0	2	1
4	5	3	65	40	0	0	0	0	1	1
5	5	3	68	42	0	0	0	0	0	0
6	5	3	67	42	0	0	0	0	1	1
7	4	3	62	39	0	0	0	0	2	1
8	4	2	57	35	0	0	0	0	3	2
9	4	2	108	67	0	0	0	0	9	5

Rec.: Based on ADRS curves developed using the recommended site factors

Table J.58 Analyses results in case of SEE at central pile top and bottom with seismic loading in transverse direction.

Bent #	FORCES AND MOMENTS- EQ_{TRANS}									
	Longitudinal				Transverse				Axial (kips)	
	Shear X (kips)		Moment Y (kips-ft)		Shear Y (kips)		Moment X (kips-ft)			
	Design	Rec.	Design	Rec.	Design	Rec.	Design	Rec.	Design	Rec.
1	0	0	0	0	8	5	123	75	0	0
2	0	0	0	0	15	9	287	177	0	0
3	0	0	0	0	22	14	447	276	0	0
4	0	0	0	0	29	18	614	379	0	0
5	0	0	0	0	32	19	670	413	0	0
6	0	0	0	0	29	18	632	390	0	0
7	0	0	0	0	25	16	517	319	0	0
8	0	0	0	0	17	10	322	199	0	0
9	0	0	0	0	55	34	1391	857	0	0

Rec.: Based on ADRS curves developed using the recommended site factors

Table J.59 Analyses results in case of SEE at central pile top with seismic loading in transverse direction.

Bent #	DISPLACEMENTS							
	EQ_{LONG}				EQ_{TRANS}			
	Global X (ft)		Global Y (ft)		Global X (ft)		Global Y (ft)	
	Design	Recommended	Design	Recommended	Design	Recommended	Design	Recommended
1	0.0530	0.0327	0.0000	0.0000	0.0000	0.0000	0.0784	0.0481
2	0.0575	0.0355	0.0000	0.0000	0.0000	0.0000	0.1831	0.1128
3	0.0621	0.0383	0.0000	0.0000	0.0000	0.0000	0.3037	0.1874
4	0.0655	0.0404	0.0000	0.0000	0.0000	0.0000	0.4270	0.2635
5	0.0673	0.0415	0.0000	0.0000	0.0000	0.0000	0.4844	0.2989
6	0.0667	0.0412	0.0000	0.0000	0.0000	0.0000	0.4565	0.2817
7	0.0633	0.0391	0.0000	0.0000	0.0000	0.0000	0.3525	0.2175
8	0.0585	0.0361	0.0000	0.0000	0.0000	0.0000	0.2080	0.1282
9	0.0493	0.0304	0.0000	0.0000	0.0000	0.0000	0.0762	0.0467

Table J.60 Analyses results in case of SEE at central pile top with seismic loading in both longitudinal and transverse directions, LC1 and LC2.

		FORCES AND MOMENTS														
		Longitudinal						Transverse						Axial (kips)		
		Shear X (kips)			Moment Y (kips-ft)			Shear Y (kips)			Moment X (kips-ft)					
Bent #	Load Case	Design	Rec.	Difference (%)	Design	Rec.	Difference (%)	Design	Rec.	Difference (%)	Design	Rec.	Difference (%)	Design	Rec.	Difference (%)
1	LC1	4	2	-44.09	52	32	-38.75	2	1	-43.66	37	23	-38.89	3	2	-38.53
	LC2	1	1	-44.09	15	9	-38.75	8	5	-43.66	123	75	-38.89	1	1	-38.54
2	LC1	4	2	-42.43	55	34	-38.54	5	3	-39.08	86	53	-38.29	2	1	-38.65
	LC2	1	1	-42.44	17	10	-38.54	15	9	-39.08	287	177	-38.29	1	0	-38.65
3	LC1	4	3	-39.16	61	38	-38.34	7	4	-39.00	134	83	-38.35	2	1	-39.09
	LC2	1	1	-39.16	18	11	-38.34	22	14	-39.00	447	276	-38.35	0	0	-39.09
4	LC1	5	3	-38.55	65	40	-38.29	9	5	-38.34	184	114	-38.29	1	1	-39.89
	LC2	1	1	-38.55	20	12	-38.29	29	18	-38.34	614	379	-38.29	0	0	-39.90
5	LC3	5	3	-38.40	68	42	-38.28	9	6	-39.05	201	124	-38.36	0	0	-46.26
	LC4	2	1	-38.40	20	13	-38.28	32	19	-39.05	670	413	-38.36	0	0	-46.27
6	LC5	5	3	-38.40	67	42	-38.28	9	5	-38.62	190	117	-38.32	1	1	-40.66
	LC6	2	1	-38.40	20	12	-38.28	29	18	-38.62	632	390	-38.32	0	0	-40.67
7	LC7	4	3	-39.01	62	39	-38.33	8	5	-38.93	155	96	-38.36	2	1	-39.68
	LC8	1	1	-39.01	19	12	-38.33	25	16	-38.93	517	319	-38.36	1	0	-39.68
8	LC9	4	2	-41.92	57	35	-38.51	5	3	-38.98	97	60	-38.30	3	2	-41.48
	LC10	1	1	-41.92	17	10	-38.51	17	10	-38.98	322	199	-38.30	1	1	-41.48
9	LC11	4	2	-49.61	108	67	-38.64	17	10	-38.47	417	257	-38.41	9	5	-44.19
	LC12	1	1	-49.61	33	20	-38.64	55	34	-38.47	1391	857	-38.41	3	2	-44.19

Rec.: Based on ADRS curves developed using the recommended site factors

Table J.61 Analyses results in case of SEE at central pile top with seismic loading in both longitudinal and transverse directions, LC1 and LC2.

		DISPLACEMENTS					
		Global X (ft)			Global Y (ft)		
Bent #	Load Case	Design	Rec.	Difference (%)	Design	Rec.	Difference (%)
1	LC1	0.0530	0.0327	-38.3131	0.0235	0.0144	-38.6562
	LC2	0.0159	0.0098	-38.3131	0.0784	0.0481	-38.6562
2	LC1	0.0575	0.0355	-38.2992	0.0549	0.0339	-38.3770
	LC2	0.0173	0.0106	-38.2992	0.1831	0.1128	-38.3770
3	LC1	0.0621	0.0383	-38.2884	0.0911	0.0562	-38.2977
	LC2	0.0186	0.0115	-38.2884	0.3037	0.1874	-38.2977
4	LC1	0.0655	0.0404	-38.2828	0.1281	0.0791	-38.2841
	LC2	0.0196	0.0121	-38.2828	0.4270	0.2635	-38.2841
5	LC3	0.0673	0.0415	-38.2796	0.1453	0.0897	-38.2910
	LC4	0.0202	0.0125	-38.2796	0.4844	0.2989	-38.2910
6	LC5	0.0667	0.0412	-38.2798	0.1369	0.0845	-38.2865
	LC6	0.0200	0.0123	-38.2798	0.4565	0.2817	-38.2865
7	LC7	0.0633	0.0391	-38.2873	0.1058	0.0653	-38.2871
	LC8	0.0190	0.0117	-38.2873	0.3525	0.2175	-38.2871
8	LC9	0.0585	0.0361	-38.2969	0.0624	0.0385	-38.3524
	LC10	0.0175	0.0108	-38.2969	0.2080	0.1282	-38.3524
9	LC11	0.0493	0.0304	-38.2844	0.0229	0.0140	-38.6705
	LC12	0.0148	0.0091	-38.2844	0.0762	0.0467	-38.6705

Rec.: Based on ADRS curves developed using the recommended site factors

APPENDIX K

COMPARISON OF SHAKE2000 AND DMOD2000 RESULTS BASED ON CONDITIONS IN CHARLESTON

K.1 Introduction

Nonlinear site response analysis can provide more accurate results compared to the equivalent linear or linear analysis if the nonlinear model parameters can be obtained and modeled accurately for situations where a profile experiences nonlinear behavior due to either larger loading or softer materials. However, because of the lack of knowledge in determining the necessary model parameters and the limitations of the stress-strain models, the nonlinear analysis procedure has always been the least used or preferred by practitioners (Stewart et al. 2008).

The seismic site coefficient models for Charleston and the South Carolina Coastal Plain (SCCP) presented in Chapters 2 and 3, respectively, were developed based upon thousands of one-dimensional equivalent linear and nonlinear site response analysis results. Equivalent linear analyses were conducted for $PGA_{outcrop} \leq 0.3$g using SHAKE2000 and nonlinear analyses were conducted for $PGA_{outcrop} > 0.3$g using DMOD2000 for all the soil profiles generated considering mean and ±3 standard deviations. This decision was, in part, based on the assumption that all profiles will behave nonlinearly for loading with higher amplitude (higher $PGA_{outcrop}$) which may be valid for a given soil profile. However, a number of profiles were considered for developing site coefficient model by varying the V_S values of the profile to take into account the possible variations in the soil properties. Such variations include softer (low V_S) and stiffer (high V_S) profiles. In such situation, it can be expected that softer profiles may undergo higher level of nonlinearity compared to stiffer profiles for a given loading condition (i.e., for a given $PGA_{outcrop}$ value), indicating that both loading and material properties of the soil profile must be taken into consideration when deciding the analysis procedure. Thus, a guideline to choose nonlinear analysis over equivalent linear analysis has to be developed for obtaining accurate seismic parameters for the design of transportation systems.

In this appendix, a site coefficient model similar to the one presented in Chapter 2 has been developed for the Charleston area based only on DMOD2000 simulations for the entire $PGA_{outcrop}$ band of 0.05 g to 0.5 g and compared with the model presented in Chapter 2. This comparison offers a scope to evaluate the performance of equivalent linear and nonlinear codes for a range of loadings ($PGA_{outcrop}$ range) and soil property variations (V_{S100ft} range).

K.2 Background Review

Nonlinear site response analysis procedure requires additional material model parameters (e.g., reference shear strain, Rayleigh damping coefficients, other fitting coefficients etc.) that are, often, difficult to obtain for a given project site from standard geotechnical site investigation program. On the other hand, the procedure for determining the nonlinear model parameters when the experimental data are available is poorly understood and/or documented (Kramer 1996; Stewart et al. 2008; Snow 2008). One of the key components in nonlinear site response analysis is the constitutive model that represents the stress-strain relationship of the soil in the numerical modeling. The loading, unloading and reloading behaviors are important for accurately capturing the behavior of a soil when subjected to cyclic loading. Over the years, a broad range of constitutive models have been developed for conducting nonlinear analysis in one- and multiple-dimensions considering fundamental features of soil behavior such as pore water pressure development and dissipation, anisotropy or dilation. The list includes advanced sophisticated models (Prevost 1989; Li et al. 1997; McKenna and Fenves 2001) and simplified models (Lee and Finn 1978; Matasović and Ordóñez 2011; Hashash 2011). In general, the number of model parameters increases with the sophistication of the model but captures the soil behavior more accurately. The simplified hyperbolic models developed by Matasović and Ordóñez (2011) and Hashash (2011) are used in DMOD2000 and DEEPSOIL, respectively. These two codes are widely used by practitioners for conducting nonlinear one-dimensional site response analysis.

Based on benchmarking studies conducted by Stewart et al. (2008) and others (Kwok et al. 2007; Stewart et al. 2006; Stewart and Kwok 2008) it is concluded that most of the nonlinear site response analysis codes have poor documentation and less accessible to practitioners. Stewart et al. (2008) primarily worked on the nonlinear model parameter selection protocols to develop a framework for using nonlinear codes and made the following key suggestions:

- Outcropping motion should be used as input with an assumption of elastic base;
- Full Rayleigh damping should be used if available in the code; and
- Modulus reduction curve matching is suggested to set the parameters for the backbone curve and if available, to match both the modulus-reduction and damping curves simultaneously.

From the study conducted by Stewart et al. (2008) to verify the above suggestions, it was found that the depth-to-bedrock affects the computed surface responses and the responses computed using equivalent linear code deviate from that of nonlinear code at around 0.1 g to 0.2 g as $PGA_{outcrop}$. The comparison of the results from different nonlinear analysis codes, in-general, agreed well with each other.

Hashash et al. (2010) and Stewart et al. (2008) reported under-prediction in the high frequency ranges by nonlinear analysis procedure. Moreover, nonlinear analysis has issues with the small strain damping (Rayleigh) and hysteretic damping estimation. Both Phillips and Hashash (2009) and Hashash et al. (2010) reported that Rayleigh damping has the tendency to dampen the system in case of deep profiles and thus computed responses may be under-predicted. Moreover, the hyperbolic constitutive model parameters calibrated by matching the measured modulus-reduction curve showed significant deviation for damping curve. The model produced higher damping than the experimental estimate at large strains and thus introduced further under-prediction of the actual site response. Phillips and Hashash (2009) proposed a frequency independent small strain damping model to overcome the former and a reduction factor to overcome the later. The reduction factor which modifies the extended Masing (1926) loading/unloading stress-strain relationship increases the flexibility of the model to match both the modulus reduction and damping curves simultaneously. Both of these modifications are implemented in another widely used nonlinear site response analysis tool, DEEPSOIL. It should be noted that DMOD2000 version used in this study lacks these updates and therefore the results presented in this study may differ from that of more accurate codes.

Recently, Matasović and Hashash (2012) made a comprehensive survey to collect information on the current practice and also the methods available for evaluating the influence of local ground conditions on the site specific earthquake design ground motions. Based on the collected information it has been identified that practitioners prefer using equivalent linear codes over nonlinear counterparts due to familiarity with the old and rather easily understood method. Matasović and Hashash (2012) made a series of recommendations on the code usage protocols and also a list of suggestions for future research. They felt the urge for further benchmarking works to make the nonlinear code a more familiar tool for users with limited experience. Another point raised by Matasović and Hashash (2012) is the need for a well-defined guideline to effectively select appropriate code for the project in hand by the practitioners. The survey

revealed that there is a large controversy on this matter in the community. Kramer and Paulsen (2004) claimed that equivalent linear codes can be used up-to 1-2 % strain level and 0.3-0.4 g accelerations ($PGA_{outcrop}$). Their paper was a result from a survey done among the practitioners working around the world including the USA. SCDOT (2008) also recommended the similar guideline for using equivalent linear codes in seismic site response analysis.

A study by Tokimatsu and Sugimoto (2008) found strong nonlinearity of a Holocene sand dune (V_S = 1,017-1,148 ft/s) at a depth of about 230 ft experiencing a shear strain of about 0.3 % from a down-hole array data during the 2007 Niigata-ken Cheutsu-oki earthquake. The surface responses computed using nonlinear and equivalent linear approaches were found to diverge at strong ground motions (higher amplitude shaking) and/or at soft sites (lower V_S). Hashash et al. (2010), Hartzell et al. (2004) and Ardoino et al. (2008) recommended nonlinear approaches for soft soil sites which experiences nonlinear behavior even at lower $PGA_{outcrop}$ ranges. Moreover, Hartzell et al. (2004) found nonlinear approaches to be the best predictor in case of site classes D and E. Matasović and Hashash (2012) claimed nonlinear and equivalent linear approaches starts to diverge at 0.1-0.2% strains and after 0.5% responses calculated by equivalent linear approach are no more reliable. Their survey revealed a trend for using nonlinear site response tools in cases of Site Classes E and F. Most practitioners, usually, use equivalent linear codes up to 1 % strains although experts (Matasović and Hashash 2012) strongly differed from that opinion. They claimed that, by a strain of 1%, soils would be too close to the failure and a high level of nonlinearity is expected.

K.3 Geology and Seismology of Charleston

The geology and seismology for Charleston has already been covered in Chapter 2.

K.4 Soil Profile and Material Properties

All twenty eight V_S profiles presented in Chapter 2 are used for the analysis presented in this study. The mean and mean±1σ (σ represents standard deviation) variations of shear modulus with shear strain (G/G_{max}-γ) and damping with shear strain (D-γ) curves for all the profiles are also considered similar to Chapter 2. However in the development of the analysis type (equivalent linear or nonlinear) presented in Section K.10 only mean G/G_{max}-γ and D-γ cases are considered.

K.5 Ground Motions

All ground motions described in Chapter 2 are also used in this study. However, additional simulations are conducted for $PGA_{outcrop}$ levels of 0.05 g, 0.1 g, 0.2 g and 0.3 g using DMOD2000 considering only the SEE (2% probabilities of exceedance in 50 years) motions. As concluded in Chapter 2, the FEE (10% probabilities of exceedance in 50 years) and SEE motions provided similar responses and thus only SEE motions are considered for the added simulations performed in this study.

K.6 Non-Linear Site Response Analysis Tool

DMOD2000 incorporates the Modified KZ model or MKZ model (Matasović and Vucetic 1993a) to define the initial backbone curve (Figure K.1) in the simulation. The normalized MKZ model is given by:

$$\tau^* = \frac{G^*_{max}\gamma}{1+\alpha(\frac{G^*_{max}}{\tau^*_{max}}\gamma)^s} \tag{K.1}$$

where α and s are two curve fitting constants added to the Kondner and Zelasko (1963) (KZ) model, $G^*_{max}=G_{max}/\sigma'_{vc}$, $\tau^*_{max}= \tau_{max}/\sigma'_{vc}$, σ'_{vc} is the initial vertical effective stress, G_{max} is the initial (maximum) shear modulus and τ_{max} is the shear strength of the soil. The material degradation with repeated cycle is then incorporated into this model by using degradation index functions (Matasović and Vucetic 1993b) as shown in Figure K.1.

The MKZ model calculates the hysteretic damping β as follows using the Masing (1926) rules (Matasović and Vucetic, 1993a):

$$\beta = \frac{4\int_0^{\gamma_{co}} f(\gamma)d\gamma}{\pi f(\gamma_{co})\gamma_{co}} - \frac{2}{\pi} \tag{K.2}$$

where γ_{co} is the strain amplitude at which β is calculated and $f(\gamma)=\tau$ is the initial backbone curve.

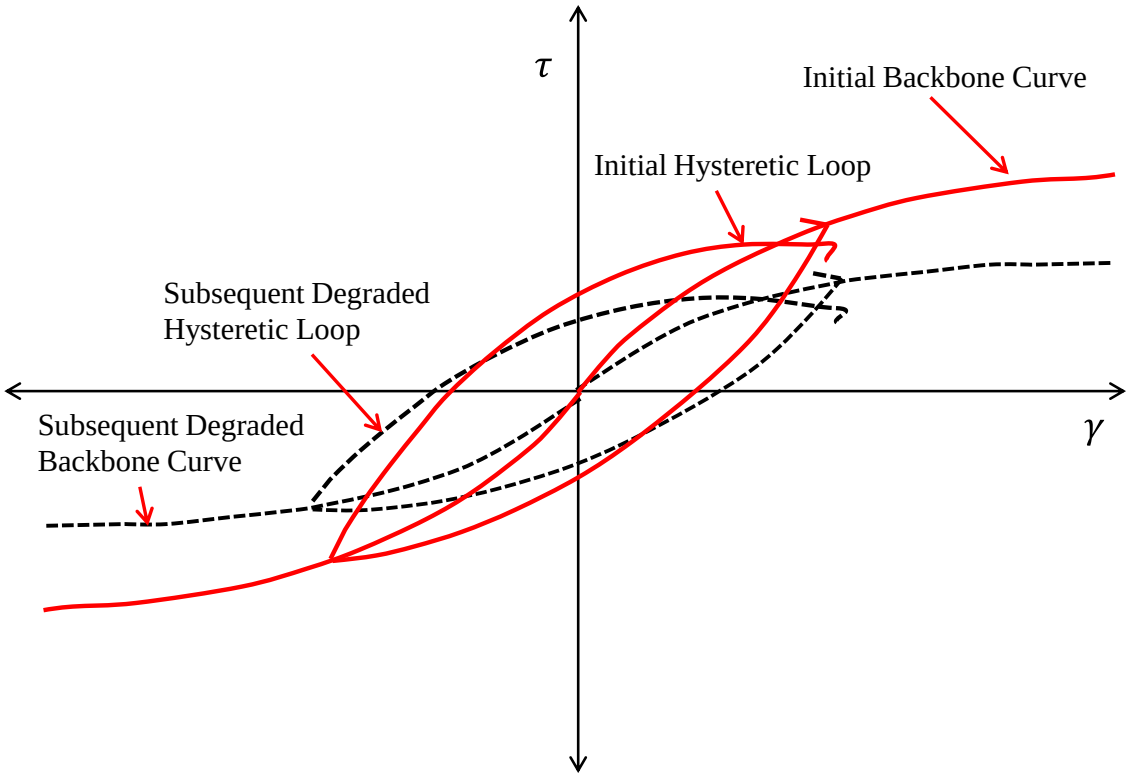

Figure K.1 Stress-strain behavior during first cycle and a subsequent cycle (based on Stewart et al. 2008).

For the calibration of the MKZ model parameters (α and s), three options are available in DMOD2000: 'modulus reduction fitting', 'modulus reduction and damping fitting', and 'damping fitting'. The 'modulus reduction fitting' was used in this research following the guideline suggested by Stewart et al. (2008). In the modulus reduction matching procedure, the MKZ model matches the experimental modulus reduction curve very well but shows significant deviation when the measured damping is compared with predicted damping at higher strains. This difference in predicted damping is primarily due to the inability of the simplified model (MKZ) to independently fit the damping-shear strain relationship.

Presented in Equation K.3 is the equation of motion in terms of matrix notations solved in DMOD2000. Time marching is conducted using the Newmark's β method.

$$\mathbf{M}\ddot{\mathrm{u}} + \mathbf{C}\dot{\mathrm{u}} + \mathbf{K}\mathrm{u} = \mathbf{f} \tag{K.3}$$

where **M** is the mass matrix, **C** is the viscous damping matrix, **K** is the nonlinear stiffness matrix, **f** is the excitation at the base of the layer and u, $\dot{\mathrm{u}}$ and $\ddot{\mathrm{u}}$ are the relative displacement, velocity

and acceleration vectors, respectively. It should be noted that the damping matrix in Equation K.3 is externally incorporated to control the vibration of the system. In this code, the damping is calculated as a mass and stiffness proportional damping through full Rayleigh damping formulation (Hudson et al. 1994). The viscous damping matrix, **C** is expressed as a function of mass and stiffness as follows:

$$\mathbf{C} = \alpha_R \mathbf{M} + \beta_R \mathbf{K} \tag{K.4}$$

where α_R and β_R are calculated using Equations K.5 and K.6, respectively (Matasović and Ordóñez 2011).

$$\alpha_R = \xi_{tar} \left(\frac{4\pi}{T} \right) \left(\frac{n}{(n+1)} \right) \tag{K.5}$$

$$\beta_R = \left(\xi_{tar} T \right) \left(\frac{1}{\pi (n+1)} \right) \tag{K.6}$$

where ξ_{tar} is the target damping ratio obtained through calibration and the range is 0.1 to 5%, T is the fundamental period of the soil profile given by $T = 4H / V_{s,avg}$, H is the total depth of the soil profile considered, $V_{s,avg}$ is the weighted average of the shear wave velocity of the profile-layers and n is an odd integer (1, 3, 5, 7 etc.) multiplier of fundamental frequency to generate frequency corresponding to a higher mode (obtained through calibration).

The first frequency is the natural frequency of the soil profile (first mode) and the second one is related to a higher mode. ξ_{tar} is the low strain damping of each of the soil layers. DMOD2000 requires a single ξ_{tar} value as an input (rather than setting ξ_{tar} for each of the layers) for the entire profile for the simulation. Therefore, calibration is required to obtain a suitable pair of ξ_{tar} and n. This calibration is done by running DMOD2000 at low $PGA_{outcrop}$ (so that the system practically behaves linearly) and adjusting ξ_{tar} and n until the response spectrum matches well with the corresponding SHAKE2000 response. Presented in Figures K.2(a), (b) and (c) are such comparisons of spectral accelerations computed using the equivalent linear code SHAKE2000 and the nonlinear code DMOD2000 at low $PGA_{outcrop}$s for three different V_{S100ft} values.

In the process of the site coefficient model generation using DMOD2000 presented in Chapters 2 and 3, a $PGA_{outcrop}$ of 0.1 g was selected to perform the calibration of n and ξ_{tar} for all the profiles with varying V_{S100ft} values. It was assumed that, at this level of excitation, the system

behavior would remain in the linear zone and thus DMOD2000 responses can be matched with the corresponding SHAKE2000 responses to successfully calibrate n and ξ_{tar}. Figure K.2(a) shows calibration process for the reference profile (V_{S100ft} = 968 ft/s) at $PGA_{outcrop}$ of 0.1 g and it was observed that any of the n and ξ_{tar} combinations (5, 0.5), (7, 0.5) and (7, 0.75) produce acceptable matching with the SHAKE2000 response.

For this apprendix, differences between the DMOD2000 and SHAKE2000 responses are observed for lower velocity profiles, with $PGA_{outcrop}$ values of 0.05 g and 0.1 g. This suggests that for softer profiles nonlinearity begins at $PGA_{outcrop}$ much lower than 0.05g. From the two profiles with low V_{S100ft} values (328 and 660 ft/s) considered, it is found that $PGA_{outcrop}$ of 0.001 g is small enough to obtain the correct level of loading to keep the system within linear zone. Figure K.2(b) and K.2(c) present these two cases for calibration at 0.001 g shaking level and the same n and ξ_{tar} combinations (5, 0.5), (7, 0.5) and (7, 0.75) were still found to produce acceptable matching. This confirms that the set of calibration parameters used for DMOD2000 simulations for the generation of site coefficient models (Chapters 2 and 3) is optimal. The purpose of selecting multiple pairs of n and ξ_{tar} was to avoid numerical issues. In some cases especially for simulations with higher $PGA_{outcrop}$ values, DMOD2000 runs failed to complete. In such situations, the numerical instability was overcome by using a different set of n and ξ_{tar} from the set of acceptable pairs.

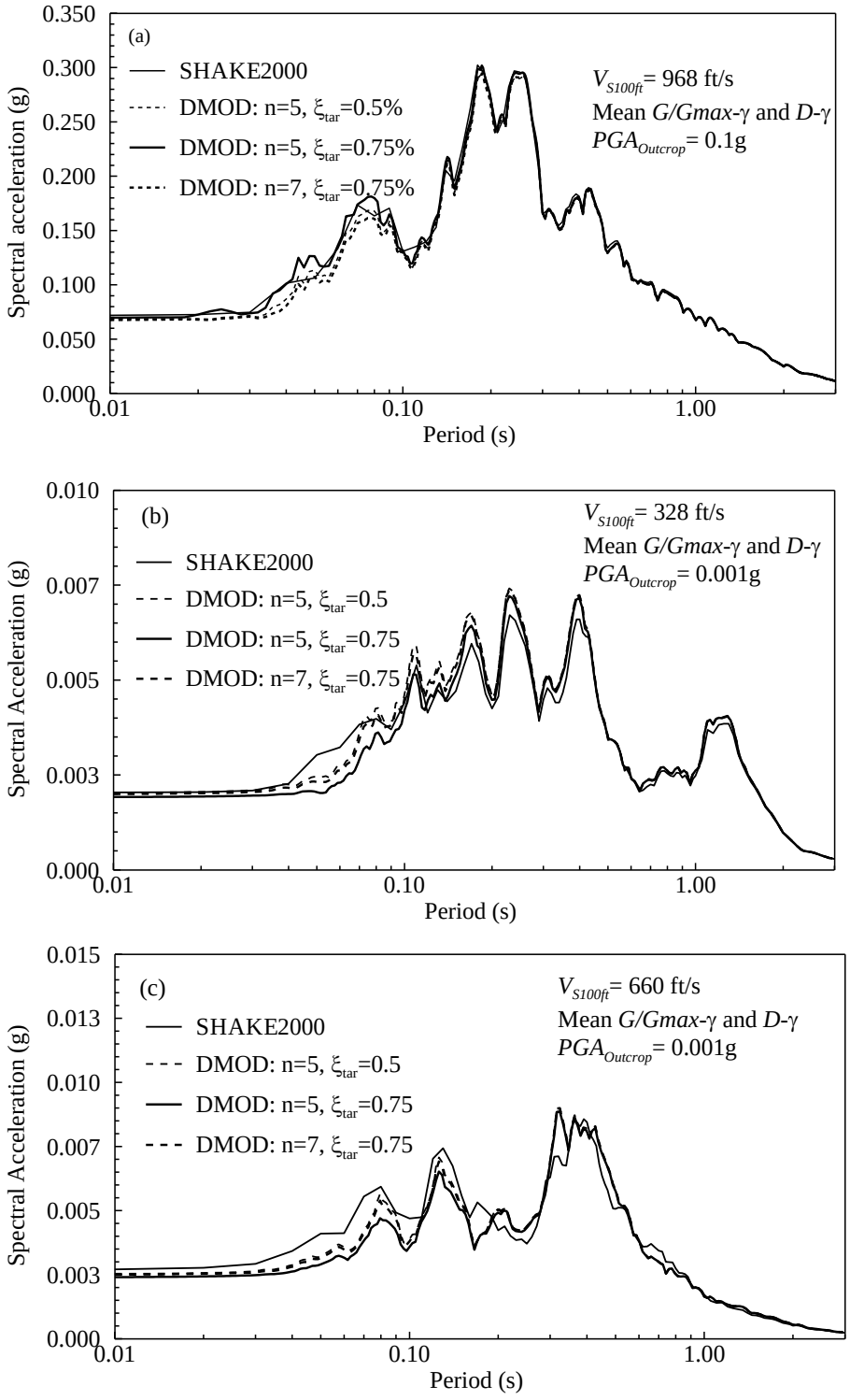

Figure K.2 Calibration procedure: (a) V_{S100ft} = 968 ft/s at $PGA_{outcrop}$ = 0.1 g; (b) V_{S100ft} = 328 ft/s at $PGA_{outcrop}$ = 0.001 g; (c) V_{S100ft} = 660 ft/s at $PGA_{outcrop}$ = 0.001 g.

K.7 Comparison of Responses Generated Using DMOD2000 and SHAKE2000

As mentioned earlier, in the process of generating the site coefficient model for SCCP, SHAKE2000 was used for ground motions scaled to $PGA_{outcrop}$ = 0.05, 0.1, 0.2 and 0.3 g and DMOD2000 was used for $PGA_{outcrop}$ = 0.4 g and 0.5 g. This is based upon the assumption that SHAKE2000 would produce acceptable results up to $PGA_{outcrop}$ of 0.3 g regardless of the properties of the soil profiles. In this appendix, an attempt is made to verify this assumption by performing additional DMOD2000 simulations of the 0.05, 0.1, 0.2 and 0.3 g cases for Charleston and to compare with the corresponding SHAKE2000 results. A separate tentative site coefficient model is developed following the procedure presented in Chapter 2 and then the model parameters are compared with the proposed values in Chapter 2. In addition, the profile maximum shear strains are also plotted for all cases to help explain the differences observed in responses from these two codes.

K.8 Generation of Site Coefficient Model Based on DMOD2000 Results

The procedure followed in developing site coefficient model for Charleston and presented in Chapter 2 is followed in developing the site coefficient model based on DMOD2000 simulation results.

First, the site coefficient (F) for six spectral period ranges: T$\leq$ 0.01 s as for F_{PGA}, T=0.01-0.4 s for $F_{0.2}$ (or F_a), T=0.41-0.8 s for $F_{0.6}$, T=0.81-1.2 s for F_1 (or F_v), T=1.21-2.0 s for $F_{1.6}$ and T=2.01-4.0 s for F_3, are computed and averaged over the corresponding ranges. These coefficients are then averaged over all motions used and plotted versus corresponding V_{S100ft} and grouped for six different $S_{outcrop}$ values corresponding to each spectral period range. Presented in Figures K.3, K.4, K.5, K.6, K.7 and K.8 are the F-V_{S100ft} plots for F_{PGA}, $F_{0.2}$, $F_{0.6}$, F_1, $F_{1.6}$ and F_3 cases, respectively.

Similar to the F-V_{S100ft} plots based on equivalent linear results for $PGA_{outcrop} \leq 0.3$ g, the data points obtained from DMOD2000 show the same three distinct features. They are: (a) an increasing trend of F *with* V_{S100ft} for low V_{S100ft} values, (b) a zone of peak F, and (c) a decreasing trend of F *with* V_{S100ft} beyond the peak. Thus, the same form of the equations developed in Chapter 2 is used to fit the F- V_{S100ft} data. For the sake of completeness, the equations are presented below:

When $V_{S100ft} < V_{S100ftP}$, the median value of F value is expressed by the following relationship (Chapter 2):

$$F = \left(\frac{F_p}{V_{S100\,ftP}} \right) V_{S100\,ft} \qquad \text{for all values of } T \text{ when } V_{S100ft} < V_{S100ftP} \tag{K.7}$$

where F_p is the peak F value, T is the spectral period and $V_{S100ftP}$ is the V_{S100ft} corresponding to F_p. F_p and $V_{S100ftP}$ are obtained using the following expressions (Chapter 2):

$$F_p = x_1 S_{Outcrop} + x_2 \tag{K.8}$$

$$V_{S100\,ftP} = x_3 S_{Outcrop} + x_4 \tag{K.9}$$

where x_1, x_2, x_3 *and* x_4 are regression coefficients.

When $V_{S100ft} \geq V_{S100ftP}$, the recommended median F value can be obtained by the following expressions (Chapter 2):

$$F = \frac{\left(F_p - 1\right)\left(2500 - V_{S100\,ft}\right)}{2500 - V_{S100\,ftP}} + 1 \qquad \text{when } T \leq 0.2\ s \text{ and } V_{S100ft} \geq V_{S100ftP} \tag{K.10a}$$

$$F = a + b\,\mathrm{e}^{cV_{S100ft}} \qquad \text{when } T > 0.2\ s \text{ and } V_{S100ft} \geq V_{S100ftP} \tag{K.10b}$$

where a is a regression coefficient. The regression coefficients b and c are calculated using the following relationships from Chapter 2:

$$b = \frac{1-a}{e^{2500c}} \tag{K.11a}$$

$$c = \frac{\ln\left(\dfrac{1-a}{F_p - a}\right)}{2500 - V_{S100\,ftP}} \tag{K.11b}$$

To fit the DMOD2000 data with these equations, a two-step procedure is followed. First, a residual analysis is performed to fit the median curves for the individual sub-set of data from Figures K.3-K.8. Secondly, linear regression analysis is performed to fit F_p versus $S_{outcrop}$ and $V_{S100ftP}$ versus $S_{outcrop}$ to obtain x_1, x_2, x_3 *and* x_4 coefficients. As for the residual analysis, the computed medians of the residuals are very close to 1.0 proving the central tendencies of the corresponding median relationships. The coefficients of the above equations for these fitting are tabulated in Table K.1. Moreover, the 95% and 5% bounds are also generated in a similar fashion to Chapter 2 and tabulated in Table K.1. The coefficient '*a*' is kept unchanged as part of

the recommended model. The rest of the coefficients based on DMOD2000 simulations are somewhat different. The coefficients from the recommended model are mentioned in each cell in parentheses for better visualization of the difference between these two models. For further details of the fitting procedure the reader is suggested to review Chapter 2.

The intention of developing the site coefficient model based on DMOD2000 results is to compare with the model based on SHAKE2000 simulation results. However, the data points from DMOD2000 simulations for $PGA_{outcrop}$ of 0.4g and 0.5g are being considered for both cases (in this appendix and also in Chapter 2). This is done for the sake of consistency and also to avoid any potential bias on the developed model in this appendix and thus the original goal of comparing the site coefficient models from both the codes persists.

Table K.1 Regression coefficients of the seismic site coefficient model based on DMOD2000 simulations.

Spectral period, T (s)	$S_{outcrop}$	x_1 (g^{-1})	x_2	x_3 (g^{-1}. ft/s)	x_4 (ft/s)	a	$Z_{0.95}$	$Z_{0.05}$
0.0	$PGA_{outcrop}$	-1.386 (-1.88)*	1.621 (1.99)	887 (1178)	572 (466)	-	1.48 (1.38)	0.44 (0.64)
0.2	S_s	-0.756 (-0.83)	1.972 (2.05)	274 (344)	678 (577)	0.65	1.47 (1.48)	0.45 (0.63)
0.6	$S_{0.6}$	-2.523 (-3.53)	2.684 (3.09)	454 (679)	600 (512)	0.85	1.39 (1.40)	0.55 (0.70)
1.0	S_1	-2.500 (-4.16)	2.886 (3.76)	406 (417)	481 (505)	0.90	1.46 (1.40)	0.60 (0.68)
1.6	$S_{1.6}$	-4.917 (-5.36)	3.217 (3.86)	1058 (649)	371 (397)	0.97	1.38 (1.40)	0.57 (0.68)
3.0	$S_{3.0}$	-4.389 (-8.20)	2.100 (2.80)	1134 (1292)	278 (262)	0.99	1.17 (1.30)	0.75 (0.65)

* Numbers in parentheses are the coefficients from the recommended model in Chapter 2. Coefficient 'a' is kept the same for both the models.

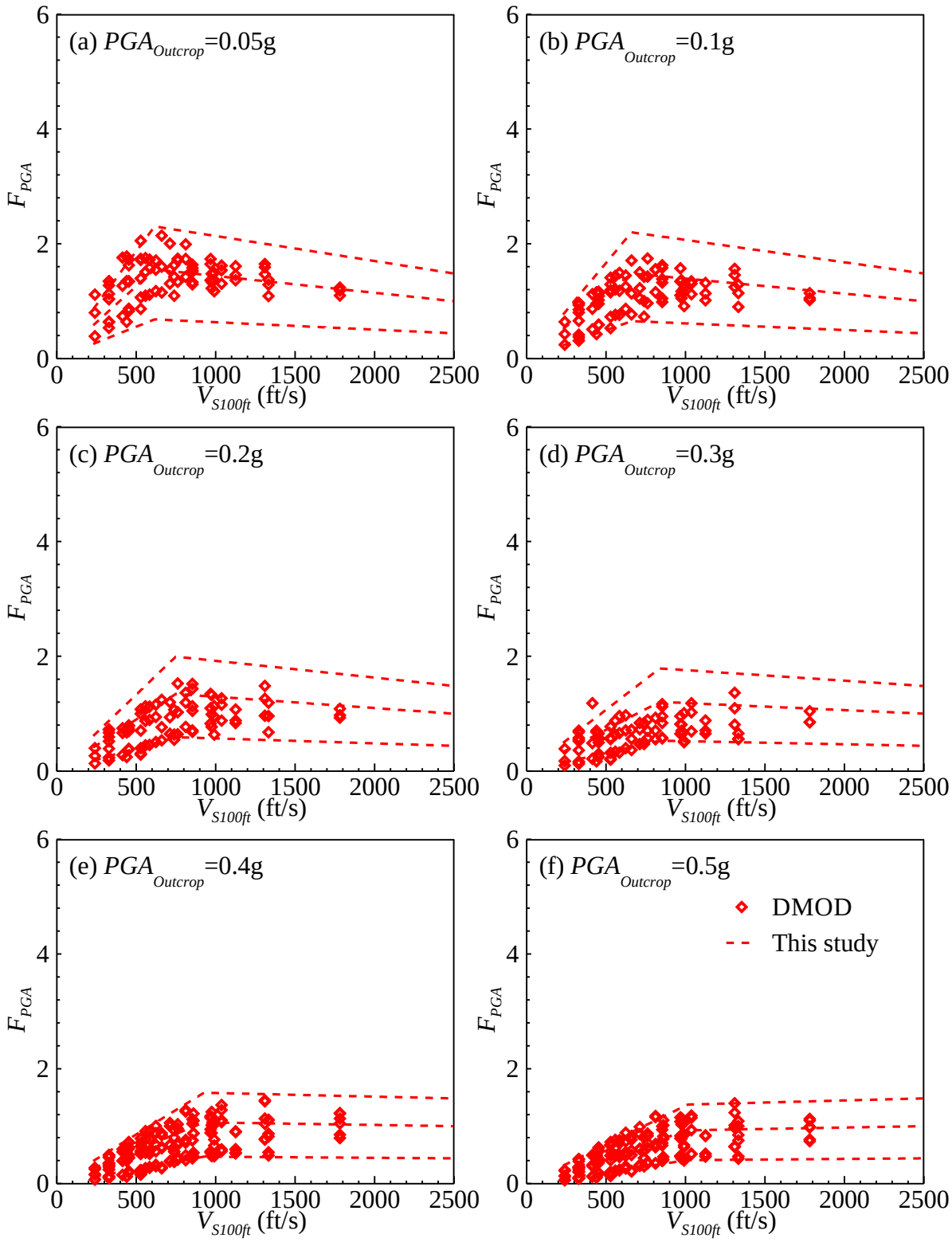

Figure K.3 Site coefficient model based on DMOD2000 data points for F_{PGA}.

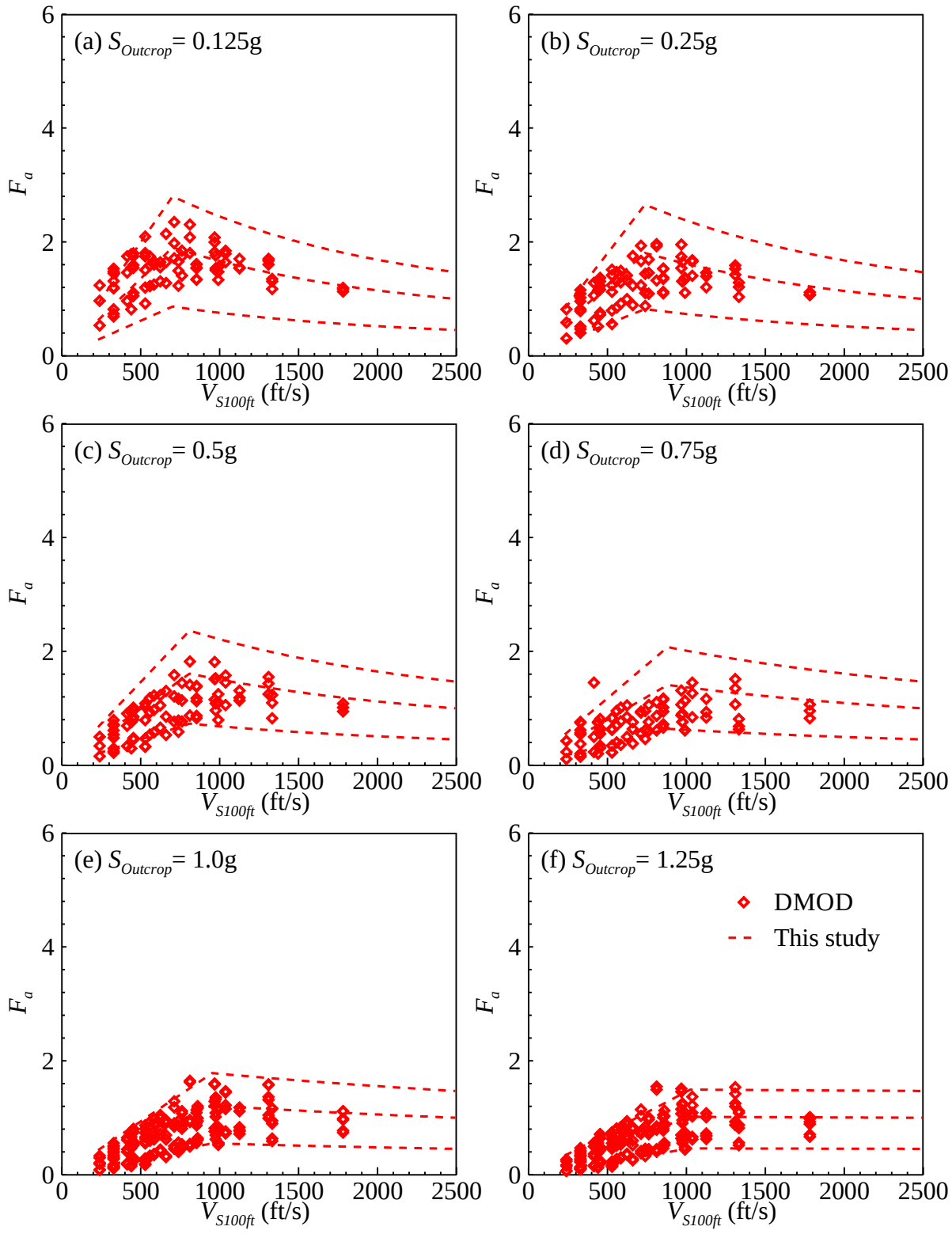

Figure K.4 Site coefficient model based on DMOD2000 data points for F_a or $F_{0.2}$.

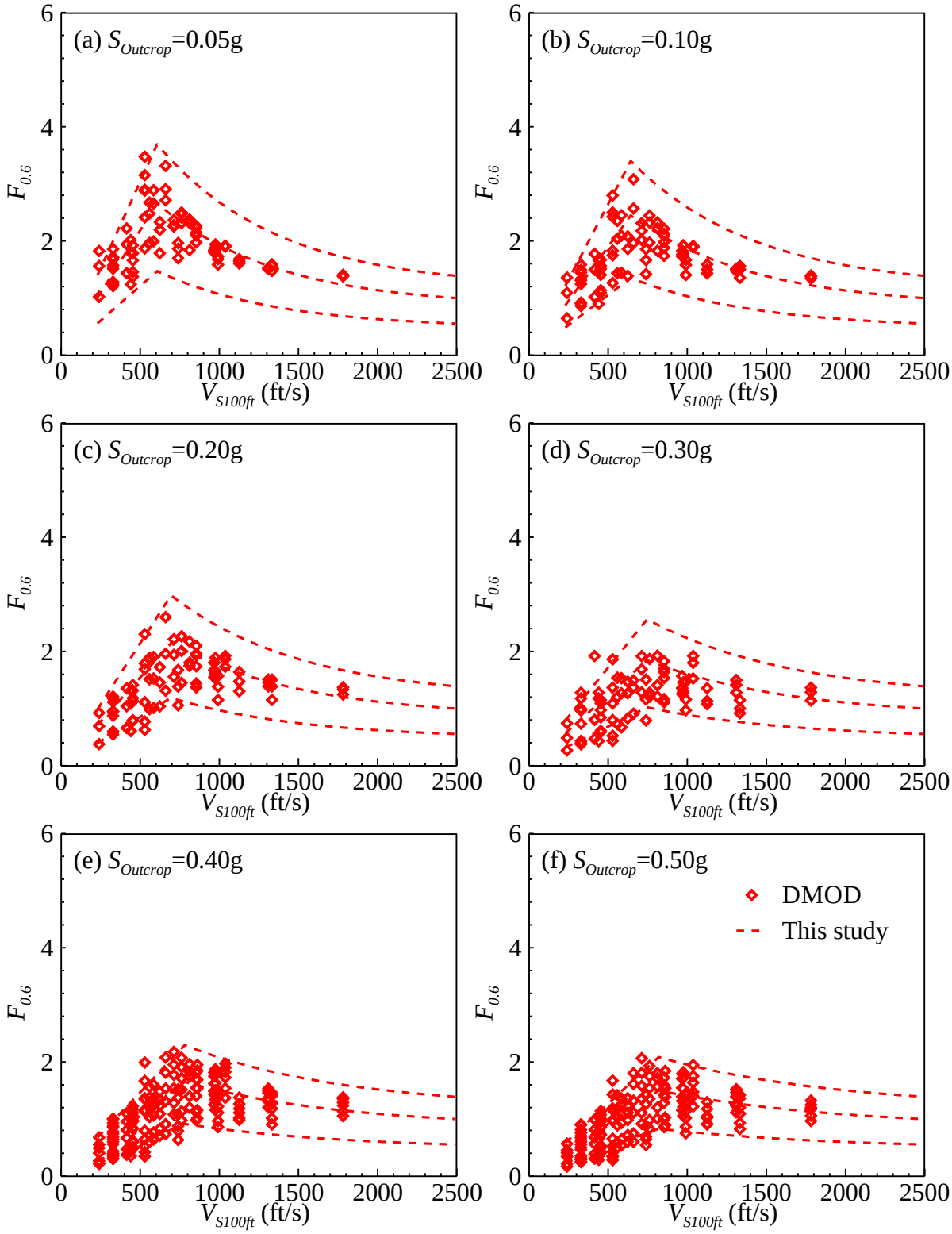

Figure K.5 Site coefficient model based on DMOD2000 data points for $F_{0.6}$.

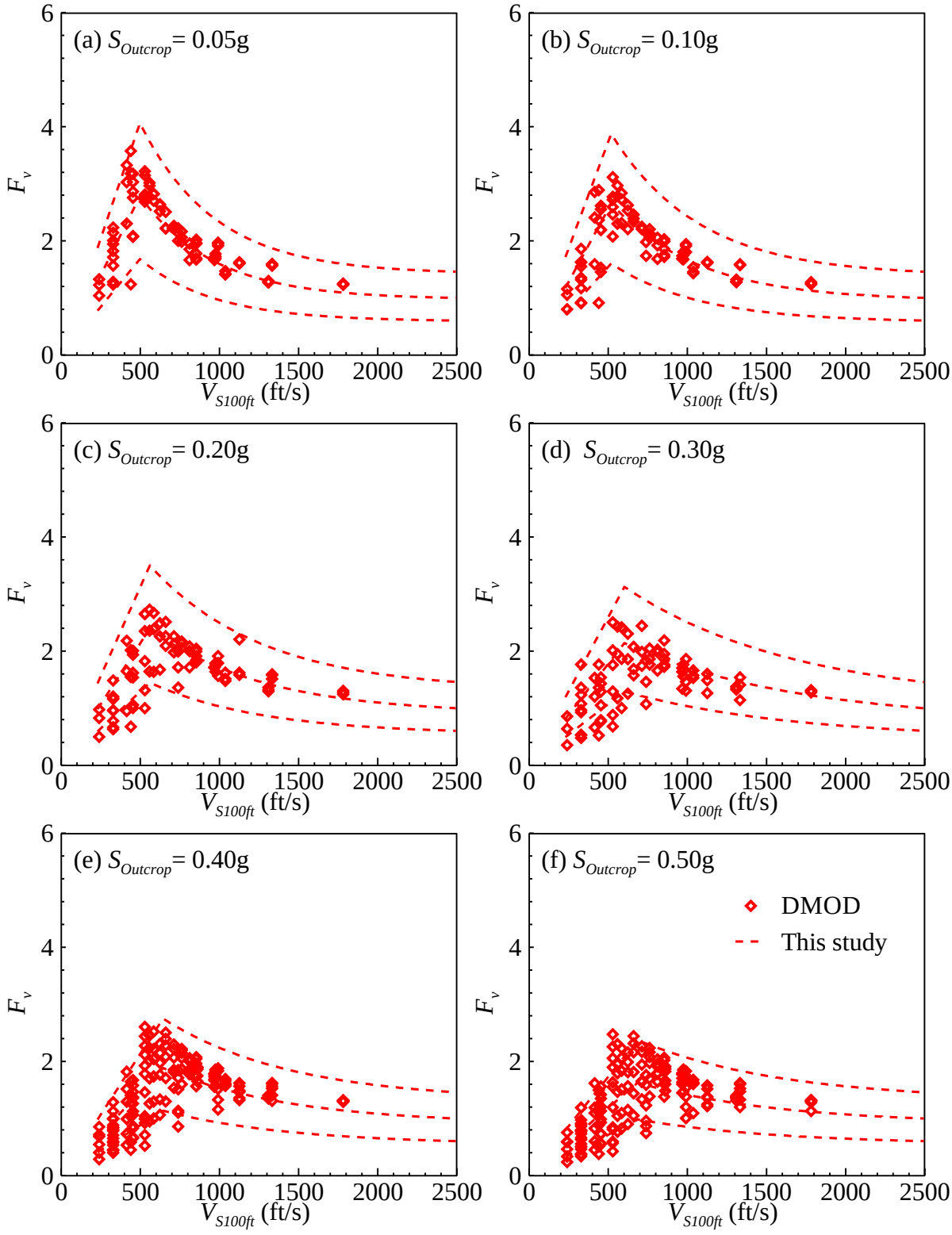

Figure K.6 Site coefficient model based on DMOD2000 data points for F_v or F_1.

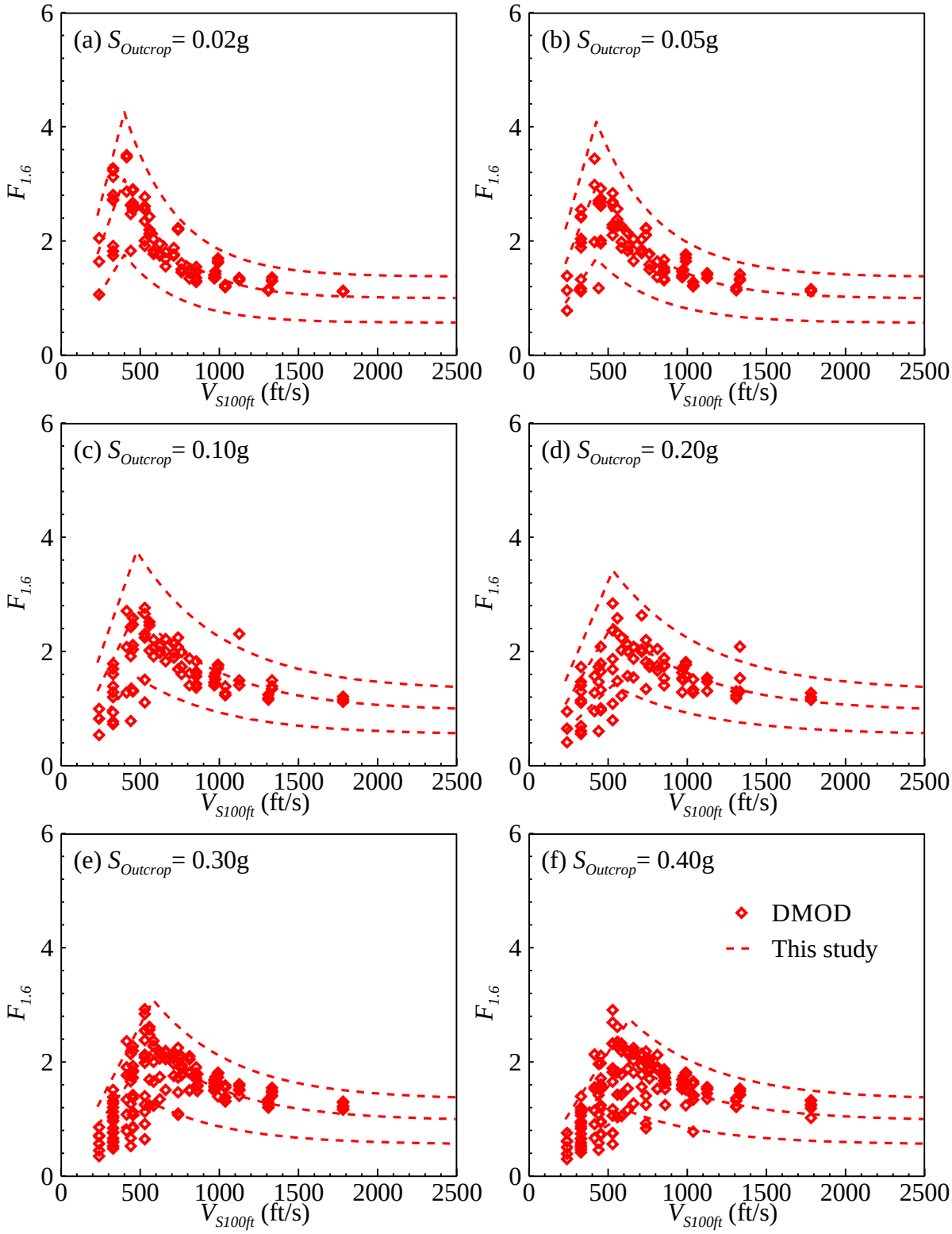

Figure K.7 Site coefficient model based on DMOD2000 data points for $F_{1.6}$.

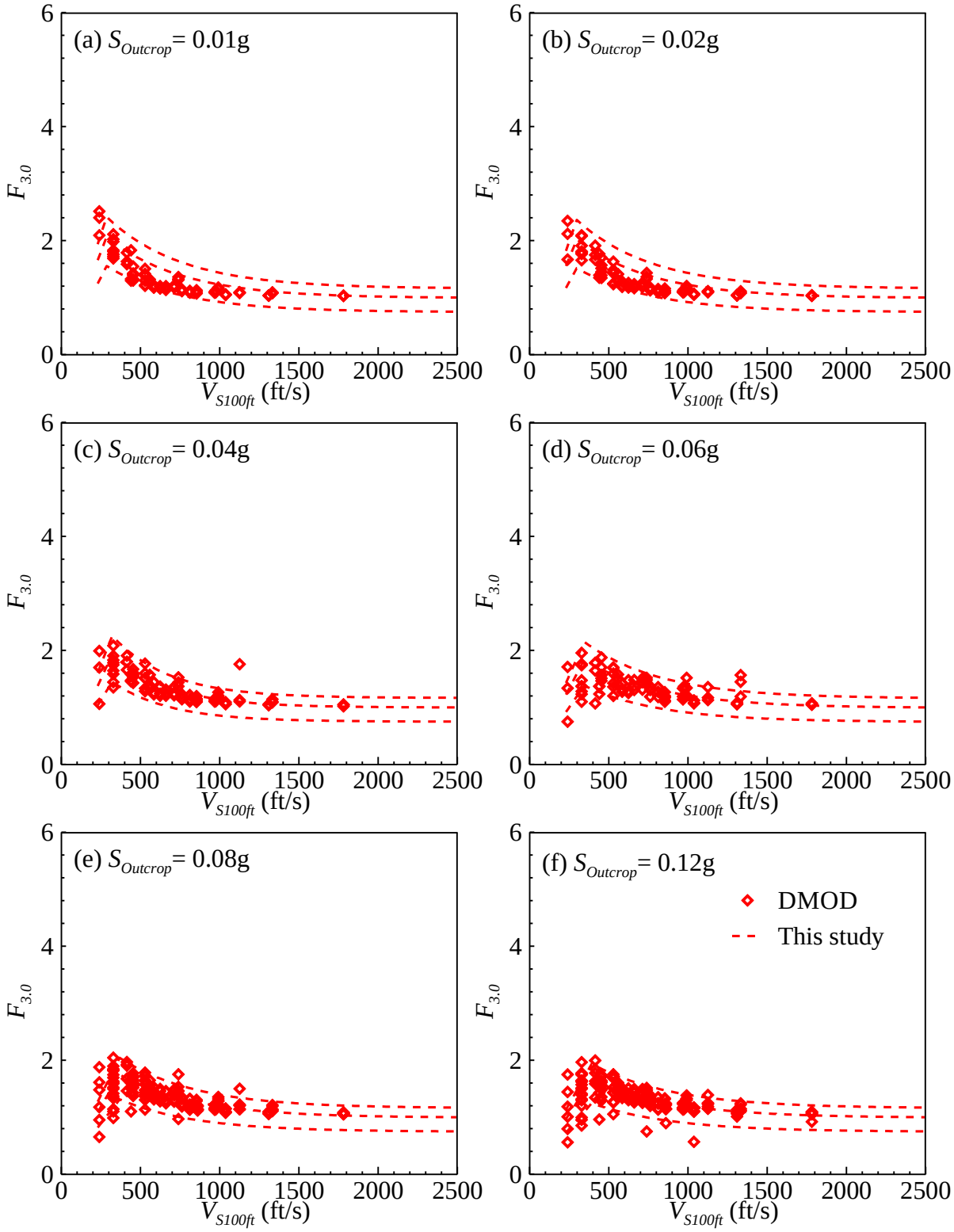

Figure K.8 Site coefficient model based on DMOD2000 data points for F_3.

K.9 Discussion

As seen in the Figures K.3-K.8, the fitted 95% and 5% bands mostly capture the data points reasonably well for all the cases. As compared to the quality of the fit of the proposed model with the corresponding data, here the fitting has been improved. In the case of the recommended model (Chapter 2 and corresponding appendix), the 95% line overestimates for some of the cases, i.e. in the sub-plots of $PGA_{outcrop}$ =0.05 g and 0.1 g for F_{PGA} and also F_a, regions of the data being over-estimated by the 95% line can be seen. The 95% lines based on DMOD2000 results (this appendix) captures those cases better. As a result, the number of data points falling above the 95% line has been reduced. One possible reason is that in the case of the recommended model, for each F case, first four $S_{outcrop}$ sub-cases were fitted based on only SHAKE2000 data points and the last two $S_{outcrop}$ sub-cases were fitted based on DMOD2000 data points. On the other hand, in this section, all cases are fitted based on data from a single program DMOD2000. Thus, better continuity of the data with $S_{outcrop}$ variation for each F case is observed when a single code is used to produce the data which results in better fitting. Point to be noted here that only the SEE motions is considered for the first four $PGA_{outcrop}$ cases (0.05, 0.1, 0.2 and 0.3 g) in this study while both SEE and FEE motions were considered during SHAKE2000 analyses, as was mentioned before. Chances are that this could be another reason of better fitting of the data by the model developed in this study although less probable.

K.9.1 Comparison of the Site Coefficient Models

After generation of the site coefficient model based on only DMOD2000 data points, the fitted curves based on DMOD200 results only are plotted and compared with the corresponding curves from the proposed site coefficient model in Chapter 2 in Figures K.9, K.10, K.11, K.12, K.13 and K.14 for the F_{PGA}, $F_{0.2}$, $F_{0.6}$, F_1, $F_{1.6}$ and F_3 cases, respectively.

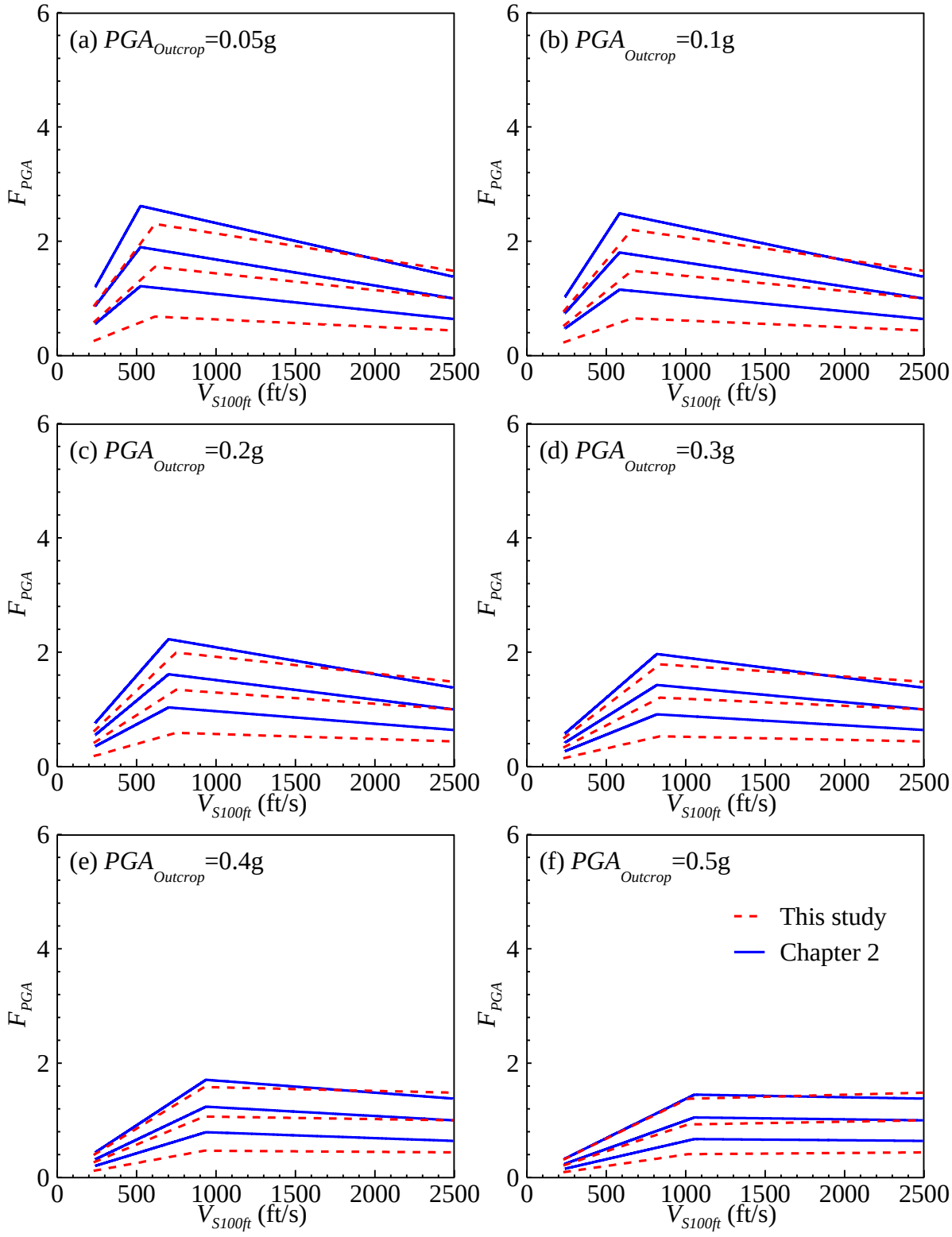

Figure K.9 Comparison of the recommended site coefficient model (Chapter 2) with the model based on DMOD2000 data points in the case of F_{PGA}.

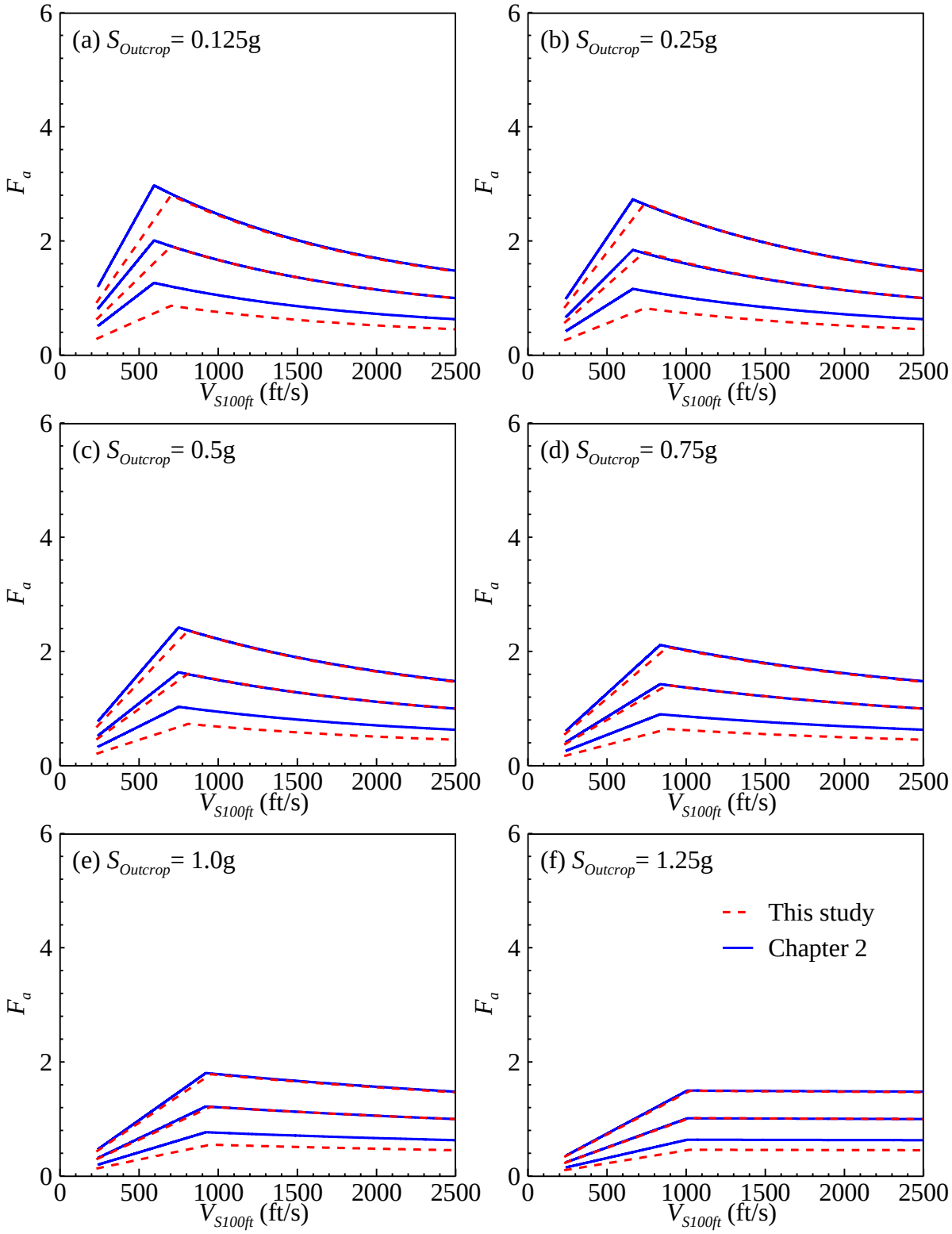

Figure K.10 Comparison of the recommended site coefficient model (Chapter 2) with the model based on DMOD2000 data points in the case of F_a or $F_{0.2}$.

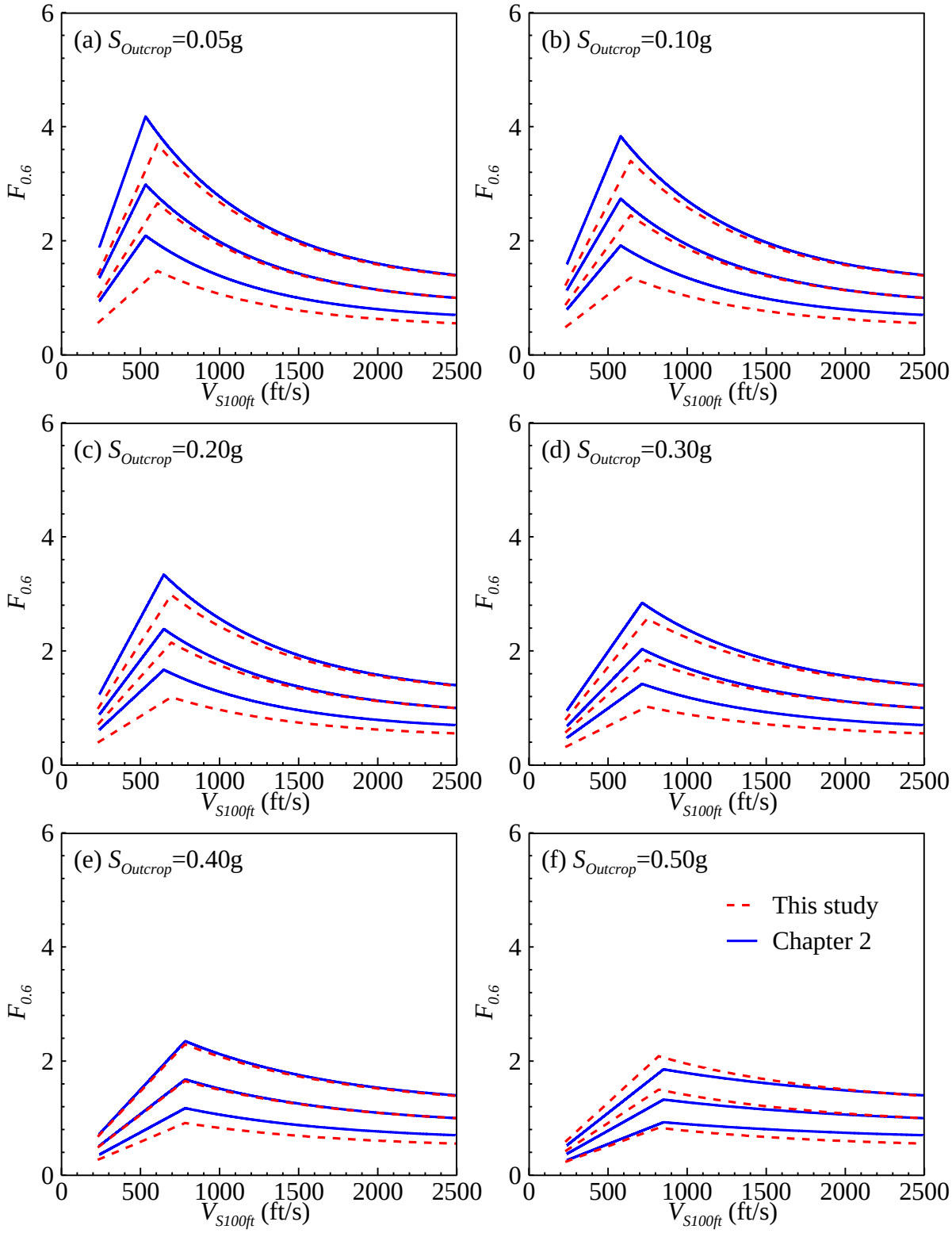

Figure K.11 Comparison of the recommended site coefficient model (Chapter 2) with the model based on DMOD2000 data points in the case of $F_{0.6}$.

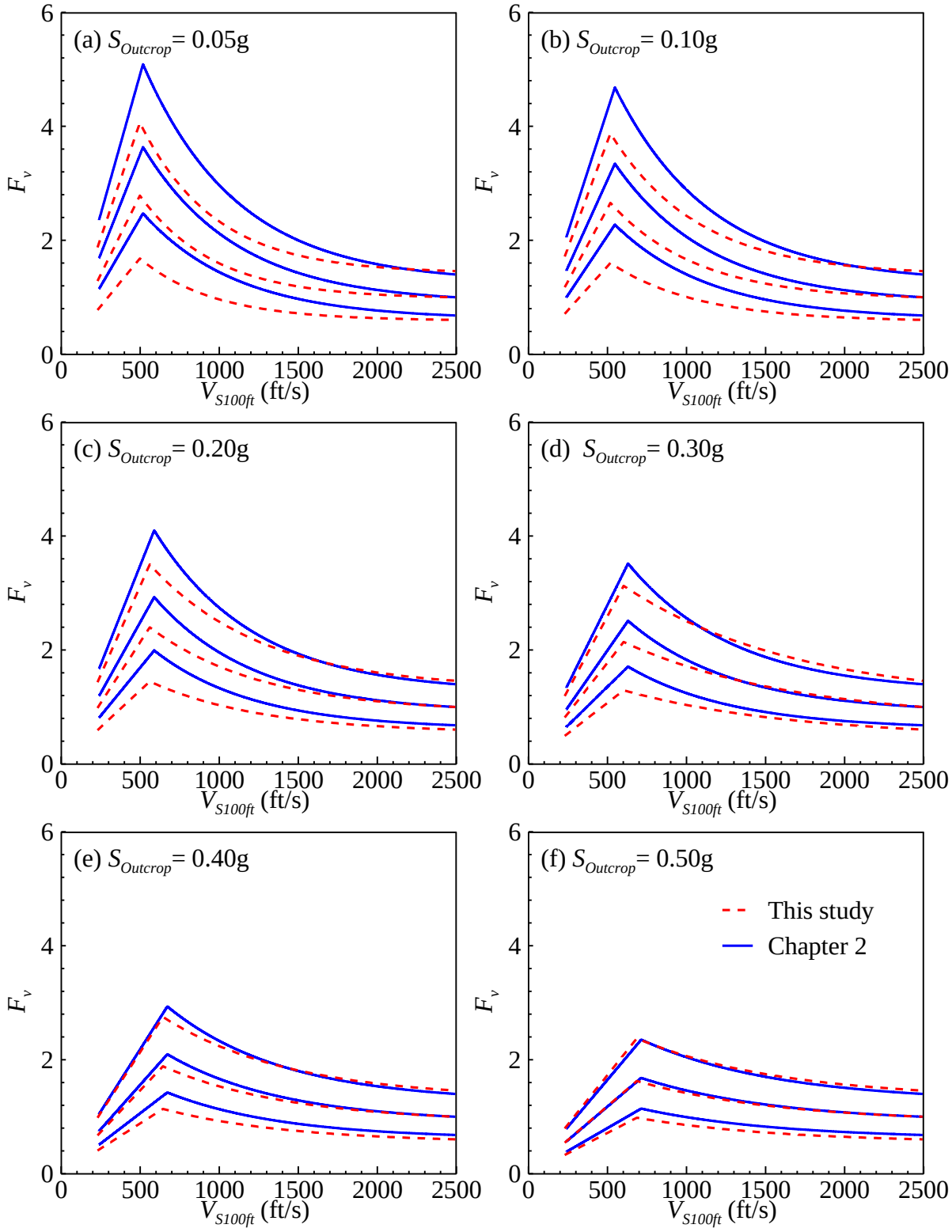

Figure K.12 Comparison of the recommended site coefficient model (Chapter 2) with the model based on DMOD2000 data points in the case of F_v or F_1.

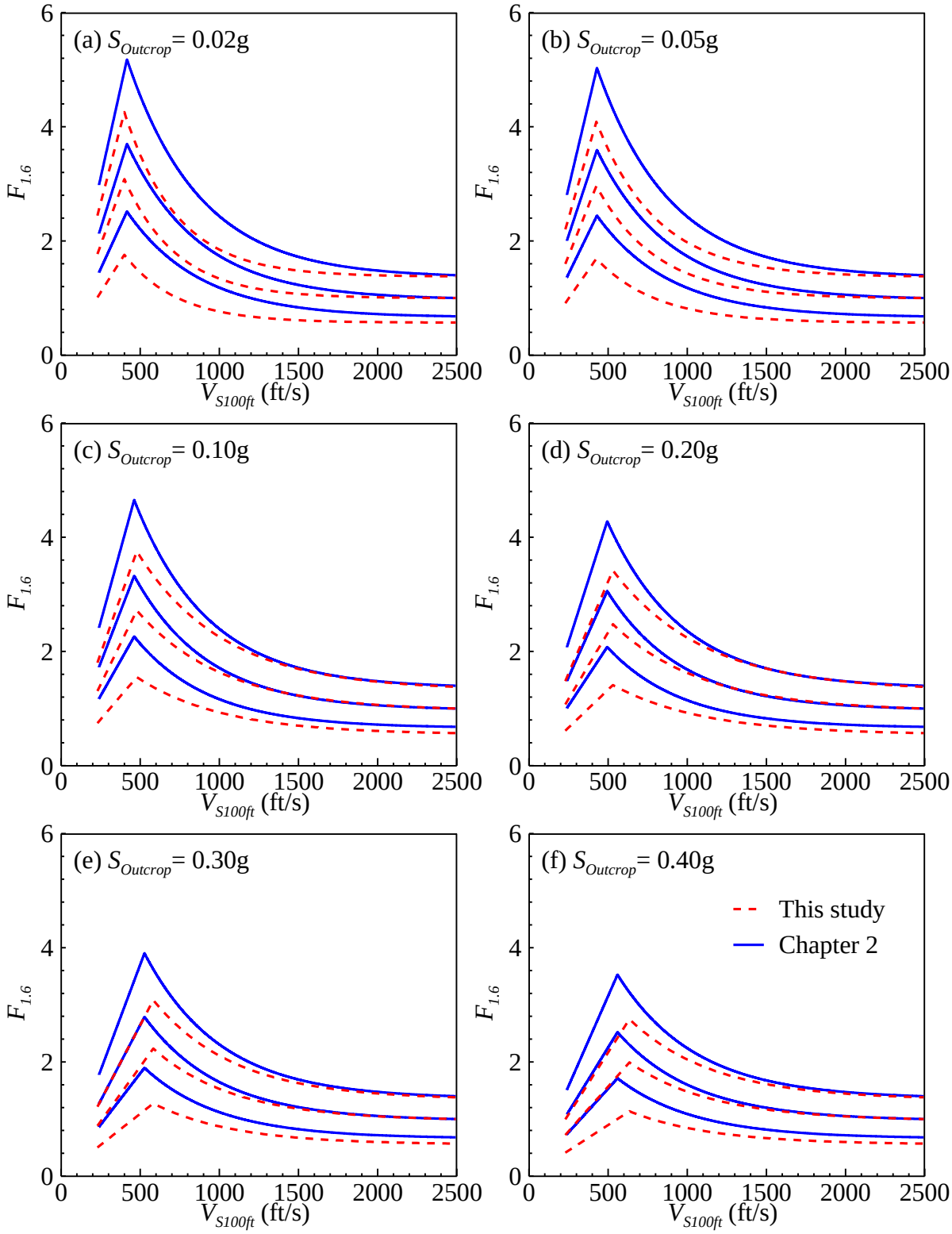

Figure K.13 Comparison of the recommended site coefficient model (Chapter 2) with the model based on DMOD2000 data points in the case of $F_{1.6}$.

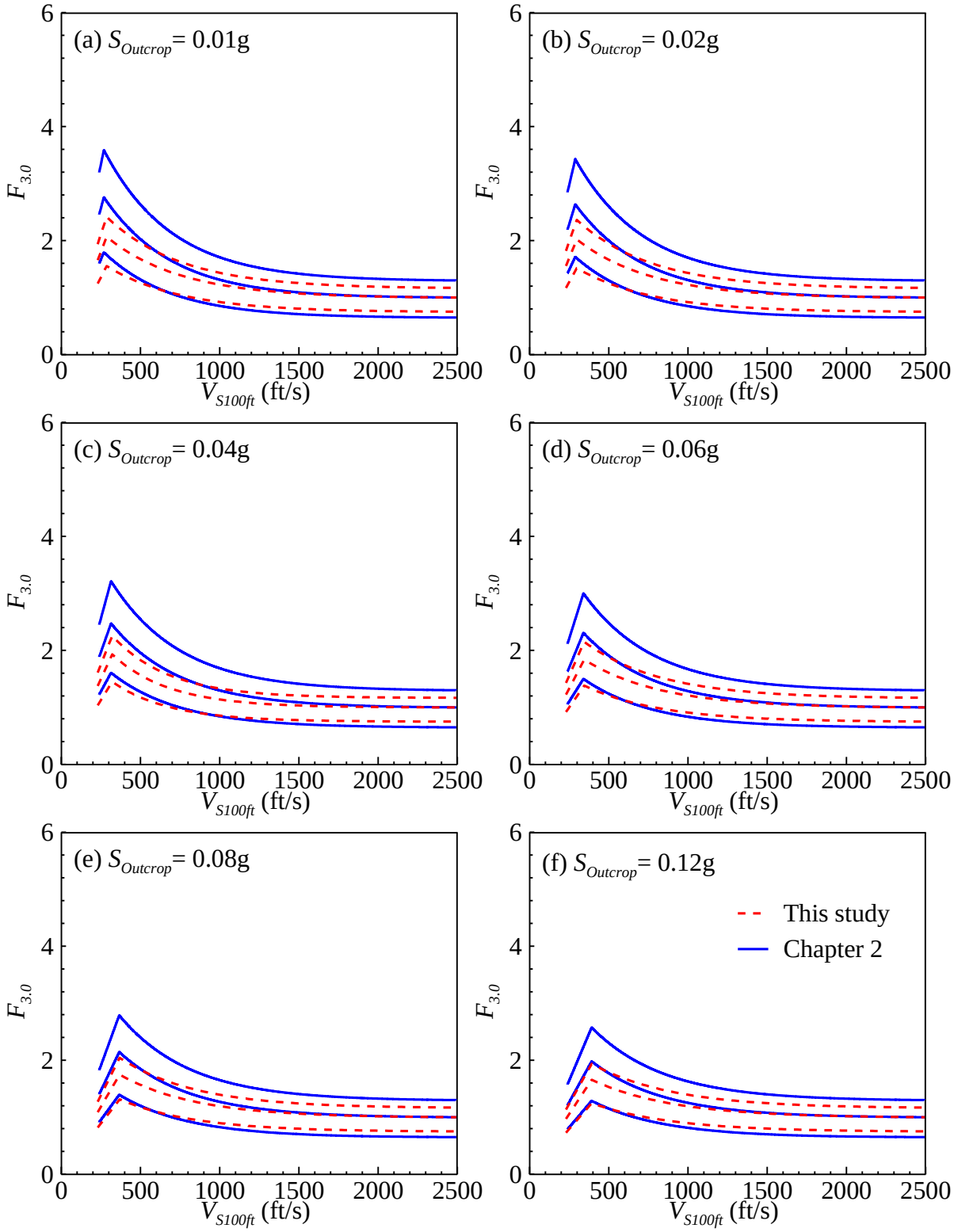

Figure K.14 Comparison of the recommended site coefficient model (Chapter 2) with the model based on DMOD2000 data points in the case of F_3.

As seen in Figures K.9-K.14, the 'Chapter 2' lines often plot above the lines from 'This study'. Although the sub-cases with low $S_{outcrop}$ values show significant amount of differences between these two sets of lines, they are expected to match originally. The difference between these two sets of lines increases from F_{PGA} to F_3 and decrease with the increment of $S_{outcrop}$ level. In some cases, the peak value from this study has shifted with respect to the V_{S100ft} axis compared to the proposed model which results in change in V_{S100ft}. Moreover, a quick check of the ratio of these two sets of curves reveals the fact that the difference generally increases with the decrease of V_{S100ft}. This may indicates that the profile began to behave nonlinearly at lower $S_{outcrop}$ level for the low V_{S100ft} profiles. However, the lines from the recommended model of site coefficients (Chapter 2) falling above the model completely based on nonlinear (DMDO2000) simulations confirms safety and/or adequacy of the recommended model (Chapter 2) of site coefficients. In addition, as discussed earlier, DMOD2000 is expected to predict overly damped responses due to it's theoretical limitations (i.e. limitations oriented to the MKZ model calibration and also the Rayleigh damping techniques) which could be a possible reason for the observed lower site coefficients calculated using the DMOD2000 results.

Furthermore, it should be noted here that the ground motions used to develop the model of this appendix are considering only the SEE variations for the first four sub-sets of $S_{outcrop}$ variations of each F-V_{S100ft} plots and both SEE and FEE variations are considered for the last two sub-sets of $S_{outcrop}$ variations in the F-V_{S100ft} plots (see Figures K.3-K.14). Thus the model developed based on DMDO2000 simulations has been developed with less number of data points. However, this should be a reasonable assumption as there was no observed difference in the responses from these two types of motions as discussed in Chapter 2.

K.9.2 Profile Maximum Strain

To further investigate soil nonlinearity, the profile maximum shear strain is generated for each DMOD2000 simulations. Profile maximum shear strain is the maximum shear strain experienced by any of the layers of the soil profile during the entire excitation period. Figure K.15 presents a profile maximum shear strain versus V_{S100ft} plot for the whole band of $PGA_{outcrop}$ levels (i.e. 0.05, 0.1, 0.2, 0.3, 0.4 and 0.5g). These maximum shear strain values are the average over all 12 motions for each of the V_{S100ft} cases (i.e. each of the twenty-eight V_{S100ft} profiles considered).

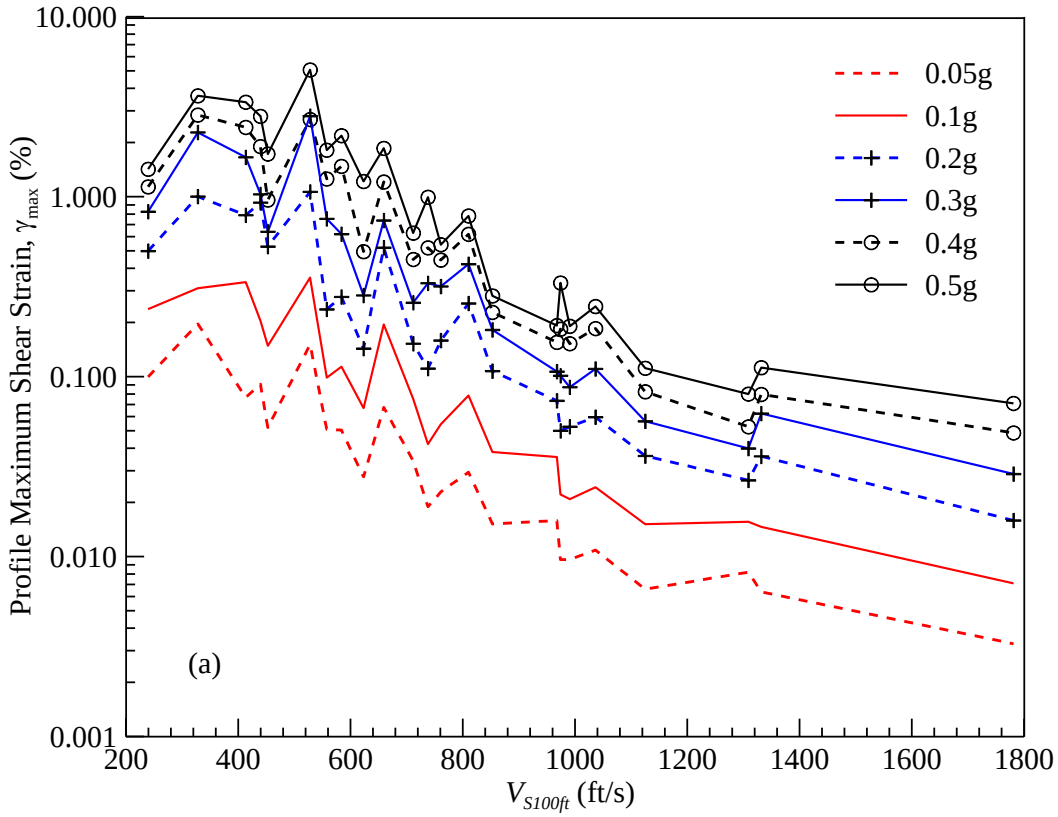

Figure K.15 Profile maximum shear strain versus V_{S100ft} plot for $PGA_{outcrop}$ levels of 0.05, 0.1, 0.2, 0.3, 0.4 and 0.5 g.

As observed in Figure K.15, higher strain is observed in low velocity profiles, especially for V_{S100ft} values around 656 ft/s or lower. Matasović and Hashash (2012) claimed nonlinearity starts at 0.1-0.2 % shear strains and after 0.5 % responses calculated by equivalent linear approach are no more reliable. The estimated profile maximum strain versus V_{S100ft} plot (Figure K.15) shows that the low velocity profiles (V_{S100ft} values mostly below 656 ft/s) experience shear strain larger than 0.1 % strains even for $PGA_{outcrop}$ of 0.05 g and in cases of 0.3, 0.4 and 0.5 g it is much higher than that 0.5 % strain threshold set by Matasović and Hashash (2012). Further analysis (presented later in Section K.10) revealed that even at the 0.1% strain level SHAKE2000 and DMOD2000 showed considerable amount of differences in responses based on DMOD2000. These results supports the differences observed in the site coefficient models, especially in the low V_{S100ft} cases as presented in the previous section. The low velocity profiles are predicted to be in the nonlinear zone even at small amplitudes which is beyond the capability of SHAKE2000 and causes the responses from DMOD2000 and SHAKE2000 to deviate. This demonstrates the need to develop a threshold which guides the user to decide whether to choose

a nonlinear or an equivalent linear program to perform accurate site response analysis with minimal effort. A simplified chart for choosing the appropriate simulation tool (nonlinear or equivalent linear) within a certain percentage difference is presented in the next section.

K.10 Development of Design Tool

As stated earlier, practitioners often assume that the equivalent linear analysis procedure is adequate for $PGA_{outcrop}$ < 0.4 g and/or the strain is within 1-2 %. Recently, Kaklamanos et al. (2013) attempted to develop a threshold to define the applicability of equivalent linear code by comparing simulation results with strong motion measurements. They found that the equivalent-linear code produced acceptable estimates up to 0.4 % strain and/or up to 0.1 g $PGA_{outcrop}$. However, the shear strain is not a direct input parameter; instead it is estimated from trial simulations. Thus, trial simulations conducted with inappropriate nonlinear model parameters may results in inaccurate shear strain values resulting in choosing an inappropriate code. Therefore, using shear strain as one of the parameters may not be appropriate. It is worth noting that some practitioners use site class as a parameter to choose simulation tool (Matasović and Hashash 2012). In this study, an attempt has been made to develop a guideline using V_{S100ft} as one of the parameters instead of shear strains. It should be noted that V_{S100ft} is one of the input parameters and is readily available for the user. For this section only, simulations conducted with the mean G/G_{max}-γ and D-γ profiles were considered.

K.10.1 Development Steps

The following is the step-by-step procedure followed to develop the design tool:

- First, the area enclosed by the response spectra with the 'Period' axis, from 0 s up to 10 s is calculated from both of the SHAKE2000 and DMOD2000 for all 12 ground motions of each of the V_{S100ft} cases.
- Second, the arithmetic average of the area under the response spectra from all 12 motions is calculated for each V_{S100ft} case.
- Then, for each V_{S100ft}, ratio of the corresponding averaged area from SHAKE2000 and DMOD2000 results are calculated.
- These area ratios are then grouped into six $PGA_{outcrop}$ levels and plotted against V_{S100ft}. Figure K.16 presents the area ratio versus V_{S100ft} plot for all $PGA_{outcrop}$. It is observed that the ratios show a clear deviation from the 10 % bound of '1.0' at around 656 ft/s or

below, especially in cases of $PGA_{outcrop}$ levels of 0.05, 0.1, 0.2 and 0.3 g. For $PGA_{outcrop}$ levels of 0.4 and 0.5 g, such deviation starts from even higher velocity. This supports the earlier observations in this study as low velocity profiles started to experience non-linearity at a very small loading while the stiffer profiles (i.e. with higher velocity) stayed within linear zone even at greater loadings. Thus high amount of shear strain and therefore much difference in the calculated site coefficients from the equivalent linear and nonlinear codes in the cases of softer profiles even at smaller loadings is an expected outcome. Another feature observed in Figure K.16 is the deviations are mostly on the 'upper' side of 1.0 which confirms the conservativeness and applicability of the proposed model even at the low velocity profiles. The following equation has been developed to fit all of the sub-plots in Figure K.16 based on regression analysis:

$$\text{Area ratio, SHAKE/DMOD} = 4.5\left(V_{S100\,ft}\right)^{a} + b \tag{K.12a}$$

where,

$$a = (-0.3888)PGA_{Outcrop}^{\ (-0.2369)} \tag{K.12b}$$

$$b = \begin{cases} (-0.4)PGA_{Outcrop} + 0.98, \textit{ when } PGA_{Outcrop} \le 0.2g \\ 0.80, \textit{ when } PGA_{Outcrop} \ge 0.2g \end{cases} \tag{K.12c}$$

The equation fits most of sub-plots fairly. The coefficient of determination, R^2 values also support the quality of these fits.

- Finally, a design chart is created by plotting V_{S100ft} versus $PGA_{outcrop}$ and then dividing them into four different regions (0.9 < Area ratio ≤ 1.0, 1.0 < Area ratio ≤ 1.1, 1.1 < Area ratio ≤ 1.2 and Area ratio > 1.2). These ranges are distinguished by using four different colors in Figure K.17. From this chart regions of variation of the responses from these two codes being less than 10 %, within 10 to 20 % and above 20 % can be easily distinguished. Higher velocity cases fell within 10 % variation for up to $PGA_{outcrop}$ of 0.4 g whereas low velocity profiles fell within 20 % or even greater ranges even at low $PGA_{outcrop}$ such as 0.1g. $PGA_{outcrop}$ above 0.4 g mostly showed more than 20% variation for all the profiles. An attempt is made to differentiate these ≤ 10 %, > 10 % and ≤ 20 %, >20% zones with three significant color patches. These regions should be helpful in deciding whether to use nonlinear or equivalent linear site response analysis. The fitted equation should also give an estimate of the expected deviations in the predicted response that could occur.

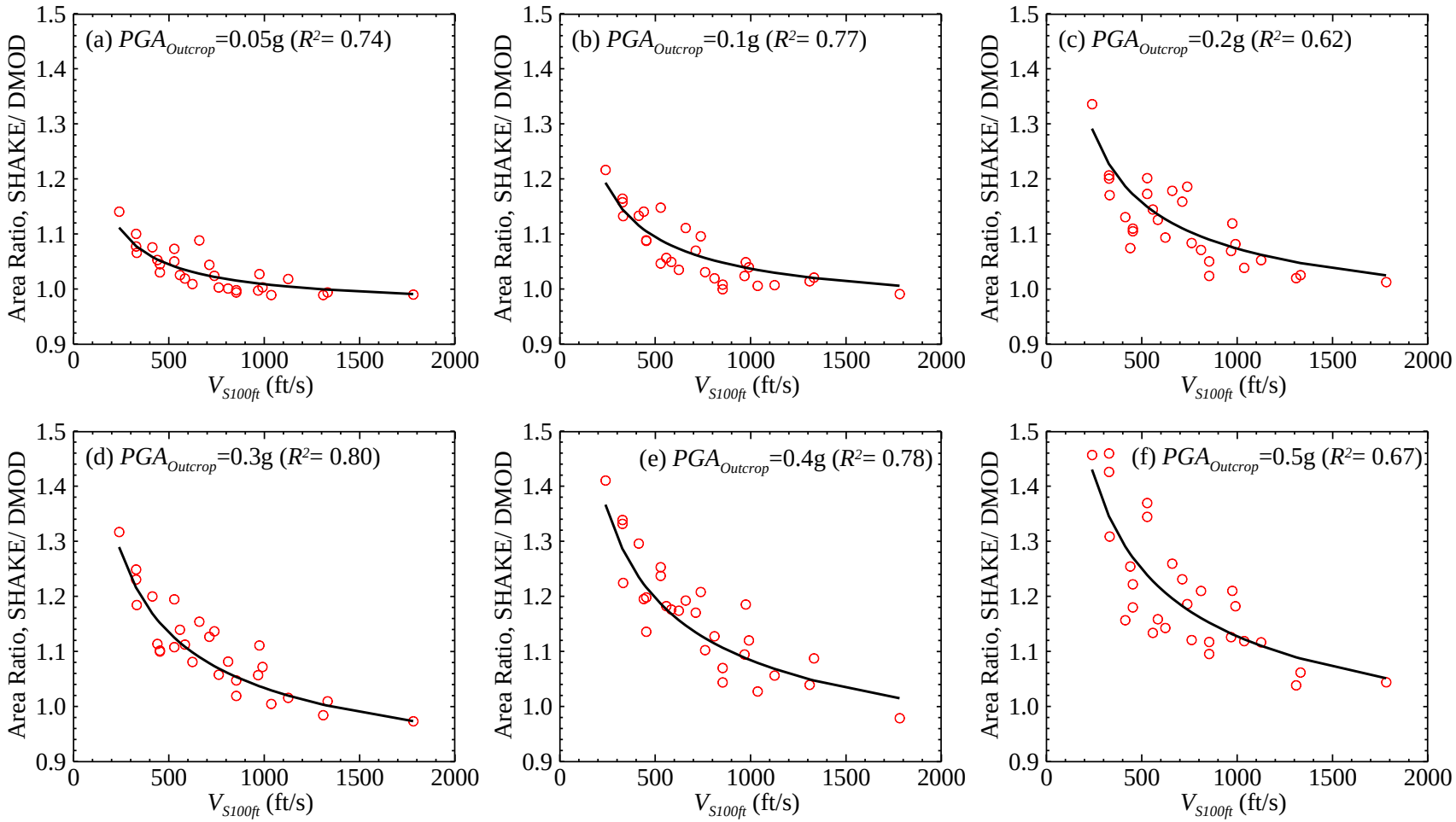

Fitting Equation: Area ratio, SHAKE/DMOD $= 4.5\left(V_{S100\,ft}\right)^{a} + b$

where, $a = (-0.3888)PGA_{Outcrop}{}^{(-0.2369)}$ and $b = \begin{cases} (-0.4)PGA_{Outcrop} + 0.98, \text{ when } PGA_{Outcrop} \le 0.2g \\ 0.80, \text{ when } PGA_{Outcrop} \ge 0.2g \end{cases}$

Figure K.16 Plots showing variation of the area ratios between SHAKE2000 and DMOD2000 with V_{S100ft} for $PGA_{outcrop}$= 0.05, 0.1, 0.2, 0.3, 0.4 and 0.5 g and the respective regressed lines.

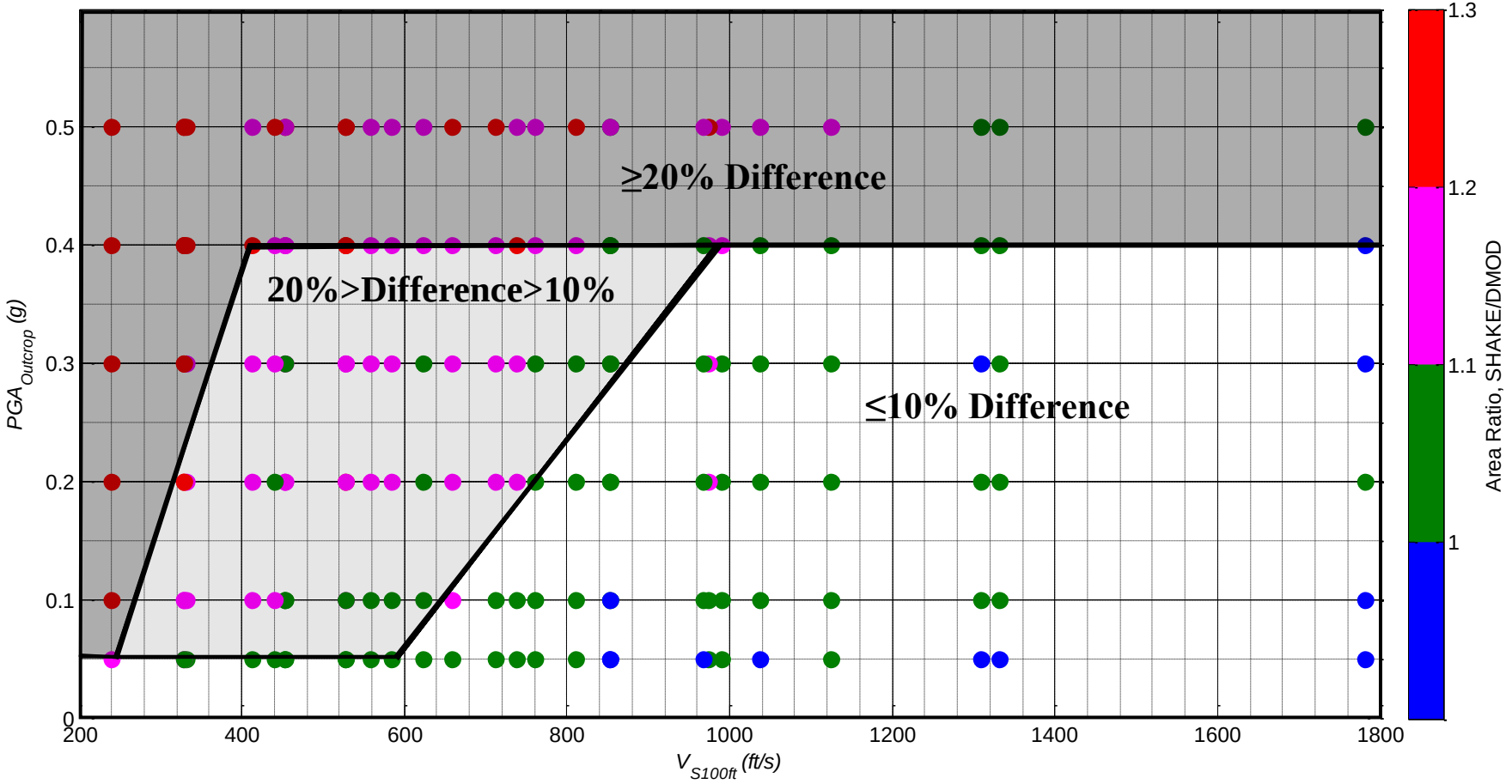

Fitting Equation: Area ratio, SHAKE/DMOD $= 4.5\left(V_{S100\,ft}\right)^{a} + b$

where, $a = (-0.3888)PGA_{Outcrop}{}^{(-0.2369)}$ and $b = \begin{cases} (-0.4)PGA_{Outcrop} + 0.98, \text{ when } PGA_{Outcrop} \le 0.2g \\ 0.80, \text{ when } PGA_{Outcrop} \ge 0.2g \end{cases}$

Figure K.17 Design chart developed with regions showing variation of the ratios between SHAKE2000 and DMOD2000 with V_{S100ft} for $PGA_{outcrop}$= 0.05, 0.1, 0.2, 0.3, 0.4 and 0.5 g.

K.10.2 Application

Together the fitted equation (Equation K.12) and the design chart (Figure K.17) is a tentative guide on deciding the most appropriate site response tool for the project in hand. The design chart provides a guidance to make decision on whether to choose nonlinear code (DMOD2000) or equivalent linear code (SHAKE2000) and the expected difference in the computed responses from these codes. The equation can be used to get an estimate of how much the SHAKE2000 analysis response could differ from the DMOD2000 response. Thus, the user can make a knowledgeable decision based on the significance of the project in hand by knowing the exact magnitude of the expected difference. The tool requires the user to know the $PGA_{outcrop}$ and the profile V_{S100ft} which are likely to be available to the user.

K.10.3 Limitations

It should be noted that the nonlinear model (MKZ model) parameters are calibrated by matching the G/G_{max}-γ curve instead of matching both G/G_{max}-γ and D-γ. The limitation regarding this matching technique is it generates higher damping especially at larger shear strain ranges than the experimental estimates. Although the technique 'matching only G/G_{max}-γ' is recommended by a previous well-known benchmarking study (Stewart et al., 2008), the computed responses using DMOD2000 can under-predict the actual scenario because of higher damping applied to the profile during the simulation. Further study by matching both G/G_{max}-γ and D-γ is needed to validate the proposed model.

K.11 Summary

Nonlinear site response analysis has been the least applied by the practitioners in the past due to lack of understanding of the model, model parameter calibration techniques and poor documentation of the nonlinear analysis procedures. In this appendix, the responses computed using SHAKE2000 and DMOD2000 are compared for a range of $PGA_{outcrop}$ and V_{S100ft} values considering conditions in Charleston. A site coefficient model was developed to fit the data generated using DMOD2000 analysis outcomes and compared with that of the SHAKE2000 outcomes. The comparison of these two models revealed that, in general, the model based on SHAKE2000 analysis results (presented in Chapter 2) shows conservative values compared to that of DMOD2000 results. Differences in the computed responses were observed even at

$PGA_{outcrop}$ as low as 0.05 g for softer profiles (low V_{S100ft}). This may be due to nonlinear behavior of the profile at such a low $PGA_{outcrop}$ and/or due to the difference in theories implemented in the equivalent linear and nonlinear codes considered. Such differences were mostly significant for profiles with lower V_{S100ft} values which also support the fact that softer profiles are more prone to nonlinear behavior at very low excitation. The study of profile maximum shear strain of the entire simulation time history also showed higher strain values in the case of low V_{S100ft} profiles at small $PGA_{outcrop}$ value which confirms the earlier observation of difference in site coefficients computed using these two models.

All these comparison raised the question: what condition requires the application of a nonlinear program over an equivalent linear program? To address this question, a unique design chart has been developed for Charleston. It requires the profile V_{S100ft} and the $PGA_{outcrop}$ of the ground motion. The tentative tool may guide the user to make a knowledgeable decision by knowing the expected deviation between the nonlinear and equivalent linear responses. Although this decision making tool has been developed only based on conditions specific to Charleston and based on DMOD2000 analysis results, a similar tool can also be generated for any other parts of the world.

Although it was found that the site coefficients based on SHAKE2000 can be as much as (or more) 20 % higher than that of DMOD2000, the results of this appendix support the site coefficient models presented in Chapters 2-4 because the curves based on the combination of SHAKE2000 and DMOD2000 results provide reasonable yet conservative site coefficients for practical design. Therefore, the site coefficient models presented in Chapters 2-4 are recommended for engineering practice. Additional investigation is required to address the limitations within the equivalent-linear and non-linear programs used.

APPENDIX L[1]

PARTIAL FIELD VALIDATION OF THE RECOMMENDED SEISMIC SITE COEFFICIENT MODEL FOR THE SCCP

[1] A similar version of the material presented in this appendix is included in a paper published in the *Bulletin of Seismological Society of America*. Aboye, S.A., Andrus, R.D., Ravichandran, N., Bhuiyan, A.H., Harman, N., and Martin, J.R., "A New Seismic Site Coefficient Model Based on Conditions in the South Carolina Coastal Plain", 2014, Vol. 104, Issue 6, doi: 10.1785/0120140005, in press.

Partial field validation of the seismic site coefficient model is possible using borehole-geotechnical and strong motion data from the 1989 Loma Prieta Earthquake as reported in Borcherdt (1994). Presented in Figure L.1 are the F_a values for 35 near-field sites in the San Francisco Bay area plotted with the NEHRP F_a. Figures L.1a and L.1b present the same information, except the former is plotted with a log-log scale, as used in the original presentation of Borcherdt (1994), and the latter is plotted with a linear scale. The plotted F_a values were derived as average Fourier spectra values normalized with respect to nearby sites underlain by firm to hard rock of the Franciscan Formation with peak ground surface accelerations ≈ 0.1 g.

Also presented in Figure L.1 are the median, 5% lower bound and 95% upper bound V_{S30}-F_a curves predicted using the recommended site coefficient model developed in Chapter 3 assuming S_s = 0.25 g and average T_m and T_{330ft} values typical of the San Francisco Bay area. T_m is computed from four strong motion recordings at sites underlain by the Franciscan Formation (i.e., South San Francisco, Yerba Buena Island, Piedmont Jr. High, and Rincon Hill stations) obtained from the Pacific Earthquake Engineering Research (PEER) ground motion database. The T_m values for the four recordings range from 0.61 to 0.68 s, with an average value of 0.64 s. Average values of V_{S100ft}, V_{S330ft} and T_{330ft} are estimated using V_S profiles from seven other strong motion stations on soil sites (i.e., Alameda Naval Air Station, Gilroy 2 (EPRI), Gilroy 2 (USGS), Oakland Outer Harbor, San Fransisco International Airport, Treasure Island, and VA Hospital Palo Alto). The V_{S100ft}, V_{S330ft} and T_{330ft} values at these seven sites range from 564 to 1,158 ft/s, 817 to 1,575 ft/s and 0.83 to 1.61 s, respectively. K_{H1} and K_{H2} are assumed to equal 1.0, because the depth to soft rock is greater than 330 ft at all seven strong motion stations on soil sites.

It can be seen in Figure L.1 that the site coefficient model developed in this study better predicts the plotted Loma Prieta F_a values, than do the NEHRP F_a values. The partial validation presented in Figure L.1 with independent field data from the Loma Prieta earthquake provides additional strong support for the use of the recommended site coefficient model developed in Chapter 3, instead of the NEHRP F_a.

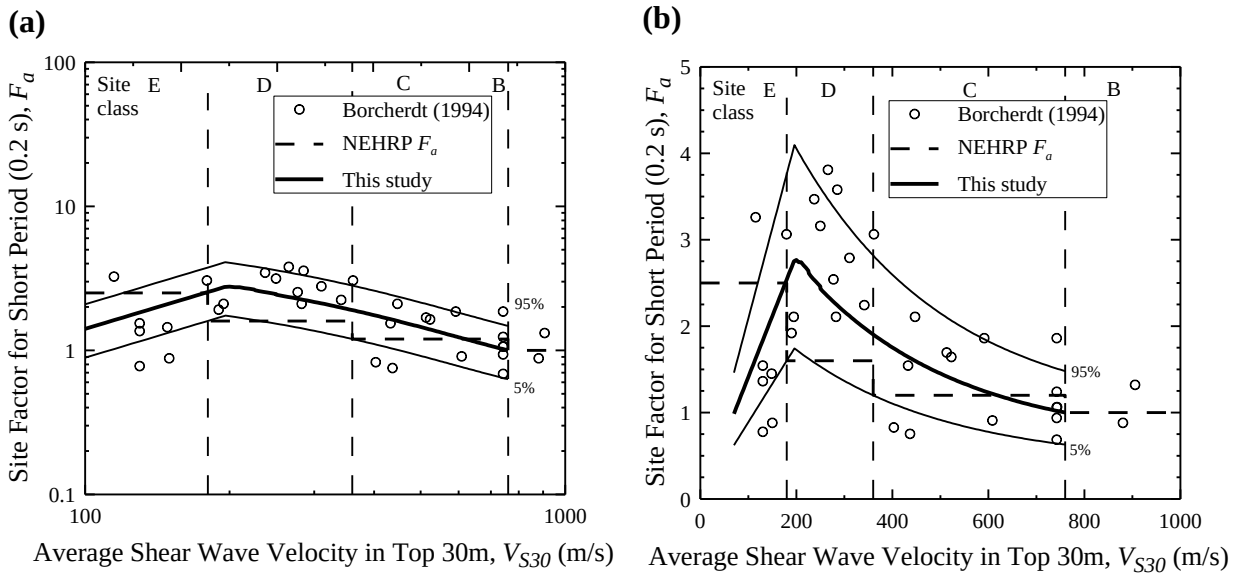

Figure L.1 Validation of the V_{S30}-F_a (or V_{S100ft}-F_a) predictive relationship developed in this study using data from the 1989 Loma Prieta earthquake.

REFERENCES

Aboye, S., Andrus, R. D., Ravichandran, N., Bhuiyan, A., and Harman, N. (2011). "Site factors for estimating peak ground acceleration in Charleston, South Carolina, based on V_{S30}," *Proc., 4th IASPEI/IAEE International Symposium: Effects of Surface Geology on Seismic Motion*, University of California Santa Barbara, CA, http://esg4.eri.ucsb.edu/.

Aboye, S., Andrus, R. D., Ravichandran, N., Bhuiyan, A., and Harman, N. (2015). "Seismic site factors and design response spectra based on conditions in Charleston, South Carolina," *Earthquake Spectra*, **31**, doi: 10.1193/041912eqs163m, in press. (Published online ahead of print 25 November 2013.)

American Association of State Highway and Transportation Officials, AASHTO (2011a). *LRFD Bridge Design Specifications*, 2nd Edition, AASHTO, Washington, D.C, 286 p.

American Association of State Highway and Transportation Officials, AASHTO (2011b). "LRFD seismic analysis and design of transportation geotechnical features and structural foundations," *Publication No. FHWA-NHI-11-032*, GEC No. 3, Washington, D.C.

American Society of Civil Engineers, ASCE (2010). *Minimum Design Loads for Buildings and Other Structures, ASCE Standard 7-10*, Reston, VA, 650 p.

Andrus, R. D., Fairbanks, C. D., Zhang, J., Camp III, W. M., Casey, T. J., Cleary, T. J., and Wright, W. B. (2006). "Shear-wave velocity and seismic response of near-surface sediments in Charleston, South Carolina," *Bulletin of the Seismological Society America*, **95**(5), 1897-1914.

Ardoino, F., Traverso, C. M., and Parker, E. J. (2008). "Evaluation of site response for deepwater field," **Proc.,** *Geotechnical Earthquake Engineering and Soil Dynamics IV*, ASCE, Reston, VA, 1-10.

ATC/MCEER (2003a). "Design examples: Recommended LRFD guidelines for the seismic design of highway bridges," *Report No. MCEER/ATC-49*, Applied Technology Council and Multidisciplinary Center for Earthquake Engineering Research Center, Redwood City, CA.

ATC/MCEER (2003b). "Specifications: Recommended LRFD guidelines for the seismic design of highway bridges," *Report No. MCEER/ATC-49*, Applied Technology Council and Multidisciplinary Center for Earthquake Engineering Research Center, Redwood City, CA.

Atkinson, G. M., and Boore, D. M. (1995). "Ground motion relations for eastern North America," *Bulletin of the Seismological Society America*, **85**(1), 17-30.

Bakun, W. H., and Hopper, M. G. (2004). "Magnitudes and locations of the 1811-1812 New Madrid, Missouri, and the 1886 Charleston, South Carolina, earthquakes." *Bulletin of the Seismological Society America,* **94**(1), 64-75.

Bollinger, G. (1975). "A catalog of southeastern United States earthquake 1754 through 1974." *Virginia Polytechnical Institute and State University, Research Division Bulletin,* 101, 68 p.

Bollinger, G. A. (1977). "Reinterpretation of the intensity data for the 1886 Charleston, South Carolina, earthquake," *Studies Related to the Charleston, South Carolina, Earthquake of 1886: A Preliminary Report, U.S.G.S. Prof. Paper 1028*, D. W. Rankin (editor), United States Geological Survey, Reston, VA, 17-32.

Boore, D. M., Joyner, W. B., and Fumal, T. E. (1994). "Estimation of response spectra and peak acceleration from western North American earthquakes: An Interim Report," *U.S.G.S. Open-File Report*, vol 2, Merlo Park, CA, 94-124.

Borcherdt, R. D. (1994). "Estimates of site-dependent response spectra for design (methodology and justification)," *Earthquake Spectra*, **10**(4), 617-653.

Borcherdt, R. D. (2002). "Empirical evidence for site coefficients in building-code provisions," *Earthquake Spectra,* **18**(2), 189-218.

Building Seismic Safety Council, BSSC (1995). "NEHRP recommended provisions for seismic regulations for new buildings (1994 edition)," *Federal Emergency Management Agency, FEMA* 222A/223A, Building Seismic Safety Council, Washington, D.C.

Building Seismic Safety Council, BSSC (2010). "NEHRP recommended provisions for seismic regulations for new buildings and other structures (2009 edition)," *Federal Emergency Management Agency, FEMA P-749*, Building Seismic Safety Council, Washington, D.C.

Chapman, M. C. (2006). "User's guide to SCENARIO_PC and SCDOTSHAKE," Report to the South Carolina Department of Transportation, Columbia, SC.

Chapman, M. C., Martin , J. R., Olgun, C. G., and Beale, J. N. (2006). "Site-response models for Charleston, South Carolina and vicinity developed from shallow geotechnical investigations," *Bulletin of the Seismological Society America*, **96**(2), 467-489.

Chapman, M. C., and Talwani, P. (2002). "Seismic hazard mapping for bridge and highway design," Report to the South Carolina Department of Transportation, Columbia, SC.

Choi, Y. and Stewart, J. P. (2005). "Nonlinear site amplification as function of 30 m shear wave velocity," *Earthquake Spectra*, **21**(1), 1-30.

Côté, R. N. (2006). *City of Heroes: The Great Charleston Earthquake of 1886*, Corinthian Books, Mt. Pleasant, SC, 542 p.

Cramer, C. H., and Boyd, O. S. (2011). "Why the New Madrid Earthquakes are M7-8 and the Charleston earthquake is ~M7," *American Geophysical Union, Fall Meeting 2011*, San Francisco, CA, December 5-9, S22A-04.

Crouse, C. B. (2011). "Effects of local geology on earthquake ground motions: from research to engineering practice and building codes," *Proc., 4th IASPEI/IAEE International Symposium: Effects of Surface Geology on Seismic Motion*, University of California Santa Barbara, CA, http://esg4.eri.ucsb.edu/.

CSI (2009). *CSI Analysis Reference Manual. Version 14.2.2*, Computers and Structures Inc. Walnut Creek, CA.

Dobry, R., Martin, G. M., Parra, E., and Bhattacharya, A. (1994). "Development of site-dependent ratios of elastic response spectra (RRS) and site categories for building seismic codes," *Proc. NCEER, SEAOC, BSSC Workshop on Site Response during Earthquakes and Seismic Code Provisions*, University of Southern California, Los Angeles, CA.

Dobry, R., Borcherdt, R. D., Crouse, C. B., Idriss, I. M., Joyner, W. B. Martin, G. R., Power, M. S., Rinne, E. E., and Seed R. B. (2000). "New site coefficients and site classification system used in recent building seismic code provisions," *Earthquake Spectra*, **16**(1), 41-67.

DuBar, J. R. (1987). "Geology of the Dongola 7.5-minute quadrangle, Horry and Marion Counties, South Carolina," South Carolina Geological Survey, **31**(1), Columbia, SC, 15 p.

Durá-Gómez, I., and Talwani, P. (2009). "Finding faults in the Charleston area, South Carolina: 1. Seismological Data," *Seismological Research Letters*, **80**(5), 883–900.

Dutton, C. E. (1889). "The Charleston earthquake of August 31, 1886," *U.S.G.S., Ninth Annual Report 1887-1888*, Washington, D.C., 203-528.

Fairbanks, C. D., Andrus, R. D., Camp III, W. M., and Wright, W. B. (2008). "Dynamic periods and building damage at Charleston, South Carolina during the 1886 earthquake," *Earthquake Spectra*, **24**(4), 867-888.

Hartzell, S., Bonilla, L. F., and Williams, R. A. (2004). "Prediction of nonlinear soil effects," *Bulletin of the Seismological Society America*, **94**(5), 1609-1629

Hashash, Y. M. A., Tsai, C. C., Phillips, C., and Park, D. (2008). "Soil-column depth-dependent seismic site coefficients and hazard maps for the upper Mississippi Embayment," *Bulletin of the Seismological Society America*, **98**(4), 2004-2021.

Hashash, Y. M., Phillips, C., and Groholski, D. R. (2010). "Recent advances in non-linear site response analysis," *Proc., Fifth International Conference on Recent Advances in Geotechnical Earthquake Engineering and Soil Dynamics*, held in San Diego, CA, May 24-29, Paper No. OSP 4.

Hashash, Y. M. A. (2011). *DEEPSOIL v5.0, User Manual and Tutorial.* University of Illinois at Urbana-Champaign, Urbana, IL, < www.illinois.edu/~deepsoil >.

Hatcher, R. D., Howell, D. E., and Talwani, P. (1977). "Eastern piedmont fault system: speculations and its extent," *Geology*, **5**, 636-640.

Heidari, T., and Andrus, R. D. (2010). "Mapping liquefaction potential of aged soil deposits in Mount Pleasant, South Carolina," *Engineering Geology,* **112**(1-4), 1-12.

Hudson, M., Idriss, I. M., and Beikae, M. (1994). "QUAD4M: a computer program to evaluate the seismic response of soil structures using finite element procedures and incorporating a compliant base," Center for Geotechnical Modeling, Department of Civil and Environmental Engineering University of California at Davis.

Idriss, I. M. (1990). "Response of soft soil sites during earthquake," *Proc., H. Bolton Seed Memorial Symp.*, vol. 2, BiTechPublishers Ltd., Richmond, British Columbia, Canada, pp. 273–289.

International Codes Council, ICC (2012). *International Building Code (IBC)*, Falls Church, VA, 328 p.

Johnston, A. C. (1996). "Seismic moment assessment of earthquakes in stable continental regions, III. New Madrid 1811-1812, Charleston 1886 and Lisbon 1755," *Geophysical Journal International*, **126**(2), 314-344.

Joyner, W. B., Fumal, T. E., and Glassmoyer, G. (1994). "Empirical spectral response ratios for strong motion data from the 1989 Loma Prieta, California, earthquake," *Proc. NCEER, SEAOC, BSSC Workshop on Site Response during Earthquakes and Seismic Code Provisions*, University of Southern California, Los Angeles, CA, November 18 - 20.

Kaklamanos, J., Bradley, B. A., Thompson, E. M., and Baise, L. G. (2013). "Critical Parameters Affecting Bias and Variability in Site-Response Analyses Using KiK-net Downhole Array Data," *Bulletin of the Seismological Society of America*, **103**(3), 1733-1749.

Kondner, R. L., and Zelasko, J. S. (1963). "A hyperbolic stress-strain formulation of sands," *Proc., 2nd Pan American Conference on Soil Mechanics and Foundation Engineering*, Sao Paulo, Brazil, 289–324.

Kramer, S. L. (1996). *Geotechnical Earthquake Engineering*, Prentice-Hall, Upper Saddle River, NJ, 653 p.

Kramer, S. L., and Paulsen, S. B. (2004). "Practical use of geotechnical site response models", *NSF/PEER Int. Workshop on Uncertainties in Nonlinear Soil Properties and their Impact on Modeling Dynamic Soil Response*, March 18-19, University of California, Berkeley, CA.

Krinitzsky, E. L., and Dunbar, J. B. (1990). "Geological-Seismological Evaluation of Earthquake Hazards at Hartwell and Clemson Upper and Lower Dams, South Carolina," *Technical Report GL-90-11*, Department of the Army, Waterways Experiment Station, Corps of Engineers, Vicksburg, MS.

Krinitzsky, E. L., and Dunbar, J. B. (1992). "Earthquake Hazards at Hartwell and the Clemson Upper and Lower Dams, Georgia-South Carolina," *South Carolina Geology*, **34**(1-2): 39-52.

Kwok, O. L. A., Stewart, J. P., Hashash, Y. M. A., Matasovic, N., Pyke, R. M., Wang, Z. L., and Yang, Z. (2007). "Use of exact solutions of wave propagation problems to guide implementationof nonlinear seismic ground response analysis procedures," *Journal Geotechnical and Geoenvironmental Engineering*, ASCE, **133**(11), 1385–1398.

Lee, M. K., and Finn, W. D. L. (1978). "DESRA-2, Dynamic effective stress response analysis of soil deposits with energy transmitting boundary including assessment of liquefaction potential," *Soil Mechanics Series No. 36*, Department of Civil Engineering, University of British Columbia, Vancouver, Canada.

Lester, A. P., and Chapman, M. C. (2005). An examination of site response in Columbia, South Carolina, *Seismological Research Letters*, **76**(1), 118 p.

Li, X., Wang, Z. L., and Shen, C. K. (1997). SUMDES. A nonlinear procedure for response analysis of horizontally layered sites subjected to multi-directional earthquake loading. Department of Civil Engineering, University of California at Davis.

Martin, J. R., II, and Clough, G. W. (1994). "Seismic parameters from liquefaction evidence," *Journal of Geotechnical Engineering,* **120**(8), 1345-1361.

Masing, G. (1926). Eigenspannungen und verfestigung beim messing (Self-stretching and hardening for brass), Proceedings, Second International Congress on Applied Mechanics, Zurich, Switzerland, 332-335 (in German).

Matasović, N. (1993). "Seismic response of composite horizontally-layered soil deposits," *Ph.D. Dissertation,* Civil Eng. Dept., University of California, Los Angeles, CA, 483 p.

Matasović, N., and Vucetic, M. (1993a). "Cyclic characterization of liquefiable sands*," Journal of Geotechnical Engineering,* ASCE, Vol. **119**(11), 1805-1822.

Matasović, N., and Vucetic, M. (1993b). Seismic response of horizontally layered soil deposits. Report No. ENG 93-182, School of Engineering and Applied Science, University of California, Los Angeles.

Matasović, N., and Ordóñez, G. A. (2011). "D-MOD2000: A Computer program for seismic response analysis of horizontally layered soil deposits, earthfill dams and solid waste landfills, user's manual," Geomotions, LLC, Lacey, WA, 172 p., http://www.geomotions.com.

Matasovic, N., and Hashash, Y. (2012). "Practices and procedures for site-specific evaluations of earthquake ground," *NCHRP Synthesis 428,* Transportation Research Board, Washingtion, D.C., 78 p. (*http://onlinepubs.trb.org/onlinepubs/nchrp/nchrp_syn_428.pdf*)

Maybin, A. H., III, and Nystrom, P. G., Jr. (1995). "Generalized geologic map of South Carolina," South Carolina Department of Natural Resources, Geology Map 1.

McCartan, L., Lemon, E. M., and Weems, R. E. (1984). "Geologic map of the area between Charleston and Orangeburg, South Carolina," *USGS Misc. Investigations Series Map I-1472,* United States Geological Survey, Reston, VA.

McKenna F., and Fenves, G. (2001). "The OpenSees command language manual: version 1.2," Pacific Earthquake Engineering Research Center, University of California at Berkeley, http://OpenSees.berkeley.edu.

Moses, C. (2002). "Geologic mapping of the central portion of the Myrtle Beach 7.5-minute Quadrangle," *Proc., 37th South-Central Section and 52nd Southeastern Section GSA Joint Annual Meeting*, Memphis, March 12-13.

Odum, J. K., Williams, R. A., Stepheson, W. J., and Worley, D. M. (2003). "Near-surface S-wave and P-wave seismic velocities of primary geological formations on the Piedmont and Atlantic Coastal Plain of South Carolina," *USGS Open-File Report 03-043*, United States Geological Survey, Reston, VA, 14 p.

Owens, J. P. (1989). "Geologic map of the Cape Fear region, Florence 1° x 2° quadrangle and northern half of the Georgetown 1° x 2° quadrangle, North Carolina and South Carolina, 1:250,000," *Misc. Investigations Series, Map I-1948-A*, United States Geological Survey, Reston, VA.

Ordóñez, G. A. (2011). "SHAKE2000: A computer program for the 1D analysis of geotechnical earthquake engineering problems, user's manual," Geomotions, LLC, Lacey, WA, 250 p.

Park, D., and Hashash, Y. M. A. (2005). "Estimation of seismic factors in the Mississippi Embayment: II. Probabilistic seismic hazard with nonlinear site effects," *Soil Dynamics and Earthquake Engineering*, **25**(2), 145-156.

Park, D., Dong, K., Chang-Gyun, J., and Taehyo, P. (2012). "Development of probabilistic seismic site coefficients of Korea," *Soil Dynamics and Earthquake Engineering*, **43**(1), 247-260.

Phillips, C., and Hashash, Y. (2009). "Damping formulation for nonlinear 1D site response analyses," *Soil Dynamics and Earthquake Engineering*, 2**9**(7), 1143-1158.

Power, M. S., and Chiou, S.-J., (2000). "National Representation of Seismic Ground Motion for New and Existing Highway Facilities," Unpublished Report, Multidisciplinary Center for Earthquake Engineering Research, University at Buffalo, Buffalo, NY.

Power, M. S., Mayes, R. L., and Friedland, I. M. (1998). "National representation of seismic ground motion for new and existing highway facilities," *Proc. CD-ROM, Sixth National Conference on Earthquake Engineering*, Earthquake Engineering Research Institute, Oakland, CA.

Prevost, J. H. (1989). "DYNA1D: A computer program for nonlinear site response analysis, technical documentation," National Center of Earthquake Engineering Research, Sunny at Buffalo, NY.

Prowell, D. C. (1996). "Geologic map of the Savannah River Site, Aiken, Allendale, and Barnwell counties South Carolina," USGS *Misc. Field Studies Map: 2300,* United States Geological Survey, Reston, VA.

Pyke, R. M. (1979). "Nonlinear models for irregular cyclic loadings," *Journal Geotechnical Engineering Division*, **105**(6), 715-726.

Rathje, E. M., Abrahamson, N. A., and Bray, J. D. (1998). " Simplified frequency content estimates of earthquake ground motions, *Journal of Geotechnical and Geoenvironmental Engineering*, **124**(2), 150-159.

Rodriguez-Marek, A., Bray, J. D., and Abrahamson, N. A. (2001). "An empirical geotechnical seismic site response procedure," *Earthquake Spectra*, **17**(1), 65-87.

Schnabel, P. B., Lysmer, J., and Seed, H. B. (1972). "SHAKE: a computer program for earthquake response analysis of horizontally layered sites," *Report EERC 72-12,* University of California, Berkeley, CA.

Seed, R. B., Dickenson, S., and Mok, C. M. (1994). "Site effects on strong shaking and seismic risk: recent developments and their impact on seismic design codes and practice," *Proc., Structures Congress XII,* vol. 1, American Society of Civil Engineers, Reston, VA 573–578.

Seyhan, E., and Stewart, J. P. (2012). "Site response in NEHRP provisions and NGA models," *Proc., 2012 GeoCongress, Geotechnical Engineering State of the Art and Practice,* ASCE, Reston, VA, 359-379.

Silva, W., Darragh, R., Gregor, N., Martin, G., Abrahamson, N., and Kircher, C. (2000). "Reassessment of site coefficients and near-fault factors for building code provisions," *NEHRP Program Report 98-HQ-GR-1010,* United States Geological Survey, Merlo Park, CA.

Silva, W., Wang, I., Siegel, T., Gregor, N., Darragh, R., and Lee, R. (2003). "Ground motion and liquefaction simulation of the 1886 Charleston, South Carolina, earthquake," *Bulletin of the Seismological Society of America,* **93**(6), 2717-2736.

Snow, R.W., II (2008). "Comparison of nonlinear and equivalent-linear site response analysis for soft-soil sites along the Wasatch Front and site-specific response predictions for the Legacy Parkway," *Ph.D. Dissertation*, University of Utah, Salt Lake City, UT.

South Carolina Department of Natural Resources, SCDNR (2005). *Generalized Geologic Map of South Carolina*, South Carolina Department of Natural Resources and South Carolina Geological Survey, Columbia, SC.

South Carolina Department of Transportation, SCDOT (2008a). *Geotechnical Design Manual*. Version 1.0, South Carolina Department of Transportation, Columbia, SC.

South Carolina Department of Transportation, SCDOT (2008b). *SCDOT Seismic Design Specification of Highway Bridges*, Version 2.0, South Carolina Department of Transportation, Columbia, SC.

South Carolina Department of Transportation, SCDOT (2010). *Geotechnical Design Manual*, Version 1.1, South Carolina Department of Transportation, Columbia, SC. (http://www.scdot.org/doing/bridge/geodesignmanual_details.shtml, accessed March 2012).

Stewart, J. P., and Kwok, O. L. A. (2008). "Nonlinear seismic ground response analysis: code usage protocols and verification against vertical array data," *Proc. 4th Decennial Geotechnical Earthquake Engineering and Soil Dynamics Conference*, ASCE, Sacramento, CA.

Stewart, J. P., S. Chiou, J. D. Bray, R. W. Graves, P. G. Somerville, and N. A. Abrahamson (2001). "Ground motion evaluation procedures for performance-based design," *PEER Report 2001/09*, Pacific Earthquake Engineering Research Center, University of California, Berkeley, CA.

Stewart, J. P., Liu, A. H., and Choi, Y. (2003). "Amplification factors for spectral acceleration in tectonically active regions," *Bulletin of the Seismological Society America*, **93**(1), 332-352**.**

Stewart, J. P., Kwok, O. L. A., Hashash, Y. M. A., Matasovic, N., Pyke, R., Wang, Z. L., and Yang, Z. (2006). "Overcoming hurdles that limit the application of nonlinear seismic ground response analysis in engineering practice," *Proc., 5th National Seismic Conference on Bridges and Highways*, San Francisco, CA.

Stewart, J. P., Kwok, A. O., Hashash, Y. M. A., Matasovic, N., Pyke, R., Wang, Z., and Yang, Z. (2008). "Benchmarking of nonlinear geotechnical ground response analysis procedures," *Report PEER 2008/04*, Pacific Earthquake Engineering Research Center, University of California at Berkeley.

Stokoe II, K. H., Darendeli, M. B., Gilbert, R. B., Menq, F.-Y., and Choi, W.-K. (2004). "Development of a new family of normalized modulus reduction and material damping curves," *Proc., NSF/PEER Int. Workshop on Uncertainties in Nonlinear Soil Properties and their Impact on Modeling Dynamic Soil Response*, University of California, Berkeley, CA.

Talwani, P. (1986). "Seismotectonics of the Charleston region," *Proc., 3rd U.S. National Conference on earthquake engineering*, Vol. 1, Earthquake Engineering Research Institute, Oakland, CA, 15-24.

Talwani, P., and Gassman, S. L. (2008). "The use of paleoliquefaction features in seismic hazard assessment-the Charleston experience." *Proc. 6th National Seismic Conf. Bridge and Highways*, July 28-30, Charleston, SC, MCEER, Buffalo, NY.

Talwani, P., and Schaeffer, W. T. (2001). "Recurrence rates of large earthquakes in the South Carolina Coastal Plain based on paleoliquefaction data," *Journal Geophysical Research*, **106**(b4), 6621-6642.

Tokimatsu, K., and Sugimoto, R. (2008). "Strain-dependent soil properties estimated from downhole array recordings at Kashiwazaki-Kariwa Nuclear Power Plant during the 2007 Niigata-Ken Chuetsu-Oki earthquake," *Geotechnical Earthquake Engineering and Soil Dynamics IV*, American Society of Civil Engineers, Reston, VA. (http://ascelibrary.org/doi/pdf/10.1061/40975(318)25)

Toro, G. (1995). "Probabilistic models of site velocity profiles for generic and site-specific ground motion amplification studies," Department of Nuclear Energy Brookhaven National Laboratory, Upton, NY.

Weems, R. E., and Lewis, W. C. (2002). "Structural and tectonic setting of the Charleston, South Carolina, region: Evidence from the Tertiary stratigraphic record," *Geological Society of America Bulletin*, **114**(1), 24–42.

Weems, R. E., Lewis, W. C., and Lemon, E. M., Jr. (2014). "Surficial geologic map of the Charleston region, Berkeley, Charleston, Colleton, Dorchester, and Georgetown Counties, South Carolina," *USGS Open-file Report 2013-1030*, Scale 1:1,000,000, United States Geological Survey, Reston VA, http://dx.doi.org/10.3133/ofr20131030.

Wheeler, R. L., and Cramer, C. H. (2000). "Preliminary estimate of the amplification of possible earthquake ground motion at a site in Charleston County, South Carolina," *USGS Open-file Report 00-048,* United States Geological Survey, Reston, VA.

Zhang J., Andrus, R. D., and Juang, C. H. (2005). "Normalized shear modulus and material damping ratio relationships," *Journal Geotechnical and Geoenvironmental Engineering*, **131**(4), 453-464.

Zhang J., Andrus, R. D., and Juang, C. H. (2008). "Model uncertainty in normalized shear modulus and damping relationships," *Journal Geotechnical and Geoenvironmental Engineering*, **134**(1), 24-36.